TRC1901

# Spatial Analysis of Benefits of Site-Specific Ground Motion Response Analysis

Ashraf Elsayed, Ph.D., P.E.
Shahram Pezeshk, Ph.D., P.E.
Nima Nazemi, Ph.D. Candidate
Ali Farhadi, Ph.D. Candidate
Naeem Khoshnevis, Ph.D.

Arkansas State University

University of Memphis

Final Report

March 2021

Final Report

# Spatial Analysis of Benefits of Site-Specific Ground Motion Response Analysis

(Research Project No. TRC1901)

for:

Arkansas Department of Transportation

Prepared by:

Ashraf Elsayed, Ph.D., P.E.

*Department of Civil Engineering*
Arkansas State University

Shahram Pezeshk, Ph.D., P.E.
Nima Nazemi, Ph.D. Candidate
Ali Farhadi, Ph.D. Candidate
Naeem Khoshnevis, Ph.D.

*Department of Civil Engineering*
The University of Memphis

March 2021

Disclaimer:
This report represents the views of the authors, who are responsible for the factual accuracy of the information presented herein. The views expressed here do not necessarily reflect the views of the Arkansas Department of Transportation.

# TECHNICAL REPORT DOCUMENTATION PAGE

| 1. Report No.<br>TRC1901 | 2. Government Accession No. | 3. Recipient's Catalog No. |
|---|---|---|
| **4. Title and Subtitle**<br>Spatial Analysis of Benefits of Site-Specific Ground Motion Response Analysis | | **5. Report Date**<br>March 2021<br>**6. Performing Organization Code** |
| **7. Author(s)**<br>Ashraf Elsayed, Ph.D., P.E.<br>Shahram Pezeshk, Ph.D., P.E.<br>Nima Nazemi, Ph.D. Candidate<br>Ali Farhadi, Ph.D. Candidate<br>Naeem Khoshnevis, Ph.D. | | **8. Performing Organization Report No.** |
| **9. Performing Organization Name and Address**<br>Arkansas State University, PO Box 1740, State University, AR 72467<br>University of Memphis, 263 Administration Building, Memphis TN 38152 | | **10. Work Unit No.**<br>**11. Contract or Grant No.** |
| **12. Sponsoring Agency Name and Address**<br>Arkansas Department of Transportation<br>PO Box 2261<br>Little Rock, AR 72203-2261 | | **13. Type of Report and Period Covered**<br>FINAL (07/19-03/21)<br>**14. Sponsoring Agency Code** |

**15. Supplementary Notes**
Project performed in cooperation with the Federal Highway Administration


**16. Abstract**

The general procedure of the American Association of State Highway and Transportation Officials (AASHTO) LRFD Bridge Design Specifications, or AASHTO Guide Specifications for Load and Resistance Factor Design (LRFD) Seismic Bridge Design is sufficient to determine seismic hazard and site response. However, it is appropriate and may be necessary to perform site-specific hazard analyses for cases involving special aspects of seismic hazard such as long duration earthquakes, critical or essential bridges, specific soil site classes, and near-fault conditions. The result of site-specific hazard analyses may be used as justification for a reduction in the spectral acceleration determined from the general procedure representing the uniform seismic hazard. The results from TRC1603 (Wood et al. 2019) and results from MBTC3032 (Cox et al. 2012) indicate that seismic demands can be reduced in portions of Arkansas by conducting a site-specific ground motion response analysis (SSGMRA).

The purpose of this study is to develop a series of Geographic Information System (GIS) maps that can be used by the Arkansas Department of Transportation (ARDOT) engineers and planners to determine when site-specific ground motion response analysis (SSGMRA) should be conducted. This project also provides information about possible cost savings if an SSGMRA is performed. To achieve this goal, this research is built upon the work completed in TRC1603 and included obtaining shear-wave velocity (Vs) profiles for 20 sites. These 20 sites will be in addition to 15 surveyed sites included in the TRC1603 project and 16 sites surveyed in the TRC0803 project (Elsayed et al., 2008).


| 17. Key Words | 18. Distribution Statement |
|---|---|
| Site-Specific Ground motion Response Analysis, Multi-Channel Spectral Analysis of Surface Waves, Refraction Microtremor, Probabilistic Seismic Hazard Analysis, Ground Motion Selection and Matching. | No restrictions. This document is available through the National Technical Information Service, Springfield, VA 22161. |

| 19. Security Classification. (of this report) | 20. Security Classification (of this page) | 21. No. of Pages | 22. Price |
|---|---|---|---|
| Unclassified | Unclassified | 386 | |

# SI* (MODERN METRIC) CONVERSION FACTORS

## APPROXIMATE CONVERSIONS TO SI UNITS

| Symbol | When You Know | Multiply By | To Find | Symbol |
|---|---|---|---|---|
| | | **LENGTH** | | |
| in | inches | 25.4 | millimeters | mm |
| ft | feet | 0.305 | meters | m |
| yd | yards | 0.914 | meters | m |
| mi | miles | 1.61 | kilometers | km |
| | | **AREA** | | |
| $in^2$ | square inches | 645.2 | square millimeters | $mm^2$ |
| $ft^2$ | square feet | 0.093 | square meters | $m^2$ |
| $yd^2$ | square yard | 0.836 | square meters | $m^2$ |
| ac | acres | 0.405 | hectares | ha |
| $mi^2$ | square miles | 2.59 | square kilometers | $km^2$ |
| | | **VOLUME** | | |
| fl oz | fluid ounces | 29.57 | milliliters | mL |
| gal | gallons | 3.785 | liters | L |
| $ft^3$ | cubic feet | 0.028 | cubic meters | $m^3$ |
| $yd^3$ | cubic yards | 0.765 | cubic meters | $m^3$ |
| | | NOTE: volumes greater than 1000 L shall be shown in $m^3$ | | |
| | | **MASS** | | |
| oz | ounces | 28.35 | grams | g |
| lb | pounds | 0.454 | kilograms | kg |
| T | short tons (2000 lb) | 0.907 | megagrams (or "metric ton") | Mg (or "t") |
| | | **TEMPERATURE (exact degrees)** | | |
| $^oF$ | Fahrenheit | 5 (F-32)/9<br>or (F-32)/1.8 | Celsius | $^oC$ |
| | | **ILLUMINATION** | | |
| fc | foot-candles | 10.76 | lux | lx |
| fl | foot-Lamberts | 3.426 | $candela/m^2$ | $cd/m^2$ |
| | | **FORCE and PRESSURE or STRESS** | | |
| lbf | poundforce | 4.45 | newtons | N |
| $lbf/in^2$ | poundforce per square inch | 6.89 | kilopascals | kPa |

## APPROXIMATE CONVERSIONS FROM SI UNITS

| Symbol | When You Know | Multiply By | To Find | Symbol |
|---|---|---|---|---|
| | | **LENGTH** | | |
| mm | millimeters | 0.039 | inches | in |
| m | meters | 3.28 | feet | ft |
| m | meters | 1.09 | yards | yd |
| km | kilometers | 0.621 | miles | mi |
| | | **AREA** | | |
| $mm^2$ | square millimeters | 0.0016 | square inches | $in^2$ |
| $m^2$ | square meters | 10.764 | square feet | $ft^2$ |
| $m^2$ | square meters | 1.195 | square yards | $yd^2$ |
| ha | hectares | 2.47 | acres | ac |
| $km^2$ | square kilometers | 0.386 | square miles | $mi^2$ |
| | | **VOLUME** | | |
| mL | milliliters | 0.034 | fluid ounces | fl oz |
| L | liters | 0.264 | gallons | gal |
| $m^3$ | cubic meters | 35.314 | cubic feet | $ft^3$ |
| $m^3$ | cubic meters | 1.307 | cubic yards | $yd^3$ |
| | | **MASS** | | |
| g | grams | 0.035 | ounces | oz |
| kg | kilograms | 2.202 | pounds | lb |
| Mg (or "t") | megagrams (or "metric ton") | 1.103 | short tons (2000 lb) | T |
| | | **TEMPERATURE (exact degrees)** | | |
| $^oC$ | Celsius | 1.8C+32 | Fahrenheit | $^oF$ |
| | | **ILLUMINATION** | | |
| lx | lux | 0.0929 | foot-candles | fc |
| $cd/m^2$ | $candela/m^2$ | 0.2919 | foot-Lamberts | fl |
| | | **FORCE and PRESSURE or STRESS** | | |
| N | newtons | 0.225 | poundforce | lbf |
| kPa | kilopascals | 0.145 | poundforce per square inch | $lbf/in^2$ |

*SI is the symbol for the International System of Units. Appropriate rounding should be made to comply with Section 4 of ASTM E380.
(Revised March 2003)

CONTENTS

LIST OF FIGURES

LIST OF TABLES

LIST OF ABBREVIATIONS

AASHTO - American Association of State Highway and Transportation Officials

AF – Amplification Factor

ARDOT - Arkansas Department of Transportation

CEUS - Central and Eastern United States

CUS - Central United States

EPRI - Electric Power Research Institute

EQL - Equivalent Linear

FAS - Fourier Amplitude Spectrum

ft - feet

GIS - Geographic Information System

GMM – Ground Motion Model

GMPE - Ground-Motion Prediction Equations

IDS – Inverse Distance Weighting

LRFD – Load and Resistance Factor Design

m - meter

MASW - Multi-Channel Spectral Analysis of Surface Waves

NSHMP - National Seismic Hazard Mapping Project

PGA – Peak Ground Acceleration

PSHA - Probabilistic Seismic Hazard Analysis

ReMi - Refraction Microtremor

RVT - Random Vibration Theory

SA – Spectral Acceleration

SASW – Spectral Analysis of Surface Waves

SCPT – Seismic Cone Penetration Testing

SSGMRA - Site-Specific Ground Motion Response Analysis

UHS – Uniform Hazard Spectrum

USGS - United States Geological Survey

# EXECUTIVE SUMMARY

The purpose of this study is to develop a series of Geographic Information System (GIS) maps that can be used by the Arkansas Department of Transportation (ARDOT) engineers and planners to determine whether site-specific ground motion response analysis (SSGMRA) should be conducted. This project also provides information about possible cost savings if SSGMRA is performed. To achieve this goal, this research is built upon the work completed in TRC1603 and includes obtaining shear-wave velocity ($V_s$) profiles for 20 sites. These 20 sites will be in addition to 15 surveyed sites included in the TRC1603 project and 16 sites surveyed in the TRC0803 project (Elsayed et al. 2008).

This page is intentionally left blank.

# CHAPTER 1. INTRODUCTION

## 1.1 INTRODUCTION

The general procedure of the American Association of State Highway and Transportation Officials (AASHTO) LRFD Bridge Design Specifications, 9th Edition, or AASHTO Guide Specifications for Load and Resistance Factor Design (LRFD) Seismic Bridge Design is sufficient to determine seismic hazard and site response. However, it is appropriate and may be necessary to perform site-specific hazard analyses for cases involving special aspects of seismic hazard such as long duration earthquakes, critical or essential bridges, specific soil site classes, and near-fault conditions. The result of site-specific hazard analyses may be used as justification for a reduction in the spectral acceleration determined from the general procedure representing the uniform seismic hazard. The results from TRC1603 (Wood et al. 2019) and results from MBTC3032 (Cox et al. 2012) indicate that seismic demands can be reduced in portions of Arkansas by conducting a site-specific ground motion response analysis (SSGMRA), which is expected to have economic benefits regarding the construction of bridges and embankments.

An SSGMRA is required for Site Class F sites as defined by AASHTO Specifications. Furthermore, site-specific ground motion response analyses are required for deep soil deposits or relatively thin soil (<15 m per AASHTO 2015) deposits over rock. Pezeshk and Hashash (2003) and Park et al. (2004) noted a shift of the design response spectrum to larger periods when site-specific ground motion response analyses were performed in deep soil sites. Cox et al. (2012) [MBTC3032] stated that "Site-specific ground motion response analyses have been conducted for an example bridge site in Blytheville, Arkansas. Results from the site-specific analyses clearly show that the generic seismic design forces could have been reduced by the AASHTO-allowed 33 percent if these site-specific analyses had been performed prior to design. Similar results are expected for short-period bridges throughout Northeast Arkansas, where probabilistic seismic hazards are generally dominated by a single earthquake scenario and subsurface conditions are relatively homogenous."

An SSGMRA consists of evaluating the hazard and its effects on bridges being analyzed or designed by (1) characterizing the subsurface soils, (2) determining probabilistic seismic hazard analysis at the rock level, (3) determining the site effects, and (4) obtaining ground motions of a design response spectrum. According to AASHTO LRFD Bridge Design Specifications, the intent of conducting a site-specific hazard study is to develop ground motions and response spectra that are more accurate for local seismic and site conditions than can be determined from the United States Geological Survey (USGS) hazard maps.

One-dimensional equivalent-linear or non-linear procedures are commonly used for site-specific site response analyses. A one-dimensional analysis is generally based on the assumption that soils and ground surfaces are laterally uniform and horizontal. Ground motions are modeled by vertically propagating shear-waves through soil layers. The influence of vertical motions, surface waves, laterally non-uniform soil conditions, incoherence, and spatial variation of ground motions are not accounted for in a one-dimensional analysis. Personnel performing site-specific studies should provide detailed information on how the appropriate input parameters for the site-specific response analysis are selected. The input

parameters that are typically required for both nonlinear and equivalent-linear site-specific response analysis include a suite of ground-motion time histories, soil layering, depth-to-rock, dynamic properties for each layer such as the shear-wave velocity of each layer and half-space, soil and rock small strain parameters, unit weight of each layer, shear modulus degradation, and damping curves for each layer. The depth-to-rock is an essential parameter in SSGMRA and will be an important parameter to consider in this study. Figure 1 shows the geology of Arkansas and the depth to bedrock within various regions. This figure is provided to show a general overview of the study region geology.

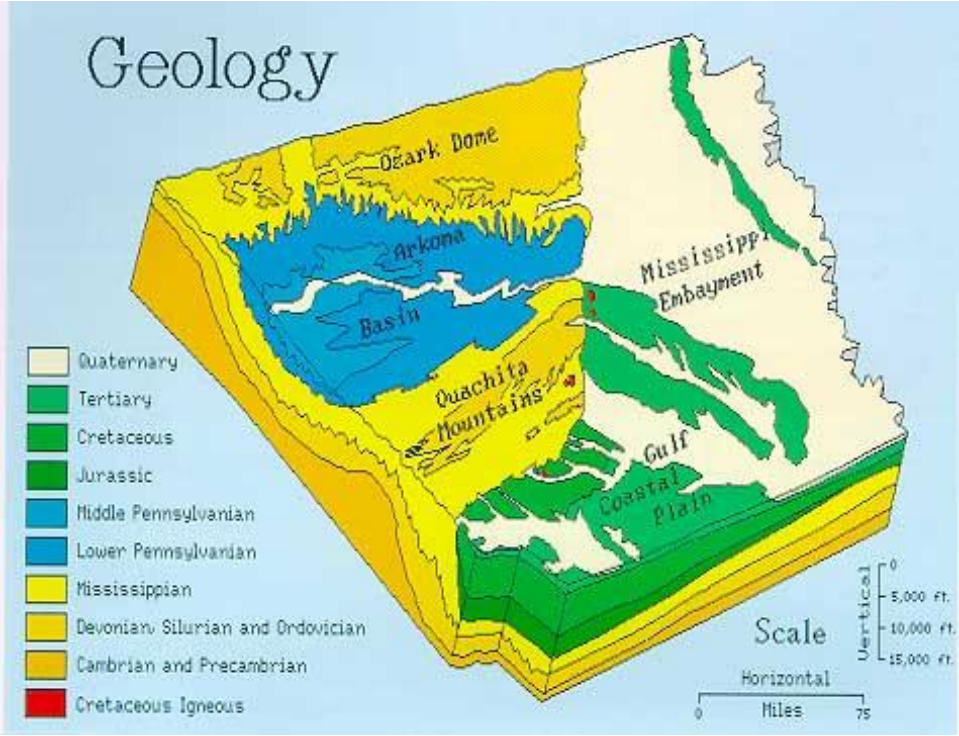


**Figure 1. Smith, R.M, "Geology Map", in *The Atlas of Arkansas*, University of Arkansas Press, 1989, United States Department of Agriculture Forest Service, https://www.fs.usda.gov/detail/ouachita/learning/nature-science/?cid=fsm9_039800**

# CHAPTER 2. SITE SELECTION AND SITE INVESTIGATION

## 2.1 BACKGROUND

This report provides detailed results of a two-year research project. The central objective of this project is the dynamic characterization of 20 selected sites spread over the northeastern quarter of Arkansas. The boundaries of the study area were discussed and approved with the TRC1901 Subcommittee. Figure 2 demarcates the study area limited to the red lines and the state boundary.

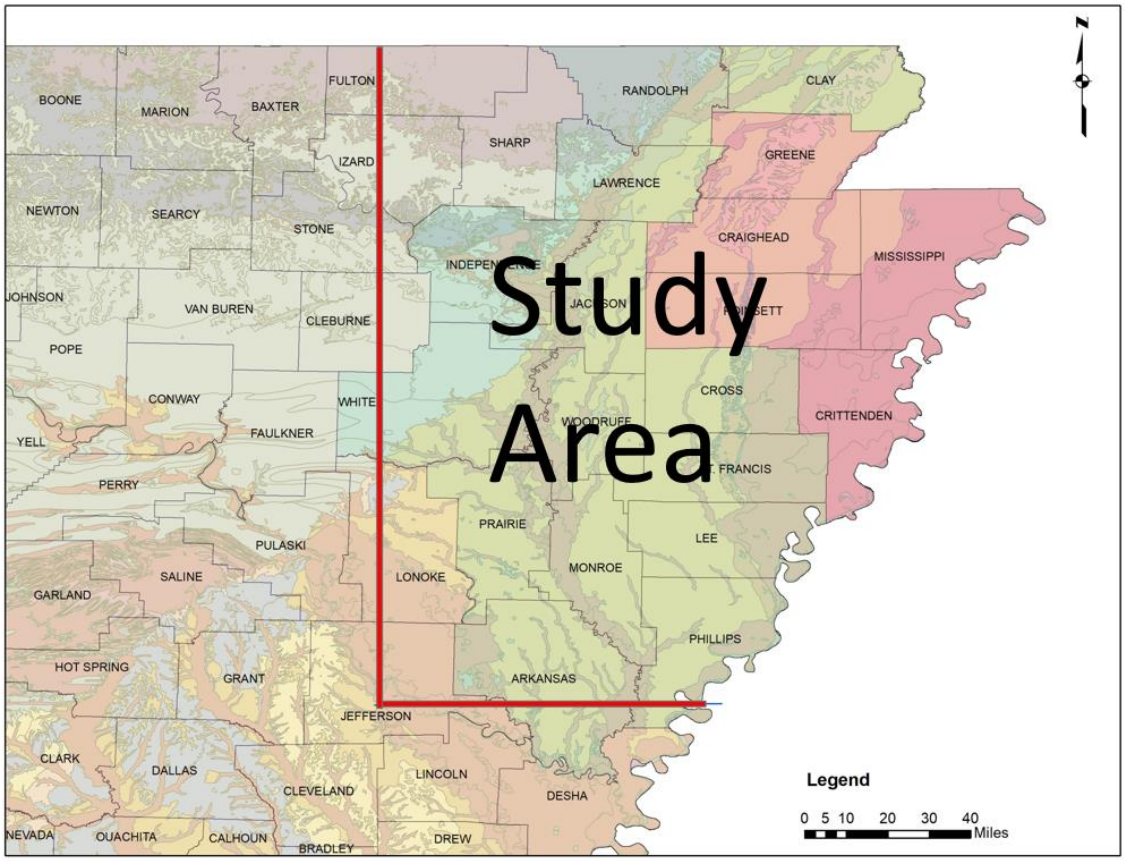


**Figure 2. The Study Area**

Most of the study area falls within the Mississippi embayment. There are six major geological/geographical features in the state of Arkansas: Ozark Mountains, Arkansas Valley, Ouachita Mountains, West Gulf Coastal Plain, Mississippi Alluvial Plain, and Crowley's Ridge (Figure 3). Given the local geological settings, a total of 20 sites were selected, in addition to available data from 15 sites in the TRC1603 project. In addition, TRC0803 (Elsayed et al. 2008) surveyed 15 sites using Multi-channel spectral analysis of surface waves (MASW).

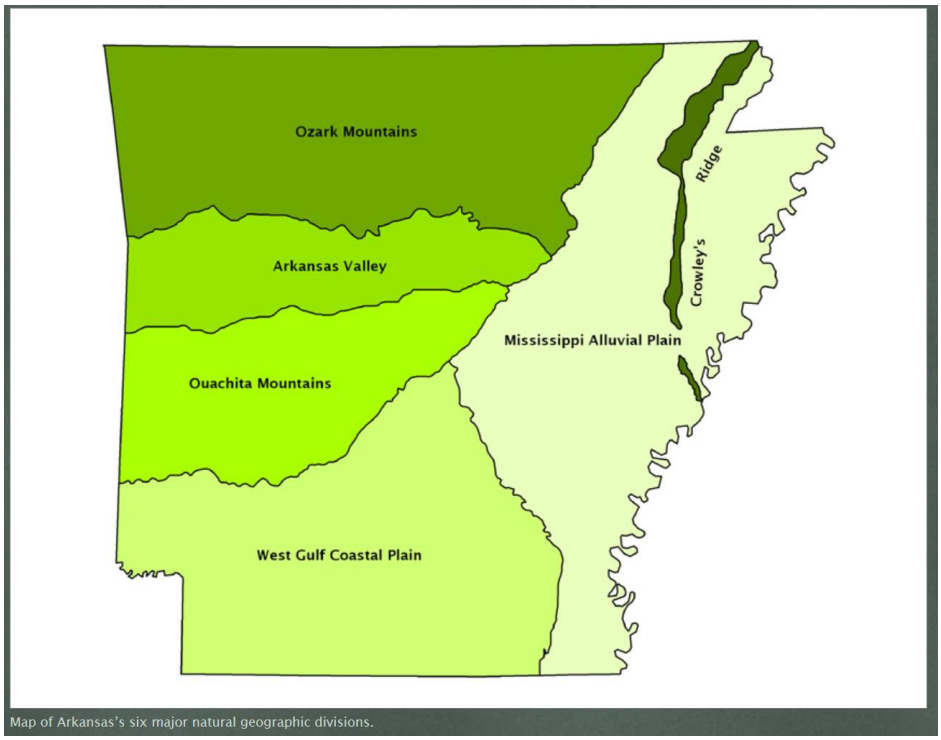


**Figure 3. Reed, David, "Map of Arkansas' six major natural geographic divisions", n.d., https://encyclopediaofarkansas.net/media/arkansas-natural-divisions-6333/**

Site selection was based on the location of current or potential ARDOT bridge locations. Dynamic site characterization seismic surveys were performed at 20 sites spatially distributed within Northeast Arkansas. Selected test sites were reviewed and approved by the Subcommittee. Included in Table 1 are the nearest ARDOT job number, route number, longitude, latitude, and county name of all 20 selected sites. In addition, two alternate sites were chosen in case one or two of the selected sites were inaccessible for any reason. Included in Table 2 is information regarding these two alternate sites. However, we did not need to use these alternative sites.

Properties of near-surface soil is fundamental information for performing site-specific seismic evaluation. Subsurface soil structure amplifies or diminishes certain ranges of seismic wave frequencies. Thus, it is important to obtain insight into the mechanical and geological features of the study area. Sites in this study were selected on the location where at least one boring log is available for enhancing and verifying our field MASW surveys. The black dots show the locations of available boring logs. In Figure 4, the red dots pinpoint the location of ARDOT future bridge projects. Green checkmarks in Figure 5 show the locations of future bridge projects that were selected.

Figure 6 shows the 20 sites selected for subsurface surveys. In Figure 7, data from TRC0803 and TRC1603 in green and blue dots are shown relative to our 20 candidate sites. To ensure the maximum data coverage over the study area, we calculated the Euclidian distance over the available, and proposed sites in Figure 8. In a complete format, proposed sites, boring data, future bridge sites, and other TRC projects are shown in Figure 9.

**Table 1. Sites Selected to Perform Dynamic Site Characterization**

| No. | Job# | Route | County | Lat | Long |
|---|---|---|---|---|---|
| 1 | 110390 | 50 | St. Francis | 35.01236 | -90.62815 |
| 2 | 110570 | 131 | Lee | 34.83260 | -90.60298 |
| 3 | 110616 | 78 | Lee | 34.70548 | -90.95934 |
| 4 | FA5415 | CR350 | Phillips | 34.50562 | -90.85035 |
| 5 | 110536 | 49 | Phillips | 34.50300 | -90.60545 |
| 6 | 050189 | 13 | White | 35.20006 | -91.80905 |
| 7 | F06233 | 31-Lonoke Maintenance Yard | Lonoke | 34.80495 | -91.88576 |
| 8 | 020047 | 31 | Jefferson | 34.41130 | -91.89755 |
| 9 | FA7315 | CR790 (Dagget Rd) | Woodruff | 35.36044 | -91.49505 |
| 10 | 110670 | 49 | Monroe | 34.90926 | -91.19669 |
| 11 | 110391 | 146 | Monroe | 34.57475 | -91.14614 |
| 12 | 020417 | 33 | Arkansas | 34.45413 | -91.32131 |
| 13 | 050321 | 56 | Izard | 36.17804 | -91.73953 |
| 14 | 100993 | 166 | Randolph | 36.31981 | -90.91261 |
| 15 | 100870 | 34 | Greene | 36.18635 | -90.33812 |
| 16 | 100723 | 148 | Mississippi | 35.86319 | -89.83975 |
| 17 | 100642 | 226 | Craighead | 35.79525 | -90.98321 |
| 18 | BR5607 | CR611 (Bayourd) | Poinsett | 35.49315 | -91.00196 |
| 19 | 110289 | 64 | Woodruff | 35.27009 | -91.23689 |
| 20 | BR1907 | CR 344 (Elmer Legg Rd) | Cross | 35.35866 | -90.75855 |

**Table 2. Two Alternate Sites**

| No. | Job# | Lat | Long | County |
|---|---|---|---|---|
| 1 | 020326 | 34.514106 | -91.53945 | Arkansas |
| 2 | 110123 | 34.668655 | -91.368809 | Monroe |

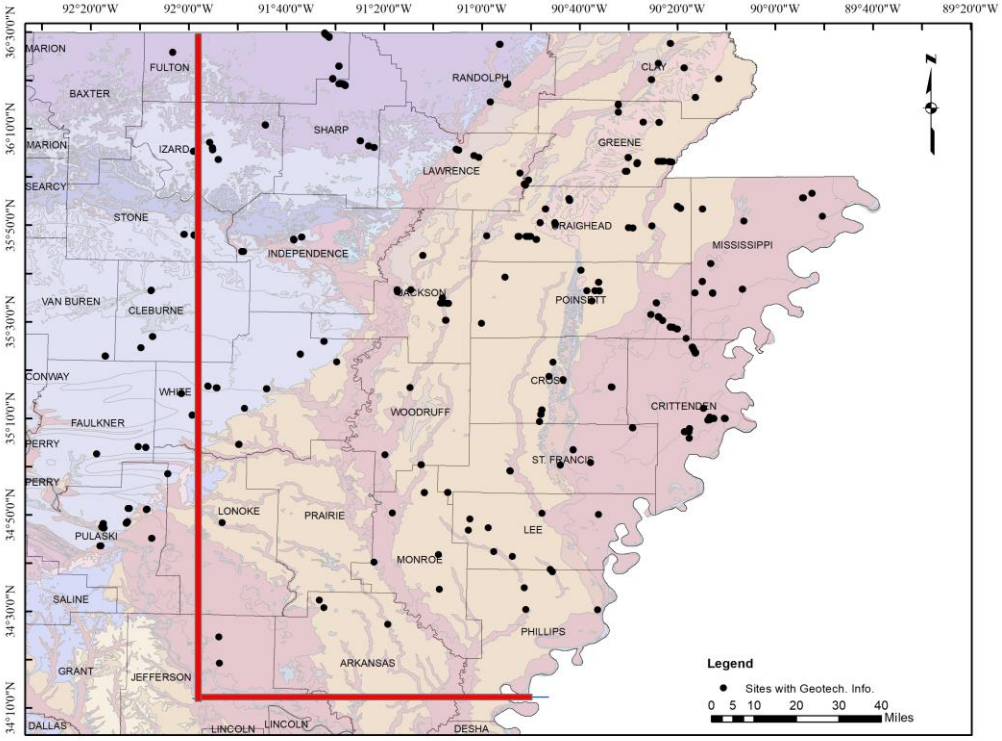


**Figure 4. Locations of Sites with Available Geotechnical Information**

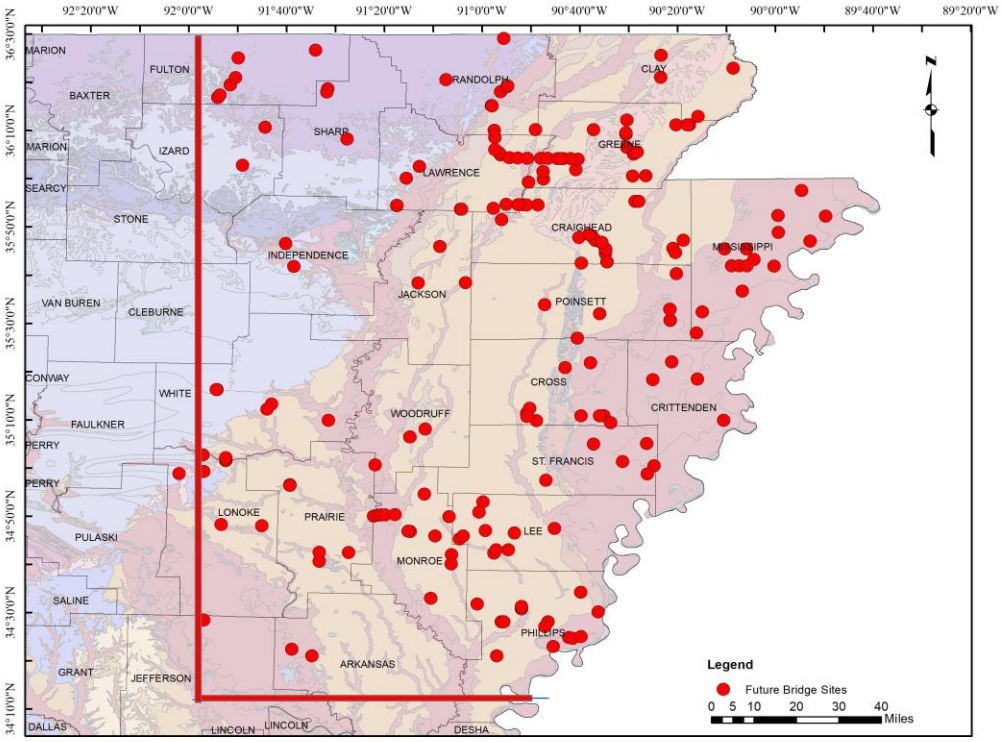


**Figure 5. Locations of Future Bridge Sites**

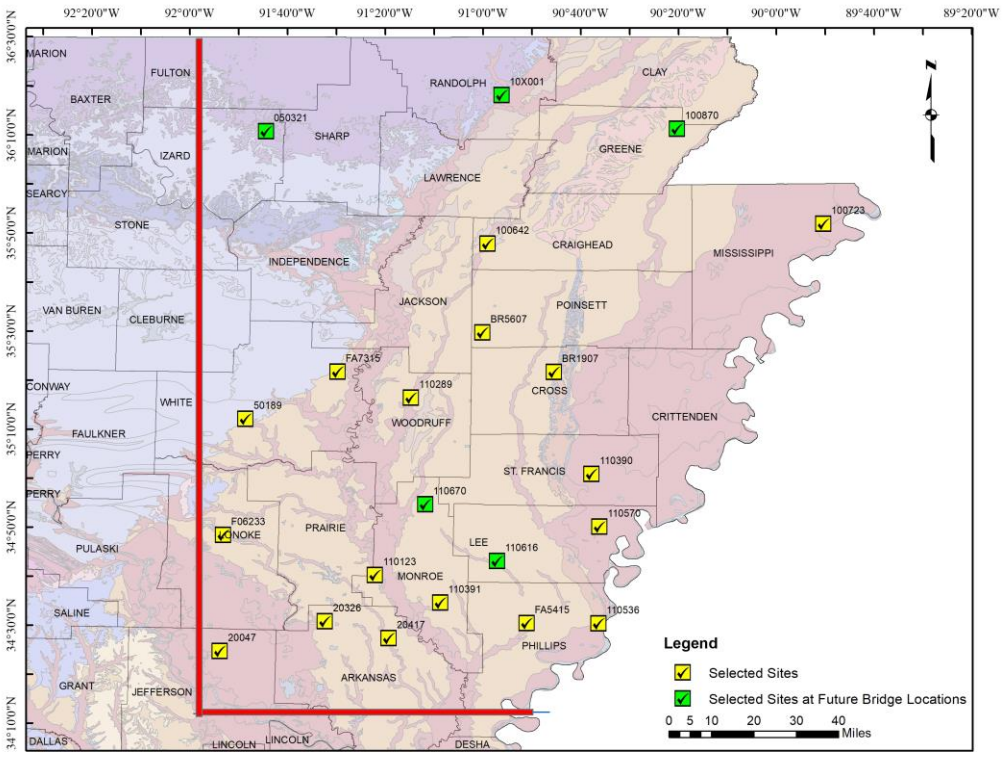


**Figure 6. Locations of the 20 Selected Sites**

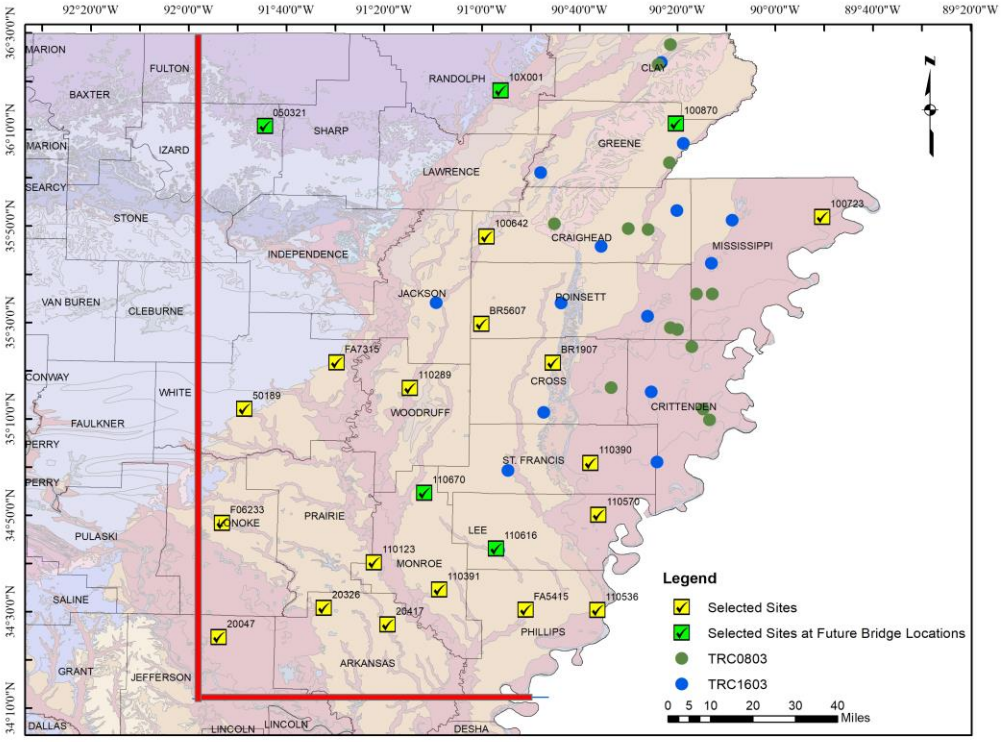


**Figure 7. Locations of Proposed Sites and sites Investigated by TRC1603 and TRC0803 Projects**

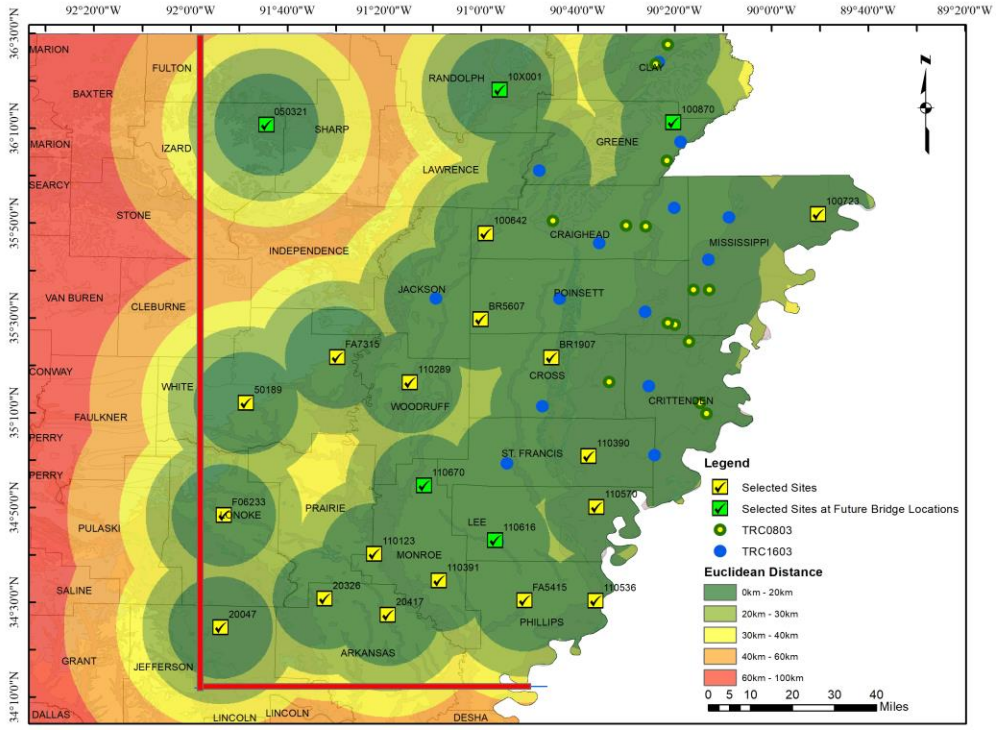


**Figure 8. Euclidean Distance of TRC0803, TRC1603, and TRC1901 Selected Sites**

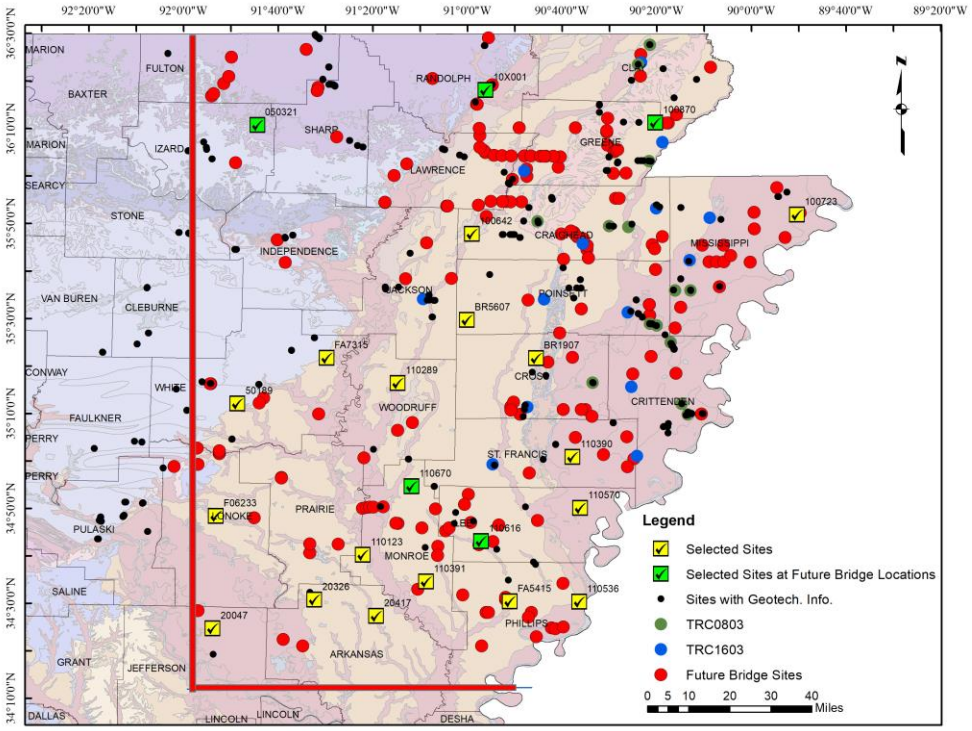


**Figure 9. Locations of Proposed Sites, Available Boring Logs, Future Bridge Sites, and Sites Investigated by TRC1603 and TRC0803 Projects**

## 2.2 OBTAINING SITE-SPECIFIC SHEAR-WAVE VELOCITY PROFILES

Near-surface shear-wave velocity ($V_s$) has been recognized as a key variable to be considered in SSGMRA, liquefaction resistance evaluations, and ground motion amplification studies. In general, borehole logging, such as downhole or crosshole seismic surveys, is considered the standard for obtaining $V_s$ data. However, drilling, casing, and logging to the required depths are expensive. In recent years, this has resulted in the development of several surface non-invasive geophysical exploration techniques to obtain shallow $V_s$. MASW (i.e., Pezeshk and Zarrabi, 2005; Rix et al., 2002) and Refraction Microtremor (ReMi) are two of the procedures that have gained popularity in recent years in estimating $V_s$ and layer thicknesses of soil profiles. Both MASW and ReMi are non-invasive soil characterization methods that use surface wave propagation characteristics. A good overview of the MASW procedure can be found in Hosseini and Pezeshk (2015), Hosseini (2014), Rix et al. (2002), Hebeler (2001), and Teague et al. (2018). Stephenson et al. (2005) provide a comparison of MASW and ReMi results with boreholes. Both MASW and ReMi procedures utilize a linear array of vertically oriented sensors. Both procedures, compared with other noninvasive methods (e.g., reflection and refraction), may provide proper resolution and more flexibility for near-surface media (Foti 2000). The general MASW procedure that has been used by several investigators is described below:

- Wave generation of a principal vertical ground motion using either an impulsive (hammer) or a continuous (shaker) source.
- Manual or computer-controlled recording of the received signals by spectrum analyzer, seismograph, or other specialized software.
- Spectral analysis of the recorded time-series data which results in the development of a dispersion curve – the curve of variation of phase velocity (Rayleigh wave velocity) with frequency (or wavelength).
- Inversion of dispersion curves to estimate the shear-wave velocity-depth profiles.

MASW and ReMi differ fundamentally in their recorded source signal type. MASW is an active-source technique requiring signals from a source such as a sledgehammer. The $V_s$ profile is obtained from the Rayleigh wavefield generated by a source. Conversely, ReMi is a passive technique, recording ambient noise or microtremors being present in the urban environment. A shear-wave velocity profile is obtained by identifying the fundamental mode of the Rayleigh wave field within the microtremors.

As discussed earlier, 20 sites were selected in coordination with the Project Subcommittee considering seismicity, geological composition, future bridge sites, representation of the geological composition of Arkansas, accessibility, and the availability of standard penetration test (SPT) data. At each of the selected sites, two types of non-invasive testing procedures (MASW and ReMi) were performed to obtain shear-wave velocity profiles.

### 2.3 REFRACTION MICROTREMOR (REMI)

The ReMi technique used in this research is based on the method described by Louie (2001). The ReMi method is designed to analyze ambient seismic waves recorded by a linear array of common seismic refraction recording equipment.

Louie (2001) used an array of up to 48 8-Hz geophones spaced from 8 to 20 m apart. The total depth measured is a function of the density of geophones, spread length, and frequency content of recorded noise events, and the number and the frequency of measurements. The geophones are pushed into the ground and can be up to 20 degrees off vertical and still produce accurate results (Louie, 2001). The ReMi procedure uses ambient noise to produce average one-dimensional shear wave profiles down to depths over 100 ft.

The ReMi method analyzes the traces from the individual geophones and is based on the slant-stack ($p$-$\tau$) transform presented by Thorson and Claerbout (1985). This transformation takes multiple seismic records of amplitude relative to distance and time and converts them into amplitudes relative to ray parameter (inverse of velocity, or slowness) $P$ and intercept time. The final result is a plot of slowness versus frequency, as shown in Figure 10. Once a slowness-frequency value is picked, the slowness is inverted back into velocity and becomes a point on a dispersion curve.

In summary, the ReMi method uses the recorded background noise, or microtremors, to separate Rayleigh waves from other seismic arrivals. This allows for the determination of the true phase velocity as opposed to the apparent velocity (Louie 2001; Thorson and Claerbout 1985). The background noise is created by numerous sources and is prevalent in urban areas. In suburban or rural areas, the waves in the ground may not be strong enough to produce a high resolution. Locating the array close to nearby roads or railroad tracks in rural areas may be necessary.

For this study, a total of 24 4.5-Hz vertical geophones in a linear array were used. The spread of geophones was spaced at 10 ft for a total array length of 230 ft. Data were recorded using a sampling rate of 500 data points per second for 32 seconds of total durations. Several individual recordings were made for each location. Figure 11 shows a typical plot of the P-f (slowness – frequency) spectrum.

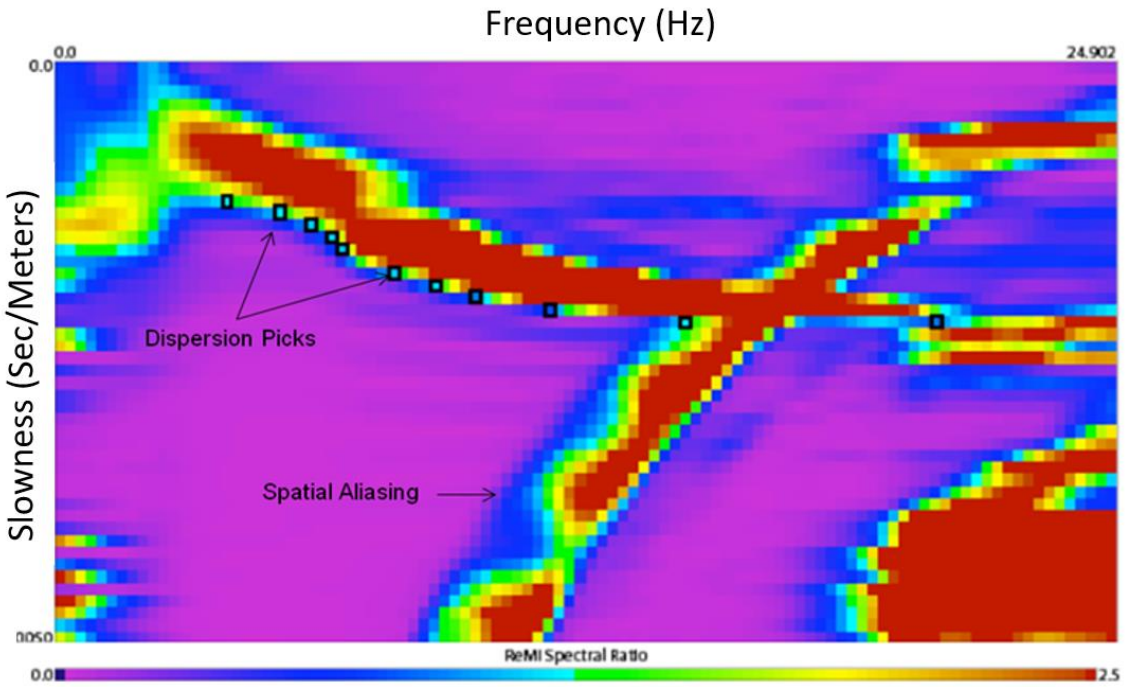


**Figure 10. Plot of Slowness-Frequency Spectrum**

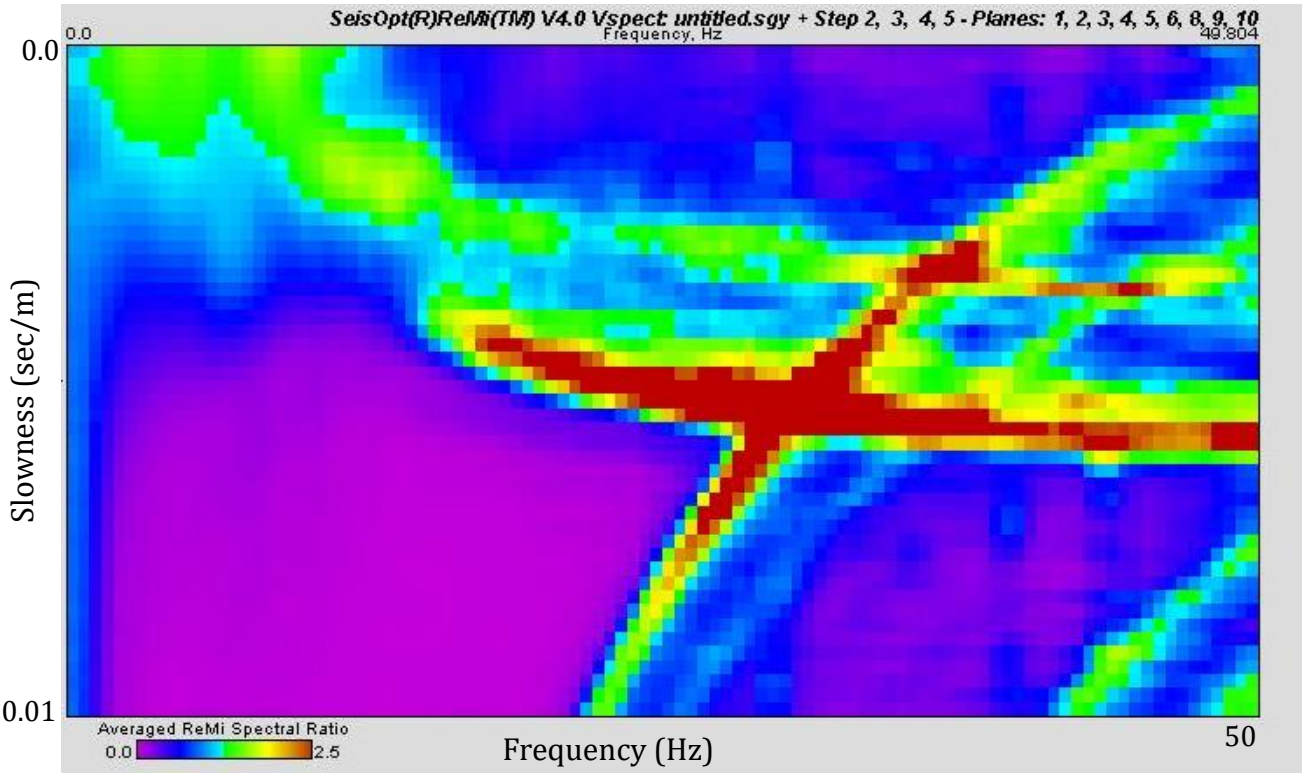


**Figure 11. A Typical Plot of Slowness-Frequency at a Study Site**

### 2.3.1 Refraction Microtremor (ReMi) Equipment and Software

The following equipment and software were used to perform the ReMi seismic survey at all selected sites:

- SeisDAQ™ ReMi™ V30+™ recording system 24 bit, the 24-channel system uses high-speed 10 Mbps Ethernet to connect to a computer; the recording system uses an internal compact flash card to store data in the unit while it is simultaneously transmitted in pseudo-realtime to host computer for storage in SEG-2, SEG-Y, or ASCII format.
- Twenty-four GS-20D 4.5 Hz geophones with split-clip take-outs, two 12-channel spread cable with 12 split-clip take outs, spaced at 8 meter (m) with 8 m lead-in and lead-out.
- SeisOpt software – ReMiVspectv4.0.

## 2.4 MULTI-CHANNEL ANALYSIS OF SURFACE WAVES (MASW) GEOPHYSICAL EXPLORATION

Rayleigh waves generate a circular particle motion in an infinite half-space. This motion's amplitude is an exponential function that is tied to frequency and wavelength. The lower frequencies (longer wavelengths) have a larger range of motion, and higher frequencies (shorter wavelengths) have a smaller range of particle motion. Consequently, higher frequency Rayleigh waves sample shallower depths and lower frequencies sample deeper through the soil layers, as shown in Figure 12. Knowing the velocity of seismic

waves is a function of soil shear-wave velocity, we can find out that different frequency ranges (phases) of Rayleigh waves will travel at different phase-velocities since they will sample different layers of soil with different seismic characteristics. This effect is called the dispersion of surface waves. Figure 13 shows the normalized vertical and horizontal particle motion exponentially decreasing with depth.

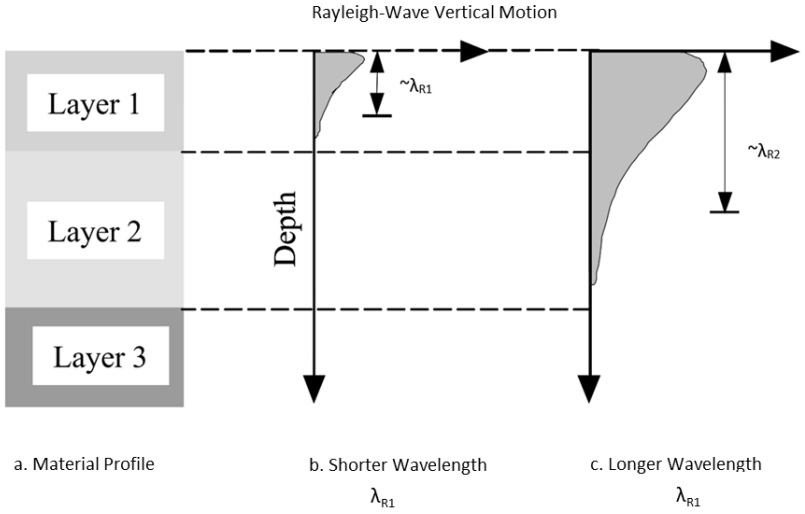


**Figure 12. Depth Sampled by Rayleigh Waves with Different Wavelengths (Stokoe II and Santamarina 2000)**

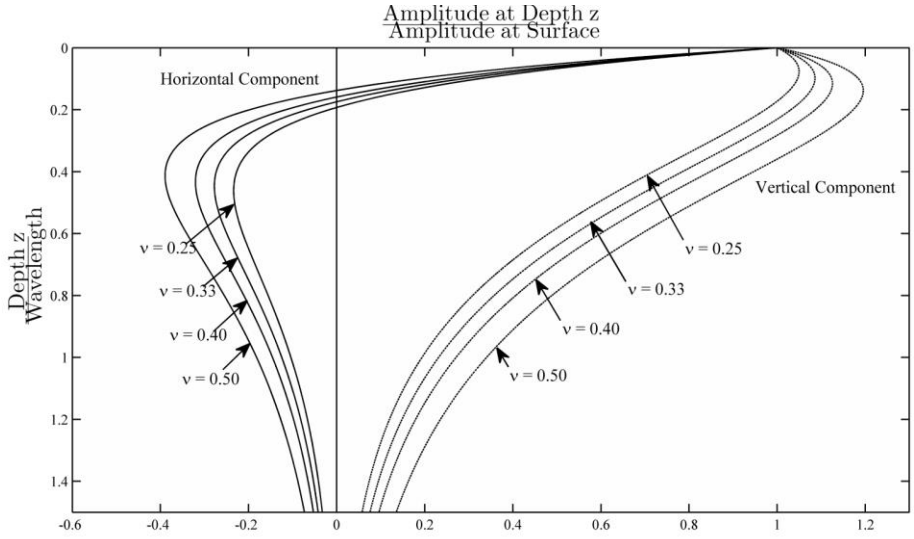


**Figure 13. Variation of Horizontal and Vertical Normalized Components of Displacements Induced by Rayleigh Waves with Normalized Depth in a Homogeneous Isotropic, Elastic Half-Space**

### 2.4.1 MASW Equipment

MASW equipment consists of the following:

- Vertical geophones to convert surface perturbations into electric analog signals (Figure 14).
- Geophone cables for all 24 geophones to transmit the electrical signals to the digitizing unit (Figure 15).
- Digitizing units that transform the electric analog signal into digital data recordable as a computer file; three (3) Geometrics Geodes® were used for this study (Figure 16).
- Data cables to transfer the digitized data into a PC (Figure 17).
- A laptop connected to the data cable to record incoming digitized signals into data files.
- A software console handling communication with the digitizers, recording the digitized signals into a file and setting parameters related to the experiment.
- A source of energy like a sledgehammer.
- A trigger attached to the hammer and an extension cable to connect the trigger to the digitizer (Figure 18).

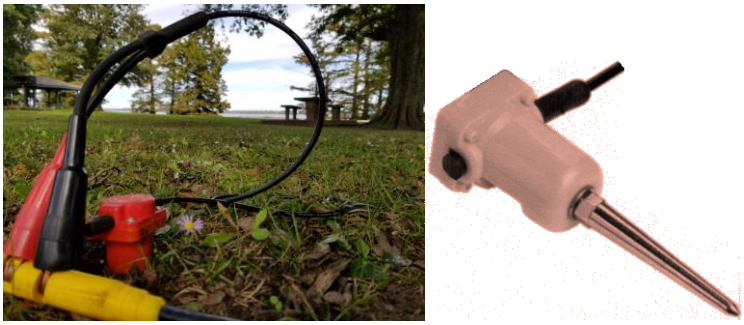

**Figure 14. Vertical Geophone with Corner Frequency of 4.5 Hz**

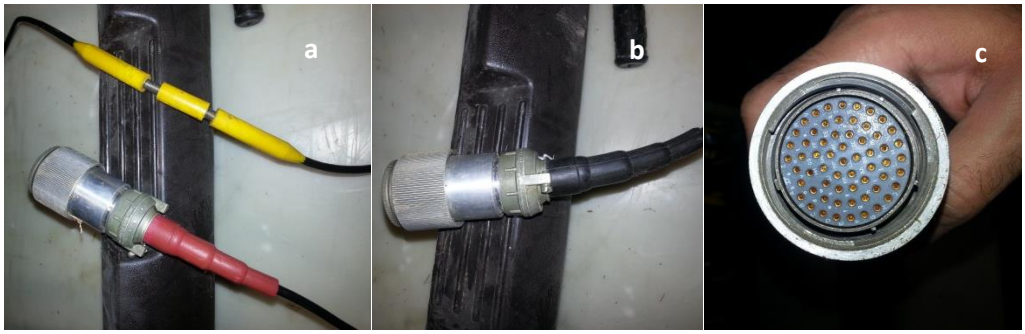


**Figure 15. Geophone Cable: (a) Red End-Connection and the Yellow Slot for Geophone Hookup, (b) Black End-Connection, and (c) Details of the End-Connection**


**Figure 16. Geometrics Geode 24 Channel Digitizer**

**Figure 17. Data Transfer Cable from Geode to Geode, or from Geode to Software Console on Laptop**

**Figure 18. The Trigger that Attaches to the Sledgehammer and Signals the Hit Time**

Once the test setup is complete, Rayleigh waves are generated by striking a metal plate with a sledgehammer at a specific location. The trigger signals the digitizer to start recording at the onset of hit time, and the digitizer sends the data from the geophones to the software console on the laptop.

### 2.4.2 Trigger Effect and Stacking

Considering the presence of noise in the recorded data, it is common practice to repeat each hit several times and stack the recorded data so that the random nature of the noise will result in the cancellation of the noise and the strengthening of the signal. It is expected that when a trigger is used, all data recorded at a different hit will have the same signal, which can be added point by point.

### 2.4.3 MASW Testing Procedure

A spread of 472 ft (144 m) linear array of 72 4.5 Hz geophones with 5.562 ft (2 m) spacings was used at all selected sites. A sledgehammer was used in all experiments as the active energy source.

An offset of 16 m from the first geophone was used, and the energy source was advanced every 4 m through the middle of the spread. Each location was shot three times.

To obtain shear-wave velocity at greater depths (e.g., lower frequency range), ambient noise was recorded using the ReMi seismic survey. An array of 24 geophones with 10 ft spacing was placed at the same location of the MASW testing site, and 32 seconds of data were acquired multiple times. The dispersion curve obtained using the MASW was augmented with the dispersion curves obtained by ReMi to better estimate the shear-wave velocity of deeper layers of the soil structure. Figure 19 shows a typical dispersion curve obtained by performing the MASW seismic survey. Figure 20a shows the energy contour resulting from ReMi analysis in the frequency-slowness domain, and Figure 20b presents a combined experimental dispersion curve from MASW and ReMi methods.

Using a combination of MASW and ReMi, the shear-wave velocity profiles of the test sites are determined. The combination of MASW and ReMi allows measurement of shear-wave velocities at greater depths than through use of the MASW survey alone.

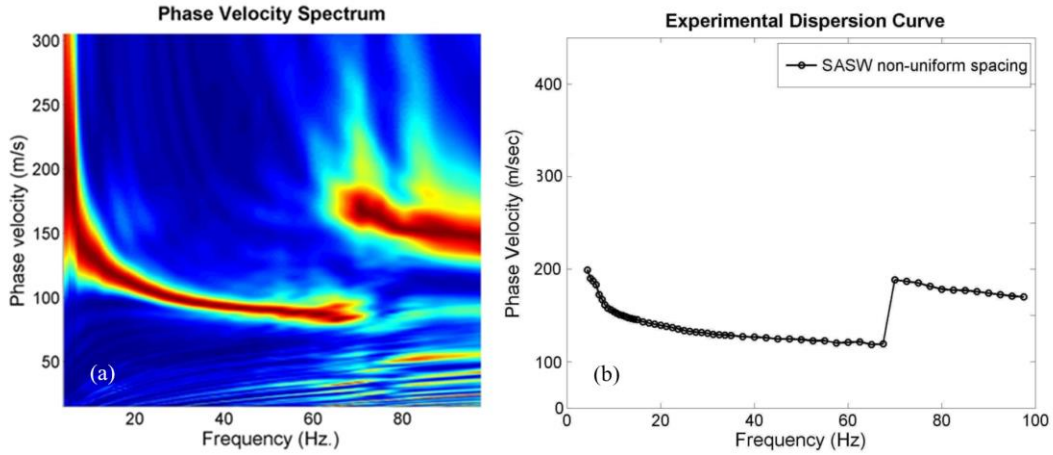


**Figure 19. Phase Velocity Dispersion Curve from MASW**

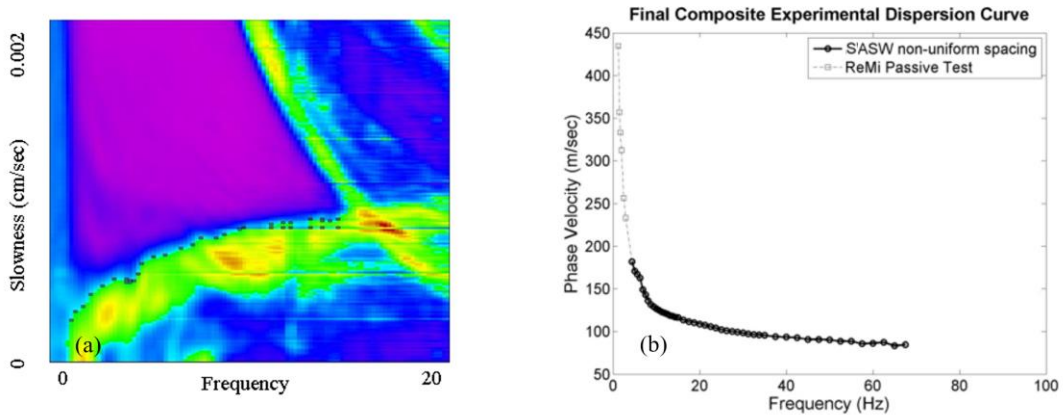


**Figure 20. (a) The ReMi Dispersion and (b) Combined Experimental Dispersion Curves from ReMi and MASW**

## 2.5 DATA PROCESSING

Data processing was performed using the SurfSeis software. The recordings were analyzed to obtain the "Overtone Images," as shown in Figure 21. The dispersion curves were automatically picked and visually checked. Figure 20b shows a combination of dispersion curves obtained from MASW and ReMi surveys. In some cases, dispersion curves from MASW are augmented with ReMi at low frequencies to collect information for greater depths. Then, the dispersion curves were inverted to obtain the shear-wave velocity profile at the tested location.

Typically, the depth of investigation is proportional to the longest wavelength captured by the instruments (Schuler 2008). For example, the depth of integration is typically 40 percent of the wavelength or 40 percent of velocity divided by frequency.

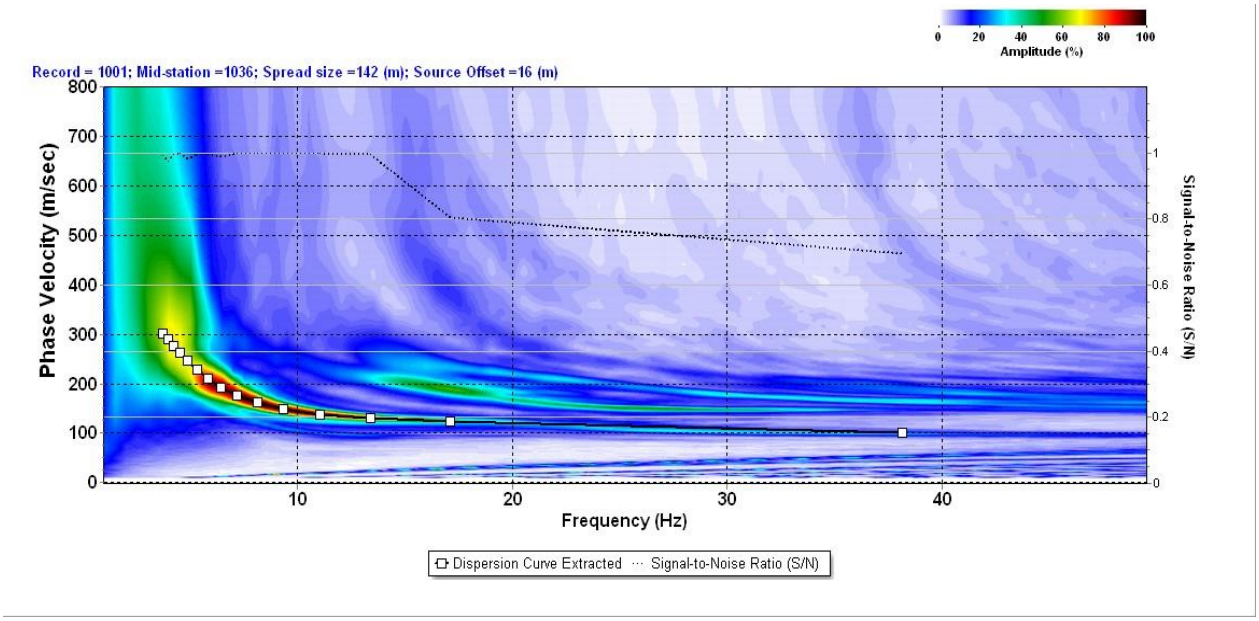


**Figure 21. A sample of the dispersion curve obtained using the surfseis software**

## 2.6 SUMMARY

The field survey results for the 20 sites surveyed are summarized in Appendix A. Appendix A contains the location and the ARDOT job number that ties the site location with an ARDOT boring log, dispersion curves, and the velocity profile for the fundamental and multiple-mode inversion. If we were not able to identify higher modes, or we had a failure in the inversion process, we only included the fundamental mode. The velocity profiles' conversion depths vary from 20 to 75 meters. The observation depth range is limited to noise levels, the range of velocities of the subsurface layers, and the corner frequency of geophones, which is 4.5 Hz.

Higher modes add extra information to the analysis and help with the non-uniqueness in the inversion process. It can also enhance the inversion resolution and increase confidence in terms of uncertainty. Yet, the depth of conversion still depends on the minimum observed frequency.

Four figures and two tables are provided for each site in Appendix A. The following is a summary of figures and tables:

1. Tables A.1, A.3, A.5, A.7, A.9, A.11, A.13, A.15, A.17, A.19, A.21, A.23, A.25, A.27, A.29, A.31, A.33, A.35, A.37, and A39 provide information about the site number, ARDOT job number, longitude, latitude, and the county name for each site tested.

2. Tables A.2, A.4, A.6, A.8, A.10, A.12, A.14, A.16, A.18, A.20, A.22, A.24, A.26, A.28, A.30, A.32, A.34, A.36, A.38, and A.40 provide the shear-wave velocity profiles obtained. In these tables, there are two sets of profiles provided: (1) the shear-wave velocity profile obtained by inverting the combined dispersion curve from MASW and ReMi, considering only the fundamental mode; and (2) the shear-wave velocity profile obtained by inverting the combined dispersion curves from MASW and ReMi, considering the fundamental mode as well as higher modes.

3. Figures A.1, A.5, A.9, A.13, A.17, A.21, A.25, A.29, A.33, A.37, A.41, A.45, A.49, A.53, A.57, A.61, A.65, A.69, A.73, and A.77 are GIS maps indicating the location of the study site within the study area. The site location is highlighted with a yellow square and a checkmark.

4. Figures A.2, A.6, A.10, A.14, A.18, A.22, A.26, A.30, A.34, A.38, A.42, A.46, A.50, A.54, A.58, A.62, A.66, A.70, A.74, and A.78 illustrate the location of the MASW and ReMi line where these experiments were conducted.

5. Figures A.3, A.7, A.11, A.15, A.19, A.23, A.27, A.31, A.35, A.39, A.43, A.47, A.51, A.55, A.59, A.63, A.67, A.71, A.75, and A.79 illustrate the shear-wave velocity versus depth at all study sites. The red curves are velocity profiles associated with the fundamental mode. If available, the orange curves are the shear-wave velocity profile associated with higher modes.

6. Figures A.4, A.8, A.12, A.16, A.20, A.24, A.28, A.32, A.36, A.40, A.44, A.48, A.52, A.56, A.60, A.64, A.68, A.72, A.76, and A.80 show dispersion curves for MASW, ReMi low energy picks, and ReMi high energy picks. If higher modes were observed, they are also shown in these figures with the same format as the fundamental mode but plotted above them.

7. Figure A.81 shows shear-wave velocity profiles obtained from all 20 sites.

Site 6 shows a relatively large shear-wave velocity profile when compared to other sites. This site is located on a rock base. Sites 13 and 14 also are located on the edges of the Mississippi embayment. The dispersion curves have sharp bends as they approach lower frequencies, suggesting a velocity contrast at shallow depths. At these locations, the boring logs were studied and verified that rock layers are at shallow depths at these locations.

At sites 5, 6, 10, 16, 17, and 20, ReMi tests did not result in a distinct dispersion curve. In these cases, we only utilized the MASW data in the analysis. In other instances, ReMi data were used for verification purposes or for augmenting the MASW data at lower frequencies to obtain deeper shear-wave velocities.

# CHAPTER 3. COLLECT SOIL BORING LOGS

## 3.1 BACKGROUND

ARDOT provided boring logs for the tested sites in electronic format. Figure 4 shows the location of sites with available boring logs that were provided for this project. Electronic copies of the provided boring logs are available as an electronic supplement to this report.

# CHAPTER 4. PERFORMING SITE-SPECIFIC ANALYSIS

## 4.1 BACKGROUND

According to AASHTO LRFD Bridge Design Specifications, 9th Edition, or AASHTO Guide Specifications for LRFD Seismic Bridge Design, the seismic hazard at a bridge site should be characterized through a Site-Specific Procedure if any one of the following conditions applies:

- The site is located within six miles of an active fault.
- The site is classified as Site Class F according to the AASHTO site classification scheme.
- Long-duration earthquakes are expected in the region.
- The importance of the bridge is such that a lower probability of exceedance should be considered.

If none of the above conditions exist, the *General Procedure* introduced in AASHTO LRFD Bridge Design Specifications should be followed to determine seismic hazard at a bridge site. Following the *General Procedure*, one may estimate spectral parameters at a bridge site by multiplying hazard values obtained for a 1000-year return period on the B/C boundary by the site factors for the applicable site class.

Preliminary results from TRC1603 (Wood et al. 2019) and results from MBTC3032 (Cox et al. 2012) indicated that seismic demands may be reduced in areas of northeast Arkansas by conducting SSGMRA, which is expected to have economic benefits regarding the construction of bridges and embankments. Therefore, it may be economically beneficial to estimate spectral parameters through a Site-Specific Procedure for sites at which the AASHTO *General Procedure* is adequate.

The objective of this study is to compare spectral parameters obtained from SSGMRA with those obtained following the *AASHTO General Procedure* to assess the possibility of reducing seismic demand when designing bridges within the northeastern Arkansas region. To this end, SSGMRA studies were performed at 51 sites within the study region. Shear-wave velocity profiles determined for 51 sites from three ARDOT projects were used. Projects TRC0803, TRC1603, and TRC1901 provide shear-wave velocity profiles for 16, 15, and 20 sites, respectively. Moreover, spectral parameters by conducting the AASHTO General Procedure were estimated. In performing SSGMRA, we used two different approaches. Finally, spectral parameters obtained from the two different approaches and the *AASHTO General Procedure* were compared to determine the economic benefits of performing SSGMRA for the construction of bridges and embankments.

## 4.2 AASHTO GENERAL PROCEDURE

The first step for calculating spectral parameters using the AASHTO General Procedure at a bridge site is to determine hazard curves at the B/C boundary. Then, the hazard values corresponding to a 1000-year return period (7 percent probability of exceedance in 75 years) should be multiplied by the deterministic site factors for the applicable site class. Site factors are determined for PGA, and spectral ordinates at 0.2 sec and 1.0 sec. Site factors for PGA, $S_s$, and $S_1$ are referred to as $F_{pga}$, $F_a$, and $F_v$, respectively.

### 4.3 REGIONAL SEISMICITY

The seismicity of the region is studied through the earthquake catalog, developed by the National Seismic Hazard Mapping Project (NSHMP) (Petersen et al., 2014). The catalog is developed by combining published catalogs to estimate the rates of future earthquakes across the Central and Eastern United States (CEUS). After removing duplicates, the NSHMP declusters the combined catalog using the Gardner and Knopoff (1974) algorithm. The final declustered catalog includes 6,259 earthquakes that took place between 1700 through 2012 with an earthquake moment magnitude ($M_w$) greater than or equal to 2.5. Figure 22 shows the United States Geological Survey (USGS) 2014 declustered catalog for CEUS.

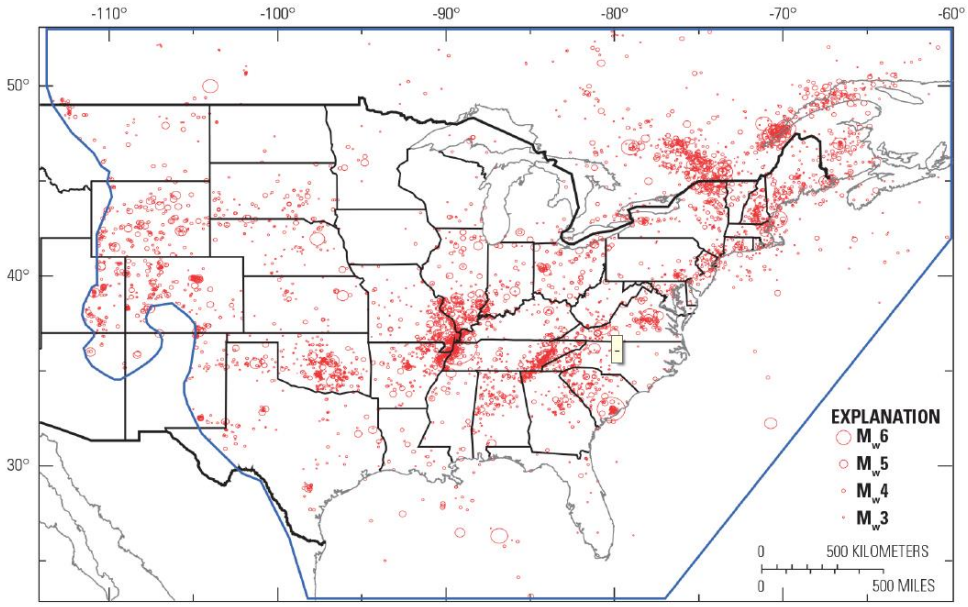


**Figure 22. USGS2014 Declustered Catalog for the Central and Eastern United States**

### 4.4 SEISMIC HAZARD ANALYSIS

A Probabilistic Seismic Hazard Analysis (PSHA) was performed to estimate the seismic ground motions for a rock condition with a shear-wave velocity of 2,500 ft/sec (760 m/sec) at the study sites. The analytical model used for the PSHA is based on models originally developed by Cornell (1968). The basic assumption of these models is that the occurrence of earthquakes in space and time within a particular seismic zone is completely random (i.e., a Poisson process). This type of probabilistic model is commonly used for seismic hazard analyses.

The two basic components of the probabilistic approach are:

1. The seismic source models, which specify the spatial, temporal, and magnitude distribution of earthquake occurrences expected in each of the seismic sources.
2. The ground-motion attenuation models, which determine the distribution of ground motions expected at a potential earthquake occurrence site (characterized by magnitude and location, among other factors) on a seismic source.

The above two components comprise the inputs to the PSHA. In the PSHA, probability-of-exceedance rates (hazard curves) are computed for a range of horizontal ground motions. These ground motions are expressed in terms of the peak ground acceleration (PGA) and five percent-damped pseudo absolute spectral accelerations ($S_a$) at various single-degree-of-freedom oscillator periods. From the probability-of-exceedance rates, the Uniform Hazard Spectrum (UHS) corresponding to average return periods of 1,000 years (7 percent probability of exceedance in 75 years) is computed.

### 4.5 SEISMIC SOURCE MODELS

The USGS 2014 seismic source models (Petersen et al. 2014) were used for this project. The USGS 2014 models addressed the causes of intraplate earthquakes in the Central and Eastern United States in two ways:

1. The seismicity-based background source models, which incorporate zones of historical seismicity in the region.
2. The fault-based seismic source models, which incorporates known and potential seismic sources.

### 4.6 GROUND MOTION MODELS

Generally, the characteristics of the source of the fault system such as distance, type, magnitude, and site conditions are used to estimate the magnitude of an earthquake parameter (spectral acceleration, peak ground acceleration, etc.) via ground-motion prediction equations (GMPEs), also known as attenuation relationships. Various GMPEs have been developed for specific regions using a database of appropriate ground motion records. The ground motion models, used in the USGS 2014 report, updated to generate national seismic hazard maps for the Central and Eastern United States, are considered in this project (Petersen et al. 2014). A logic tree approach was used to develop hazard maps. The logic tree weights are based on the distance and the geometric spreading term used by each model. The models with a faster geometric spreading term are given more weight. The New Madrid seismic zone is the most likely seismic source that could affect the considered sites. Therefore, the attenuation relationships which are not applicable beyond 500 km are removed, and weights are renormalized. Tables 3 and 4 list the selected GMPEs from the USGS 2014 models with their associated weights.

**Table 3. The Considered Ground Motion Prediction Equations**

| USGS 2014 GMM | Abbreviation | Weights | | Long Distances ( > 500 km ) |
|---|---|---|---|---|
| | | RLME** | Grid Source | |
| 1. Frankel et al. (1996) | F96 | 0.16 | 0.06 | ✓ |
| 2. Toro et al. (1997) | T97 | 0 | 0.13 | × |
| 3. Silva et al. (2002) | S02 | 0 | 0.06 | × |
| 4. Campbell (2003) | C03 | 0.17 | 0.13 | ✓ |
| 5. Tavakoli and Pezeshk (2005) | TP05 | 0.17 | 0.13 | ✓ |
| 6. Atkinson and Boore (2006') * | AB06’ | 0.3 | 0.25 | ✓ |
| 7. Pezeshk et al. (2011) | PZT11 | 0.2 | 0.16 | ✓ |
| 8. Atkinson (2008) * | A08’ | 0 | 0.08 | × |
| 9. Somerville et al. (2001) | S01 | 0 | 0 | × |

* The AB06' model and the A08' models are the revised version of the Atkinson and Boore (2006) and Atkinson and Boore (2008) models (Atkinson and Boore 2011).

** repeated large-magnitude earthquake (RLME)

**Table 4. The Considered Ground Motion Prediction Equations and Their Corresponding Weights**

| Seismic Source | Region | Fault Mechanism | Frankel (1996) | Toro (1999) | Silva et al. (2002) | Compbell (2003) | Tavakoli and Pezeshk (2005) | Atkinson and Boore (2006) | Pezeshk et al. (2011) | Atkinson (2008) | Sommerville (2001) |
|---|---|---|---|---|---|---|---|---|---|---|---|
| ERM-S Composite | USGS 2014 RLME Eastern Rift Margin-S | Strike Slip Fault | 0.06 | 0.11 | 0.06 | 0.11 | 0.11 | 0.22 | 0.15 | 0.08 | 0.10 |
| ERM-N Composite | USGS 2014 RLME Eastern Rift Margin-N | Strike Slip Fault | 0.06 | 0.11 | 0.06 | 0.11 | 0.11 | 0.22 | 0.15 | 0.08 | 0.10 |
| Wabash Valley Composite | USGS 2014 RLME Wabash Valley | Strike Slip Fault | 0.06 | 0.11 | 0.06 | 0.11 | 0.11 | 0.22 | 0.15 | 0.08 | 0.10 |
| New Madrid Composite | USGS 2014 New Madrid | Strike Slip Fault | 0.06 | 0.11 | 0.06 | 0.11 | 0.11 | 0.22 | 0.15 | 0.08 | 0.10 |
| Commerce Composite | USGS 2014 RLME Commerce | Strike Slip Fault | 0.06 | 0.11 | 0.06 | 0.11 | 0.11 | 0.22 | 0.15 | 0.08 | 0.10 |
| Marianna Composite | USGS 2014 RLME Marianna | Strike Slip Fault | 0.06 | 0.11 | 0.06 | 0.11 | 0.11 | 0.22 | 0.15 | 0.08 | 0.10 |
| CEUS Gridded Source | USGS 2014 CEUS Gridded Source | Strike Slip Fault | 0.06 | 0.13 | 0.06 | 0.13 | 0.13 | 0.25 | 0.16 | 0.08 | 0.00 |

## 4.7 SITE-SPECIFIC PROCEDURE

The PSHA considers all potential earthquake sources that will contribute to the seismic hazard at a specific site. The PSHA factors in contributions from all magnitudes, distances, and probabilities of occurrence for all sources. In this study, PSHA was used to estimate PGA and spectral acceleration at various periods for a B/C NEHRP site condition for a 7 percent probability of exceedance in 75 years. We obtained hazard curves for PGA and spectral accelerations at periods of 0.2 sec and 1.0 sec for a 1000-year return period. Moreover, we determined the seismic site class for the 51 sites based on the average shear-wave velocity within the upper 100 feet (ft) of the soil profiles following guidelines provided in Table 3.10.3.1-1 of AASHTO LRFD Bridge Design Specifications. PGA, $S_s$, and $S_1$ were used in line with the previously determined site class for each site to calculate site factors including $F_{pga}$, $F_a$, and $F_v$ from Table 3.10.3.2-1 through Table 3.10.3.2-3 of AASHTO. Finally, we multiplied PGA, $S_s$, and $S_1$ by $F_{pga}$, $F_a$, and $F_v$, respectively, to calculate spectral parameters. Parameters $A_s$, $S_{Ds}$, and $S_{D1}$ represent spectral parameters for PGA, and spectral periods of 0.2 sec, and 1.0 sec. Table 5 summarizes information about the 51 study sites. This table includes geographical information, the time-averaged shear-wave velocity for the top 100 ft (30 meters), seismic site class, hazard values for a return period of 1000 years at PGA, $S_s$, and $S_1$, site factors, and spectral parameters for each study site.

**Table 5. Spectral Parameters Determined from AASHTO General Procedure for the 51 Study Sites.**

| *Site* | *Project* | *Lat (°)* | *Long (°)* | *Site Class* | $\overline{V_s}(ft/s)$ | *PGA* | $S_s$ | $S_1$ | $F_{pga}$ | $F_a$ | $F_v$ | $A_s$ | $SD_s$ | $SD_1$ |
|---|---|---|---|---|---|---|---|---|---|---|---|---|---|---|
| **1** | TRC0803_1 | 35.27326 | -90.5589 | D | 869 | 0.544 | 0.910 | 0.243 | 1.000 | 1.136 | 1.913 | 0.544 | 1.034 | 0.466 |
| **2** | TRC0803_2 | 35.16262 | -90.2243 | D | 708 | 0.408 | 0.704 | 0.188 | 1.092 | 1.237 | 2.048 | 0.446 | 0.871 | 0.385 |
| **3** | TRC0803_3 | 35.39146 | -90.2734 | D | 745 | 0.664 | 1.119 | 0.281 | 1.000 | 1.052 | 1.837 | 0.664 | 1.178 | 0.517 |
| **4** | TRC0803_4 | 35.4748 | -90.3333 | D | 727 | 0.897 | 1.455 | 0.378 | 1.000 | 1.000 | 1.644 | 0.897 | 1.455 | 0.622 |
| **5** | TRC0803_5 | 35.19971 | -90.2457 | D | 628 | 0.433 | 0.763 | 0.200 | 1.067 | 1.195 | 1.999 | 0.462 | 0.912 | 0.400 |
| **6** | TRC0803_6 | 35.41504 | -90.284 | D | 667 | 0.732 | 1.209 | 0.301 | 1.000 | 1.016 | 1.798 | 0.732 | 1.229 | 0.541 |
| **7** | TRC0803_7 | 35.48047 | -90.3576 | C | 1214 | 0.928 | 1.533 | 0.393 | 1.000 | 1.000 | 1.407 | 0.928 | 1.533 | 0.553 |
| **8** | TRC0803_8 | 35.51862 | -90.4127 | D | 783 | 1.002 | 1.723 | 0.433 | 1.000 | 1.000 | 1.567 | 1.002 | 1.723 | 0.678 |
| **9** | TRC0803_9 | 35.59755 | -90.2693 | D | 809 | 1.001 | 1.730 | 0.439 | 1.000 | 1.000 | 1.561 | 1.001 | 1.730 | 0.685 |
| **10** | TRC0803_10 | 35.59754 | -90.2145 | D | 760 | 0.940 | 1.576 | 0.404 | 1.000 | 1.000 | 1.596 | 0.940 | 1.576 | 0.645 |
| **11** | TRC0803_11 | 35.84046 | -90.7532 | D | 866 | 0.383 | 0.643 | 0.179 | 1.117 | 1.285 | 2.083 | 0.428 | 0.827 | 0.373 |
| **12** | TRC0803_12 | 35.82309 | -90.5006 | D | 775 | 0.566 | 0.927 | 0.244 | 1.000 | 1.129 | 1.912 | 0.566 | 1.047 | 0.466 |
| **13** | TRC0803_13 | 35.82073 | -90.4333 | D | 785 | 0.623 | 1.031 | 0.267 | 1.000 | 1.088 | 1.867 | 0.623 | 1.121 | 0.498 |
| **14** | TRC0803_14 | 36.05171 | -90.3604 | D | 724 | 0.490 | 0.831 | 0.221 | 1.010 | 1.168 | 1.958 | 0.495 | 0.970 | 0.433 |
| **15** | TRC0803_15 | 36.39091 | -90.3992 | D | 757 | 0.394 | 0.665 | 0.183 | 1.106 | 1.268 | 2.069 | 0.436 | 0.843 | 0.378 |
| **16** | TRC0803_16 | 36.45966 | -90.3571 | D | 656 | 0.411 | 0.705 | 0.188 | 1.089 | 1.236 | 2.050 | 0.447 | 0.872 | 0.385 |
| **17** | TRC1603_1 | 36.39858 | -90.3882 | D | 774 | 0.396 | 0.672 | 0.184 | 1.104 | 1.262 | 2.064 | 0.438 | 0.849 | 0.380 |
| **18** | TRC1603_2 | 36.11861 | -90.3131 | D | 889 | 0.490 | 0.833 | 0.222 | 1.010 | 1.167 | 1.956 | 0.495 | 0.972 | 0.434 |
| **19** | TRC1603_3 | 36.01718 | -90.7995 | D | 859 | 0.322 | 0.572 | 0.159 | 1.178 | 1.342 | 2.163 | 0.379 | 0.768 | 0.345 |
| **20** | TRC1603_4 | 35.76162 | -90.5943 | D | 800 | 0.538 | 0.892 | 0.234 | 1.000 | 1.143 | 1.931 | 0.538 | 1.019 | 0.453 |
| **21** | TRC1603_5 | 35.88558 | -90.3352 | D | 872 | 0.639 | 1.075 | 0.276 | 1.000 | 1.070 | 1.848 | 0.639 | 1.150 | 0.510 |
| **22** | TRC1603_6 | 35.8525 | -90.1471 | D | 806 | 0.968 | 1.657 | 0.421 | 1.000 | 1.000 | 1.579 | 0.968 | 1.657 | 0.665 |
| **23** | TRC1603_7 | 35.70421 | -90.2175 | D | 867 | 1.059 | 1.860 | 0.488 | 1.000 | 1.000 | 1.512 | 1.059 | 1.860 | 0.737 |
| **24** | TRC1603_8 | 35.56757 | -91.1559 | D | 883 | 0.268 | 0.480 | 0.140 | 1.264 | 1.416 | 2.241 | 0.339 | 0.680 | 0.313 |
| **25** | TRC1603_9 | 35.56578 | -90.7302 | D | 973 | 0.545 | 0.905 | 0.240 | 1.000 | 1.138 | 1.920 | 0.545 | 1.030 | 0.461 |
| **26** | TRC1603_10 | 35.52005 | -90.4358 | D | 840 | 0.986 | 1.695 | 0.427 | 1.000 | 1.000 | 1.573 | 0.986 | 1.695 | 0.671 |
| **27** | TRC1603_11 | 35.18832 | -90.7895 | D | 796 | 0.364 | 0.621 | 0.175 | 1.136 | 1.304 | 2.101 | 0.414 | 0.809 | 0.367 |
| **28** | TRC1603_12 | 35.25864 | -90.4226 | D | 912 | 0.534 | 0.893 | 0.239 | 1.000 | 1.143 | 1.922 | 0.534 | 1.021 | 0.459 |
| **29** | TRC1603_13 | 34.98673 | -90.9112 | D | 979 | 0.256 | 0.452 | 0.135 | 1.288 | 1.439 | 2.261 | 0.330 | 0.650 | 0.305 |
| **30** | TRC1603_14 | 35.01591 | -90.4034 | D | 993 | 0.338 | 0.590 | 0.167 | 1.162 | 1.328 | 2.131 | 0.393 | 0.783 | 0.356 |
| **31** | TRC1603_15 | 34.711 | -90.9439 | D | 886 | 0.194 | 0.377 | 0.119 | 1.412 | 1.499 | 2.325 | 0.274 | 0.565 | 0.276 |
| **32** | TRC1901_1 | 35.01236 | -90.6282 | D | 732 | 0.312 | 0.559 | 0.161 | 1.188 | 1.353 | 2.157 | 0.371 | 0.756 | 0.347 |
| **33** | TRC1901_2 | 34.8326 | -90.603 | D | 705 | 0.252 | 0.448 | 0.136 | 1.295 | 1.441 | 2.255 | 0.327 | 0.646 | 0.307 |

**Table 5 Continued. Spectral Parameters Determined from AASHTO General Procedure for the 51 Study Sites.**

| | | | | | | | | | | | | | | |
|---|---|---|---|---|---|---|---|---|---|---|---|---|---|---|
| **33** | **TRC1901_2** | **34.8326** | **-90.603** | **D** | **705** | **0.252** | **0.448** | **0.136** | **1.295** | **1.441** | **2.255** | **0.327** | **0.646** | **0.307** |
| **34** | TRC1901_3 | 34.70548 | -90.9593 | D | 736 | 0.192 | 0.374 | 0.118 | 1.417 | 1.501 | 2.328 | 0.271 | 0.561 | 0.275 |
| **35** | TRC1901_4 | 34.50562 | -90.8504 | D | 730 | 0.174 | 0.336 | 0.111 | 1.453 | 1.531 | 2.356 | 0.252 | 0.515 | 0.262 |
| **36** | TRC1901_5 | 34.503 | -90.6055 | D | 695 | 0.179 | 0.347 | 0.112 | 1.442 | 1.523 | 2.351 | 0.258 | 0.528 | 0.264 |
| **37** | TRC1901_6 | 35.20006 | -91.8091 | B | 3673 | 0.206 | 0.378 | 0.107 | 1.000 | 1.000 | 1.000 | 0.206 | 0.378 | 0.107 |
| **38** | TRC1901_7 | 34.80495 | -91.8858 | D | 934 | 0.160 | 0.288 | 0.093 | 1.480 | 1.569 | 2.400 | 0.237 | 0.453 | 0.224 |
| **39** | TRC1901_8 | 34.4113 | -91.8976 | D | 755 | 0.113 | 0.226 | 0.080 | 1.574 | 1.600 | 2.400 | 0.178 | 0.361 | 0.193 |
| **40** | TRC1901_9 | 35.36044 | -91.4951 | D | 726 | 0.204 | 0.382 | 0.116 | 1.392 | 1.494 | 2.337 | 0.284 | 0.571 | 0.270 |
| **41** | TRC1901_10 | 34.90926 | -91.1967 | D | 935 | 0.196 | 0.375 | 0.116 | 1.408 | 1.500 | 2.336 | 0.276 | 0.562 | 0.271 |
| **42** | TRC1901_11 | 34.57475 | -91.1461 | D | 685 | 0.168 | 0.323 | 0.108 | 1.463 | 1.542 | 2.369 | 0.246 | 0.498 | 0.255 |
| **43** | TRC1901_12 | 34.45413 | -91.3213 | D | 789 | 0.142 | 0.276 | 0.097 | 1.516 | 1.579 | 2.400 | 0.215 | 0.436 | 0.232 |
| **44** | TRC1901_13 | 36.17804 | -91.7395 | C | 2355 | 0.176 | 0.341 | 0.109 | 1.200 | 1.200 | 1.691 | 0.211 | 0.409 | 0.184 |
| **45** | TRC1901_14 | 36.31981 | -90.9126 | C | 2045 | 0.277 | 0.512 | 0.144 | 1.123 | 1.195 | 1.656 | 0.311 | 0.612 | 0.238 |
| **46** | TRC1901_15 | 36.18635 | -90.3381 | D | 698 | 0.436 | 0.768 | 0.205 | 1.064 | 1.193 | 1.990 | 0.464 | 0.916 | 0.408 |
| **47** | TRC1901_16 | 35.86319 | -89.8398 | E | 523 | 0.918 | 1.468 | 0.381 | 0.900 | 0.900 | 2.478 | 0.826 | 1.321 | 0.943 |
| **48** | TRC1901_17 | 35.79525 | -90.9832 | D | 786 | 0.303 | 0.549 | 0.155 | 1.197 | 1.361 | 2.180 | 0.363 | 0.747 | 0.338 |
| **49** | TRC1901_18 | 35.49315 | -91.002 | D | 815 | 0.333 | 0.582 | 0.164 | 1.167 | 1.335 | 2.144 | 0.389 | 0.776 | 0.352 |
| **50** | TRC1901_19 | 35.27009 | -91.2369 | D | 760 | 0.237 | 0.419 | 0.125 | 1.325 | 1.465 | 2.300 | 0.315 | 0.613 | 0.287 |
| **51** | TRC1901_20 | 35.35866 | -90.7586 | D | 818 | 0.479 | 0.829 | 0.223 | 1.021 | 1.168 | 1.954 | 0.489 | 0.969 | 0.436 |

## 4.8 SITE-SPECIFIC GROUND MOTION RESPONSE ANALYSIS

A near-surface low-velocity layer has a significant effect on seismic waves' frequency, content, and amplitude. Amplification, deamplificaiton, and shift in resonant frequency are essential factors in designing bridges and buildings. Devastating damage after Micheocan, Mexico (1985), Kalmat, Greece (1989), Loma Perieta, California, USA (1989), Roodbar-Manjil, Iran (1990), and other earthquakes highlight the importance of comprehensive site response analyses in engineering practices. In this study, we used two approaches to perform SSGMRA:

- SSGMRA using an equivalent linear (EQL) approach.
- SSGMRA using a fully probabilistic approach, which is also referred to as Approach 3 (App3) in the literature.

### 4.8.1 SSGMRA Using an Equivalent Linear (EQL) Approach

This project's goal is to conduct probabilistic seismic hazard analyses incorporating site effects. A large level of uncertainty is associated with near-surface material properties and the parameters that control

the dynamic response. Figure 23 illustrates steps to follow when performing a time series site-specific study. Details of the approach are discussed later through a case study.

### 4.8.2 SSGMRA Using a Fully Probabilistic Approach (App3)

The considered fully probabilistic approach is characterized by higher levels of sophistication in which the rock hazard is convolved with the probability density function of the amplification to calculate the surface ground motions. Uncertainties associated with the site characterization are addressed via Monte Carlo randomization.

In this approach, the surface hazard curves ($HC^{Surface}$) are computed by convolving the $HC^{Rock}$ with the probability density function for the amplification factors (AFs). The variability and uncertainty in both the site response and the rock hazard are incorporated using the convolution process, and the computed probabilities at rock level are fully preserved and transferred to the surface ground motions. The AFs in this approach were developed as a function of the spectral accelerations at rock level ($Sa_r$). Following the Bazzuro and Cornell (2004b) formulation, the $HC^{Surface}$ is calculated as:

$$HC^{Surface}(z) = \sum_{x_j} P\left[ AF > \frac{z}{x_j} \mid x_j \right] p_{Sa_r}(x_j) \tag{1}$$

where *z* is the desired ground motion level at the surface, $P[\mathrm{AF} > z / x_j \mid x_j]$ is the conditional probability for which AF is greater than $z / x_j$ for a given $Sa_r = x_j$, and $p_{Sa_r}(x_j)$ is the annual probability of exceedance for $Sa_r = x_j$. Each ground motion at rock level will contribute to the hazard for each ground motion at a surface level using Equation (2). The AF is assumed to be lognormally distributed. Therefore, $P[\mathrm{AF} > z / x_j]$ can be calculated as:

$$P\left[ AF > \frac{z}{x_j} \right] = \hat{\Phi}\left( \frac{\ln[\frac{z}{x}] - \mu_{\ln \mathrm{AF}|Sa_r = x_j}}{\sigma_{\ln \mathrm{AF}|Sa_r = x_j}} \right) \tag{2}$$

where $\hat{\Phi}$ is the standard Gaussian cumulative distribution function, $\mu_{\ln \mathrm{AF}|x}$ and $\sigma_{\ln \mathrm{AF}|x}$ are the median value and the standard deviation of AF for a given $Sa_r = x_j$, respectively. In calculating Equation (2), both the $HC^{Rock}$ and the AFs are required to be spanned over a wide range of $Sa_r$. This is due to the fact that a particular ground motion equal to *z* at surface level may be exceeded by either a small rock motion noticeably amplified by the nearly linear soil response or by a large rock motion significantly deamplified by the nonlinear behavior of the soil (McGuire et al. 2001; Cramer 2004; Bazzurro and Cornell 2004; Haji-Soltani and Pezeshk 2017).

### 4.8.3 Defining Input Motions

A number of rock input ground motions are needed to estimate the distribution parameters of AFs (i.e., $\mu_{\ln AF}$ and $\sigma_{\ln AF}$). A wide exponentially-spaced range of PGA amplitudes is selected from the PGA $HC^{Rock}$. Figure 24 illustrates steps to follow when performing SSGMRA using a fully probabilistic approach. A case study, discussed later, details the application of this fully probabilistic approach.

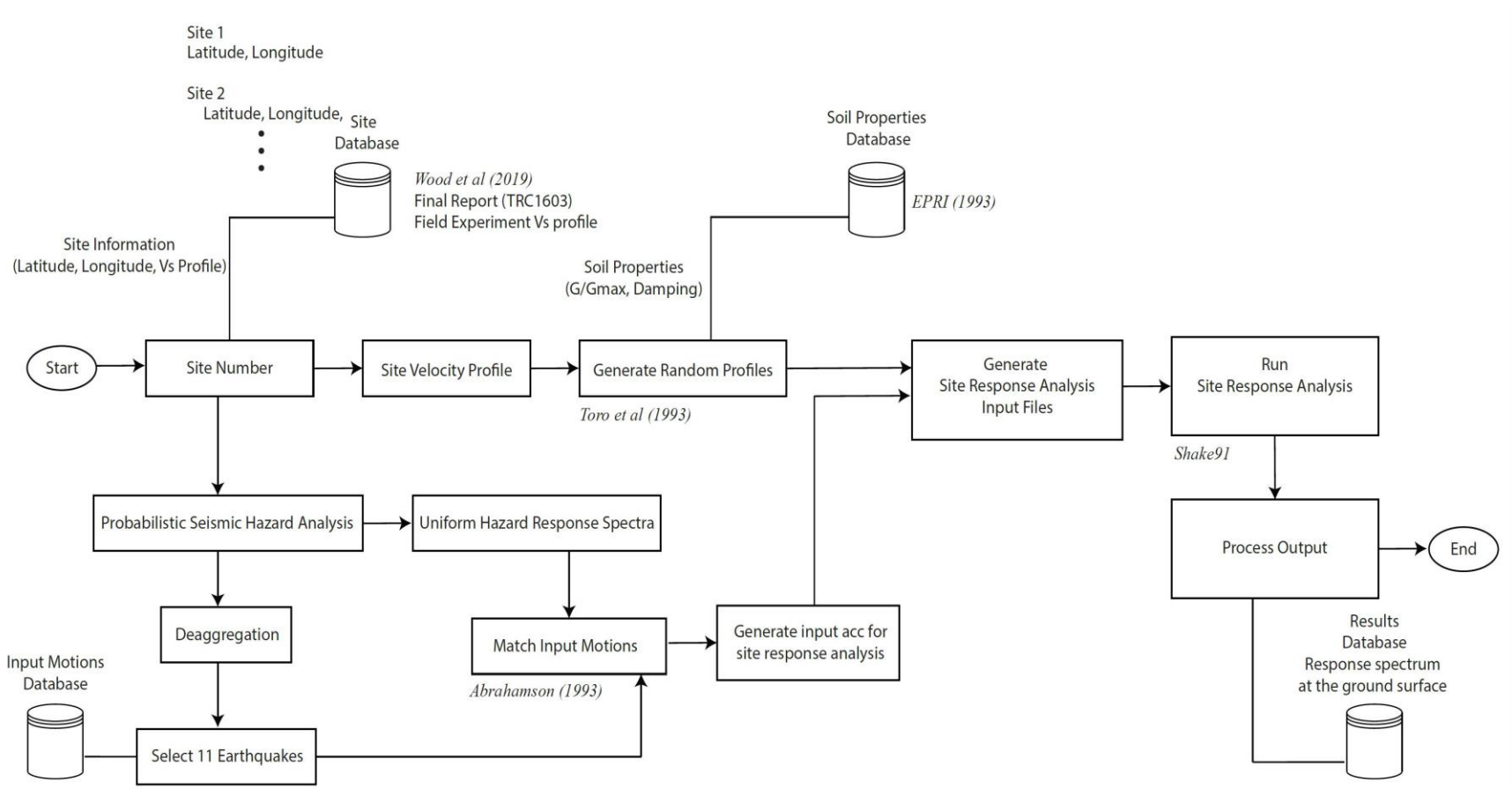


**Figure 23. Steps in Performing SSGMRA Using an Equivalent Linear Approach**

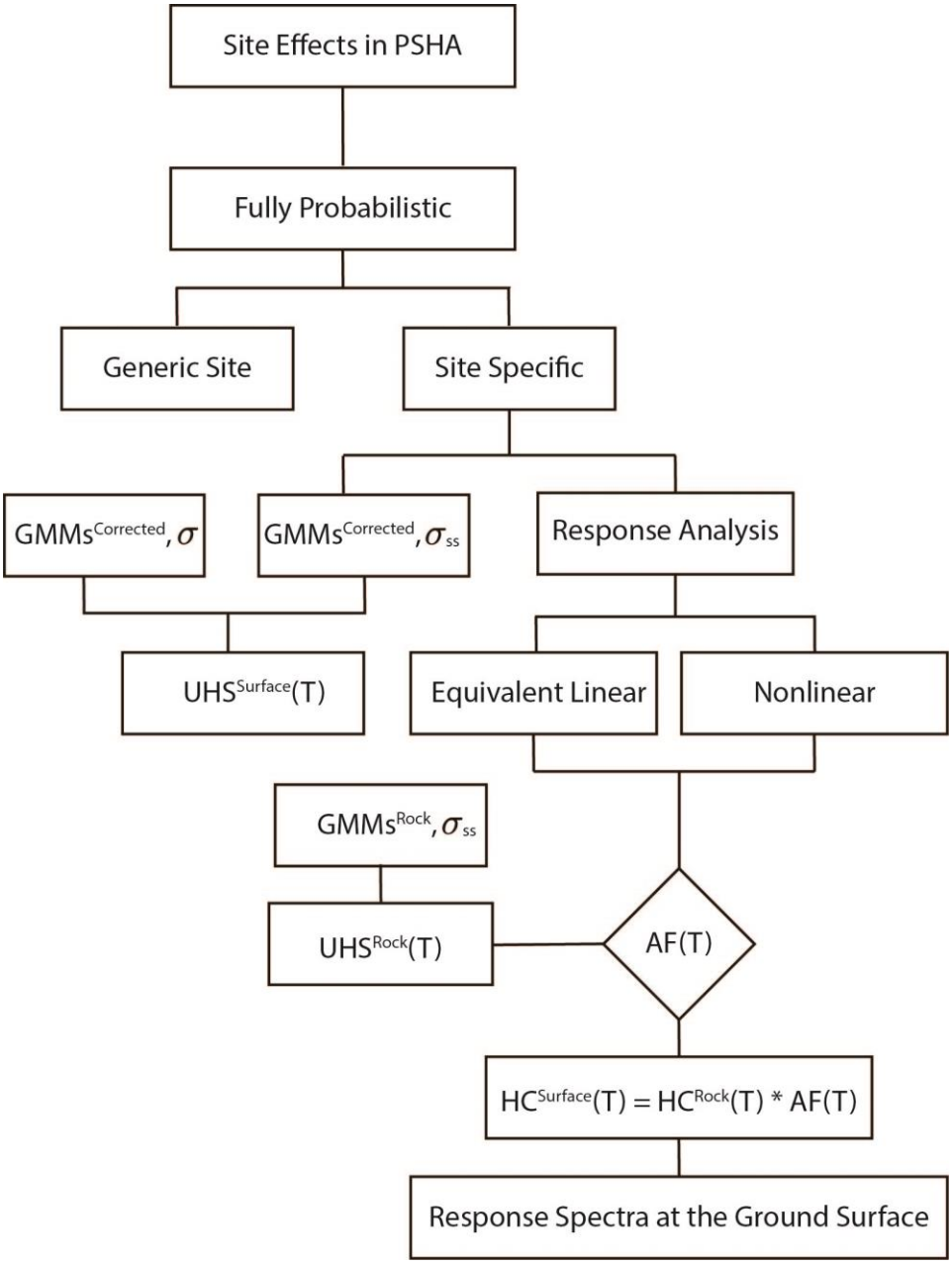


**Figure 24. Steps in performing SSGMRA Using a Fully Probabilistic Approach**

Both procedures have common features, which include: (1) development of base shear-wave velocity profile, (2) randomization of the base shear-wave velocity profile, and (3) nonlinear dynamic soil properties.

### 4.8.4 Development of the Base-Case Shear-Wave Velocity Profiles

Base-case profiles are available for all 51 sites' shallower portions. These profiles were estimated through non-invasive geophysical measurements such as MASW and ReMi testing. To construct a base-case profile, the velocity profile that represents the reference site condition should be extended to a deeper geologic unit. To extend the shallower portion of the velocity profile to the deeper portion, the 3D velocity model developed for Central United States (CUS) was used. The CUS 3D velocity model was developed by Ramirez-Guzman et al. (2012) and is a result of several efforts in previous years including Allen and Wald (2007), Chung and Rogers (2010), Cramer et al. (2004), Ginzburg et al. (1983), Gomberg et al. (2003), Bradley (2003), Mooney et al. (1983), Prodehl et al. (1984), and Stewart (1968). In the following section, the adopted methodology to represent aleatory variability in base-case profiles through randomizations will be explained.

### 4.8.5 Randomizing Shear-Wave Velocity Profiles

In this study, the model developed by Toro (1996) to randomize the base shear-wave velocity profiles was utilized. Random field models assume a lognormal distribution for the shear-wave velocity at any depth and consider velocities of adjacent layers as correlated. Toro (1996) also developed a model for randomizing layer thicknesses, but that model was not used in this study. The statistical parameters required for the generation of the velocity profiles are the baseline shear-wave velocity profile, the standard deviation of the natural log of the shear-wave velocity $\sigma_{ln_{Vs}}$, and the interlayer correlation parameters $\rho_{200}$, $d_0$, b, $\rho_0$, and Δ. In addition, to prevent unrealistic randomized velocity profiles, a bound of $\pm 2\sigma_{ln_{Vs}}$ is imposed throughout the profile. Model parameters developed by Toro (1996) are given for different generalized National Hazard Reduction Program (NEHRP) site classes in Table 6.

**Table 6. Parameters for Toro (1996) Model for the Shear-Wave Velocity Randomization**

| | USGS Site Class | | | |
|---|---|---|---|---|
| **Parameters** | **Class A** | **Class B** | **Class C** | **Class D** |
| $\sigma_{ln_{Vs}}$ | 0.36 | 0.27 | 0.31 | 0.37 |
| $\rho_{200}$ | 0.42 | 1.0 | 0.98 | 0.50 |
| $d_0$ | 0.0 | 0.0 | 0.0 | 0.0 |
| **b** | 0.063 | 0.293 | 0.344 | 0.744 |
| $\rho_0$ | 0.95 | 0.97 | 0.99 | 0.00 |
| **Δ** | 3.4 | 3.8 | 3.9 | 5.0 |

Among parameters introduced by Toro (1996), the sigma component ($\sigma_{ln_{Vs}}$) is large and represents the variability for the whole site class. To evaluate the influence of the sigma component on the result of site response analysis, we computed soil hazard curves for Site 11 provided in the TRC1603 projects for different values of the sigma component. Results are shown in Figure 25 for PGA and three spectral periods, including spectral accelerations at 0.2, 1.0, and 2 sec. Following values suggested by Toro (1996), a sigma value of 0.37 should be considered for this site as it is classified as Site Class D. We further reduced sigma by 50 percent ($\sigma_{ln_{Vs}} = 0.18$) and 80 percent ($\sigma_{ln_{Vs}} = 0.08$) and computed soil hazard curves to assess the impact of the sigma component on the site response analysis. It can be seen from Figure 25. that considering a larger variability will reduce the hazard in a given return period for short to median spectral periods. For larger spectral periods, the impact of the standard deviation of the natural log of the shear-wave velocity is minimal across the majority of return periods.

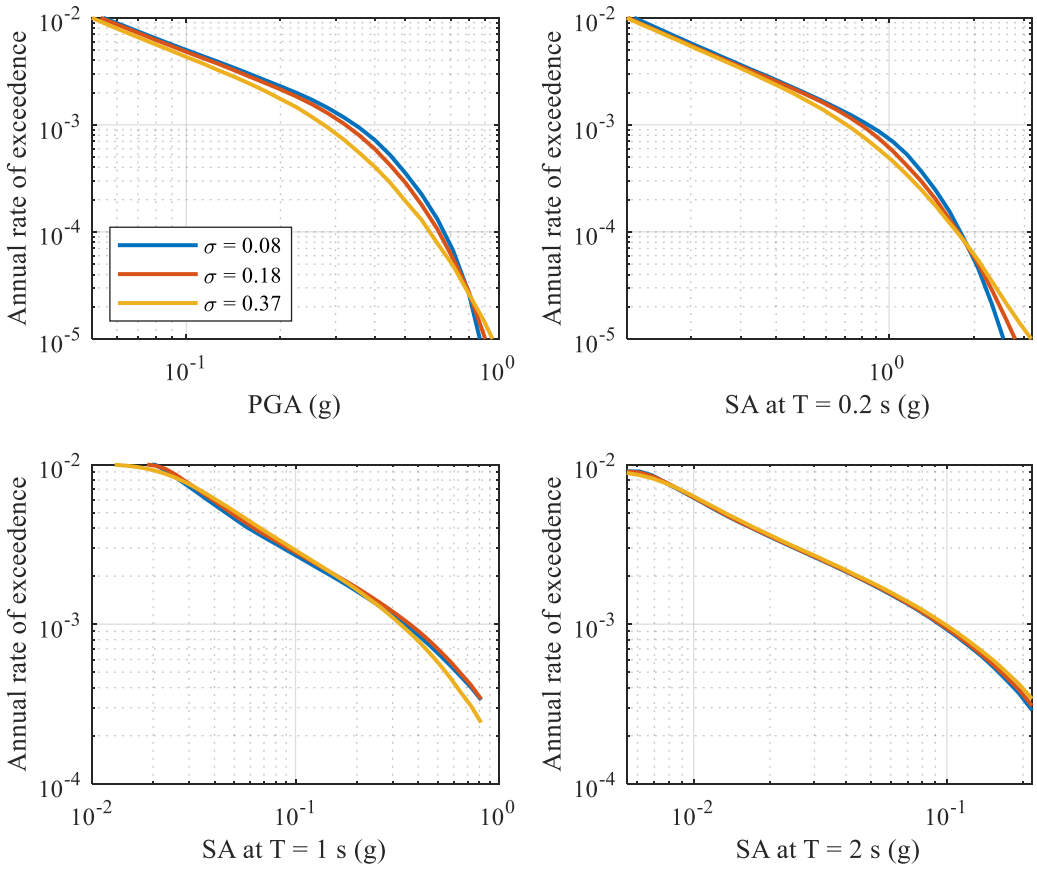


**Figure 25. Evaluating the Influence of the Standard Deviation of the Natural Log of the Shear-Wave Velocity on the Site Response Analysis. The Legend in the top Left Hand Figure Applies to all Figures**

Rathje et al. (2010) suggested that the standard deviation of the natural log of the shear-wave velocity is typically large for most site-specific studies and should be estimated from multiple measured profiles across the site or from the knowledge of geology/variability across the site. In this study, we considered the values suggested by Toro (1996) due to a lack of reliable estimations of shear-wave velocities in the vicinity of study sites.

### 4.8.6 Nonlinear Dynamic Material Properties

The impact of the nonlinear response of near-surface materials on input ground motions is a crucial element of site response analysis. There are epistemic uncertainty and aleatory variability in the nonlinear properties of the soil materials. Electric Power Research Institute (EPRI 2013) recommends using the two sets of generic modulus reduction and hysteretic damping curves to characterize the epistemic uncertainty in nonlinear dynamic material properties for both soil and firm rock sites. For soil sites, for instance, the two sets of proposed curves are the Electric Power Research Institute (EPRI 1993) and Peninsular Range (Silva et al. 1996; Walling et al. 2008). The EPRI (1993) curves represent a moderate

degree of nonlinearity while the Peninsular Range curves reflect more linear, cyclic shear strain dependencies. The Peninsular Range curves represent a subset of the EPRI (1993) soil curves with the 51 to 120 ft (15 to 37 m) EPRI (1993) curves applied to the 0 to 50 ft (0 to 15 m) depth range and the EPRI (1993) 501 to 1,000 ft (153 to 305 m) curve applied to the 51 to 500 ft (15 to 152 m) depth range, below which a rock half-space is used. To evaluate the influence of considering different sets of generic modulus reduction and hysteretic damping curves on the result of site response analysis, we computed soil hazard curves at Site 11 of the TRC1603 project for two sets of material properties suggested by EPRI (2013). Results are shown in Figure 26 for four periods and across a range of return periods. As it can be observed from Figure 26, considering EPRI (1993) curves for the site response analysis yielded smaller hazard values than those obtained when linear Peninsular Range curves were considered. Therefore, considering a larger level of nonlinearity in the site response analysis reduces the hazard in a given return period for short to median spectral periods. However, the impact of the nonlinear properties of the soil materials is minimal for longer spectral periods.

EPRI (2013) suggested that the two sets of soil curves should be given equal weights to represent a reasonable accommodation of epistemic uncertainty in nonlinear dynamic material properties for the generic types of soils found at most CEUS sites. In this study, we followed the EPRI (2013) procedure and gave equal weights to the two sets of soil curves to adequately capture epistemic uncertainty in nonlinear dynamic material properties.

The aleatory variability of the two sets of curves (EPRI and Peninsular Range) will be considered by randomizing modulus reduction and hysteretic damping curves for each of the randomized velocity profiles of the base-case profile. Following Silva et al. (1996), a log-normal distribution is assumed with the standard deviation of the natural log of 0.15 and 0.30 at a cyclic shear strain of 0.03 percent for modulus reduction and hysteretic damping, respectively. Similar to the randomization of velocity profiles, the standard deviation of the natural log is truncated at $\pm 2\sigma$. The truncation is necessary to prevent modulus reduction or damping models that are not physically realizable.

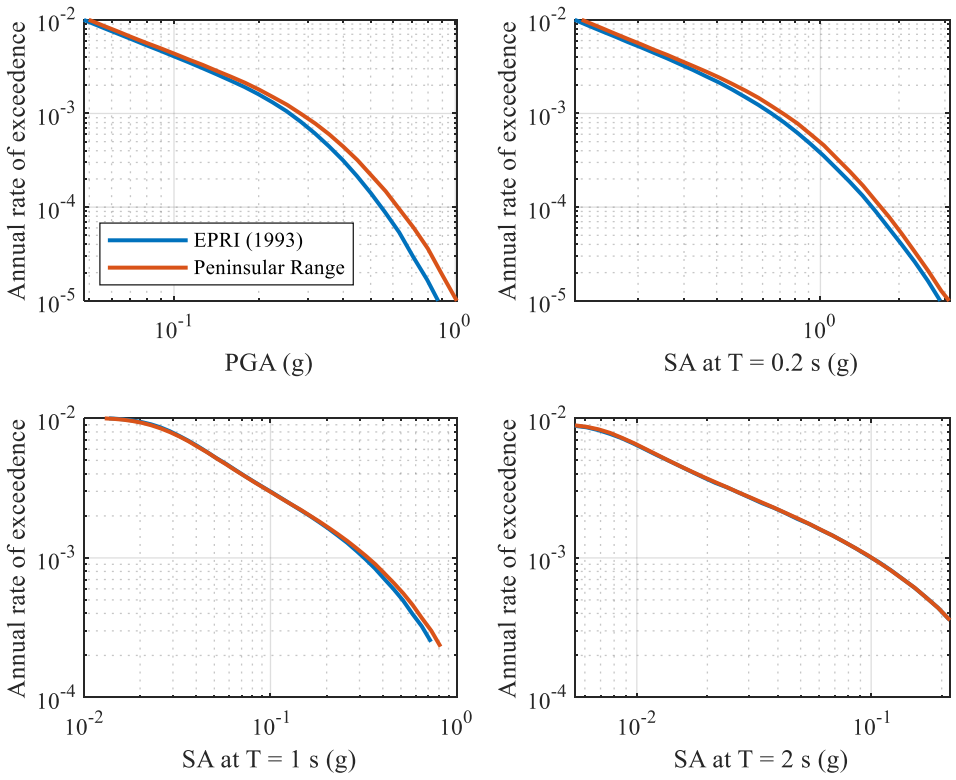


**Figure 26. Evaluating the Influence of the Nonlinear Properties of the Soil Materials on the Site Response Analysis. The Legend in the top Left Hand Figure Applies to all Figures**

### 4.8.7 Layer Unit Weights

Only an approximate estimate of the soil unit weight is considered necessary because it plays a minor role in site-specific amplification (EPRI 2013). Therefore, following EPRI (2013), we considered a simple model based on the shear-wave velocity to determine layer unit weight. Table 7 provides an example base-case velocity profile for Site 11 of the TRC1901 project. This table includes shear-wave velocity, layer thickness, layer depth, and the estimated layer unit weight information.

**Table 7. An Example of a Base-Case Shear Wave Velocity Profile**

| Depth (ft) | Thickness (ft) | Shear-Wave Velocity (ft/sec) | Unit Weight ($lb/ft^3$) |
|---|---|---|---|
| 8 | 8 | 482 | 114.75 |
| 12 | 4 | 581 | 114.75 |
| 25 | 13 | 620 | 114.75 |
| 39 | 15 | 745 | 114.75 |
| 69 | 30 | 860 | 114.75 |
| 157 | 89 | 1129 | 114.75 |
| 184 | 26 | 1916 | 119.77 |
| 272 | 89 | 1955 | 119.77 |
| 436 | 164 | 1975 | 119.77 |
| 650 | 213 | 1995 | 119.77 |
| 1066 | 417 | 2014 | 119.77 |
| 1411 | 344 | 2018 | 119.77 |
| 1575 | 164 | 2080 | 119.77 |
| 1739 | 164 | 2142 | 119.77 |
| 1903 | 164 | 2208 | 119.77 |
| 2198 | 295 | 2493 | 130.97 |

## 4.9 CASE STUDY

To provide details of the approaches used, we selected one site and provided details regarding:

1. The AASHTO general procedure.
2. SSGMRA using a fully probabilistic approach.
3. SSGMRA using an equivalent linear (EQL) approach.

The selected site for the case study is Site 1 of the TRC0803 project (TRC0803_1). Figure 27 shows the geographical location of the study site (site_001) within the study region. This site has the latitude and longitude of 35.2736° and -90.55888° and is located in Cross County. The closest boring log to this site has the job number of 110288.

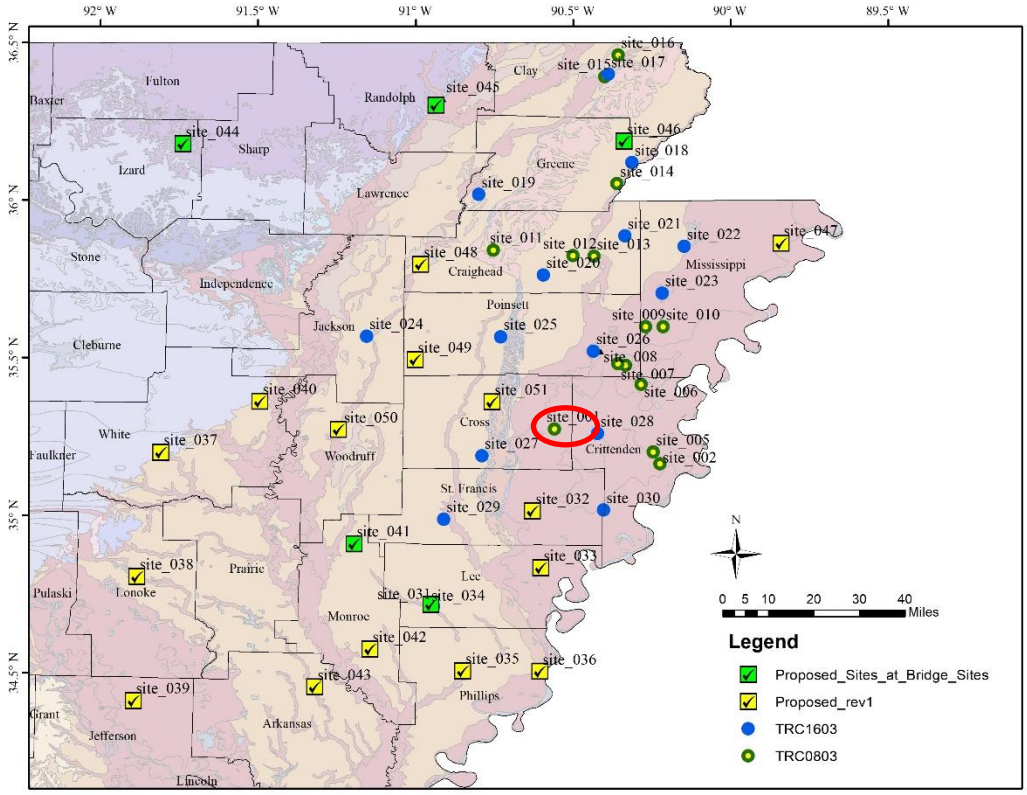


**Figure 27. Location of the Case Study Site (Site 1)**

### 4.9.1 AASHTO General Procedure

According to AASHTO General Procedure, spectral parameters can be obtained for a study site in three steps.

#### *4.9.1.1 The First Step of AASHTO General Procedure*

The first step of the AASHTO General Procedure for calculating spectral parameters at a bridge site is to determine hazard values at the B/C boundary for a 1,000-year return period (7 percent probability of exceedance in 75 years) at PGA and spectral ordinates of 0.2 sec and 1.0 sec. We obtained hazard curves for the study sites from the USGS Unified Hazard Tool for the B/C boundary condition. Then, we used hazard curves obtained from the USGS hazard tool to obtain PGA and spectral accelerations at periods of 0.2 sec and 1.0 sec for the 1000-year return period.

The required input parameters are Site Class, Return Period, Latitude and Longitude of the study site, and the edition of the hazard model. The selected edition will provide deaggregation results in addition to hazard curves. Figure 28 shows the uniform hazard spectrum and hazard curves for various spectral ordinates and seismic sources.

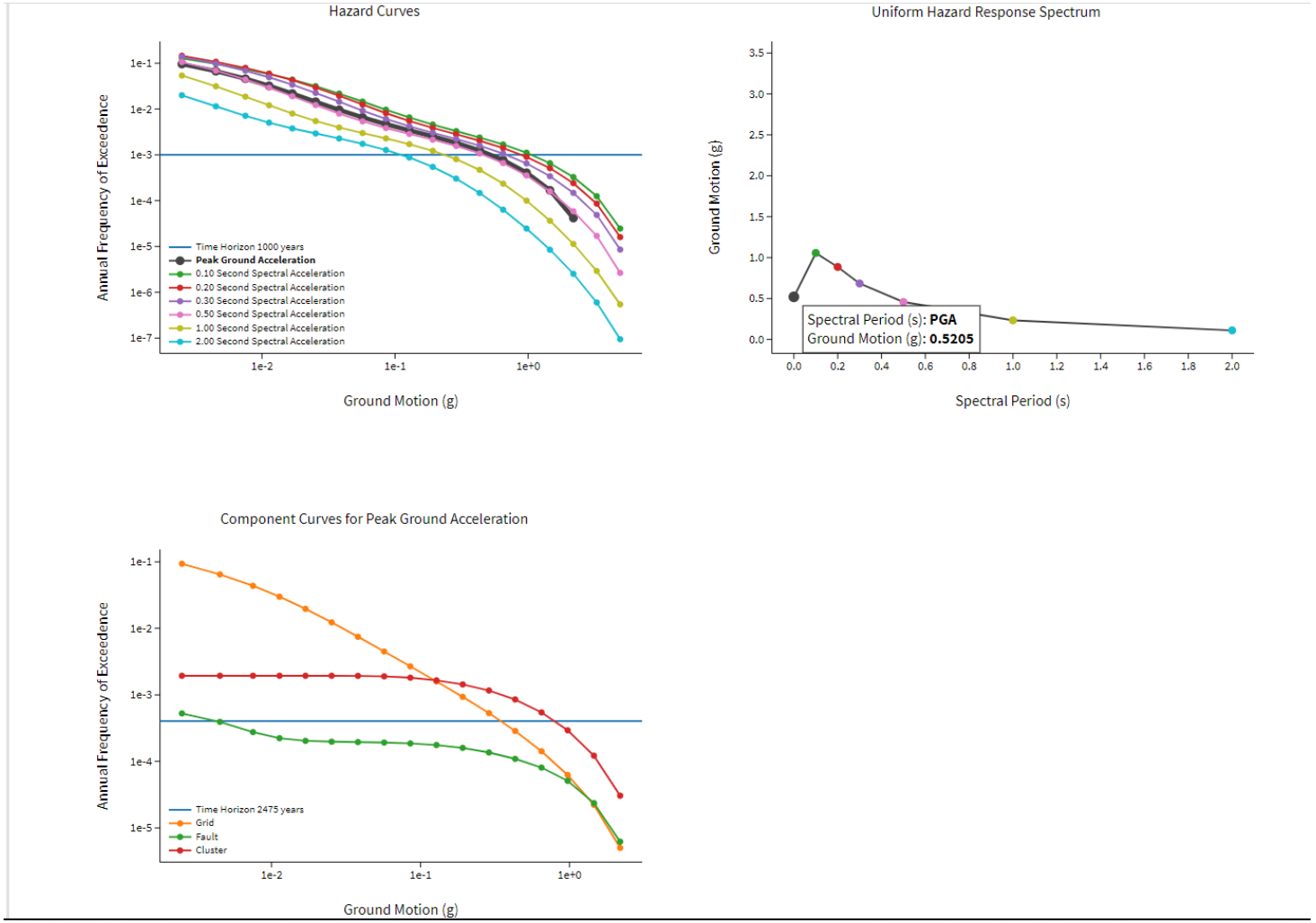


**Figure 28. Outputs of the USGS Unified Hazard Tool**

*4.9.1.2 The Second Step of the AASHTO General Procedure*

The second step of AASHTO General Procedure is to compute site factors for spectral accelerations determined from the previous step. Site factors for *PGA*, $S_s$, and $S_1$ are referred to as $F_{pga}$, $F_a$, and $F_v$, respectively. Site factors can be determined from Table 3.10.3.2-1 through Table 3.10.3.2-3 of the AASHTO LRFD Bridge Design Specifications. To implement these tables and compute site factors, we need to know the Site Class at the study site and spectral accelerations from the previous step. We determined Site Class for the case study, as well as the remaining 50 sites, based on the average shear-wave velocity for the upper 100 ft of the soil profiles and following guidelines provided in Table 3.10.3.1-1 of the AASHTO LRFD Bridge Design Specifications. The shear-wave velocity values within the top 100 ft used to determine site classification of the study site are summarized in Table 8.

**Table 8. Shallow Velocity Profile of the Case Study Site**

| Depth (ft) | Shear -Wave Velocity (ft/s) |
|---|---|
| 2.49 | 787.40 |
| 7.51 | 623.36 |
| 12.50 | 606.96 |
| 17.49 | 606.96 |
| 22.80 | 754.59 |
| 27.99 | 787.40 |
| 33.01 | 787.40 |
| 38.29 | 820.21 |
| 43.50 | 853.02 |
| 48.49 | 853.02 |
| 53.51 | 918.64 |
| 58.50 | 918.64 |
| 63.48 | 918.64 |
| 68.50 | 951.44 |
| 73.49 | 951.44 |
| 78.51 | 1017.06 |
| 83.50 | 1181.10 |
| 88.48 | 1181.10 |
| 93.50 | 1312.34 |
| 98.49 | 1312.34 |

*4.9.1.3 The Third Step of the AASHTO General Procedure*

In the third step, spectral accelerations of the first step should be multiplied by their corresponding site factors determined from the second step to compute spectral parameters. In other words, one should multiply *PGA*, $S_s$, and $S_1$ by $F_{pga}$, $F_a$, and $F_v$, respectively, to calculate spectral parameters. $A_s$, $S_{Ds}$, $S_{D1}$ represent spectral parameters for *PGA*, and spectral periods of 0.2 sec and 1.0 sec, respectively.

For the study site, the time-averaged shear-wave velocity of the top 100 ft (30 m) is determined to be 869 ft/sec (265 m/sec). Therefore, this site is classified as a Site Class D. Using the USGS Unified Hazard Tool, *PGA*, $S_s$, and $S_1$ of the study site are determined to be 0.544 g, 0.910 g, and 0.243 g, respectively (g is gravitation acceleration). Moreover, the $F_{pga}$, $F_a$, and $F_v$ values were determined to be 1.0, 1.136, and 1.913, respectively. Therefore, the AASHTO spectral parameters for the study site based on the AASHTO general procedure will be 0.544 g, 1.034 g, and 0.466 g, respectively.

## 4.10 SSGMRA USING A FULLY PROBABILISTIC APPROACH

The SSGMRA fully probabilistic approach is performed in three steps:

1. Calculating the hazard curve for the reference site condition.
2. Developing the probability density function of amplification factors.
3. Calculating the hazard curve at the soil surface for the desired hazard level.

### 4.10.1 Calculating the Hazard Curve for the Reference Site Condition

The first step of this approach is to perform a Probabilistic Seismic Hazard Analysis (PSHA) that reflects an outcropping (rock at the ground surface) reference site condition. In this study, we used the B/C boundary condition as the reference site condition. Similar to the first step of AASHTO General Procedure for obtaining spectral parameters, we used the USGS Unified Hazard Tool for B/C boundary conditions as the reference site condition to obtain hazard curves for the Case Study and the remaining 50 study sites. The same B/C boundary conditions were used for both approaches.

### 4.10.2 Development of the Probability Density Function of Amplification Factors

The equivalent linear (EQL) method can be used through the Monte Carlo Simulation to develop the probability density function of the amplification factors. In other words, a set of site response analyses using the EQL method should be performed for a given site to develop the probability density function of the amplification factors. Such a set of site response analyses will properly model the aleatory variability and the epistemic uncertainty of the dynamic properties of the soil materials and shear-wave velocity profile of the site in the development of the probability density function for amplification factors.

The EQL analysis may be performed through a time-series approach by specifying the acceleration-time series as the input rock motion. A suite of motions is needed to develop a stable estimate of the response due to motion-to-motion variability. Alternatively, the random vibration theory (RVT) approach can be utilized for the EQL analysis, such that only a Fourier amplitude spectrum (FAS) is required as input, and the selection of a set input motion is avoided. The EQL method requires the following information:

- The shear-wave velocity profile of the site.
- The nonlinear stress-strain response of the soil.
- An input rock motion.

In the following subsections, we will describe these three steps in detail, and we will explain how the aleatory variability and the epistemic uncertainty of the dynamic properties of the soil materials and shear-wave velocity profile of the site are captured.

### 4.10.3 The Shear-Wave Velocity Profile of the Case Study Site

The shear-wave velocity profiles are available for the shallower portion of all 51 sites. These profiles were estimated through non-invasive geophysical measurements such as the MASW and the ReMi seismic surveys. However, we should extend the velocity profile to a deeper geologic unit that represents the reference site condition (B/C boundary). To extend the shallower portion of the velocity profile to the deeper portion, we used the USGS 3D velocity model developed for CUS.

We used the Ramirez-Guzman et al. (2012) report, which is the result of several efforts in previous years including Allen and Wald (2007), Chung and Rogers (2010), Cramer et al. (2004), Ginzburg et al. (1983), Gomberg et al. (2003), Bradley (2003), Mooney et al. (1983), Prodehl et al. (1984), and Stewart (1968). Their model covers a large region of the United States and includes several urban areas, including Little Rock, AR; Evansville, IN; Memphis, TN; Nashville, TN; Louisville, KY; and St. Louis, MO. The CUS 3D velocity model is parameterized by extending the physical properties of most of the well-defined units, to less well-constrained areas, in the Mississippi embayment and the CUS. Outside the embayment and the urban areas mentioned above, where shallow $V_s$ measurements are sparse, the $V_{s30}$ information derived from the correlation between $V_{s30}$ and topographic slope (Allen and Wald 2007; 2009) is used to estimate velocities.

For the case study site, for instance, the shear-wave velocity profiles are available for the top 100 ft (30 m) for all 51 sites. For depths below 100 ft, we used the report by Ramirez-Guzman et al. (2012) and obtained the velocity of deeper geologic units down to the B/C boundary. The full profile of the case study site is summarized in Table 9. Table 9 is an extension to Table 8 and provides the velocity profile down to the reference site condition.

The velocity profile of the study site is randomized to properly consider the aleatory variability associated with the shear-wave velocity, as discussed earlier. The randomized velocity profiles for the case study site are shown in Figure 29. In this figure, the light color represents each of the randomized soil profiles, the red color represents the mean of random profiles, and the blue color represents the original profile.

**Table 9. Velocity Profile of the Case Study Site Down to B/C Boundary Site Condition**

| Depth (ft) | *Shear-Wave Velocity* (ft/sec) |
|---|---|
| 2.49 | 787.40 |
| 7.51 | 623.36 |
| 12.50 | 606.96 |
| 17.49 | 606.96 |
| 22.80 | 754.59 |
| 27.99 | 787.40 |
| 33.01 | 787.40 |
| 38.29 | 820.21 |
| 43.50 | 853.02 |
| 48.49 | 853.02 |
| 53.51 | 918.64 |
| 58.50 | 918.64 |
| 63.48 | 918.64 |
| 68.50 | 951.44 |
| 73.49 | 951.44 |
| 78.51 | 1017.06 |
| 83.50 | 1181.10 |
| 88.48 | 1181.10 |
| 93.50 | 1312.34 |
| 98.49 | 1312.34 |
| 262.47 | 1325.46 |
| 426.51 | 1505.91 |
| 590.55 | 1581.36 |
| 754.59 | 1663.39 |
| 918.64 | 1748.69 |
| 1082.68 | 1870.08 |
| 1246.72 | 1922.57 |
| 1410.76 | 1975.07 |
| 1574.80 | 2027.56 |
| 1738.85 | 2083.33 |
| 1902.89 | 2139.11 |
| 2066.93 | 2194.88 |
| 2230.97 | 2253.94 |
| 2460.63 | 2493.44 |

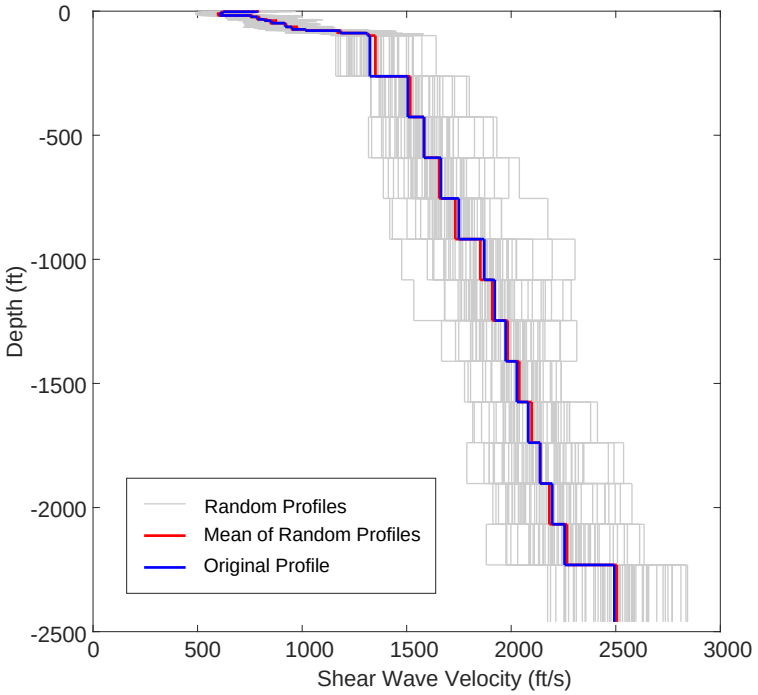


**Figure 29. Randomized Shear-Wave Velocity Profiles for the Case Study Site**

### 4.10.4 The Nonlinear Stress-Strain Response of the Soil

The impact of the nonlinear response of near-surface materials on input ground motions is a crucial element of site response analysis. For the shallower portion of the study sites, information from boring logs can be used to determine soil type. When there is no boring log near the site, or the boring log does not provide information for depths representing the B/C boundary condition, a generic soil type is considered. In this study, we used the *G*/*Gmax* and the damping curves suggested by Chang et al. (1992) to define soil layers for which information from a boring log is available. Chang et al. (1992) specified five soil types, including *S1*, *S2*, *S3*, *C1*, and *C2*. Different soil types can be assigned to various layers of the site profile based on the information from the boring log close to the site. For the Case Study site, for instance, the closest project has the job number of 110288. Figures 30 to 32 show a boring log from that job. The boring is terminated at this site at around 100 ft. We assigned soil types defined by Chang et al. (1992) to layers down to 100 ft (30 m). The results are summarized in Table 10. Tables 11 and 12 define soil types S1, S2, S3, C1, and C2 provided in Table 10. In these tables, $e_{max}$ is the maximum void ratio, $e_{min}$ is the minimum void ratio, $G_s$ is the specific gravity of soil solids, $I_P$ is the plasticity index, and *LL* is the liquid limit of the soils.

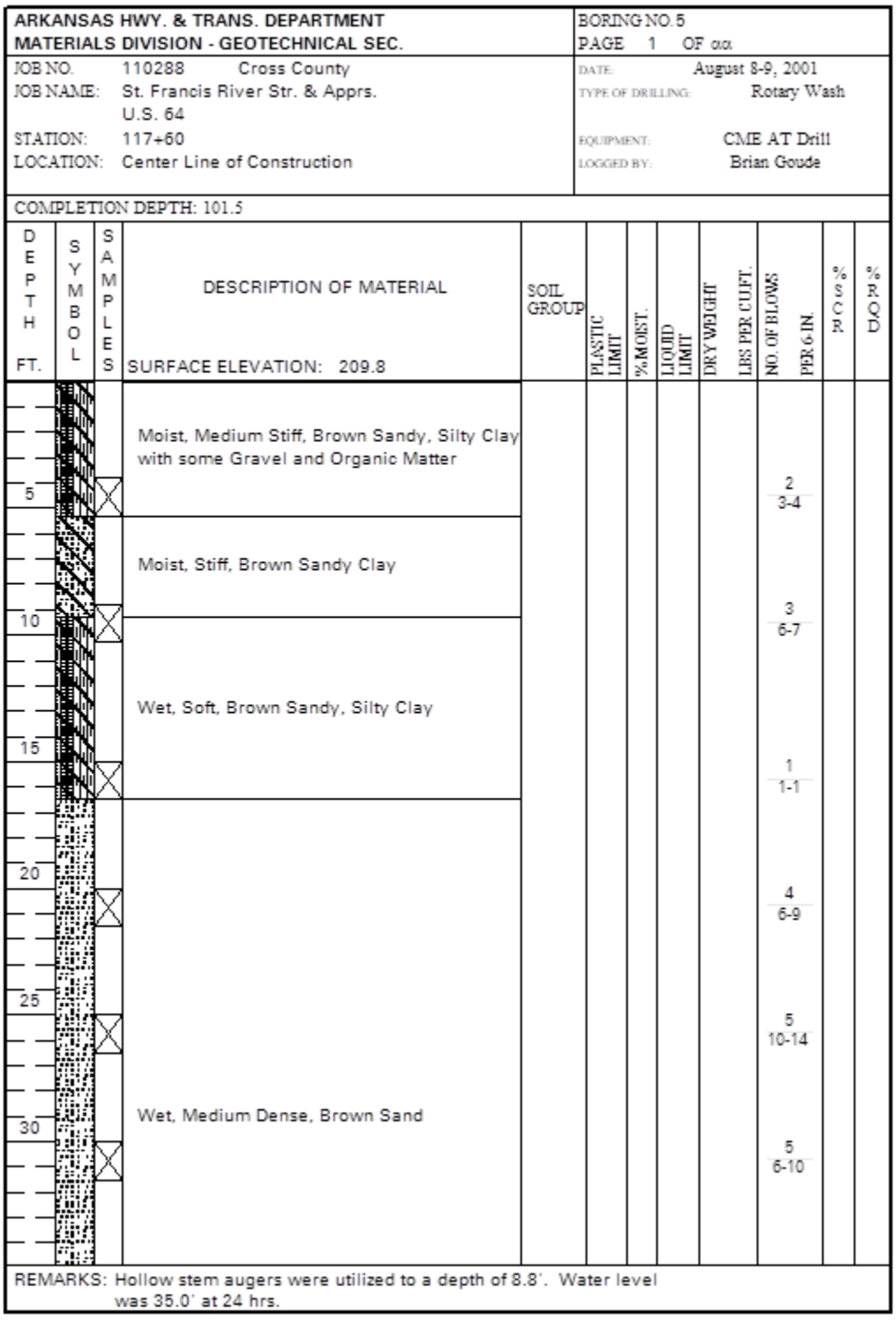


**Figure 30. Boring Log Information from Job 110288 Used for the Case Study Site for the Top 35 ft**

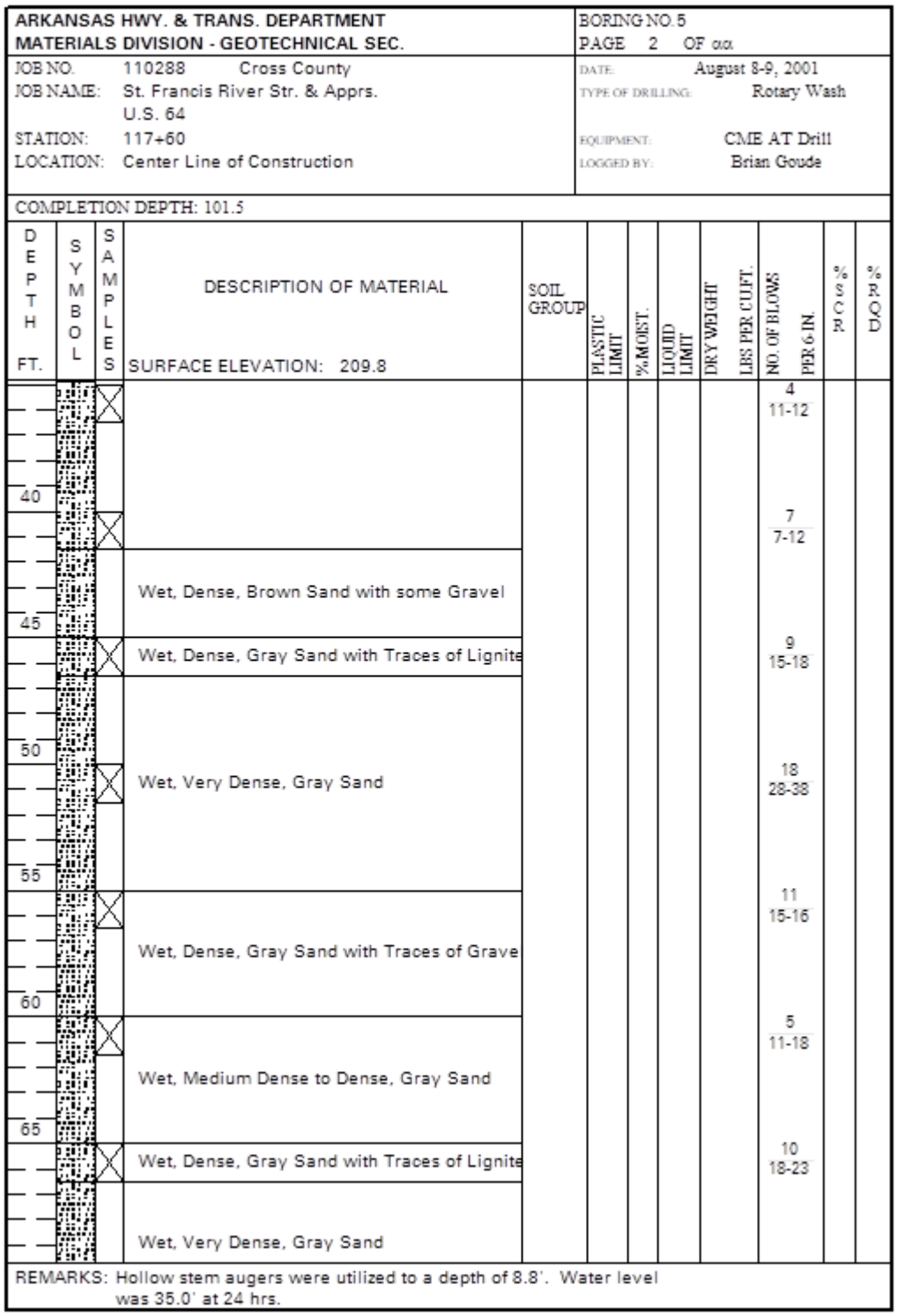

ARKANSAS HWY. & TRANS. DEPARTMENT
MATERIALS DIVISION - GEOTECHNICAL SEC.

BORING NO. 5
PAGE 2 OF αα

JOB NO. 110288 Cross County
JOB NAME: St. Francis River Str. & Apprs. U.S. 64
STATION: 117+60
LOCATION: Center Line of Construction

DATE: August 8-9, 2001
TYPE OF DRILLING: Rotary Wash
EQUIPMENT: CME AT Drill
LOGGED BY: Brian Goude

COMPLETION DEPTH: 101.5

| DEPTH FT. | SYMBOL | SAMPLES | DESCRIPTION OF MATERIAL | SOIL GROUP | PLASTIC LIMIT | %MOIST. | LIQUID LIMIT | DRY WEIGHT LBS PER CU.FT. | NO. OF BLOWS PER 6 IN. | % SCR | % RQD |
|---|---|---|---|---|---|---|---|---|---|---|---|
| | | | SURFACE ELEVATION: 209.8 | | | | | | | | |
| | | X | | | | | | | 4<br>11-12 | | |
| 40 | | X | | | | | | | 7<br>7-12 | | |
| | | | Wet, Dense, Brown Sand with some Gravel | | | | | | | | |
| 45 | | X | Wet, Dense, Gray Sand with Traces of Lignite | | | | | | 9<br>15-18 | | |
| 50 | | X | Wet, Very Dense, Gray Sand | | | | | | 18<br>28-38 | | |
| 55 | | X | Wet, Dense, Gray Sand with Traces of Grave | | | | | | 11<br>15-16 | | |
| 60 | | X | Wet, Medium Dense to Dense, Gray Sand | | | | | | 5<br>11-18 | | |
| 65 | | X | Wet, Dense, Gray Sand with Traces of Lignite | | | | | | 10<br>18-23 | | |
| | | | Wet, Very Dense, Gray Sand | | | | | | | | |

REMARKS: Hollow stem augers were utilized to a depth of 8.8'. Water level was 35.0' at 24 hrs.

**Figure 31. Boring Log Information from Job 110288 Used for the Case Study Site for Depths Between 35 ft and 70 ft**

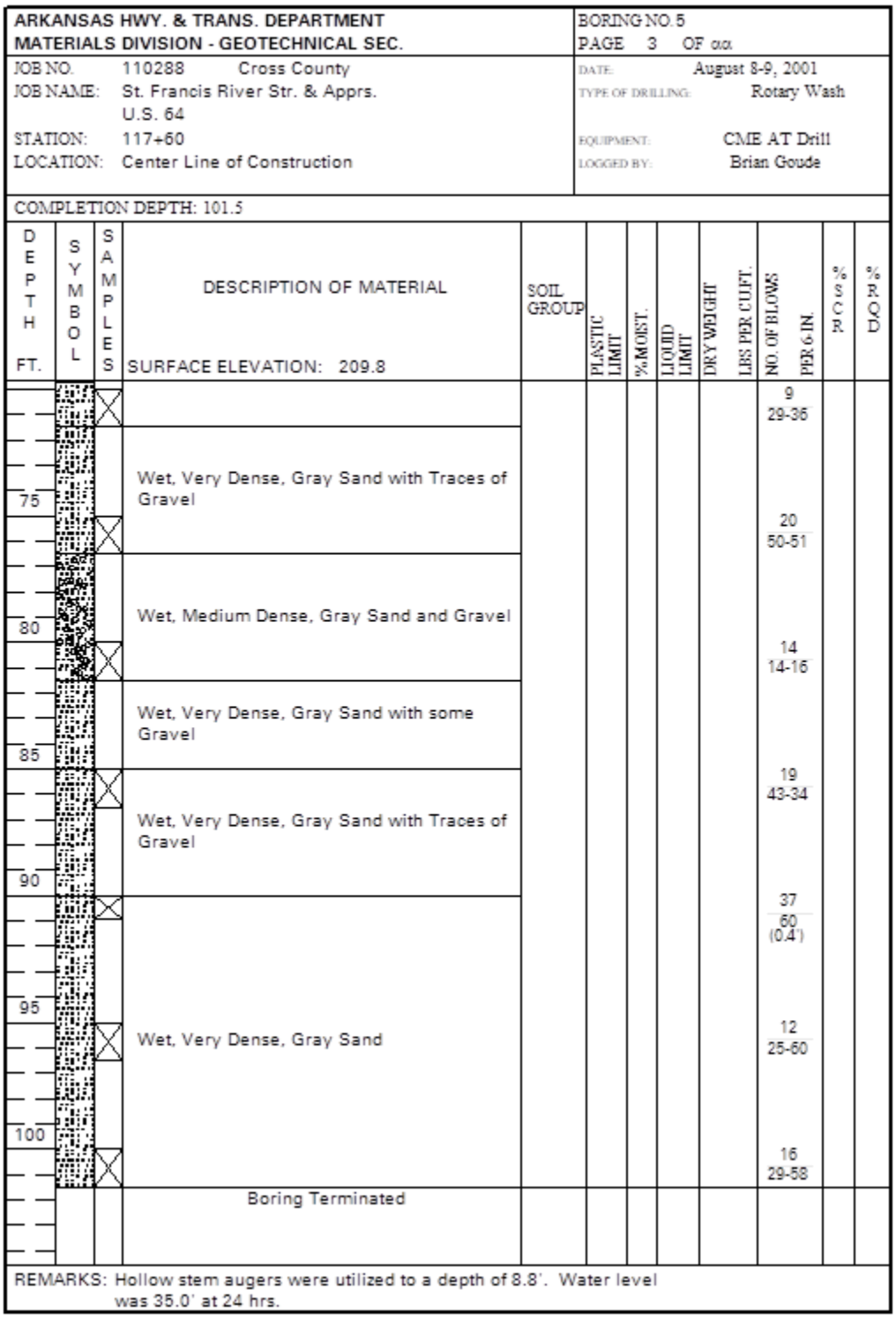


**Figure 32. Boring Log from Job 110288 Used Information for the Case Study Site for Depths Between 70 ft and 100 ft**

**Table 10. Soil Type for Layers of the Case Study Profile from Job 110288 Boring Log**

| Depth (ft) | Thickness (ft) | Soil Type |
|---|---|---|
| 2.49 | 2.50 | C2 |
| 7.51 | 5.00 | C2 |
| 12.50 | 5.00 | C2 |
| 17.49 | 5.00 | S2 |
| 22.80 | 5.30 | S2 |
| 27.99 | 5.20 | S2 |
| 33.01 | 5.00 | S2 |
| 38.29 | 5.30 | S2 |
| 43.50 | 5.20 | S2 |
| 48.49 | 5.00 | S2 |
| 53.51 | 5.00 | S2 |
| 58.50 | 5.00 | S2 |
| 63.48 | 5.00 | S2 |
| 68.50 | 5.00 | S2 |
| 73.49 | 5.00 | S2 |
| 78.51 | 5.00 | S2 |
| 83.50 | 5.00 | S2 |
| 88.48 | 5.00 | S2 |
| 93.50 | 5.00 | S2 |
| 98.49 | 5.00 | S2 |

**Table 11. Information for Sandy Soil Types**

| Soil Type | Description | Unified Soil Classification | $e_{max}$ | $e_{min}$ | $G_s$ |
|---|---|---|---|---|---|
| S1 | Silt, poorly graded fine sand | ML, MH,SP-SM | 0.88 | 0.47 | 2.62 |
| S2 | Fine to medium sand | SM,SP, SP-SM | 0.93 | 0.48 | 2.64 |
| S3 | Fine to coarse sand | SP-SW-SM-GP | 0.79 | 0.38 | 2.60 |

**Table 12. Information for Clay Soil Types**

| Soil Type | Description | Unified Soil Classification | $I_p$ | *LL* | $G_s$ |
|---|---|---|---|---|---|
| C1 | High plasticity fat clay | CH, CL-CH | 44 | 70 | 2.58 |
| C2 | Silty to sandy clay | CL,CL-ML | 14 | 33 | 2.58 |

EPRI (2013) recommends using two sets of generic modulus reductions and hysteretic damping curves to characterize the epistemic uncertainty in nonlinear dynamic material properties for both soil and firm rock sites. For soil sites, for instance, the two sets of proposed curves are the EPRI (1993) and the Peninsular Range (Silva et al. 1996; Walling et al. 2008). The EPRI (1993) curves represent a moderate degree of nonlinearity while the Peninsular Range curves reflect more linear, cyclic shear strain dependencies. The Peninsular Range curves represent a subset of the EPRI (1993) soil curves with the 51 to 120 ft (15 to 37 m) EPRI (1993) curves applied to the 0 to 50 ft (0 to 15 m) depth range and the EPRI (1993) 501 to 1,000 ft (153 to 305 m) curve applied to the 51 to 500 ft (15 to 152 m) depth range, below which linear behavior is assumed. EPRI (2013) suggested that the two sets of soil curves should be given equal weights to represent a reasonable accommodation of the epistemic uncertainty in the nonlinear dynamic material properties for the generic types of soils found at most CEUS sites. In this study, we followed the EPRI (2013) procedure and gave equal weights to the two sets of soil curves to adequately capture the epistemic uncertainty in the nonlinear dynamic material properties. Table 13 summarizes the specification of $G/G_{max}$ models and damping models for layers of the case study site profile. These models are plotted in Figure 33 and Figure 34.

**Table 13. $G/G_{max}$ and Damping Models Specified for Layers of the Case Site Profile With no Available Soil Information from Boring Logs**

| Depth (ft) | Thickness (ft) | Soil Type 1 | Damp. Type 1 | Soil Type 2 | Damp. Type 2 |
|---|---|---|---|---|---|
| 262.47 | 163.98 | EPRI 1993 250-500 ft | EPRI 1993 250-500 ft | Peninsular 50-500 ft | Peninsular 50-500 ft |
| 426.51 | 164.04 | EPRI 1993 250-500 ft | EPRI 1993 250-500 ft | Peninsular 50-500 ft | Peninsular 50-500 ft |
| 590.55 | 164.04 | EPRI 1993 500-1000 ft | EPRI 1993 500-1000 ft | Linear | Damp0p1 |
| 754.59 | 164.04 | EPRI 1993 500-1000 ft | EPRI 1993 500-1000 ft | Linear | Damp0p1 |
| 918.64 | 164.04 | EPRI 1993 500-1000 ft | EPRI 1993 500-1000 ft | Linear | Damp0p1 |
| 1082.68 | 164.04 | Linear | Damp0p1 | Linear | Damp0p1 |
| 1246.72 | 164.04 | Linear | Damp0p1 | Linear | Damp0p1 |
| 1410.76 | 164.04 | Linear | Damp0p1 | Linear | Damp0p1 |
| 1574.80 | 164.04 | Linear | Damp0p1 | Linear | Damp0p1 |
| 1738.85 | 164.04 | Linear | Damp0p1 | Linear | Damp0p1 |
| 1902.89 | 164.04 | Linear | Damp0p1 | Linear | Damp0p1 |
| 2066.93 | 164.04 | Linear | Damp0p1 | Linear | Damp0p1 |
| 2230.97 | 164.04 | Linear | Damp0p1 | Linear | Damp0p1 |
| 2460.63 | 229.66 | Linear | Damp0p1 | Linear | Damp0p1 |

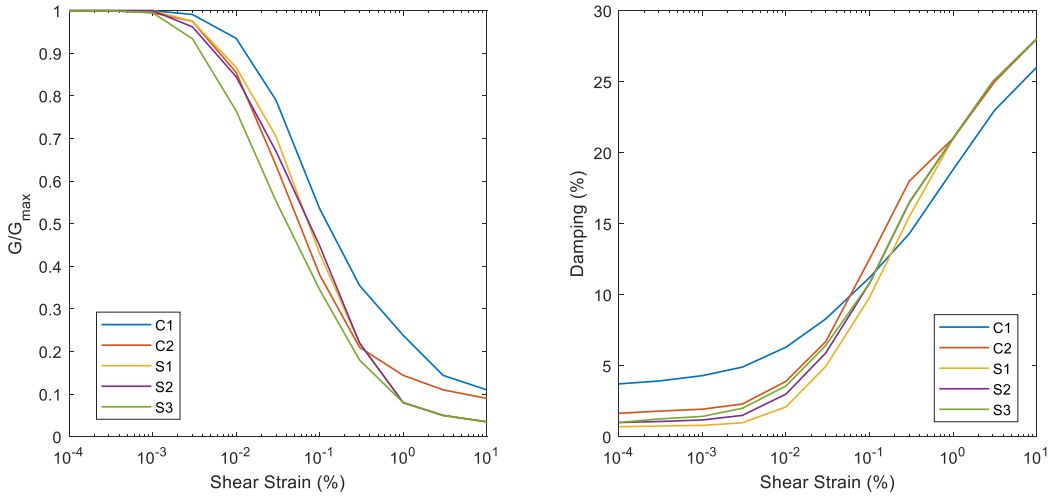


**Figure 33. $G/G_{max}$ and Damping Chang et al. (1992)**

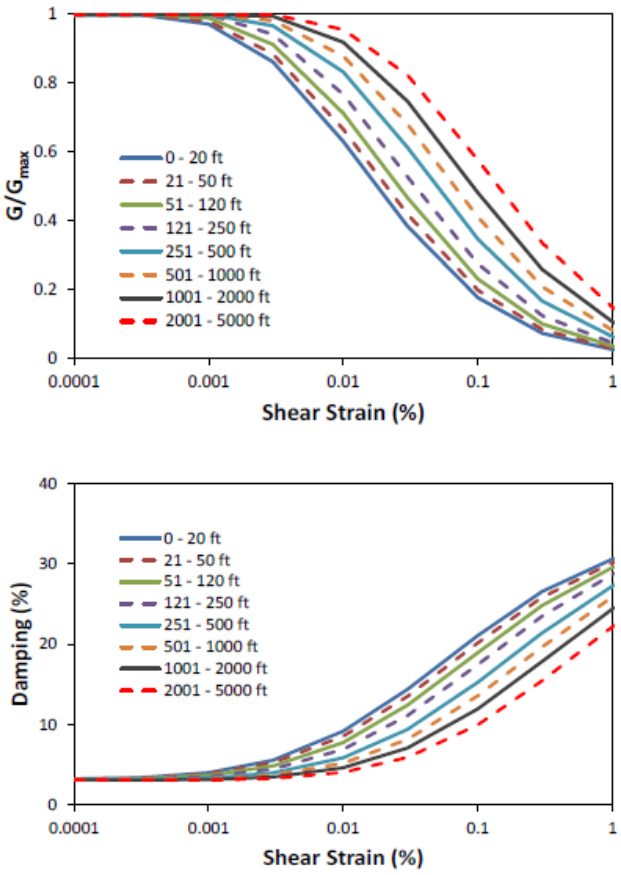


**Figure 34. $G/G_{max}$ and Damping Curves Specified by EPRI (1993)**

The aleatory variability of different curves will be considered by randomizing the modulus reduction and hysteretic damping curves for each of the randomized velocity profiles of the base-case profile. Following Silva et al. (1996), a log-normal distribution is assumed with the standard deviation of the natural log of 0.15 and 0.30 at a cyclic shear strain of 0.03 percent for modulus reduction and hysteretic damping, respectively. Similar to the randomization of velocity profiles, the standard deviation of the natural log is truncated at ±2σ. The truncation is necessary to prevent modulus reduction or damping models that are not physically realizable.

### 4.11 THE INPUT ROCK MOTION USING A FULLY PROBABILISTIC APPROACH

Performing the EQL analysis requires specifying the acceleration-time series as the input rock motion. A suite of motions is needed to develop a stable estimate of the response due to motion-to-motion variability. Alternatively, the RVT approach can be used for the EQL analysis, such that only a FAS is required as input, and the selection of a set input motion is avoided.

For this study, a point-source seismological model is considered. In the point-source model, the total FAS of the horizontal ground motion displacement can be expressed as (Boore, 2003):

$$Y(M_0, R, f) = E(M_0, f) \cdot P(R, f) \cdot G(f) \quad (3)$$

where $M_0$ is the seismic moment (dyne·cm), $R$ is the source-to-site distance (km), $f$ is the frequency (Hz), $E(M_0, f)$ is the source spectrum, $P(R, f)$ is the path effect, and $G(f)$ represents the local site effects. Different components of FAS are described in the following subsections.

#### 4.11.1 Source Term

A set of parameters are required to describe the source term. Earthquake magnitude ($M$), source spectrum model, stress parameter ($\Delta\sigma$), source velocity ($\beta_s$), and source density ($\rho_s$) are the necessary parameters that should be defined to calculate the source term. Earthquake magnitude has little impact on the results of site response analysis because, in the site response analysis, the source-to-site distance is changed to obtain a ground motion intensity that matches the target hazard value. Therefore, a larger magnitude will be accompanied by a larger distance compared to a smaller-magnitude earthquake to generate controlling motion. The source spectral model can be described by assuming a single-corner- or double-corner-frequency model. To be consistent with the EPRI suggested approach, we gave equal weights to the two sets of source spectrum models to adequately capture the epistemic uncertainty in this parameter. In this study, we used the stress parameter of Boore and Thompson (2015). We assumed the stress drop to be equal to 400 bar.

#### 4.11.2 Path Term

The path term $P(R, f)$ in Equation 3 can be decomposed into two components, commonly referred to as the geometric attenuation and the anelastic attenuation. The geometric spreading represents the amplitude decay caused by the increasing distance from the source. The anelastic attenuation, quantified by the quality factor $Q$, models the amplitude attenuation due to scattering and the conversion of the elastic wave energy to heat and is usually found to be frequency-dependent. The path-attenuation

parameters that were suggested by EPRI (2013) and those considered in Chapman et al. (2014) are given in Table 14. In this study, we will consider the path term quantified by Chapman et al. (2014) while conducting site response analysis. Pezeshk et al. (2018) also used the path-attenuation term developed by Chapman et al. (2014) in their Central and Eastern North America (CENA) seismological model.

**Table 14. Path-Attenuation Term Study Compared to Those Suggested by EPRI (1993)**

| Study | Geometric Spreading | | | Anelastic Attenuation |
|---|---|---|---|---|
| **EPRI (1993)** | $R^{-1.0}$ | *for* | $R \le 60$ km | $Q(f) = 670f^{0.33}$ |
| | $R^{-0.5}$ | *for* | $R > 60$ km | |
| **Chapman *et al.* (2014)** | $R^{-1.3}$ | *for* | $R \le 60$ km | $Q(f) = 440f^{0.47}$ |
| | $R^{0}$ | *for* | $60 \le R < 120$ km | |
| | $R^{-0.5}$ | *for* | $R \le 60$km | |

### 4.11.3 Site Term

The site effect, *G(f)* in Equation 3, can be separated into site amplification factors and a near-surface attenuation term, which models the near-surface damping effects and is independent of the path. We employed the model of Anderson and Hough (1984) for near-source attenuation, which is described as a low-pass filter and is defined by the decay slope of the spectrum at high frequencies, *kappa* ($\kappa_0$) (at near-source distances). Anderson and Hough (1984) have introduced *kappa* as a parameter that controls the shape of the Fourier acceleration amplitude spectrum of ground-motion recordings at high frequencies. In accordance with Anderson and Hough (1984), spectrum decays exponentially as:

$$a(f) = A_0 \exp(-\pi\kappa f) \qquad for \quad f > f_E \tag{4}$$

In this equation, *a(f)* is the amplitude spectrum at the frequency *f*, $A_0$ is the source and path-dependent amplitude, $f_E$ is the frequency above which the spectral shape is indistinguishable from exponential decay, and $\kappa$ (*kappa*) is the spectral decay parameter. In other words, *kappa* accounts for the path-independent decay of the high frequency in ground motions. It is clear in Equation 4, for frequencies above $f_E$, *kappa* controls the spectrum decay. Moreover, the amplitude fall-off is approximately linear on a $log[a(f)]$ versus *f* plot. Therefore, one should calculate the slope of the fit to the spectra at the high frequencies (in frequency/log-amplitude space) using the linear least-squares to obtain the *kappa* parameter.

The site *kappa* is an important parameter in developing the input motion since it may significantly impact the spectrum of the controlling motion. Due to this fact, uncertainties associated with *kappa* should be characterized appropriately. Epistemic uncertainties associated with site *kappa* can be captured through the development of the mean base case value as well as two upper-case and lower-case values. The development of the base case for the site *kappa* largely depends on the study region and characteristics of the site of interest. Boore and Campbell (2017) suggested a range of *kappa* values for B/C boundary conditions in CUS. They suggested kappa to be between 0.01 sec and 0.03 sec. The *kappa* parameter has

a significant impact on the results of site response analysis for PGA and has smaller impact at larger periods. In this study, we assumed *kappa* to be 0.02 sec while performing the site-specific seismic hazard analysis, which is compatible with the average *kappa* value for the Central United States.

### 4.12 THE INPUT ROCK MOTION FOR SSGMRA USING AN EQUIVALENT LINEAR APPROACH

The Time Series approach requires specifying the acceleration-time series as the input rock motion. A suite of motions is needed to develop a stable estimate of the response due to motion-to-motion variability. The selection of input motions is based on deaggregation results. Deaggregation is an output of the PSHA that determines the combination of different earthquake scenarios (pairs of earthquake magnitude and distance) to the overall hazard. Selected input motions should be similar to the earthquake scenario that contributes the most to the overall hazard level. The USGS Unified Hazard Tool provides deaggregation results for a given site within the United States.

Figure 35 provides deaggregation information for the study site. As it is clear from this figure, the dominant scenario can be specified by an earthquake with a mean magnitude of 7.26 and a mean distance of 28.2 km. We repeated this procedure and analyzed deaggregation results for all 51 study sites to determine the dominant earthquake scenarios. We noticed that some sites share relatively the same earthquake scenarios. Accordingly, we divided the entire study region into five subregions and assigned a different set of 11 earthquakes for two horizontal directions (a total of 22-time series) to each subregion. Figure 36 shows the mentioned subregions and sites that can be included in each subregion. According to Figure 36, we included the case study site within the Zone 3 region. Table 15 provides the mean moment magnitude and mean distance based on de-aggregation for each of the zones shown in Figure 36. Table 16. provides a set of 11 pairs of time series selected for this subregion. In this table, each row represents two recorded horizontal components of a single motion.

Deaggregation of Seismic Hazard at One Period of Spectral Acceleration
Data from Dynamic: Conterminous U.S. 2014 (v4.1.4)
PSHA Deaggregation. Percent contributions.
site: Test
latitude: 35.274°E
longitude: 90.559°W
imt: Peak Ground Acceleration
vs30 = 760 m/s (B/C boundary)
return period: 1000 yrs.
This deaggregation corresponds to: Total
Summary statistics for PSHA PGA deaggregation, r=distance, ε=epsilon:
Deaggregation targets:
Return period: 1000 yrs

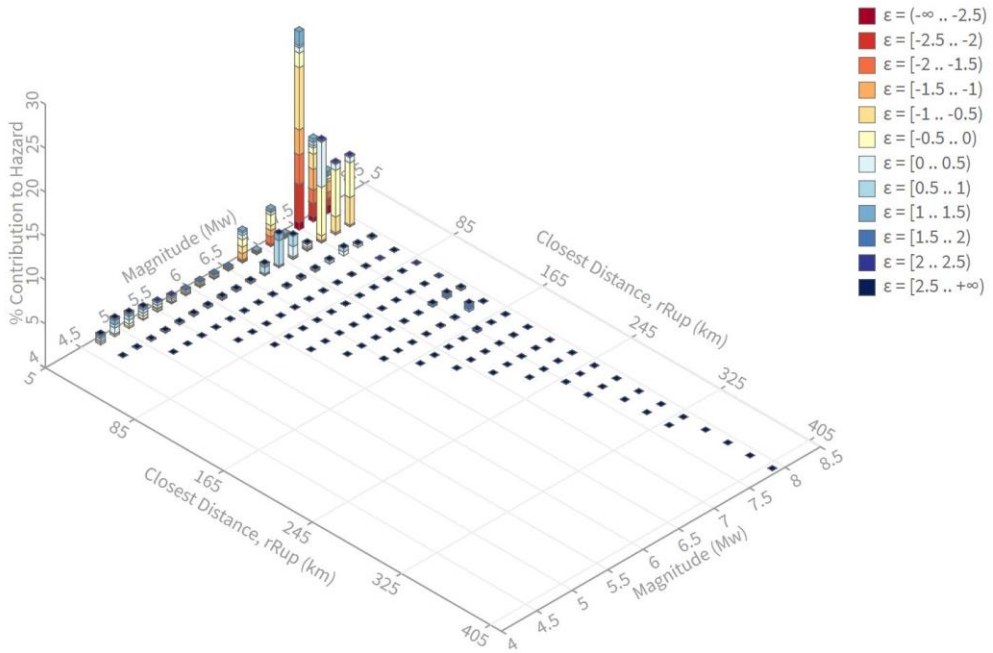


Exceedance rate: 0.001 $yr^{-1}$
PGA ground motion: 0.52032123 g
Recovered targets:
Return period: 1005.5097 yrs
Exceedance rate: 0.00099452053 $yr^{-1}$
Totals:
Binned: 100 percent
Residual: 0 percent
Trace: 0.56 percent
Mean (over all sources):
m: 7.26
r: 28.2 km
$\varepsilon_0$: -0.35 σ
Mode (largest m-r bin):
m: 7.5
r: 18.5 km
$\varepsilon_0$: -1.03 σ
Contribution: 22.59 percent
Mode (largest m-r-$\varepsilon_0$ bin):
m: 7.5
r: 19.16 km
$\varepsilon_0$: -0.69 σ
Contribution: 7.08 percent

**Figure 35. Deaggregation Result for the Case Study Site**

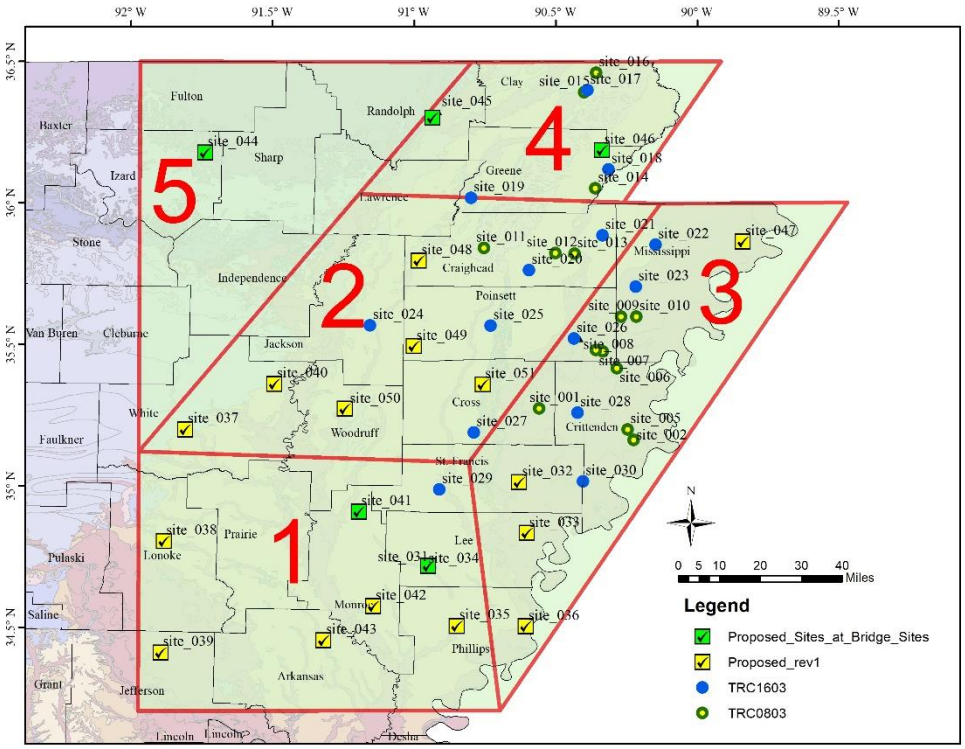


**Figure 36. Dividing the Study Region into Five Subregions Based on the Deaggregation results. Dominant Earthquake Scenarios are Similar for Sites Within Each Subregion**

**Table 15. Mean Moment Magnitude and Mean Distance for Each of the Five Zones**

| | Zone 1 | Zone 2 | Zone 3 | Zone 4 | Zone 5 |
|---|---|---|---|---|---|
| Mean **M** | 7.50 | 7.51 | 7.51 | 7.51 | 7.50 |
| Mean R | 154.50 | 82.40 | 62.50 | 64.95 | 162.19 |

**Table 16. Selected Ground-Motion Records for Performing SSGMRA Using the EQL Approach**

| No. | First Component | Second Component |
|---|---|---|
| **1** | RSN1577_CHICHI_TTN025-E | RSN1577_CHICHI_TTN025-N |
| **2** | RSN1161_KOCAELI_GBZ000 | RSN1161_KOCAELI_GBZ270 |
| **3** | RSN1245_CHICHI_CHY102-E | RSN1245_CHICHI_CHY102-N |
| **4** | RSN1256_CHICHI_HWA002-N | RSN1256_CHICHI_HWA002-W |
| **5** | RSN1485_CHICHI_TCU045-E | RSN1485_CHICHI_TCU045-N |
| **6** | RSN1582_CHICHI_TTN032-E | RSN1582_CHICHI_TTN032-N |
| **7** | RSN1585_CHICHI_TTN040-N | RSN1585_CHICHI_TTN040-W |
| **8** | RSN1587_CHICHI_TTN042-N | RSN1587_CHICHI_TTN042-W |
| **9** | RSN1613_DUZCE_1060-N | RSN1613_DUZCE_1060-E |
| **10** | RSN1787_HECTOR_HEC000 | RSN1787_HECTOR_HEC090 |
| **11** | RSN1633_MANJIL_ABBAR—L | RSN1633_MANJIL_ABBAR--T |

The next phase of SSGMRA using the EQL approach is to match the selected time series to the uniform hazard response spectrum (UHRS) of the reference site. Figure 37 shows the UHRS of the case study site for a return period of 1000 years. Hazard values for this return period are available at PGA and spectral ordinates of 0.1, 0.2, 0.3, 0.5, 1.0, 2.0, and 5.0 sec. We interpolated hazard values for the remaining spectral periods based on the eight known hazard values at the mentioned spectral ordinates.

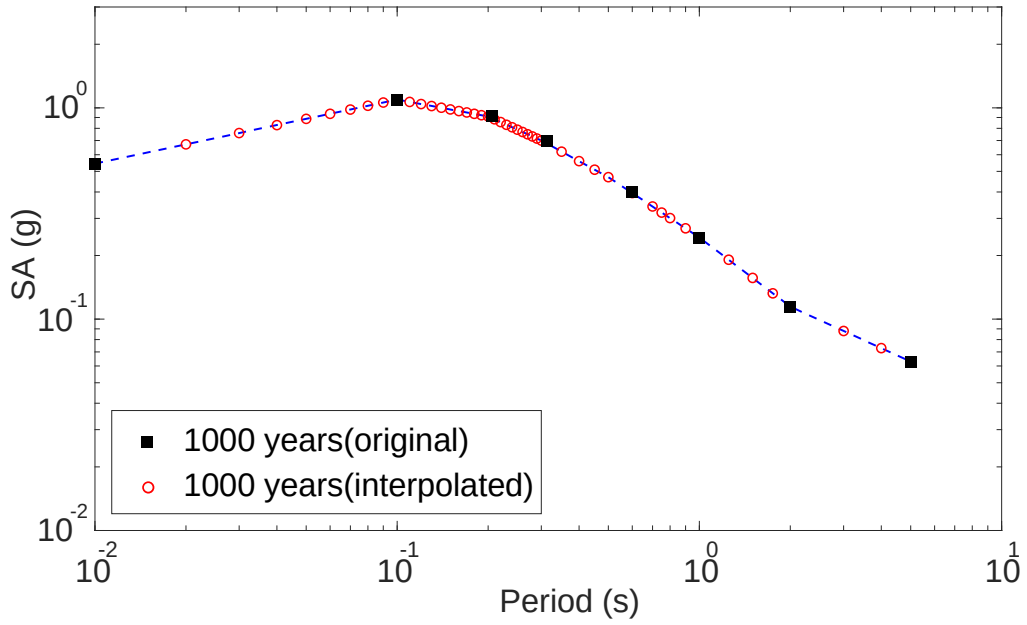


**Figure 37. The Uniform Hazard Response Spectrum (UHRS) of Study Site 1 at the B/C Boundary Condition**

Figure 38 shows the seed ground motion (RSN1577_CHICHI_TTN025-E) and the scaled ground motion as well as the response spectra for the target (UHRS), the seed, and the matched case. We used the Abrahamson (1993) procedure to match the seed motion to the target spectrum. The matched motion is the one that is used in the EQL analysis. This figure illustrates the "target spectrum" obtained from a probabilistic seismic hazard analysis (PSHA) shown in dotted green line in the top figure, the response spectrum of the matched ground motion shown in solid red in the top figure, and the response spectrum of the selected ground motion (seed) before spectrum matching in purple in the top figure. The other figures shown below represent acceleration, velocity, and displacement of the seed earthquake (in blue) and the matched earthquake in red.

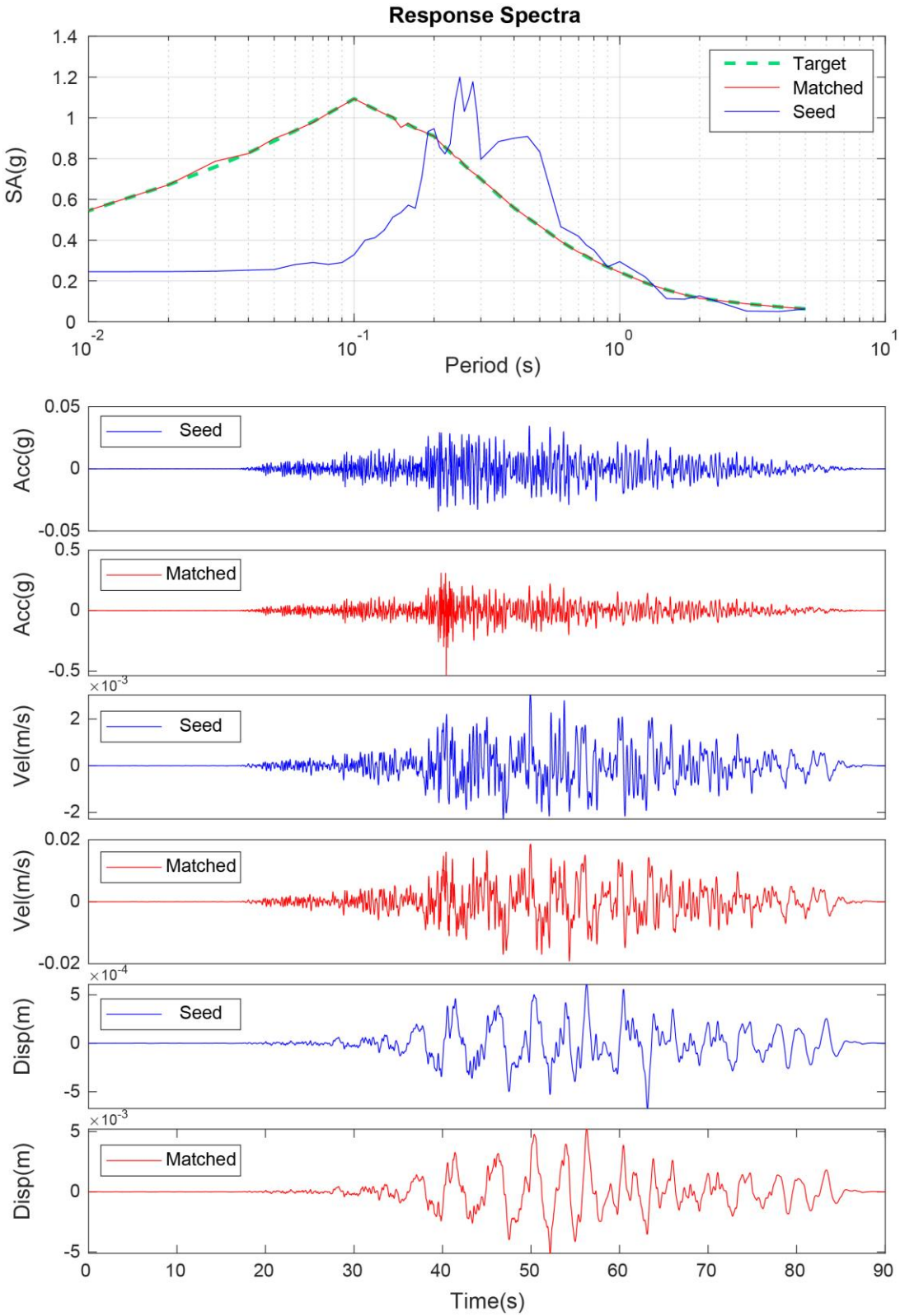


**Figure 38. Matching Spectrum of Seed Motion to the Target Spectrum (UHS). The Middle Subplot Shows the Seed Motion, and the Bottom Subplot Indicates the Matched Motion**

## 4.13 CALCULATING THE HAZARD CURVE ON THE SOIL SURFACE FOR THE DESIRED HAZARD LEVEL

Both SSGMRA using the EQL approach and a fully probabilistic approach were used for the Site 1 case study. For a fully probabilistic approach, both Equations 1 and 2 are used in line with each other to compute soil surface hazard curves. Both equations involve integrations that can be replaced by the Monte Carlo simulation as an alternative approach. In the Monte Carlo approach, we can average over the results of a large number of simulations that represent the variability of soil profiles and dynamic properties of the soil materials to compute hazard values on the soil surface. In the time series analysis, we performed 2640 analyses for a single site. We performed 1320 analyses for 22 input motions and 60 randomized shear-wave velocity profiles (22 x 60). The same analyses were performed for two different combinations of soil types (two sets of soil types were considered for layers with no information from boring logs). For the fully probabilistic approach, however, a fewer number of analyses are required. The number of analyses for the fully probabilistic approach is 22 times less than the time series analysis because this method does not require the selection of input motions.

Figure 39 shows the shear-wave velocity profile of the case study site as well as response spectra for:

- Random soil profiles.
- Mean of 60 random soil profiles for 11 earthquakes.
- Mean plus and minus of one standard deviation of all 60 random soil profiles for 11 earthquakes.
- Results of the SSGMRA fully probabilistic approach and the SSGMRA equivalent linear approach.
- Result of general AASHTO procedure.
- Other site analysis results are shown in Appendix B.

Both SSGMRA and fully probabilistic results typically fall within one plus and minus standard deviation of the SSGMRA equivalent linear approach.

## 4.14 SUMMARY

The longitude and the latitude, site class, and $V_{s30}$ for all 51 sites are provided in Table 17. Table 18 provides acceleration coefficients following AASHTO LRFD Design Specifications for all 51 sites. Table 19 provides acceleration coefficients obtained following the site-specific procedure outlined in this report.

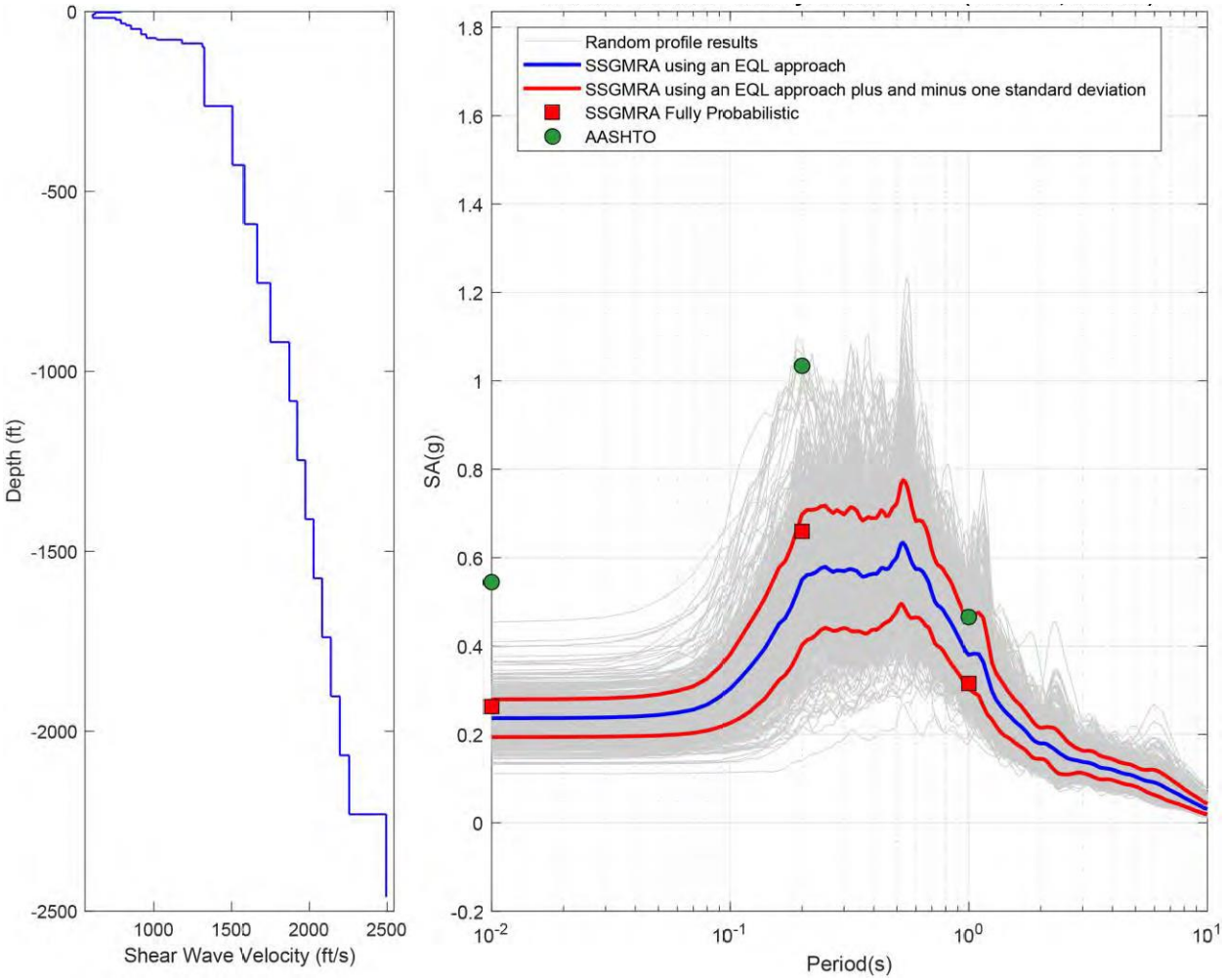


**Figure 39. Left Panel: Shear-Wave Velocity Profile for Site 1; and Right Panel: Results of SSGMRA Using a Fully Probabilistic Approach, SSGMRA Using an Equivalent Linear Approach, SSGMRA Using an Equivalent Linear Approach Plus and Minus One Standard Deviation, and AASHTO Using a General Approach**

**Table 17. The Longitude and the Latitude, Site Class, and $V_{s30}$ for All Study Sites**

| Project | Latitude | Longitude | Site_Class | VS30 |
|---|---|---|---|---|
| TRC0803_1 | 35.27326 | -90.55888 | D | 264.92 |
| TRC0803_2 | 35.16262 | -90.22425 | D | 215.81 |
| TRC0803_3 | 35.39146 | -90.27344 | D | 227.02 |
| TRC0803_4 | 35.4748 | -90.33327 | D | 221.69 |
| TRC0803_5 | 35.19971 | -90.24574 | D | 191.38 |
| TRC0803_6 | 35.41504 | -90.28398 | D | 203.31 |
| TRC0803_7 | 35.48047 | -90.35757 | C | 370.14 |
| TRC0803_8 | 35.51862 | -90.41266 | D | 238.55 |
| TRC0803_9 | 35.59755 | -90.26931 | D | 246.64 |
| TRC0803_10 | 35.59754 | -90.21449 | D | 231.62 |
| TRC0803_11 | 35.84046 | -90.75316 | D | 264.05 |
| TRC0803_12 | 35.82309 | -90.5006 | D | 236.37 |
| TRC0803_13 | 35.82073 | -90.43327 | D | 239.16 |
| TRC0803_14 | 36.05171 | -90.36039 | D | 220.66 |
| TRC0803_15 | 36.39091 | -90.39922 | D | 230.75 |
| TRC0803_16 | 36.45966 | -90.35708 | D | 199.81 |
| TRC1603_1 | 36.398583 | -90.388175 | D | 235.98 |
| TRC1603_2 | 36.118611 | -90.313083 | D | 270.86 |
| TRC1603_3 | 36.017175 | -90.799475 | D | 261.76 |
| TRC1603_4 | 35.761622 | -90.594256 | D | 243.82 |
| TRC1603_5 | 35.885581 | -90.335186 | D | 265.74 |
| TRC1603_6 | 35.8525 | -90.147089 | D | 245.75 |
| TRC1603_7 | 35.704214 | -90.217497 | D | 264.29 |
| TRC1603_8 | 35.567572 | -91.155928 | D | 269.25 |
| TRC1603_9 | 35.565781 | -90.730197 | D | 296.47 |
| TRC1603_10 | 35.52005 | -90.435811 | D | 256.02 |
| TRC1603_11 | 35.188317 | -90.789519 | D | 242.70 |
| TRC1603_12 | 35.258642 | -90.422603 | D | 277.99 |
| TRC1603_13 | 34.986725 | -90.911181 | D | 298.55 |
| TRC1603_14 | 35.015908 | -90.403436 | D | 302.66 |
| TRC1603_15 | 34.711003 | -90.943864 | D | 270.03 |
| TRC1901_1 | 35.01236 | -90.62815 | D | 223.20 |
| TRC1901_2 | 34.8326 | -90.60298 | D | 214.99 |
| TRC1901_3 | 34.70548 | -90.95934 | D | 224.26 |
| TRC1901_4 | 34.50562 | -90.85035 | D | 222.42 |
| TRC1901_5 | 34.503 | -90.60545 | D | 211.96 |
| TRC1901_6 | 35.20006 | -91.80905 | B | 1119.57 |
| TRC1901_7 | 34.80495 | -91.88576 | D | 284.71 |
| TRC1901_8 | 34.4113 | -91.89755 | D | 230.14 |
| TRC1901_9 | 35.36044 | -91.49505 | D | 221.33 |
| TRC1901_10 | 34.90926 | -91.19669 | D | 284.94 |
| TRC1901_11 | 34.57475 | -91.14614 | D | 208.85 |
| TRC1901_12 | 34.45413 | -91.32131 | D | 240.55 |
| TRC1901_13 | 36.17804 | -91.73953 | C | 717.82 |
| TRC1901_14 | 36.31981 | -90.91261 | C | 623.27 |
| TRC1901_15 | 36.18635 | -90.33812 | D | 212.71 |
| TRC1901_16 | 35.86319 | -89.83975 | E | 159.37 |
| TRC1901_17 | 35.79525 | -90.98321 | D | 239.60 |
| TRC1901_18 | 35.49315 | -91.00196 | D | 248.52 |
| TRC1901_19 | 35.27009 | -91.23689 | D | 231.73 |
| TRC1901_20 | 35.35866 | -90.75855 | D | 249.40 |

## Table 18. Acceleration Coefficients Based on AASHTO LRFD Bridge Design Specifications, 9th Edition, or AASHTO Guide Specifications for LRFD Seismic Bridge Design

| Project | BC Boundary Hazard Values | | | Site Factors Factor | | | AASHTO Hazard Values | | | AASHTO Hazard Values (Map) | | |
|---|---|---|---|---|---|---|---|---|---|---|---|---|
| | PGA | SA0.2s | SA1.0s | Fpga | Fa | Fv | PGA | SA0.2s | SA1.0s | PGA | SA0.2s | SA1.0s |
| TRC0803_1 | 0.544 | 0.910 | 0.243 | 1.000 | 1.136 | 1.913 | 0.544 | 1.034 | 0.466 | 0.545 | 1.038 | 0.449 |
| TRC0803_2 | 0.408 | 0.704 | 0.188 | 1.092 | 1.237 | 2.048 | 0.446 | 0.871 | 0.385 | 0.465 | 0.880 | 0.442 |
| TRC0803_3 | 0.664 | 1.119 | 0.281 | 1.000 | 1.052 | 1.837 | 0.664 | 1.178 | 0.517 | 0.726 | 1.212 | 0.553 |
| TRC0803_4 | 0.897 | 1.455 | 0.378 | 1.000 | 1.000 | 1.644 | 0.897 | 1.455 | 0.622 | 0.873 | 1.478 | 0.584 |
| TRC0803_5 | 0.433 | 0.763 | 0.200 | 1.067 | 1.195 | 1.999 | 0.462 | 0.912 | 0.400 | 0.488 | 0.912 | 0.453 |
| TRC0803_6 | 0.732 | 1.209 | 0.301 | 1.000 | 1.016 | 1.798 | 0.732 | 1.229 | 0.541 | 0.767 | 1.276 | 0.564 |
| TRC0803_7 | 0.928 | 1.533 | 0.393 | 1.000 | 1.000 | 1.407 | 0.928 | 1.533 | 0.553 | 0.875 | 1.504 | 0.578 |
| TRC0803_8 | 1.002 | 1.723 | 0.433 | 1.000 | 1.000 | 1.567 | 1.002 | 1.723 | 0.678 | 0.899 | 1.620 | 0.582 |
| TRC0803_9 | 1.001 | 1.730 | 0.439 | 1.000 | 1.000 | 1.561 | 1.001 | 1.730 | 0.685 | 0.967 | 1.687 | 0.639 |
| TRC0803_10 | 0.940 | 1.576 | 0.404 | 1.000 | 1.000 | 1.596 | 0.940 | 1.576 | 0.645 | 0.967 | 1.656 | 0.656 |
| TRC0803_11 | 0.383 | 0.643 | 0.179 | 1.117 | 1.285 | 2.083 | 0.428 | 0.827 | 0.373 | 0.439 | 0.840 | 0.394 |
| TRC0803_12 | 0.566 | 0.927 | 0.244 | 1.000 | 1.129 | 1.912 | 0.566 | 1.047 | 0.466 | 0.583 | 1.047 | 0.486 |
| TRC0803_13 | 0.623 | 1.031 | 0.267 | 1.000 | 1.088 | 1.867 | 0.623 | 1.121 | 0.498 | 0.649 | 1.151 | 0.519 |
| TRC0803_14 | 0.490 | 0.831 | 0.221 | 1.010 | 1.168 | 1.958 | 0.495 | 0.970 | 0.433 | 0.523 | 0.978 | 0.467 |
| TRC0803_15 | 0.394 | 0.665 | 0.183 | 1.106 | 1.268 | 2.069 | 0.436 | 0.843 | 0.378 | 0.432 | 0.845 | 0.368 |
| TRC0803_16 | 0.411 | 0.705 | 0.188 | 1.089 | 1.236 | 2.050 | 0.447 | 0.872 | 0.385 | 0.440 | 0.864 | 0.373 |
| TRC1603_1 | 0.396 | 0.672 | 0.184 | 1.104 | 1.262 | 2.064 | 0.438 | 0.849 | 0.380 | 0.434 | 0.849 | 0.370 |
| TRC1603_2 | 0.490 | 0.833 | 0.222 | 1.010 | 1.167 | 1.956 | 0.495 | 0.972 | 0.434 | 0.513 | 0.975 | 0.465 |
| TRC1603_3 | 0.322 | 0.572 | 0.159 | 1.178 | 1.342 | 2.163 | 0.379 | 0.768 | 0.345 | 0.371 | 0.756 | 0.335 |
| TRC1603_4 | 0.538 | 0.892 | 0.234 | 1.000 | 1.143 | 1.931 | 0.538 | 1.019 | 0.453 | 0.560 | 1.025 | 0.470 |
| TRC1603_5 | 0.639 | 1.075 | 0.276 | 1.000 | 1.070 | 1.848 | 0.639 | 1.150 | 0.510 | 0.682 | 1.202 | 0.544 |
| TRC1603_6 | 0.968 | 1.657 | 0.421 | 1.000 | 1.000 | 1.579 | 0.968 | 1.657 | 0.665 | 0.900 | 1.604 | 0.671 |
| TRC1603_7 | 1.059 | 1.860 | 0.488 | 1.000 | 1.000 | 1.512 | 1.059 | 1.860 | 0.737 | 0.979 | 1.761 | 0.665 |
| TRC1603_8 | 0.268 | 0.480 | 0.140 | 1.264 | 1.416 | 2.241 | 0.339 | 0.680 | 0.313 | 0.340 | 0.683 | 0.318 |
| TRC1603_9 | 0.545 | 0.905 | 0.240 | 1.000 | 1.138 | 1.920 | 0.545 | 1.030 | 0.461 | 0.550 | 1.030 | 0.455 |
| TRC1603_10 | 0.986 | 1.695 | 0.427 | 1.000 | 1.000 | 1.573 | 0.986 | 1.695 | 0.671 | 0.878 | 1.600 | 0.573 |
| TRC1603_11 | 0.364 | 0.621 | 0.175 | 1.136 | 1.304 | 2.101 | 0.414 | 0.809 | 0.367 | 0.416 | 0.809 | 0.376 |
| TRC1603_12 | 0.534 | 0.893 | 0.239 | 1.000 | 1.143 | 1.922 | 0.534 | 1.021 | 0.459 | 0.551 | 1.026 | 0.460 |
| TRC1603_13 | 0.256 | 0.452 | 0.135 | 1.288 | 1.439 | 2.261 | 0.330 | 0.650 | 0.305 | 0.329 | 0.652 | 0.311 |
| TRC1603_14 | 0.338 | 0.590 | 0.167 | 1.162 | 1.328 | 2.131 | 0.393 | 0.783 | 0.356 | 0.388 | 0.781 | 0.366 |
| TRC1603_15 | 0.194 | 0.377 | 0.119 | 1.412 | 1.499 | 2.325 | 0.274 | 0.565 | 0.276 | 0.275 | 0.564 | 0.274 |
| TRC1901_1 | 0.312 | 0.559 | 0.161 | 1.188 | 1.353 | 2.157 | 0.371 | 0.756 | 0.347 | 0.372 | 0.749 | 0.348 |
| TRC1901_2 | 0.252 | 0.448 | 0.136 | 1.295 | 1.441 | 2.255 | 0.327 | 0.646 | 0.307 | 0.321 | 0.644 | 0.308 |
| TRC1901_3 | 0.192 | 0.374 | 0.118 | 1.417 | 1.501 | 2.328 | 0.271 | 0.561 | 0.275 | 0.274 | 0.561 | 0.273 |
| TRC1901_4 | 0.174 | 0.336 | 0.111 | 1.453 | 1.531 | 2.356 | 0.252 | 0.515 | 0.262 | 0.251 | 0.515 | 0.257 |
| TRC1901_5 | 0.179 | 0.347 | 0.112 | 1.442 | 1.523 | 2.351 | 0.258 | 0.528 | 0.264 | 0.258 | 0.526 | 0.262 |
| TRC1901_6 | 0.206 | 0.378 | 0.107 | 1.000 | 1.000 | 1.000 | 0.206 | 0.378 | 0.107 | 0.216 | 0.387 | 0.158 |
| TRC1901_7 | 0.160 | 0.288 | 0.093 | 1.480 | 1.569 | 2.400 | 0.237 | 0.453 | 0.224 | 0.228 | 0.445 | 0.196 |
| TRC1901_8 | 0.113 | 0.226 | 0.080 | 1.574 | 1.600 | 2.400 | 0.178 | 0.361 | 0.193 | 0.180 | 0.360 | 0.199 |
| TRC1901_9 | 0.204 | 0.382 | 0.116 | 1.392 | 1.494 | 2.337 | 0.284 | 0.571 | 0.270 | 0.276 | 0.559 | 0.244 |
| TRC1901_10 | 0.196 | 0.375 | 0.116 | 1.408 | 1.500 | 2.336 | 0.276 | 0.562 | 0.271 | 0.278 | 0.565 | 0.271 |
| TRC1901_11 | 0.168 | 0.323 | 0.108 | 1.463 | 1.542 | 2.369 | 0.246 | 0.498 | 0.255 | 0.245 | 0.498 | 0.252 |
| TRC1901_12 | 0.142 | 0.276 | 0.097 | 1.516 | 1.579 | 2.400 | 0.215 | 0.436 | 0.232 | 0.216 | 0.436 | 0.233 |
| TRC1901_13 | 0.176 | 0.341 | 0.109 | 1.200 | 1.200 | 1.691 | 0.211 | 0.409 | 0.184 | 0.213 | 0.409 | 0.180 |
| TRC1901_14 | 0.277 | 0.512 | 0.144 | 1.123 | 1.195 | 1.656 | 0.311 | 0.612 | 0.238 | 0.306 | 0.613 | 0.244 |
| TRC1901_15 | 0.436 | 0.768 | 0.205 | 1.064 | 1.193 | 1.990 | 0.464 | 0.916 | 0.408 | 0.474 | 0.916 | 0.432 |
| TRC1901_16 | 0.918 | 1.468 | 0.381 | 0.900 | 0.900 | 2.478 | 0.826 | 1.321 | 0.943 | 0.849 | 1.349 | 0.879 |
| TRC1901_17 | 0.303 | 0.549 | 0.155 | 1.197 | 1.361 | 2.180 | 0.363 | 0.747 | 0.338 | 0.368 | 0.748 | 0.341 |
| TRC1901_18 | 0.333 | 0.582 | 0.164 | 1.167 | 1.335 | 2.144 | 0.389 | 0.776 | 0.352 | 0.393 | 0.779 | 0.359 |
| TRC1901_19 | 0.237 | 0.419 | 0.125 | 1.325 | 1.465 | 2.300 | 0.315 | 0.613 | 0.287 | 0.312 | 0.616 | 0.291 |
| TRC1901_20 | 0.479 | 0.829 | 0.223 | 1.021 | 1.168 | 1.954 | 0.489 | 0.969 | 0.436 | 0.498 | 0.960 | 0.429 |

**Table 19. Acceleration Coefficients Based on the Site-Specific Studies at All 51 Sites**

| Project | Site-Specific Values | | | Site-Specific Values (GIS-Maps) | | |
|---|---|---|---|---|---|---|
| | PGA | SA0.2s | SA1.0s | PGA | SA0.2s | SA1.0s |
| TRC0803_ | 0.260 | 0.615 | 0.408 | 0.260 | 0.615 | 0.414 |
| TRC0803_ | 0.210 | 0.412 | 0.383 | 0.209 | 0.412 | 0.401 |
| TRC0803_ | 0.261 | 0.494 | 0.507 | 0.253 | 0.484 | 0.510 |
| TRC0803_ | 0.265 | 0.413 | 0.640 | 0.386 | 0.666 | 0.617 |
| TRC0803_ | 0.206 | 0.408 | 0.457 | 0.208 | 0.409 | 0.427 |
| TRC0803_ | 0.243 | 0.472 | 0.497 | 0.255 | 0.474 | 0.534 |
| TRC0803_ | 0.745 | 1.790 | 0.537 | 0.586 | 1.604 | 0.601 |
| TRC0803_ | 0.266 | 0.403 | 0.637 | 0.340 | 0.440 | 0.685 |
| TRC0803_ | 0.709 | 1.530 | 1.050 | 0.664 | 1.509 | 0.929 |
| TRC0803_ | 0.344 | 0.613 | 0.821 | 0.389 | 0.634 | 0.875 |
| TRC0803_ | 0.244 | 0.533 | 0.324 | 0.239 | 0.534 | 0.335 |
| TRC0803_ | 0.272 | 0.541 | 0.516 | 0.275 | 0.544 | 0.497 |
| TRC0803_ | 0.315 | 0.679 | 0.534 | 0.314 | 0.677 | 0.553 |
| TRC0803_ | 0.229 | 0.406 | 0.503 | 0.239 | 0.412 | 0.475 |
| TRC0803_ | 0.310 | 0.618 | 0.436 | 0.284 | 0.596 | 0.424 |
| TRC0803_ | 0.225 | 0.471 | 0.435 | 0.226 | 0.469 | 0.437 |
| TRC1603_ | 0.245 | 0.471 | 0.428 | 0.265 | 0.491 | 0.428 |
| TRC1603_ | 0.415 | 1.100 | 0.399 | 0.386 | 1.084 | 0.417 |
| TRC1603_ | 0.293 | 0.766 | 0.299 | 0.289 | 0.766 | 0.294 |
| TRC1603_ | 0.347 | 0.873 | 0.426 | 0.341 | 0.870 | 0.435 |
| TRC1603_ | 0.304 | 0.607 | 0.552 | 0.313 | 0.611 | 0.579 |
| TRC1603_ | 0.683 | 1.600 | 0.834 | 0.672 | 1.596 | 0.794 |
| TRC1603_ | 0.428 | 0.761 | 0.873 | 0.439 | 0.766 | 0.873 |
| TRC1603_ | 0.188 | 0.454 | 0.263 | 0.186 | 0.453 | 0.277 |
| TRC1603_ | 0.321 | 0.793 | 0.418 | 0.319 | 0.793 | 0.422 |
| TRC1603_ | 0.386 | 0.715 | 0.826 | 0.344 | 0.691 | 0.698 |
| TRC1603_ | 0.239 | 0.553 | 0.371 | 0.238 | 0.552 | 0.363 |
| TRC1603_ | 0.358 | 0.941 | 0.410 | 0.351 | 0.939 | 0.409 |
| TRC1603_ | 0.229 | 0.471 | 0.208 | 0.228 | 0.471 | 0.221 |
| TRC1603_ | 0.287 | 0.732 | 0.243 | 0.284 | 0.731 | 0.265 |
| TRC1603_ | 0.201 | 0.439 | 0.198 | 0.192 | 0.428 | 0.207 |
| TRC1901_ | 0.156 | 0.312 | 0.324 | 0.158 | 0.312 | 0.317 |
| TRC1901_ | 0.116 | 0.158 | 0.302 | 0.117 | 0.158 | 0.292 |
| TRC1901_ | 0.177 | 0.360 | 0.213 | 0.185 | 0.371 | 0.207 |
| TRC1901_ | 0.106 | 0.244 | 0.214 | 0.107 | 0.244 | 0.214 |
| TRC1901_ | 0.135 | 0.259 | 0.219 | 0.133 | 0.259 | 0.219 |
| TRC1901_ | 0.161 | 0.357 | 0.106 | 0.161 | 0.357 | 0.114 |
| TRC1901_ | 0.131 | 0.249 | 0.171 | 0.131 | 0.249 | 0.168 |
| TRC1901_ | 0.108 | 0.239 | 0.157 | 0.108 | 0.239 | 0.157 |
| TRC1901_ | 0.154 | 0.286 | 0.302 | 0.154 | 0.286 | 0.290 |
| TRC1901_ | 0.146 | 0.256 | 0.197 | 0.147 | 0.257 | 0.202 |
| TRC1901_ | 0.111 | 0.236 | 0.218 | 0.112 | 0.236 | 0.213 |
| TRC1901_ | 0.099 | 0.176 | 0.186 | 0.098 | 0.176 | 0.187 |
| TRC1901_ | 0.240 | 0.419 | 0.110 | 0.240 | 0.419 | 0.108 |
| TRC1901_ | 0.333 | 0.834 | 0.146 | 0.333 | 0.834 | 0.150 |
| TRC1901_ | 0.179 | 0.403 | 0.348 | 0.196 | 0.404 | 0.366 |
| TRC1901_ | 0.214 | 0.315 | 0.424 | 0.222 | 0.319 | 0.450 |
| TRC1901_ | 0.236 | 0.579 | 0.374 | 0.233 | 0.579 | 0.359 |
| TRC1901_ | 0.169 | 0.359 | 0.344 | 0.169 | 0.360 | 0.341 |
| TRC1901_ | 0.146 | 0.320 | 0.315 | 0.146 | 0.320 | 0.310 |
| TRC1901_ | 0.223 | 0.431 | 0.431 | 0.225 | 0.432 | 0.424 |

# CHAPTER 5. GROUND SURFACE CONTOUR MAPS

## 5.1 BACKGROUND

The 51 sites or the sample data points are used to cover the entire study region. Using ESRI ArcGIS (http://www.arcgis.com), one can apply predictive spatial analysis techniques to interpolate between available data points and create contour maps. A variety of interpolation approaches are available in ArcGIS, and they will almost always generate different outputs. Therefore, the selection of the interpolation method is of great importance. The appropriate method can be selected based on the distribution of the sample data points and the phenomenon that is being studied.

Interpolation methods can be categorized into two groups: deterministic and geostatistical approaches. In the deterministic approach, contour maps are generated based on mathematical formulas and a set of measured data points. Therefore, deterministic methods may yield significantly different outputs depending on the selected methodology and the number of data points used to make predictions. Geostatistical methods are based on statistics and designed for advanced predictions.

One deterministic approach available in ArcGIS is the Inverse Distance Weighting (IDW) method. This method is used when the observed data points densely populate the entire study region. In the IDW method, unknown cell values are predicted based on the linear-weighted combination of a set of nearby sample data points. The weights are assigned according to the distance of input sample data points from the output cell. Data points with a large distance from the unknown cell will be assigned smaller weights than those closer to the unknown cell. Figures 40 and 41 show the two contour maps indicating the percentage change of PGA when the site-specific approach is used instead of the general procedure. Figure 40 is prepared using IDW methods and based on eight nearby data points, while Figure 41 indicates the same map based on four nearby data points. As it can be observed from Figures 40 and 41, the difference between the two maps is more highlighted where limited data points exist. In the top left corner of the contour maps, for instance, the IDW method primarily depends on the selection of the number of nearby data points used to determine the unknown cell values. In some instances when a large number of neighboring data points exist, the method may produce a smooth map that ignores some local changes.

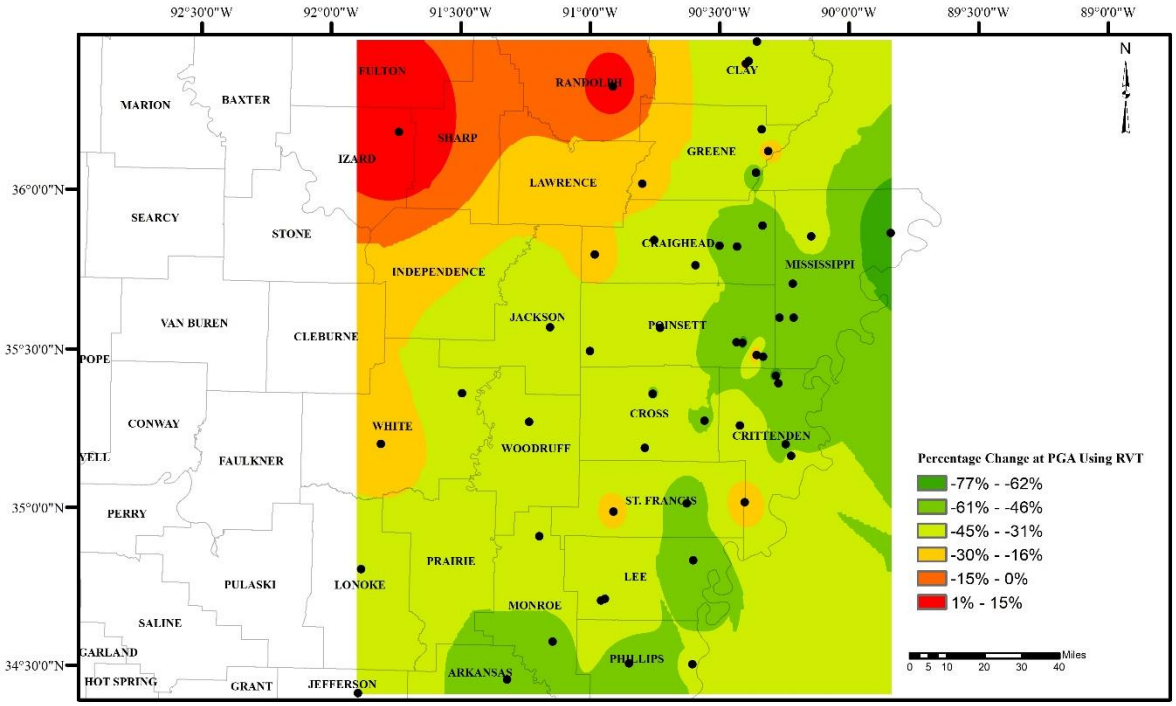


**Figure 40. Percentage Change of PGA When the Site-Specific Approach is Used Instead of the General Procedure for Site Response Analysis. IDW Method Considering Eight Nearby Points is Used to Prepare This Contour Map**

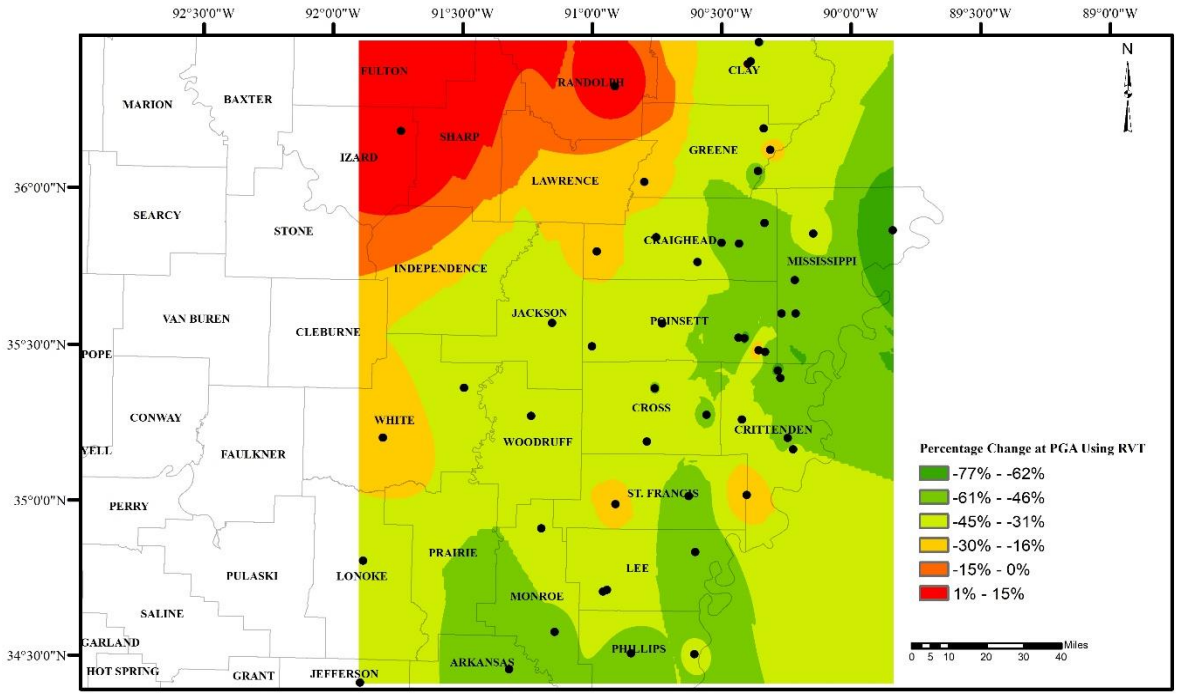


**Figure 41. Percentage Change of PGA When the Site-Specific Approach is Used Instead of the General Procedure for Site Response Analysis. The IDW Method Considering Four Nearby Points is Used to Prepare This Contour Map**

The Spline method is another deterministic approach implemented in ArcGIS. This method uses a mathematical function to minimize the curvature of the output surface contour map, and there are two variations of this approach: Regularized and Tension. Tension Spline would result in a smoother surface. This method predicts ridges and valleys in the data and is suitable for predicting smoothly varying surfaces such as temperature. Figures 42 and 43 show the two contour maps that indicate the percentage change of PGA when the site-specific approach is used instead of the general procedure. Figure 42 is prepared using the Tension variation of the Spline method and is based on eight nearby data points. Figure 43 indicates the same map based on four nearby data points. The level of difference between two maps prepared using the Spline method (Figures 42 and 43) is more than the difference between two maps prepared using the IDW method (Figures 40 and 41). Accordingly, the Spline approach shows a higher sensitivity to the number of nearby points than the IDW method.

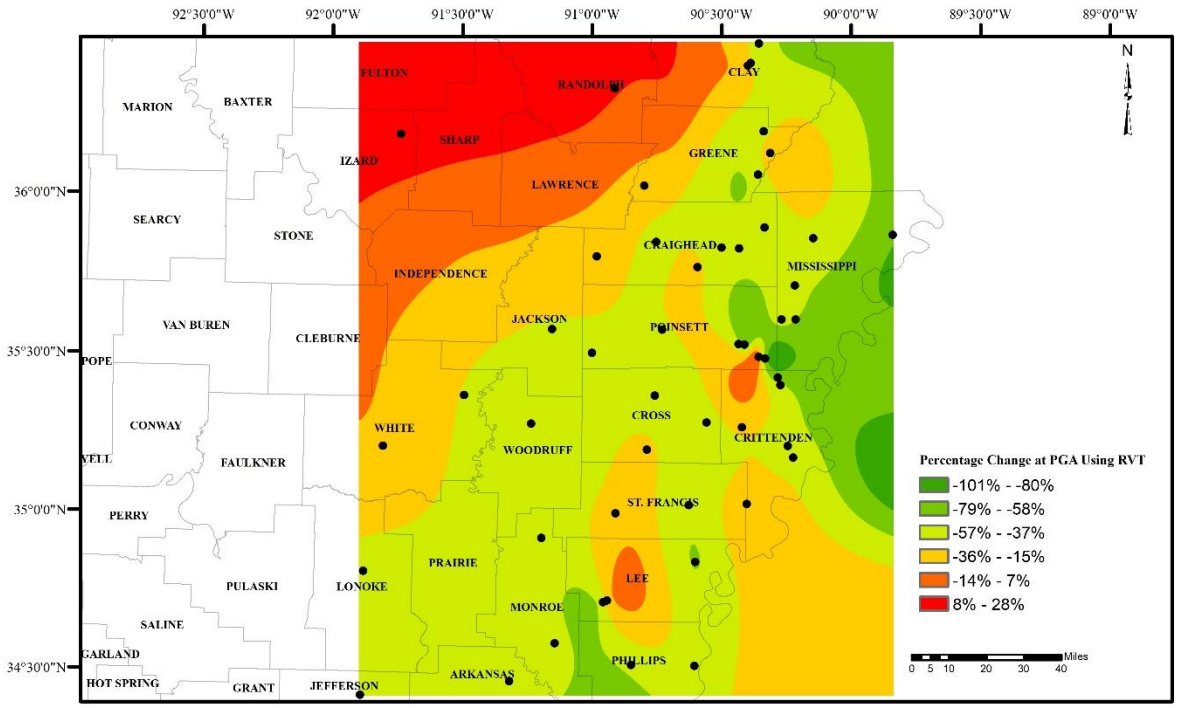


**Figure 42. Percentage Change of PGA When the Site-Specific Approach is Used Instead of the General Procedure for Site Response Analysis. Tension Spline Method Considering Eight Nearby Points is Used to Prepare This Contour Map**

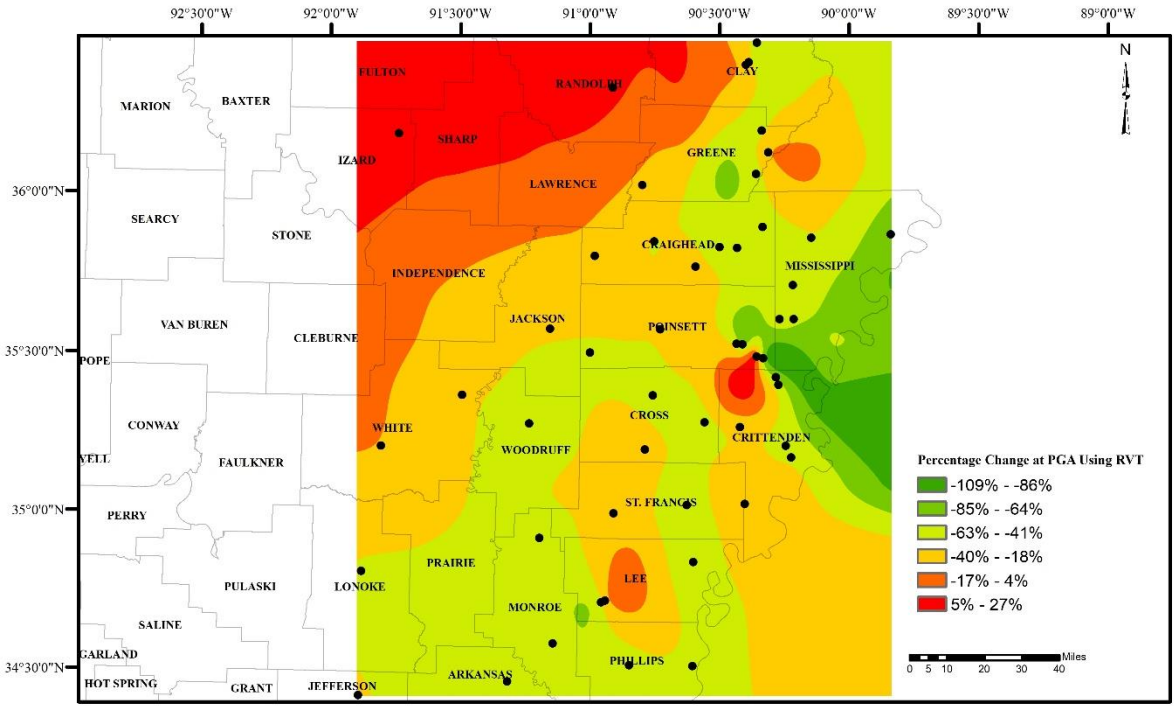


**Figure 43. Percentage Change of PGA When the Site-Specific Approach is Used Instead of the General Procedure for Site Response Analysis. Tension Spline Method Considering Four Nearby Points is Used to Prepare This Contour Map**

Kriging is another methodology for interpolation to prepare contour maps in ArcGIS. The kriging approach is a powerful statistical method that assumes data points to be spatially correlated. Kriging fits a function to a specified number of data points or data points within a certain radius. This approach is most appropriate when spatially correlated distance or directional bias in the data is known. Kriging method is often used for application in soil science and geology. Like the Spline approach, there are two variants to the kriging approach. The options of the kriging approaches are: ordinary kriging and universal kriging. Ordinary kriging assumes no prior trend in the data and is used more often than universal kriging, which considers the overriding trend in the data. Figures 44 to 46 show the contour maps for the percentage change in PGA between two different site response analysis approaches. In these figures, the ordinary kriging approach is applied, considering all points within 10 miles and three semivariogram models, including linear, circular, and spherical. Figure 44 to 46 represent linear, circular, and spherical semivariogram models, respectively. According to these figures, the three semivariogram models do not show significant differences. Figure 44 to 46 are not compatible with observed data points in some cases. For example, for the site located in the northwest corner of the study area, the observed change in PGA is around 15 percent, while the map represents a value between -4 percent to 6 percent. This could be attributed to the selected radius (10 miles) for interpolation. We reduced the radius to 1 mile and

prepared Figure 47 to see how decreasing the radius may affect the result. Reducing the radius to 1 mile alleviated the shortcoming of the larger radius of 10 miles for the data point in the top left corner of the study area. We did not use the universal kriging approach because we are not aware of any prior trend in the data points.

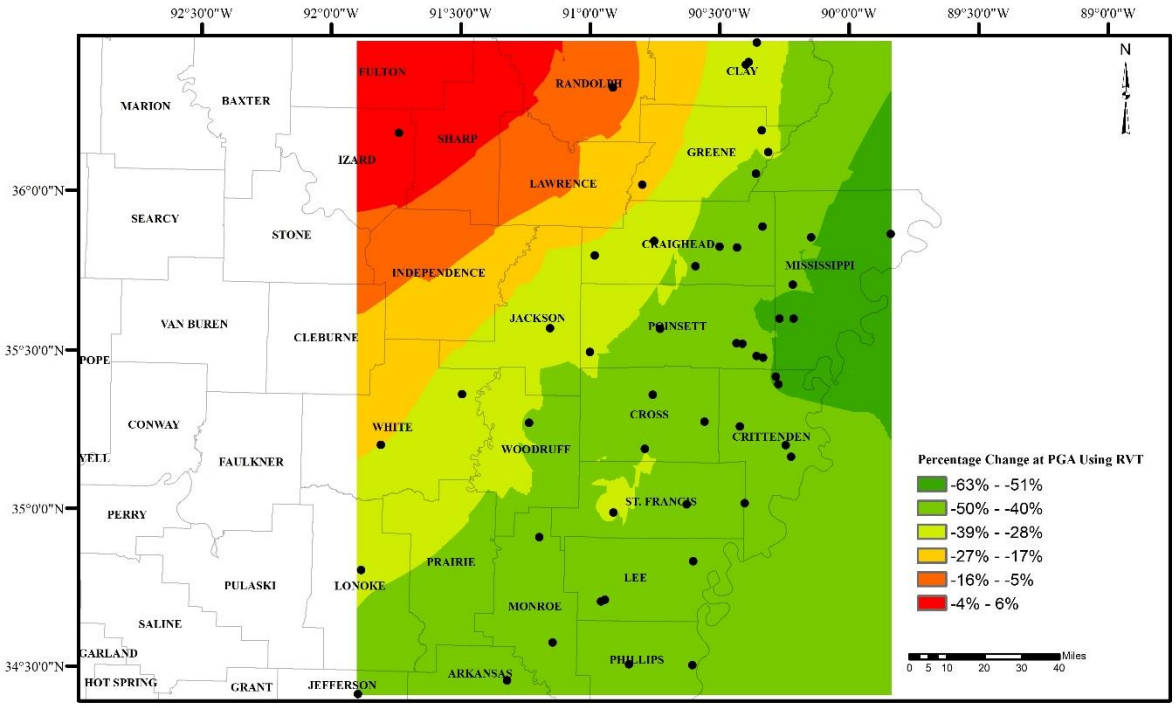


**Figure 44. Percentage Change of PGA When the Site-Specific Approach is Used Instead of the General Procedure for Site Response Analysis. The Ordinary Kriging Method Considering Data Points Within 10 Miles and Linear Semivariogram Model is Used to Prepare This Contour Map**

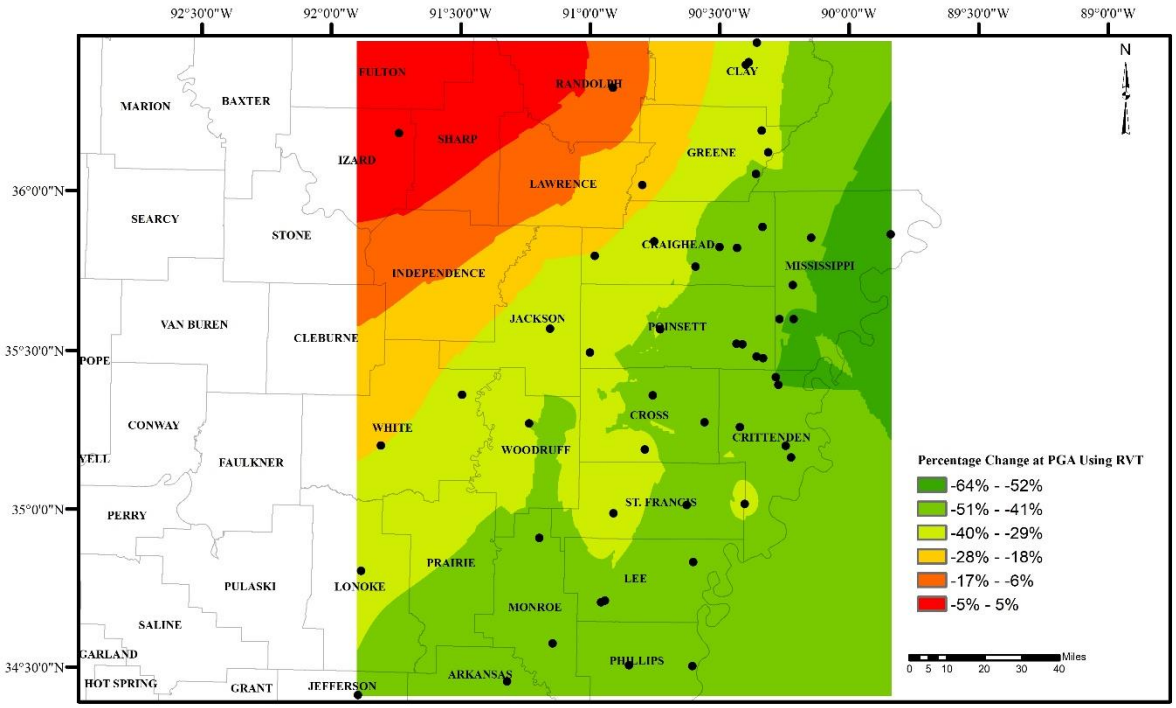


**Figure 45. Percentage Change of PGA When the Site-Specific Approach is Used Instead of the General Procedure for Site Response Analysis. The Ordinary Kriging Method Considering Data Points Within 10 Miles and Circular Semivariogram Model is Used to Prepare This Contour Map**

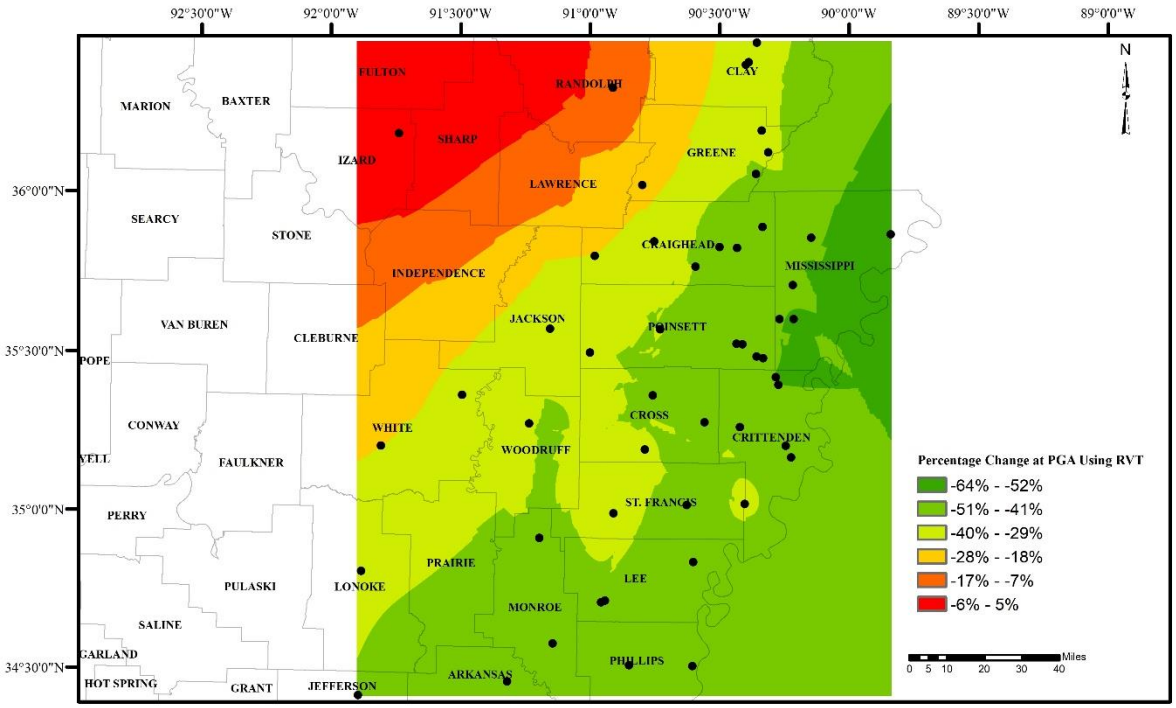


**Figure 46. Percentage Change Of PGA When the Site-Specific Approach Was Used Instead of the General Procedure for Site Response Analysis. The Ordinary Kriging Method Considering Data Points Within 10 Miles and Spherical Semivariogram Model Was Used to Prepare This Contour Map**

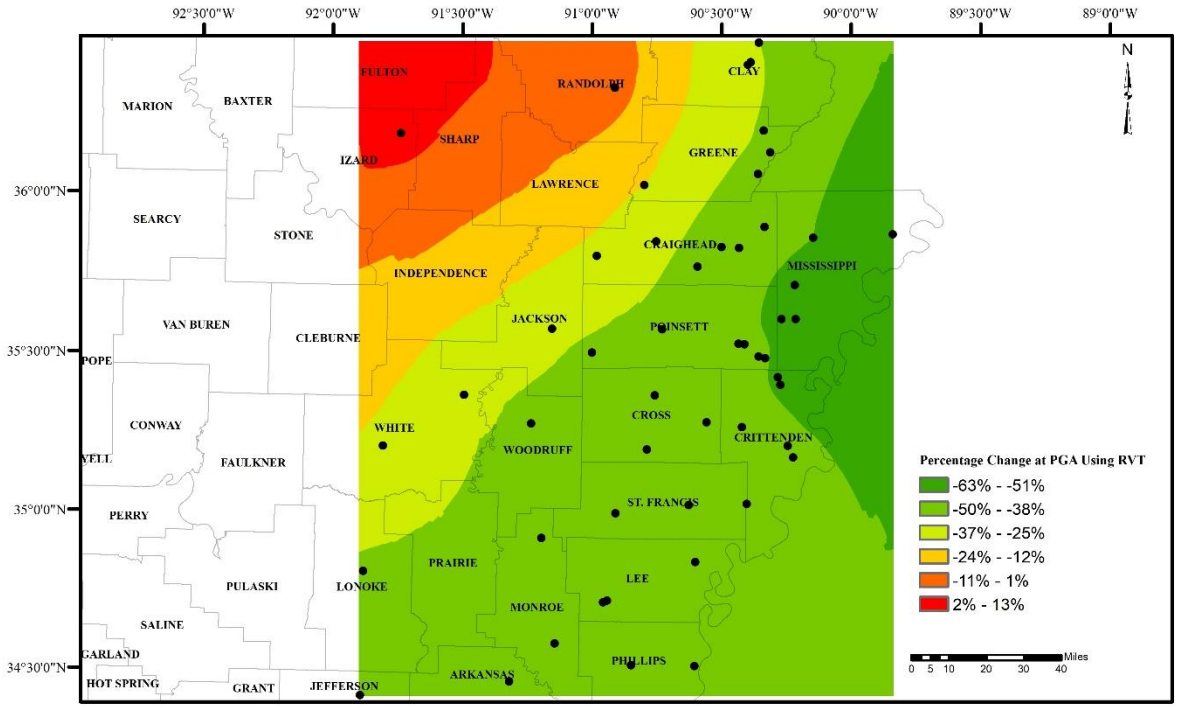


**Figure 47. Percentage Change of PGA When the Site-Specific Approach is Used Instead of the General Procedure for Site Response Analysis. The Ordinary Kriging Method Considering Data Points Within One Mile and Circular Semivariogram Model Was Used to Prepare This Contour Map**

The Natural Neighbor interpolation method is another method implemented within ArcGIS to perform spatial analysis and prepare contour maps. This method has many positive features and can be used for both interpolation and extrapolation. The Natural Neighbor interpolation method is the most suitable for scattered data points. Figure 48 represents the contour map prepared following the Natural Neighbor interpolation method. ArcGIS does not require the user to provide many inputs or select between various options while using this approach. The Natural Neighbor approach did not provide information for cells outside the boundary constructed with the available observed data points. The observed data points are in good agreement with the contour map prepared by this approach.

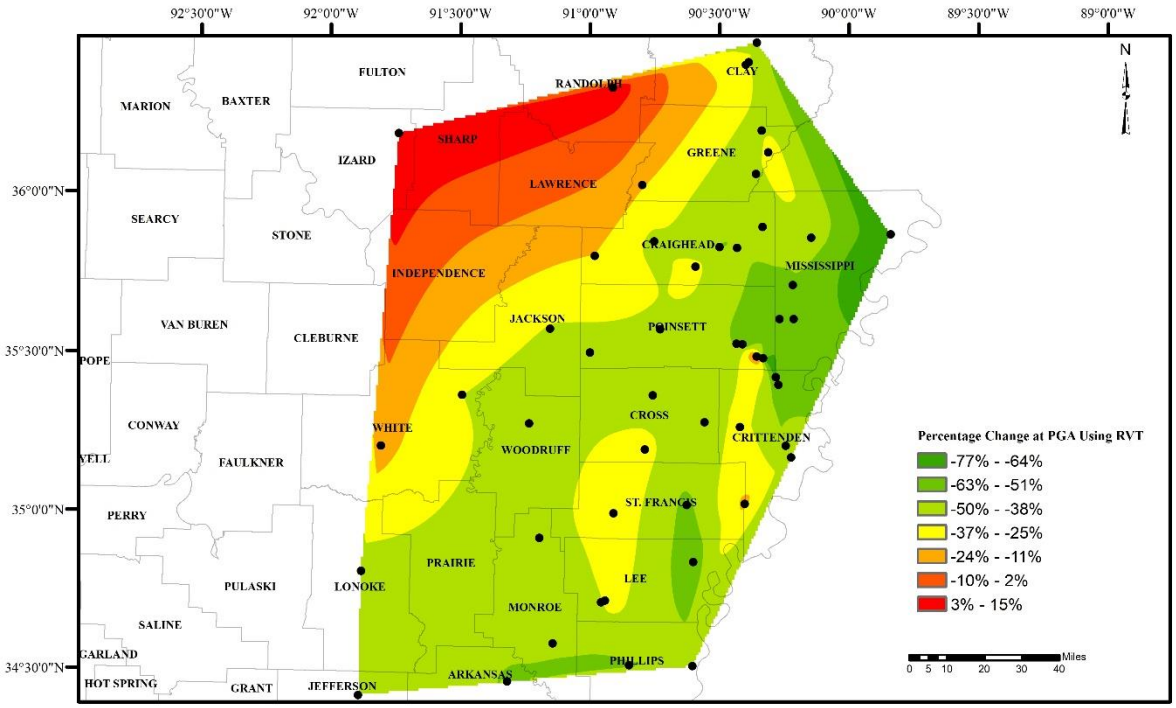


**Figure 48. Percentage Change of PGA When the Site-Specific Approach is Used Instead of the General Procedure for Site Response Analysis. The Natural Neighbor Method Was Used to Prepare This Contour Map**

There is another interpolation method in ArcGIS that is simple. This method is referred to as the Topo to Raster interpolation approach. This is specifically designed to work intelligently with contour inputs. Figure 49 shows the contour map of the percentage change in PGA when the site-specific approach is used instead of the general procedure using the Topo to Raster approach. According to this figure, the Topo to Raster method is in good agreement with the observed data points. The contour map prepared using the Topo to Raster method is as accurate as of the Natural Neighbor approach. In addition, unlike the Natural Neighbor method, the Topo to Raster interpolation predicts reasonable values for unknown cells outside the boundary represented by the observed data points. In the Topo to Raster method, boundaries between different classes are smoother than those of the Natural Neighbor approach.

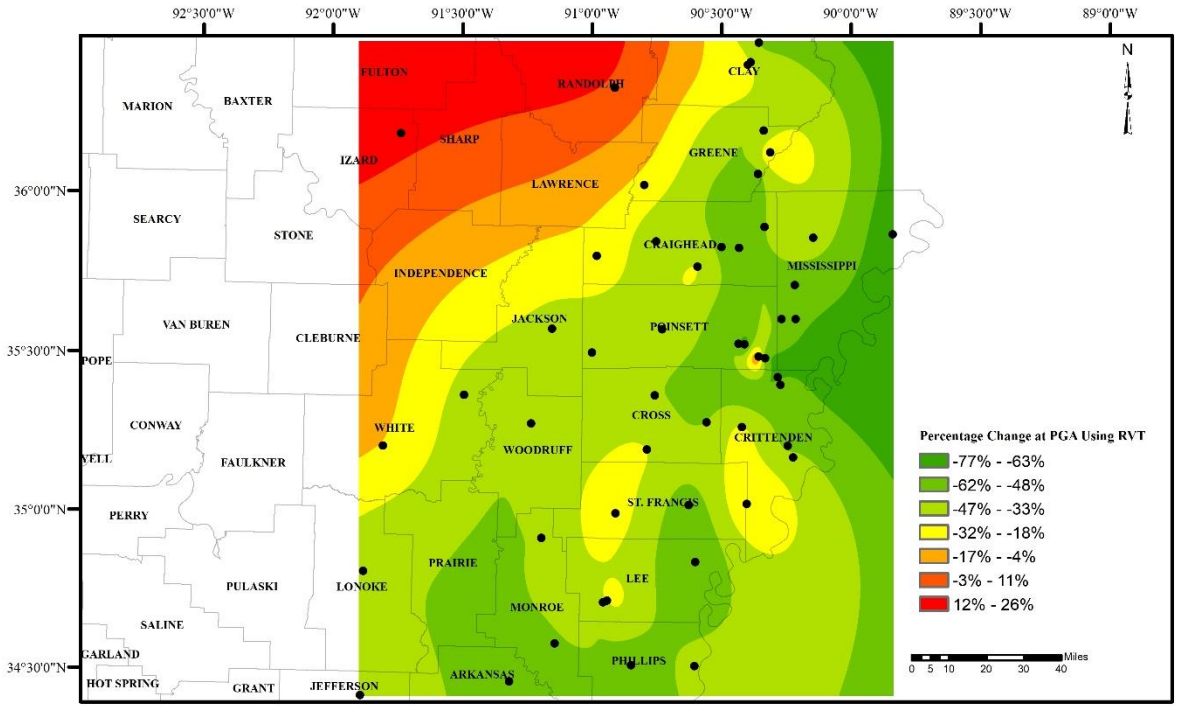


**Figure 49. Percentage Change of PGA When the Site-Specific Approach is Used Instead of the General Procedure for Site Response Analysis. The Topo to Raster Method Was Used to Prepare This Contour Map**

## 5.2 RECOMMENDED CONTOUR MAPS

The Topo to Raster method works well for contour data inputs and outperforms other interpolation methods for this specific application. Consequently, we recommend using the Topo to Raster method to draft final contour maps in this chapter. We cropped contour maps to only show counties of Arkansas with available data points and prepared contour maps for other spectral periods.

The project's goal was to conduct probabilistic seismic hazard analyses incorporating site effects. For this study, two approaches were implemented: (1) SSGMRA using a fully probabilistic approach [hereafter referred to as Method 1], and (2) SSGMRA using an equivalent linear approach [hereafter referred to as Method 2]. Final deliverables are a series of contour maps for three approaches discussed in the previous section: (1) Method 1, (2) Method 2, and (3) the AASHTO LRFD Bridge Design Specifications. All contour maps are cropped to only show counties of Arkansas with available data points and prepared contour maps. The Percent Changes noted in the figures indicate the difference between spectral accelerations estimated using the particular method and accelerations determined using the AASHTO LRFD Bridge Design Specifications method.

The following is a list of recommended maps:

Figure 72. Difference Between Method 2 and the AASHTO LRFD Bridge Design Specifications for SA of 0.2 sec.

Figure 73. Difference Between Method 2 and the AASHTO LRFD Bridge Design Specifications for SA 1.0 of sec.

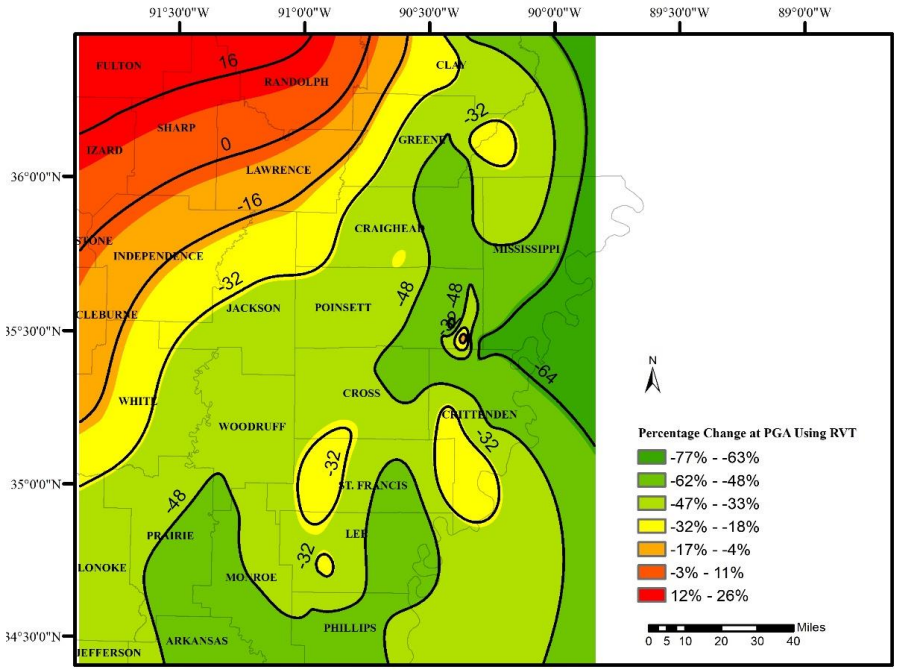


**Figure 50. Percentage Change of PGA Based on Method 1**

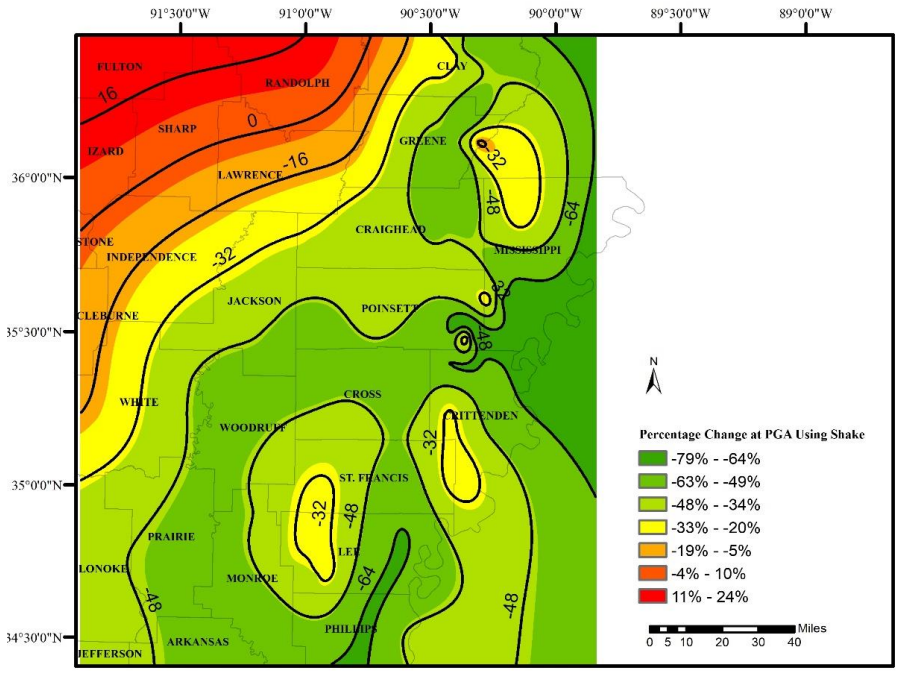


**Figure 51. Percentage Change of PGA Based on Method 2**

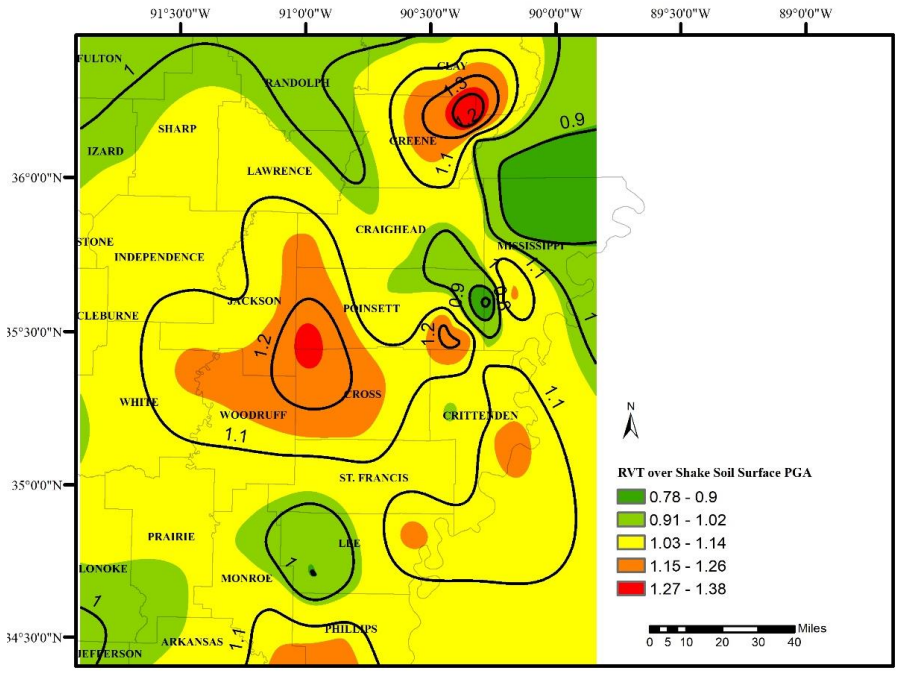


**Figure 52. The ratio of Method 1 Soil Surface PGA to Method 2 Soil Surface PGA**

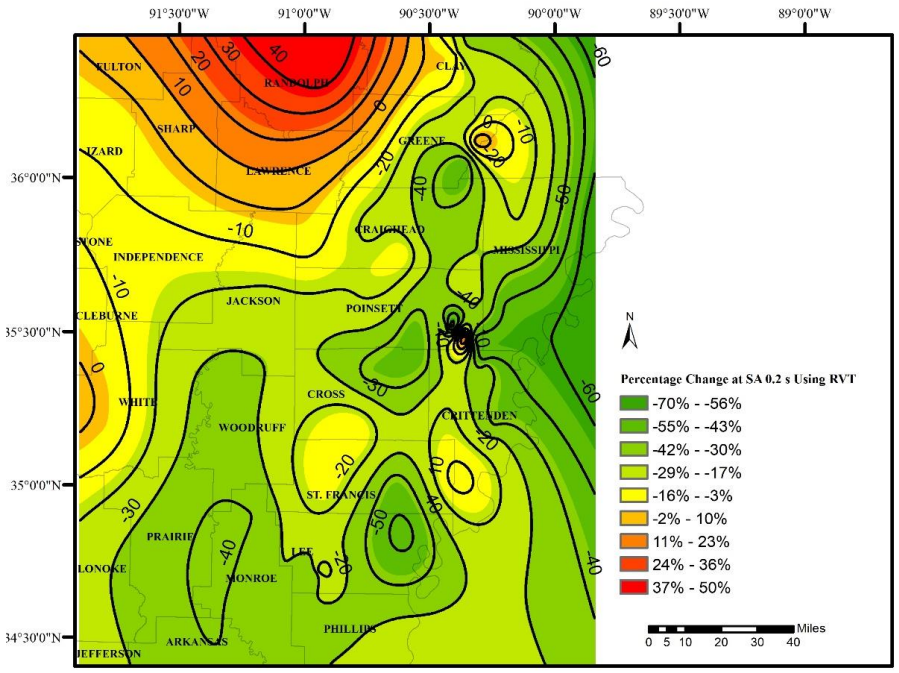


**Figure 53. Percentage Change of SA at 0.2 sec Based on Method 1**

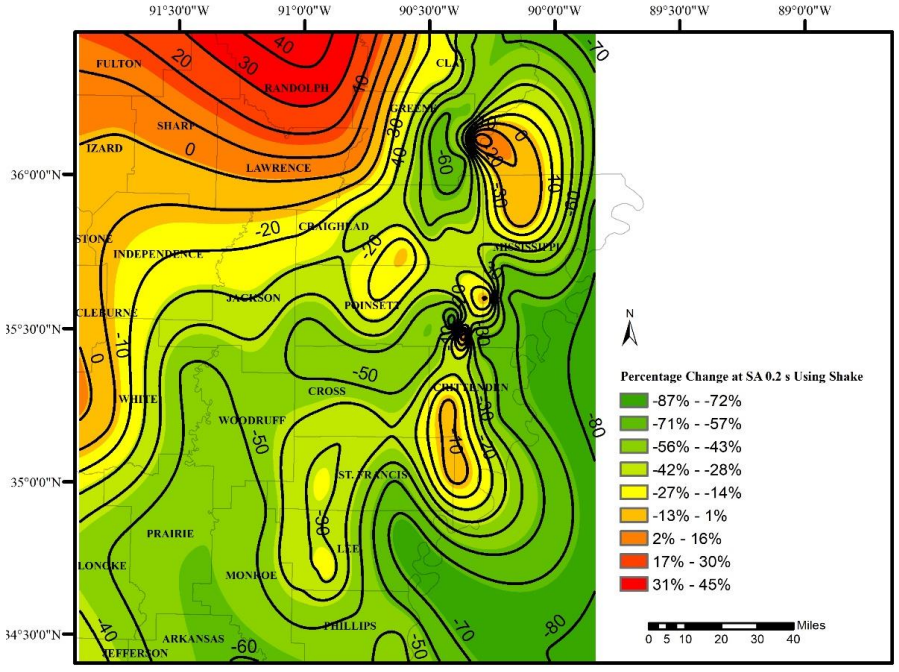


**Figure 54. Percentage Change of SA at 0.2 sec Based on Method 2**

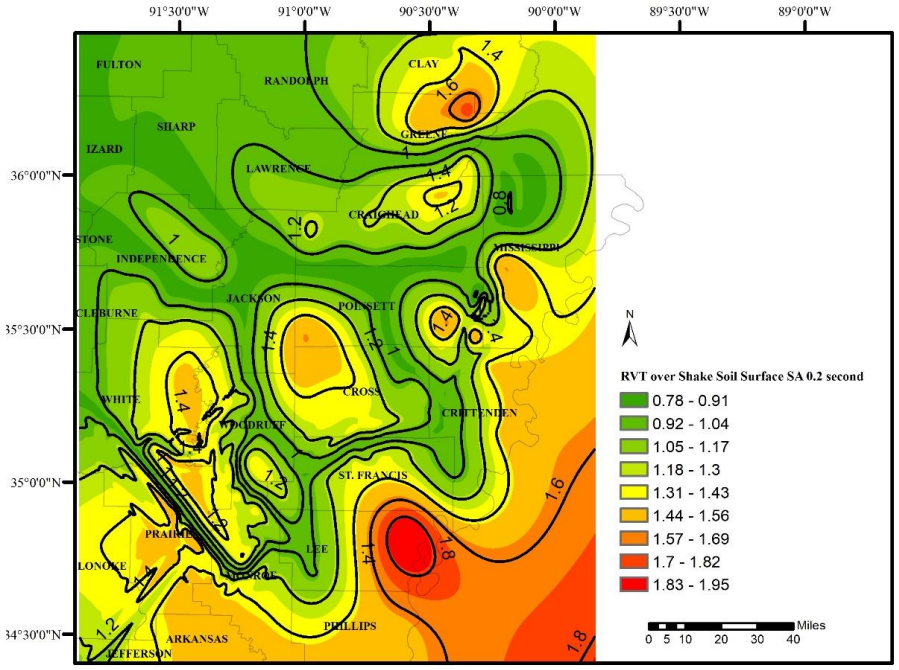


**Figure 55. The Ratio of Method 1 Soil Surface SA 0.2 sec to Method 2 Soil Surface SA 0.2 sec**

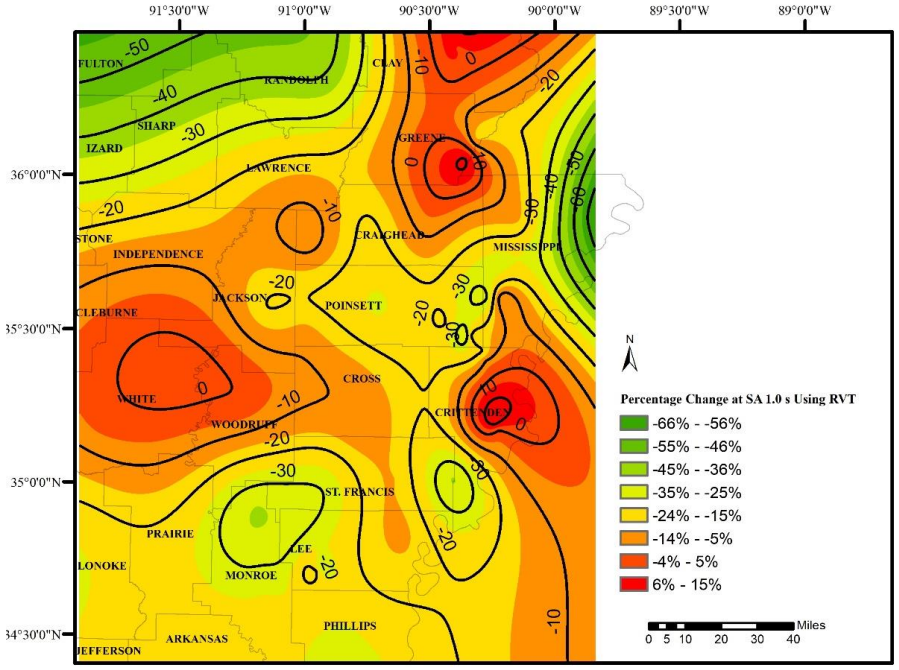


**Figure 56. Percentage Change of SA at 1.0 sec Based on Method 1**

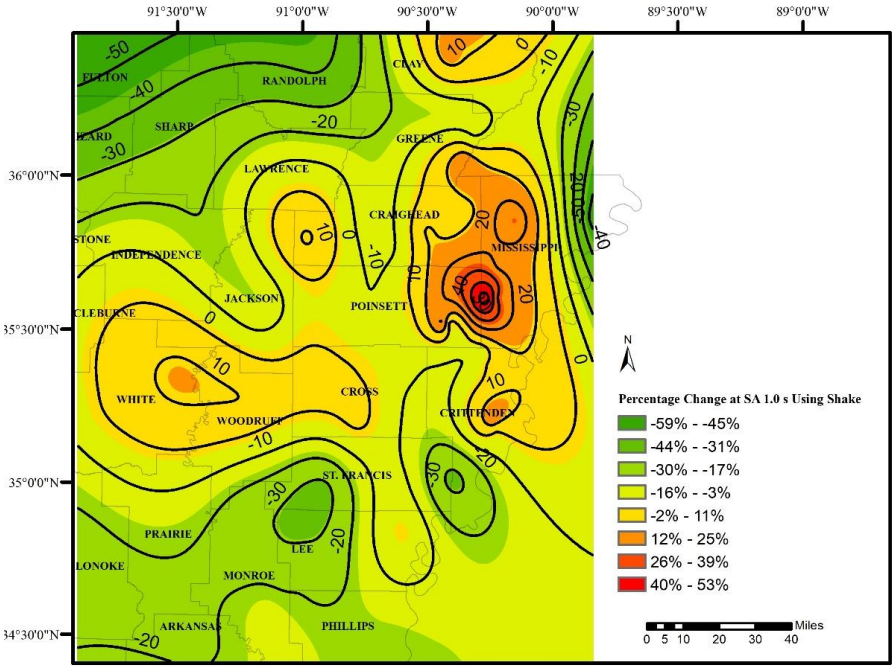


**Figure 57. Percentage Change of SA of 1.0 sec Based on Method 2**

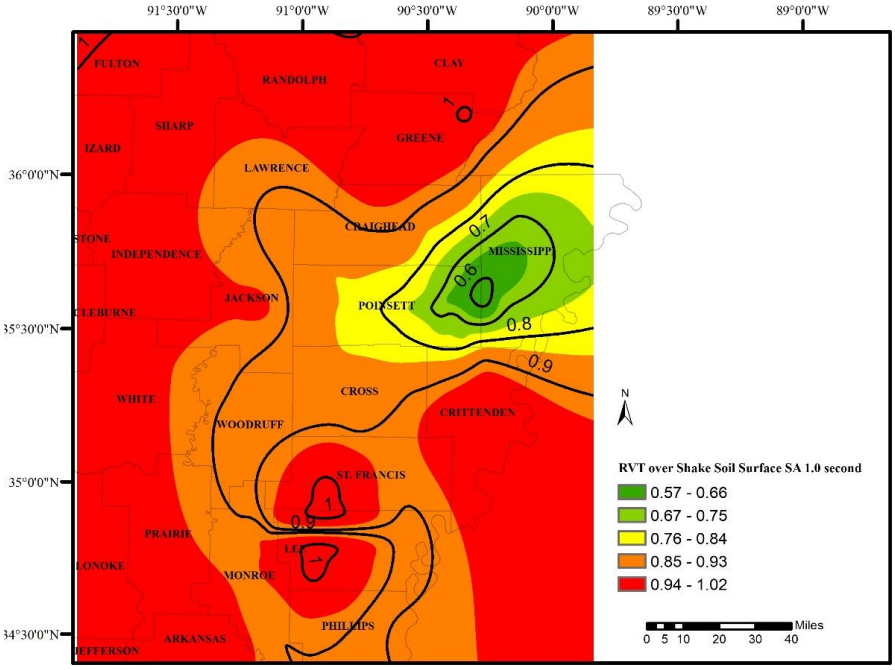


**Figure 58. The Ratio of Method 1 Soil Surface SA at 1.0 sec to Method 2 Soil Surface SA at 1.0 sec**

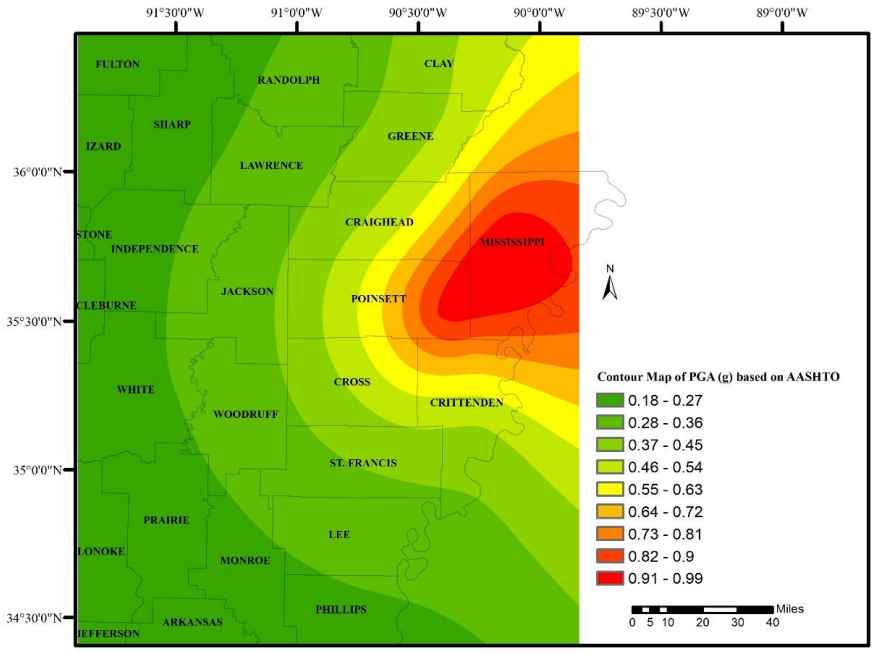


**Figure 59. PGA Contour Map Based on AASHTO LRFD Bridge Design Specifications**

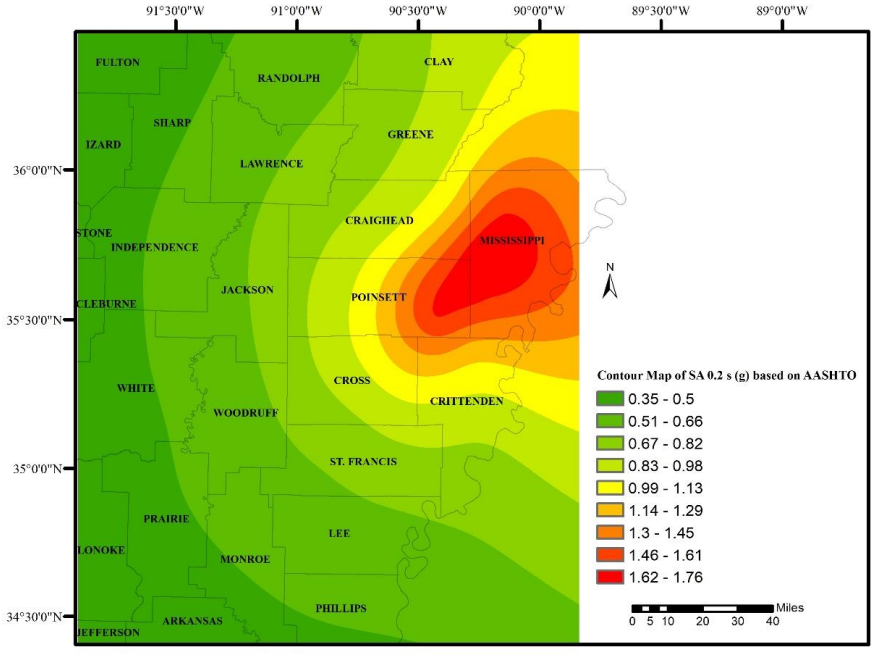


**Figure 60. SA of 0.2 sec Contour Map Based on the AASHTO LRFD Bridge Design Specifications**

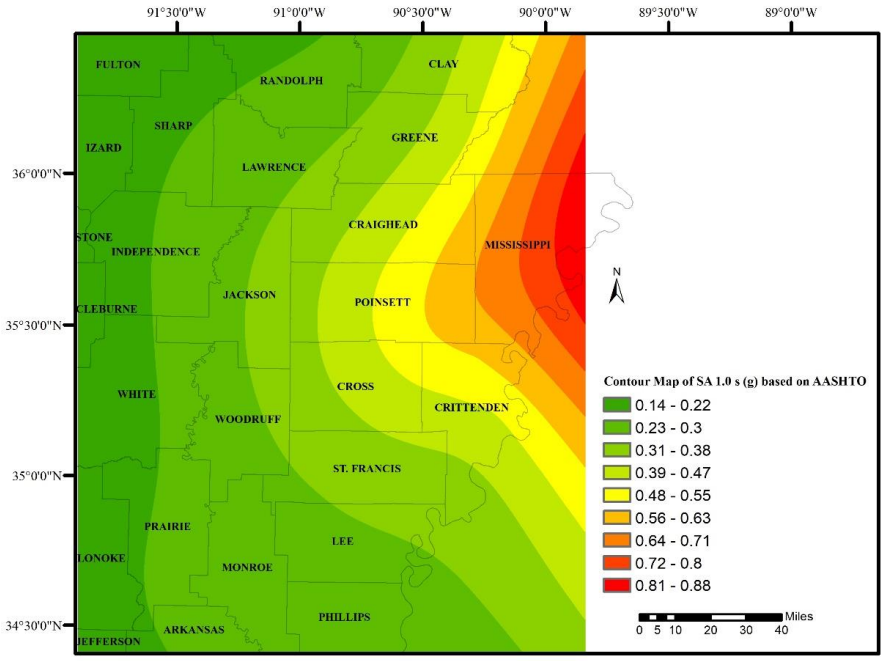


**Figure 61. SA of 1.0 sec Contour Map Based on the AASHTO LRFD Bridge Design Specifications**

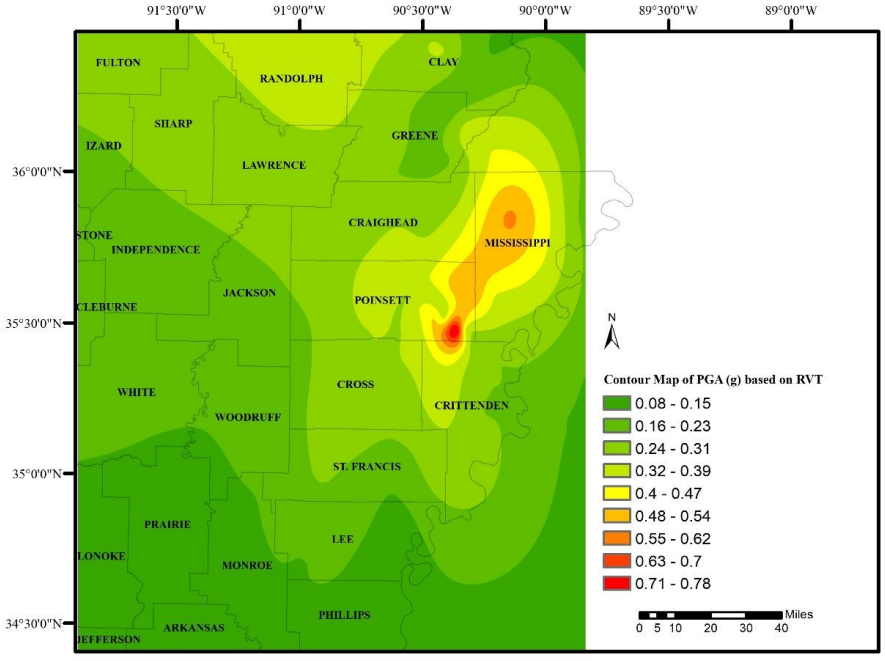


**Figure 62. PGA Contour Map Based on Method 1**

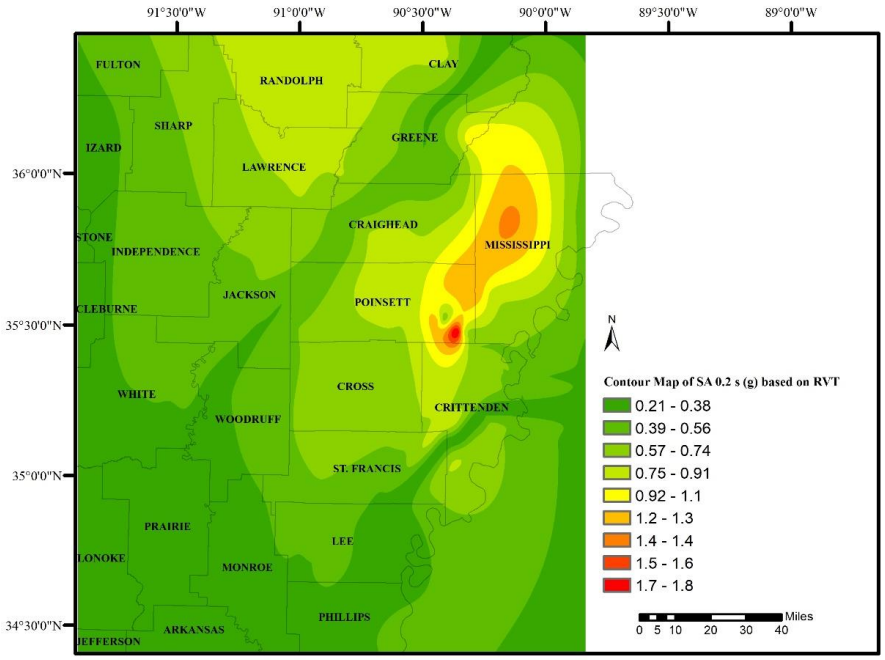


**Figure 63. SA of 0.2 sec Contour Map Based on Method 1**

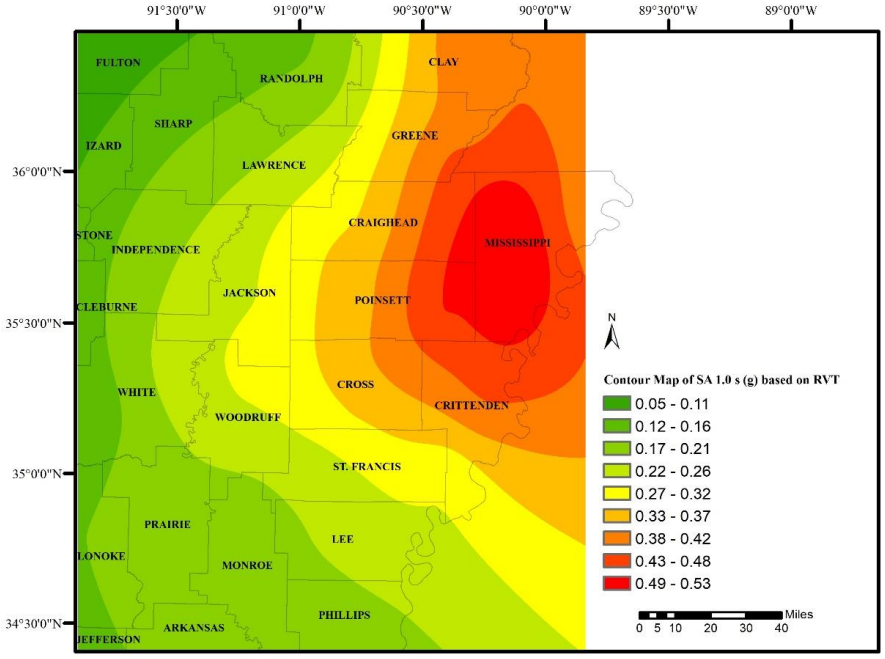


**Figure 64. SA of 1.0 sec Contour Map Based on Method 1**

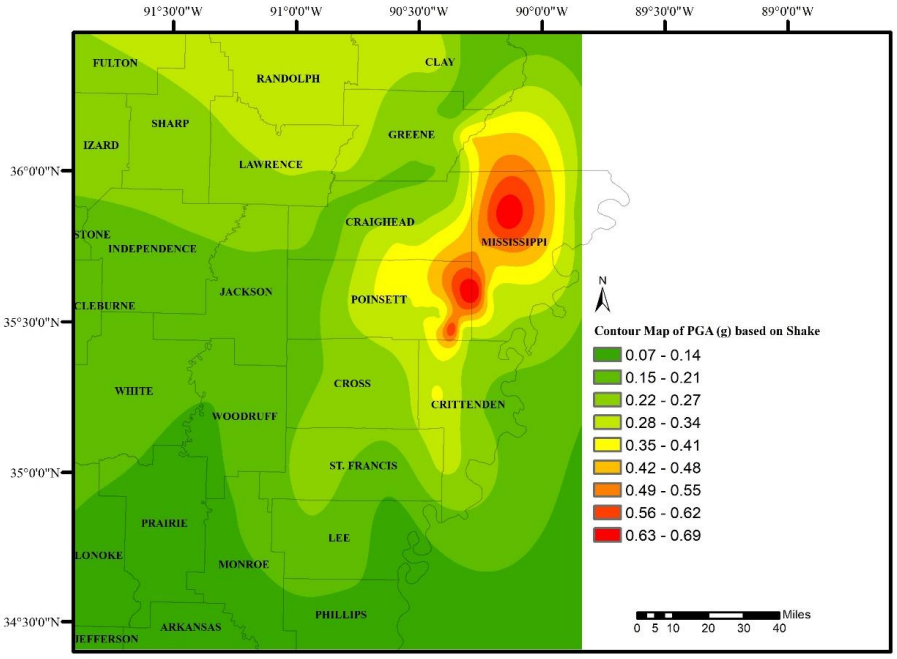


**Figure 65. PGA Contour Map Based on Method 2**

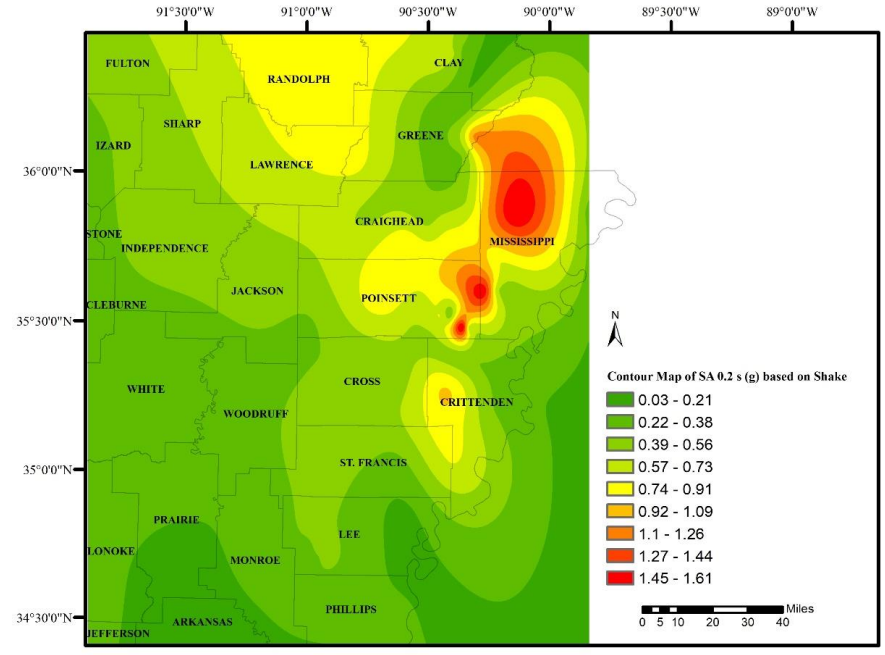


**Figure 66. SA 0.2 of sec Contour Map Based on Method 2**

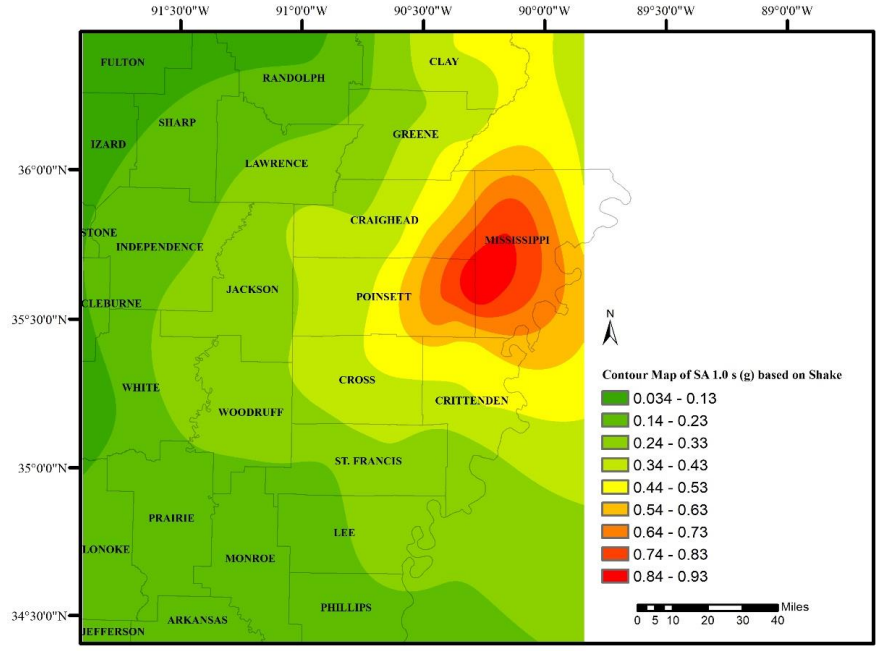


**Figure 67. SA of 1.0 sec Contour Map Based on Method 2**

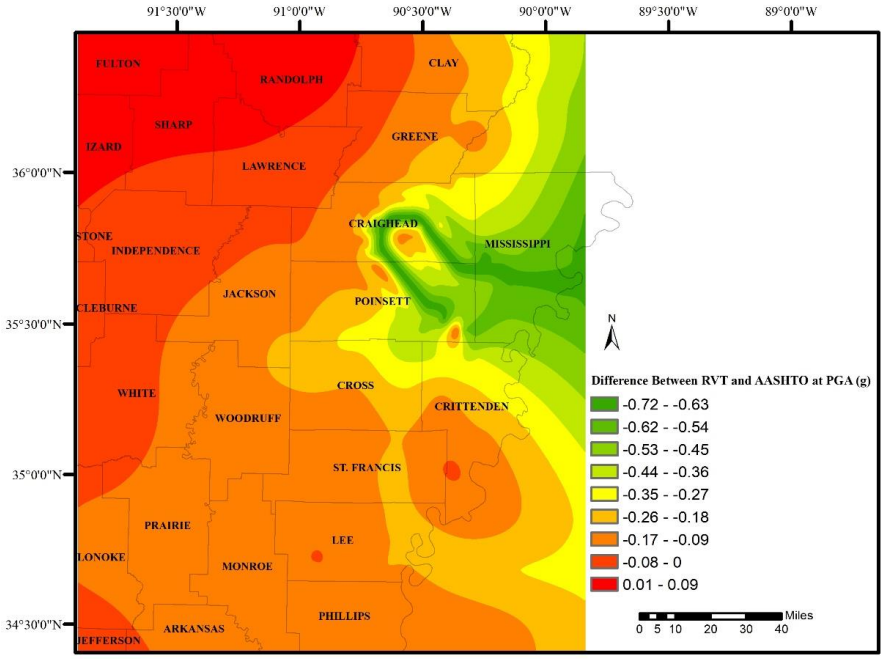


**Figure 68. Difference Between Method 1 and the AASHTO LRFD Bridge Design Specifications for PGA**

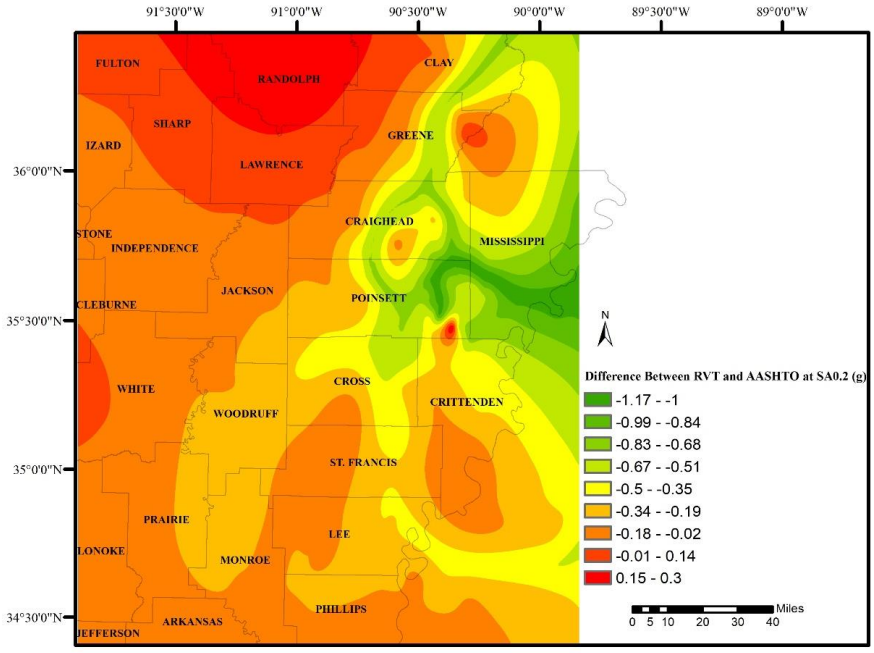


**Figure 69. Difference Between Method 1 and the AASHTO LRFD Bridge Design Specifications for SA of 0.2 sec**

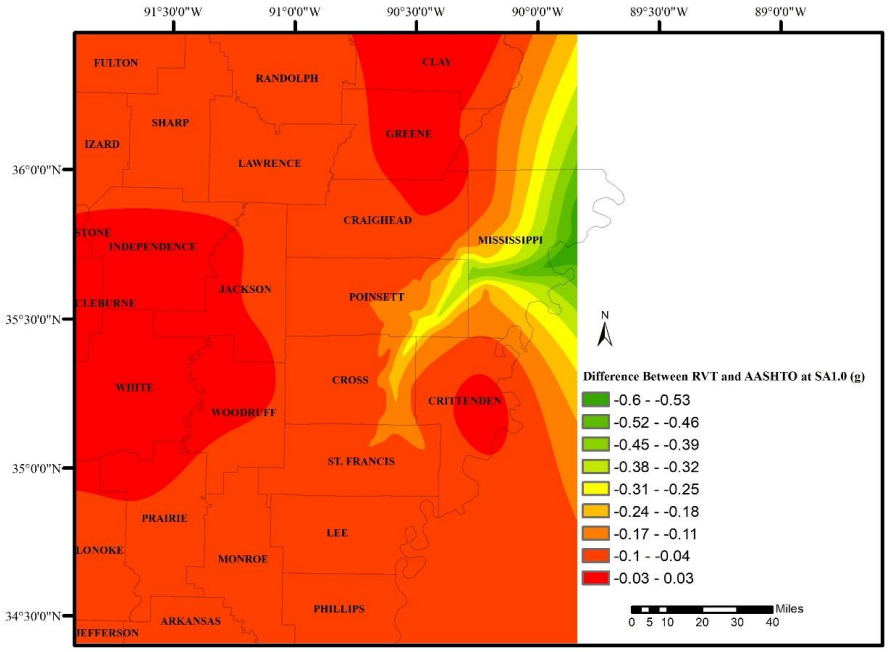


**Figure 70. Difference Between Method 1 and the AASHTO LRFD Bridge Design Specifications for SA of 1.0 sec**

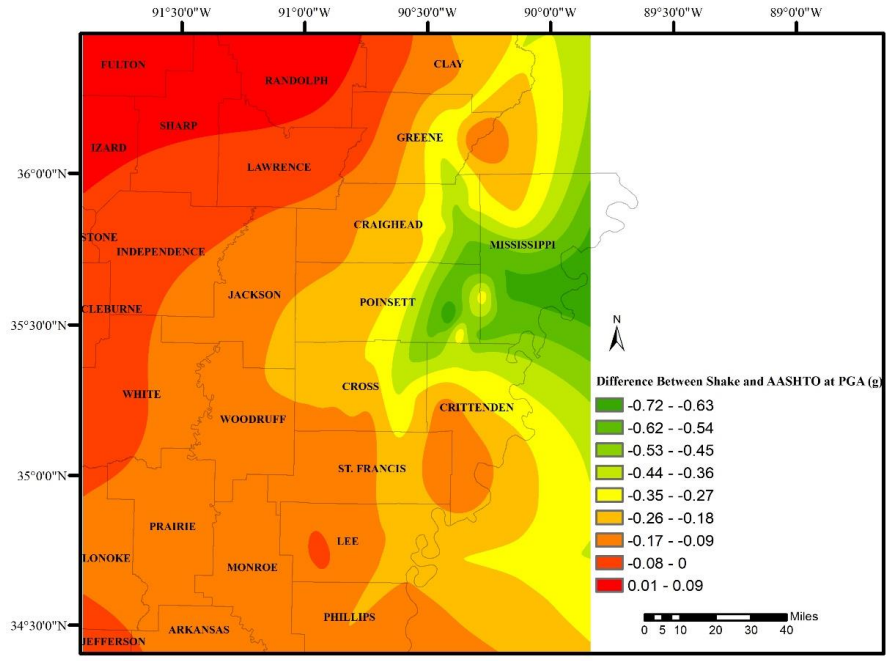


**Figure 71. Difference Between Method 2 and the AASHTO LRFD Bridge Design Specifications for PGA**

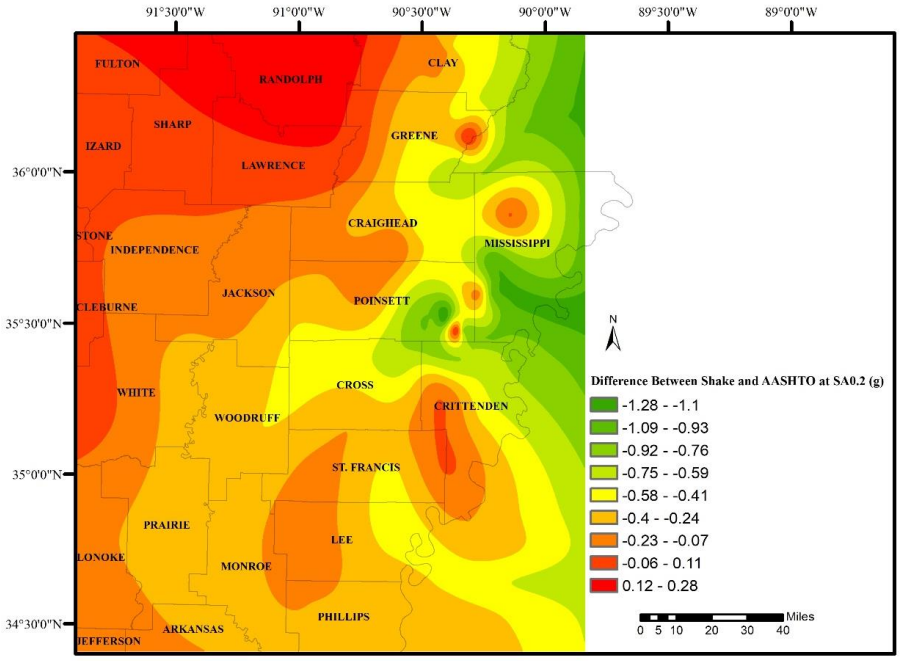


**Figure 72. Difference Between Method 2 and the AASHTO LRFD Bridge Design Specifications for SA of 0.2 sec**

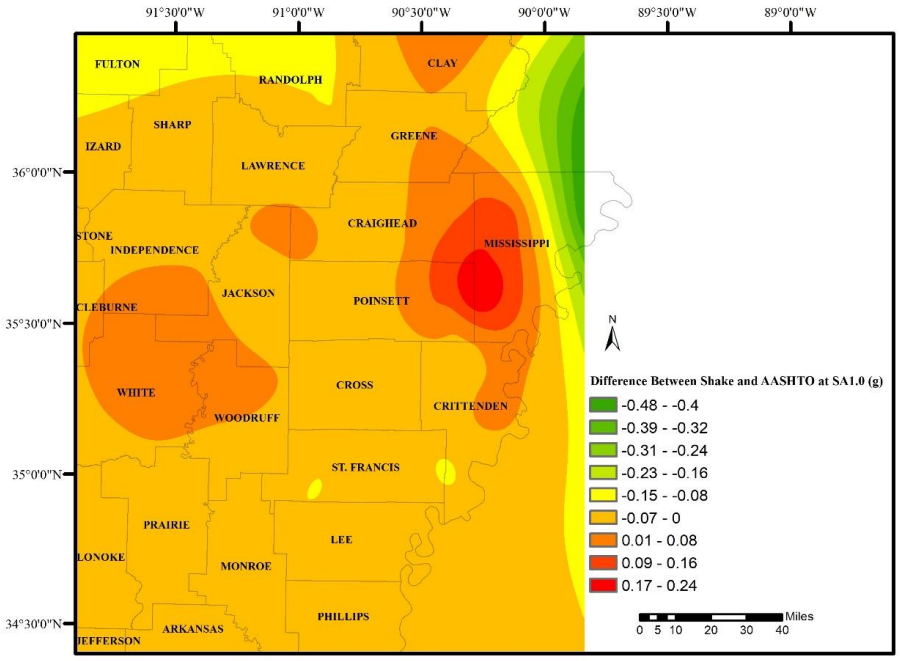


**Figure 73. Difference Between Method 2 and the AASHTO LRFD Bridge Design Specifications for SA 1.0 of sec**

Based on the methods discussed in this section, the research team recommends using the maps identified as Method 2 for estimating PGA and spectral accelerations in Northeast Arkansas. A step-by-step procedure for how to use these maps is included in the implementation report.

### 5.3 POTENTIAL COST SAVING

As part of this project, potential savings are estimated based on the Ketchum et al. (2004) recommendations. Ketchum et al. (2004) recommendations are not directly applicable to steel bridges in Northeast Arkansas due to the bridge types included in their study. However, based on what was included in the TRC1603 report, there were similarities in the cost savings estimated using the Ketchum et al. method with the cost savings calculated as part of the TRC1603 for a steel girder bridge in Northeast Arkansas; thus, it is used herein in this study. Detailed cost savings of steel bridges was not part of the scope of this project. Ketchum et al. (2004) conclude that: "For the most commonly used low-overhead concrete bridges, construction cost escalates about 5 percent per 10 percent increase in PGA above a baseline cost at 0.3 g to 0.4 g PGA. For tall concrete box girder bridges, construction cost escalates about 10 percent to 12 percent per 10 percent increase in PGA above a baseline cost at 0.6 g to 0.7 g PGA."

Given that AASHTO allows up to a 33 percent reduction in PGA if the SSGMRA concludes this is appropriate, it can be assumed that there will be a 15 percent to 30 percent cost savings that may be achievable for bridges built in Arkansas.

Figures 74 and 75 show the percentage of cost that can be reduced for low-overhead concrete bridges based on the RVT and SHAKE91, respectively. For clarification, SHAKE is the name of analysis using the SHAKE software, and SHAKE91 is the version of the software used. The assumption made prior to preparing these figures is that every 10 percent reduction in PGA would be equivalent to 5 percent reduction in cost, with the maximum cost reduction of 15 percent (PGA can be reduced up to 30 percent).

$$Percent\ Reduction\ in\ PGA = \frac{PGA_{Shake\ or\ RVT} - PGA_{AASHTO}}{PGA_{AASHTO}} \times 100 \quad (5)$$

$$Percent\ Reduction\ in\ Cost = \frac{\max\left(\%\ Reduction\ in\ PGA, -30\%\right)}{2} \quad (6)$$

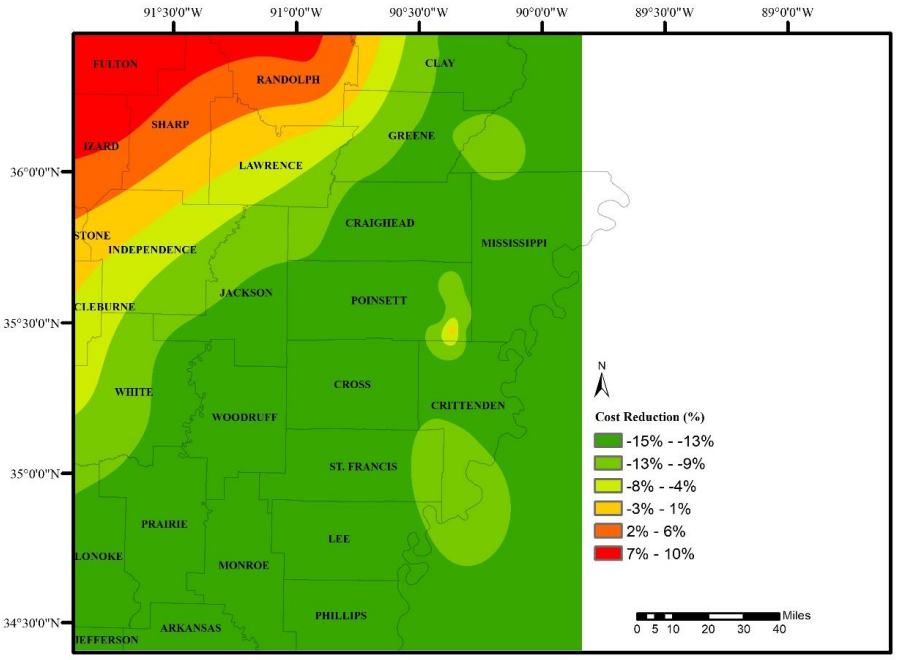


**Figure 74. Percentage of the Cost that Can be Reduced for Low-Overhead Concrete Bridges Based on the RVT Method. Negative Values Indicate Reduction and Positive Values Indicate Increase**

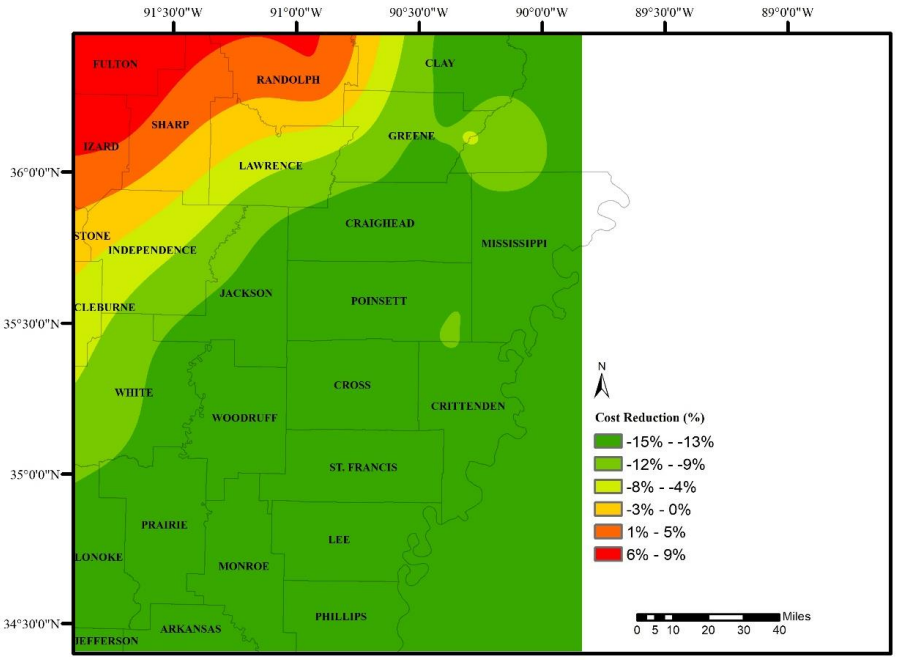


**Figure 75. Percentage of the Cost That Can be Reduced for Low-Overhead Concrete Bridges Based on the SHAKE Method. Negative Values Indicate Reduction and Positive Values Indicate Increase**

Figures 76 and 77 show the percentage of cost that can be reduced for tall concrete box girder bridges based on the RVT and SHAKE91, respectively. The assumption made prior to preparing these figures is that every 10 percent reduction in PGA would be equivalent to 10 percent reduction in cost, with the maximum cost reduction of 30 percent (PGA can be reduced up to 30 percent [Ketchum et al. 2004]).

$$Percent\ Reduction\ in\ PGA = \frac{PGA_{Shake\ or\ RVT} - PGA_{AASHTO}}{PGA_{AASTHO}} \times 100 \quad (7)$$

$$Percent\ Reduction\ in\ Cost = \max\left(\%\ Reduction\ in\ PGA, -30\%\right) \quad (8)$$

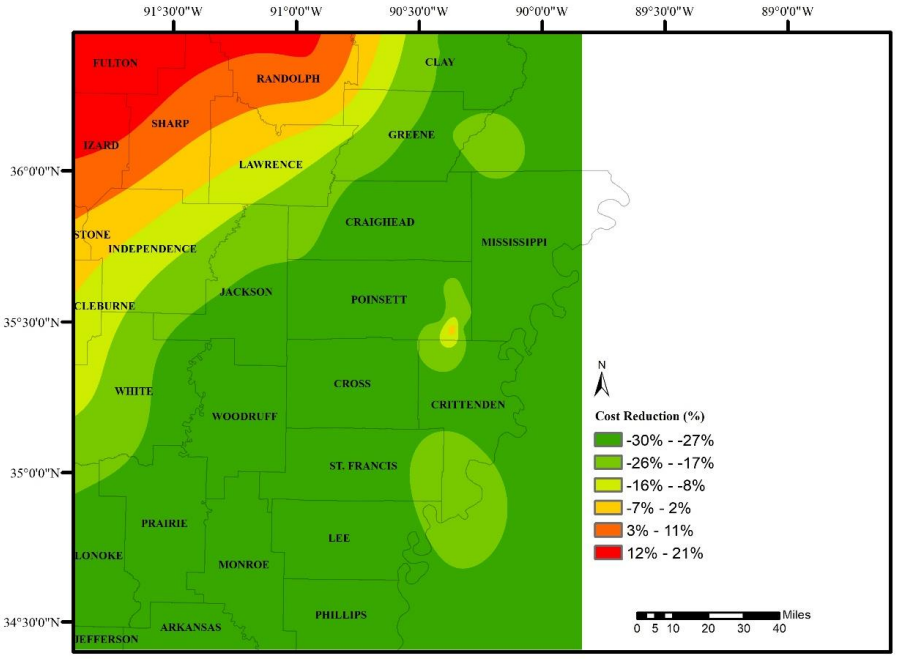


**Figure 76. Percentage of Cost Reduction for Tall Concrete Box Girder Bridges Based on the RVT Method**

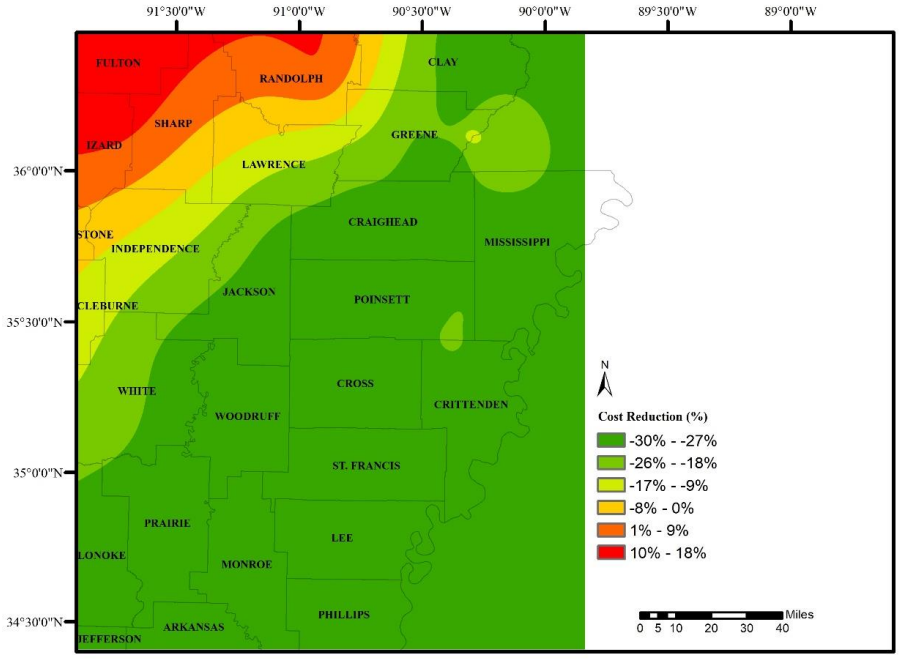


**Figure 77. Percentage of Cost Reduction for Tall Concrete Box Girder Bridges Based on the SHAKE Method**

Figures 78 and 79 show the percentage of cost that can be reduced for low-overhead concrete bridges based on the RVT and SHAKE91, respectively. The assumption made prior to preparing these figures is that every 10 percent reduction in PGA would be equivalent to 5 percent reduction in cost, with the maximum cost reduction of 15 percent (PGA can be reduced up to 30 percent). In addition, it is assumed that this bridge type should be designed for a minimum PGA of 0.3 g (Ketchum et al. 2004).

$$Percent\ Reduction\ in\ PGA = \frac{\max\left(PGA_{Shake\ or\ RVT}, 0.3\ g\right) - \max\left(PGA_{AASHTO}, 0.3\ g\right)}{\max\left(PGA_{AASHTO}, 0.3\ g\right)} \times 100 \quad (9)$$

$$Percent\ Reduction\ in\ Cost = \frac{\max\left(\%\ Reduction\ in\ PGA, -30\%\right)}{2} \quad (10)$$

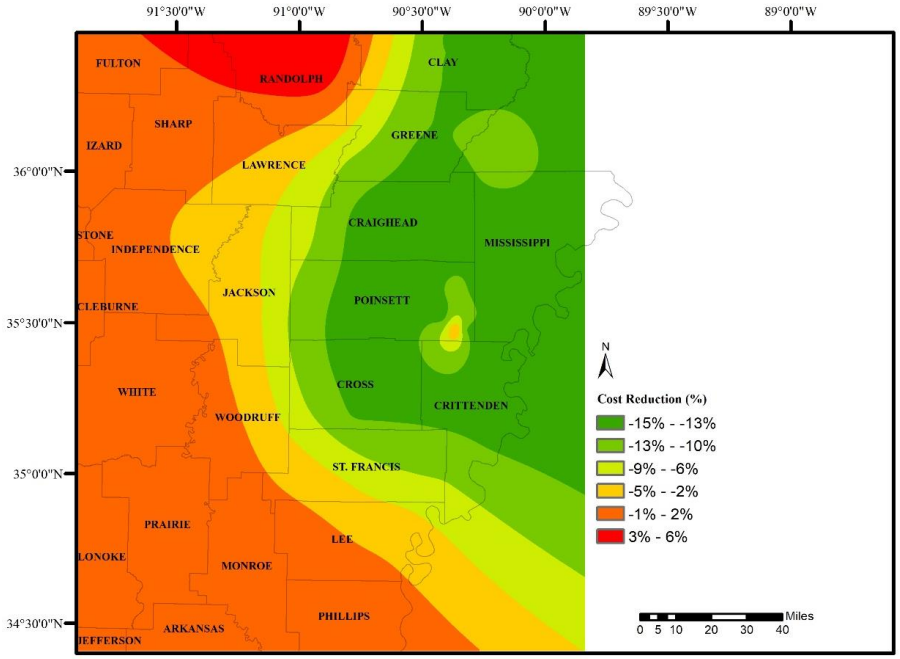


**Figure 78. Percentage of the Cost That Can Be Reduced for Low-Overhead Concrete Bridges Based on the RVT method. Negative Values Indicate a Reduction, and Positive Values Indicate Increase. A Minimum Design PGA of 0.30 g was Assumed to Prepare This Map**

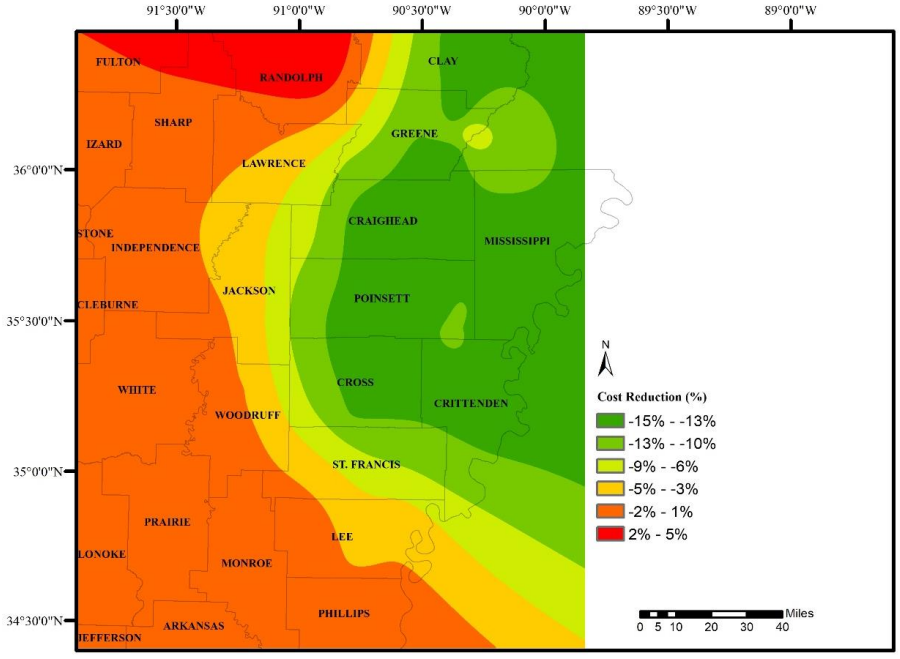


**Figure 79. Percentage of the Cost That Can be Reduced for Low-Overhead Concrete Bridges Based on the SHAKE91 Method. Negative Values Indicate a Reduction, and Positive Values Indicate Increase. A Minimum Design PGA of 0.30 g was Assumed to Prepare This Map**

Figures 80 and 81 show the percentage of cost that can be reduced for tall concrete box girder bridges based on the RVT and SHAKE91, respectively. The assumption made prior to preparing these figures is that every 10 percent reduction in PGA would be equivalent to 10 percent reduction in cost, with the maximum cost reduction of 30 percent (PGA can be reduced up to 30 percent). In addition, it is assumed that this bridge type should be designed for a minimum PGA of 0.6 g (Ketchum et al. 2004).

$$Percent\ Reduction\ in\ PGA = \frac{\max\left(PGA_{Shake\ or\ RVT}, 0.6\ g\right) - \max\left(PGA_{AASHTO}, 0.6\ g\right)}{\max\left(PGA_{AASHTO}, 0.6\ g\right)} \times 100 \quad (11)$$

$$Percent\ Reduction\ in\ Cost = \max\left(\%\ Reduction\ in\ PGA, -30\%\right) \quad (12)$$

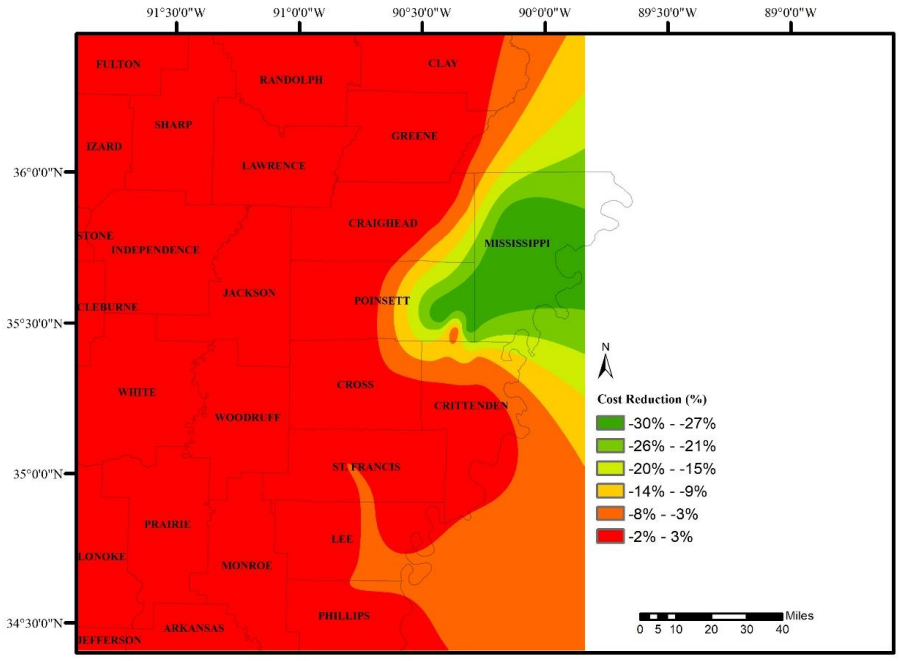


**Figure 80. Percentage of Cost Reduction for Tall Concrete Box Girder Bridges Based on the RVT Method. A Minimum Design PGA of 0.60 g was Assumed to Prepare This Map**

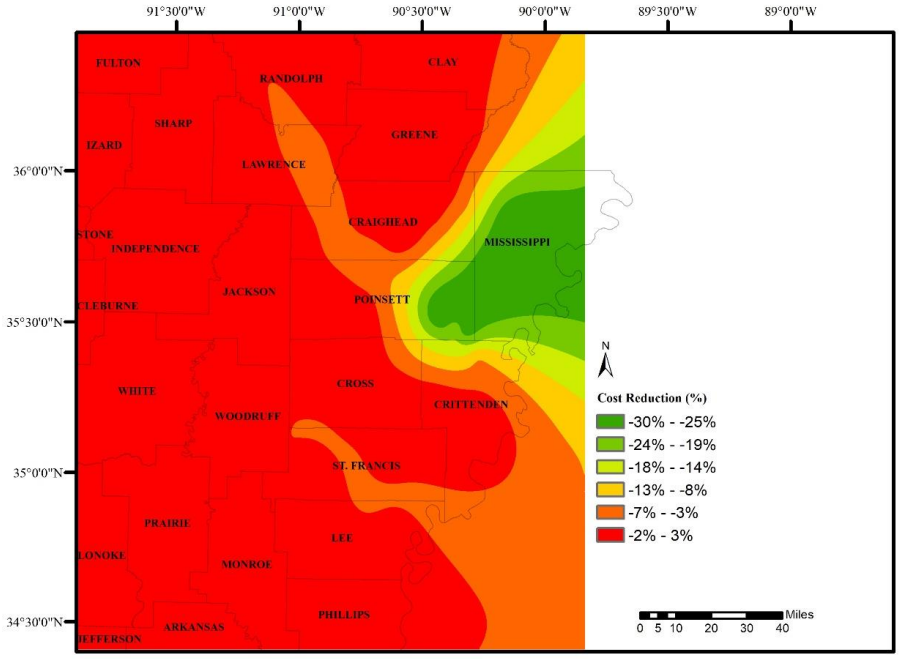


**Figure 81. Percentage of Cost Reduction for Tall Concrete Box Girder Bridges Based on the SHAKE Method. A Minimum Design PGA of 0.60 g was Assumed to Prepare This Map**

## 5.4 RECOMMENDATIONS FOR FUTURE RESEARCH

The research team recommends that ARDOT sponsors a study to perform an extensive cost comparison between bridges designed using spectral accelerations determined by the AASHTO LRFD Bridge Design Specifications and bridges designed using spectral accelerations from SSGMRA studies. This will enable ARDOT bridge designers to make more accurate decisions regarding the cost benefit of performing SSGMRA studies.

# CHAPTER 6. DEVELOPING DOCUMENTATION AND SPECIFICATIONS FOR SITES THAT NEED SITE-SPECIFIC STUDIES TO BE PERFORMED

## 6.1 INTRODUCTION

For this part of the project, the research team developed an approach for ARDOT to select qualified consultants who will perform SSGMRA investigations. Also included in this chapter are requirements to be included in the consultants' Request for Qualifications (RFQ) when an SSGMRA is required.

## 6.2 BACKGROUND

The research team searched web pages and contacted engineers at ten State Departments of Transportation (DOT) located within zones of influence of known seismic activities. We pursued answers to the following questions:

- Does the DOT have a geotechnical manual?
- Does the DOT have guidelines for performing SSGMRA?
- Does the DOT have qualification requirements for consultants who perform SSGMRA studies?

Table 20 provided information related to the questions above.

**Table 20. Summary of the Current Conditions of Specific state DOTs**

| Name of the State DOT's | Do they have a Geotechnical Manual? | Do they have specific site response analysis guidelines? |
|---|---|---|
| South Carolina | Yes | Yes |
| California | Yes | Yes |
| Washington | Yes | Yes |
| Oregon | Yes | Yes |
| Illinois | Yes | Yes |
| Kentucky | Yes | No |
| North Carolina | Yes | No |
| Virginia | Yes | No |
| Oklahoma | Yes | No |
| Utah | Yes | No |
| Tennessee | Yes | No |
| Missouri | No | No |

## 6.3 SUMMARY OF FINDINGS

Based on our search results, although the levels of details in state DOTs regarding geotechnical documents vary substantially, we did not find an indication that any of the state DOTs listed above has a prequalification procedure for consultants who perform SSGMRA studies. The following is a summary of

our relevant findings through document search and personal communications. Our focus in this section is on states located in the Central and Eastern United States (CEUS).

- Tennessee Department of Transportation (TDOT) Geotechnical Engineering Section (GES) has several geotechnical-related manuals and special provisions but no comprehensive geotechnical design manual (GDM). GES attempted to generate a geotechnical seismic manual back in 2010, but it was never completed. TDOT has a pre-qualification process to pre-approve its consultants and awards two to three on-call geotechnical engineering contracts for each of its four regions. TDOT contracts with consultants to perform SSGMRA studies.
- Likewise, the Missouri Department of Transportation (MoDOT) geotechnical engineering department neither has a comprehensive GDM, nor a procedure for performing SSGMRS studies. MoDOT awards multiple on-call geotechnical engineering contracts for each of its regions, and it contracts with consultants to perform such studies.
- Illinois DOT (IDOT) has a comprehensive geotechnical manual (GM) that includes seismic-related geotechnical design guidelines. IDOT has a general consultant pre-qualification process (not specifically for performing SSGMRA studeis), and it relies on consultants to perform geotechnical exploration and design; however, the PI could not find specific guidelines regarding performing SSGMRA studies.
- South Carolina DOT (SCDOT) has a comprehensive geotechnical design manual (GDM) that includes substantial seismic-related discussions, guidelines, and procedures regarding performing SSGMRA studies (Section 12.9 of the GDM). SCDOT performs specific SSGMRA studies in-house, specifically total-stress, one-dimensional, equivalent-linear SHAKE analyses. SCDOT also has a pre-qualification process for consultants, but not specifically for performing SSGMRA studies, and it relies on consultants on its on-call geotechnical contracts to perform these studies. Section 12.9.4 of the GDM states that for specific situations, where the SSGMRA study results in a reduction in the design response spectra below a certain threshold, the reduction can be used only if an independent third-party review (Peer Review) of the Acceleration Design Response Spectra (ADRS) curve by an individual with the expertise in the evaluation of ground motions is to be undertaken. The Peer Review shall be conducted by an individual who has a minimum of 10 years' experience in geotechnical seismic design and who shall have conducted a minimum of 7 site-specific response analyses as the lead designer. If a nonlinear analysis is performed, the Peer Reviewer shall have conducted at least three nonlinear site response analyses. The three nonlinear analyses may be included in the seven site-specific response analyses. In addition, the Peer Reviewer shall be licensed as either an engineer (PE) or geologist (PG) according to the laws of South Carolina.

Based on the search discussed above, it is the researcher's professional opinion that a pre-qualification process will serve ARDOT well regarding performing SSGMRA studies and that the SCDOT GDM guidelines in this regard can be considered when a procedure is established. ARDOT bridge design and geotechnical personnel can further consult with their SCDOT peers if ARDOT is to create a geotechnical manual.

## 6.4 DISCUSSION OF METHODS OF PERFORMING SHEAR WAVE VELOCITY PROFILING

Several methods exist for determining the shear wave velocity ($V_s$) profiles. These methods are generally divided into invasive or non-invasive (or surface) techniques. Examples of invasive techniques are Crosshole (ASTM D 4428), Downhole (ASTM D 7400), and Seismic Cone Penetration Testing (ASTM D 5778). Examples of non-invasive techniques are Refraction Microtremor (ReMi), Spectral Analysis of Surface Waves (SASW), Multichannel Analysis of Surface Waves (MASW), Passive Source Microtremor Array Measurements (MAM), and Horizontal to Vertical Spectral Ratio (HVSR), among others. The surface techniques have not been standardized by ASTM; their performance typically depends on experience, education, and research. The equipment used for performing shear wave velocity profiling also varies substantially as many types of geophones, accelerometers, and data acquisition systems are available in the market today.

Len et al. (2017) performed a study to compare the SASW and MASW and elucidated the differences between the two techniques. He concluded MASW is a superior technique. Park et al. (2007) provided detailed explanations of both active and passive MASW methods. He stated the need for passive MASW due to increased demand for increased investigation depth. He concluded it is often useful or necessary to combine dispersion images processed from both active and passive data for two reasons: (1) to enlarge the analyzable frequencies (therefore the depth) range of dispersion, and (2) to identify the modal nature of dispersion trends better.

Liu (2017) collected shear wave velocity data using SASW, MASW, and ReMi in the Greater Boston Area to determine which method gives the best estimation of the 1-D shear wave velocity profile near-surface soil. He concluded that, overall, the MASW and ReMi methods have a comparable quality of accuracy, while the SASW method is the least accurate method with the highest percentage differences in direct measurement. He also stated that MASW is the most precise method among the three methods in determining the shear wave velocities of the subsurface in the Greater Boston Area.

Cox and Beekman (2011) performed ReMi testing at three sites in Fayetteville, AR. They concluded there is a potential for significant uncertainty in shear-wave velocity ($V_s$) estimates obtained in this manner because much is unknown about the seismic wavefield that is being sampled. They found that changes in the sampled seismic wavefield, obtained through employing various array orientations at a site and inclusion of actively generated noise, resulted in significant variations in the ReMi-obtained dispersion curves and $V_s$ profiles.

Andrus et al. (2004) performed various in-situ testing techniques to obtain shear wave velocity profiles. The comparison included invasive (Crosshole, downhole and seismic CPT) and non-invasive (SASW and surface reflection/refraction) techniques. In terms of quality control and repeatability, they rated the invasive methods as “good.” In contrast, SASW was rated “good to fair” due to complex interpretation techniques at sites with large velocity contrasts. Reflection/refraction methods were rated “fair” due to the difficulties in distinguishing shear wave arrival. In terms of resolution of variability in soil deposits’ stiffness, the invasive and SASW methods were rated “good to fair” with quality decreasing with depth. In contrast, the reflection/refraction methods were rated “fair to poor”. They concluded that Crosshole is

a highly reliable test, seismic CPT also provides geotechnical information of the subsurface, and the surface reflection/refraction methods are well suited for screening large areas.

Based on the above, one can conclude that there is no universal agreement or consensus regarding the best method for obtaining $V_s$ profiles. Accordingly, the PIs' recommendations are presented as follows:

- ReMi should not be used as a stand-alone $V_s$ profiling method; it can be combined with MASW.
- MASW is superior to SASW.
- Invasive techniques such as Crosshole, downhole and seismic CPT are all suitable for $V_s$ profiling in the study area. Seismic CPT has the advantage of providing geotechnical subsurface information due to its ability to penetrate to a great depth in Northeast Arkansas.
- The methods used for $V_s$ profiling in TRC1603 (MASW, MAM, and HVSR) are all considered to be reliable methods.
- For small new bridges (single to 4-span) or bridge replacement projects, a single profile using downhole, seismic CPT, or a surface method as recommended above should be considered sufficient.
- For longer, multiple-span (more than 4) bridges and where the soil conditions are considered erratic, consideration should be given to generating more than a single $V_s$ profile.
- For essential or critical bridges, or bridges deemed by ARDOT to be relatively more important than what is described above, multiple $V_s$ profiles should be determined. If such a bridge crosses a waterway, multiple profiles should be determined on both sides of the channel.

### 6.5 ANALYSIS TYPE

SSGMRA can be performed using one, two, or three dimensions, either equivalent-linear or nonlinear domain. Several computer programs are available to perform these studies. Software examples are SHAKE, DEEPSOIL, and STRATA. Results from equivalent-linear and nonlinear analyses can be substantially different. Griffiths et al. (2016) showed that, contrary to popular belief, nonlinear analyses may not produce realistic results at high shear strains; such conditions may be expected in Northeast Arkansas.

Based on our experience, presented below are the PIs' recommendations:

- For small new bridges (single to four spans) or bridge replacement projects, a single one-dimensional, equivalent-linear analysis should be considered sufficient.
- For longer, multiple-span (more than four) bridges, a single one-dimensional, equivalent-linear analysis plus a single one-dimensional nonlinear analysis should be considered sufficient.
- For bridges deemed by ARDOT to be relatively more important than the ones described above, multiple (more than one) equivalent-linear and nonlinear analyses should be performed.
- For essential or critical bridges, we recommend that ARDOT retain a "third party" firm or person with a well-established, nationally recognized reputation to serve as the "Owner Representative" and establish guidelines for how SSGMRA studies should be performed. This firm/person should also serve as a "Peer Reviewer" of the results and recommendations on ARDOT's behalf.

- Care should be exercised upon establishing "combined envelope" response spectra when both equivalent-linear and nonlinear analyses are performed; the results of the two analyses can be substantially different.

### 6.6 ESTIMATED COST FOR SSGMRA

The cost of performing an SSGMRA study, when compared to the projected design and construction saving, should be taken into consideration when a decision to perform, or not perform, such a study is made. Sometimes, conducting the study will result in designing a safer bridge, regardless of the potential for cost-saving. Nevertheless, knowing an approximate estimate for performing the study is always helpful.

The cost for performing SSGMRA studies can vary substantially, depending on travel distance and cost, the type of field test(s) to be performed (invasive vs. non-invasive), the number of field tests, and the type and number of analyses. Based on our experience, the following cost ranges can be considered upon making a decision to perform SSGMRA studies:

- One complete site-specific study, which will include a single shear-wave velocity profile measurement using surface, seismic cone or downhole method, probabilistic seismic hazard analysis, spectrum matching, one-dimensional equivalent-linear analyses considering all uncertainties, the estimated cost would be in the range of $10,000 to $15,000.
- A Crosshole survey may have up to $10,000 of extra cost.
- For a single shear wave velocity profile, a single one-dimensional equivalent-linear analysis, and a single nonlinear analysis, the estimated cost would be in the range of $15,000 to $25,000.
- For bridges where multiple field tests and analyses are to be performed, the above estimates can be used to calculate the total cost.
- For essential or critical bridges, the "third party" mentioned in Section 6.5 above should establish the scope of work and review the cost of the SSGMRA studies to be performed.

### 6.7 CONSULTANT SELECTION

It is our understanding ARDOT will task consulting firms to perform SSGMRA studies. These firms could be bridge design firms that are tasked with designing new bridges, replacement bridges or bridge retrofits, or could be geotechnical subconsultants who have the capabilities of performing SSGMRA studies.

It is our recommendation that ARDOT establishes a pre-qualification procedure for consultants who wish to perform SSGMRA studies. ARDOT should post an advertisement on its web page to announce the intent of accepting consultant qualifications. Consultants should then submit their qualifications to ARDOT for review. ARDOT should assemble a committee for the review of such qualifications then make a decision to accept or reject them. The committee should include senior geotechnical and structural (bridge) engineers, as well as procurement and consultant services personnel. Once a list of prequalified consultants is assembled, it should be posted on the ARDOT web page.

Once a bridge replacement or a new bridge project is to be designed, either in-house by ARDOT or a consulting firm, a request to perform single or multiple SSGMRA studies should be made. If the project is

to be designed in-house, then ARDOT can contract directly with a prequalified consulting firm that can perform SSGMRA studies. If the project is to be designed by a consultant, either the consultant firm can perform the SSGMRA if it is prequalified to do that, or it can engage a subconsultant from the prequalified list.

### 6.8 CONSULTANT QUALIFICATIONS

It is the research team's recommendations that consulting firms who wish to perform SSGMRA studies for ARDOT should meet the following requirements:

- The consulting firm and the individuals who perform the study should demonstrate the ability to perform SSGMRA studies by means of individual training, course work, and experience.
- The consulting firm must have a minimum of 10 years of experience in geotechnical seismic design and shall have conducted a minimum of seven site-specific response analyses in the last five years. If a nonlinear analysis is to be performed, the consulting firm shall have conducted at least three nonlinear site response analyses.
- The consulting firm must possess the equipment and experience to perform shear-wave velocity profiling using both non-invasive and invasive techniques. Examples of non-invasive techniques include SASW, MASW, or ReMi methods. Examples of invasive techniques include downhole, Crosshole, or seismic cone penetration testing (SCPT) methods.
- The consulting firm must own the computer programs to perform ground motion analyses. This can include SHAKE, DEEPSOIL, DMOD, STRATA or other similar software. As previously mentioned, the analysis can be performed in one, two, or three dimensions. Equivalent linear or nonlinear analyses can be performed.

### 6.9 DOCUMENTS TO BE PROVIDED BY ARDOT TO THE CONSULTING FIRM PERFORMING SSGMRA

ARDOT should provide the consulting firm to perform the SSGMRA with the following documents:

- Plans showing bridge locations, including bents and abutments.
- Drawings showing approach profiles and cross-sections.
- Reports of any geotechnical exploration performed at the site.
- Any limitation an ARDOT bridge designer would have on the design response spectra (for example, SCDOT will not allow the site-specific design response spectra to be less than 70 percent of the 3-point, or code-based, method).

### 6.10 REQUEST FOR QUALIFICATIONS (RFQ)

Section 6.8 of this report includes the suggested qualification requirements for consultants who will perform SSGMRA. If ARDOT is going to prequalify consultants, an RFQ is not needed. If ARDOT is not going to do so, then the language included in Section 6.8 can be included in the RFQ.

## 6.11 REQUEST FOR PROPOSALS (RFP)

It is our understanding that engineering board rules prohibit governmental agencies from selecting/procuring an Architectural/Engineering (A/E) firm to provide professional services based on price; the selection should be solely a qualification-based selection (QBS). ARDOT, however, can advertise and post a Request for Qualifications (RFQ) when SSGMRA studies are needed. Once a list of qualified firms that can perform SSGMRA studies is established, ARDOT can evaluate estimates and reject them if the cost to perform the SSGMRA study is deemed to be too high.

# LIST OF REFERENCES


Allen, T.I., and Wald, D.J. (2007). "Topographic Slope As a Proxy For Global Seismic Site Conditions ($V_{S30}$) and Amplification Around the Globe," U.S. Geological Survey Open-File Report 2007-1357*,* U.S Department of the Interior: 69.

Andrus, R., D., Stokoe, K., H., and Juang, H. (May 2004). "Guide for Shear Wave-Based Liquefaction Potential Evaluation," *Earthquake Spectra* 20, no. 2, Earthquake Engineering Research Institute: 285-308.

ARDOT (2001). Boring Logs, Job 220288, "U.S 64 St. Francis River Structures and Approaches, Cross County".

Atkinson, G.M. (2008). "Ground-motion Prediction Equations for Eastern North America from a Referenced Empirical Approach—Implications for Epistemic Uncertainty," *Bull. Seismol. Soc. Amer.* 98, no. 2: 1,304–1,318, doi:10.1785/0120070199.

Atkinson, G.M., and Boore, D.M. (2006). "Earthquake Ground-Motion Prediction Equations for Eastern North America," *Bull. Seismol. Soc. Amer.* 96: 2,181–2,205, doi:10.1785/0120050245.

Atkinson, G.M., and Boore, D.M. "Modifications to Existing Ground-Motion Prediction Equations in Light of New Data," *Bull. Seismol. Soc. Amer.* 101, (2011): 1,121–1,135, doi:10.1785/0120100270.

Bazzurro, P., and Cornell, C. A. "Ground Motion Amplification in Nonlinear Soil Sites with Uncertain Properties," *Bull. Seismol. Soc. Amer.* 94 (2004): 2090-2109.

Boore, D. M. (2003). "Prediction of Ground Motion Using the Stochastic Method," *Pure Appl. Geophys.* 160: 635–676.

Boore, D. M., and E. M. Thompson. (2014). "Path Durations for Use in the Stochastic-Method Simulation of Ground Motions," *Bull. Seismol. Soc. Amer.* 104: 2541–2552.

Campbell, K.W. (2003). "Prediction Of Strong Ground Motion Using the Hybrid Empirical Method and Its Use in the Development Of Ground Motion (Attenuation) Relations in Eastern North America," *Bull. Seismol. Soc. Amer*. 93: 1012–1033.

Chapman, M., Pezeshk, S., Hosseini, M., and Conn, A. (2014). "Regional Study of Fourier Amplitude Drop of Lg-Wave Acceleration in Central United States," *Seismol. Res. Lett*. 85: 513.

Chung, J.W, and Rogers J. D. (2010). "GIS-Based Virtual Geotechnical Database for the St. Louis Metro Area," *Environ. Eng. Geosci.* 16, no. 2: 143-62.

Cornell, C. A. (1968). "Engineering Seismic Risk Analysis," *Bull. Seismol. Soc. Amer.* 58: 1583-1606.

Cox, B. R., Trenton, P. E., Ellis, B., and Griffiths, S. C. (2012). "Site-Specific Seismic Ground Motion Analyses for Transportation Infrastructure in the New Madrid Seismic Zone," *Mack-Blackwell Rural Transportation Center*, https://ardot.gov/System_Info_and_Research/research/Library/MBTC/MBTC3032.PDF.

Cox, B., R., and Beekman, A., N. (April 2011). "Intra-Method Variability in ReMi Dispersion Measurements and $V_s$ Estimates at Shallow Bedrock Sites" *ASCE Journal of Geotechnical and Geoenvironmental Engineering*.

Cramer, C. H. (2004). "Site-Specific Seismic-Hazard Analysis that is Completely Probabilistic," *Bull. Seismol. Soc. Amer*. 93: 1841-1846.

Cramer, C. H., Gomberg, J. S., Schweig, E. S., Waldron, B. A., and Tucker, K. (2004). The Memphis, Shelby County, Tennessee, Seismic Hazard Maps, U.S. Geological Survey Open-File Report 04-1294.

Electric Power Research Institute. (November 1993). "Guidelines for Determining Design Basis Ground Motions," *Electric Power Research Institute* 2.

Electric Power Research Institute. (May 17 2013). "Seismic Evaluation Guidance." *Electric Power Research Institute*.

Elsayed, A., S. Pezeshk, S. Stovall, and A. Kizzee. (2008). "Shear-Wave Velocity Profiling and Liquefaction Hazard Analysis," TRC0803, Final Report to State of Arkansas Highway and Transportation Department.

EPRI NP-6395-D. (1989). "Probabilistic Seismic Hazard Evaluation at Nuclear Plant Sites in the Central and Eastern United States: Resolution of the Charleston Issue," *Electric Power Research Institute*.

Foti, S. (2000). "Multistation Methods for Geotechnical Characterization Using Surface Waves," *Ph.D. Dissertation*, Politecnico di Torino.

Frankel, A. (1995). "Mapping Seismic Hazard in the Central and Eastern United States" *Seismol. Res. Lett.* 66: 8–21.

Gardner, J. K., Knopoff, L. (1974). "Is the Sequence of Earthquakes in Southern California, with Aftershocks Removed, Poissonian?" *Bull. Seismol. Soc. Amer.* 64: 1363-1367

Ginzburg, A., Mooney, W.D., Walter, A.W., Lutter, W.J., and Healy, J.H. (1983). "Deep Structure of Northern Mississippi Embayment," *AAPG Bull*. 67: 2031-2046.

Gomberg, J., Waldron, B., Schweig, E., Hwang, H., Webbers, A., Van Arsdale, A., Tucker, K., Williams, R., Street, R., Mayne, P., Stephenson, W., Odum, J., Cramer, C., Updike, R., Hutson, R., and Bradley, M. (2003). "Lithology and shear velocity in Memphis, Tennessee," *Bull. Seismol. Soc. Amer*. 93: 986-997.

Griffiths, S.C., Cox, B.R., Rathje, E.M., and Teague, D.P. (2016). "A Surface Wave Dispersion Approach for Evaluating Statistical Models that Account for Shear Wave Velocity Uncertainty," *Journal of*

*Geotechnical and Geoenvironmental Engineering* 142, no. 11.

Hashash, Y., S. Pezeshk, and D. Park. (2013). *Non-Linear Seismic Response of Deep Deposits in West Tennessee*. TDOT Report.

Hebeler, G. L. (2001). *Site Characterization in Shelby County, Tennessee Using Advanced Surface Wave Methods.* Thesis, Georgia Institute of Technology.

Hosseini, S. M., and S. Pezeshk. (2015). "A Synthetic Study into the Nature and Solution of Nonuniqueness in Surface-Wave Inverse Problems." *Bulletin of the Seismological Society of America* 105: 3167–3179.

Hosseini, S. M. (2014). "Reducing Uncertainties in the Velocities Determined by the Inversion of Phase Velocity Dispersion Curves Using Synthetics Seismograms." Ph.D. Dissertation, The University of Memphis.

http://www.idot.illinois.gov/Assets/uploads/files/Doing-Business/Manuals-Guides-&-Handbooks/Highways/Materials/Geotechnical%20Manual.pdf

https://transportation.ky.gov/OrganizationalResources/Policy%20Manuals%20Library/Geotechnical.pdf

https://connect.ncdot.gov/resources/Geological/Documents/16-03-29_Geotechnical%20Investigation%20and%20Recommendations%20Manual.pdf

https://www.tn.gov/content/dam/tn/tdot/hq-materials-tests/geotech/2016-10-15 TDOT Geotech Manual.pdf

Ketchum, M., Chang, V., and Shantz, T. (2004). "Influence of Design Ground Motion Level on Highway Bridge Costs," *Pacific Earthquake Engineering Research* (PEER) Center, Report No. Lifelines 6D01, University of California, Berkeley, California.

Lin, C-P., Lin, C-H., and Chien, C-J. (2017). "Dispersion Analysis of Surface Wave Testing – SASW vs. MASW." *Journal of Applied Geophysics* 143: 223-230.

Liu, S. (2007). "Shear Wave Velocity Analysis by Surface Wave Methods in the Boston Area" Thesis, Boston College Morrissey College of Arts and Sciences.

Louie, J. N. (2001). "Faster, Better: Shear-Wave Velocity to 100 Meters Depth from Refraction Microtremor Arrays." *Bulletin of the Seismological Society of America* 91, no. 2: 347–364.

McGuire, R.K., Silva, W.J., and Costantino, C. J. (2001). "Technical Basis for Revision of Regulatory Guidance on Design Ground Motions: Hazard and Risk-Consistent Ground Motion Spectra Guidelines," NUREG/CR- 6728, U.S. Nuclear Regulatory Commission.

Mooney, W., Andrews, M., Ginzburgh, A., Peters, D., and Hamilton, R. (1983). "Crystal Structure of the Northern Mississippi Embayment and a Comparison with other Continental Rift Zones," *Tectonophysics* 94: 327-348.

Oklahoma Department of Transportation, ed. 2015. "Geotechnical Specifications for Roadway Design." http://www.okladot.state.ok.us/roadway/Geotech/Geotechnical%20Specifications%20for%20Roadway%20Design.pdf

Oregon Department of Transportation. (April 2010). "Geotechnical Design Manual." http://www.ce.memphis.edu/7137/PDFs/Seismic%20Manual/Oregon/GDM_April_2010_2.pdf

Park, D., S. Pezeshk, and Y. Hashash. (2014). "Nonlinear Site Response of Deep Deposits in West Tennessee." 4th National Seismic Conference and Workshop on Bridges and Highways, Memphis, Tennessee, February 9-12, 2004.

Park, C., Miller, R., Xia, J., and Ivanov, J., C-J. (2007). "Multichannel Analysis of Surface Waves (MASW) – Active and Passive Methods," *The Leading Edge,* Kansas Geological Survey.

Pezeshk, S., and M. Zarrabi. (2005). "A New Inversion Procedure for Spectral Analysis of Surface Waves Using a Genetic Algorithm," *Bulletin of the Seismological Society of America*, 95 no. 5: 1801–1808.

Petersen, M. D., Moschetti, M. P., Powers, P. M., Mueller, C. S., Haller, K. M., Frankel, A. D., and Olsen, A. H. (2015). "The 2014 United States National Seismic Hazard Model," *Earthquake Spectra*, 31(1_suppl), S1–S30, https://doi.org/10.1193/120814EQS210M.

Pezeshk, S., Zandieh, A., and Tavakoli, B. (2011). "Hybrid Empirical Ground-Motion Prediction Equations for Eastern North America Using NGA Models and Updated Seismological Parameters," *Bull. Seismol. Soc. Amer.* 101: 1,859–1,870, doi:10.1785/0120100144.

Prodehl, C., Schlittenhardt, J., and Stewart, S.W. (1984). "Crystal Structure of the Appalachian Highlands in Tennessee," *Tectonophysics* 109, no 1-2: 61-76.

Ramirez-Guzman, L., Boyd, O. S., Hartzell, S., and Williams, R. A. (2012). "Seismic Velocity Model of the Central United States (Version 1): Description and Simulation of the 18 April 2008 Mt. Carmel, Illinois Earthquake," *Bull. Seismol. Soc. Amer.* 102 no. 6: 2622-2645, doi:10.1785/0120110303.

Rathje, E. M., Kottke, A. R., and Trent, W. L. (2010). "Influence of Input Motion and Site Property Variabilities on Seismic Site Response Analysis," *Journal of Geotechnical and Geoenvironmental Engineering* 607.

Reed, David, "Map of Arkansas' six major natural geographic divisions", n.d., https://encyclopediaofarkansas.net/media/arkansas-natural-divisions-6333/

Rix, G.J., and S. Romero-Hudock. (2006). "Liquefaction Potential Mapping in Memphis and Shelby County, Tennessee." *USGS Report*.

Schnable, P.B., J. Lysmer, and H.B. Seed. (1972). "SHAKE91, a Computer Program for Earthquake Response Analysis of Horizontally Layered Sites," Report No. EERC 72-12, University of California, Berkeley, California.

Silva, W.J., Abrahamson, N., Toro, G., and Costantino, C. (1996). "Description and Validation of the Stochastic Ground Motion Model", Report Submitted to Brookhaven National Laboratory, Associated Universities, Inc.

Silva, W., Gregor, N., and Darragh, R. (November 1, 2002). "Development of Regional Hard Rock Attenuation Relations for Central and Eastern North America," Pacific Engineering and Analysis Technical Report: 57.

Smith, R.M, "Geology Map," in The Atlas of Arkansas, University of Arkansas Press, 1989, United States Department of Agriculture Forest Service. https://www.fs.usda.gov/detail/ouachita/learning/nature-science/?cid=fsm9_039800

Somerville, P., Collins, N., Abrahamson, N., Graves, R., and Saikia, C. (June 30, 2001): "Ground Motion Attenuation Relations for the Central and Eastern United States—Final report, June 30, 2001: Technical Report to U.S. Geological Survey, Reston, Virginia, under Contract 99HQGR0098: 38.

South Carolina Department of Transportation. (June 2010). "Geotechnical Design Manual." https://www.scdot.org/business/pdf/geotech/archive/2010_Geotechnical_Design_Manual-Complete.pdf

Stewart, S. W. (1968). "Crustal structure in Missouri by seismic-refraction methods," *Bull. Seismol. Soc. Amer.* 58: 291-323.

Stephenson, W. J., R. A. Williams, J. K. Odum, and D. M.Worley. (2005). "Comparison of ReMi, MASW Shear-Wave Velocity Techniques with the CCOC Borehole to 100m", U.S. Geological Survey Open-File Report.

Tavakoli, B., and Pezeshk, S. (2005). "Empirical-stochastic ground-motion prediction for eastern North America,'" *Bull. Seismol. Soc. Amer.* 95: 2283–2296.

Teague, D.P., B.R. Cox, and E.M. Rathje. (2018). "Measured vs. predicted site response at the Garner Valley downhole array considering shear-wave velocity uncertainty from borehole and surface wave methods." *Soil Dynamics and Earthquake Engineering* 113: 339–355.

Thorson, J. R., and J. F. Claerbout. (1985). "Velocity-Stack and Slant-Stack Stochastic Inversion," *Journal of Geophysics* 50, no. 12: 2727–2741.

Toro, G., Abrahamson, N., and Schneider, J.F. (1997). "Model of Strong Ground Motions from Earthquake in Central and Eastern North America—Best Estimates and Uncertainties," *Seismol. Res. Lett*. 68 : 41–57.

Toro, G. (1996). "Probabilistic Models of Site Velocity Profiles for Generic and Site-Specific Ground Motion Amplification Studies," Published as an appendix in Silva et al.

Utah Department of Transportation. (January 2014). "Geotechnical Manual of Instruction." https://www.udot.utah.gov/main/uconowner.gf?n=36968203515699623

Virginia Department of Transportation. (October 2019). "Chapter III: Geotechnical Engineering," Materials Division Documents and Downloads. http://www.virginiadot.org/business/resources/Materials/bu-mat-MOI-III.pdf

Walling, M., Silva,W., and Abrahamson, N. (2008). "Nonlinear Site Amplification Factors for Constraining the NGA Models." *Earthquake Spectra* 24, no. 1: 243-255.

Washington State Department of Transportation. (January 2010). "Geotechnical Design Manual: M 46-03.01." https://dot.ca.gov/-/media/dot-media/programs/engineering/documents/geotechnical-services/geotechnical-investigations-july2017r1-a11y.pdf

Washington State Department of Transportation. (January 2010). "Geotechnical Design Manual: M 46-03.01." https://www.wsdot.wa.gov/publications/manuals/fulltext/M46-03/M46-03.01Complete.pdf

Wood, C.M., E. Baker, M. Deschenes, and A.K. Himel. (2019). "Deep Shear Wave Velocity Profiling in Northeastern, Arkansas." TRC1603*,* ARDOT Final Report.

# APPENDIX A. PROCESSED SITES

This appendix includes the test results of the investigated sites. For each site, a table is provided that includes the job number, longitude and latitude, and the county information. In addition, a GIS map is provided showing the location of the site, along with a Google map of the site, a table providing the determined shear-wave velocity profile, a figure showing the shear-wave velocity profile, and a figure showing the dispersion curves obtained using MASW and ReMi.

The inversion results for the fundamental mode are provided by red lines in figures and red headers in tables. We provided inversion results for higher modes if we detected a higher mode and successfully inverted the data. These are marked with orange lines in figures and orange headers in tables.

Dispersion curves are provided for ReMi and MASW. The gray lines with triangles and orange lines with rectangles are dispersion curve picks for the lower margin and middle picks of the ReMi overtone image. Blue triangles represent the dispersion picks for the MASW. If higher modes are detected, more than one curve is drawn in the figures. Figure A-81 includes shear-wave velocity profiles for all 20 tested sites.

**Table A-1. Site 1 Information**

| Site No. | Job Number | Latitude | Longitude | COUNTY |
|---|---|---|---|---|
| 1 | 110390 | 35.012362 | -90.628147 | St. Francis |

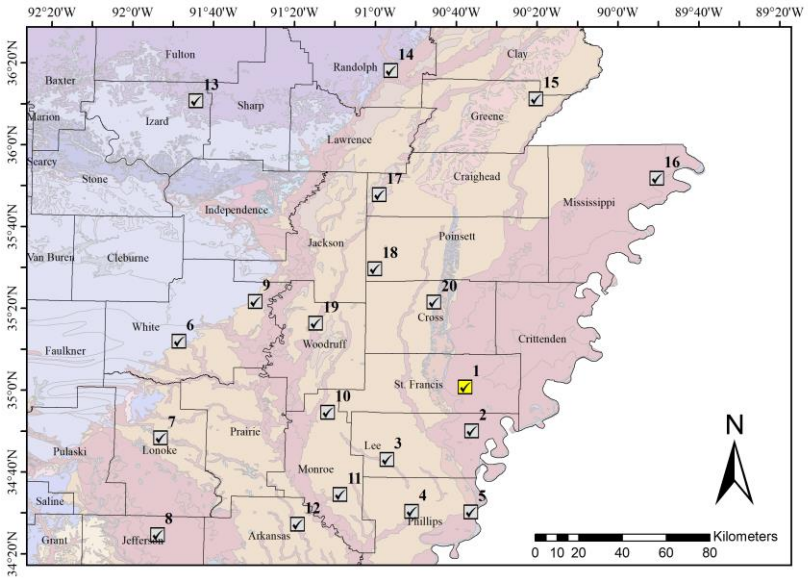


**Figure A-1. The Location of Site 1 is Highlighted in Yellow**


**Figure A-2. The Location of ReMi and MASW Lines is Highlighted in Yellow for Site 1**

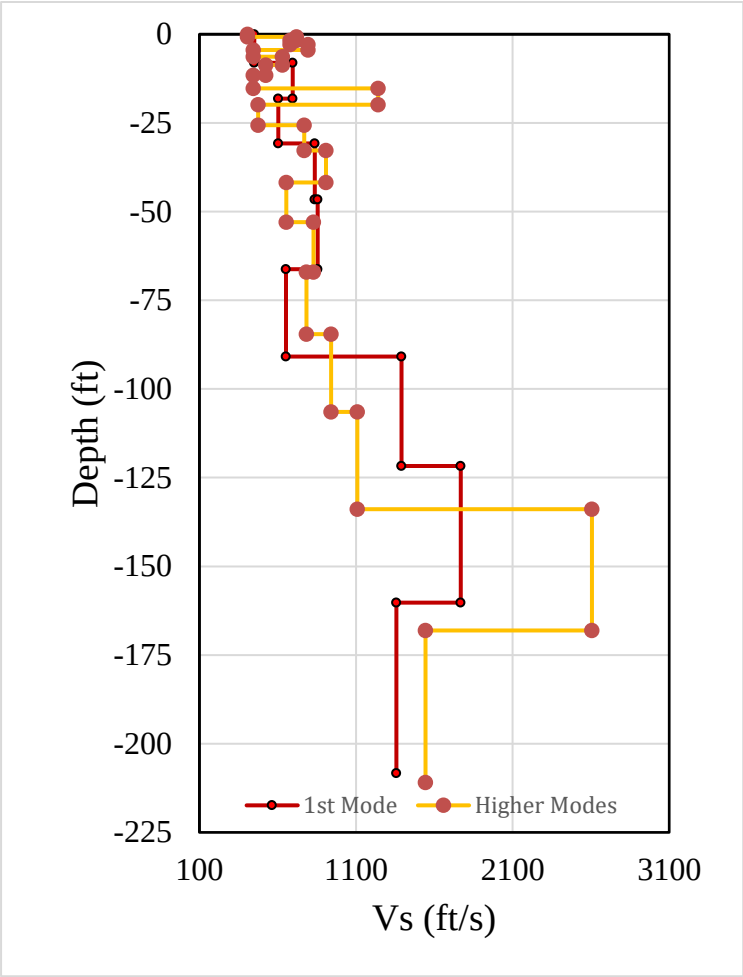


**Figure A-3. The Velocity Profile of Site 1**

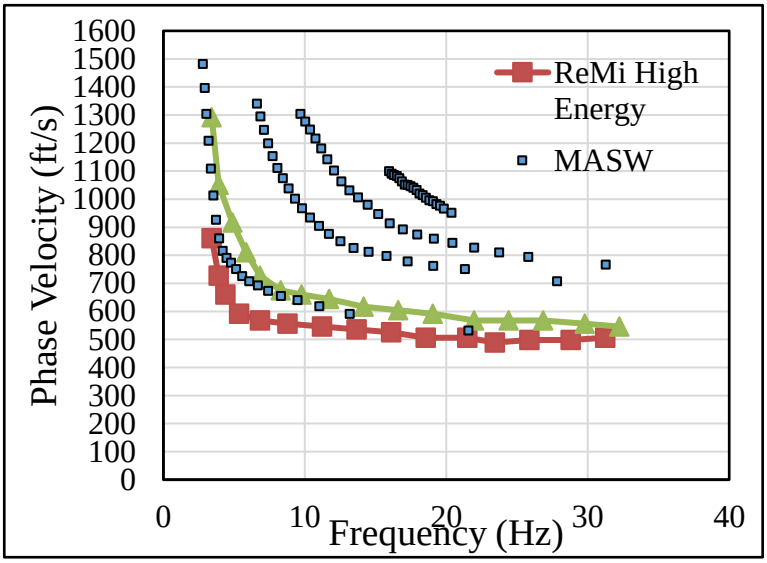


**Figure A-4. The Dispersion Curves Obtained at Site 1**

**Table A-2. Velocity Profile of Fundamental and Higher Modes for Site 1**

| 1st Mode | | Higher Modes | |
|---|---|---|---|
| Depth (ft) | Vs (ft/s) | Depth (ft) | Vs (ft/s) |
| -8.2 | 449 | -0.7 | 407 |
| -18.0 | 696 | -1.6 | 722 |
| -30.8 | 604 | -3.0 | 679 |
| -46.6 | 837 | -4.6 | 794 |
| -66.3 | 856 | -6.2 | 443 |
| -90.9 | 653 | -8.5 | 630 |
| -121.7 | 1391 | -11.5 | 525 |
| -160.1 | 1768 | -15.4 | 446 |
| -208.3 | 1358 | -20.0 | 1243 |
| | | -25.6 | 476 |
| | | -32.8 | 768 |
| | | -41.7 | 909 |
| | | -53.1 | 653 |
| | | -66.9 | 830 |
| | | -84.6 | 784 |
| | | -106.6 | 942 |
| | | -133.9 | 1109 |
| | | -168.0 | 2605 |
| | | -211.0 | 1542 |

**Table A-3. Site 2 Information**

| Site No. | Job Number | Latitude | Longitude | COUNTY |
|---|---|---|---|---|
| 2 | 110570 | 34.8326 | -90.602976 | Lee |

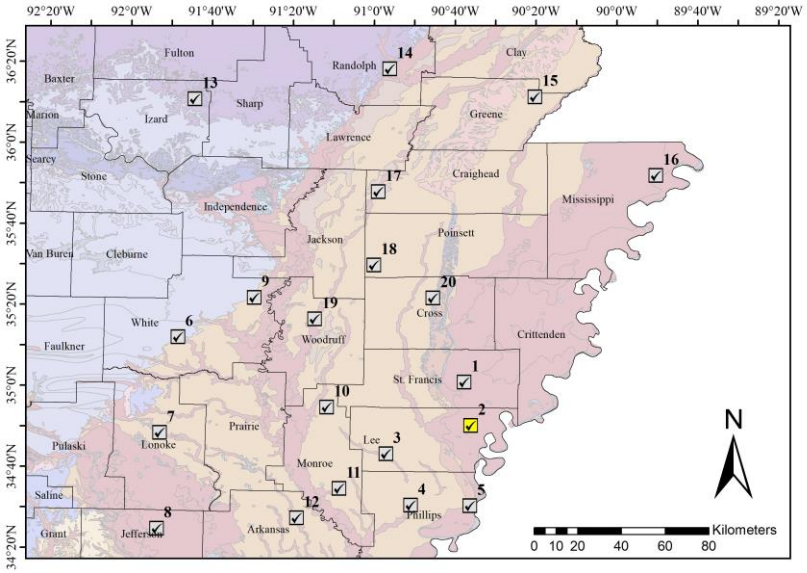


**Figure A-5. The Location of Site 2 is Highlighted in Yellow**


**Figure A-6. The Location of ReMi and MASW Lines is Highlighted in Yellow for Site 2**

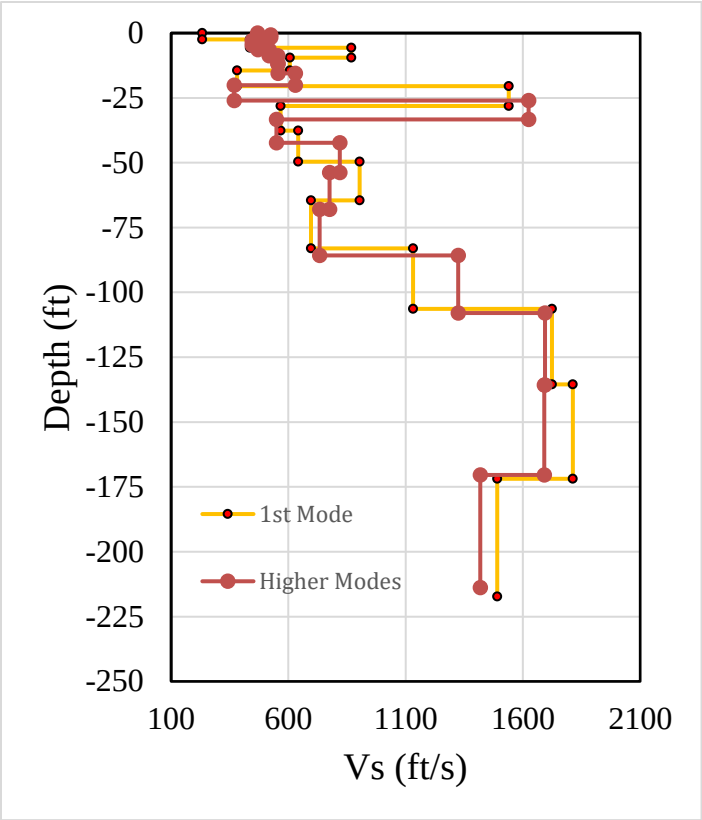


**Figure A-7. The Velocity Profile of Site 2**

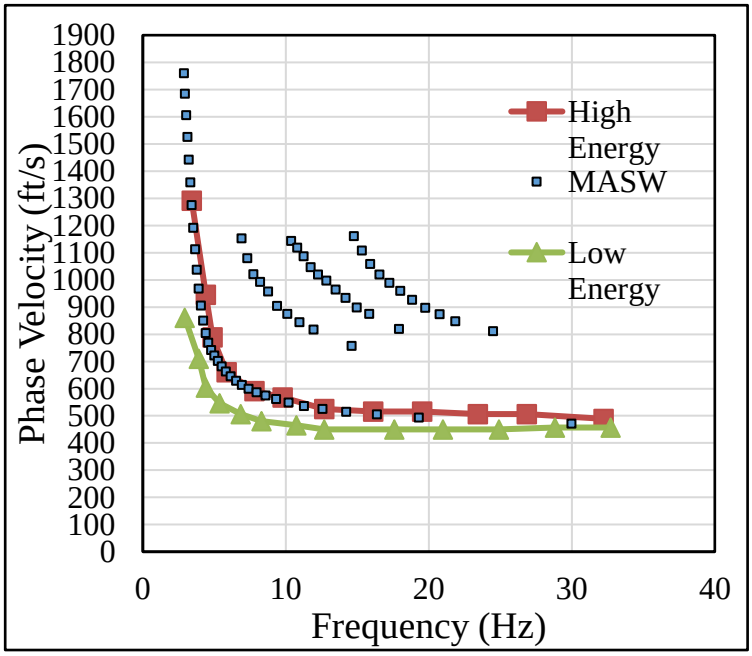


**Figure A-8. The Dispersion Curves Obtained at Site 2**

**Table A-4. Velocity Profile of Fundamental and Higher Modes for Site 2**

| 1st Mode | | Higher Modes | |
|---|---|---|---|
| Depth (ft) | Vs (ft/s) | Depth (ft) | Vs (ft/s) |
| -3 | 233 | -1 | 469 |
| -6 | 436 | -2 | 525 |
| -10 | 869 | -3 | 472 |
| -14 | 607 | -5 | 446 |
| -21 | 381 | -7 | 469 |
| -28 | 1539 | -9 | 518 |
| -38 | 568 | -12 | 554 |
| -50 | 643 | -15 | 554 |
| -65 | 902 | -20 | 630 |
| -83 | 696 | -26 | 367 |
| -106 | 1132 | -33 | 1624 |
| -135 | 1722 | -42 | 548 |
| -172 | 1814 | -54 | 820 |
| -217 | 1490 | -68 | 774 |
| -272 | 2562 | -86 | 735 |
| | | -108 | 1322 |
| | | -136 | 1693 |
| | | -170 | 1690 |
| | | -214 | 1417 |
| | | -267 | 2687 |

**Table A-5. Site 3 Information**

| Site No. | Job Number | Latitude | Longitude | COUNTY |
|---|---|---|---|---|
| 3 | 110616 | 34.705475 | -90.959335 | Lee |

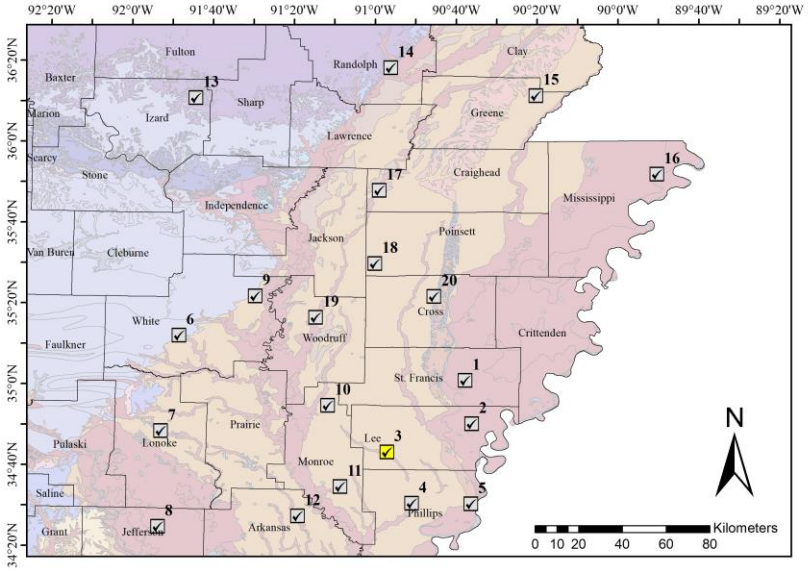


**Figure A.9. The Location of Site 3 is Highlighted in Yellow**


**Figure A-10. The Location of ReMi and MASW Lines is Highlighted in Yellow for Site 3**

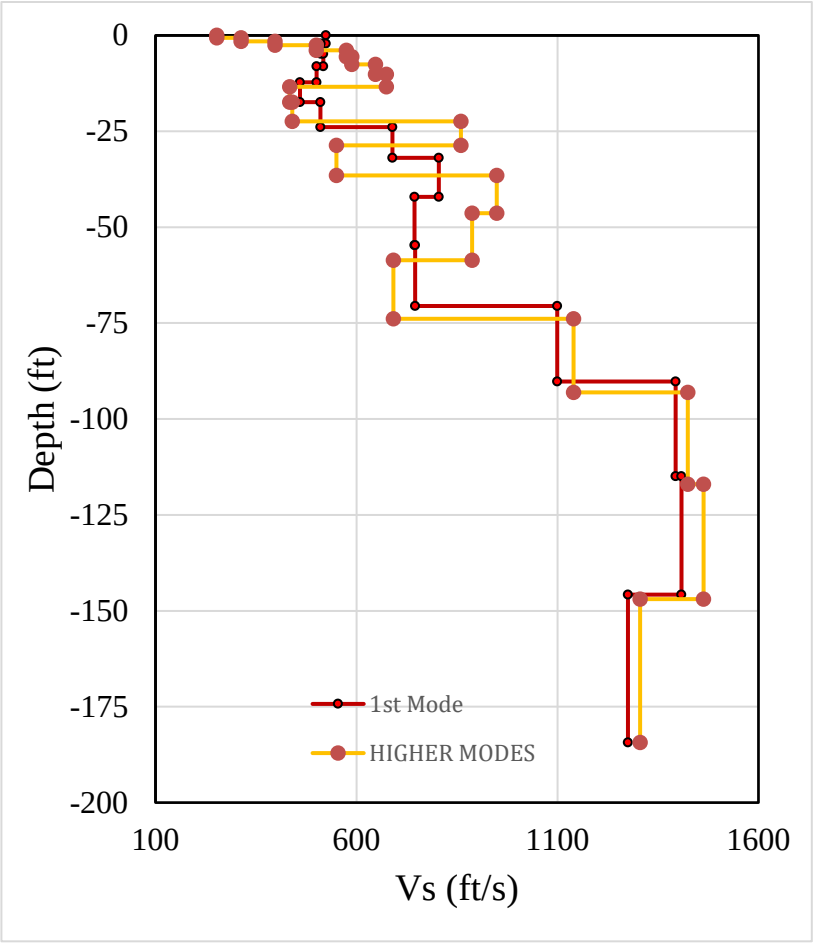


**Figure A-11. The Velocity Profile of Site 3**

**Table A-6. Velocity Profile of Fundamental and Higher Modes for Site 3**

| 1st Mode | | Higher Modes | |
|---|---|---|---|
| Depth (ft) | Vs (ft/s) | Depth (ft) | Vs (ft/s) |
| -2 | 525 | -1 | 253 |
| -5 | 512 | -2 | 312 |
| -8 | 518 | -3 | 397 |
| -12 | 502 | -4 | 499 |
| -17 | 459 | -6 | 574 |
| -24 | 512 | -8 | 587 |
| -32 | 689 | -10 | 646 |
| -42 | 804 | -13 | 676 |
| -55 | 745 | -17 | 433 |
| -71 | 745 | -22 | 440 |
| -90 | 1099 | -29 | 860 |
| -115 | 1394 | -36 | 551 |
| -146 | 1407 | -46 | 948 |
| -184 | 1276 | -59 | 889 |
| -230 | 2260 | -74 | 692 |
| | | -93 | 1138 |
| | | -117 | 1424 |
| | | -147 | 1463 |
| | | -184 | 1306 |
| | | -230 | 2172 |

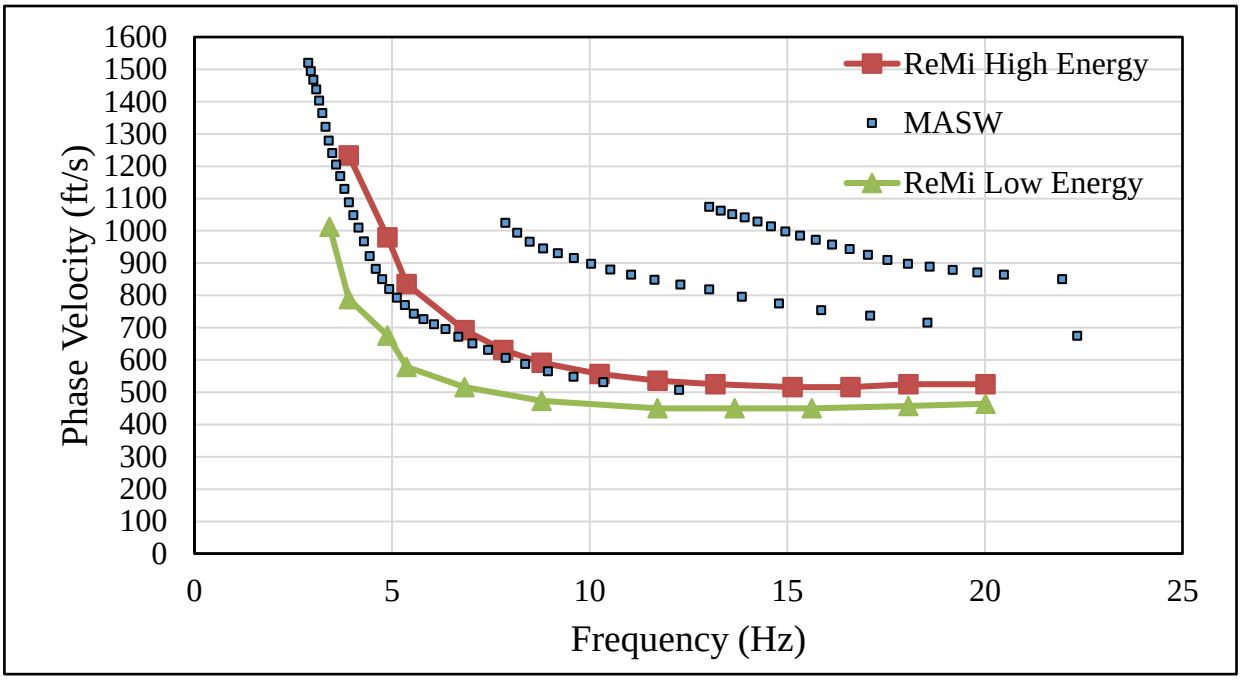


**Figure A-12. The Dispersion Curves Obtained at Site 3**

**Table A-7. Site 4 Information**

| Site No. | Job Number | Latitude | Longitude | COUNTY |
|---|---|---|---|---|
| 4 | FA5415 | 34.505615 | -90.850347 | Phillips |

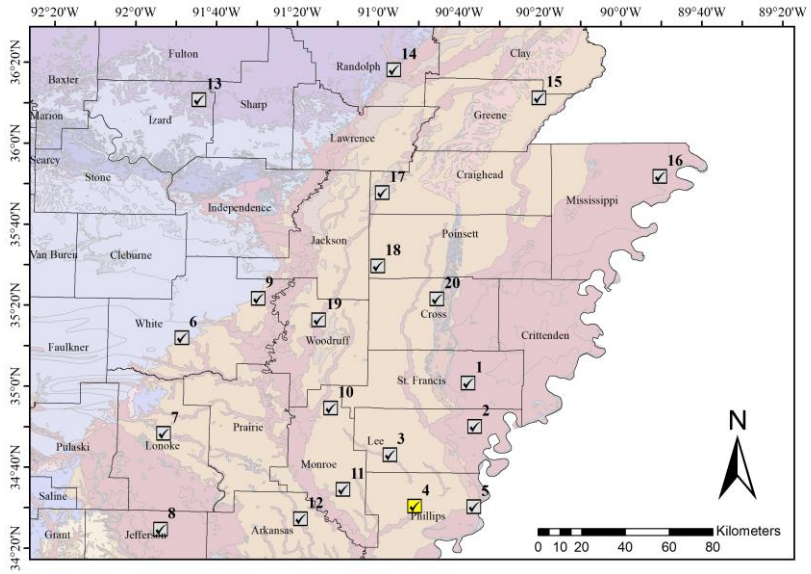


**Figure A-13. The Location of Site 4 is Highlighted in Yellow**


**Figure A-14. The Location of ReMi and MASW Lines is Highlighted in Yellow for Site 4**

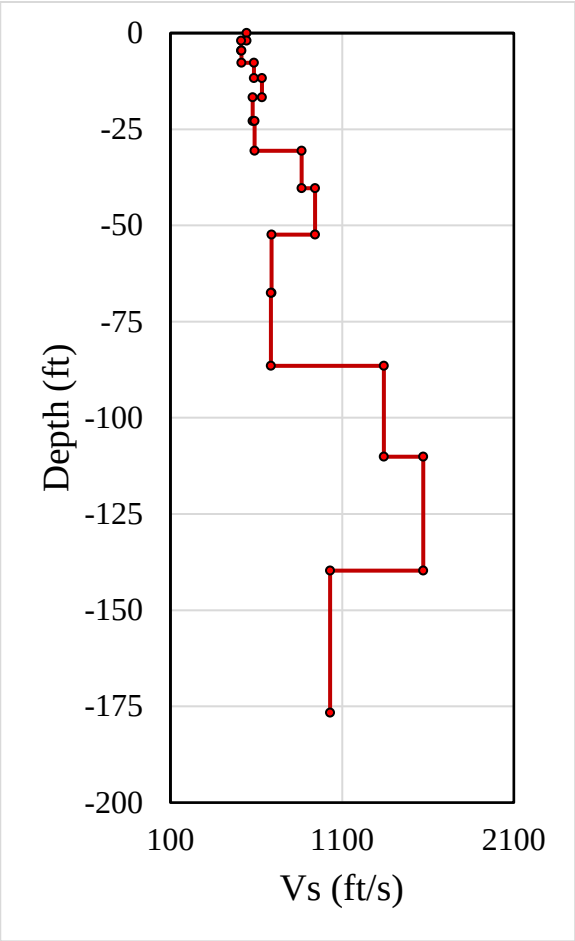


**Figure A-15. The Velocity Profile of Site 4**

**Table A.8. Velocity Profile of Fundamental and Higher Modes for Site 4. Higher modes were not detected.**

| 1st Mode | |
|---|---|
| Depth (ft) | Vs (ft/s) |
| -6 | 403 |
| -14 | 608 |
| -24 | 701 |
| -37 | 577 |
| -52 | 936 |
| -71 | 813 |
| -95 | 837 |
| -126 | 2094 |
| -163 | 2095 |
| -204 | 1591 |

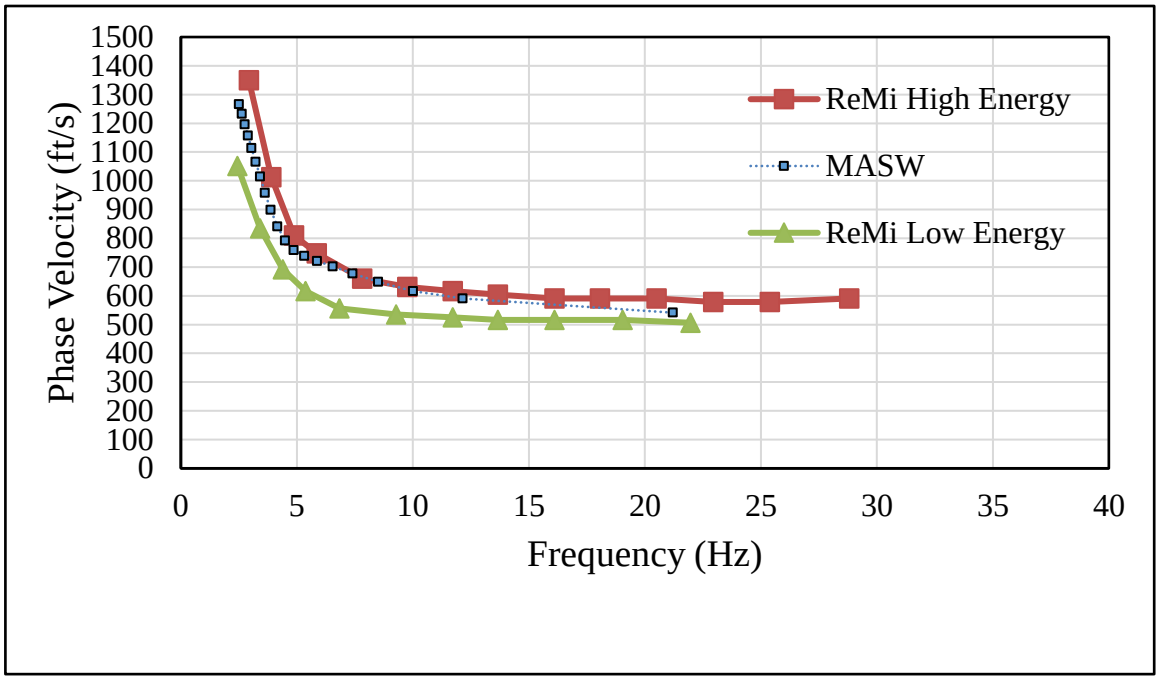


**Figure A-16. The Dispersion Curves Obtained at Site 4**

**Table A-9. Site 5 Information**

| Site No. | Job Number | Latitude | Longitude | COUNTY |
|---|---|---|---|---|
| **5** | 110536 | 34.50300 | -90.60545 | Phillips |

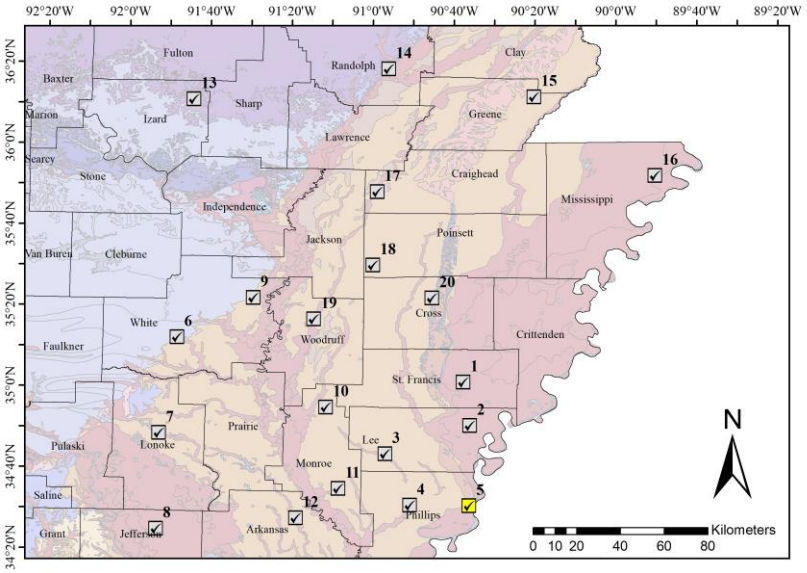


**Figure A-17. The Location of Site 5 is Highlighted in Yellow**


**Figure A-18. The Location of ReMi and MASW Lines is Highlighted in Yellow for Site 5**

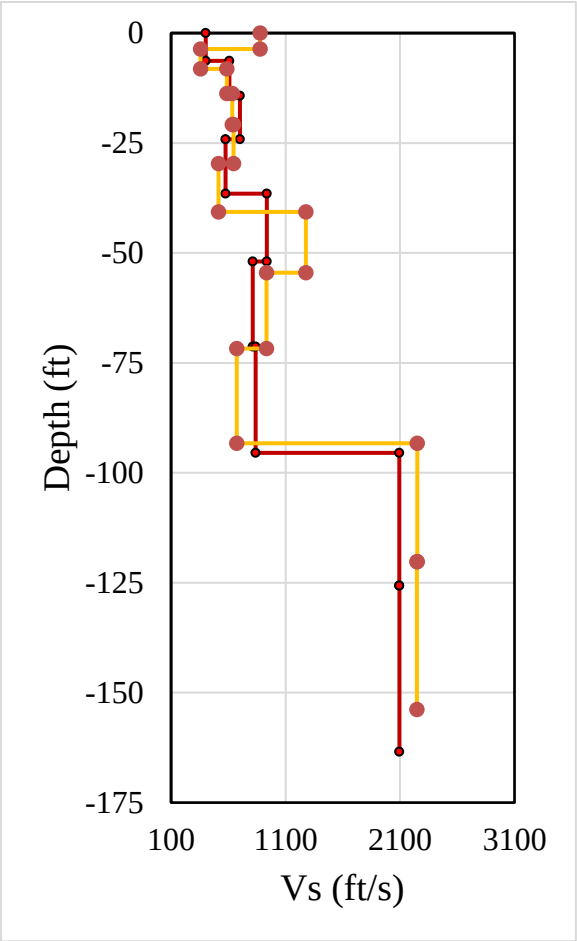


**Figure A-19. The Velocity Profile of Site 5**

**Table A-10. Velocity Profile of Fundamental and Higher Modes for Site 5**

| 1st Mode | | Higher Modes | |
|---|---|---|---|
| Depth (ft) | Vs (ft/s) | Depth (ft) | Vs (ft/s) |
| -6 | 403 | -4 | 878 |
| -14 | 608 | -8 | 358 |
| -24 | 701 | -14 | 588 |
| -36 | 577 | -21 | 635 |
| -52 | 936 | -30 | 646 |
| -71 | 813 | -41 | 515 |
| -95 | 837 | -54 | 1278 |
| -126 | 2094 | -72 | 934 |
| -163 | 2095 | -93 | 674 |
| | | -120 | 2251 |

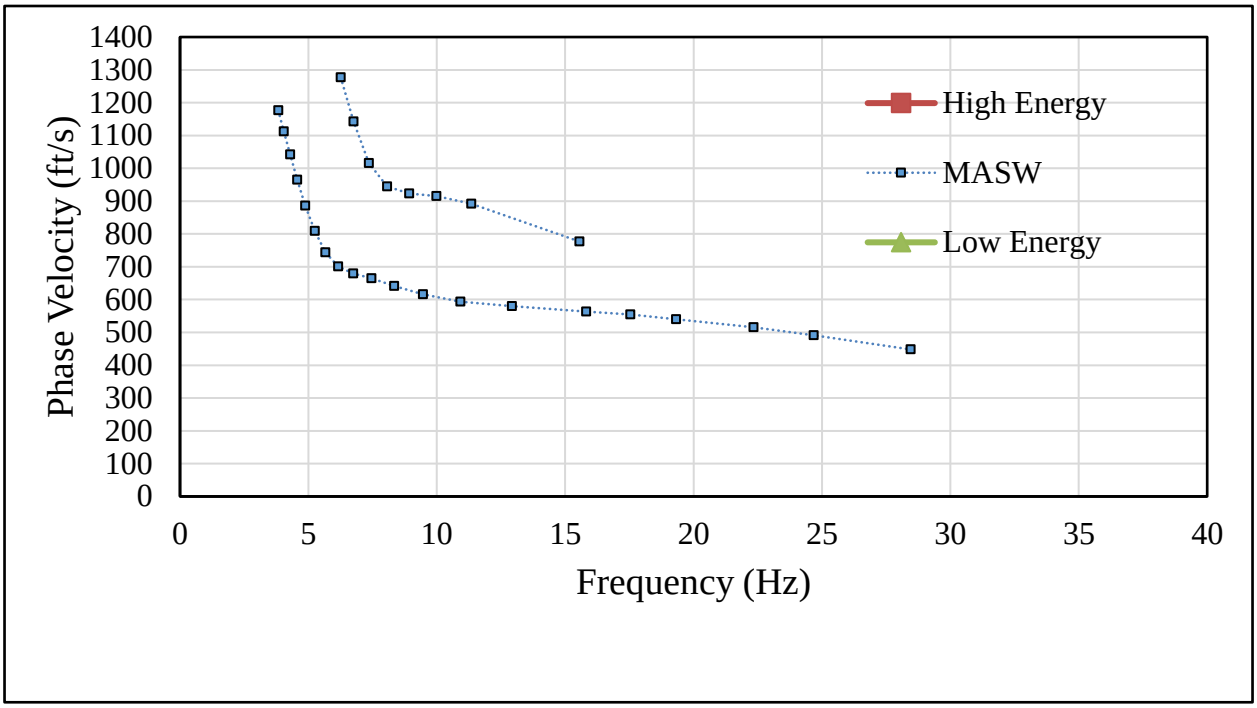


**Figure A-20. The Dispersion Curves Obtained at Site 5 (*ReMi Not Available)**

**Table A-11. Site 6 Information**

| Site No. | Job Number | Latitude | Longitude | COUNTY |
|---|---|---|---|---|
| 6 | 050189 | 35.200063 | -91.809054 | White |

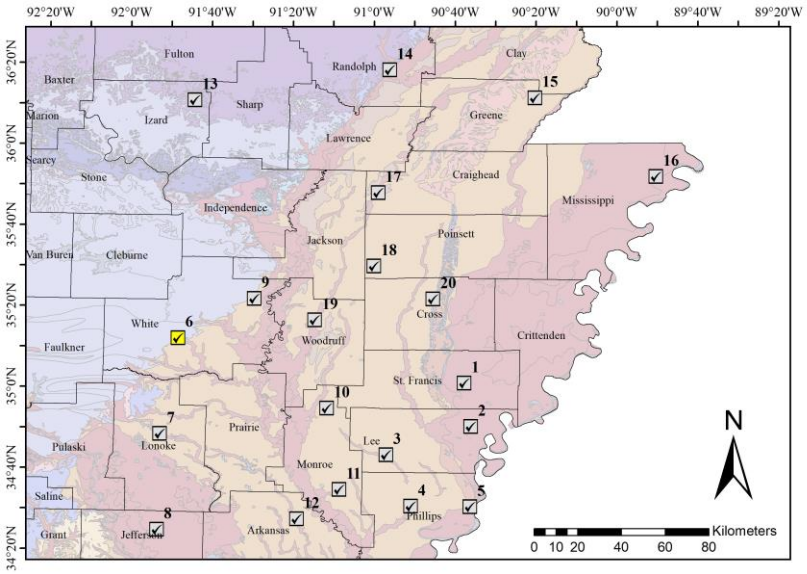


**Figure A-21. The Location of Site 6 is Highlighted in Yellow**


**Figure A-22. The Location of ReMi and MASW Lines is Highlighted in Yellow for Site 6**

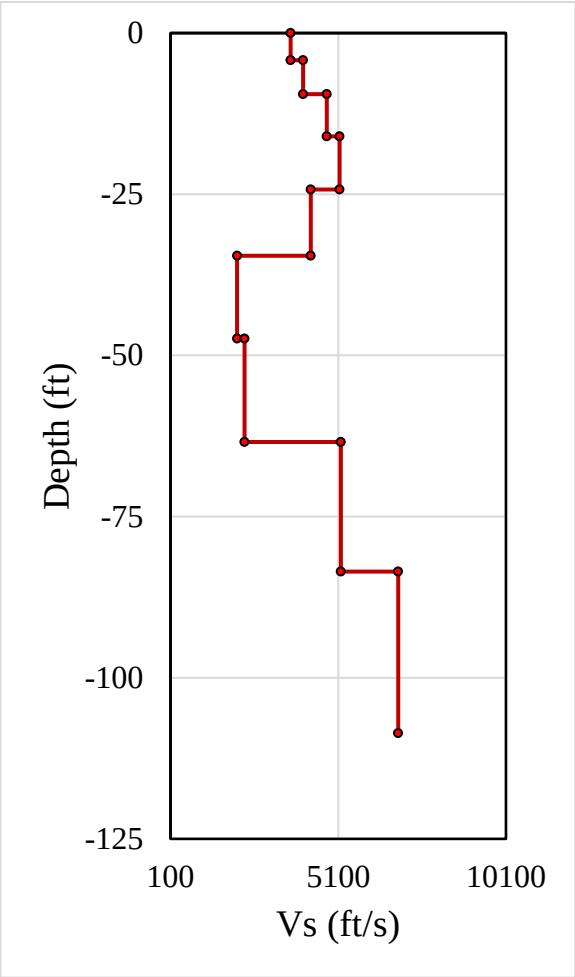


**Figure A-23. The Velocity Profile of Site 6**

**Table A-12. Velocity Profile of Fundamental and Higher Modes for Site 6. Higher modes were not detected**

| 1st Mode | |
|---|---|
| Depth (ft) | Vs (ft/s) |
| -4.21 | 3679 |
| -9.47 | 4054 |
| -16.05 | 4755 |
| -24.27 | 5135 |
| -34.55 | 4278 |
| -47.39 | 2083 |
| -63.45 | 2307 |
| -83.52 | 5174 |
| -108.61 | 6888 |
| -135.76 | 8855 |

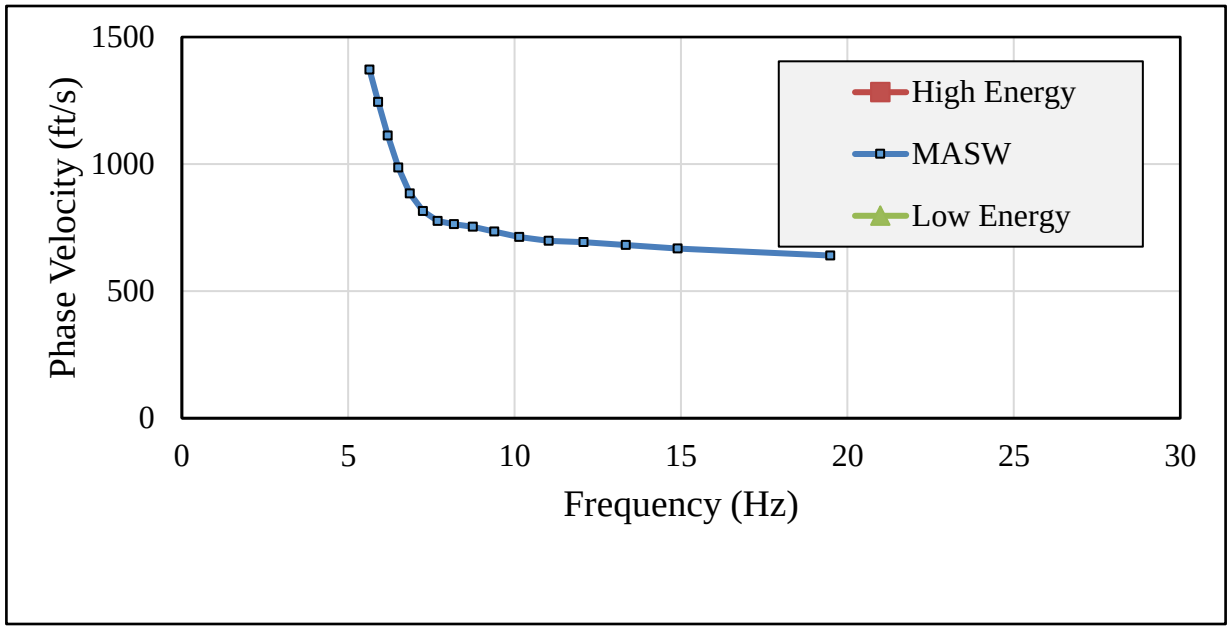


**Figure A-24. The Dispersion Curves Obtained at Site 6**

**Table A-13. Site 7 Information**

| Site No. | Job Number | Latitude | Longitude | COUNTY |
|---|---|---|---|---|
| 7 | F06233 | 34.804945 | -91.885759 | Lonoke |

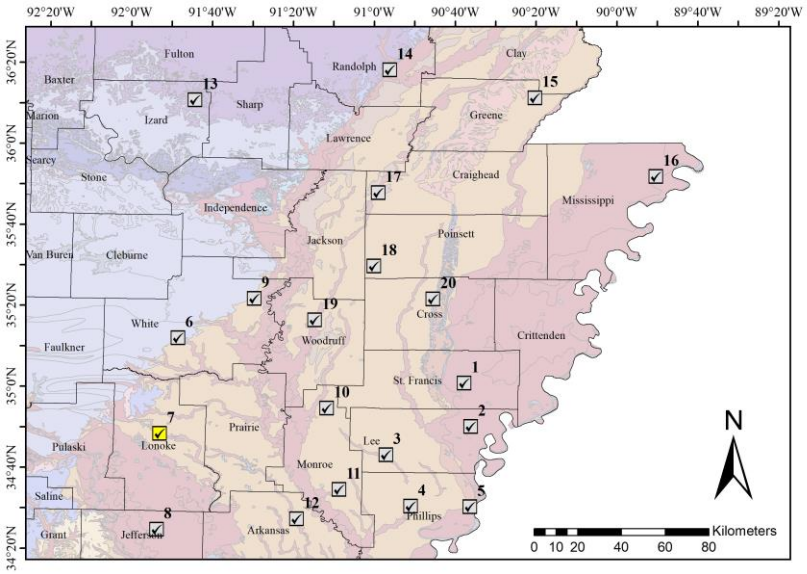


**Figure A-25. The Location of Site 7 is Highlighted in Yellow**


**Figure A-26. The Location of ReMi and MASW Lines is Highlighted in Yellow for Site 7**

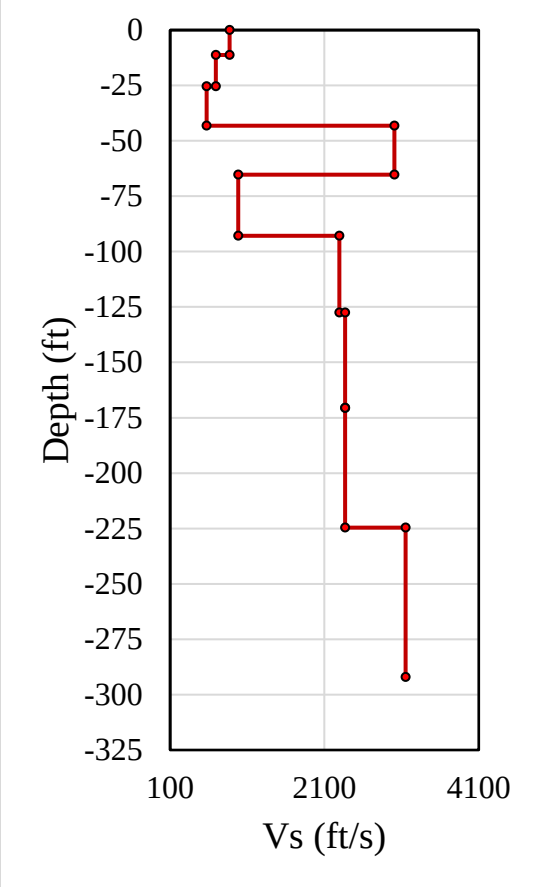


**Figure A-27. The Velocity Profile of Site 7**

**Table A-14. Velocity Profile of Fundamental and Higher Modes for Site 7. Higher modes were not detected**

| 1st Mode | |
|---|---|
| Depth (ft) | Vs (ft/s) |
| -11 | 873 |
| -26 | 689 |
| -43 | 574 |
| -65 | 3009 |
| -93 | 981 |
| -128 | 2293 |
| -171 | 2369 |
| -225 | 2365 |
| -292 | 3153 |

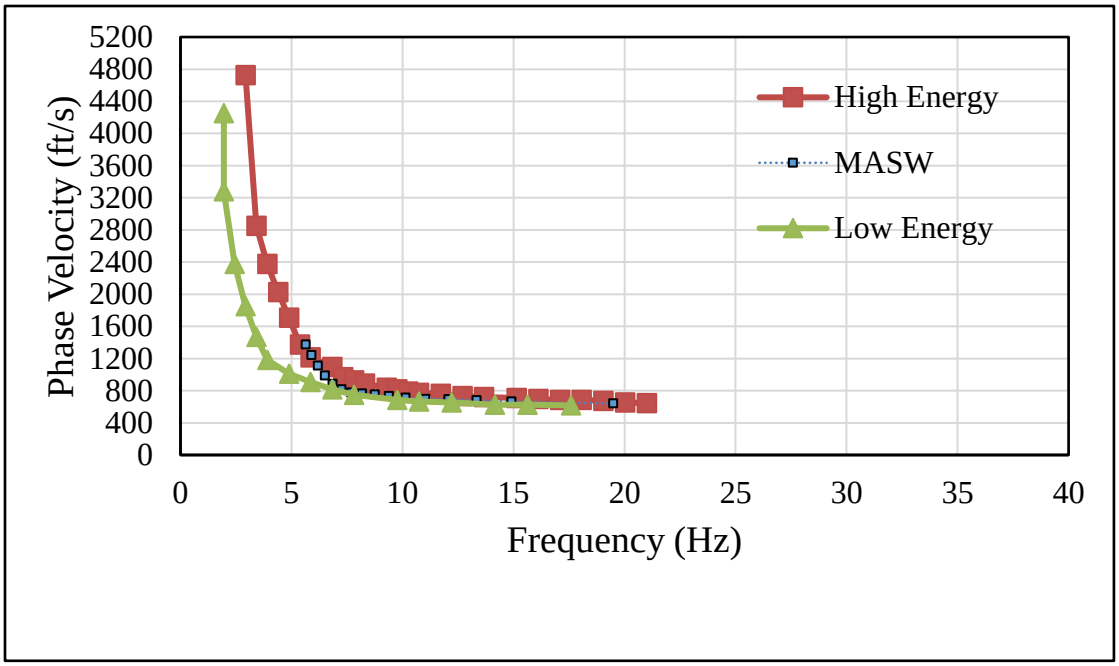


**Figure A-28. The Dispersion Curves Obtained at Site 7**

**Table A-15. Site 8 Information**

| Site No. | Job Number | Latitude | Longitude | COUNTY |
|---|---|---|---|---|
| 8 | 020047 | 34.411295 | -91.897552 | Jefferson |

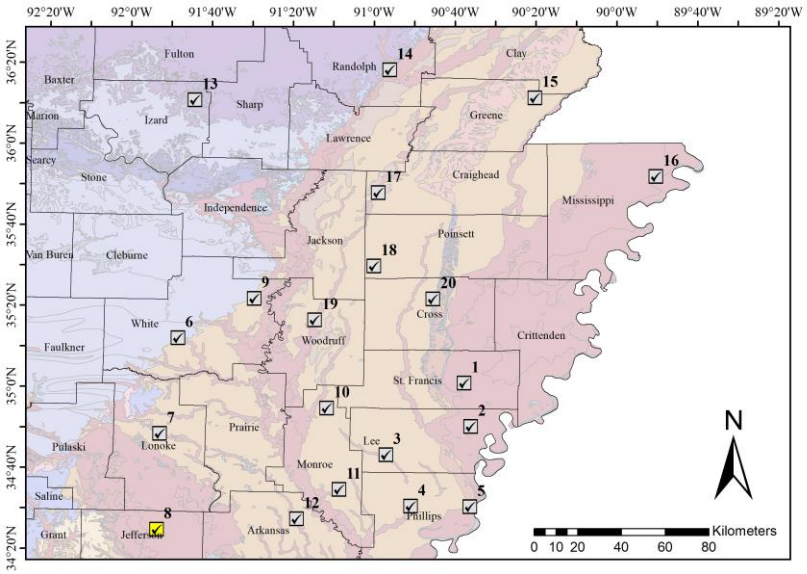


**Figure A-29. The Location of Site 8 is Highlighted in Yellow**

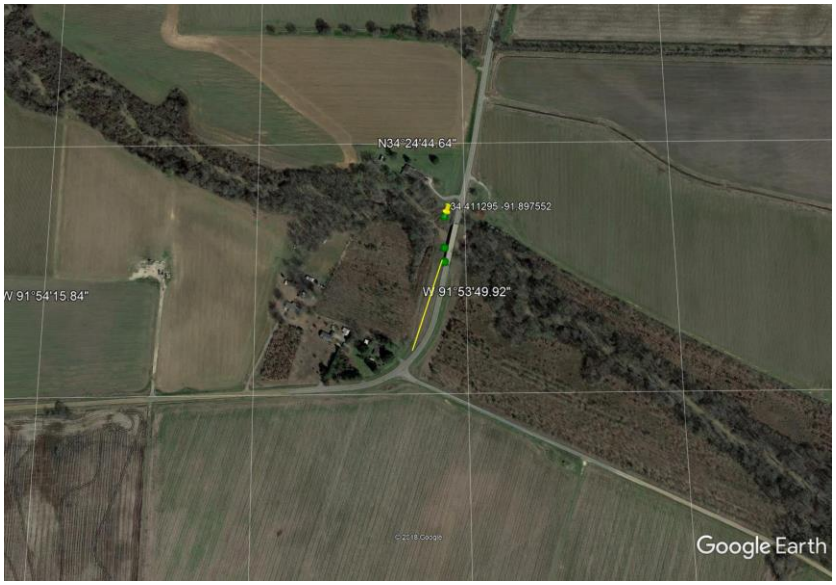


**Figure A-30. The Location of ReMi and MASW Lines is Highlighted in Yellow for Site 8**

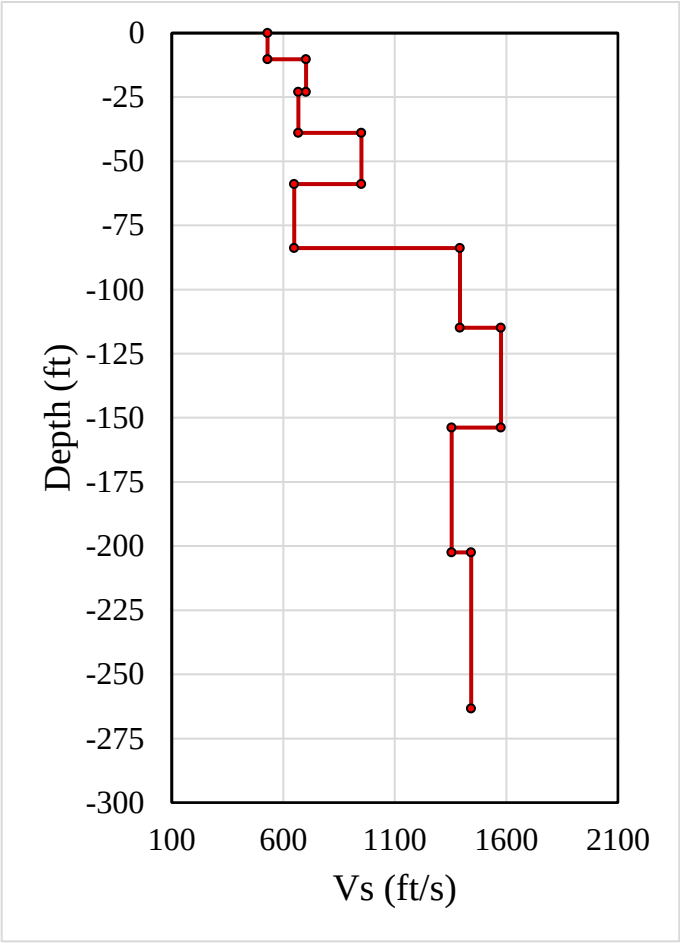


**Figure A-31. The Velocity Profile of Site 8**

**Table A-16. Velocity Profile of Fundamental and Higher Modes for Site 8. Higher modes were not detected**

| 1st Mode | |
|---|---|
| Depth(ft) | Vs (ft/s) |
| -10 | 528 |
| -23 | 702 |
| -39 | 666 |
| -59 | 948 |
| -84 | 650 |
| -115 | 1391 |
| -154 | 1575 |
| -202 | 1355 |
| -263 | 1440 |
| -329 | 2146 |

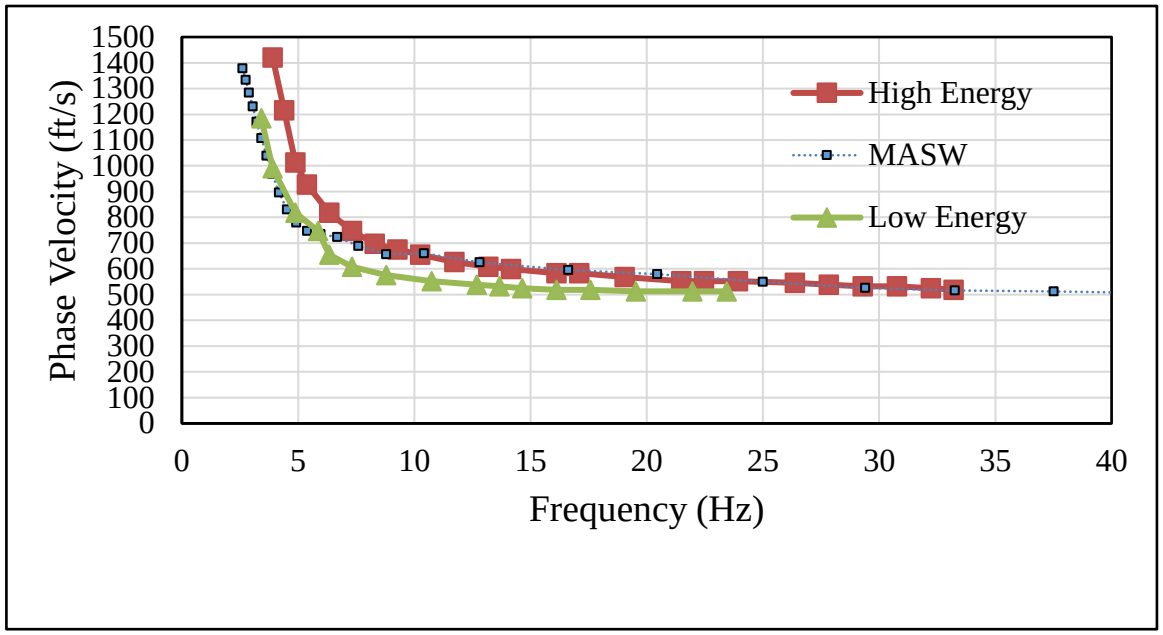


**Figure A-32. The Dispersion Curves Obtained at Site 8**

**Table A-17. Site 9 Information**

| Site No. | Job Number | Latitude | Longitude | COUNTY |
|---|---|---|---|---|
| 9 | FA7315 | 35.360437 | -91.495049 | White |

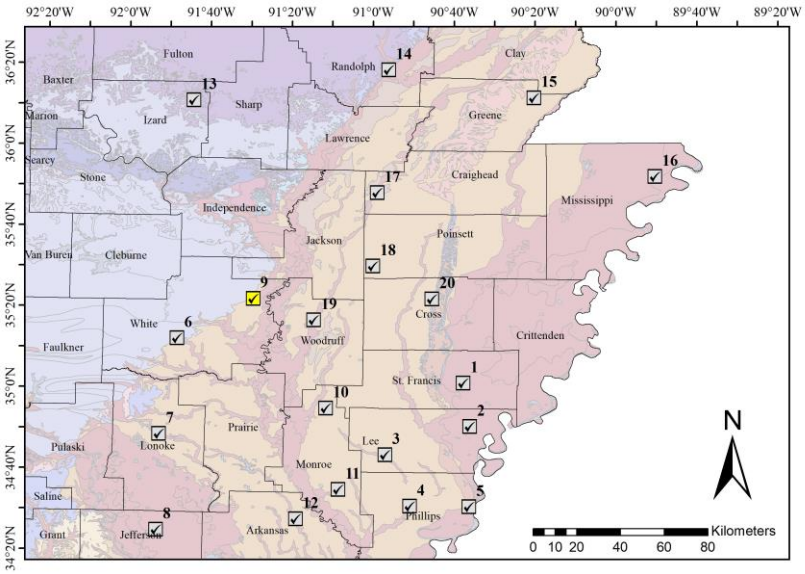


**Figure A-33. The Location of Site 9 is Highlighted in Yellow**


**Figure A-34. The Location of ReMi and MASW Lines is Highlighted in Yellow for Site 9**

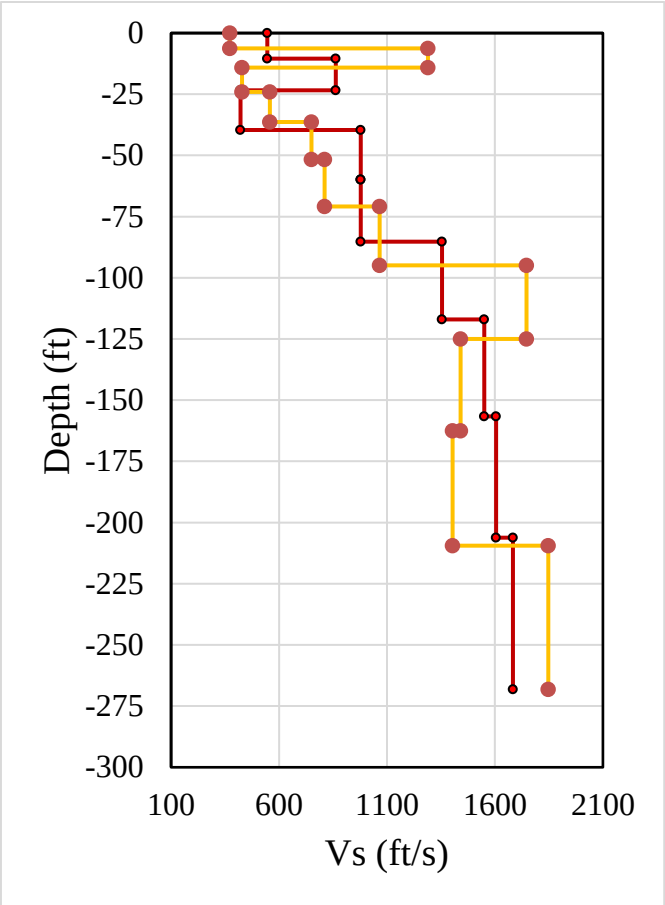


**Figure A-35. The Velocity Profile of Site 9**

**Table A-18. Velocity Profile of Fundamental and Higher Modes for Site 9**

| 1st Mode | | Higher Modes | |
|---|---|---|---|
| Depth (ft) | Vs (ft/s) | Depth (ft) | Vs (ft/s) |
| -10 | 546 | -6 | 372 |
| -23 | 863 | -14 | 1289 |
| -40 | 422 | -24 | 428 |
| -60 | 979 | -36 | 558 |
| -85 | 978 | -52 | 750 |
| -117 | 1355 | -71 | 810 |
| -157 | 1551 | -95 | 1067 |
| -206 | 1606 | -125 | 1747 |
| -268 | 1683 | -162 | 1441 |
| -335 | 2510 | -209 | 1403 |
| | | -268 | 1847 |
| | | -335 | 2545 |
| | | -6 | 372 |

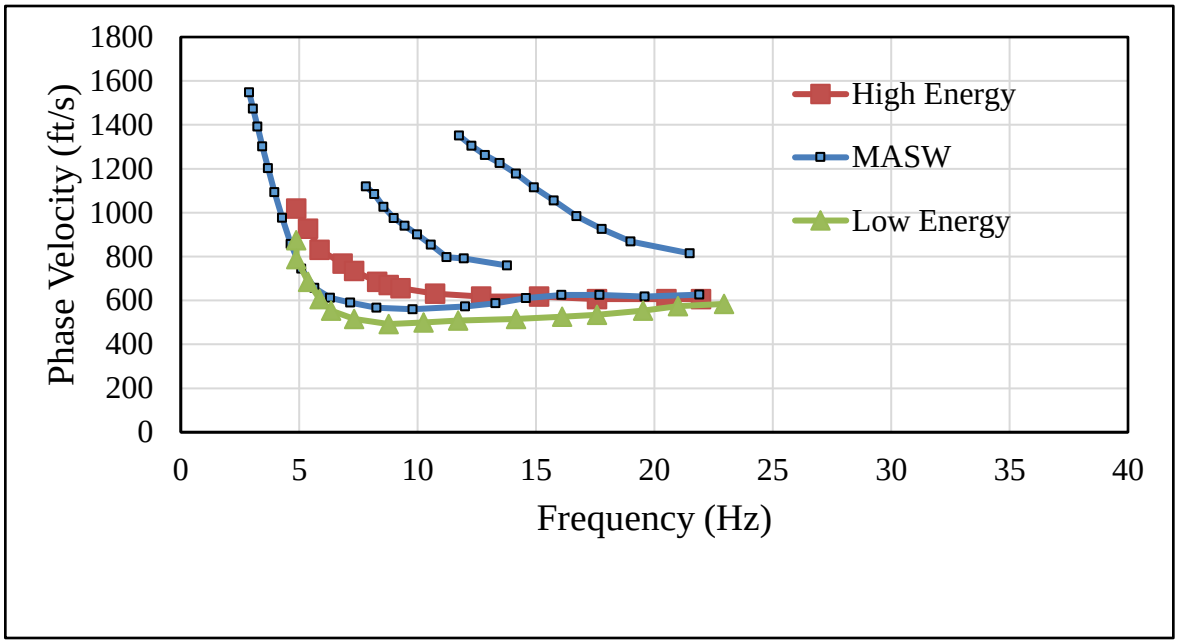


**Figure A-36. The Dispersion Curves Obtained at Site 9**

**Table A-19. Site 10 Information**

| Site No. | JobNumber | Latitude | Longitude | COUNTY |
|---|---|---|---|---|
| 10 | 110670 | 34.90926 | -91.1967 | Monroe |

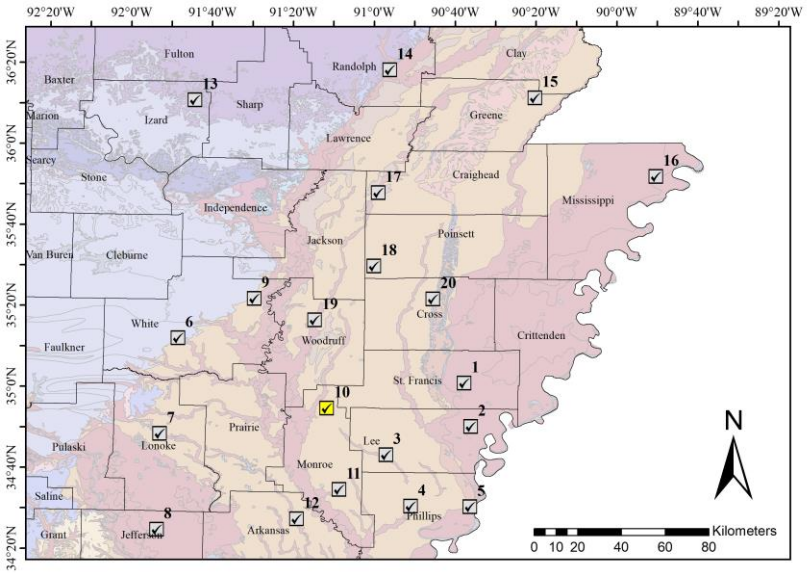


**Figure A-37. The Location of Site 10 is Highlighted in Yellow**


**Figure A-38. The Location of ReMi and MASW Lines is Highlighted in Yellow for Site 10**

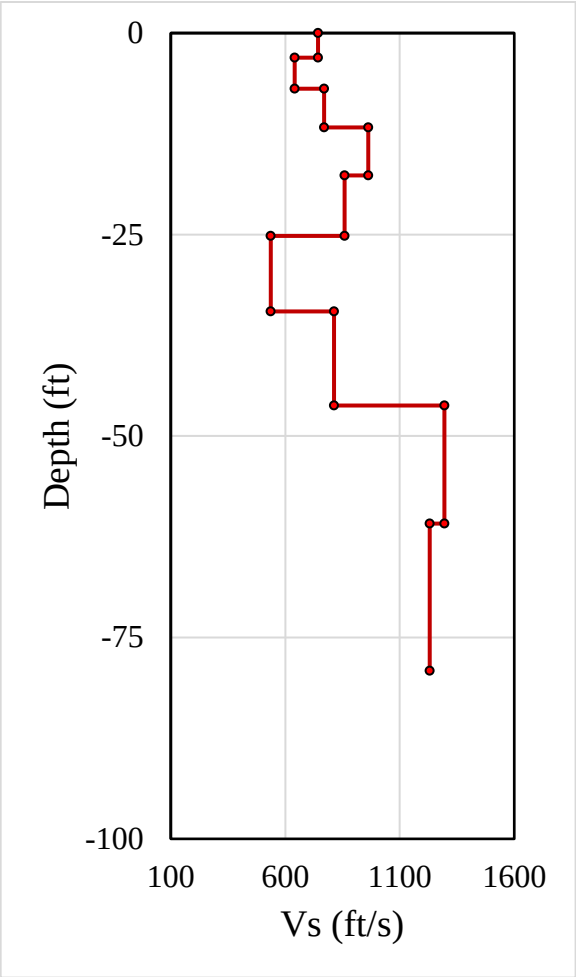


**Figure A-39. The Velocity Profile of Site 10**

**Table A-20. Velocity Profile of Fundamental and Higher Modes for Site 10. Higher modes were not detected**

| 1st Mode | |
|---|---|
| Depth(ft) | Vs (ft/s) |
| -3 | 743 |
| -7 | 640 |
| -12 | 770 |
| -18 | 962 |
| -25 | 860 |
| -35 | 537 |
| -46 | 813 |
| -61 | 1295 |
| -79 | 1231 |
| -99 | 1177 |

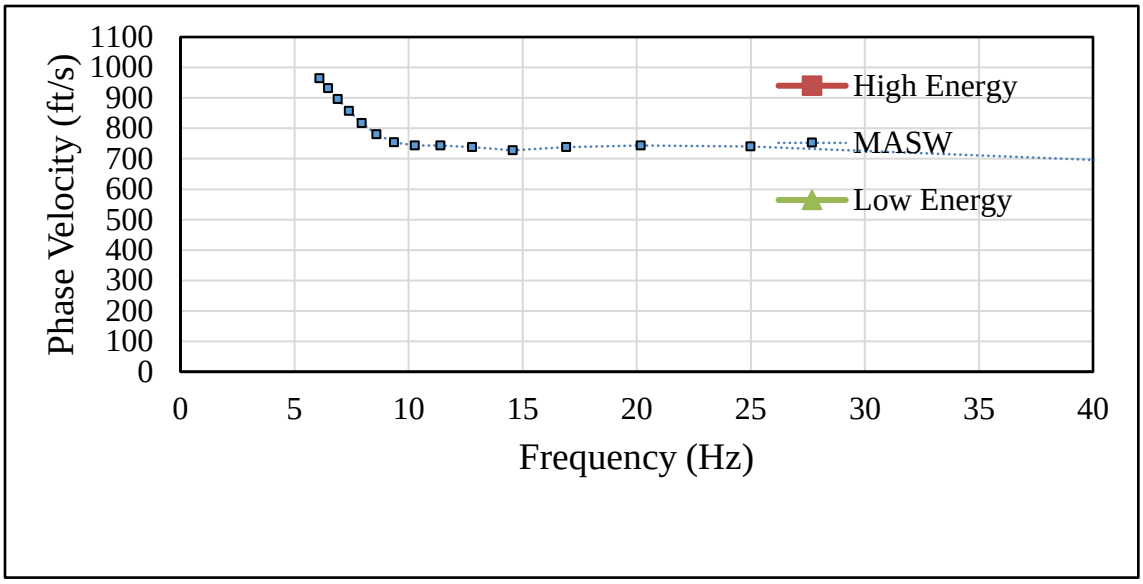


**Figure A-40. The Dispersion Curves Obtained at Site 10**

**Table A-21. Site 11 Information**

| Site No. | Job Number | Latitude | Longitude | COUNTY |
|---|---|---|---|---|
| 11 | 110391 | 34.57475 | -91.146135 | Monroe |

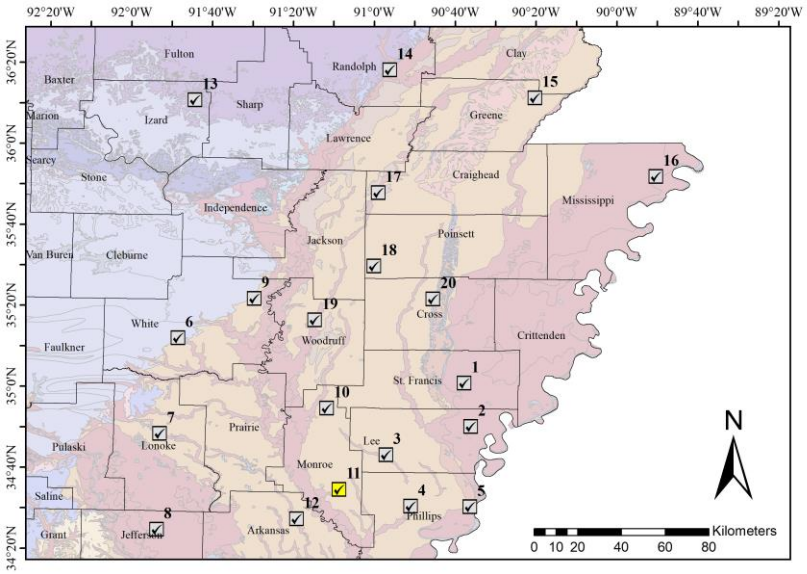


**Figure A-41. The Location of Site 11 is Highlighted in Yellow**


**Figure A-42. The Location of ReMi and MASW Lines is Highlighted in Yellow for Site 11**

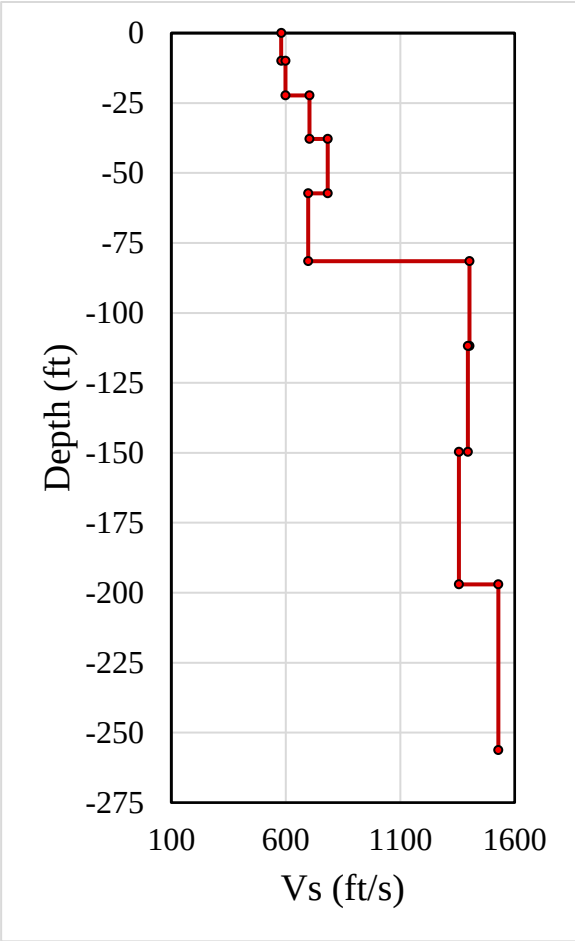


**Figure A-43. The Velocity Profile of Site 11**

**Table A-22. Velocity Profile of Fundamental and Higher Modes for Site 11. Higher modes were not detected**

| 1st Mode | |
|---|---|
| Depth (ft) | Vs (ft/s) |
| -10 | 581 |
| -22 | 600 |
| -38 | 702 |
| -57 | 784 |
| -81 | 699 |
| -112 | 1401 |
| -150 | 1394 |
| -197 | 1358 |
| -256 | 1529 |
| -320 | 2110 |

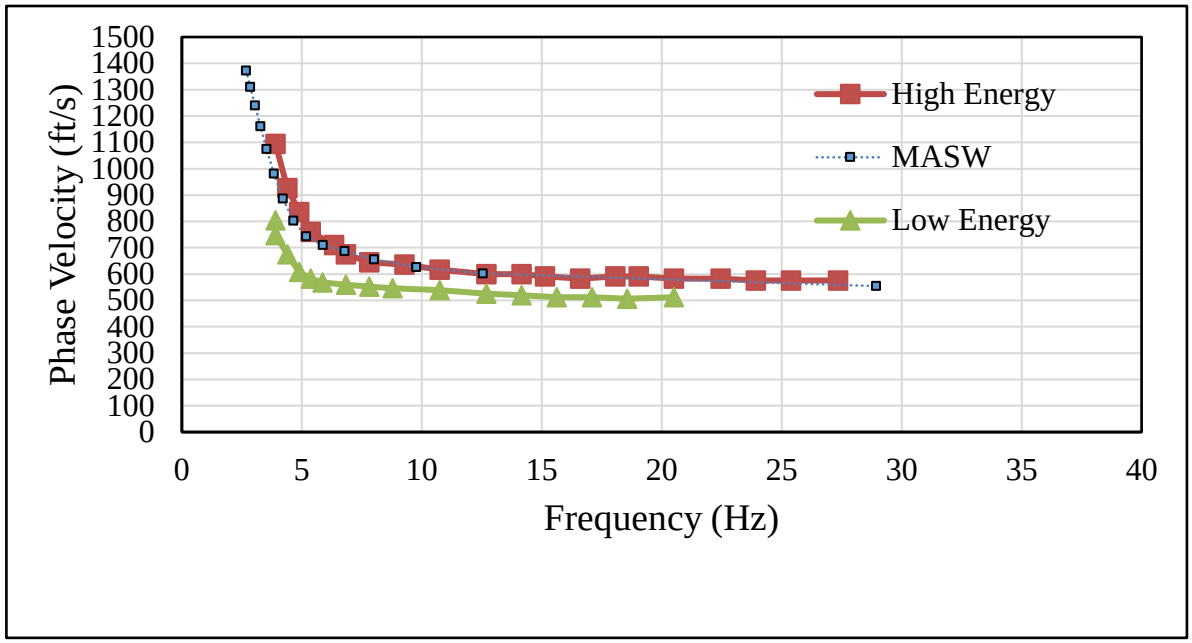


**Figure A-44. The Dispersion Curves Obtained at Site 11**

**Table A-23. Site 12 Information**

| Site No. | Job Number | Latitude | Longitude | COUNTY |
|---|---|---|---|---|
| 12 | 020417 | 34.454131 | -91.321308 | Arkansas |

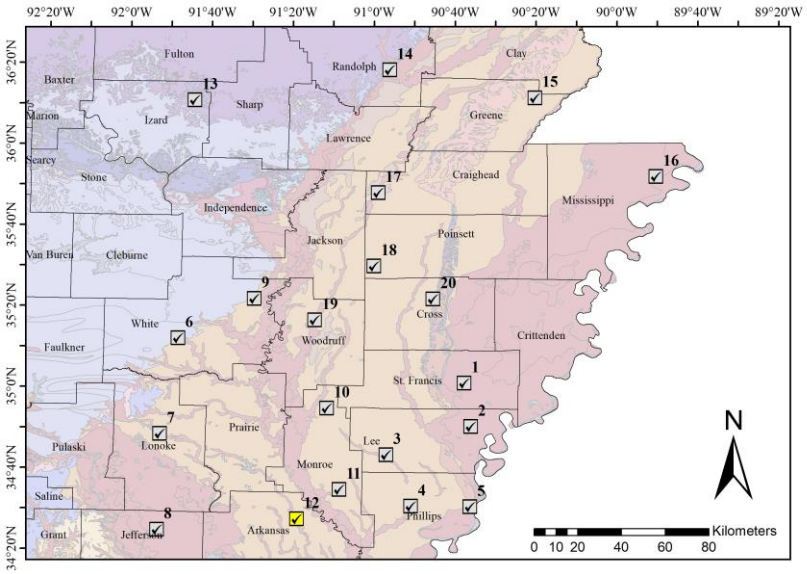


**Figure A-45. The Location of Site 12 is Highlighted in Yellow**


**Figure A-46. The Location of ReMi and MASW Lines is Highlighted in Yellow for Site 12**

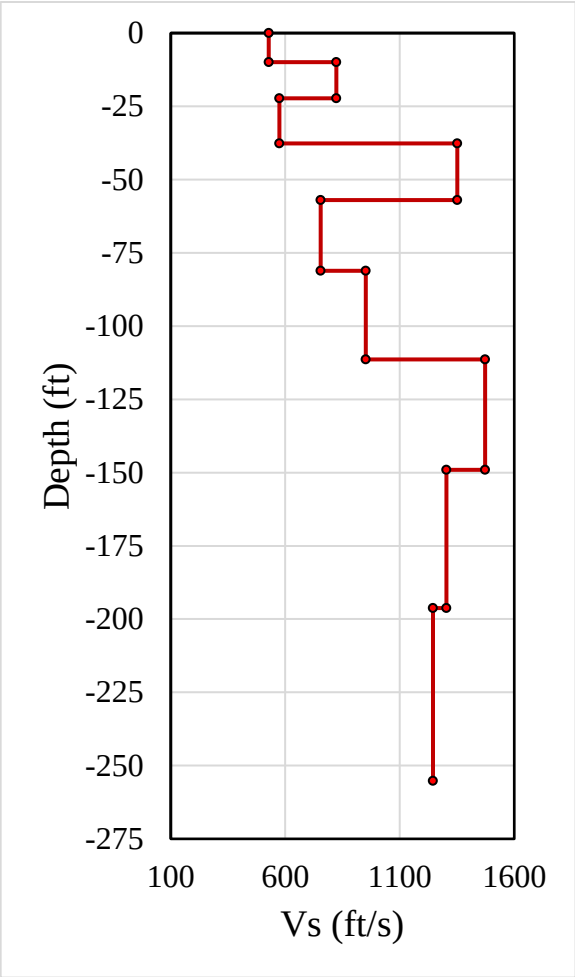


**Figure A-47. The Velocity Profile of Site 12**

**Table A-24. Velocity Profile of Fundamental and Higher Modes for Site 12. Higher modes were not detected**

| 1st Mode | |
|---|---|
| **Depth (ft)** | **Vs (ft/s)** |
| -10 | 528 |
| -22 | 823 |
| -38 | 574 |
| -57 | 1352 |
| -81 | 755 |
| -111 | 951 |
| -149 | 1473 |
| -196 | 1302 |
| -255 | 1243 |
| -319 | 1601 |

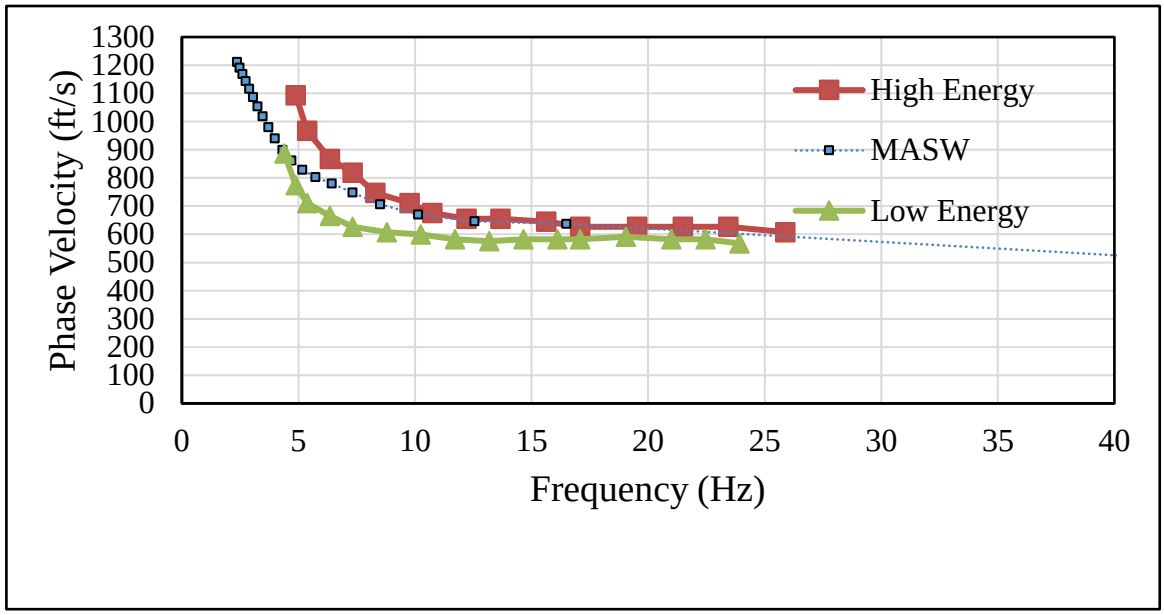


**Figure A-48. The Dispersion Curves Obtained at Site 12**

**Table A-25. Site 13 Information**

| Site No. | Job Number | Latitude | Longitude | COUNTY |
|---|---|---|---|---|
| 13 | 050321 | 36.178038 | -91.739529 | Izard |

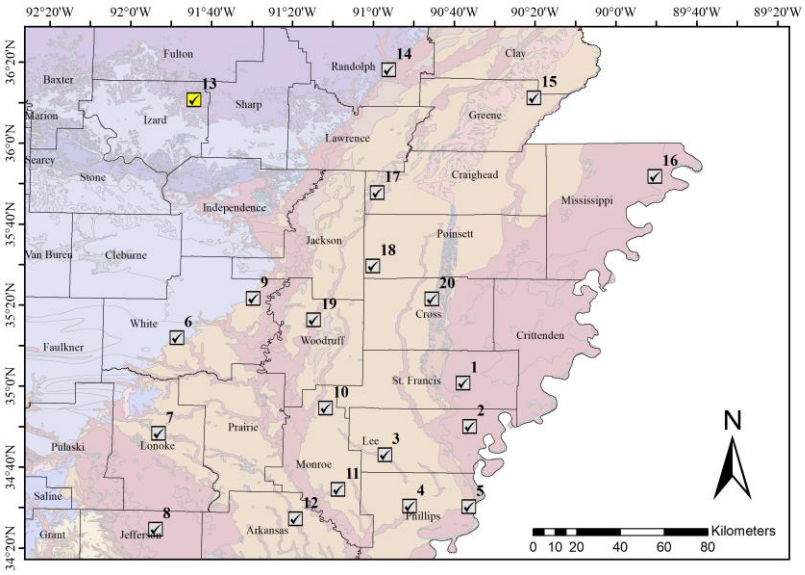


**Figure A-49. The Location of Site 13 is Highlighted in Yellow**


**Figure A-50. The Location of ReMi and MASW Lines is Highlighted in Yellow for Site 13**

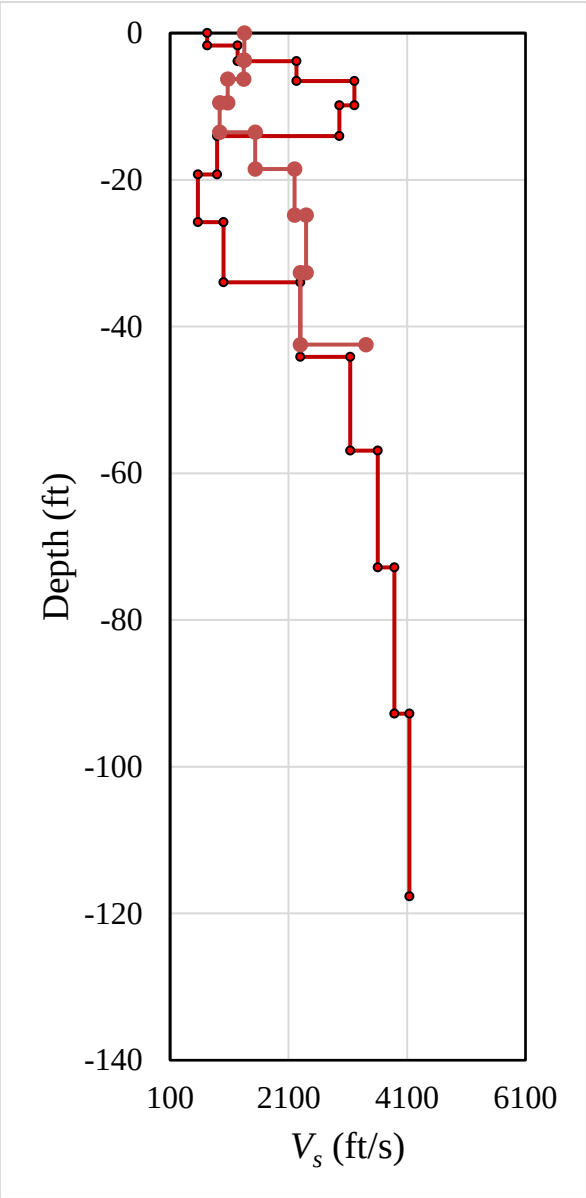


**Figure A-51. The Velocity Profile of Site 13**

**Table A-26. Velocity Profile of Fundamental and Higher Modes for Site 13**

| MODEL 1 | | MODEL 2 | |
|---|---|---|---|
| Depth (ft) | Vs (ft/s) | Depth (ft) | Vs (ft/s) |
| -2 | 729 | -2 | 1311 |
| -4 | 1242 | -4 | 1356 |
| -7 | 2235 | -6 | 1343 |
| -10 | 3212 | -10 | 1073 |
| -14 | 2959 | -13 | 937 |
| -19 | 892 | -18 | 1537 |
| -26 | 570 | -25 | 2201 |
| -34 | 1001 | -33 | 2399 |
| -44 | 2300 | -42 | 2299 |
| -57 | 3143 | -53 | 3404 |
| -73 | 3608 | | |
| -93 | 3888 | | |
| -118 | 4141 | | |
| -149 | 4471 | | |
| -186 | 6569 | | |

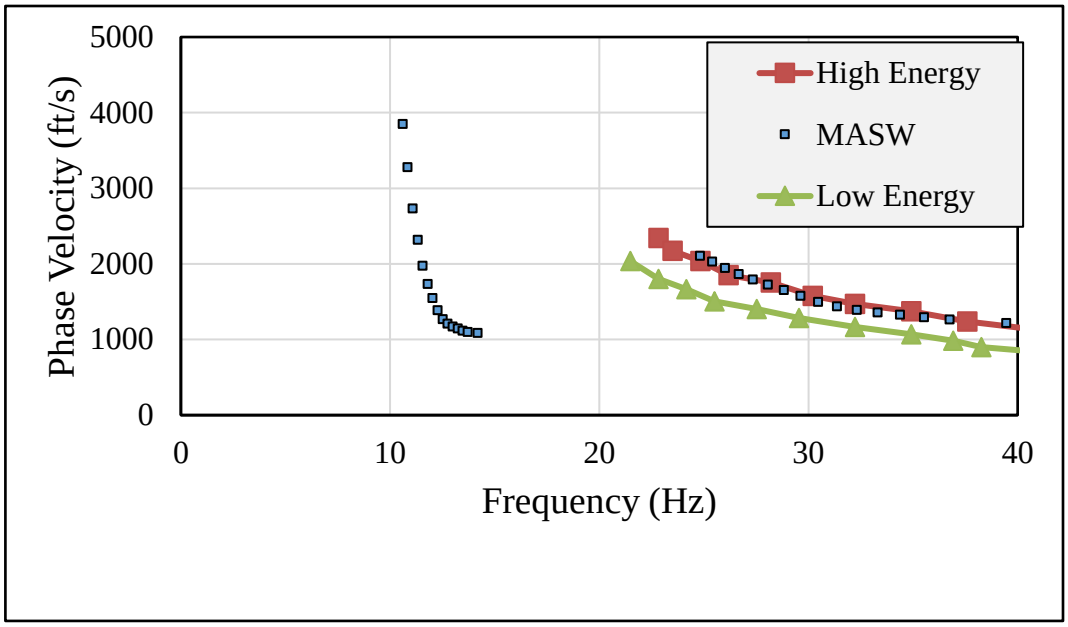


**Figure A-52. The Dispersion Curves Obtained at Site 13**

**Table A-27. Site 14 Information**

| Site No. | Job Number | Latitude | Longitude | COUNTY |
|---|---|---|---|---|
| 14 | 100993 | 36.31981 | -90.91261 | Randolph |

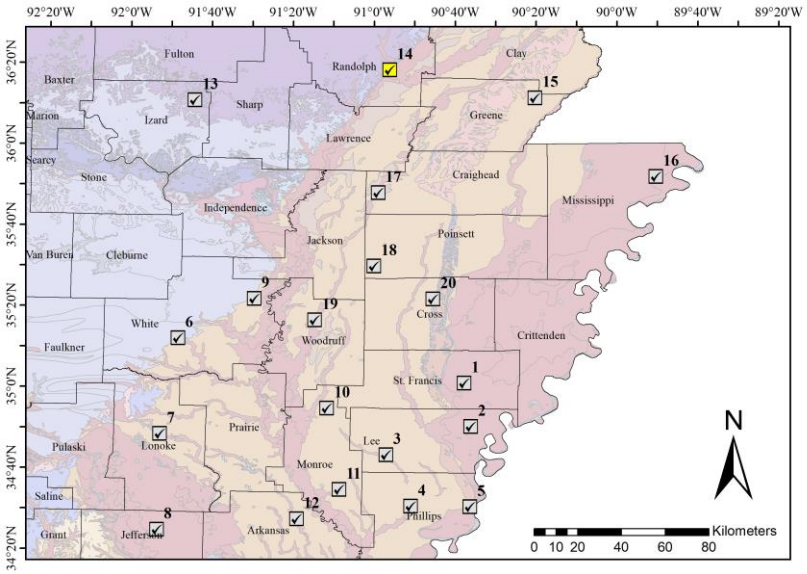


**Figure A-53. The Location of Site 14 is Highlighted in Yellow**


**Figure A-54. The Location of ReMi and MASW Lines is Highlighted in Yellow for Site 14**

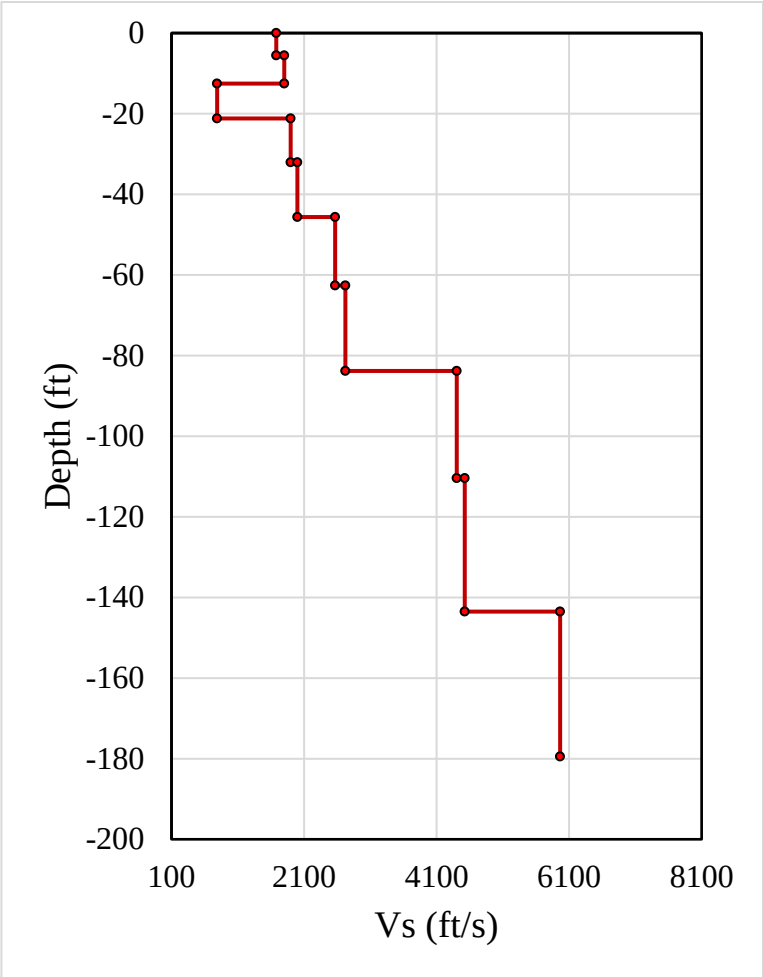


**Figure A-55. The Velocity Profile of Site 14**

**Table A-28. Velocity Profile of Fundamental and Higher Modes for Site 14. Higher modes were not detected**

| 1st Mode | |
|---|---|
| **Depth (ft)** | **Vs (ft/s)** |
| -6 | 1683 |
| -13 | 1803 |
| -21 | 789 |
| -32 | 1896 |
| -46 | 2571 |
| -63 | 2721 |
| -84 | 4405 |
| -110 | 4525 |
| -144 | 5964 |
| -179 | 5964 |

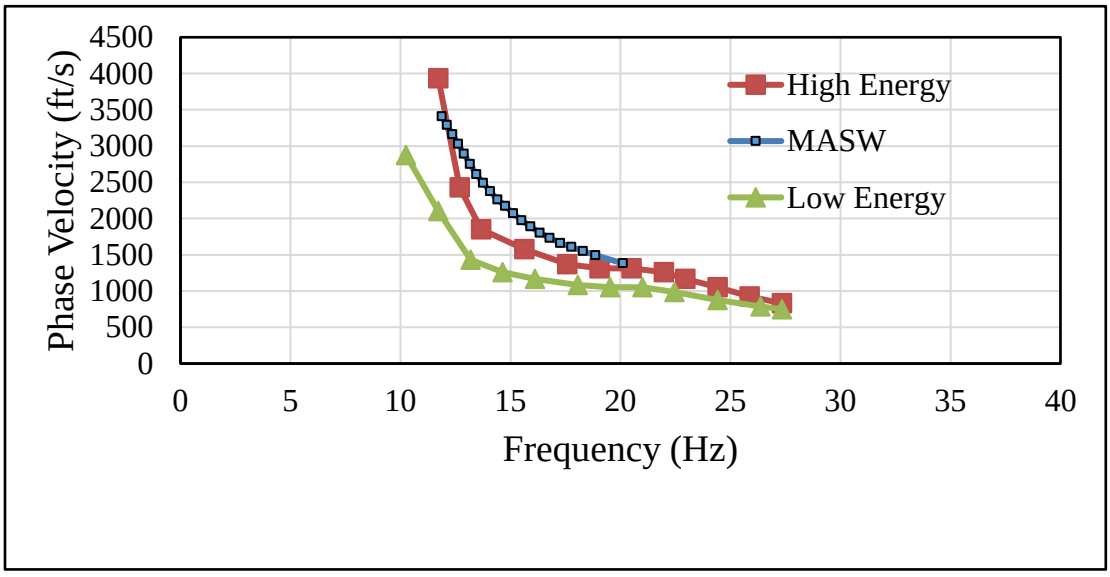


**Figure A-56. The Dispersion Curves Obtained at Site 14**

**Table A-29. Site 15 Information**

| Site No. | Job Number | Latitude | Longitude | COUNTY |
|---|---|---|---|---|
| 15 | 100870 | 36.18635 | -90.33812 | Greene |

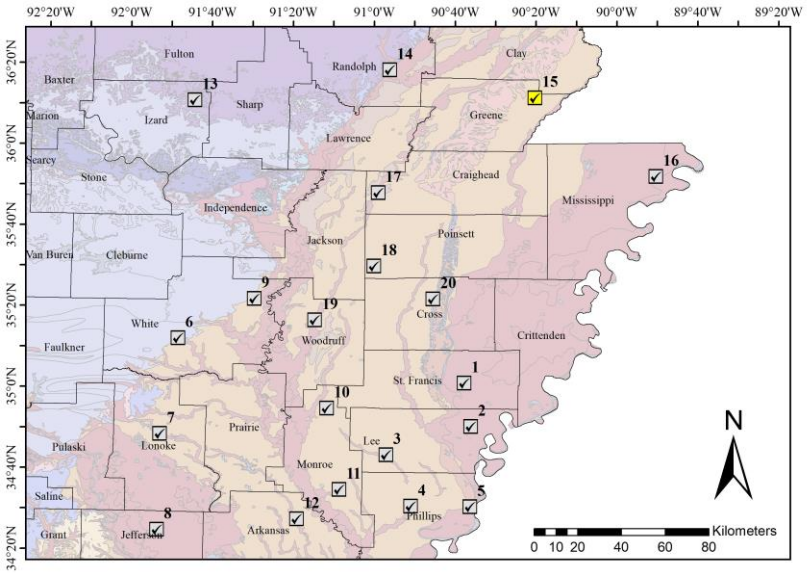


**Figure A-57. The Location of Site 15 is Highlighted in Yellow**


**Figure A-58. The Location of ReMi and MASW Lines is Highlighted in Yellow for Site 15**

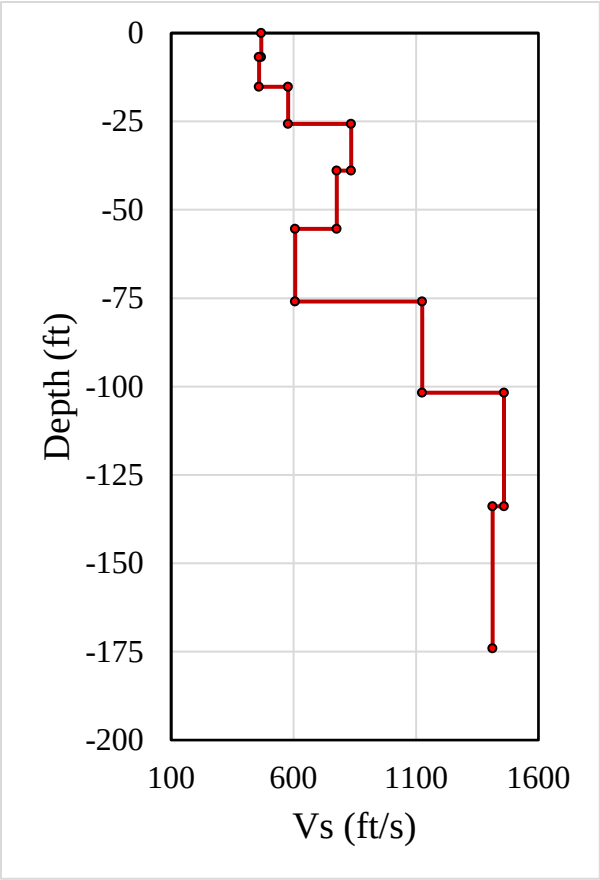


**Figure A-59. The Velocity Profile of Site 15**

**Table A-30. Velocity Profile of Fundamental and Higher Modes for Site 15. Higher Modes Were Not Detected**

| 1st Mode | |
|---|---|
| **Depth (ft)** | **Vs (ft/s)** |
| -7 | 468 |
| -15 | 459 |
| -26 | 577 |
| -39 | 835 |
| -55 | 777 |
| -76 | 607 |
| -102 | 1126 |
| -134 | 1459 |
| -174 | 1413 |

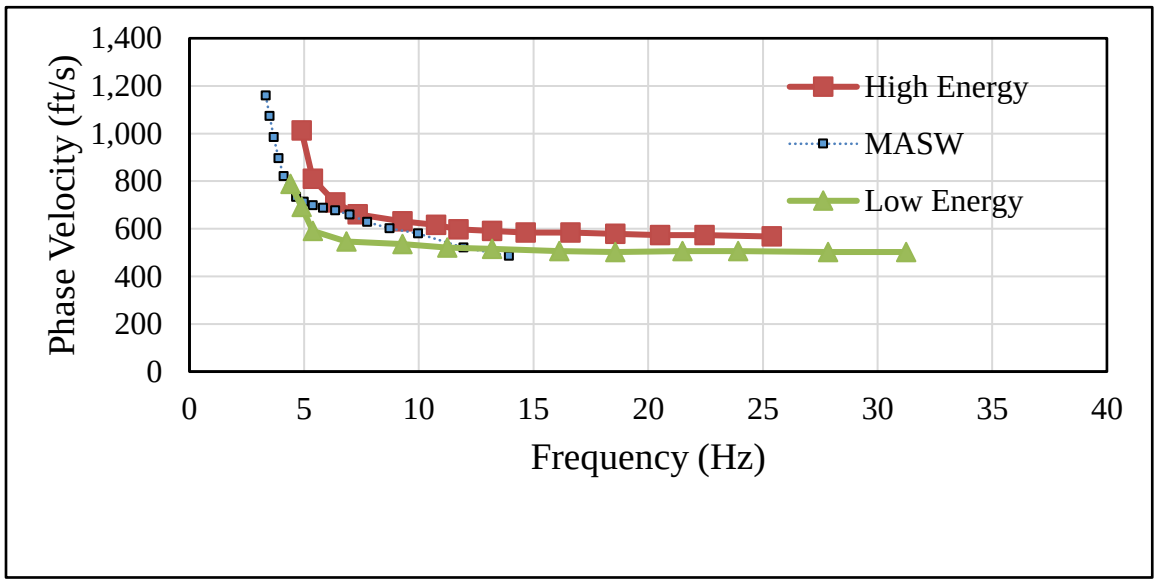


**Figure A.60. The Dispersion Curves Obtained at Site 15**

**Table A-31. Site 16 Information**

| Site No. | Job Number | Latitude | Longitude | COUNTY |
|---|---|---|---|---|
| 16 | 100721 | 35.86319 | -89.83975 | Mississippi |

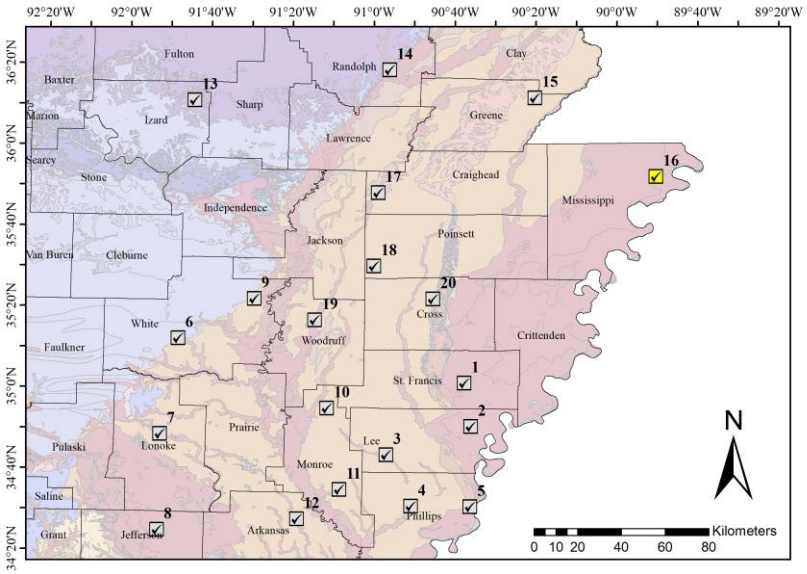


**Figure A-61. The Location of Site 16 is Highlighted in Yellow**


**Figure A-62. The Location of ReMi and MASW Lines is Highlighted in Yellow for Site 16**

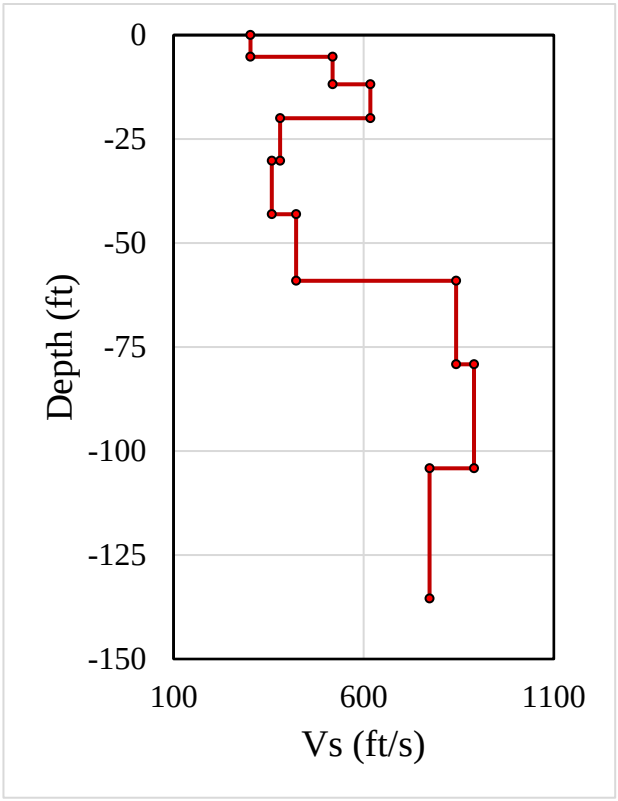


Figure A-63. The Velocity Profile of Site 16

Table A-32. Velocity Profile of Fundamental and Higher Modes for Site 16. Higher Modes Were Not Detected.

| 1st Mode | |
|---|---|
| **Depth (ft)** | **Vs (ft/s)** |
| -5 | 302 |
| -12 | 518 |
| -20 | 617 |
| -30 | 380 |
| -43 | 358 |
| -59 | 422 |
| -79 | 843 |
| -104 | 890 |
| -135 | 773 |
| -169 | 1138 |

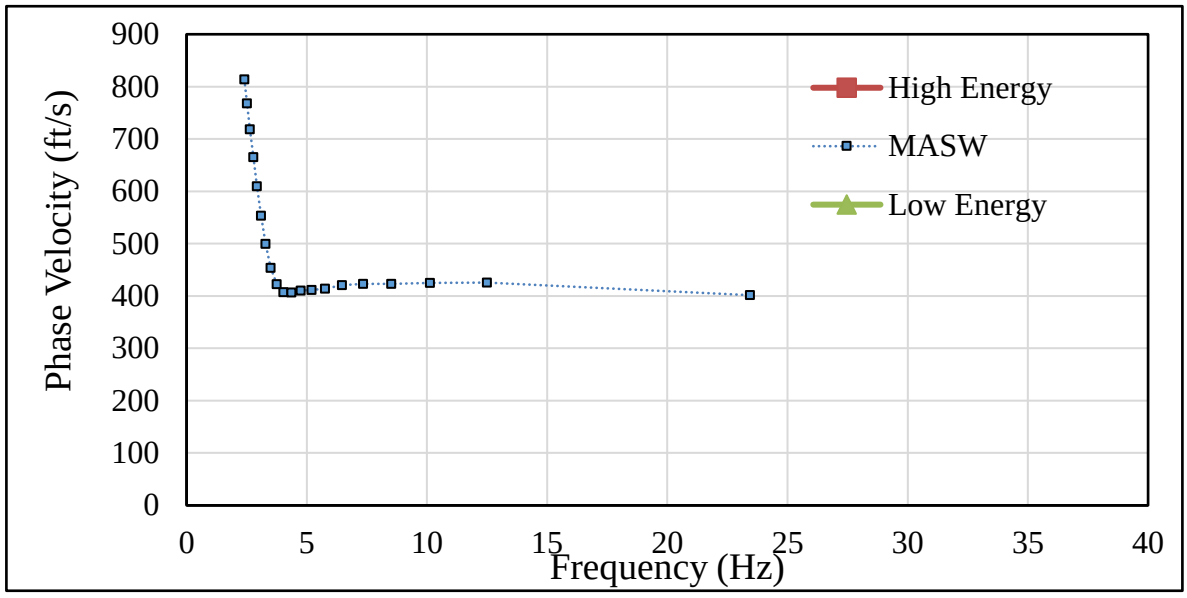


Figure A-64. The Dispersion Curves Obtained at Site 16 (ReMi Not Available)

**Table A-33. Site 17 Information**

| Site No. | Job Number | Latitude | Longitude | COUNTY |
|---|---|---|---|---|
| 17 | 100662 | 35.79525 | -90.98321 | Arkansas |

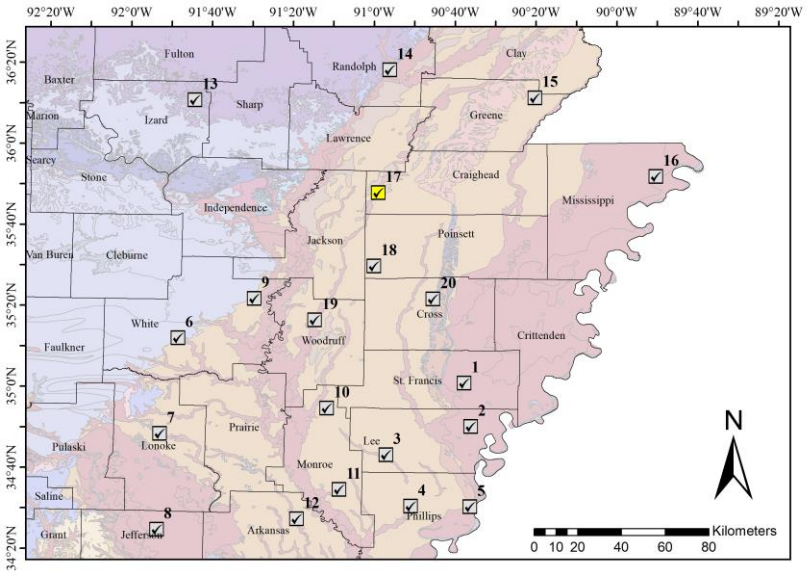


**Figure A-65. The Location of Site 17 is Highlighted in Yellow**


**Figure A-66. The Location of ReMi and MASW Lines is Highlighted in Yellow for Site 17**

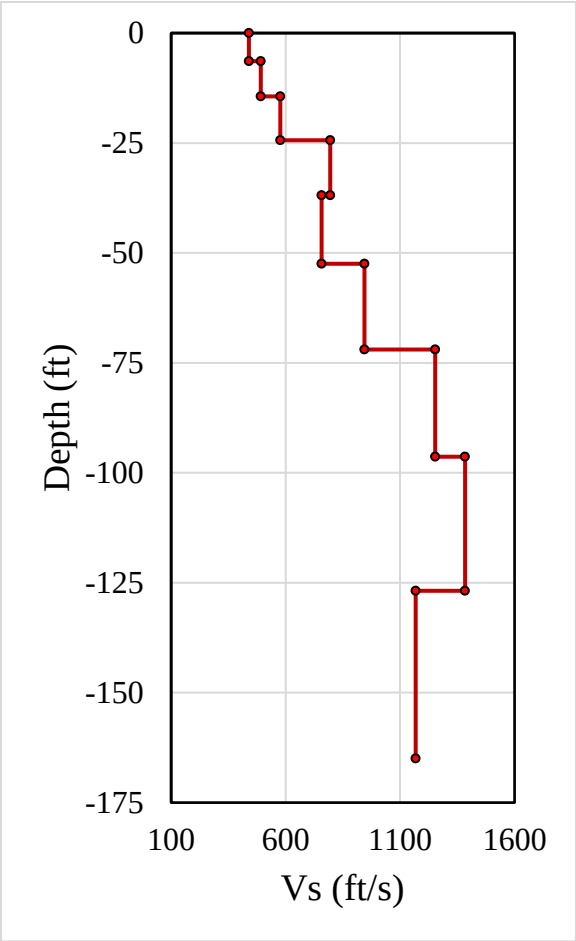


**Figure A-67. The Velocity Profile of Site 17**

**Table A-34. Velocity Profile of Fundamental and Higher Modes for Site 17. Higher Modes Were Not Detected**

| 1st Mode | |
|---|---|
| **Depth (ft)** | **Vs (ft/s)** |
| -6 | 440 |
| -14 | 491 |
| -24 | 577 |
| -37 | 795 |
| -52 | 757 |
| -72 | 944 |
| -96 | 1254 |
| -127 | 1384 |
| -165 | 1169 |
| -206 | 1508 |

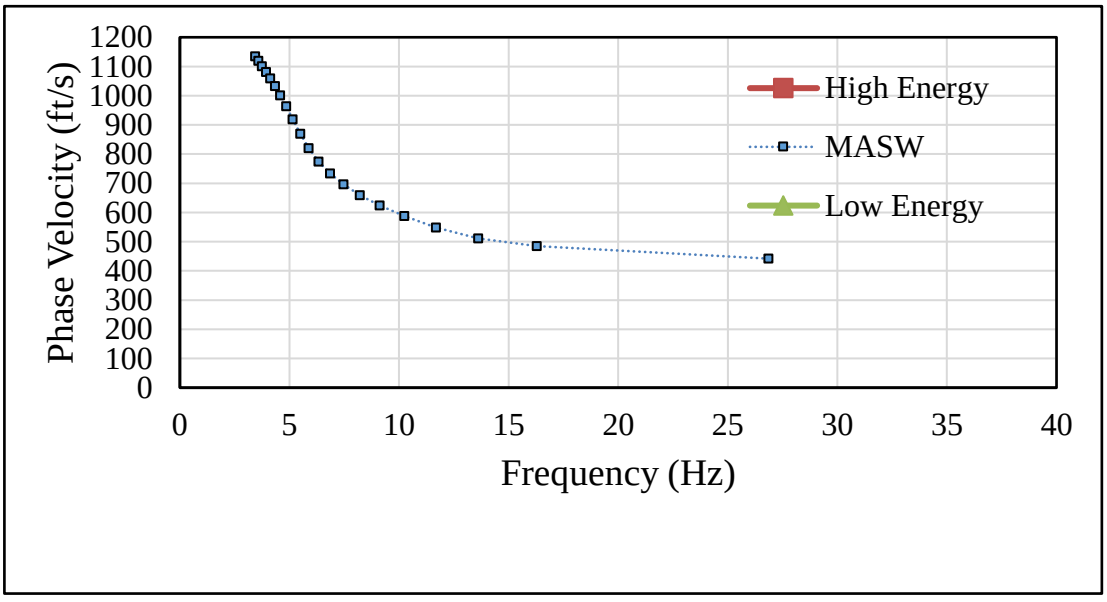


**Figure A-68. The Dispersion Curves Obtained at Site 17**

**Table A-35. Site 18 Information**

| Site No. | JobNumber | Latitude | Longitude | COUNTY |
|---|---|---|---|---|
| 18 | BR5607 | 35.49315 | -91.00196 | Poinsett |

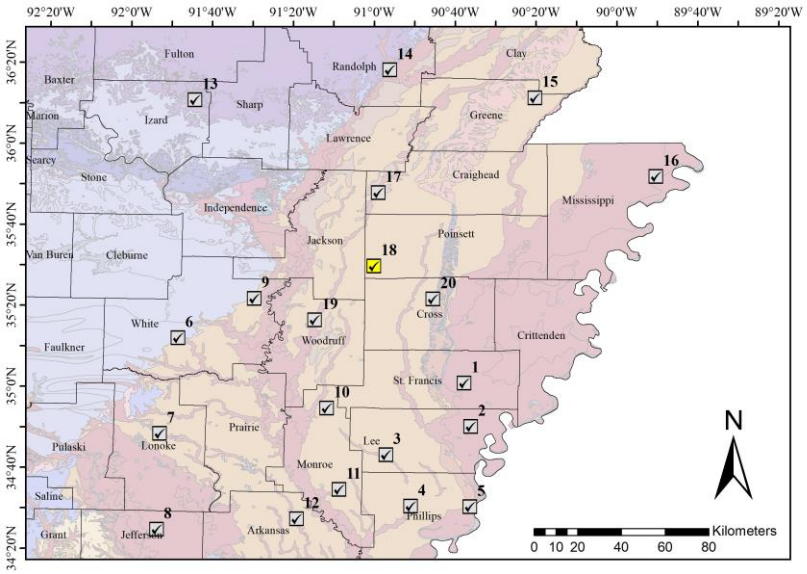


**Figure A-69. The Location of Site 18 is Highlighted in Yellow**


**Figure A-70. The Location of ReMi and MASW Lines is Highlighted in Yellow for Site 18**

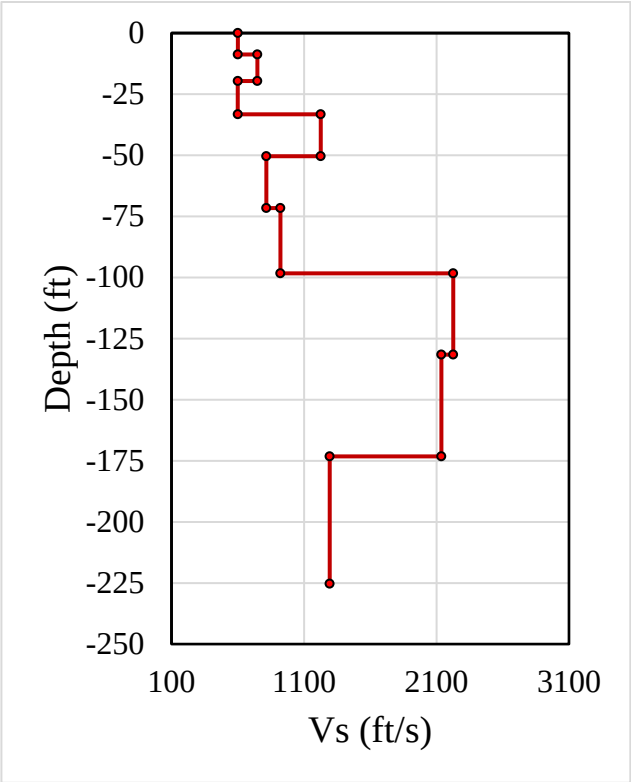


**Figure A-71. The Velocity Profile of Site 18**

**Table A-36. Velocity Profile of Fundamental and Higher Modes for Site 18. Higher Modes Were Not Detected**

| 1st Mode | |
|---|---|
| **Depth (ft)** | **Vs (ft/s)** |
| -9 | 600 |
| -20 | 749 |
| -33 | 600 |
| -50 | 1227 |
| -72 | 816 |
| -98 | 922 |
| -132 | 2226 |
| -173 | 2136 |
| -225 | 1293 |
| -282 | 2631 |

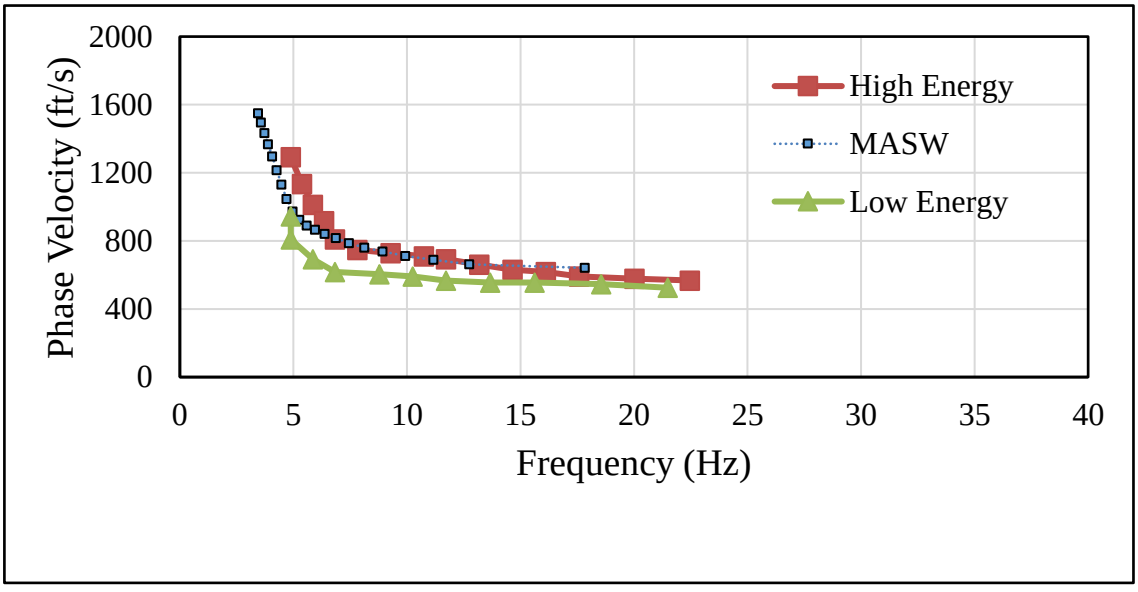


**Figure A-72. The Dispersion Curves Obtained at Site 18**

**Table A-37. Site 19 Information**

| Site No. | JobNumber | Latitude | Longitude | COUNTY |
|---|---|---|---|---|
| 19 | 110289 | 35.27009 | -91.23689 | Woodruff |

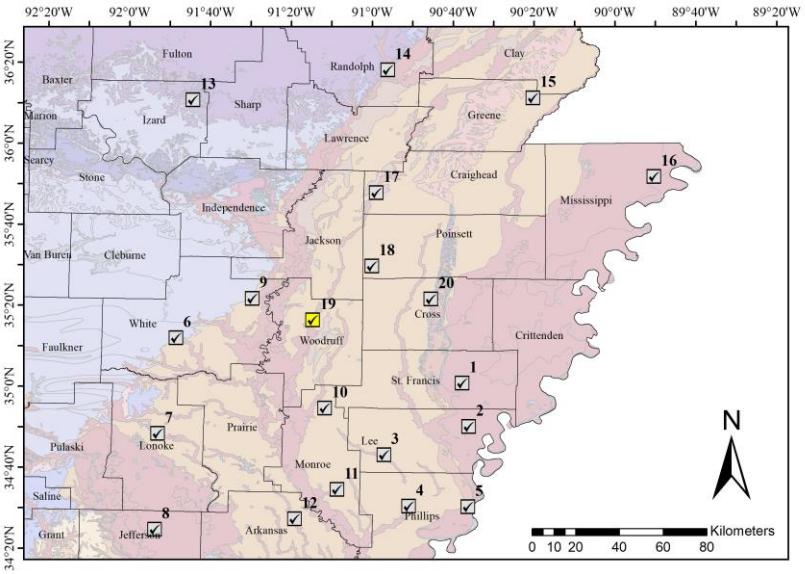


**Figure A-73. The Location of Site 19 is Highlighted in Yellow**


**Figure A-74. The Location of ReMi and MASW Lines is Highlighted in Yellow for Site 19**

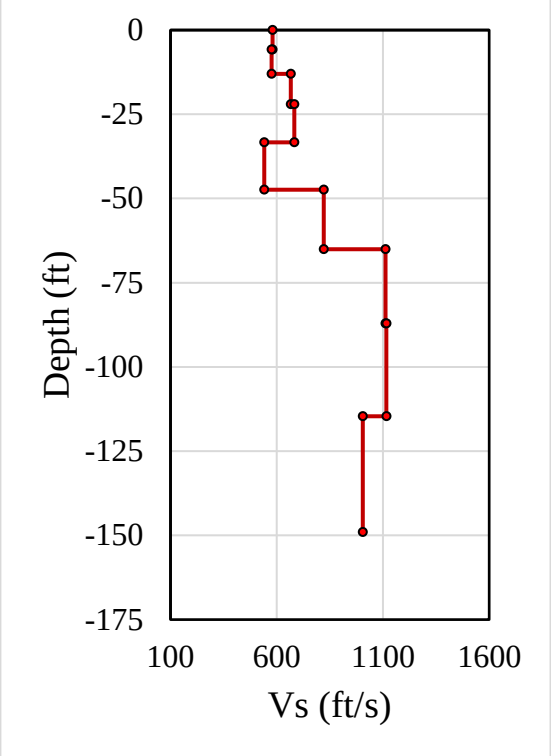


**Figure A-75. The Velocity Profile of Site 19**

**Table A-38. Velocity Profile of Fundamental and Higher Modes for Site 19. Higher Modes Were Not Detected**

| 1st Mode | |
|---|---|
| **Depth (ft)** | **Vs (ft/s)** |
| -6 | 580 |
| -13 | 575 |
| -22 | 666 |
| -33 | 682 |
| -47 | 541 |
| -65 | 822 |
| -87 | 1112 |
| -115 | 1116 |
| -149 | 1004 |
| -186 | 1495 |

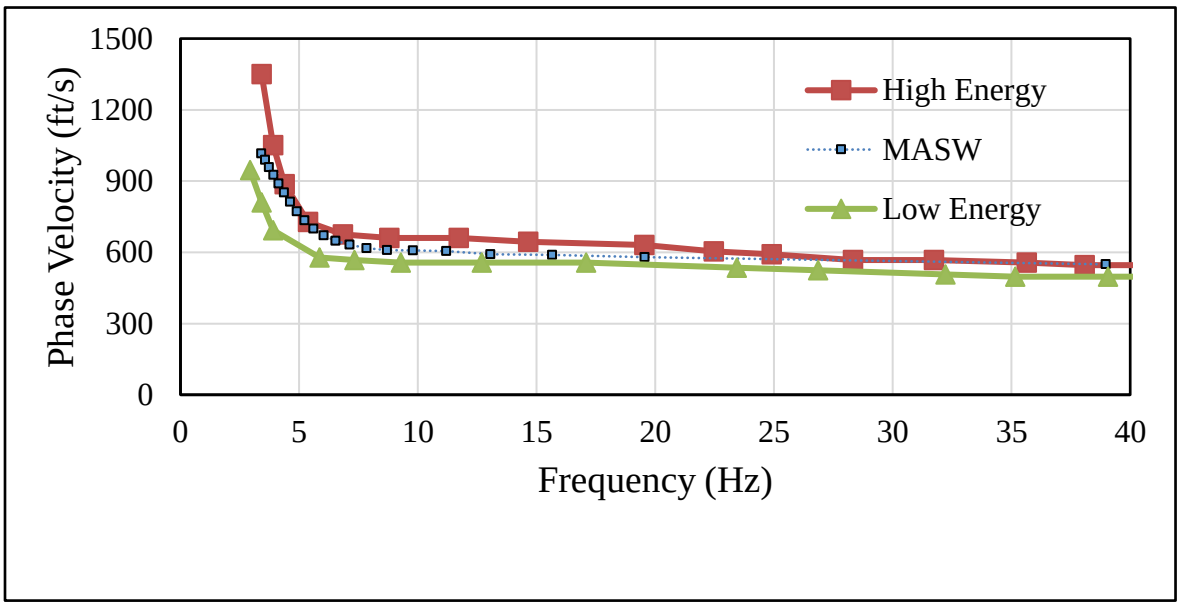


**Figure A-76. Dispersion Curves Obtained at Site 19**

**Table A-39. Site 20 Information**

| Site No. | JobNumber | Latitude | Longitude | COUNTY |
|---|---|---|---|---|
| 20 | BR1907 | 35.358664 | -90.758546 | Cross |

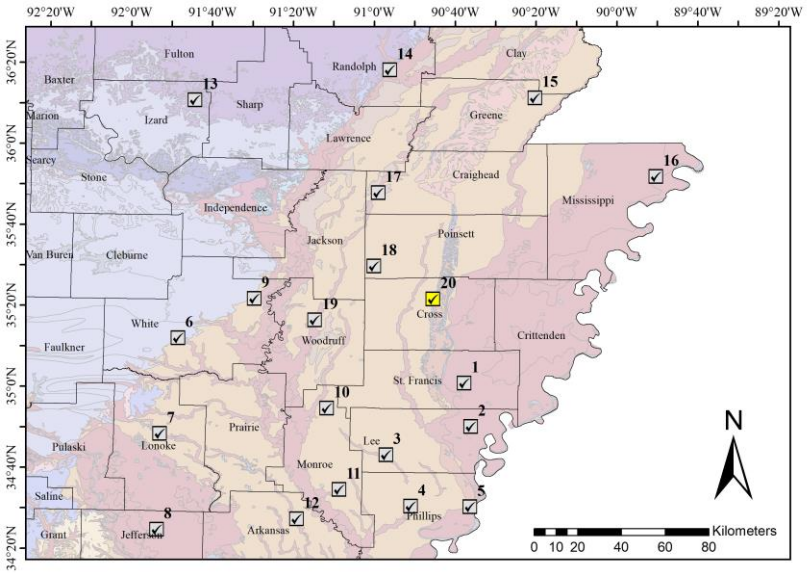


**Figure A-77. The Location of Site 20 is Highlighted in Yellow**


**Figure A-78. The Location of ReMi and MASW Lines is Highlighted in Yellow for Site 20**

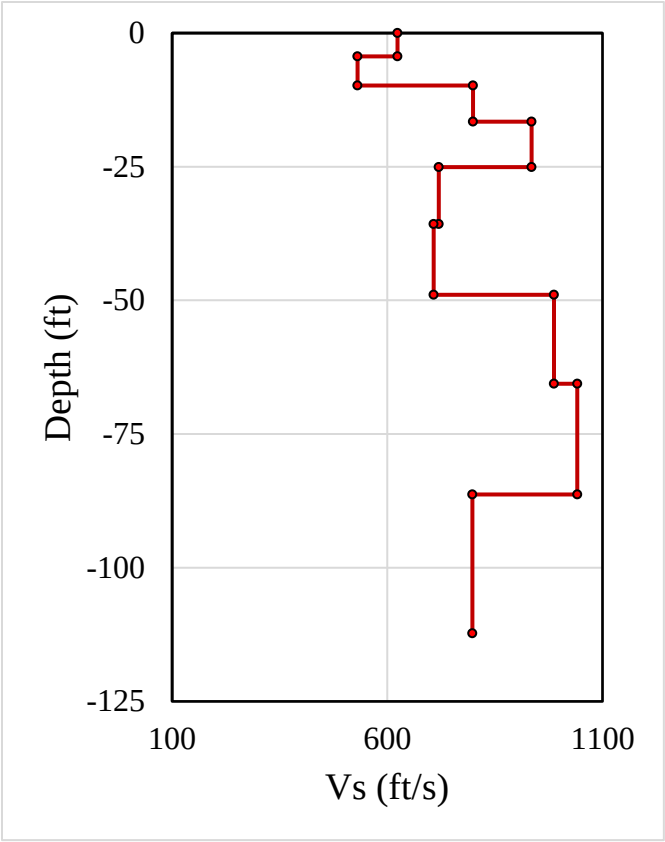


Figure A-79. Velocity Profile at Site 20.

**Table A-40. Velocity Profile of Fundamental and Higher Modes for Site 20. Higher Modes Were Not Detected.**

| 1st Mode | |
|---|---|
| **Depth (ft)** | **Vs (ft/s)** |
| -4 | 624 |
| -10 | 531 |
| -17 | 799 |
| -25 | 935 |
| -36 | 719 |
| -49 | 707 |
| -66 | 987 |
| -86 | 1041 |
| -112 | 798 |
| -140 | 1170 |

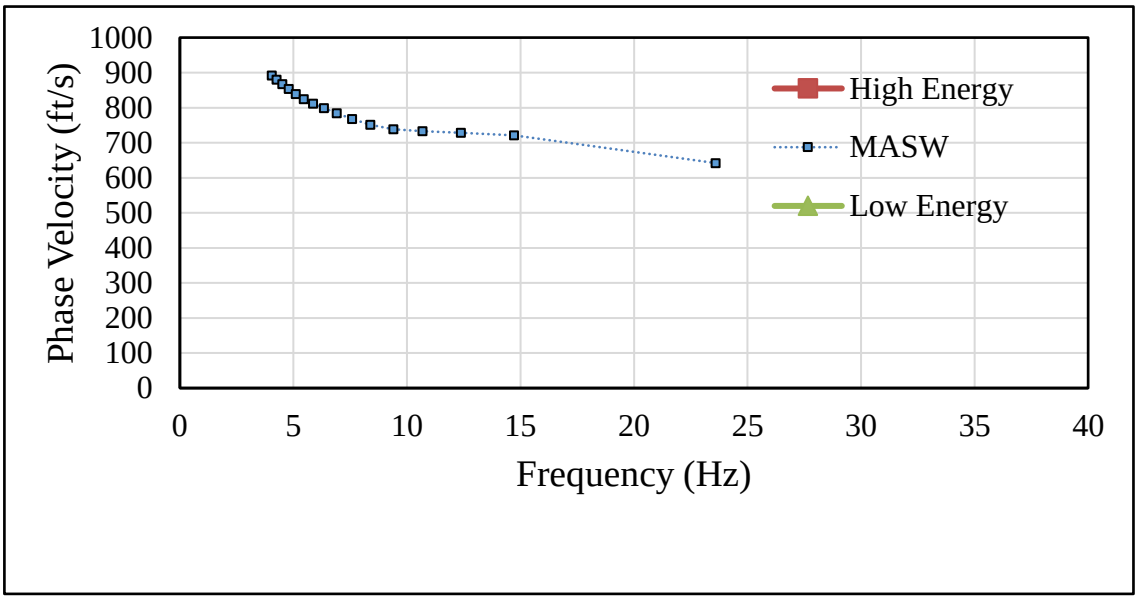


Figure A-80. Dispersion Curve Obtained at Site 20 (ReMi Not available)

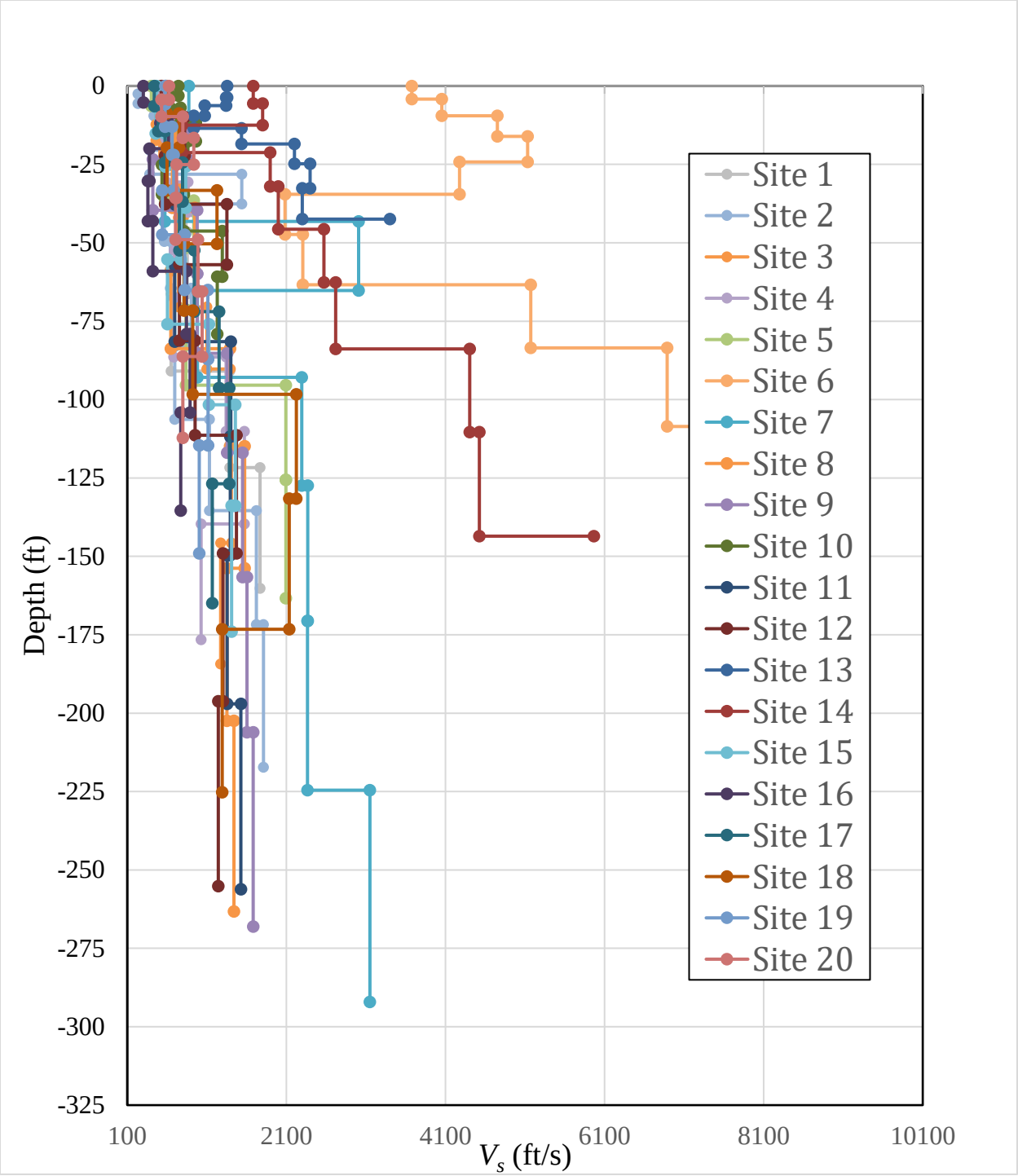


**Figure A-81. Shear-Wave Velocity Profiles of at all 20 Sites**

# APPENDIX B. SUPPLEMENTAL SITE FIGURES

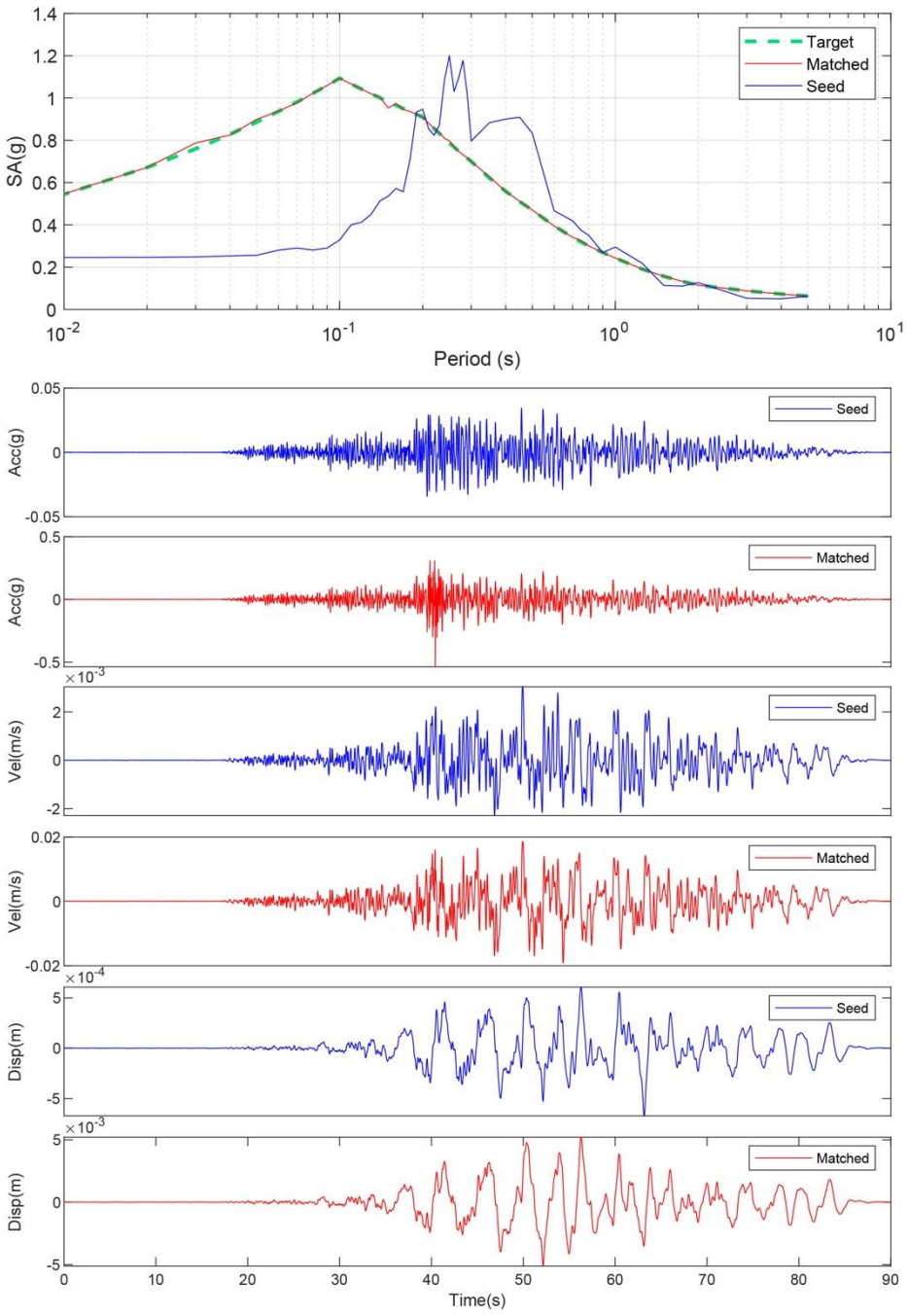


**Figure B-1. Matching Spectrum of Seed Motion (Rsn1577-Chichi-Ttn025-E) to the Target Spectrum (UHS) at Site 1. The Middle Subplot Shows the Seed Motion, and the Bottom Subplot Indicates the Matched Motion**

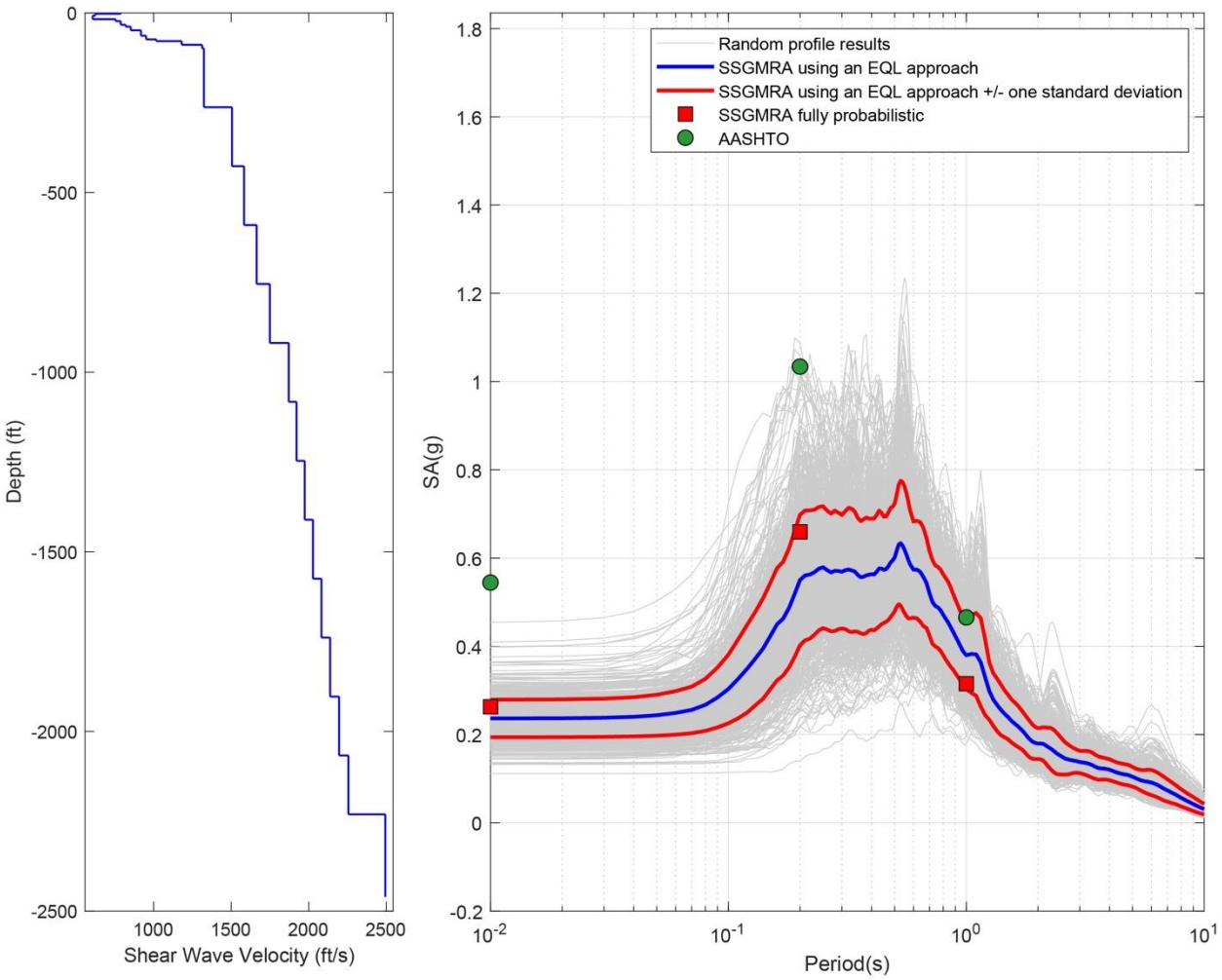


**Figure B-2. Left Panel: Shear-Wave Velocity Profile for Site 1 (Based on EPRI Soil Model); and Right Panel: Results of SSGMRA Using a Fully Probabilistic Approach, SSGMRA Using an Equivalent Linear Approach, SSGMRA Using an Equivalent Linear Approach Plus and Minus One Standard Deviation, and AASHTO General Approach**

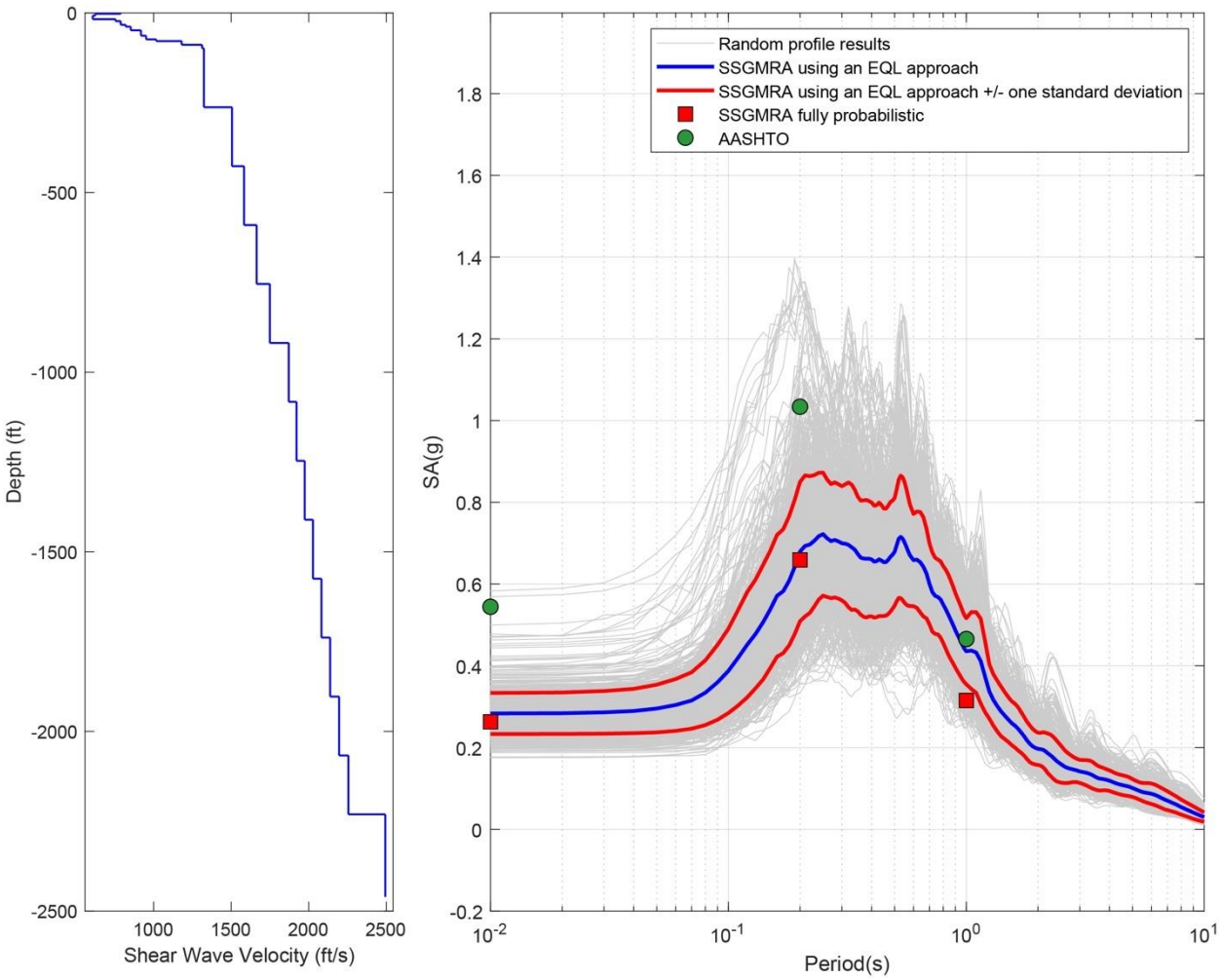


***Figure* B-3. Left Panel: Shear-Wave Velocity Profile for Site 1 (Based on Peninsular Soil Model); and Right Panel: Results of SSGMRA Using a Fully Probabilistic Approach, SSGMRA Using an Equivalent Linear Approach, SSGMRA Using an Equivalent Linear Approach Plus and Minus One Standard Deviation, and AASHTO General Approach**

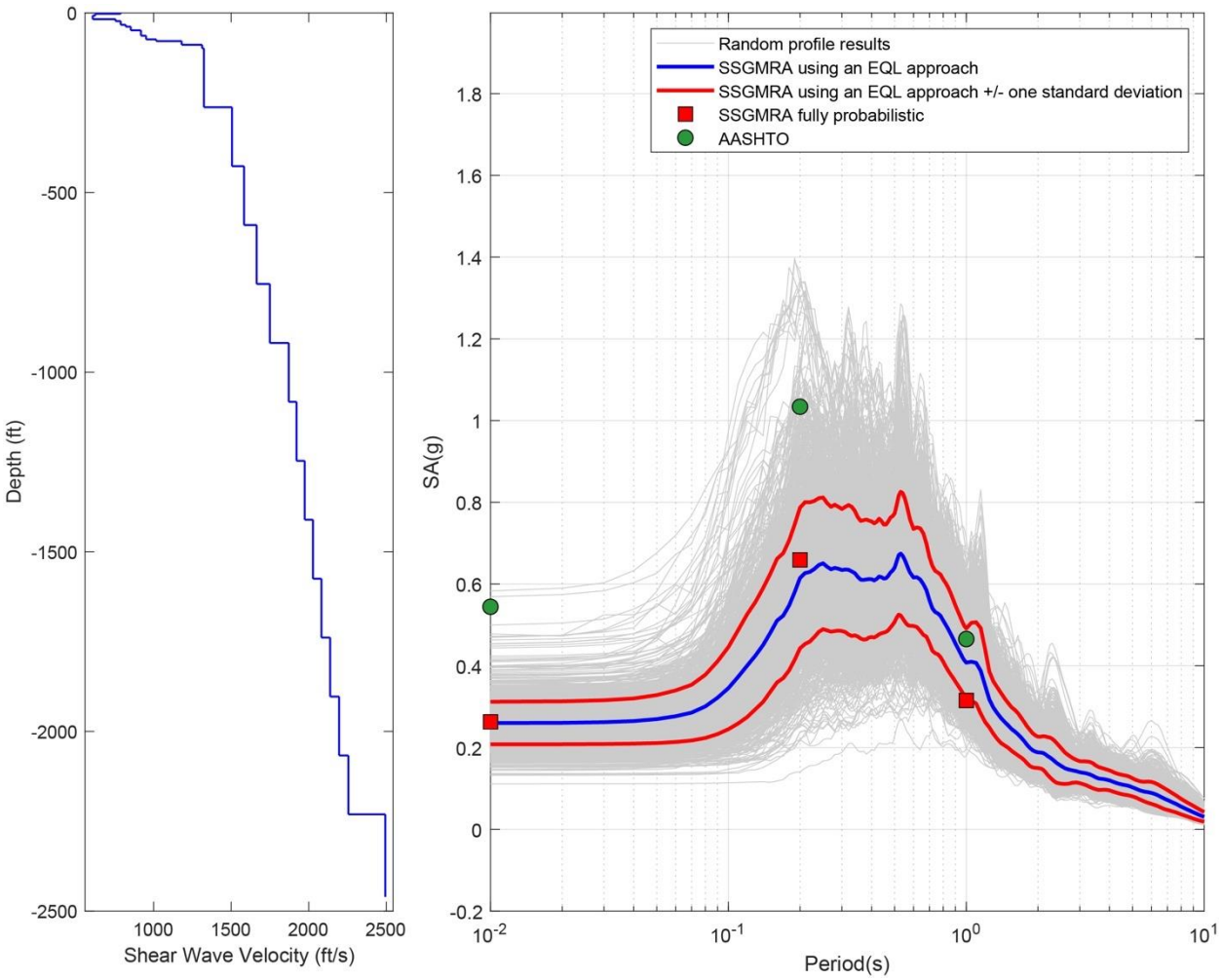


**Figure B-4. Left Panel: Shear-Wave Velocity Profile for Site 1 (Combined); and Right Panel: Results of SSGMRA Using a Fully Probabilistic Approach, SSGMRA Using an Equivalent Linear Approach, SSGMRA Using an Equivalent Linear Approach Plus and Minus One Standard Deviation, and AASHTO General Approach**

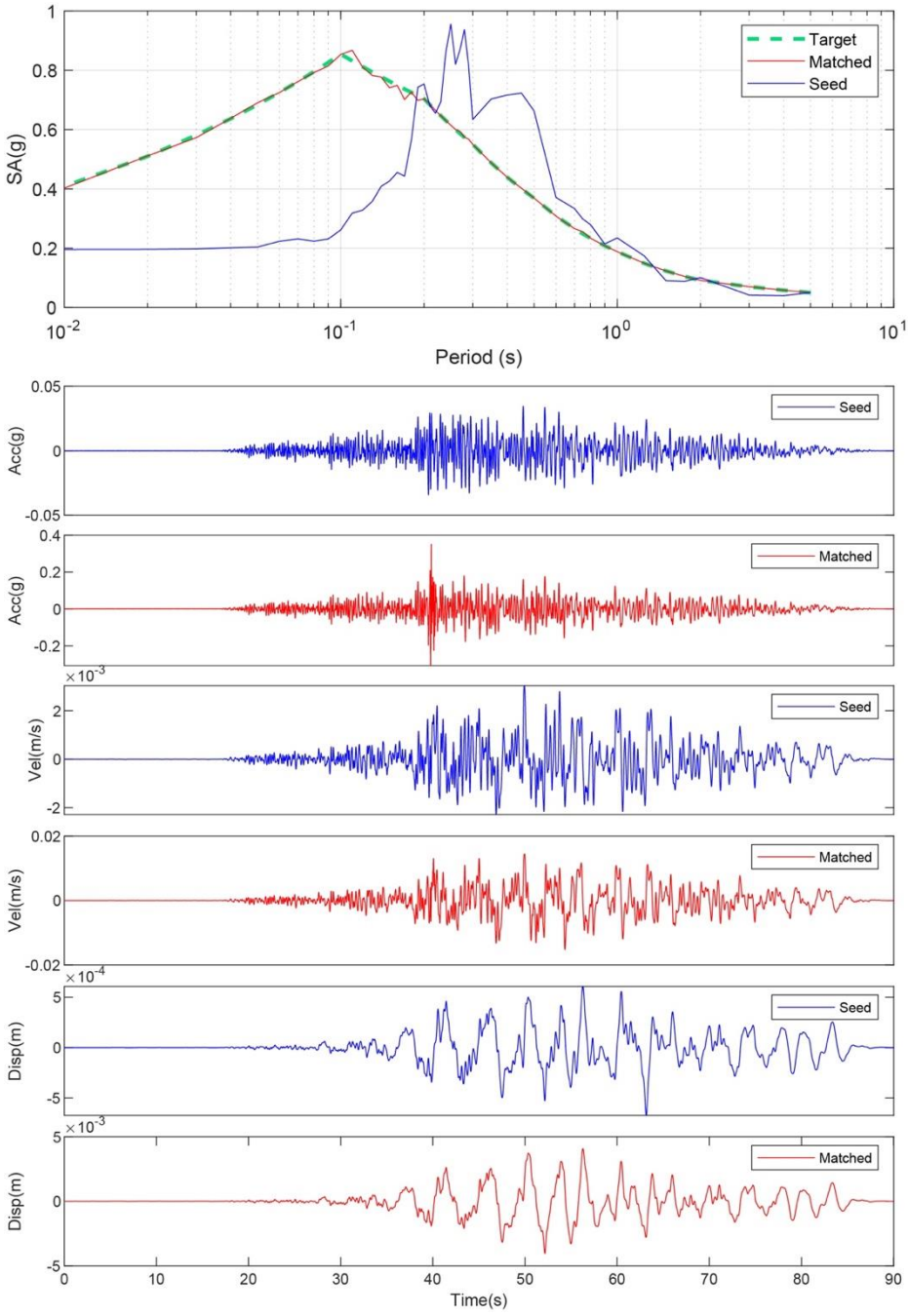


**Figure B-5. Matching Spectrum of Seed Motion (RSN1577-CHICHI-TTN025-E) to The Target Spectrum (UHS) at Site 2. The Middle Subplot Shows the Seed Motion, and the Bottom Subplot Indicates the Matched Motion**

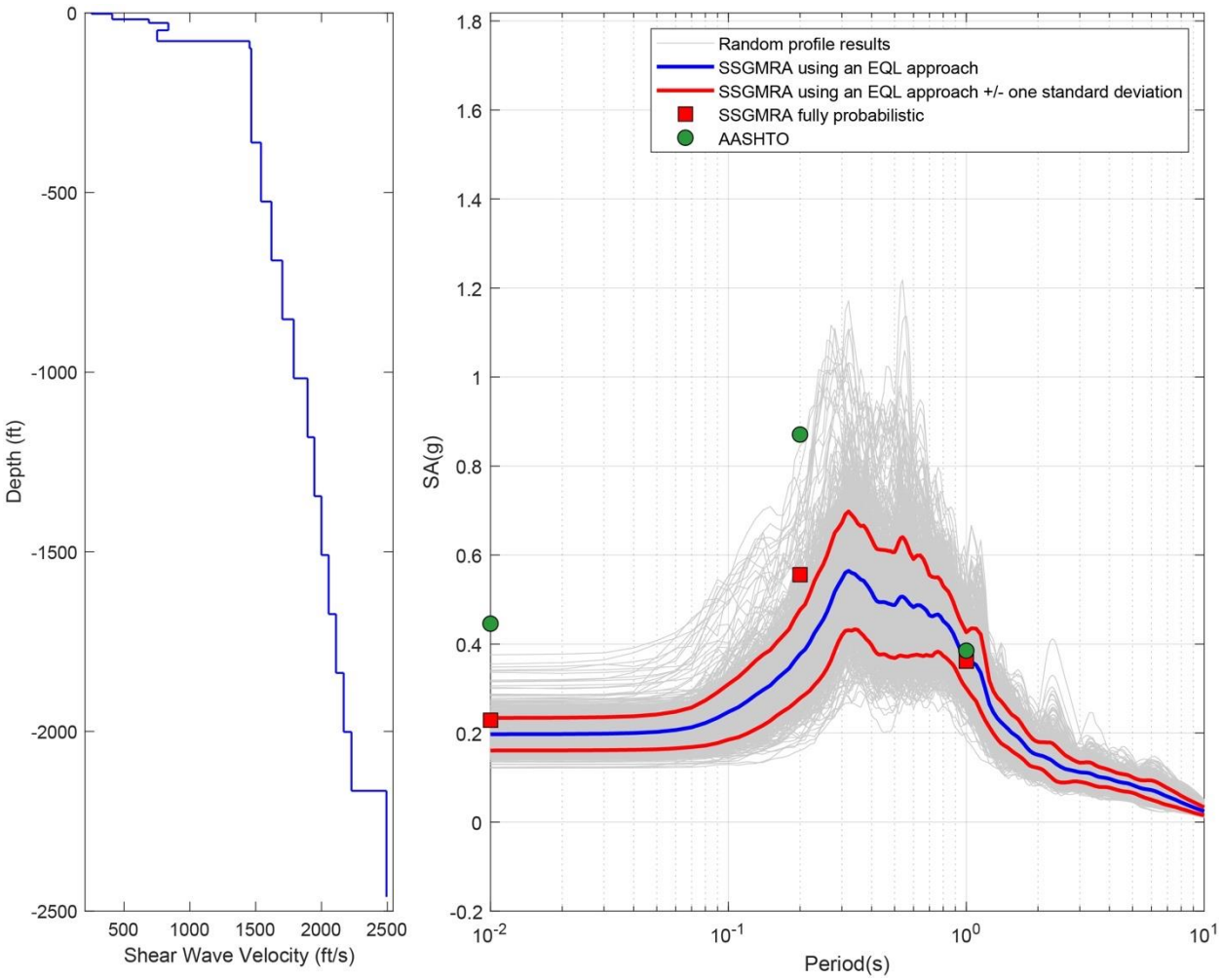


**Figure B-6. Left Panel: Shear-Wave Velocity Profile for Site 2 (Based on EPRI Soil Model); and Right Panel: Results of SSGMRA Using a Fully Probabilistic Approach, SSGMRA Using an Equivalent Linear Approach, SSGMRA Using an Equivalent Linear Approach Plus and Minus One Standard Deviation, and AASHTO General Approach**

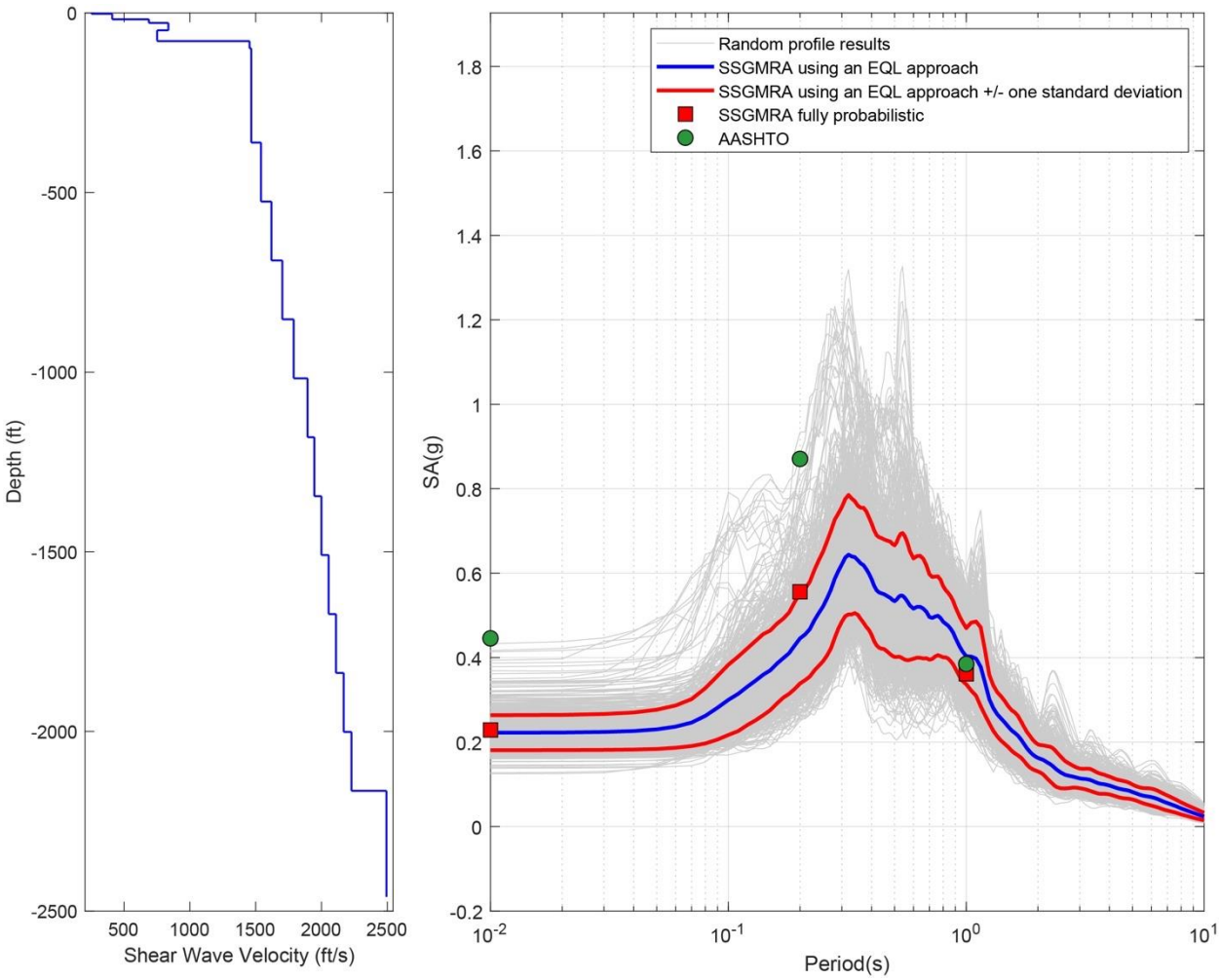


**Figure B-7. Left Panel: Shear-Wave Velocity Profile for Site 2 (Based on Peninsular Soil Model); and Right Panel: Results of SSGMRA Using a Fully Probabilistic Approach, SSGMRA Using an Equivalent Linear Approach, SSGMRA Using an Equivalent Linear Approach Plus and Minus One Standard Deviation, and AASHTO General Approach**

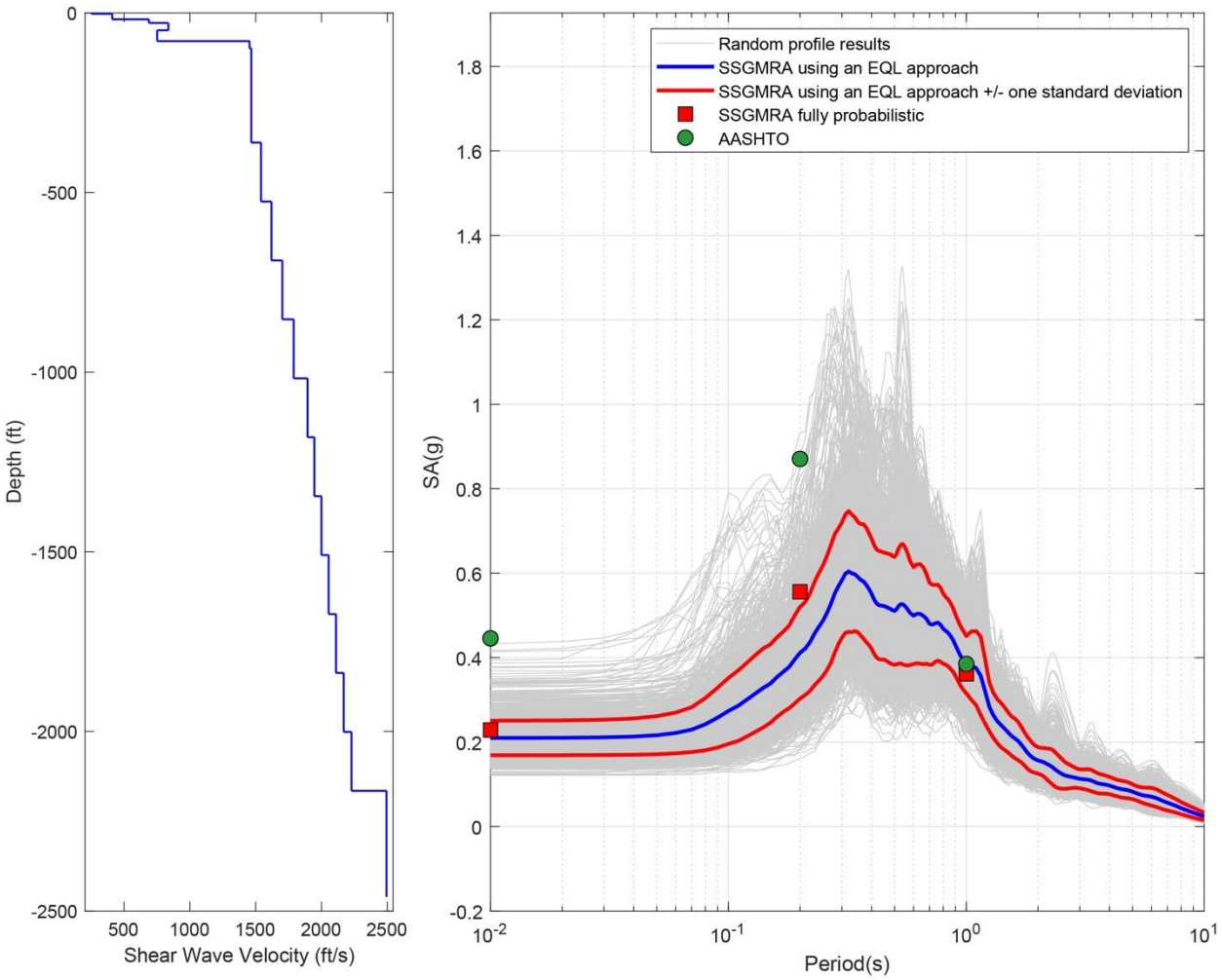


**Figure B-8. Left Panel: Shear-Wave Velocity Profile for Site 2 (Combined); and Right Panel: Results of SSGMRA Using a Fully Probabilistic Approach, SSGMRA Using an Equivalent Linear Approach, SSGMRA Using an Equivalent Linear Approach Plus and Minus One Standard Deviation, and AASHTO General Approach**

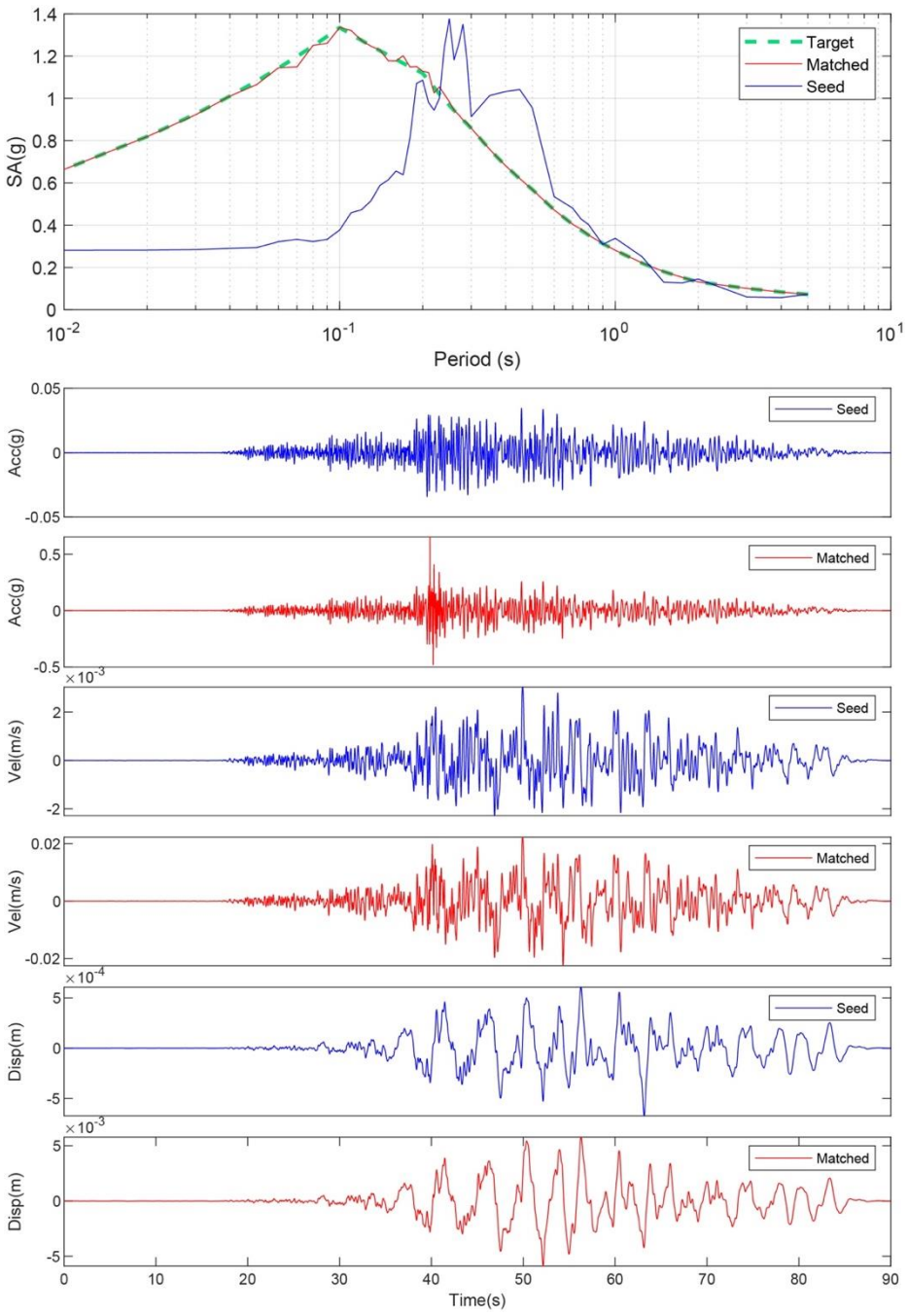


**Figure B-9. Matching Spectrum of Seed Motion (RSN1577-CHICHI-TTN025-E) to the Target Spectrum (UHS) at Site 3. The Middle Subplot Shows the Seed Motion, and the Bottom Subplot Indicates the Matched Motion**

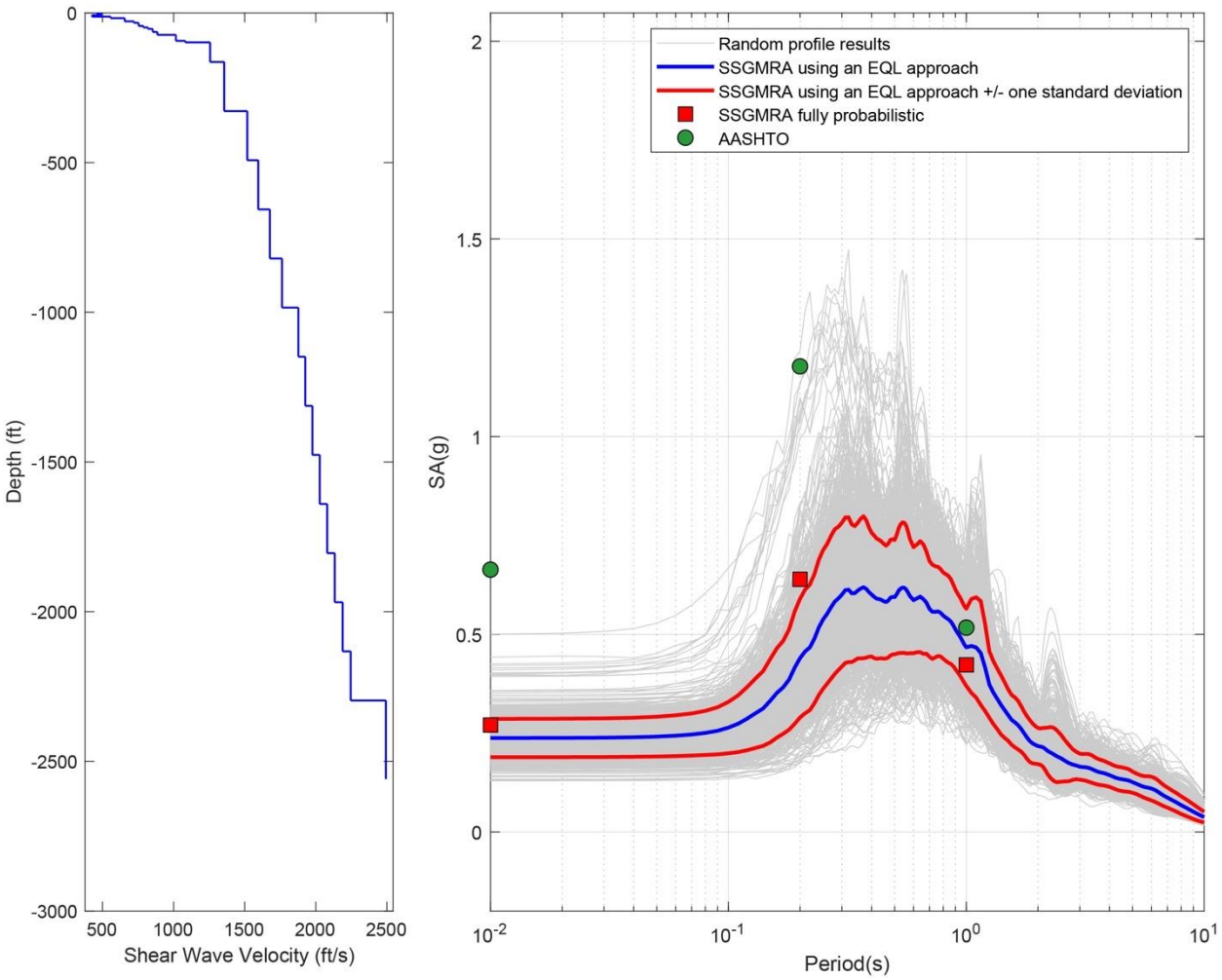


**Figure B-10. Left Panel: Shear-Wave Velocity Profile for Site 3 (Based on EPRI Soil Model); and Right Panel: Results of SSGMRA Using a Fully Probabilistic Approach, SSGMRA Using an Equivalent Linear Approach, SSGMRA Using an Equivalent Linear Approach Plus and Minus One Standard Deviation, and AASHTO General Approach**

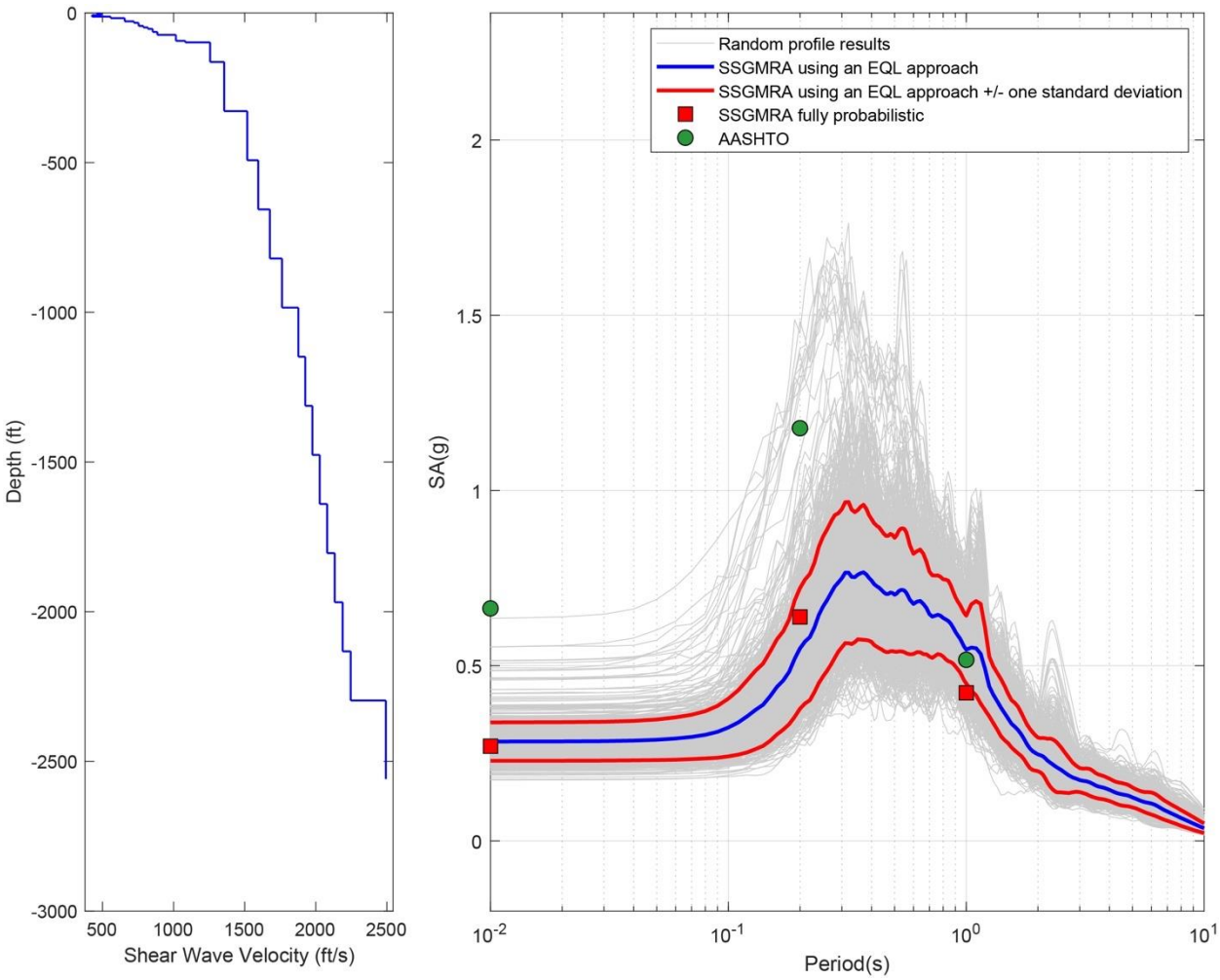


**Figure B-11. Left Panel: Shear-Wave Velocity Profile for Site 3 (Based on Peninsular Soil Model); and Right Panel: Results of SSGMRA Using a Fully Probabilistic Approach, SSGMRA Using an Equivalent Linear Approach, SSGMRA Using an Equivalent Linear Approach Plus and Minus One Standard Deviation, and AASHTO General Approach**

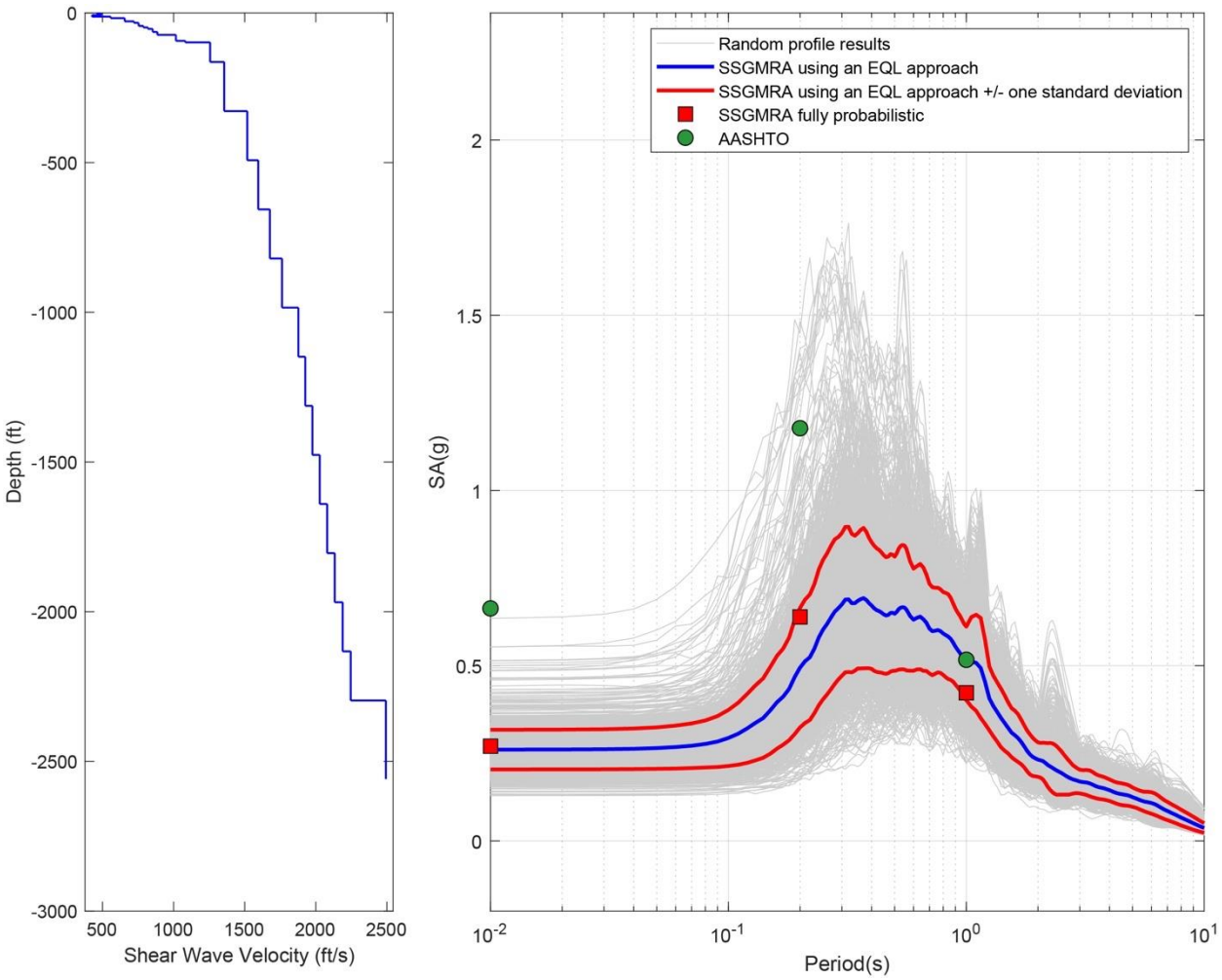


**Figure B-12. Left Panel: Shear-Wave Velocity Profile for Site 3 (Combined); and Right Panel: Results of SSGMRA Using a Fully Probabilistic Approach, SSGMRA Using an Equivalent Linear Approach, SSGMRA Using an Equivalent Linear Approach Plus and Minus One Standard Deviation, and AASHTO General Approach**

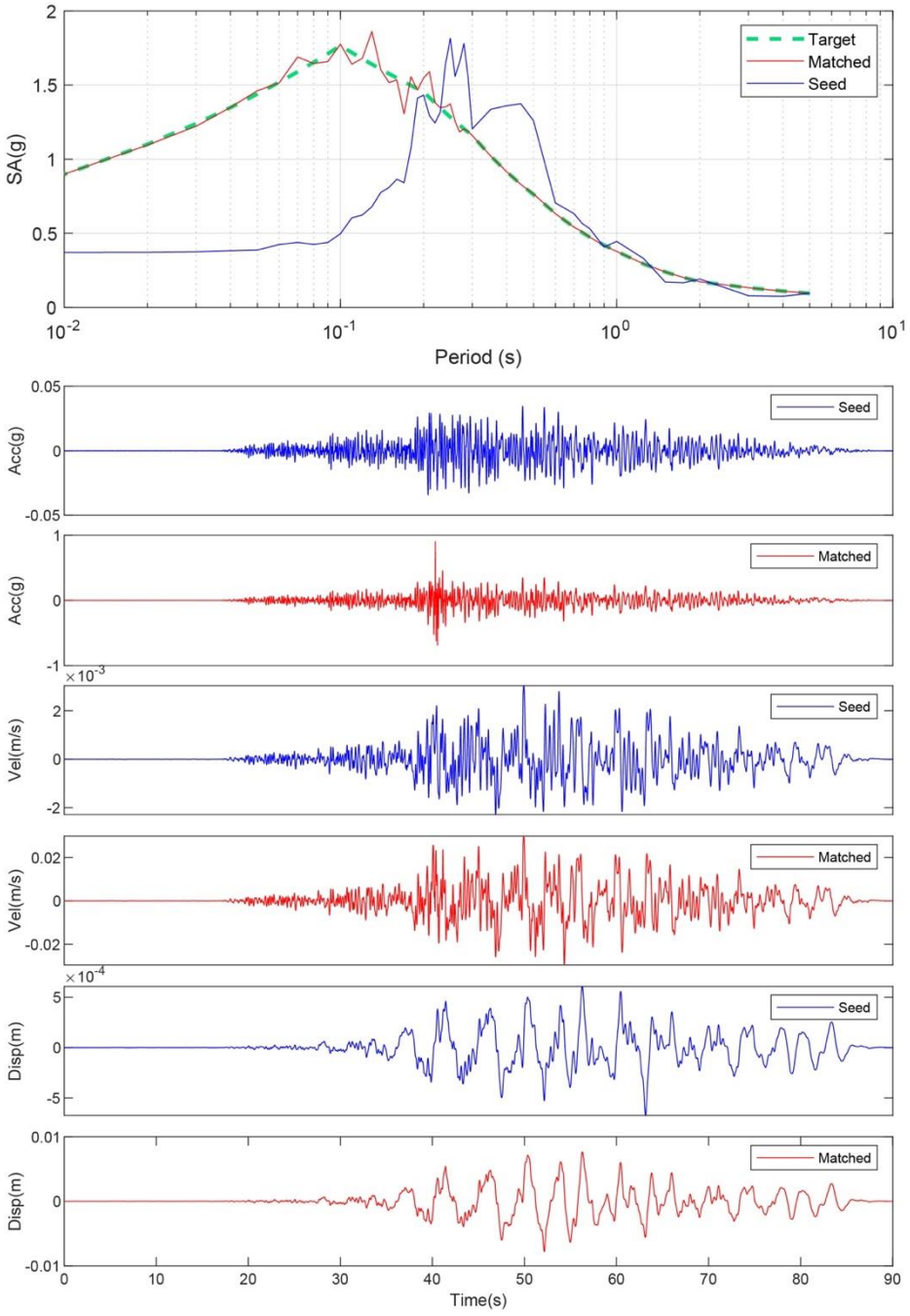


**Figure B-13. Matching Spectrum of Seed Motion (RSN1577-CHICHI-TTN025-E) to the Target Spectrum (UHS) at Site 4. The Middle Subplot Shows the Seed Motion, and the Bottom Subplot Indicates the Matched Motion**

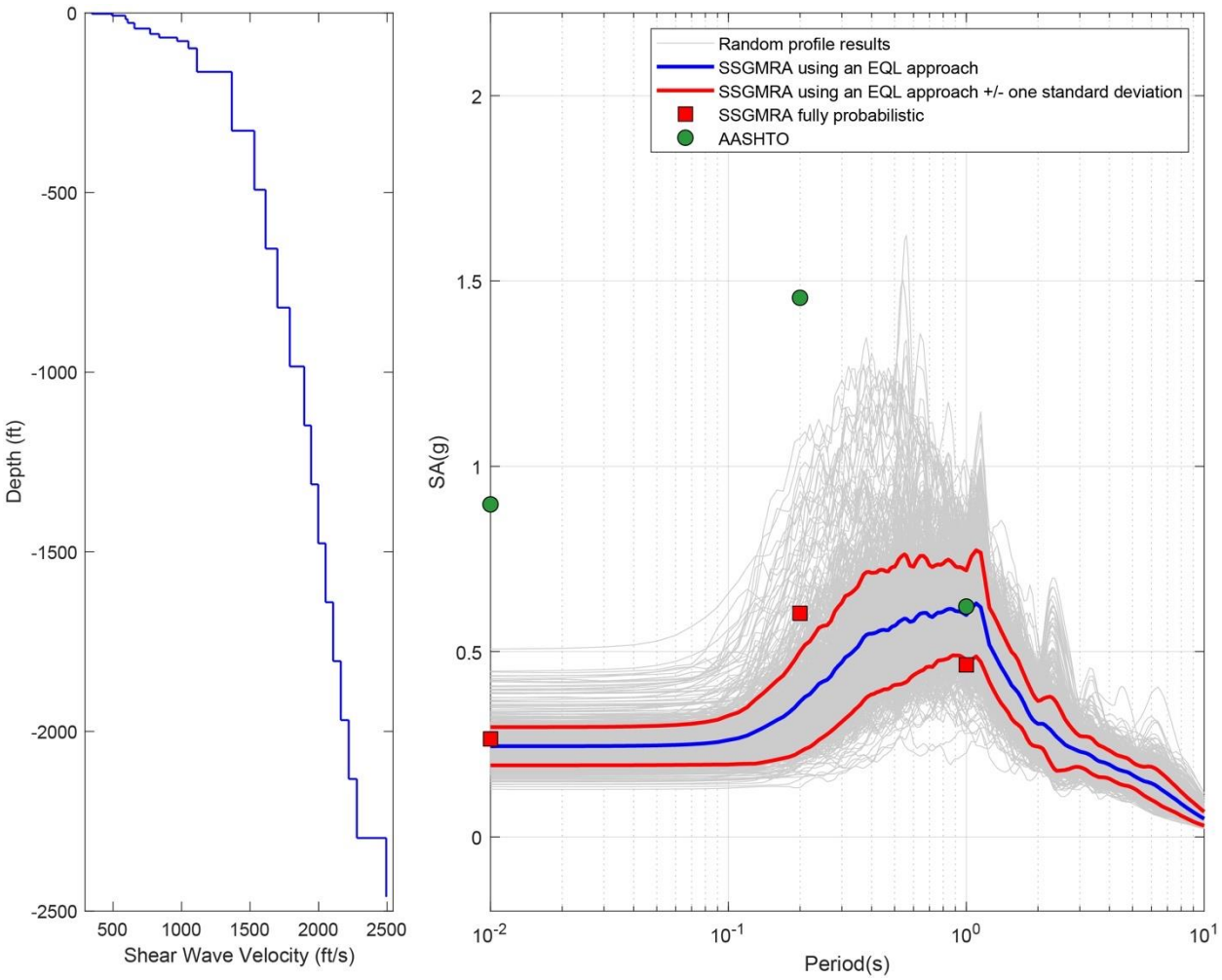


**Figure B-14. Left Panel: Shear-Wave Velocity Profile for Site 4 (Based on EPRI Soil Model); and Right Panel: Results of SSGMRA Using a Fully Probabilistic Approach, SSGMRA Using an Equivalent Linear Approach, SSGMRA Using an Equivalent Linear Approach Plus and Minus One Standard Deviation, and AASHTO General Approach**

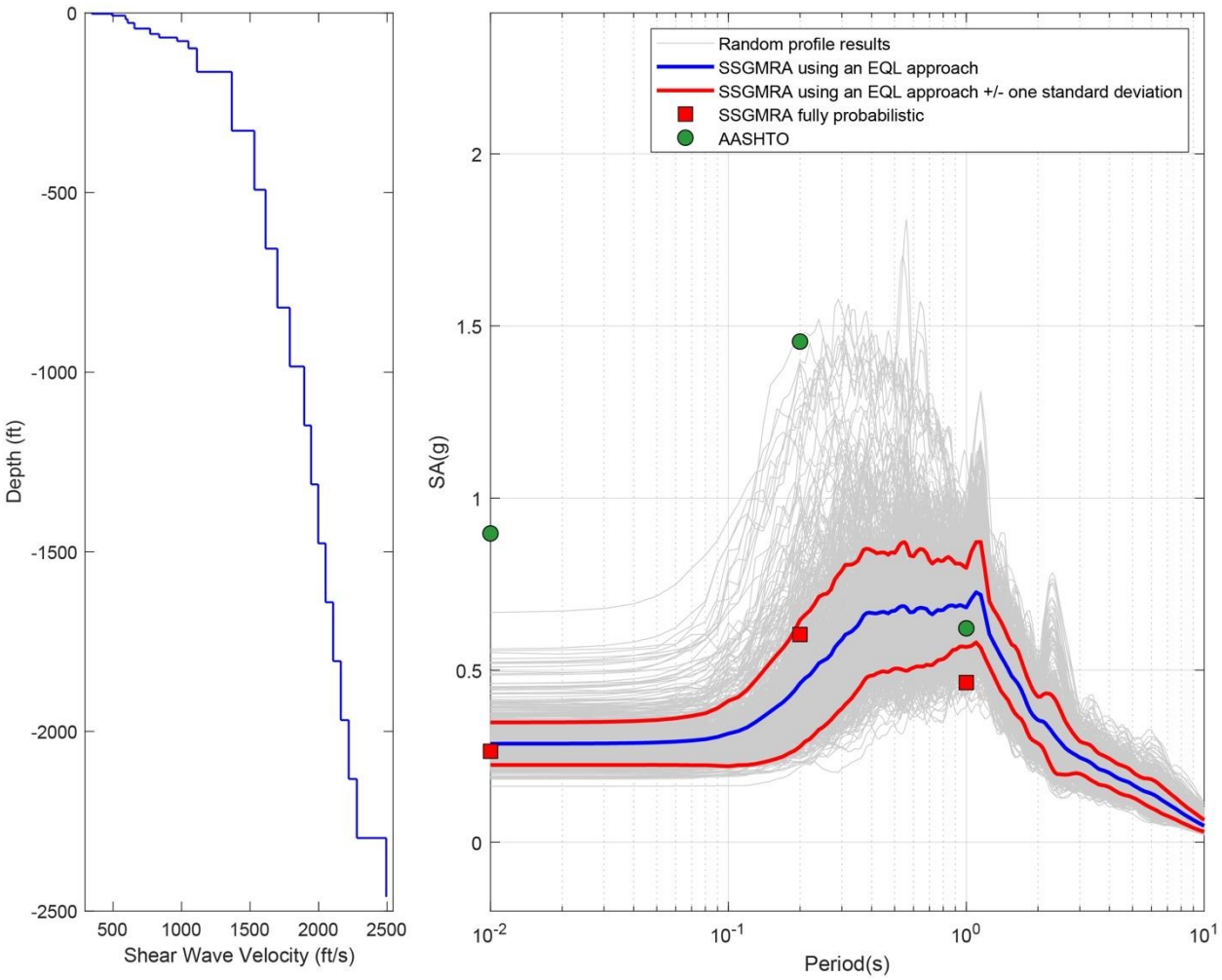


**Figure B-15. Left Panel: Shear-Wave Velocity Profile for Site 4 (Based on Peninsular Soil Model); and Right Panel: Results of SSGMRA Using a Fully Probabilistic Approach, SSGMRA Using an Equivalent Linear Approach, SSGMRA Using an Equivalent Linear Approach Plus and Minus One Standard Deviation, and AASHTO General Approach**

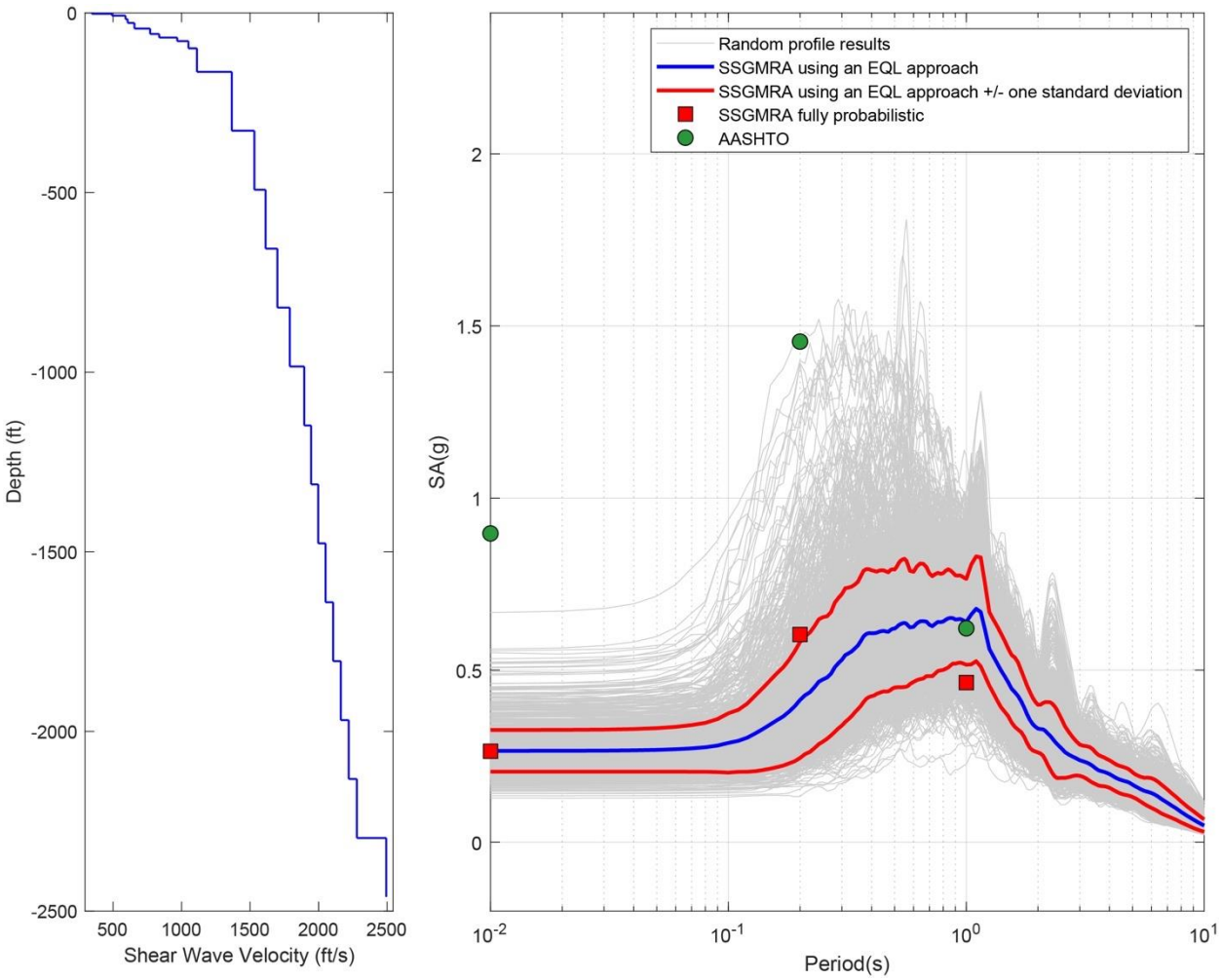


**Figure B-16. Left Panel: Shear-Wave Velocity Profile for Site 4 (Combined); and Right Panel: Results of SSGMRA Using a Fully Probabilistic Approach, SSGMRA Using an Equivalent Linear Approach, SSGMRA Using an Equivalent Linear Approach Plus and Minus One Standard Deviation, and AASHTO General Approach**

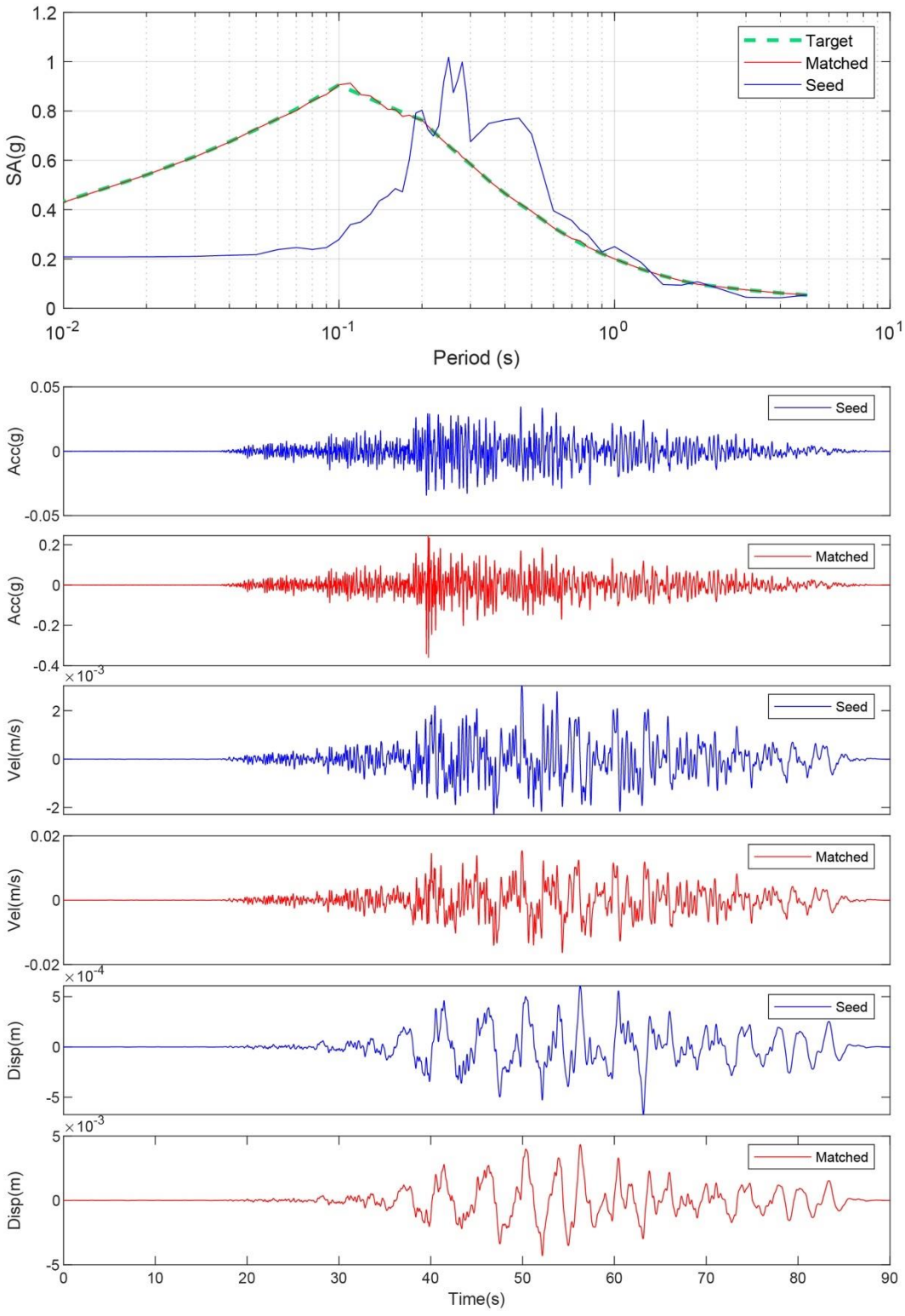


**Figure B-17. Matching Spectrum of Seed Motion (RSN1577-CHICHI-TTN025-E) to the Target Spectrum (UHS) at Site 5. The Middle Subplot Shows the Seed Motion, and the Bottom Subplot Indicates the Matched Motion**

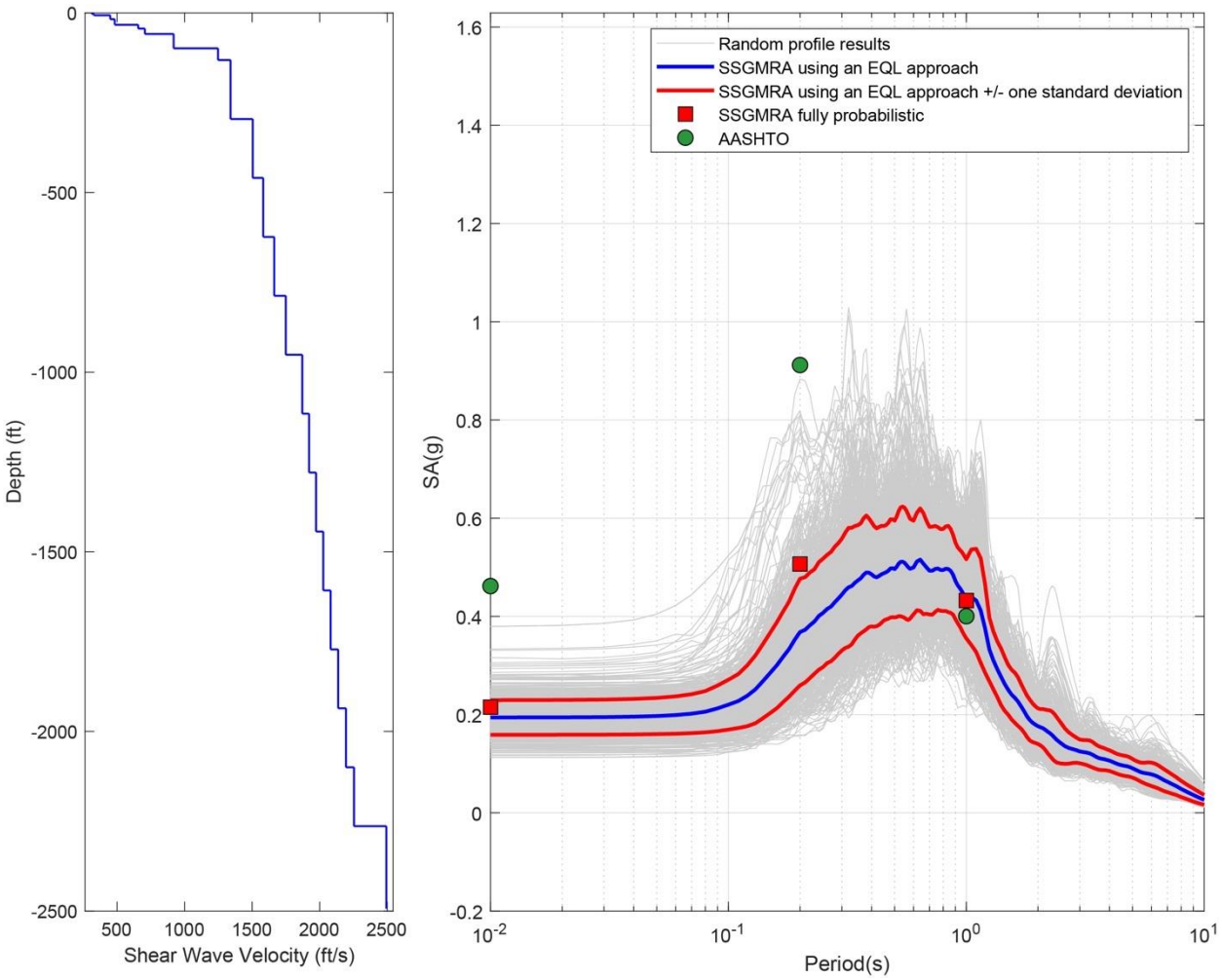


**Figure B-18. Left Panel: Shear-Wave Velocity Profile for Site 5 (Based on EPRI Soil Model); and Right Panel: Results of SSGMRA Using a Fully Probabilistic Approach, SSGMRA Using an Equivalent Linear Approach, SSGMRA Using an Equivalent Linear Approach Plus and Minus One Standard Deviation, and AASHTO General Approach**

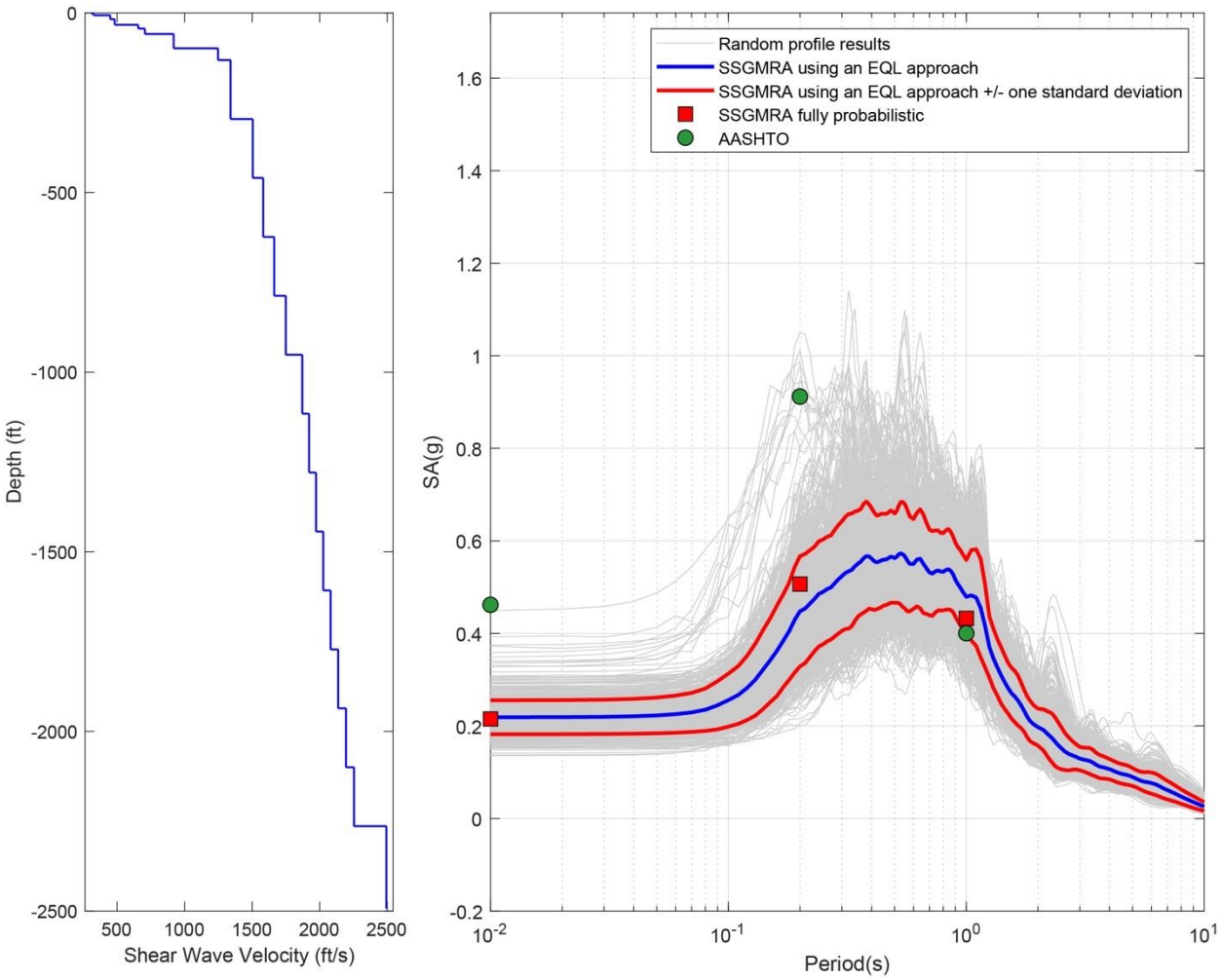


**Figure B-19. Left Panel: Shear-Wave Velocity Profile for Site 5 (Based on Peninsular Soil Model); and Right Panel: Results of SSGMRA Using a Fully Probabilistic Approach, SSGMRA Using an Equivalent Linear Approach, SSGMRA Using an Equivalent Linear Approach Plus and Minus One Standard Deviation, and AASHTO General Approach**

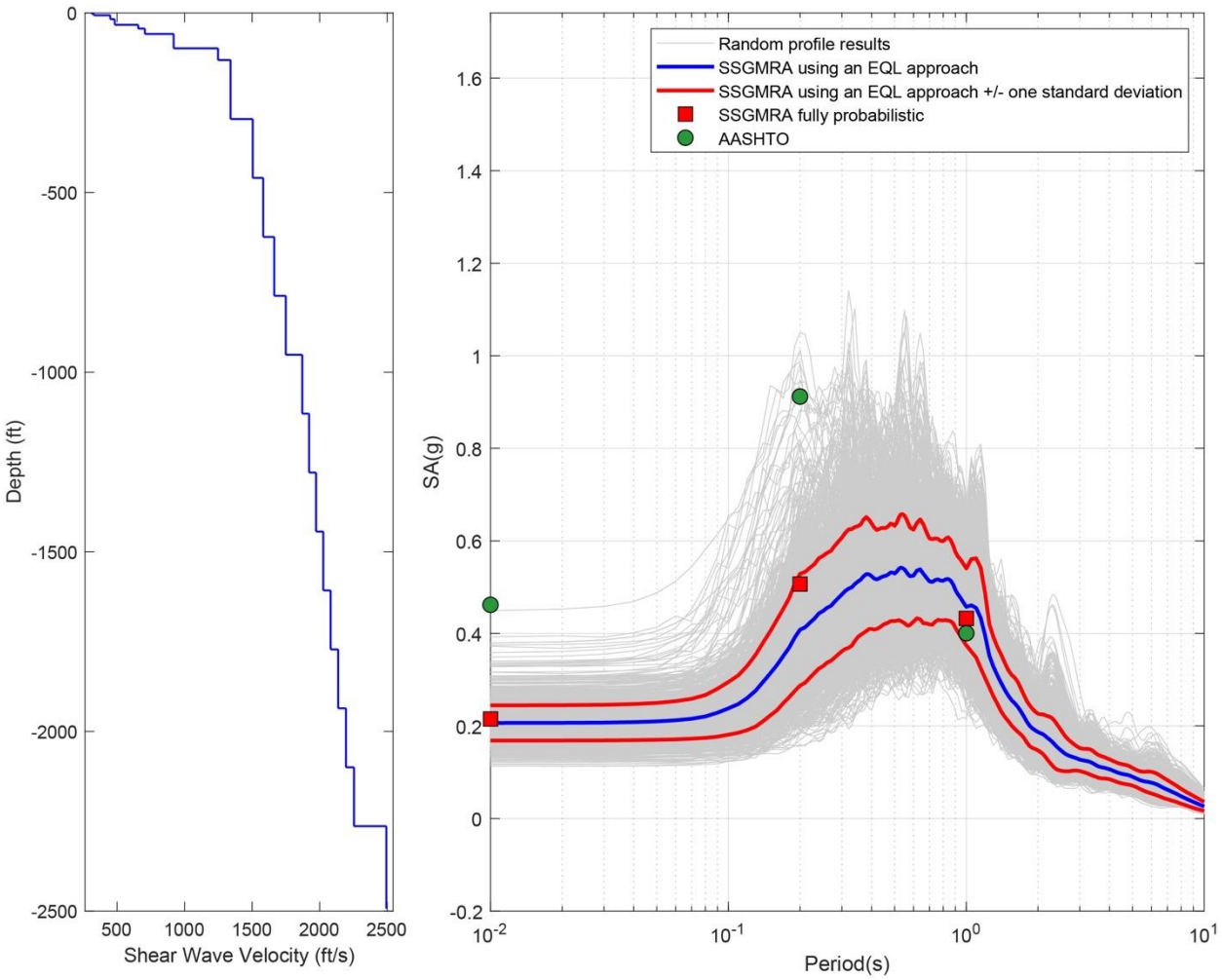


**Figure B-20. Left Panel: Shear-Wave Velocity Profile for Site 5 (Combined); and Right Panel: Results of SSGMRA Using a Fully Probabilistic Approach, SSGMRA Using an Equivalent Linear Approach, SSGMRA Using an Equivalent Linear Approach Plus and Minus One Standard Deviation, and AASHTO General Approach**

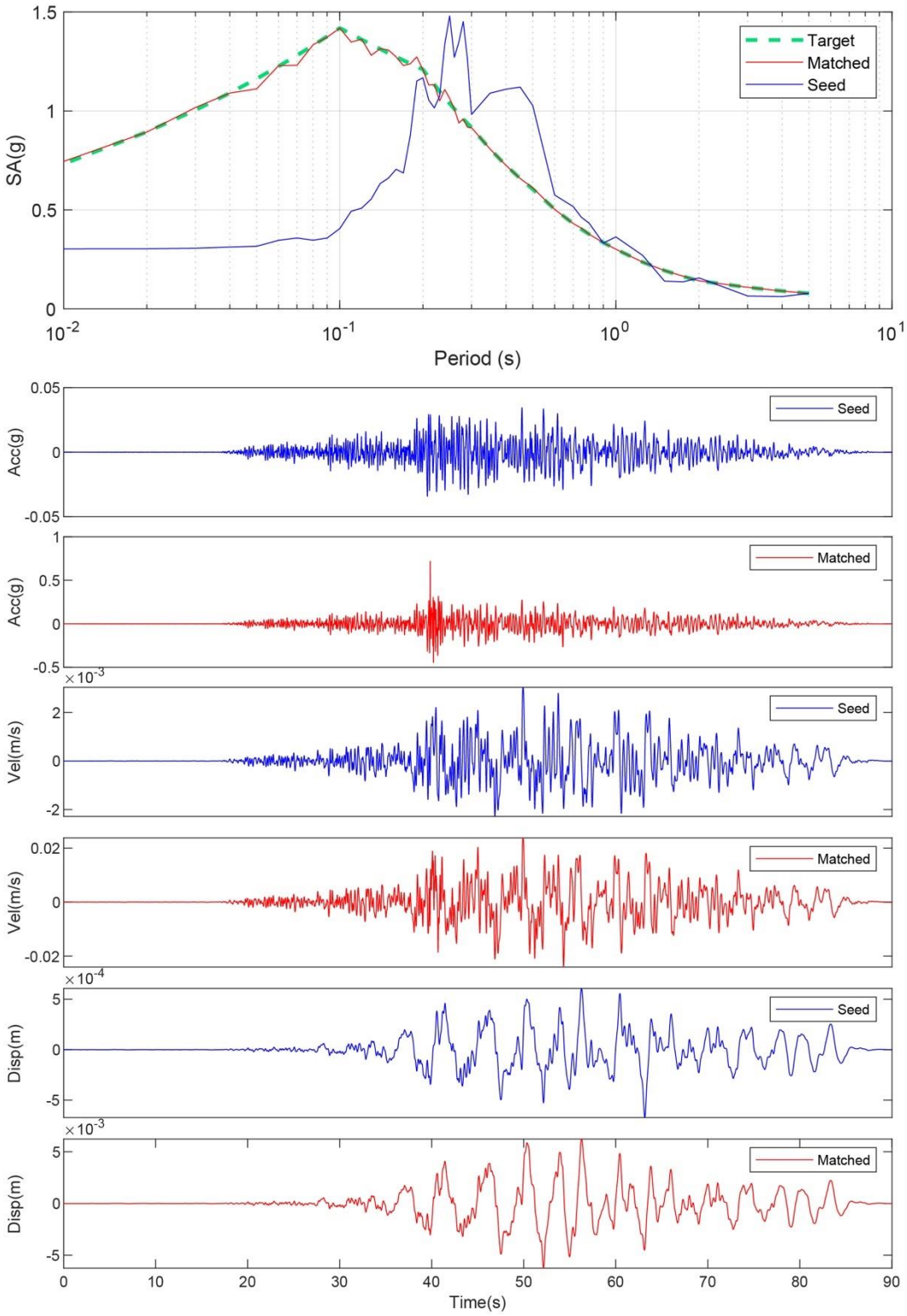


**Figure B-21. Matching Spectrum of Seed Motion (RSN1577-CHICHI-TTN025-E) to the Target Spectrum (UHS) at Site 6. The Middle Subplot Shows the Seed Motion, and the Bottom Subplot Indicates the Matched Motion**

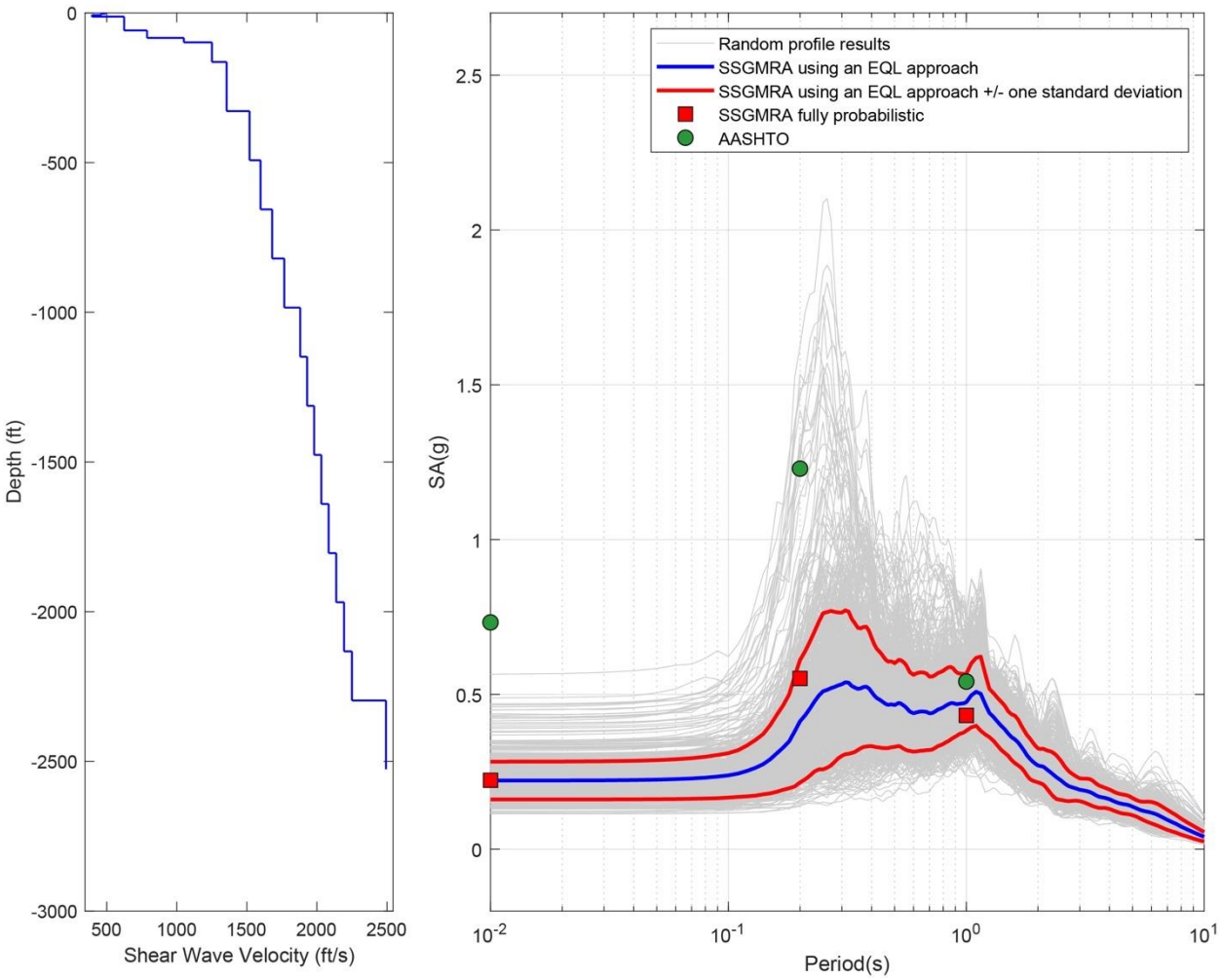


**Figure B-22. Left Panel: Shear-Wave Velocity Profile for Site 6 (Based on EPRI Soil Model); and Right Panel: Results of SSGMRA Using a Fully Probabilistic Approach, SSGMRA Using an Equivalent Linear Approach, SSGMRA Using an Equivalent Linear Approach Plus and Minus One Standard Deviation, and AASHTO General Approach**

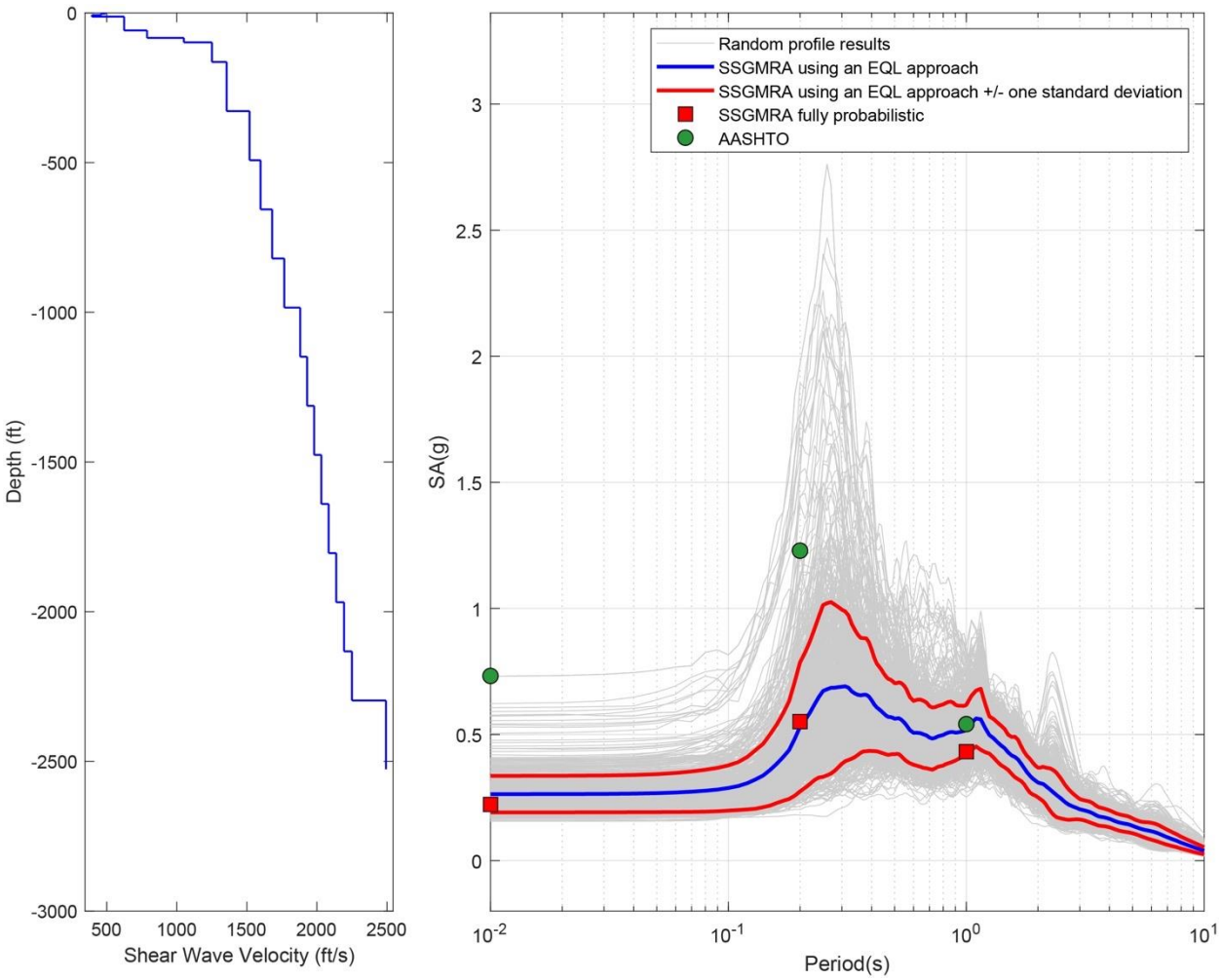


**Figure B-23. Left Panel: Shear-Wave Velocity Profile for Site 6 (Based on Peninsular Soil Model); and Right Panel: Results of SSGMRA Using a Fully Probabilistic Approach, SSGMRA Using an Equivalent Linear Approach, SSGMRA Using an Equivalent Linear Approach Plus and Minus One Standard Deviation, and AASHTO General Approach**

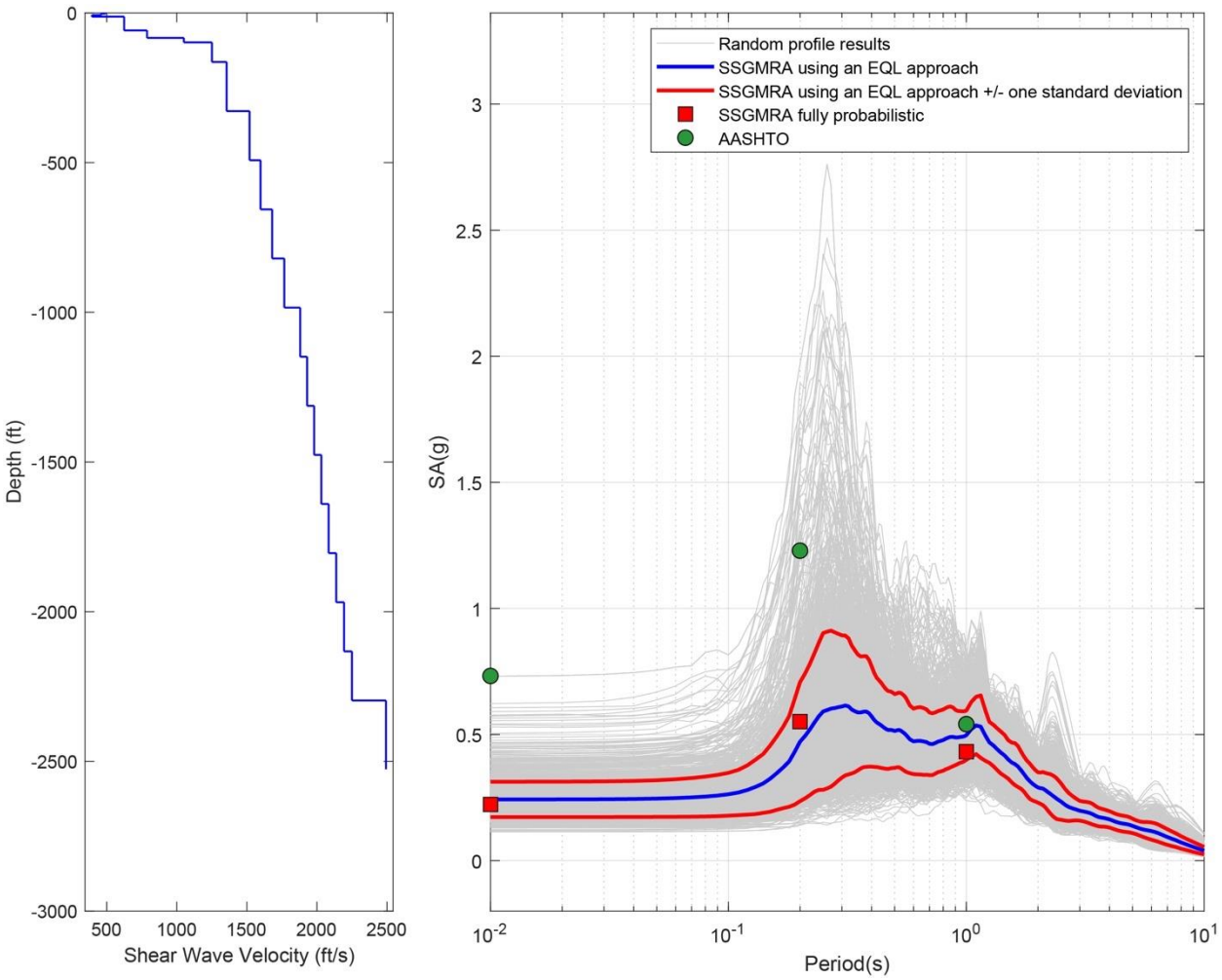


**Figure B-24. Left Panel: Shear-Wave Velocity Profile for Site 6 (Combined); and Right Panel: Results of SSGMRA Using a Fully Probabilistic Approach, SSGMRA Using an Equivalent Linear Approach, SSGMRA Using an Equivalent Linear Approach Plus and Minus One Standard Deviation, and AASHTO General Approach**

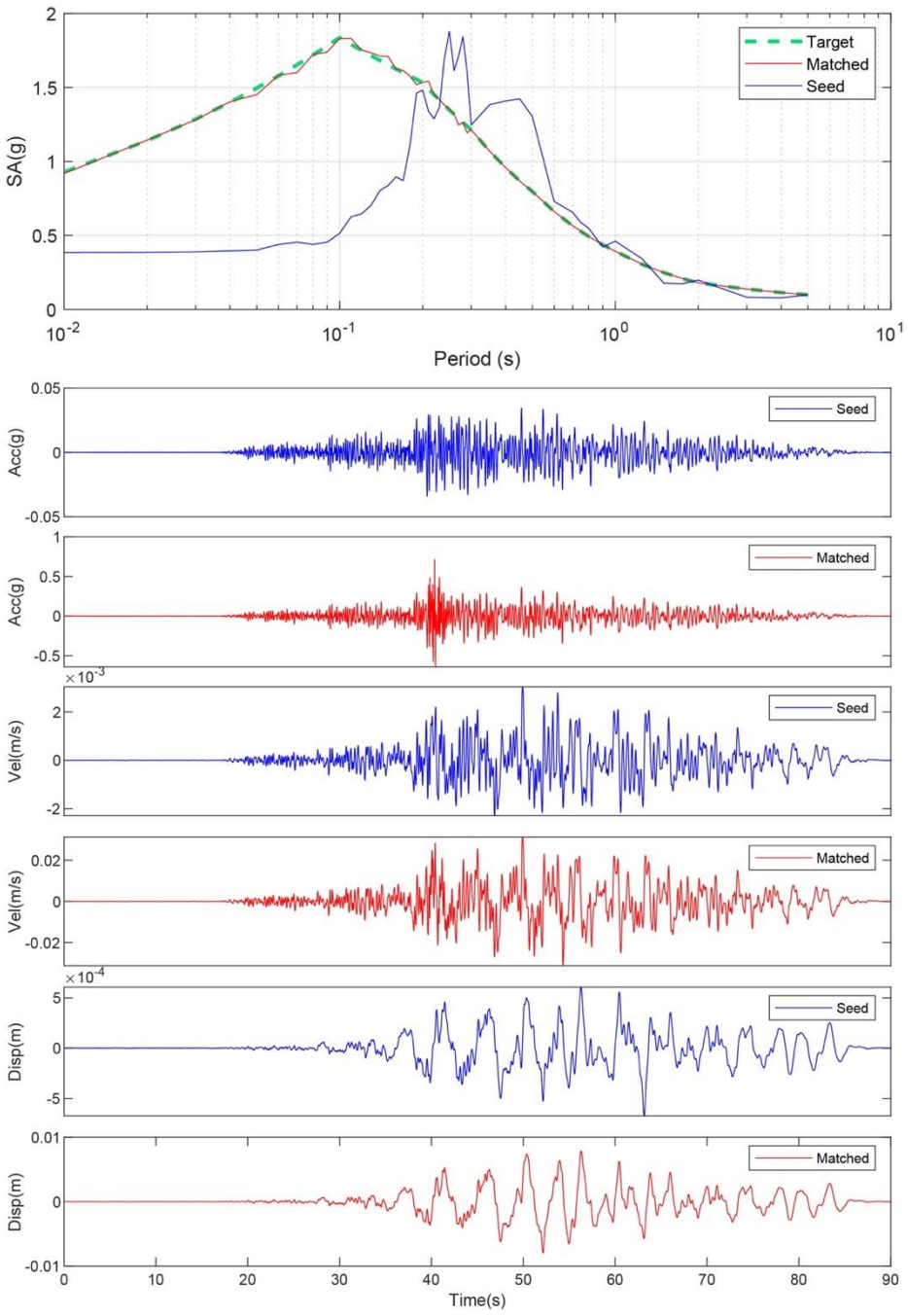


**Figure B-25. Matching Spectrum of Seed Motion (RSN1577-CHICHI-TTN025-E) to the Target Spectrum (UHS) at Site 7. The Middle Subplot Shows the Seed Motion, and the Bottom Subplot Indicates the Matched Motion**

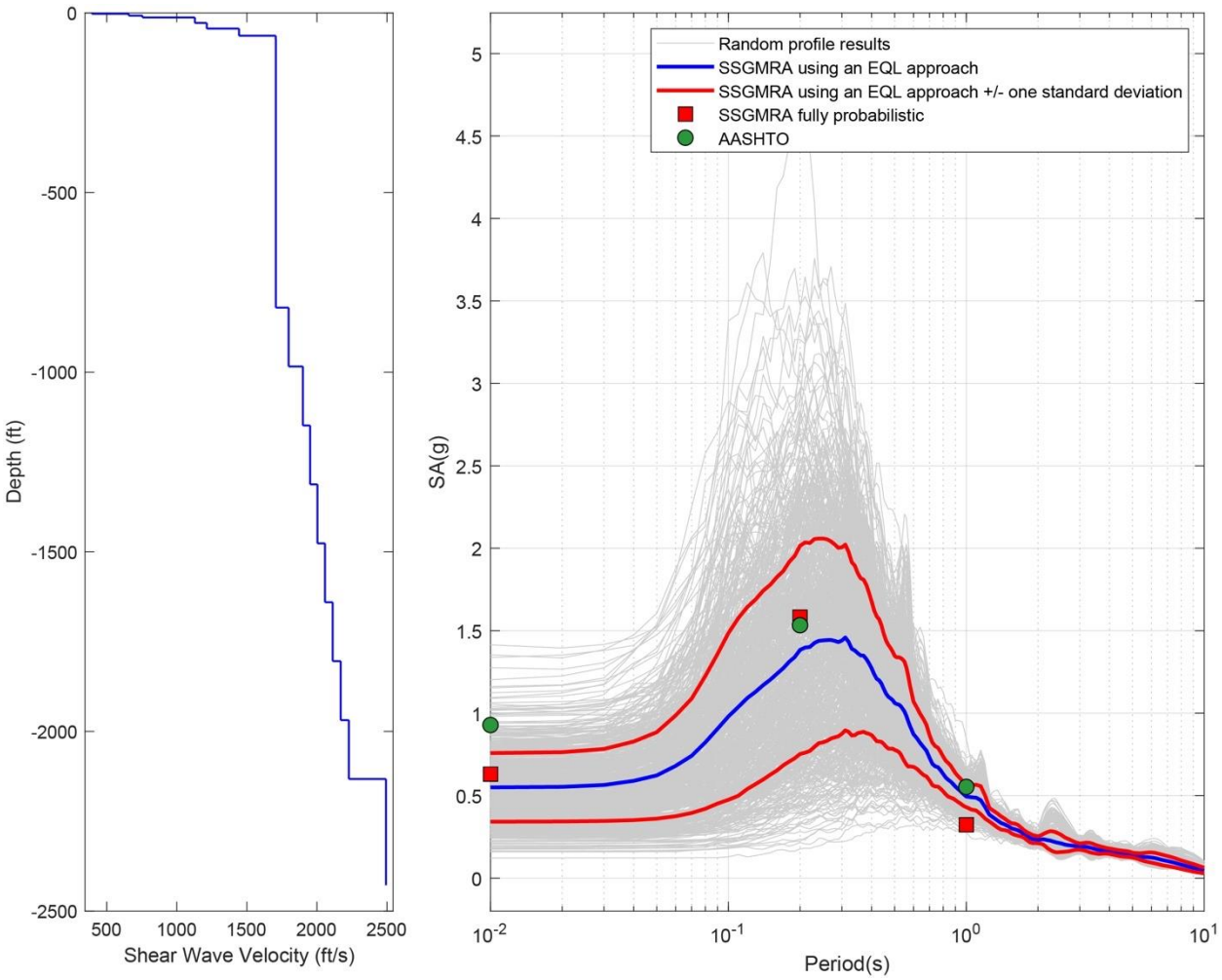


**Figure B-26. Left Panel: Shear-Wave Velocity Profile for Site 7 (Based on EPRI Soil Model); and Right Panel: Results of SSGMRA Using a Fully Probabilistic Approach, SSGMRA Using an Equivalent Linear Approach, SSGMRA Using an Equivalent Linear Approach Plus and Minus One Standard Deviation, and AASHTO General Approach**

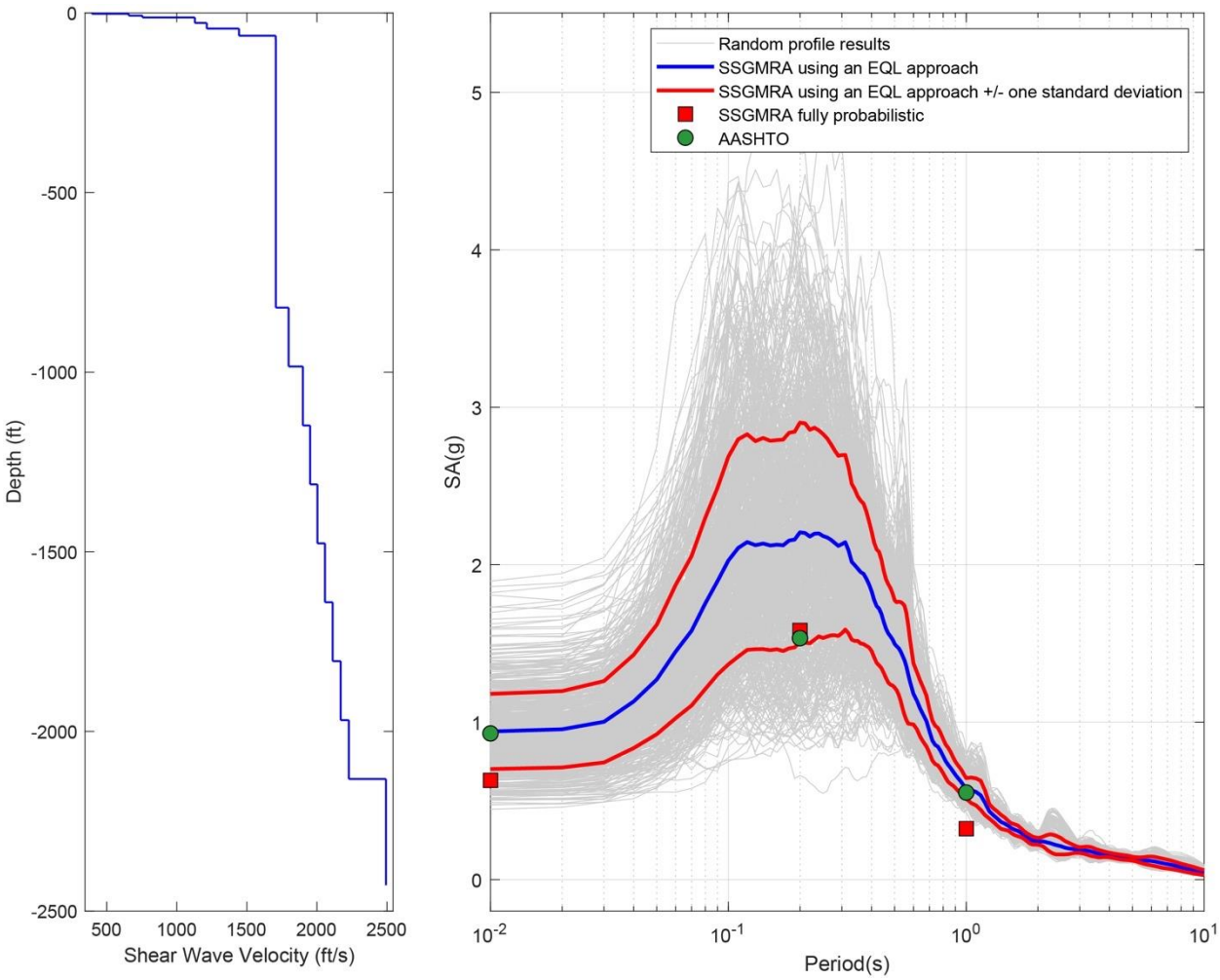


**Figure B-27. Left Panel: Shear-Wave Velocity Profile for Site 7 (Based on Peninsular Soil Model); and Right Panel: Results of SSGMRA Using a Fully Probabilistic Approach, SSGMRA Using an Equivalent Linear Approach, SSGMRA Using an Equivalent Linear Approach Plus and Minus One Standard Deviation, and AASHTO General Approach**

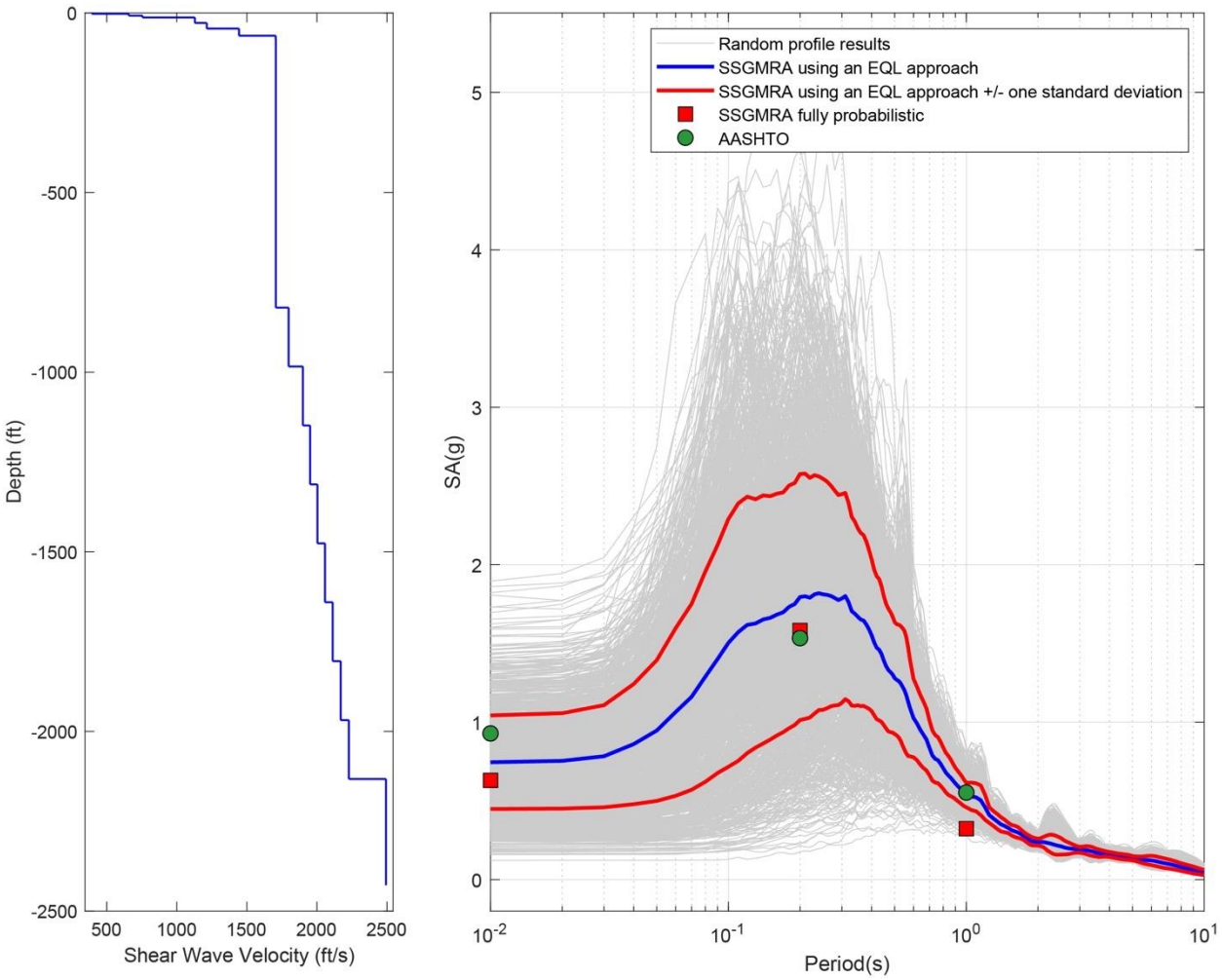


**Figure B-28. Left Panel: Shear-Wave Velocity Profile for Site 7 (Combined); and Right Panel: Results of SSGMRA Using a Fully Probabilistic Approach, SSGMRA Using an Equivalent Linear Approach, SSGMRA Using an Equivalent Linear Approach Plus and Minus One Standard Deviation, and AASHTO General Approach**

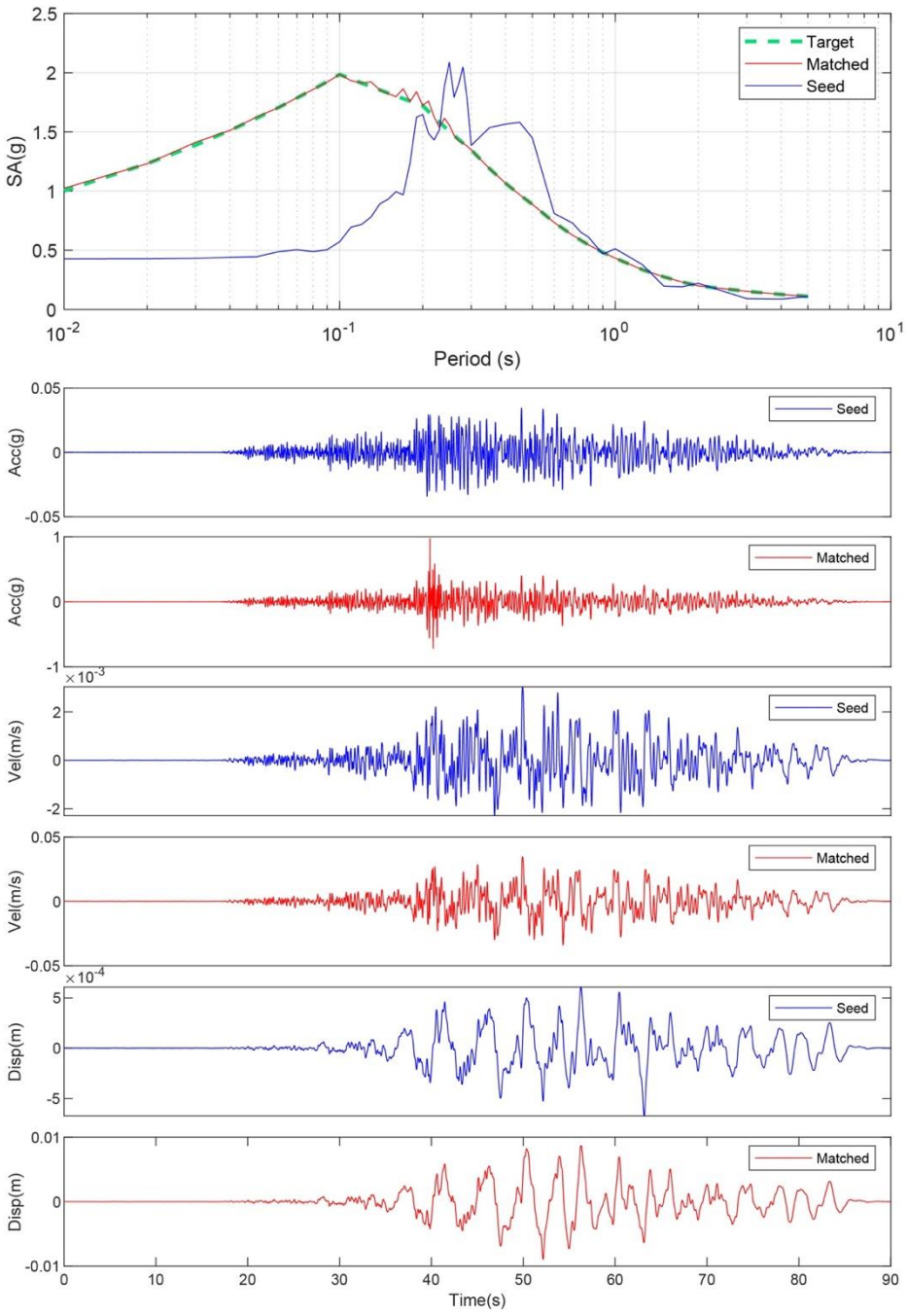


**Figure B-29. Matching Spectrum of Seed Motion (RSN1577-CHICHI-TTN025-E) to the Target Spectrum (UHS) at Site 8. The Middle Subplot Shows the Seed Motion, and the Bottom Subplot Indicates the Matched Motion**

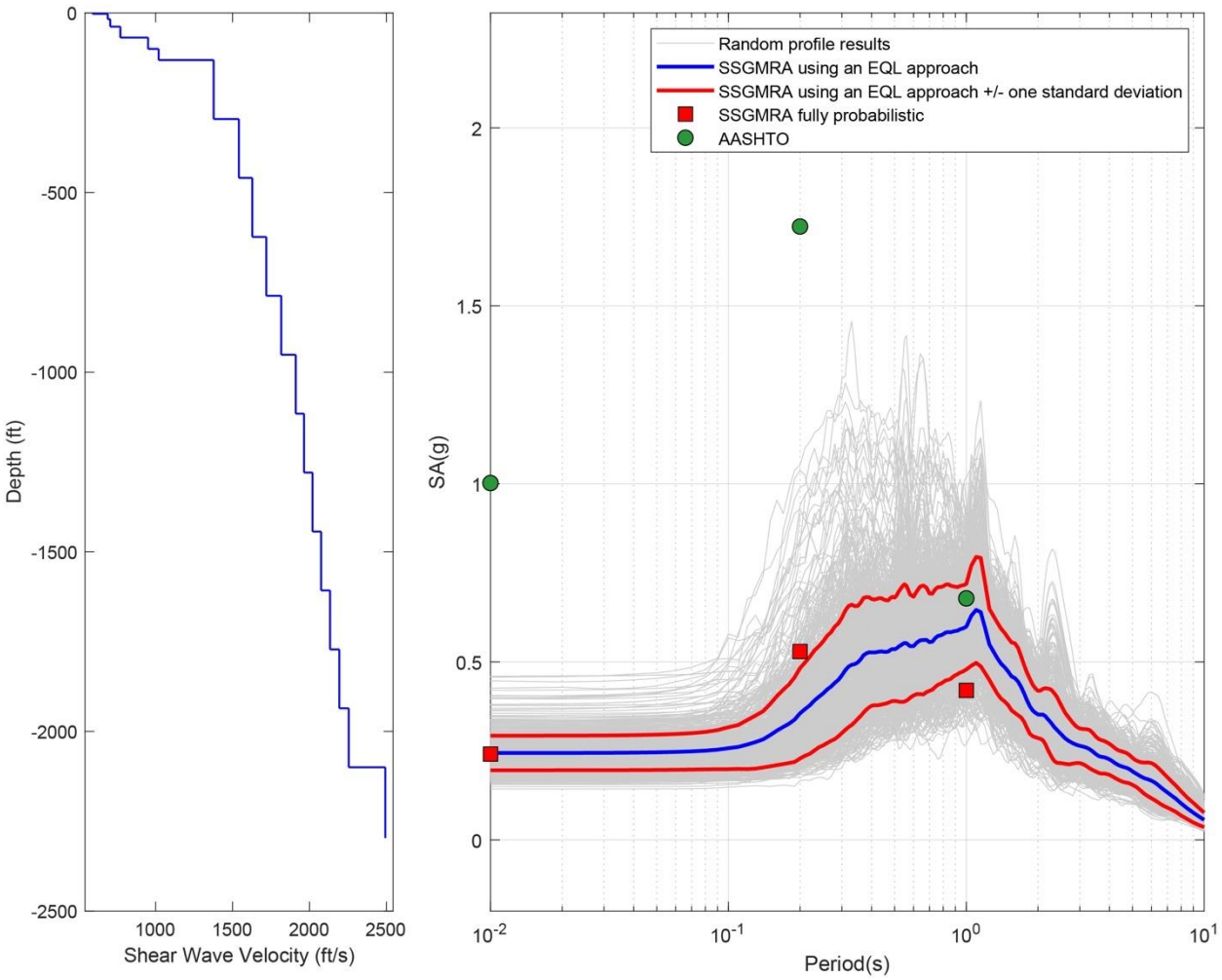


**Figure B-30. Left Panel: Shear-Wave Velocity Profile for Site 8 (Based on EPRI Soil Model); and Right Panel: Results of SSGMRA Using a Fully Probabilistic Approach, SSGMRA Using an Equivalent Linear Approach, SSGMRA Using an Equivalent Linear Approach Plus and Minus One Standard Deviation, and AASHTO General Approach**

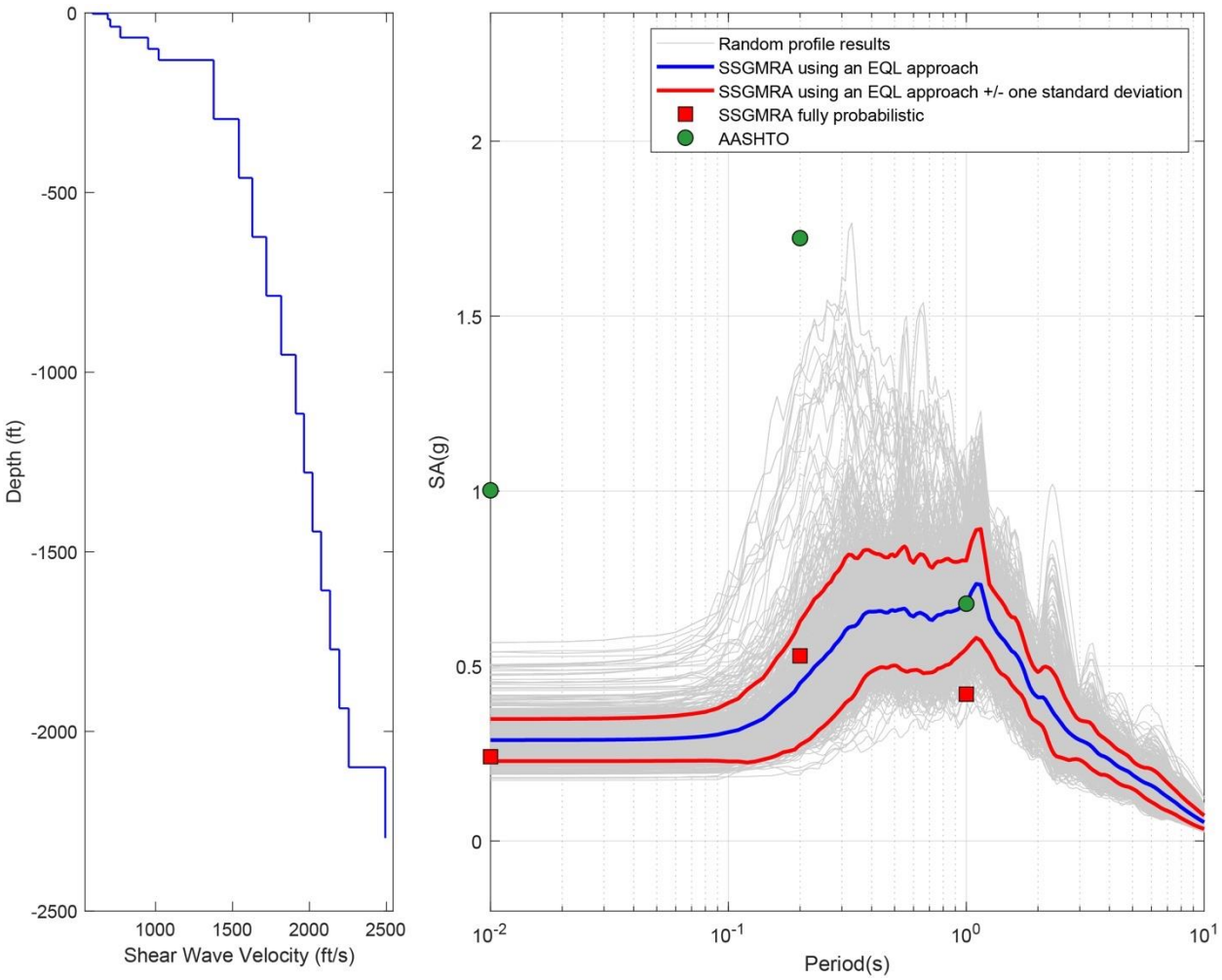


**Figure B-31. Left Panel: Shear-Wave Velocity Profile for Site 8 (Based on Peninsular Soil Model); and Right Panel: Results of SSGMRA Using a Fully Probabilistic Approach, SSGMRA Using an Equivalent Linear Approach, SSGMRA Using an Equivalent Linear Approach Plus and Minus One Standard Deviation, and AASHTO General Approach**

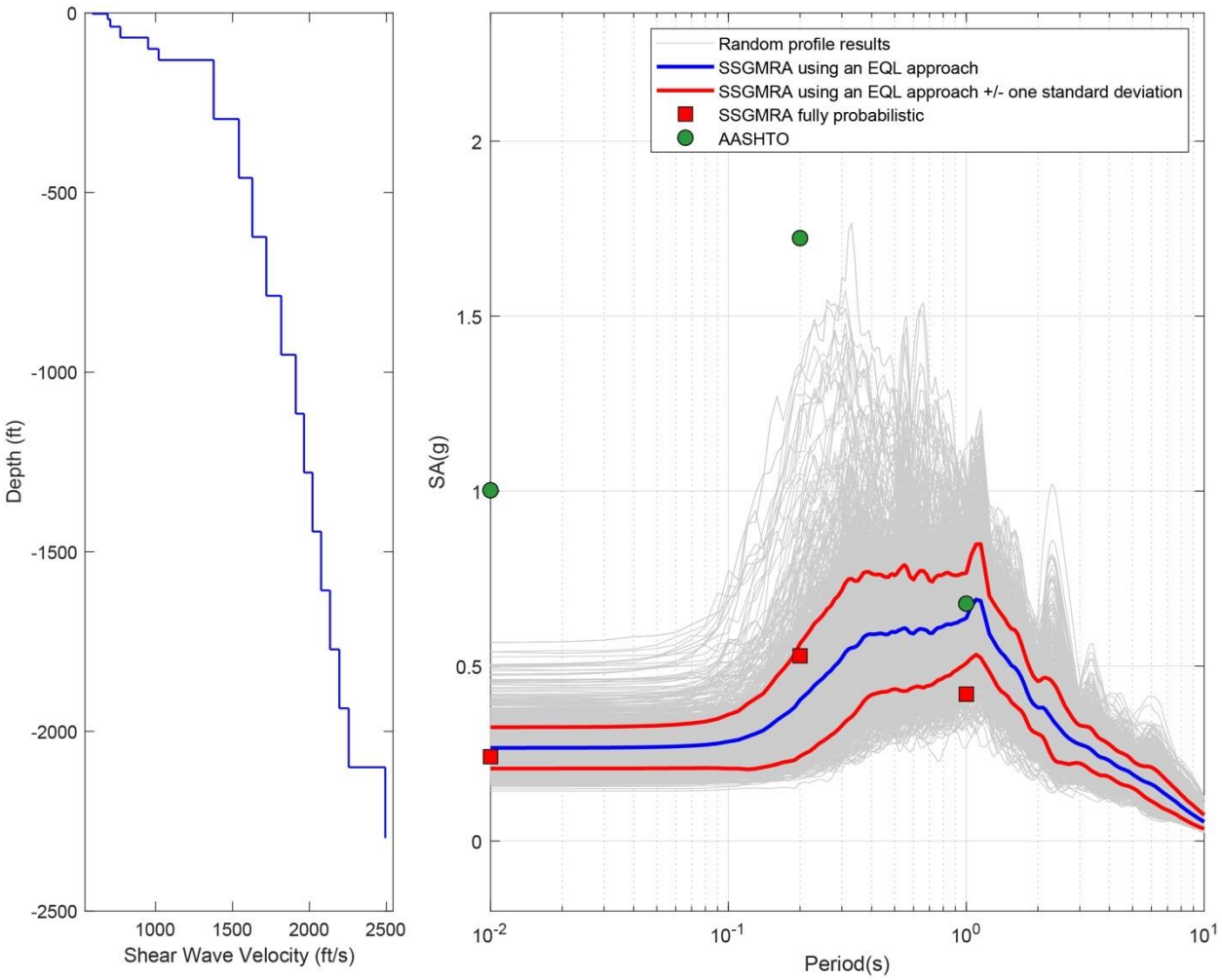


**Figure B-32. Left Panel: Shear-Wave Velocity Profile for Site 8 (Combined); and Right Panel: Results of SSGMRA Using a Fully Probabilistic Approach, SSGMRA Using an Equivalent Linear Approach, SSGMRA Using an Equivalent Linear Approach Plus and Minus One Standard Deviation, and AASHTO General Approach**

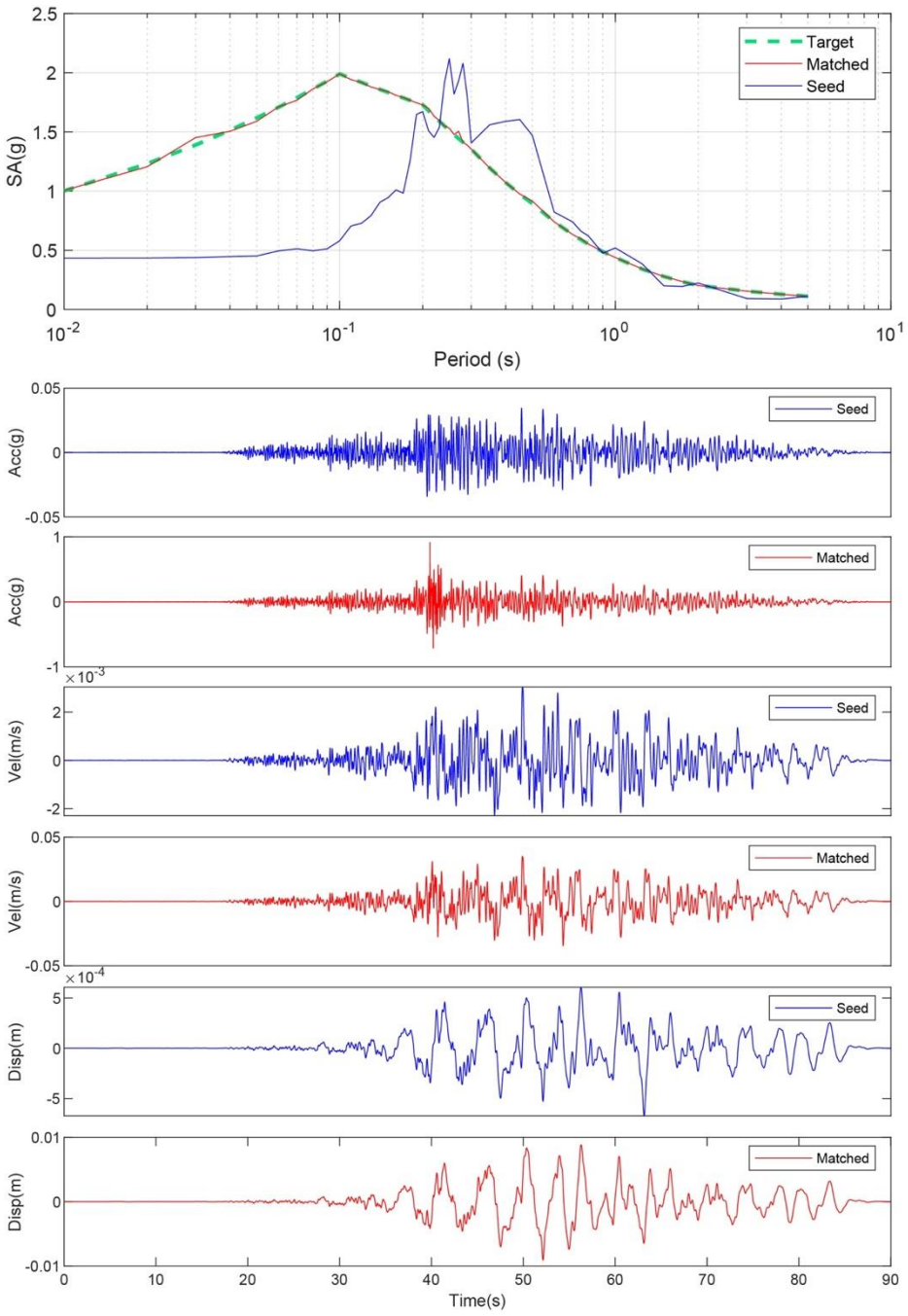


**Figure B-33. Matching Spectrum of Seed Motion (RSN1577-CHICHI-TTN025-E) to The Target Spectrum (UHS) at Site 9. The Middle Subplot Shows the Seed Motion, and The Bottom Subplot Indicates the Matched Motion**

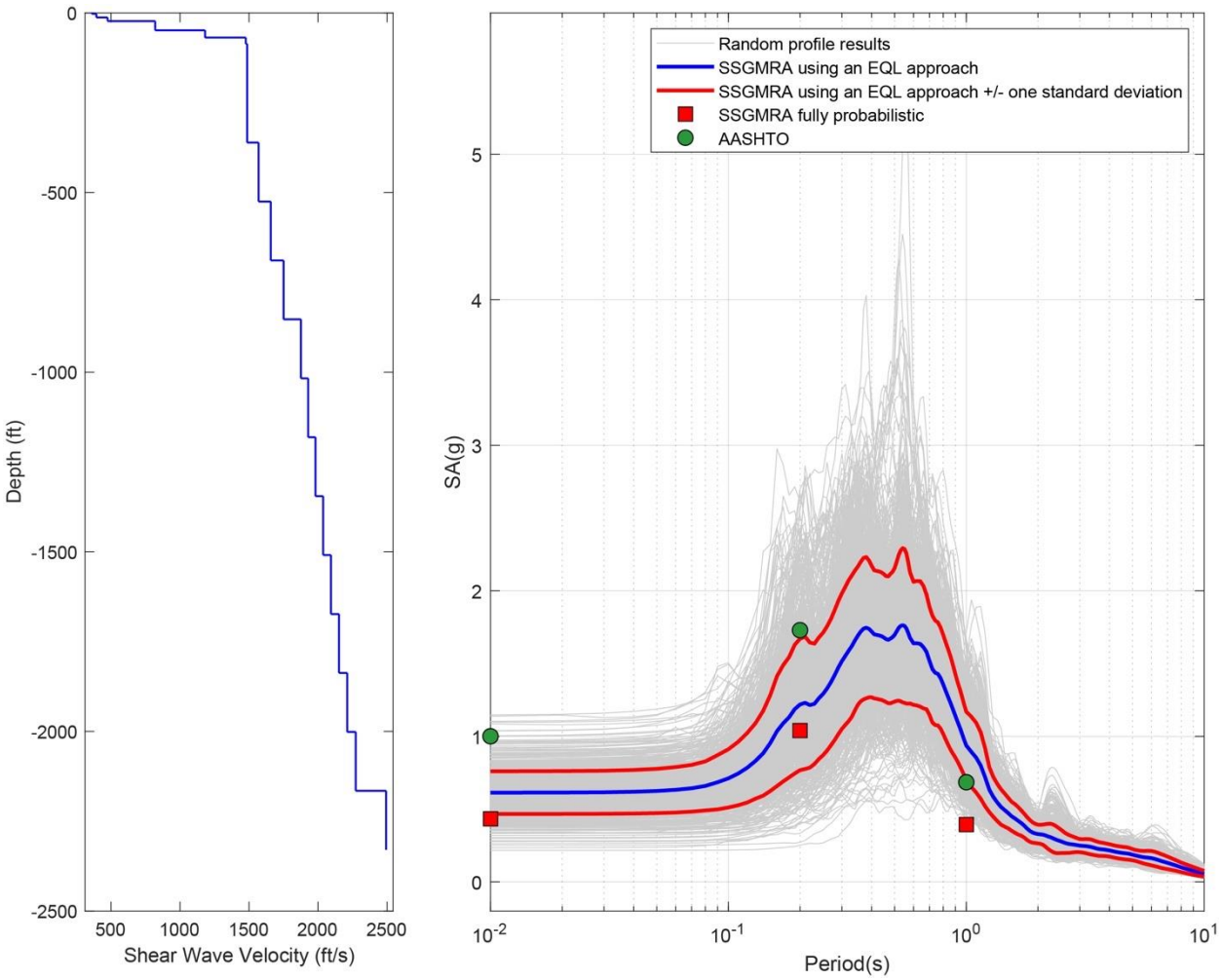


**Figure B-34. Left Panel: Shear-Wave Velocity Profile for Site 9 (Based on EPRI Soil Model); and Right Panel: Results of SSGMRA Using a Fully Probabilistic Approach, SSGMRA Using an Equivalent Linear Approach, SSGMRA Using an Equivalent Linear Approach Plus and Minus One Standard Deviation, and AASHTO General Approach**

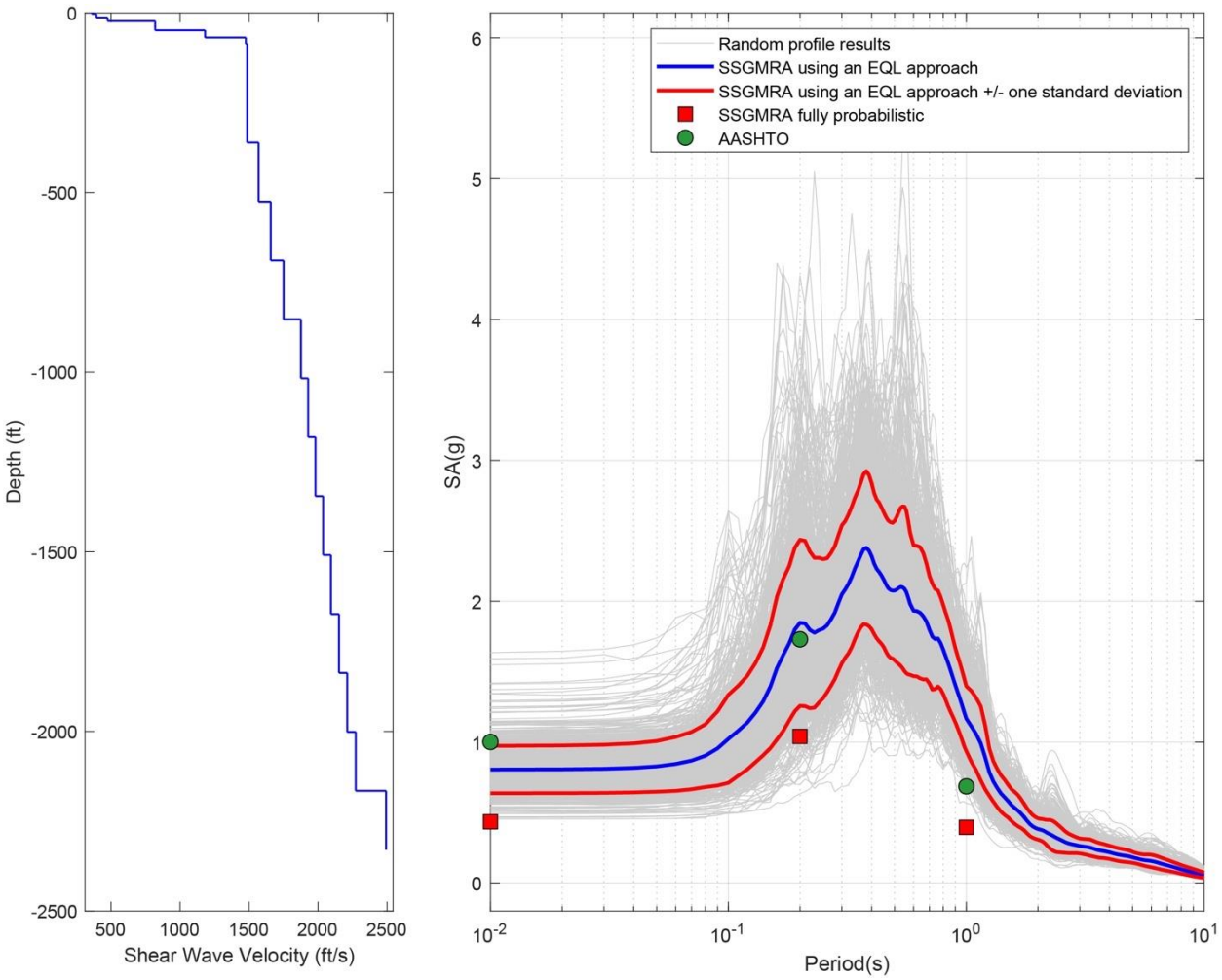


**Figure B-35. Left Panel: Shear-Wave Velocity Profile for Site 9 (Based on Peninsular Soil Model); and Right Panel: Results of SSGMRA Using a Fully Probabilistic Approach, SSGMRA Using an Equivalent Linear Approach, SSGMRA Using an Equivalent Linear Approach Plus and Minus One Standard Deviation, and AASHTO General Approach**

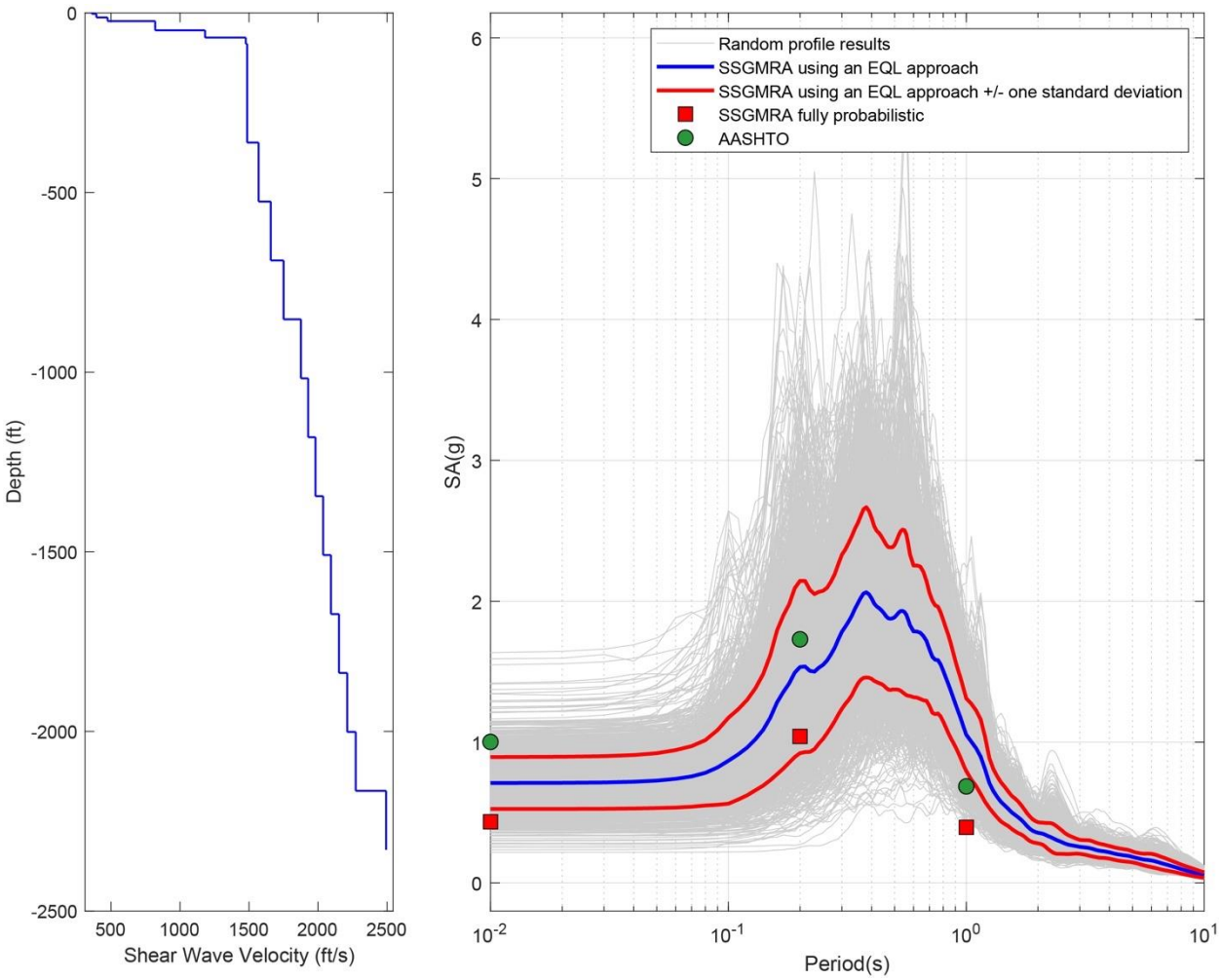


**Figure B-36. Left Panel: Shear-Wave Velocity Profile for Site 9 (Combined); and Right Panel: Results of SSGMRA Using a Fully Probabilistic Approach, SSGMRA Using an Equivalent Linear Approach, SSGMRA Using an Equivalent Linear Approach Plus and Minus One Standard Deviation, and AASHTO General Approach**

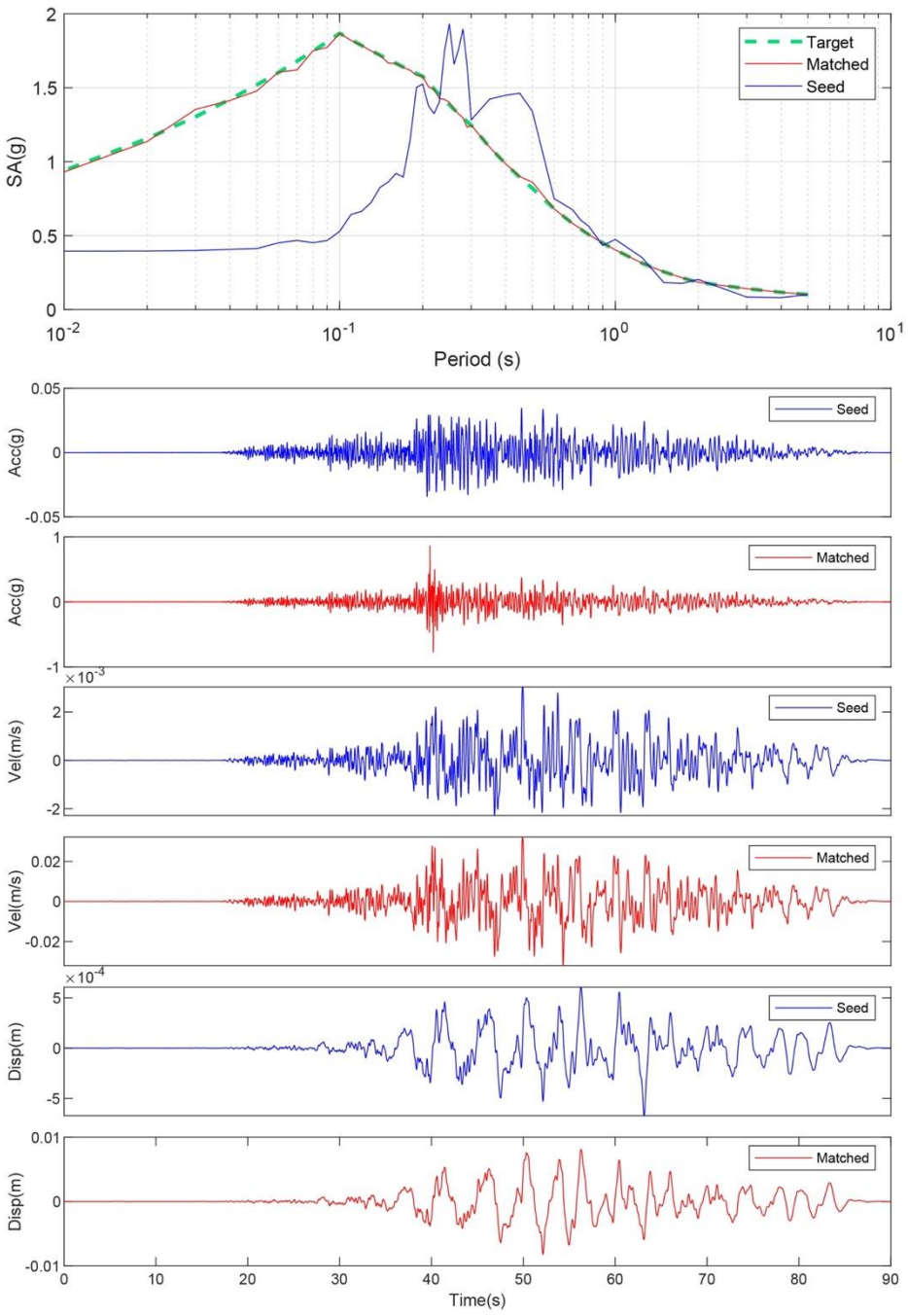


**Figure B-37. Matching Spectrum of Seed Motion (RSN1577-CHICHI-TTN025-E) to the Target Spectrum (UHS) at Site 10. The Middle Subplot Shows the Seed Motion, and the Bottom Subplot Indicates the Matched Motion**

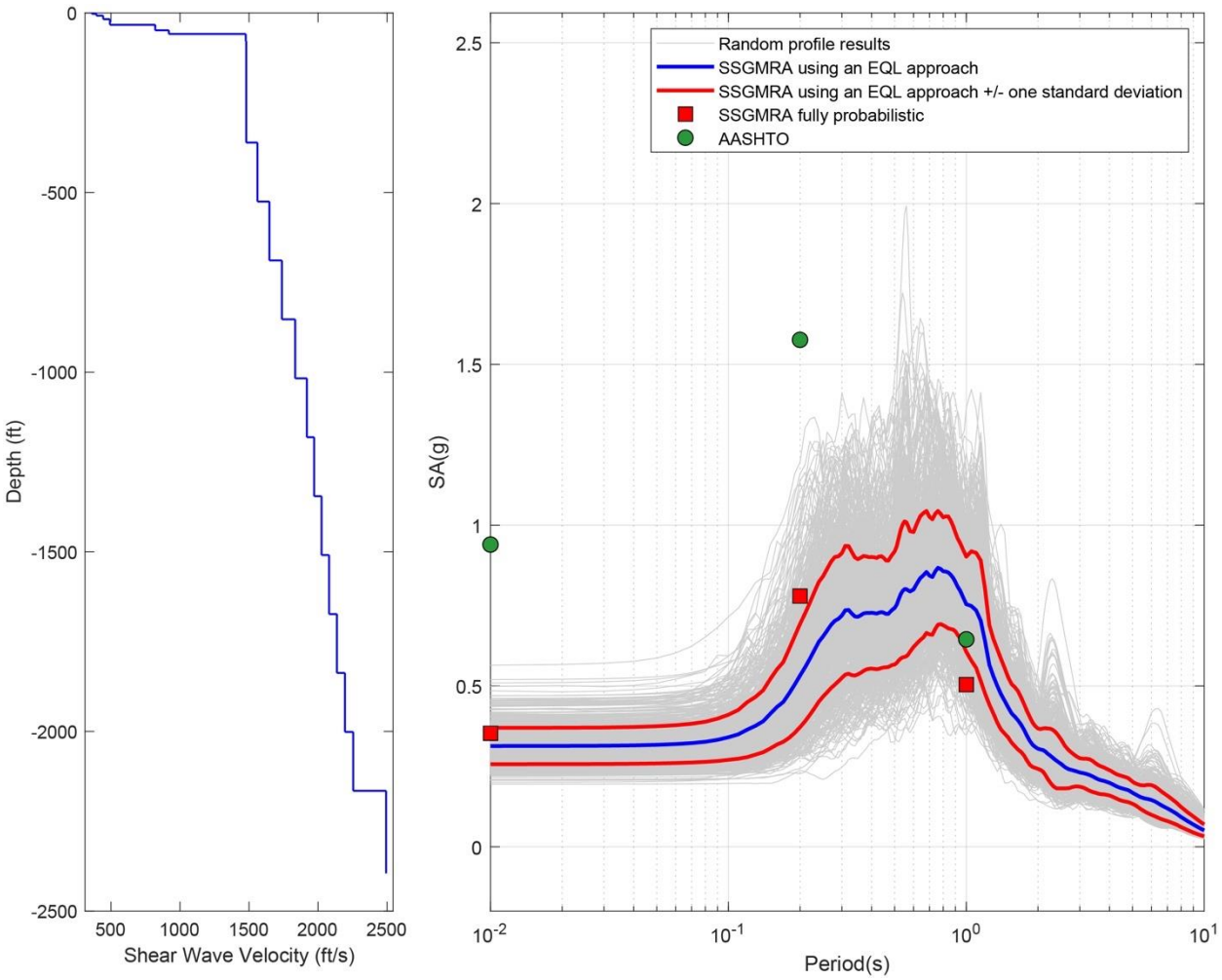


**Figure B-38. Left Panel: Shear-Wave Velocity Profile for Site 10 (Based on EPRI Soil Model); and Right Panel: Results of SSGMRA Using a Fully Probabilistic Approach, SSGMRA Using an Equivalent Linear Approach, SSGMRA Using an Equivalent Linear Approach Plus and Minus One Standard Deviation, and AASHTO General Approach**

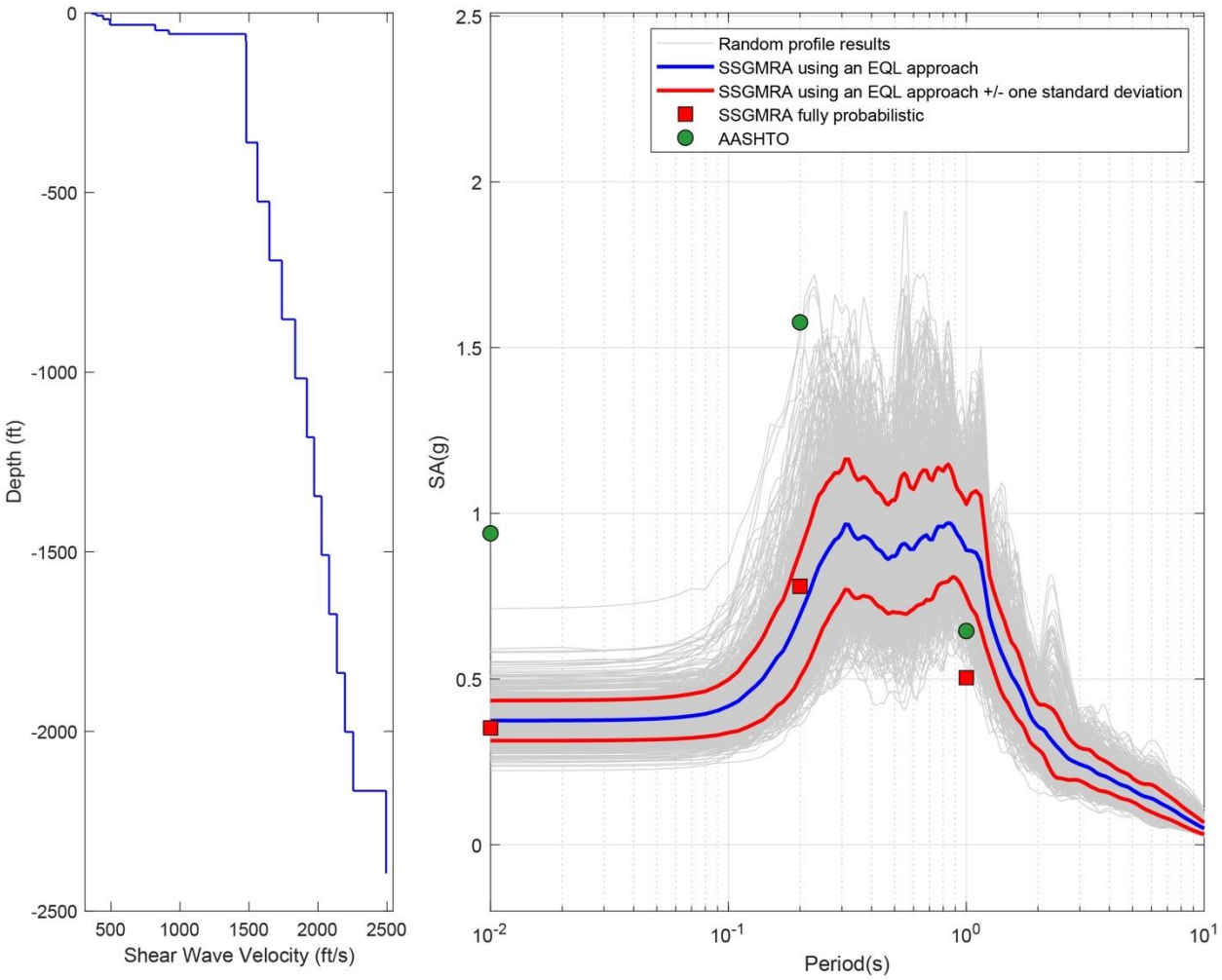


**Figure B-39. Left Panel: Shear-Wave Velocity Profile for Site 10 (Based on Peninsular Soil Model); and Right Panel: Results of SSGMRA Using a Fully Probabilistic Approach, SSGMRA Using an Equivalent Linear Approach, SSGMRA Using an Equivalent Linear Approach Plus and Minus One Standard Deviation, and AASHTO General Approach**

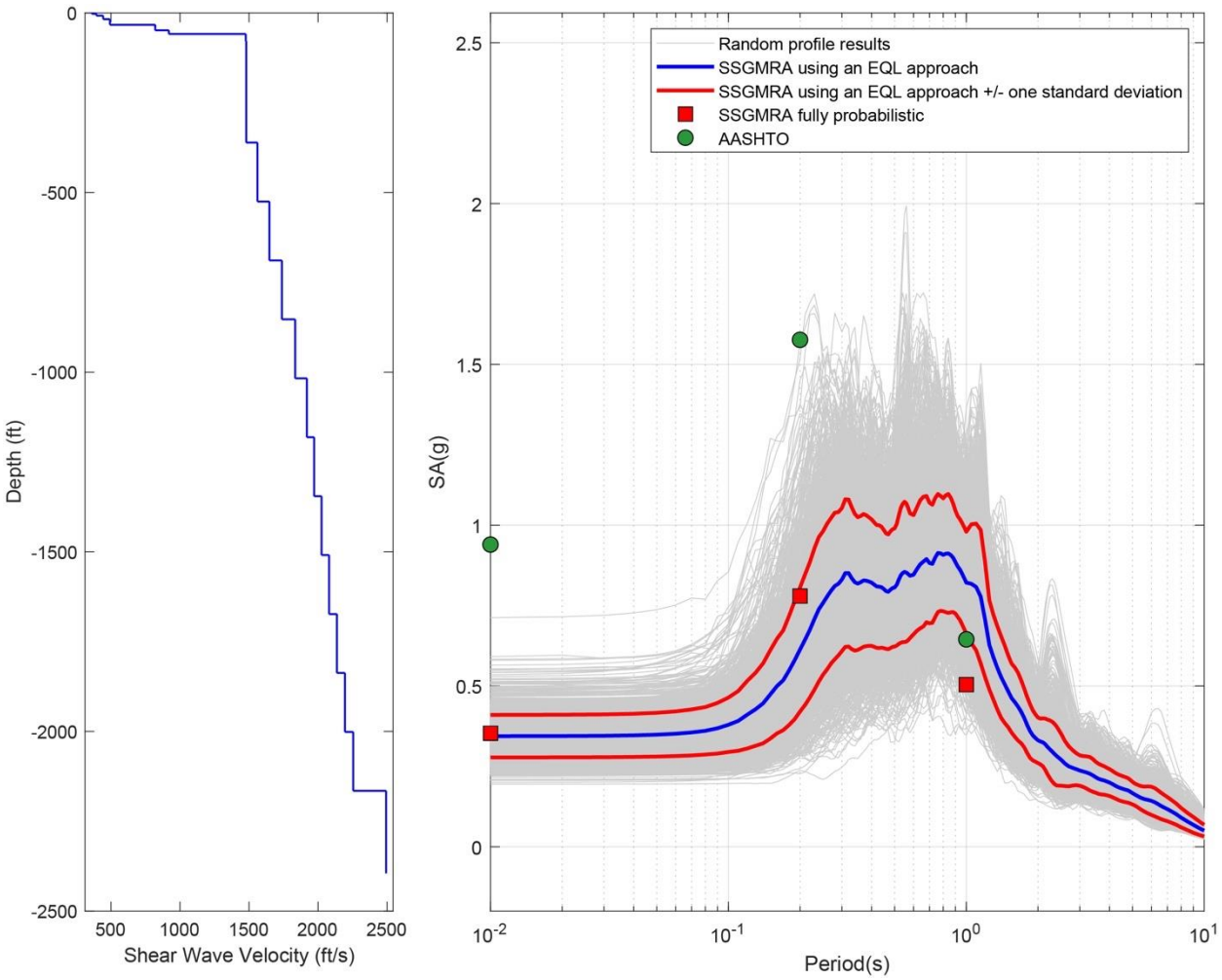


**Figure B-40. Left Panel: Shear-Wave Velocity Profile for Site 10 (Combined); and Right Panel: Results of SSGMRA Using a Fully Probabilistic Approach, SSGMRA Using an Equivalent Linear Approach, SSGMRA Using an Equivalent Linear Approach Plus and Minus One Standard Deviation, and AASHTO General Approach**

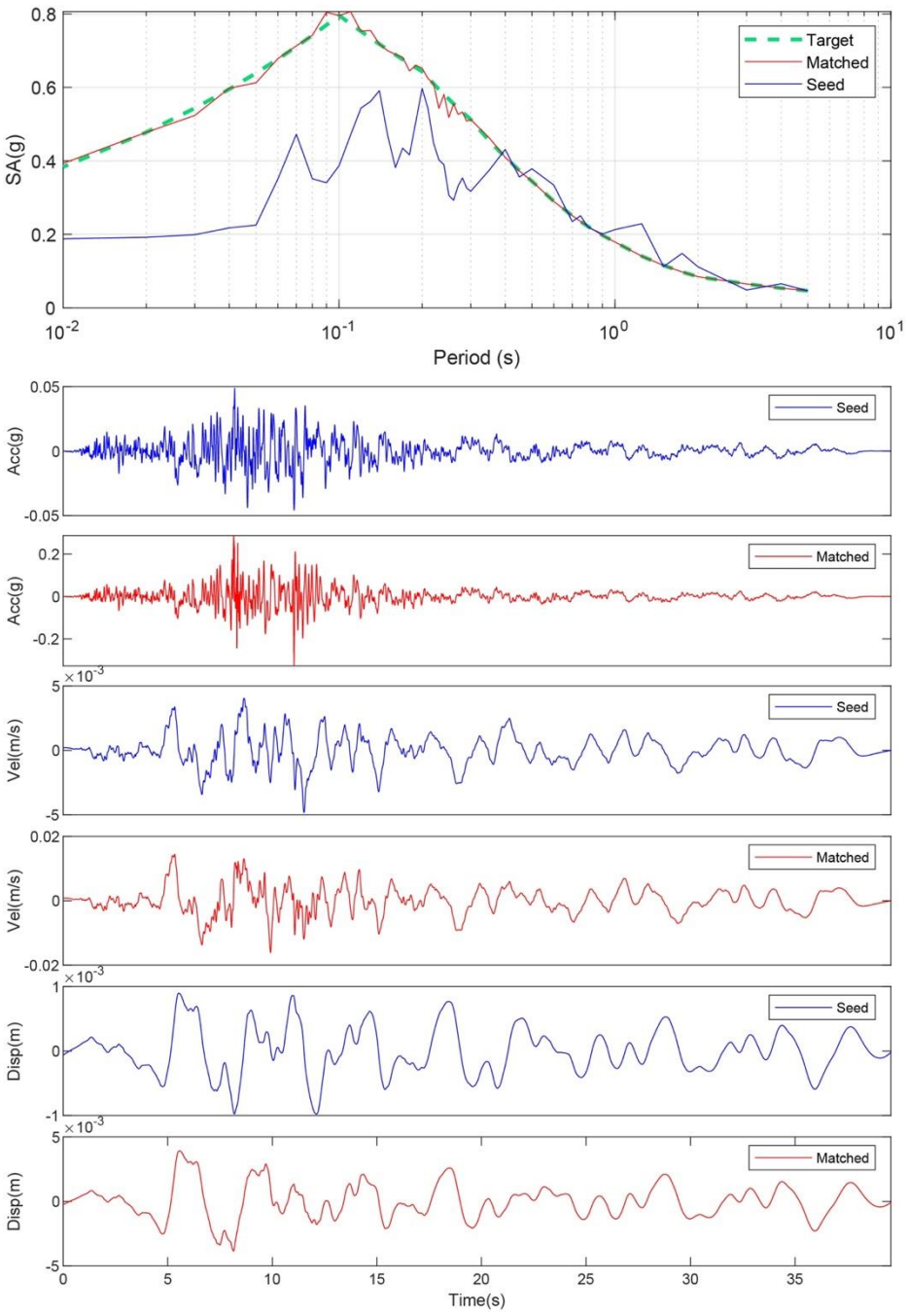


**Figure B-41. Matching Spectrum of Seed Motion (RSN774-LOMAP-HYN064) to the Target Spectrum (UHS) at Site 11. The Middle Subplot Shows the Seed Motion, and the Bottom Subplot Indicates the Matched Motion**

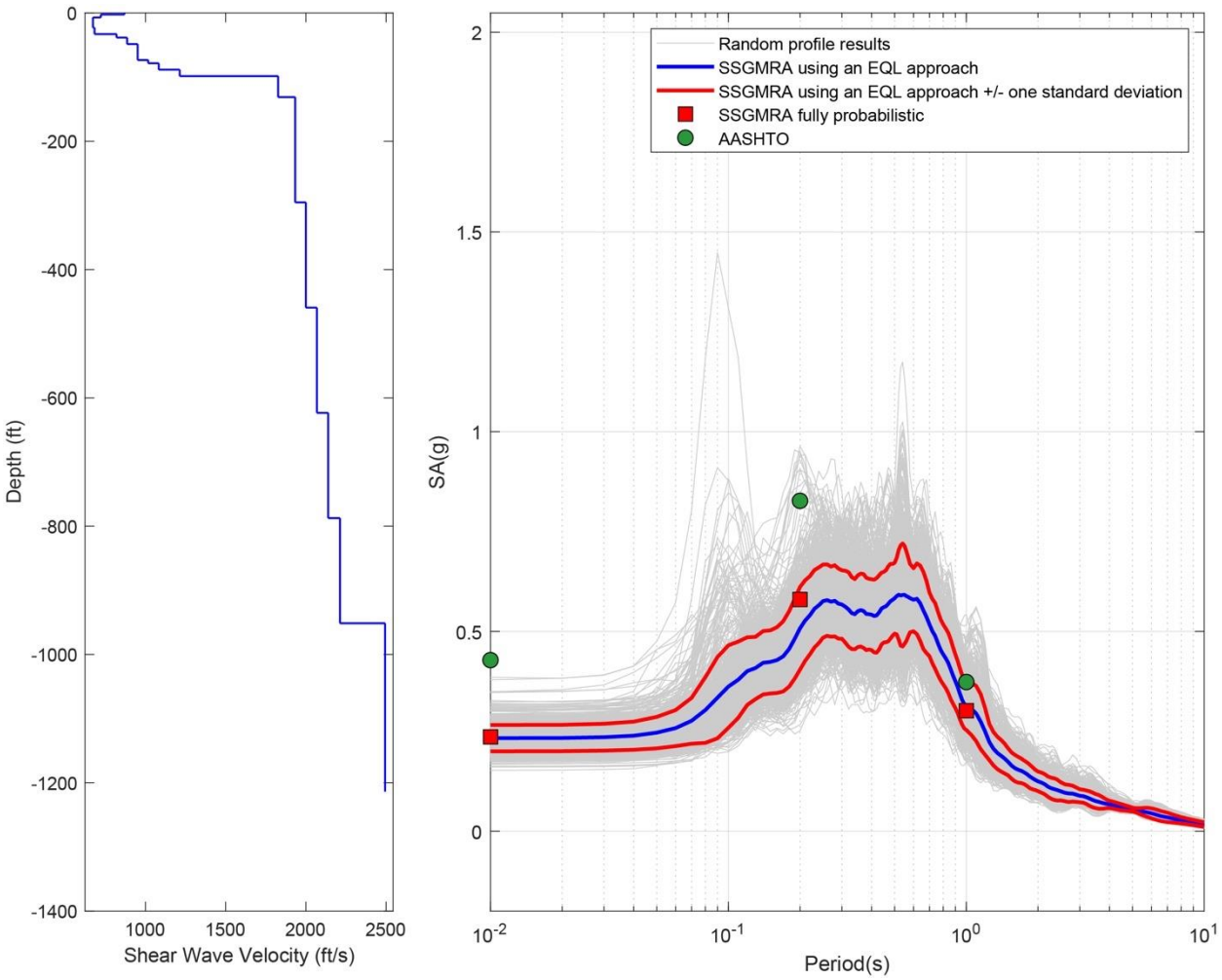


**Figure B-42. Left Panel: Shear-Wave Velocity Profile for Site 11 (Based on EPRI Soil Model); and Right Panel: Results of SSGMRA Using a Fully Probabilistic Approach, SSGMRA Using an Equivalent Linear Approach, SSGMRA Using an Equivalent Linear Approach Plus and Minus One Standard Deviation, and AASHTO General Approach**

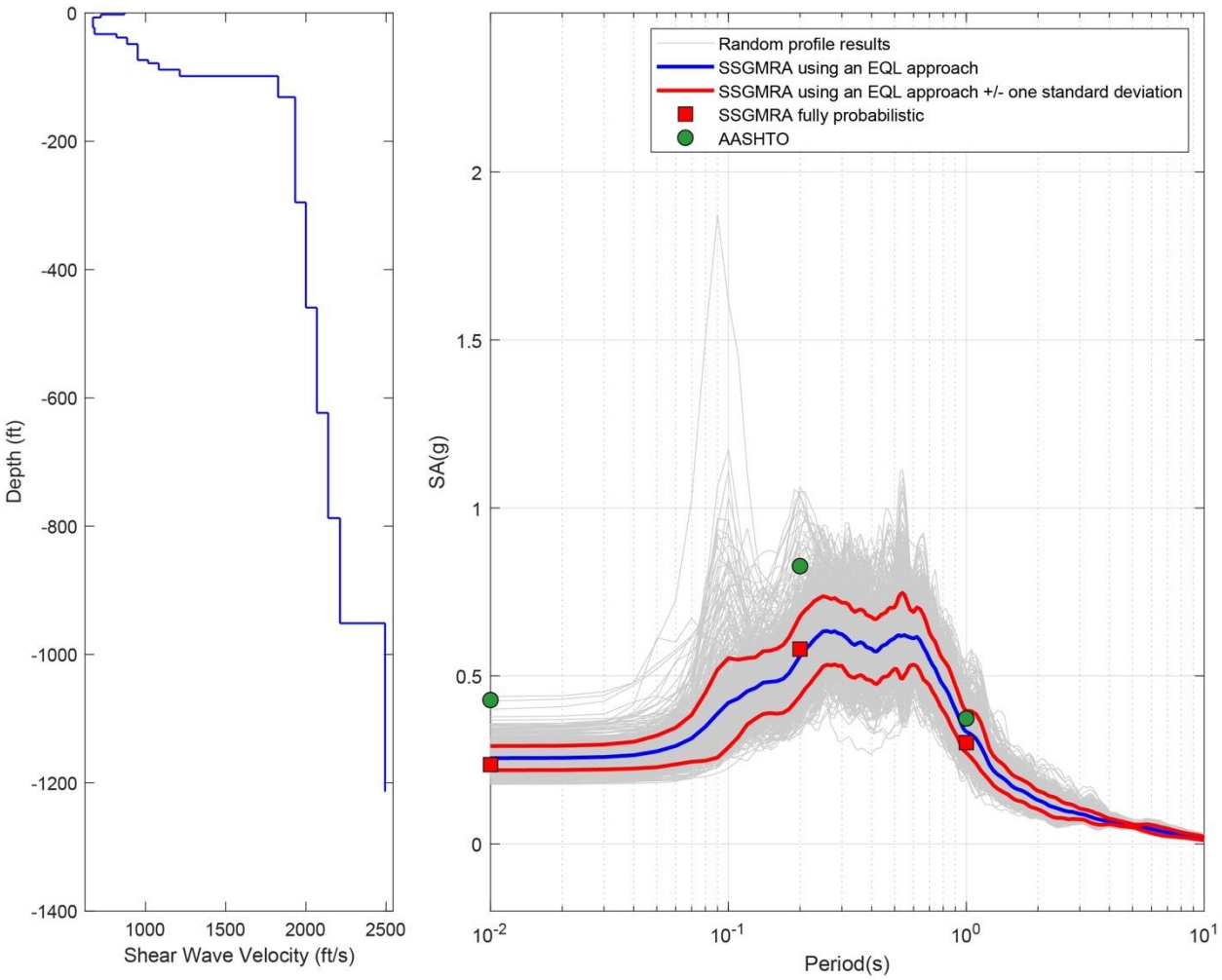


**Figure B-43. Left Panel: Shear-Wave Velocity Profile for Site 11 (Based on Peninsular Soil Model); and Right Panel: Results of SSGMRA Using a Fully Probabilistic Approach, SSGMRA Using an Equivalent Linear Approach, SSGMRA Using an Equivalent Linear Approach Plus and Minus One Standard Deviation, and AASHTO General Approach**

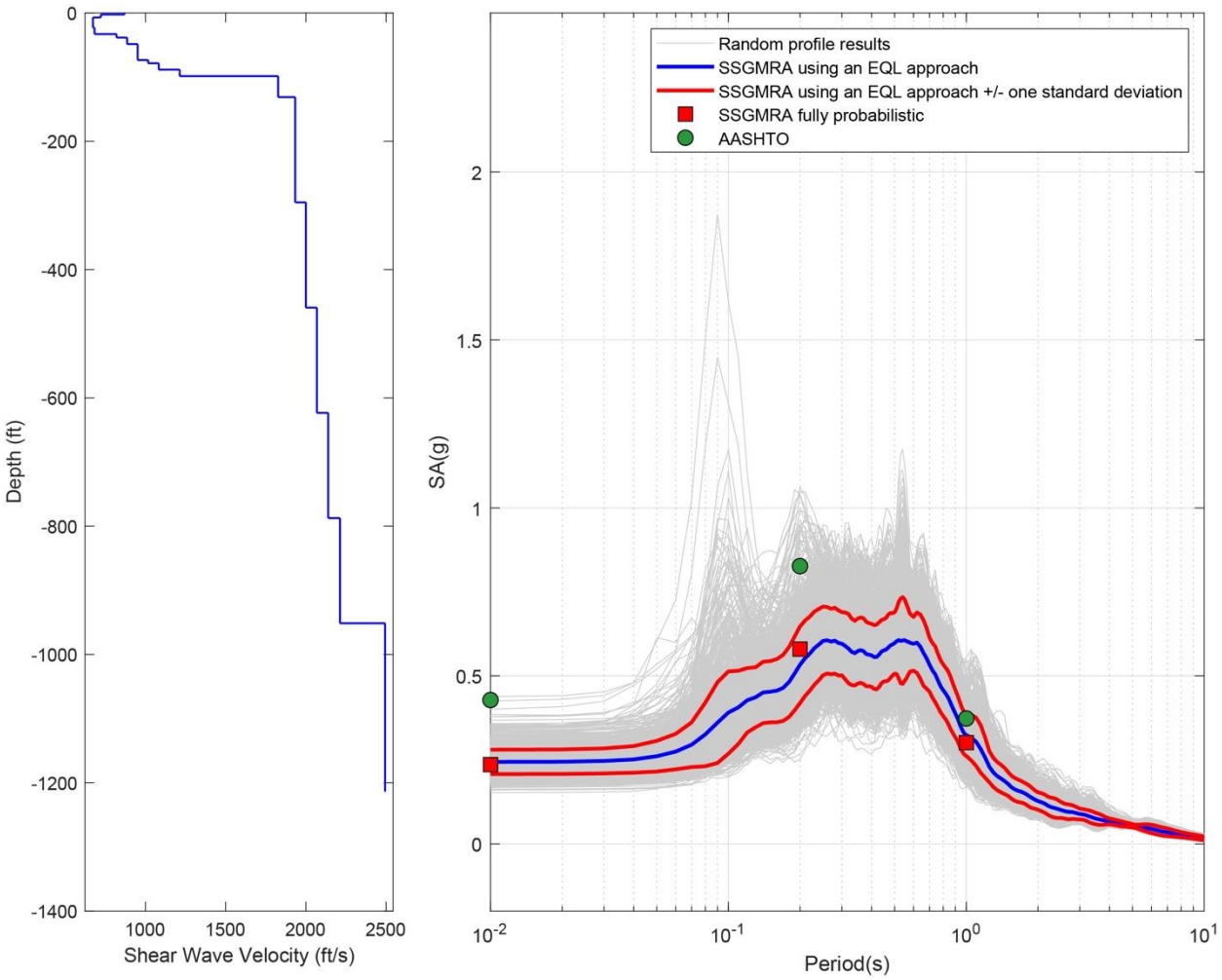


**Figure B-44. Left Panel: Shear-Wave Velocity Profile for Site 11 (Combined); and Right Panel: Results of SSGMRA Using a Fully Probabilistic Approach, SSGMRA Using an Equivalent Linear Approach, SSGMRA Using an Equivalent Linear Approach Plus and Minus One Standard Deviation, and AASHTO General Approach**

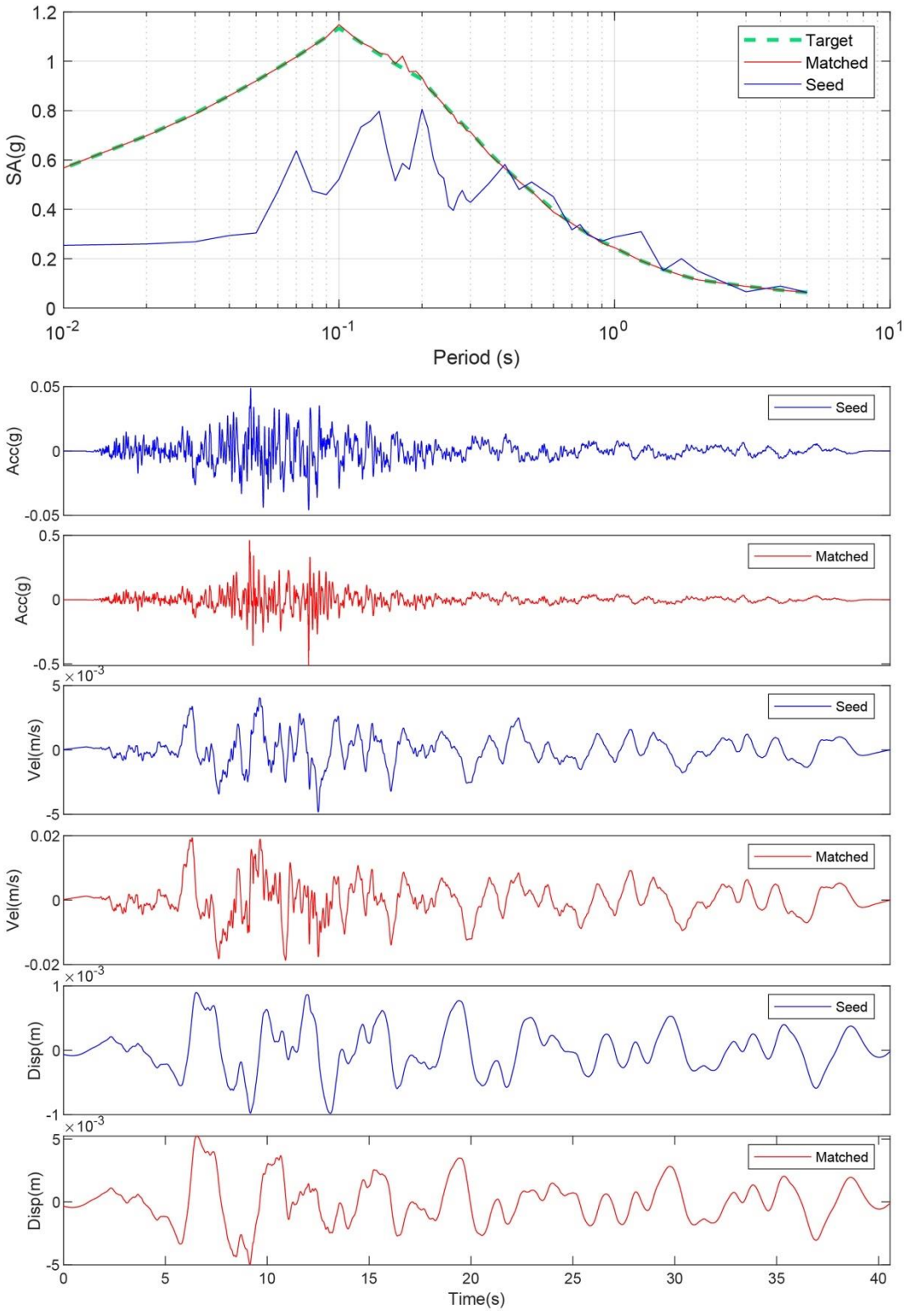


**Figure B-45. Matching Spectrum of Seed Motion (RSN774-LOMAP-HYN064) to The Target Spectrum (UHS) at Site 12. The Middle Subplot Shows the Seed Motion, and the Bottom Subplot Indicates the Matched Motion**

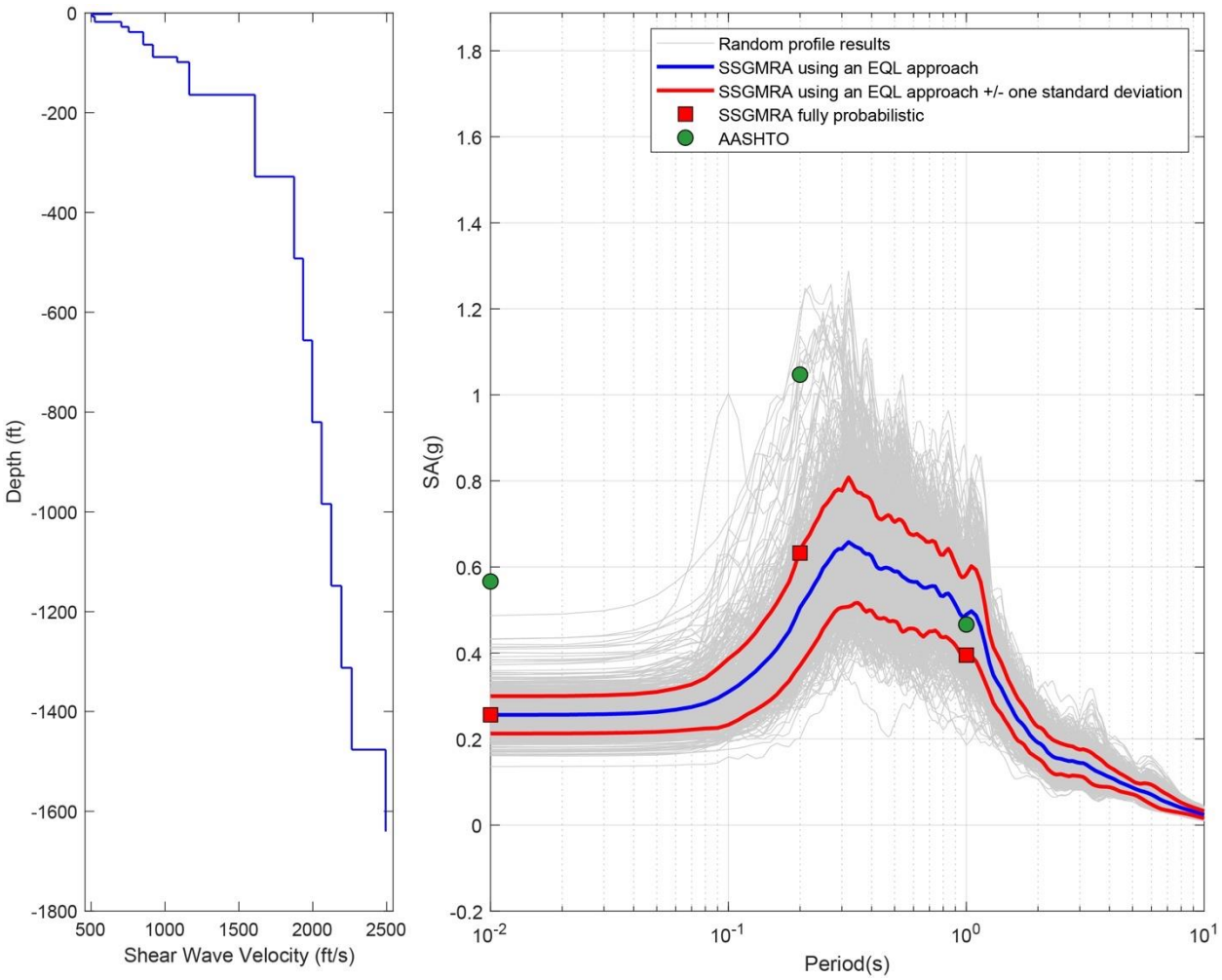


**Figure B-46. Left Panel: Shear-Wave Velocity Profile for Site 12 (Based on EPRI Soil Model); and Right Panel: Results of SSGMRA Using a Fully Probabilistic Approach, SSGMRA Using an Equivalent Linear Approach, SSGMRA Using an Equivalent Linear Approach Plus and Minus One Standard Deviation, and AASHTO General Approach**

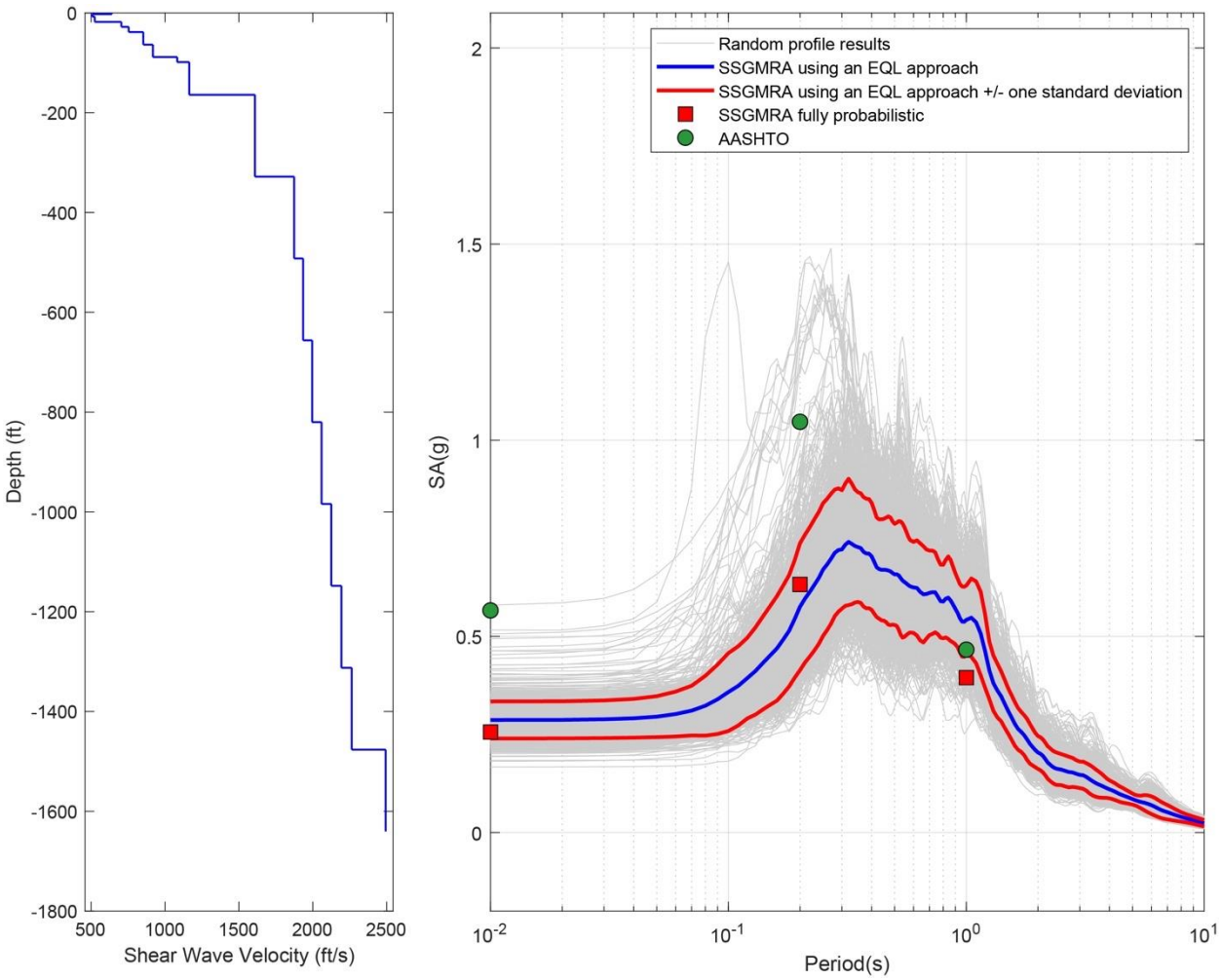


**Figure B.47 Left Panel: Shear-Wave Velocity Profile for Site 12 (Based on Peninsular Soil Model); and Right Panel: Results of SSGMRA Using a Fully Probabilistic Approach, SSGMRA Using an Equivalent Linear Approach, SSGMRA Using an Equivalent Linear Approach Plus And Minus One Standard Deviation, and AASHTO General Approach.**

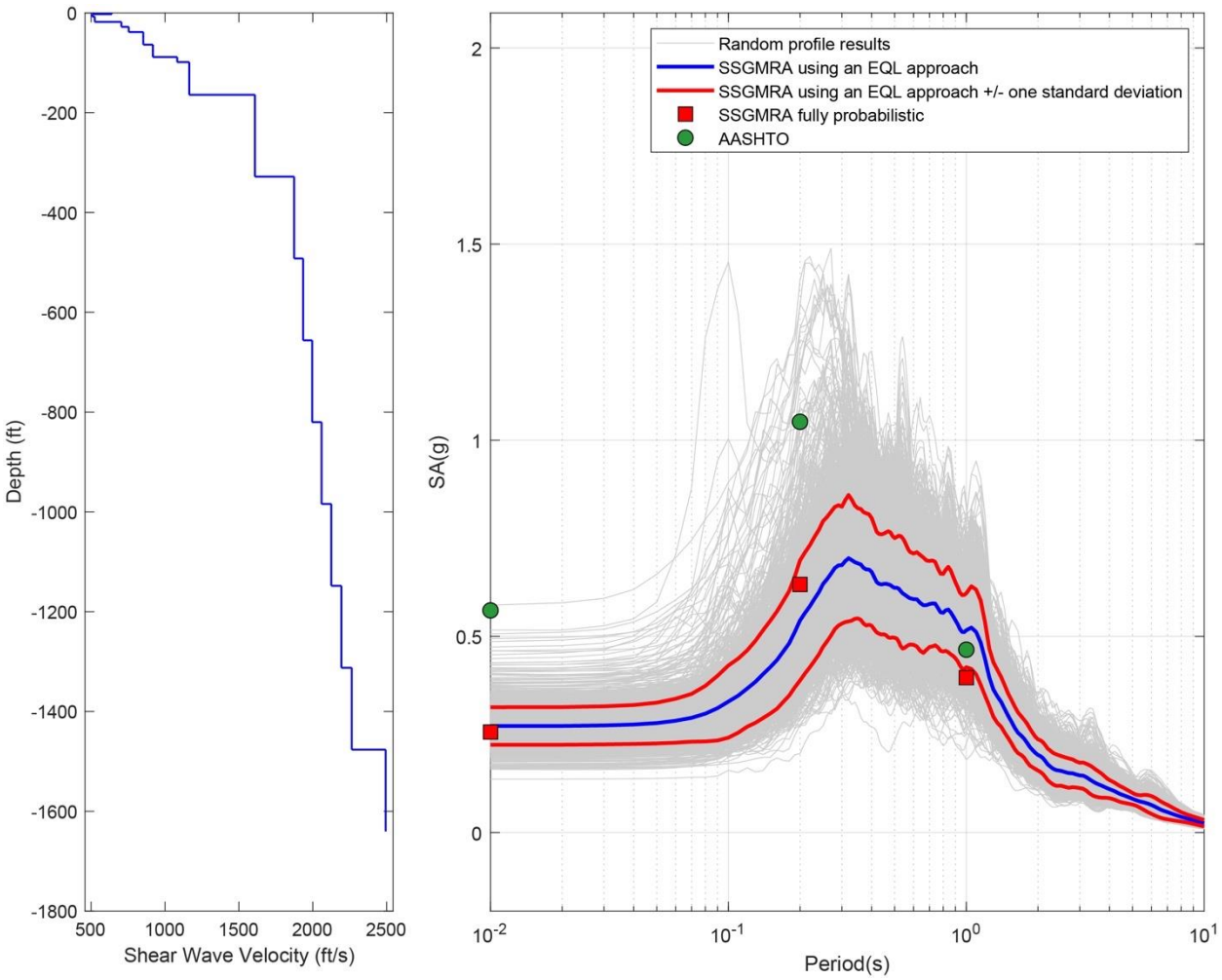


**Figure B-48. Left Panel: Shear-Wave Velocity Profile for Site 12 (Combined); and Right Panel: Results of SSGMRA Using a Fully Probabilistic Approach, SSGMRA Using an Equivalent Linear Approach, SSGMRA Using an Equivalent Linear Approach Plus and Minus One Standard Deviation, and AASHTO General Approach**

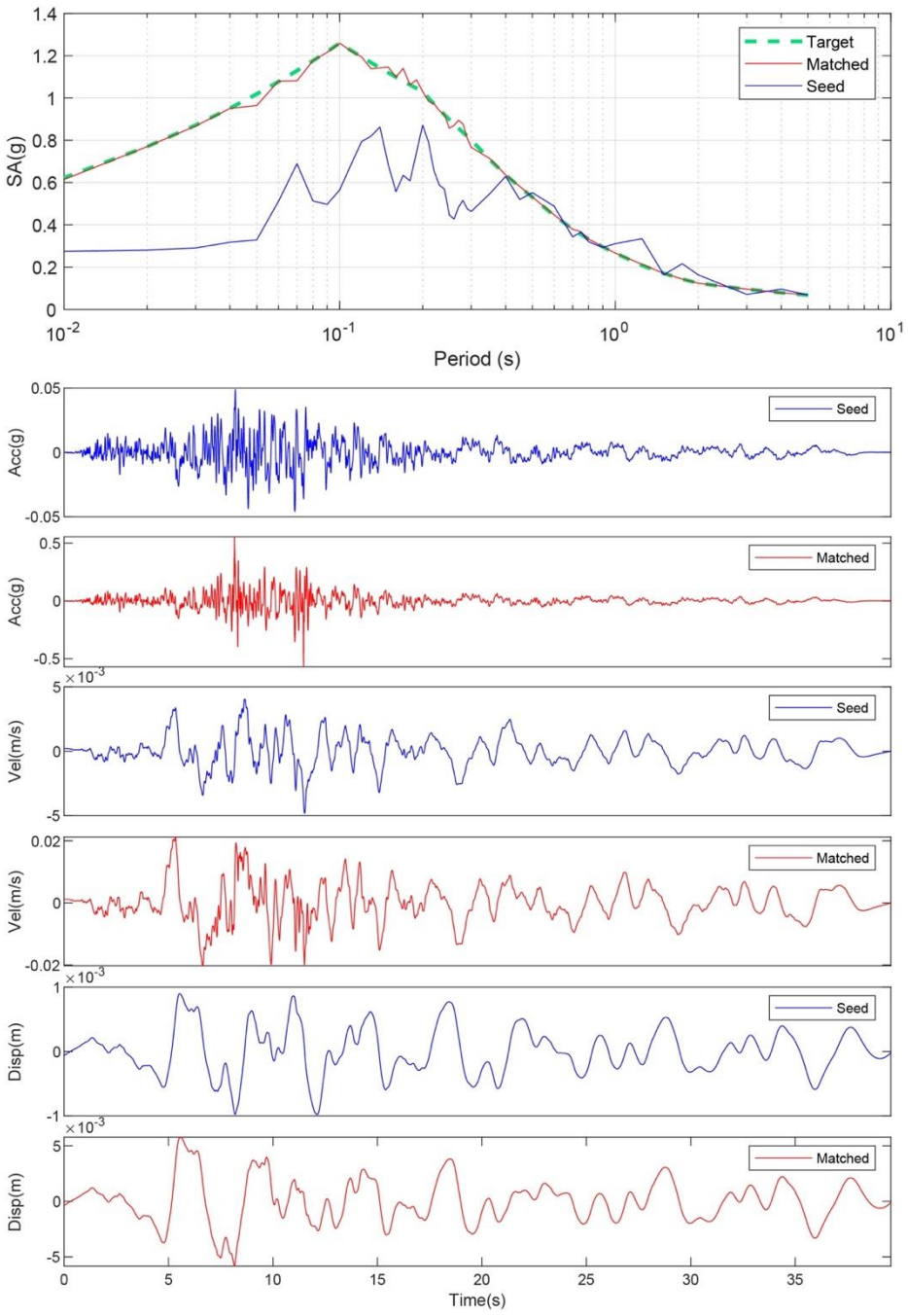


**Figure B-49. Matching Spectrum of Seed Motion (RSN774-LOMAP-HYN064) to the Target Spectrum (UHS) at Site 13. The Middle Subplot Shows the Seed Motion, and the Bottom Subplot Indicates the Matched Motion**

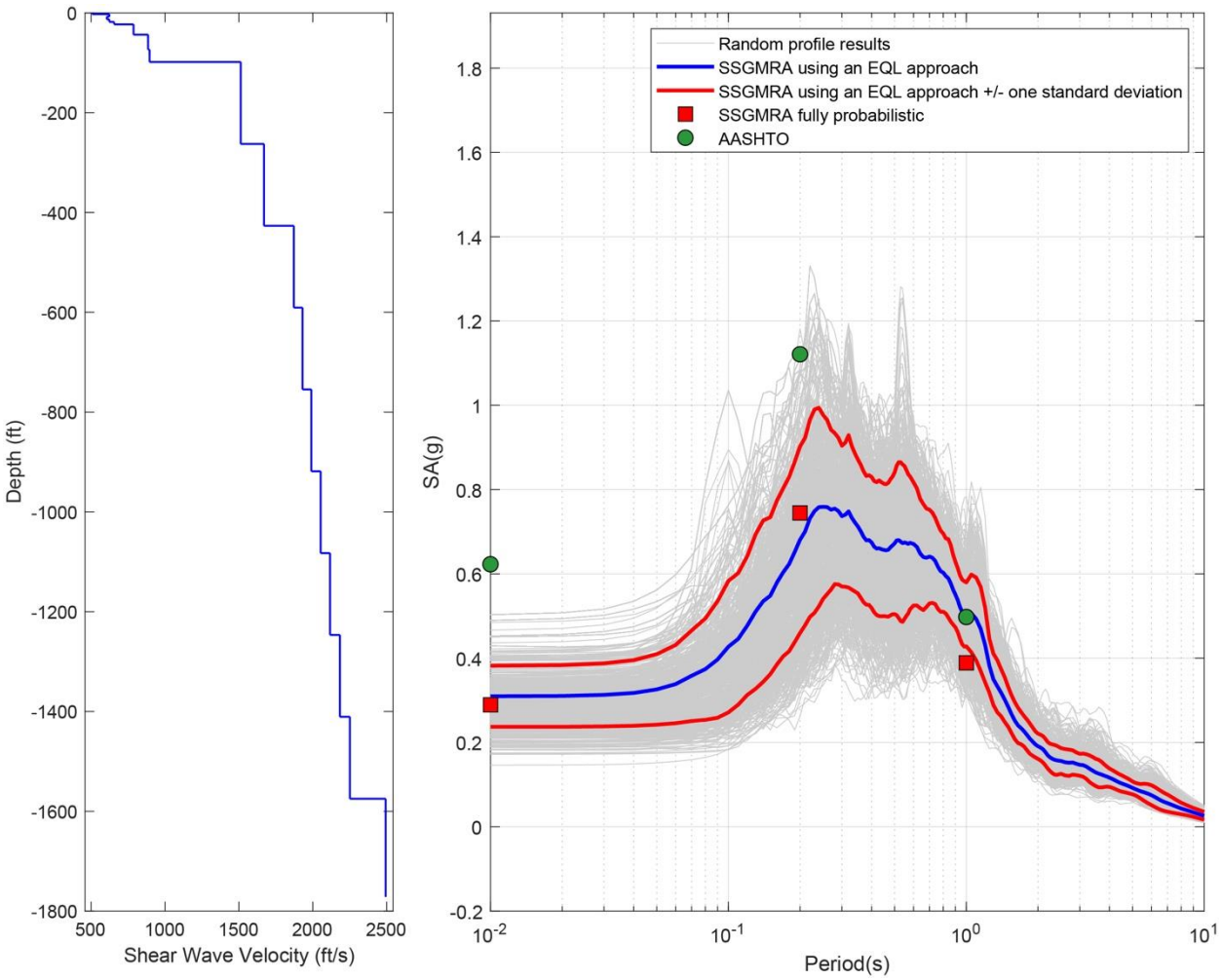


**Figure B-50. Left Panel: Shear-Wave Velocity Profile for Site 13 (Based on EPRI Soil Model); and Right Panel: Results of SSGMRA Using a Fully Probabilistic Approach, SSGMRA Using an Equivalent Linear Approach, SSGMRA Using an Equivalent Linear Approach Plus and Minus One Standard Deviation, and AASHTO General Approach**

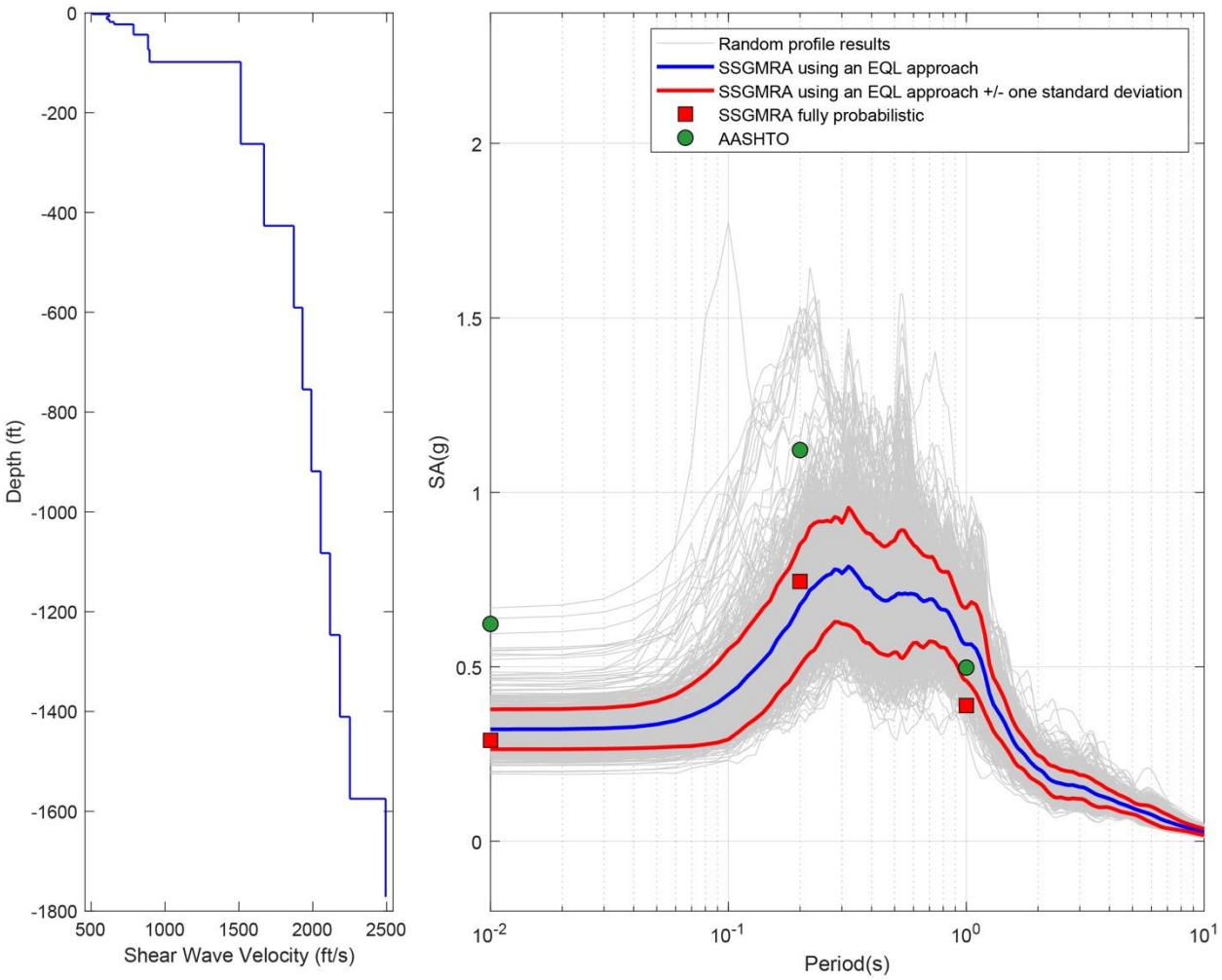


**Figure B-51. Left Panel: Shear-Wave Velocity Profile for Site 13 (Based on Peninsular Soil Model); and Right Panel: Results of SSGMRA Using a Fully Probabilistic Approach, SSGMRA Using an Equivalent Linear Approach, SSGMRA Using an Equivalent Linear Approach Plus and Minus One Standard Deviation, and AASHTO General Approach**

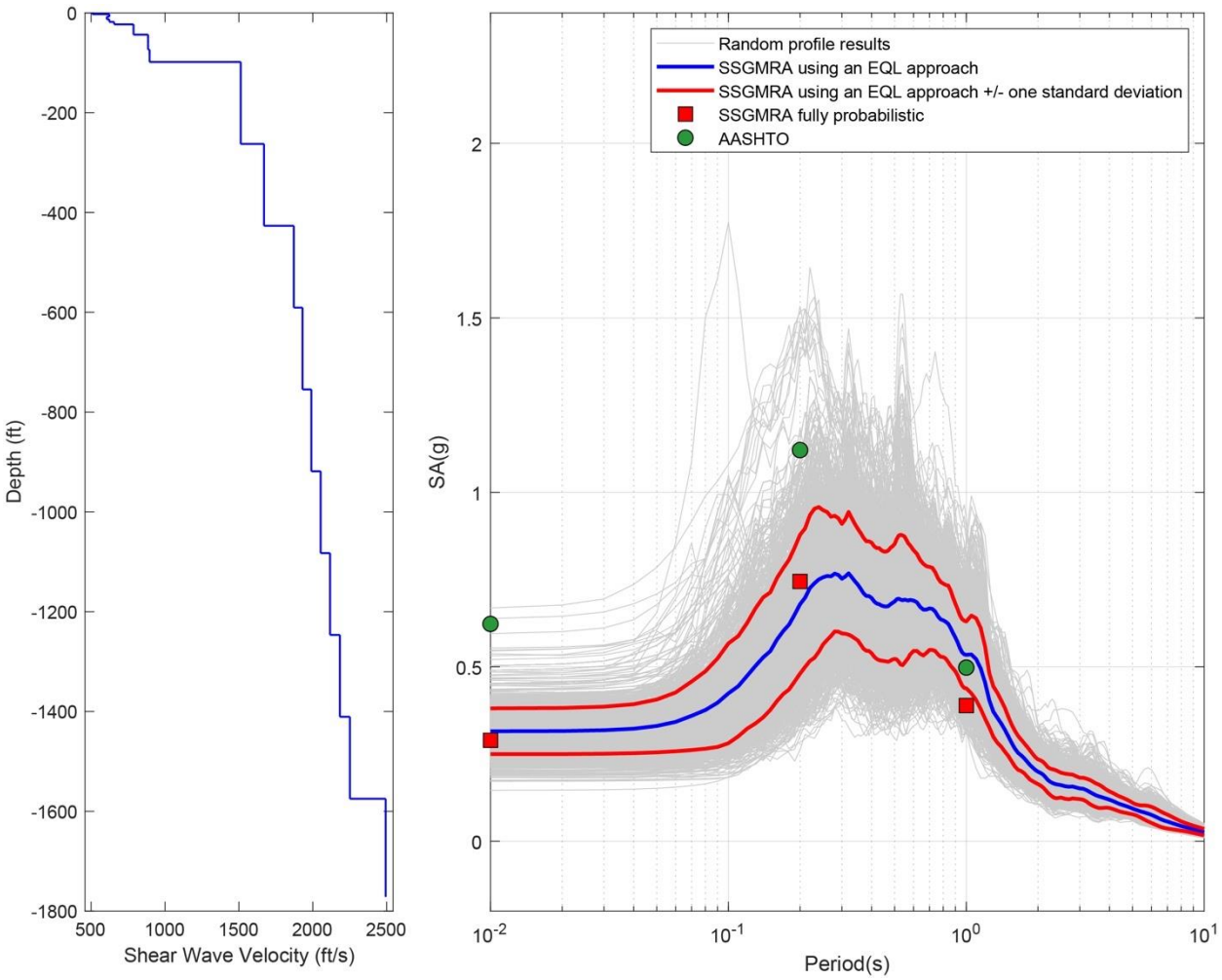


**Figure B-52. Left Panel: Shear-Wave Velocity Profile for Site 13 (Combined); and Right Panel: Results of SSGMRA Using a Fully Probabilistic Approach, SSGMRA Using an Equivalent Linear Approach, SSGMRA Using an Equivalent Linear Approach Plus and Minus One Standard Deviation, and AASHTO General Approach**

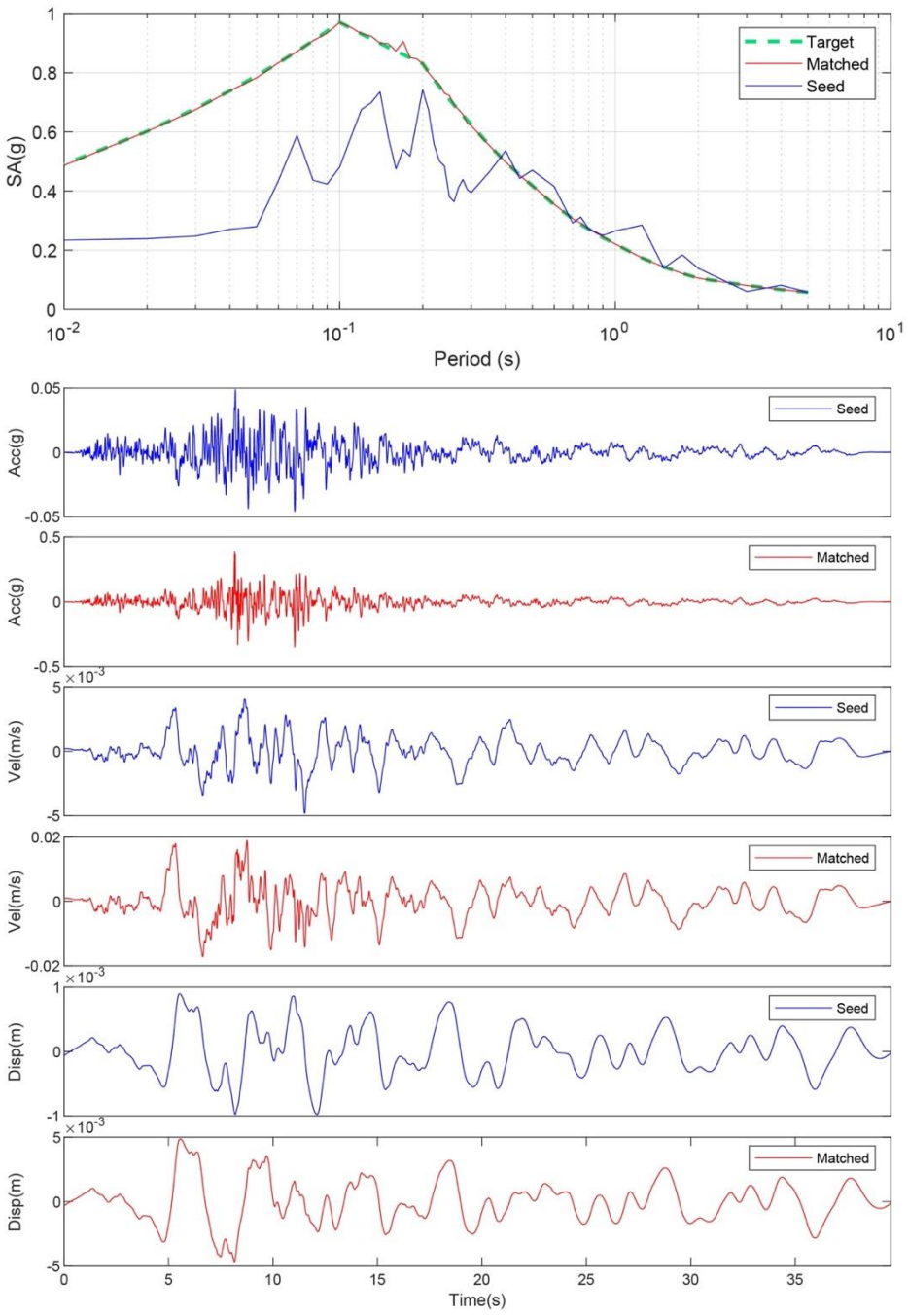


**Figure B-53. Matching Spectrum of Seed Motion (RSN774-LOMAP-HYN064) to the Target Spectrum (UHS) at Site 14. The Middle Subplot Shows the Seed Motion, and the Bottom Subplot Indicates the Matched Motion**

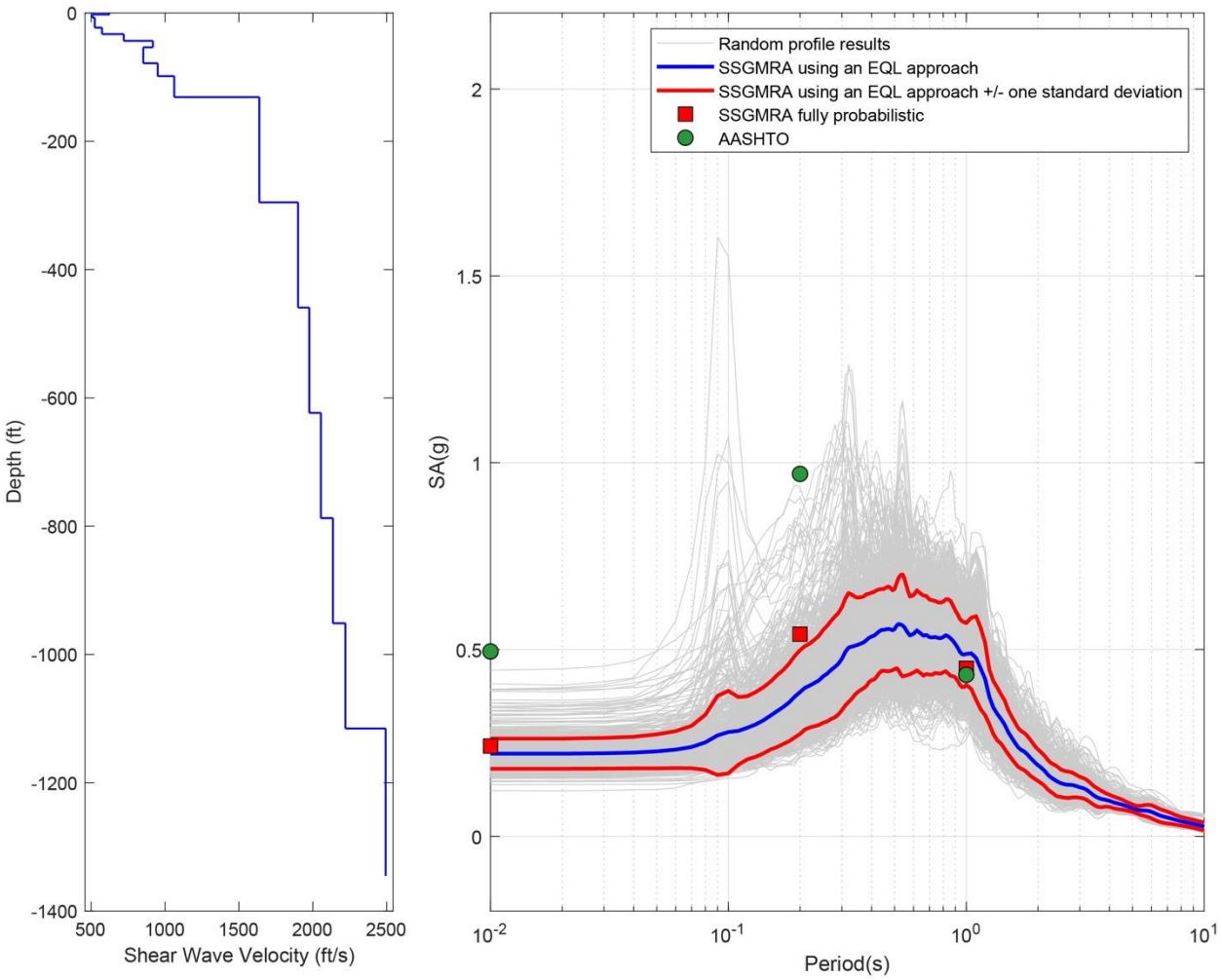


**Figure B-54. Left Panel: Shear-Wave Velocity Profile for Site 14 (Based on EPRI Soil Model); and Right Panel: Results of SSGMRA Using a Fully Probabilistic Approach, SSGMRA Using an Equivalent Linear Approach, SSGMRA Using an Equivalent Linear Approach Plus and Minus One Standard Deviation, and AASHTO General Approach**

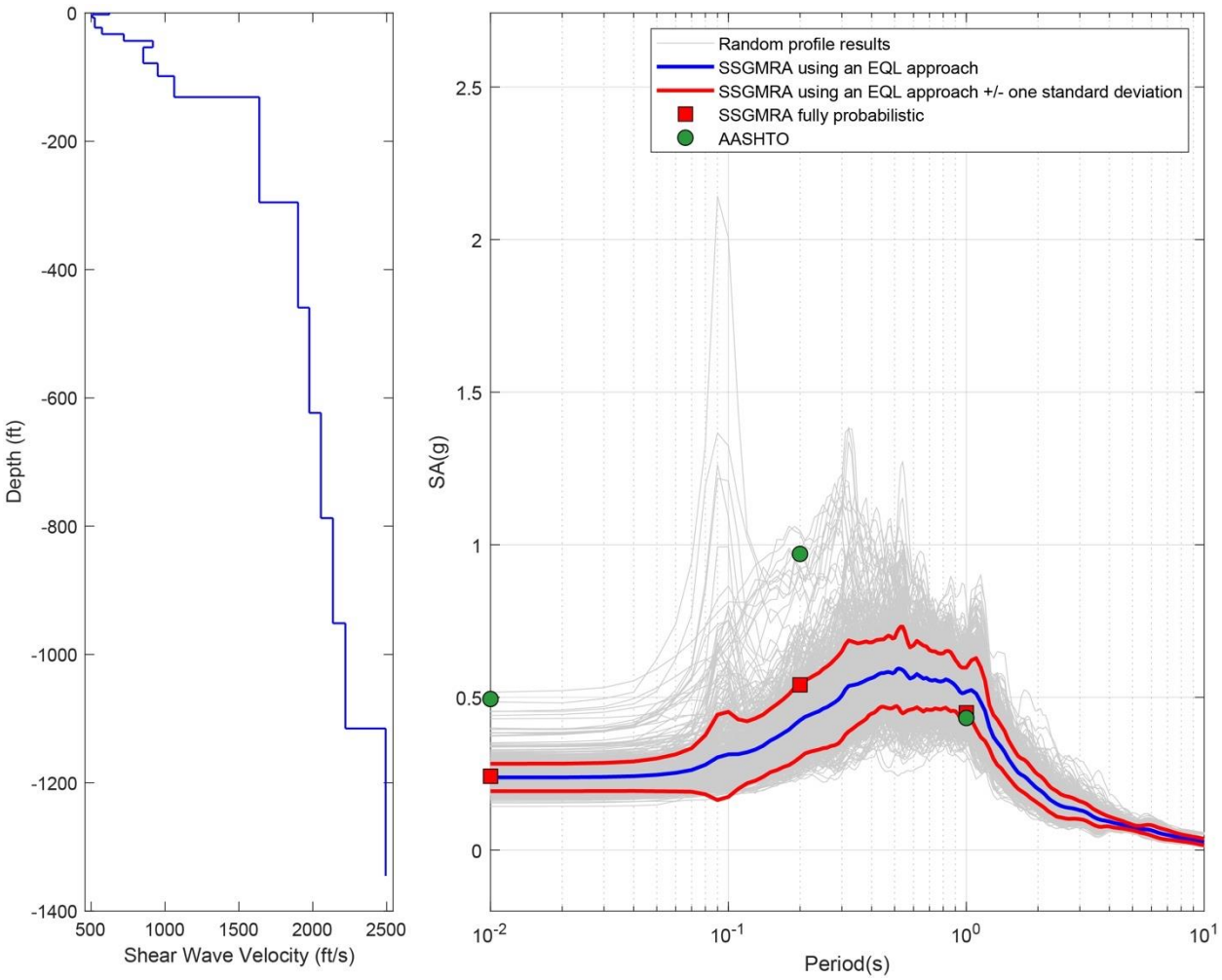


**Figure B-55. Left Panel: Shear-Wave Velocity Profile for Site 14 (Based on Peninsular Soil Model); and Right Panel: Results of SSGMRA Using a Fully Probabilistic Approach, SSGMRA Using an Equivalent Linear Approach, SSGMRA Using an Equivalent Linear Approach Plus and Minus One Standard Deviation, and AASHTO General Approach**

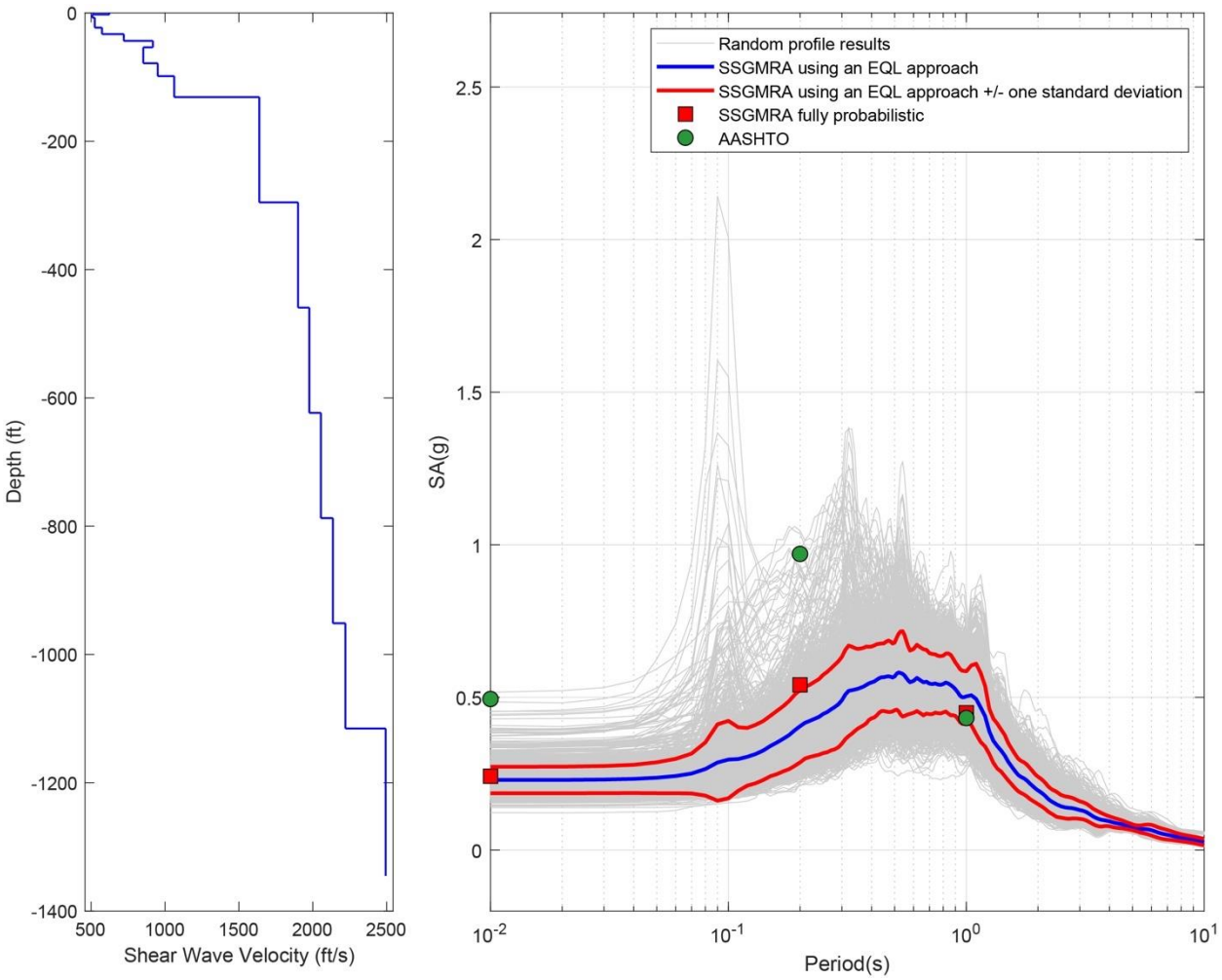


**Figure B-56. Left Panel: Shear-Wave Velocity Profile for Site 14 (Combined); and Right Panel: Results of SSGMRA Using a Fully Probabilistic Approach, SSGMRA Using an Equivalent Linear Approach, SSGMRA Using an Equivalent Linear Approach Plus and Minus One Standard Deviation, and AASHTO General Approach**

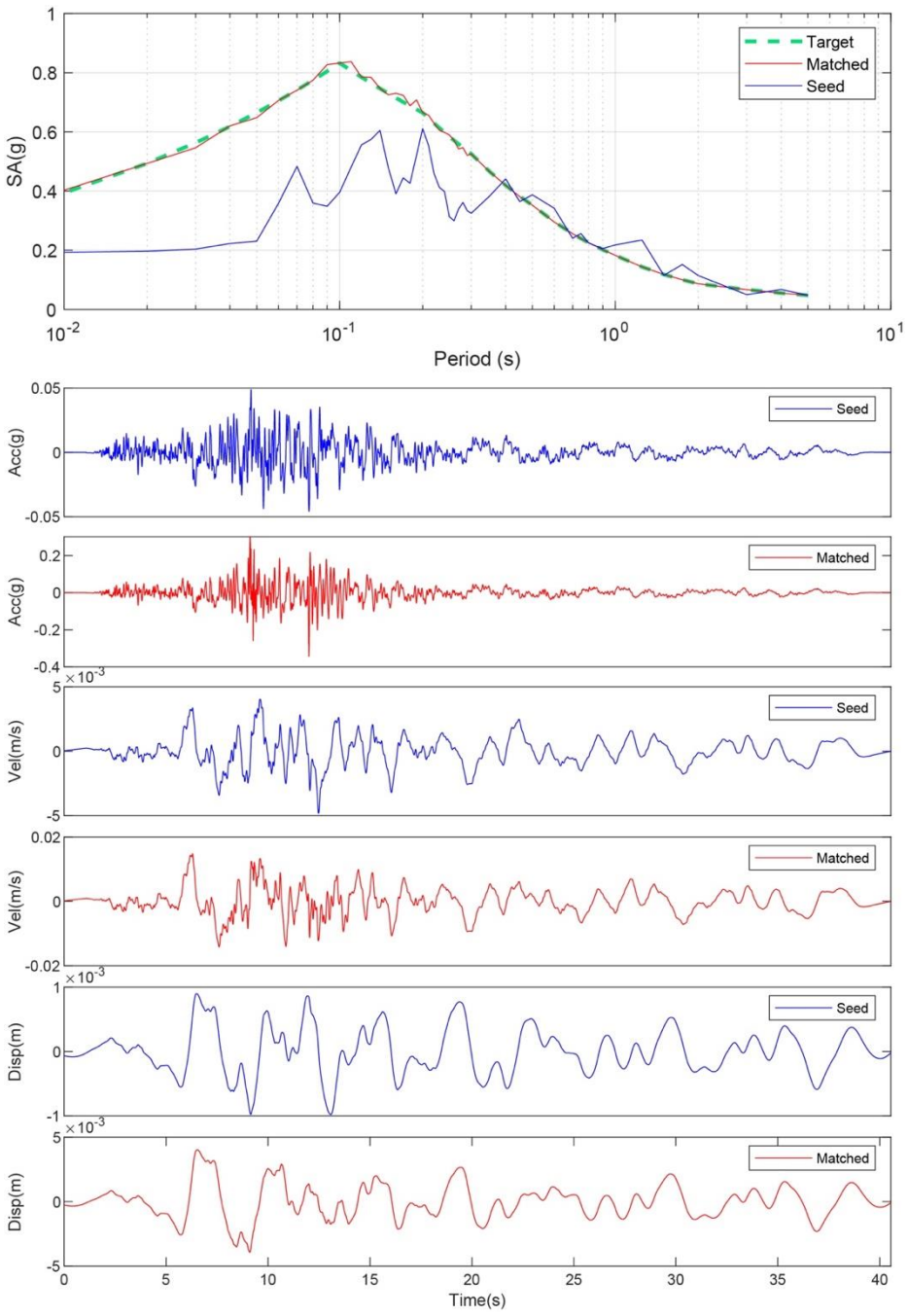


**Figure B-57. Matching Spectrum of Seed Motion (RSN774-LOMAP-HYN064) to the Target Spectrum (UHS) at Site 15. The Middle Subplot Shows the Seed Motion, and the Bottom Subplot Indicates the Matched Motion**

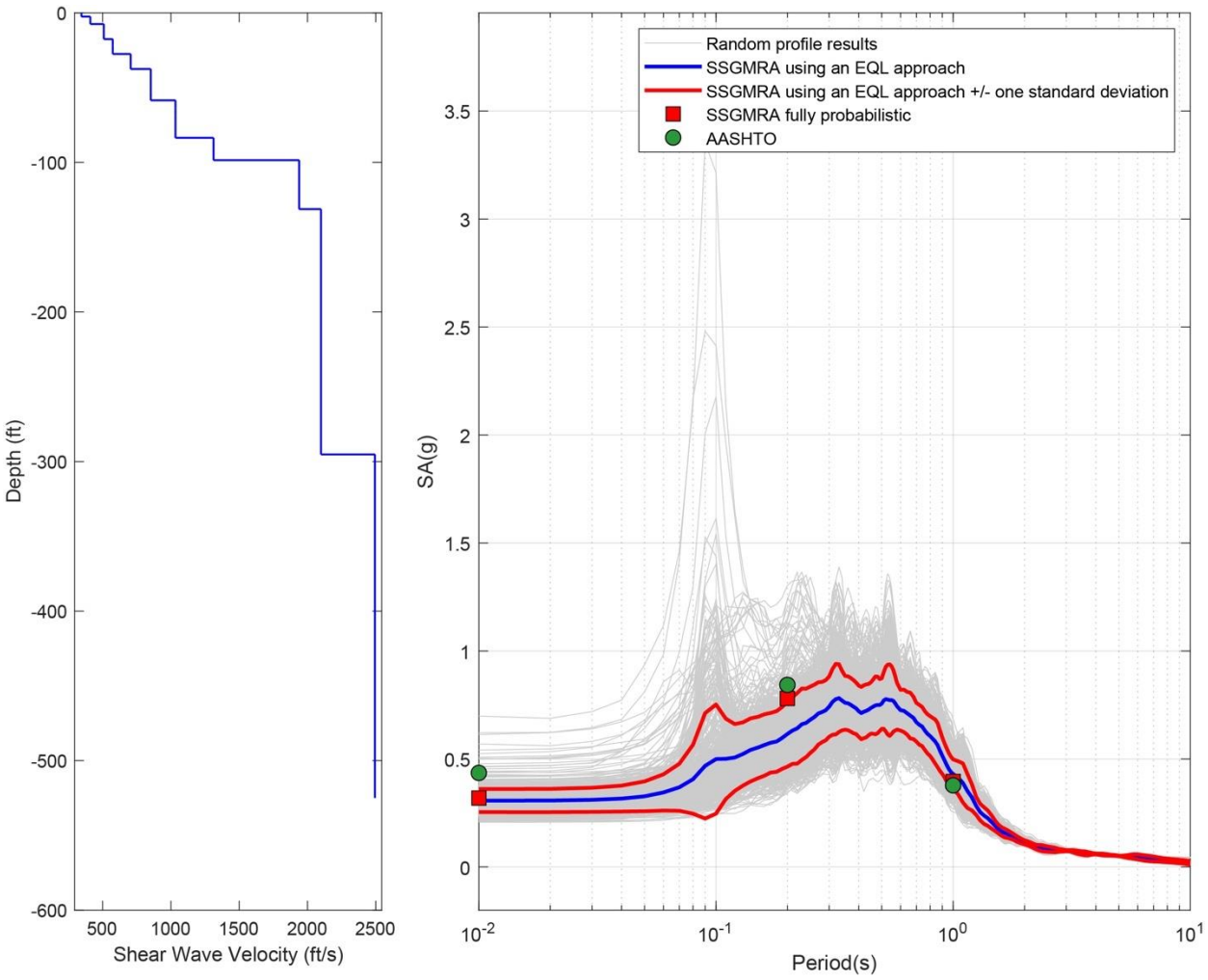


**Figure B-58. Left Panel: Shear-Wave Velocity Profile for Site 15 (Based on EPRI Soil Model); and Right Panel: Results of SSGMRA Using a Fully Probabilistic Approach, SSGMRA Using an Equivalent Linear Approach, SSGMRA Using an Equivalent Linear Approach Plus and Minus One Standard Deviation, And AASHTO General Approach**

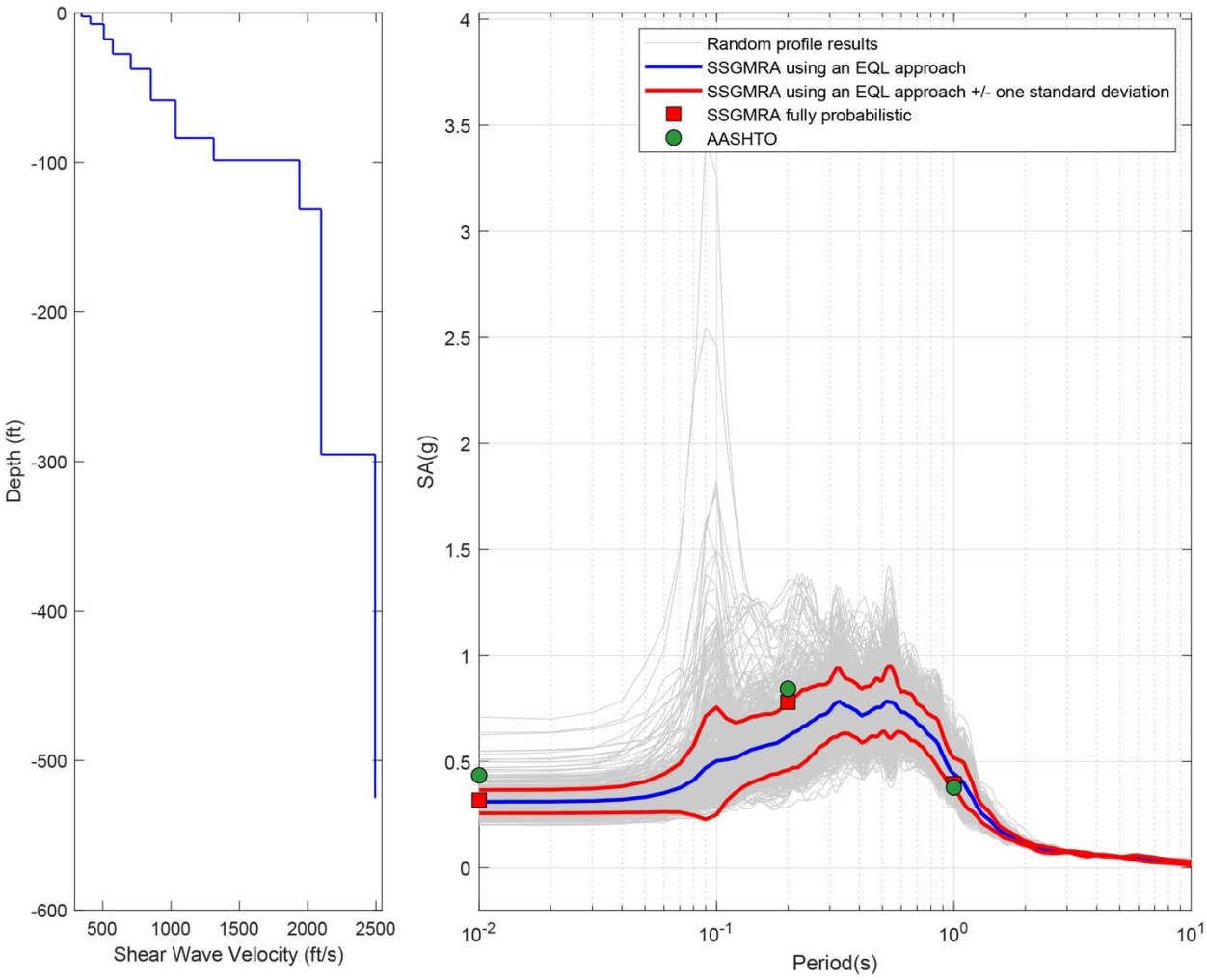


**Figure B-59. Left Panel: Shear-Wave Velocity Profile for Site 15 (Based on Peninsular Soil Model); and Right Panel: Results of SSGMRA Using a Fully Probabilistic Approach, SSGMRA Using an Equivalent Linear Approach, SSGMRA Using an Equivalent Linear Approach Plus and Minus One Standard Deviation, and AASHTO General Approach**

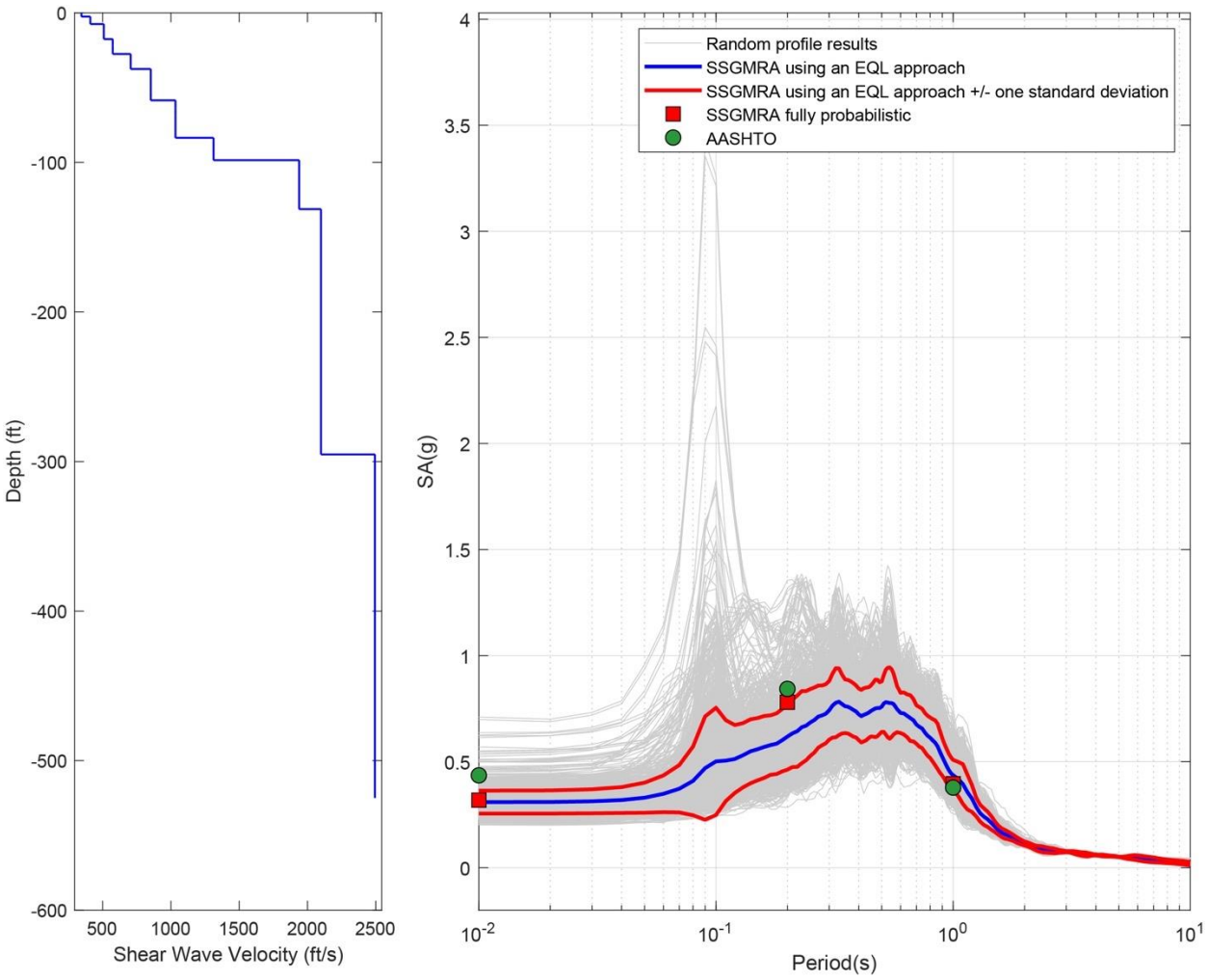


**Figure B-60. Left Panel: Shear-Wave Velocity Profile for Site 15 (Combined); and Right Panel: Results of SSGMRA Using a Fully Probabilistic Approach, SSGMRA Using an Equivalent Linear Approach, SSGMRA Using an Equivalent Linear Approach Plus and Minus One Standard Deviation, and AASHTO General Approach**

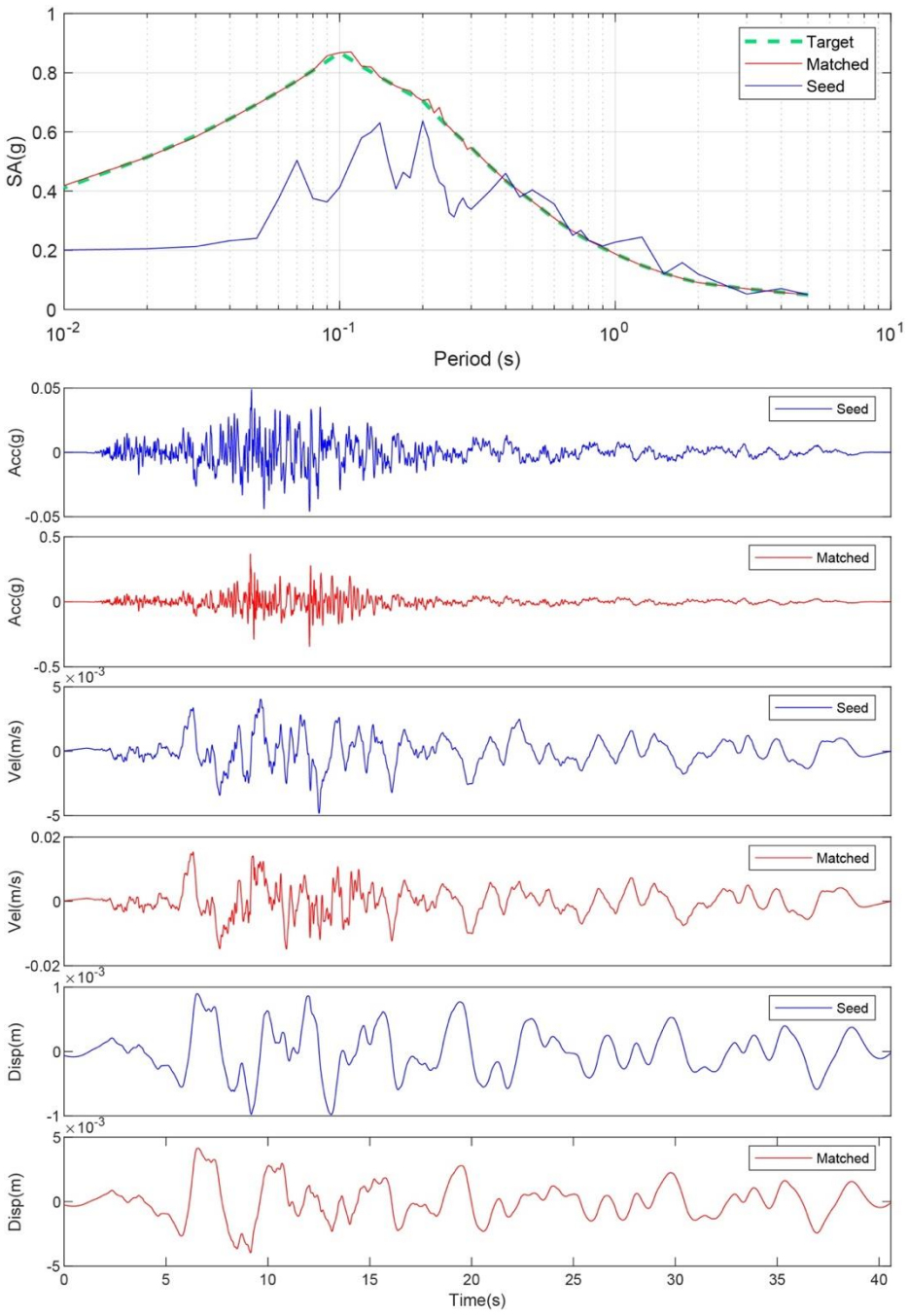


**Figure B-61. Matching Spectrum of Seed Motion (RSN774-LOMAP-HYN064) to the Target Spectrum (UHS) at Site 16. The Middle Subplot Shows the Seed Motion, and the Bottom Subplot Indicates the Matched Motion**

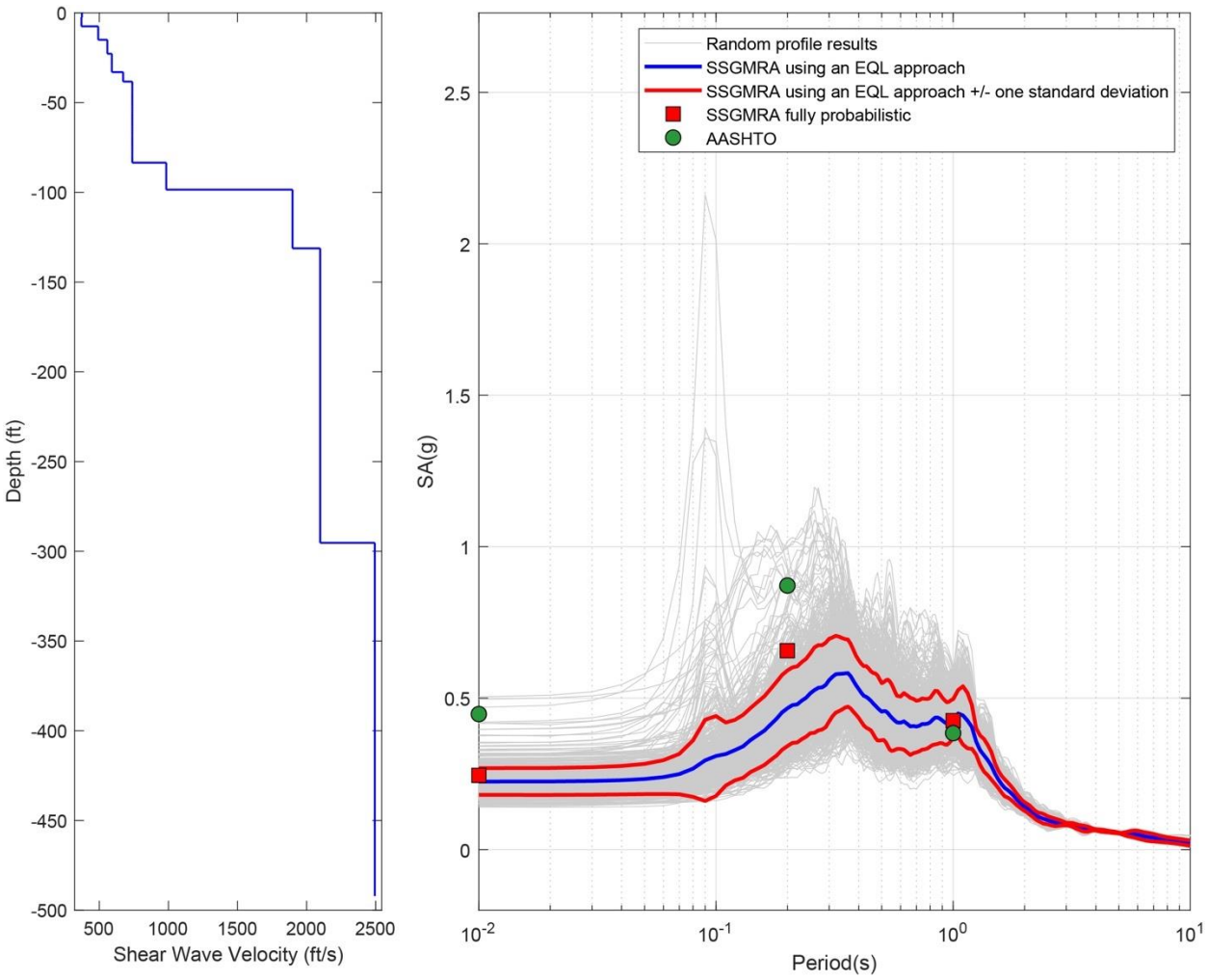


**Figure B-62. Left Panel: Shear-Wave Velocity Profile for Site 16 (Based on EPRI Soil Model); and Right Panel: Results of SSGMRA Using a Fully Probabilistic Approach, SSGMRA Using an Equivalent Linear Approach, SSGMRA Using an Equivalent Linear Approach Plus and Minus One Standard Deviation, and AASHTO General Approach**

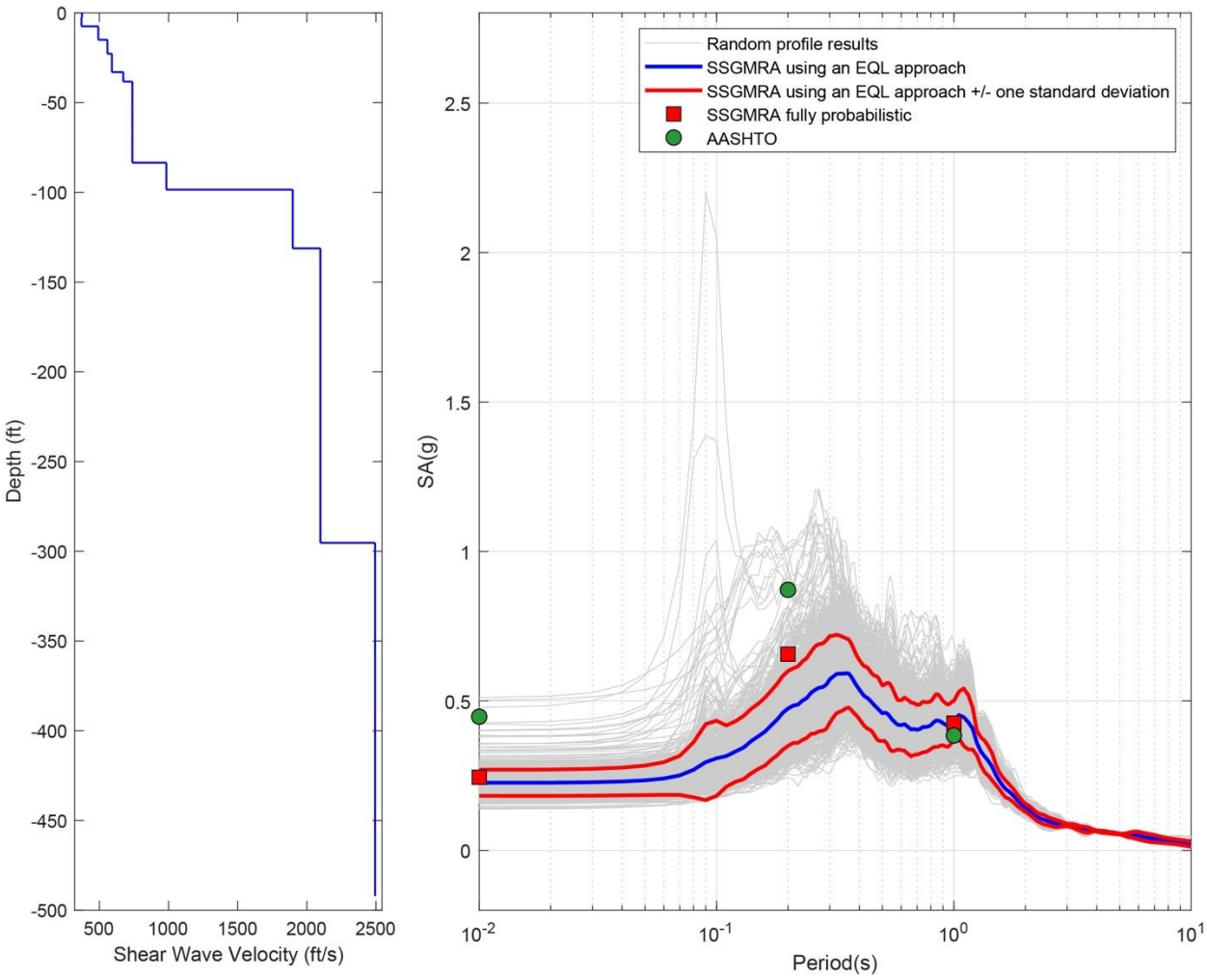


**Figure B-63. Left Panel: Shear-Wave Velocity Profile for Site 16 (Based on Peninsular Soil Model); and Right Panel: Results of SSGMRA Using a Fully Probabilistic Approach, SSGMRA Using an Equivalent Linear Approach, SSGMRA Using an Equivalent Linear Approach Plus and Minus One Standard Deviation, and AASHTO General Approach**

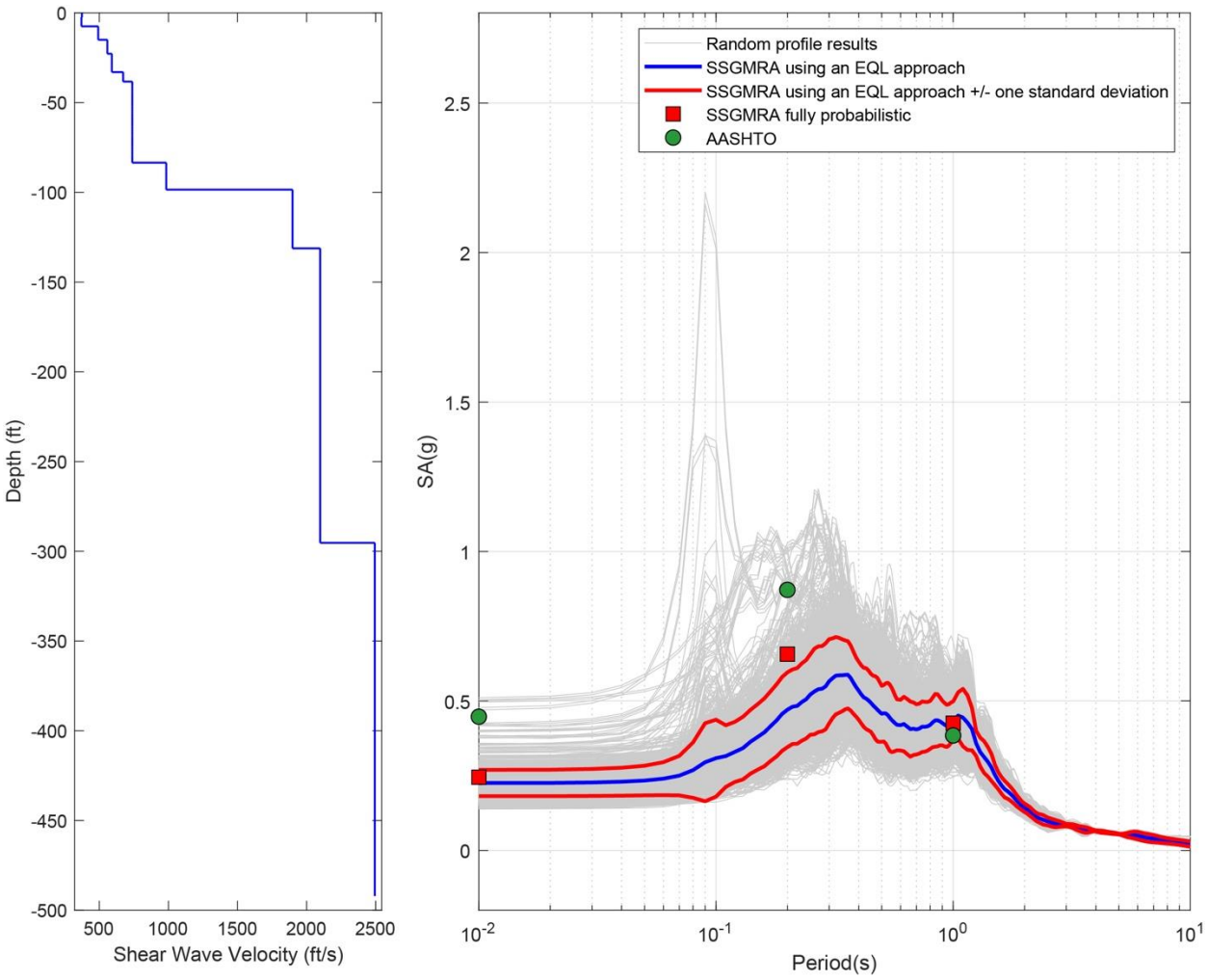


**Figure B-64. Left Panel: Shear-Wave Velocity Profile for Site 16 (Combined); and Right Panel: Results of SSGMRA Using a Fully Probabilistic Approach, SSGMRA Using an Equivalent Linear Approach, SSGMRA Using an Equivalent Linear Approach Plus and Minus One Standard Deviation, and AASHTO General Approach**

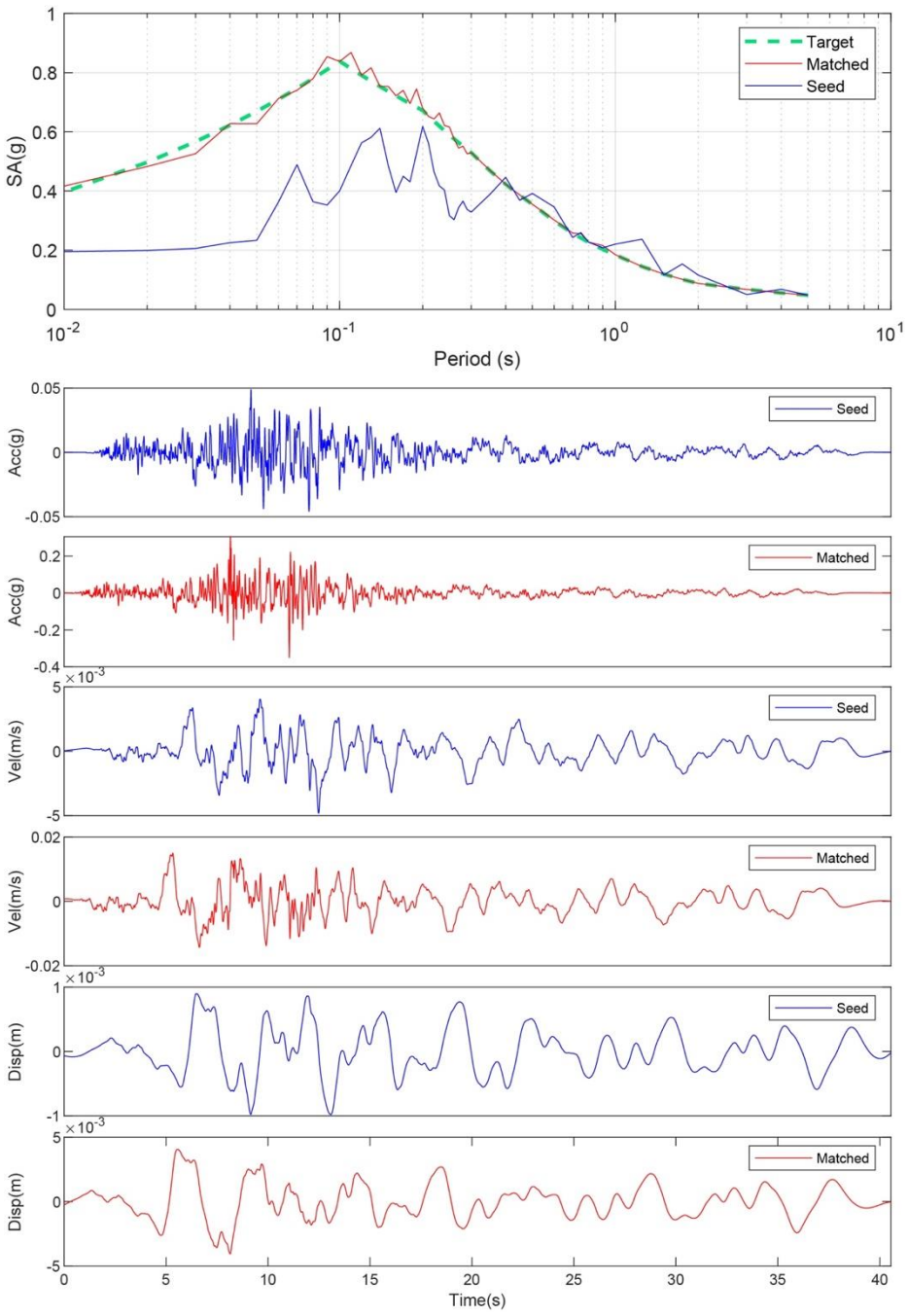


**Figure B-65. Matching Spectrum of Seed Motion (RSN774-LOMAP-HYN064) to The Target Spectrum (UHS) at Site 17. The Middle Subplot Shows the Seed Motion, and the Bottom Subplot Indicates the Matched Motion**

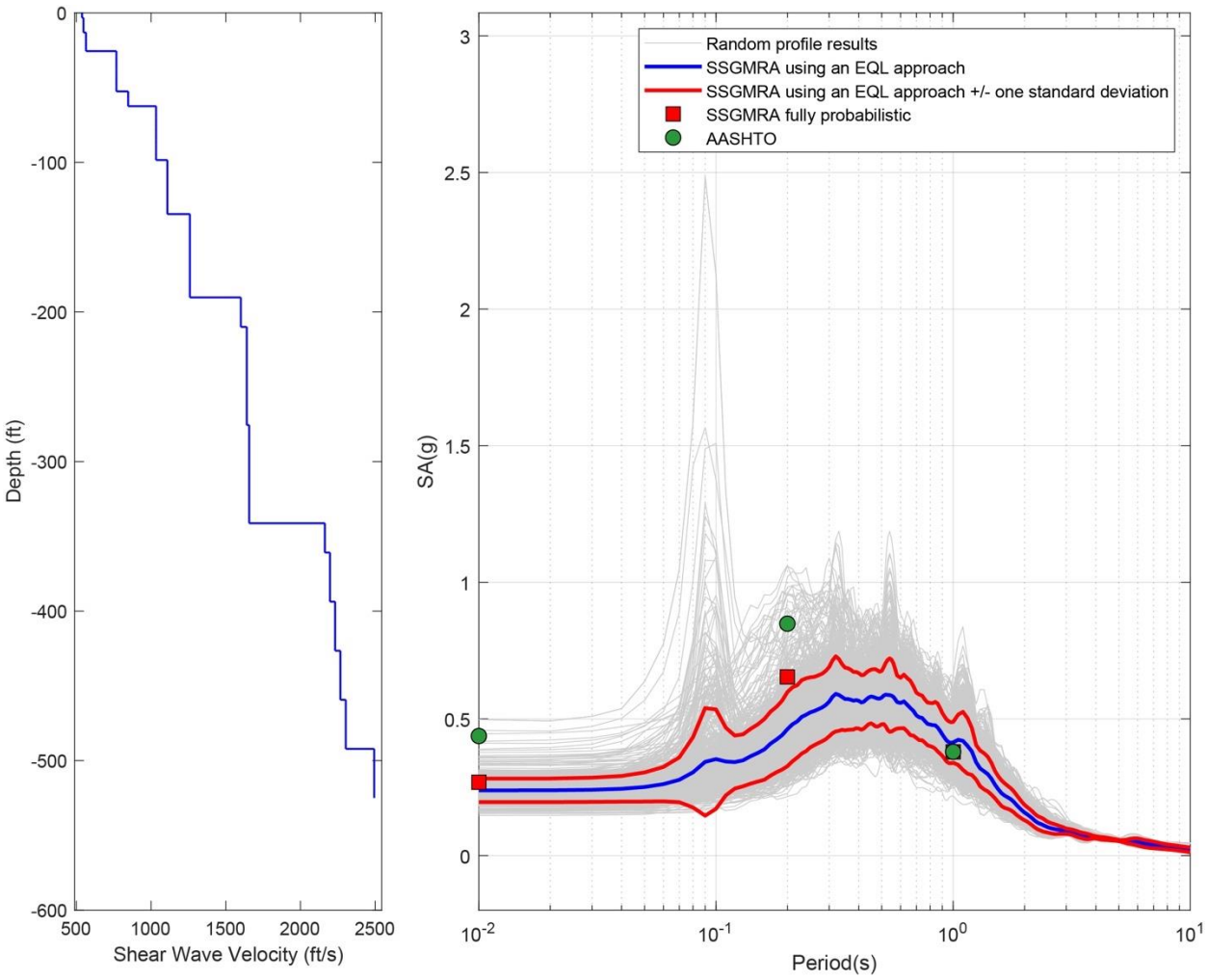


**Figure B-66. Left Panel: Shear-Wave Velocity Profile for Site 17 (Based on EPRI Soil Model); and Right Panel: Results of SSGMRA Using a Fully Probabilistic Approach, SSGMRA Using an Equivalent Linear Approach, SSGMRA Using an Equivalent Linear Approach Plus and Minus One Standard Deviation, and AASHTO General Approach**

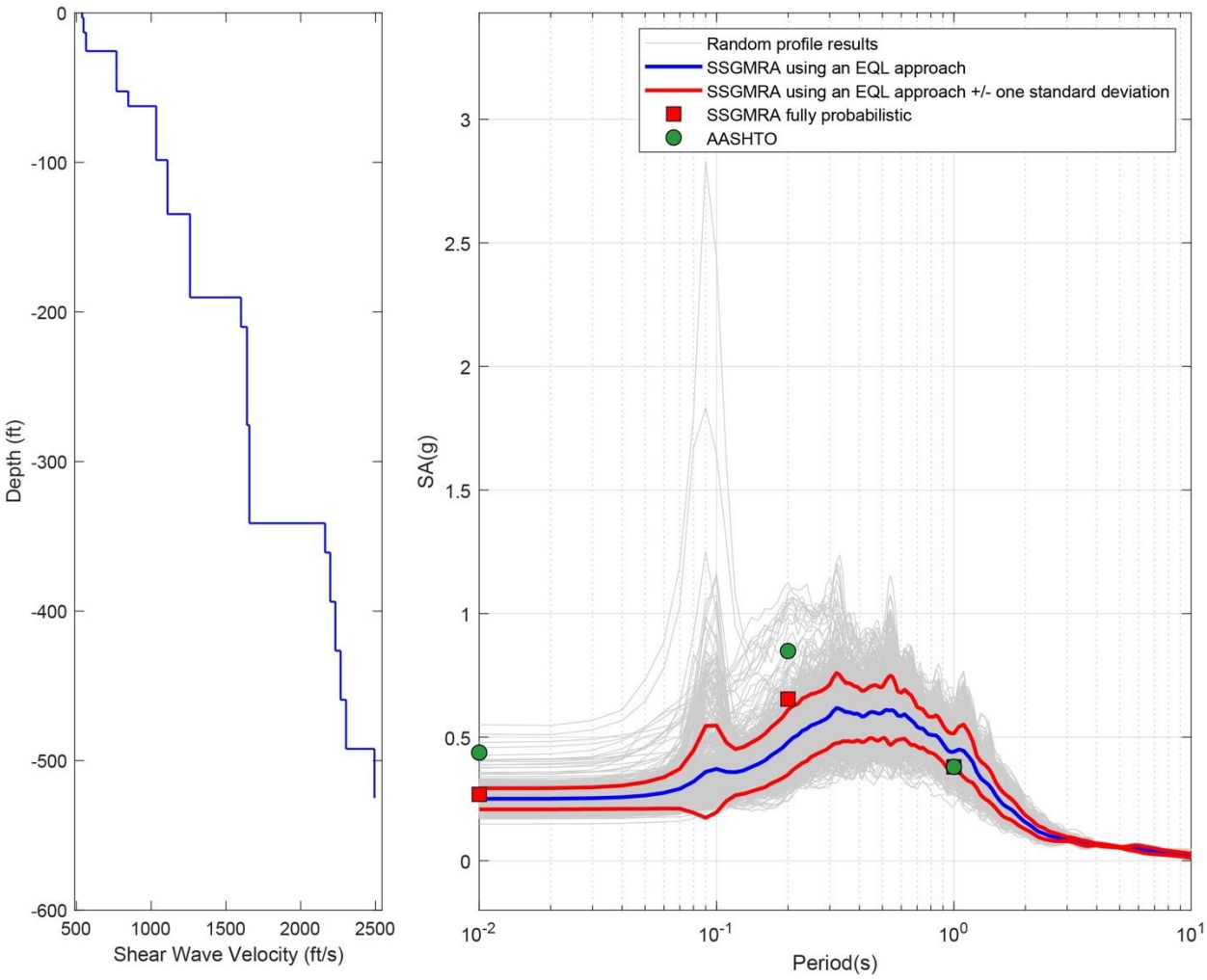


**Figure B-67. Left Panel: Shear-Wave Velocity Profile for Site 17 (Based on Peninsular Soil Model); and Right Panel: Results of SSGMRA Using a Fully Probabilistic Approach, SSGMRA Using an Equivalent Linear Approach, SSGMRA Using an Equivalent Linear Approach Plus and Minus One Standard Deviation, and AASHTO General Approach**

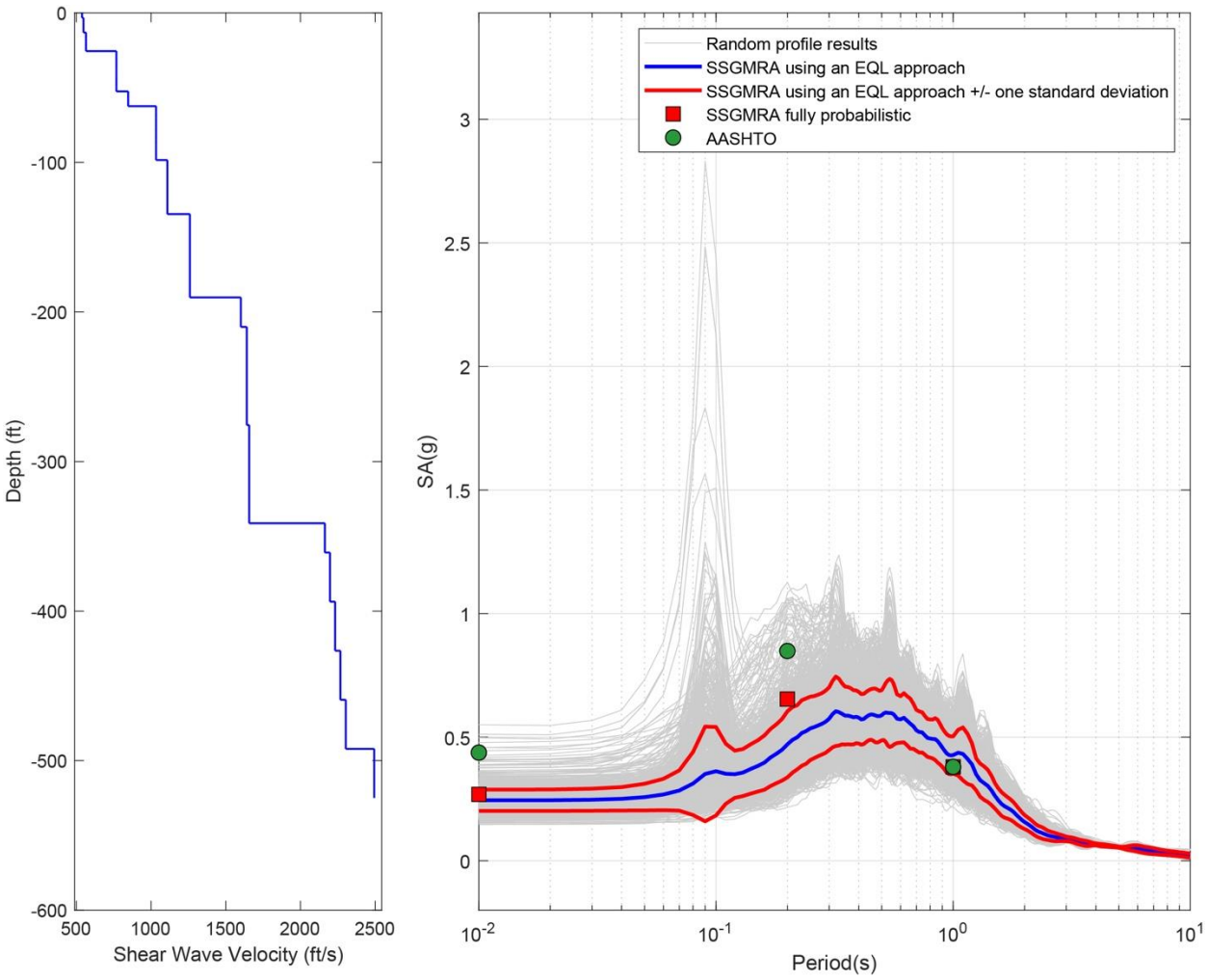


**Figure B-68. Left Panel: Shear-Wave Velocity Profile for Site 17 (Combined); and Right Panel: Results of SSGMRA Using a Fully Probabilistic Approach, SSGMRA Using an Equivalent Linear Approach, SSGMRA Using an Equivalent Linear Approach Plus and Minus One Standard Deviation, and AASHTO General Approach**

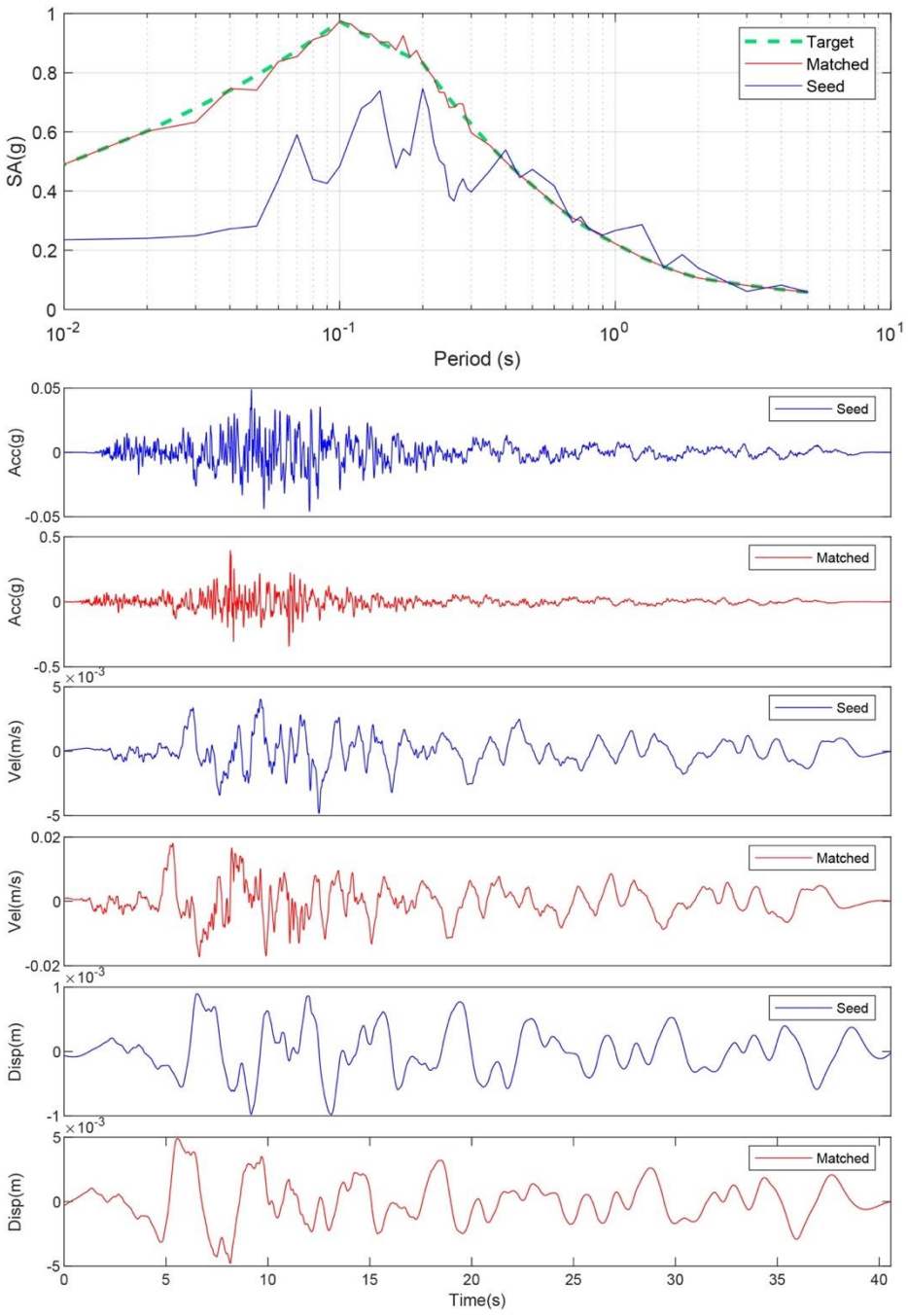


**Figure B.69 Matching Spectrum of Seed Motion (RSN774-LOMAP-HYN064) to the Target Spectrum (UHS) at Site 18. The Middle Subplot Shows the Seed Motion, and The Bottom Subplot Indicates the Matched Motion**

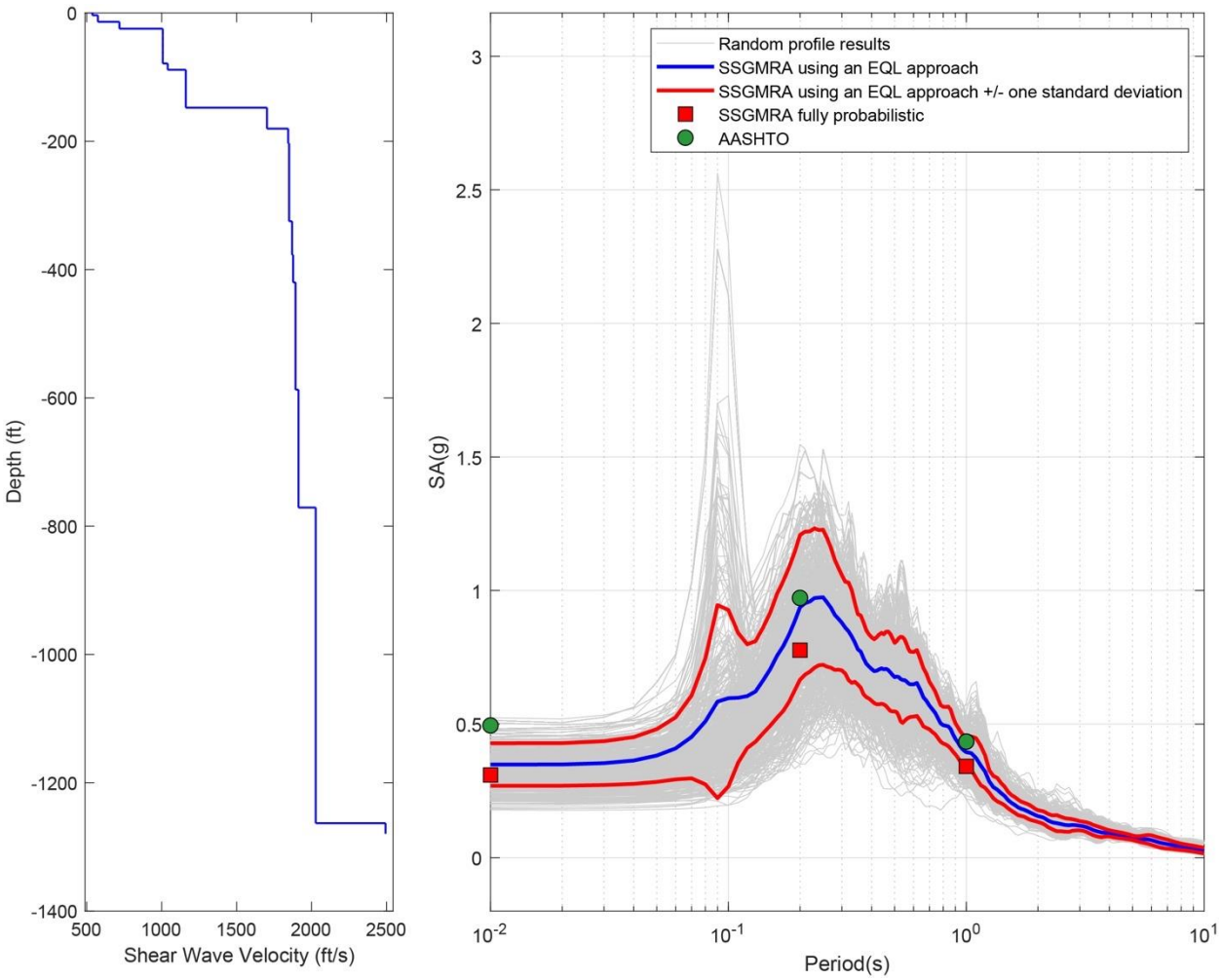


**Figure B-70. Left Panel: Shear-Wave Velocity Profile for Site 18 (Based on EPRI Soil Model); and Right Panel: Results of SSGMRA Using a Fully Probabilistic Approach, SSGMRA Using an Equivalent Linear Approach, SSGMRA Using an Equivalent Linear Approach Plus and Minus One Standard Deviation, and AASHTO General Approach**

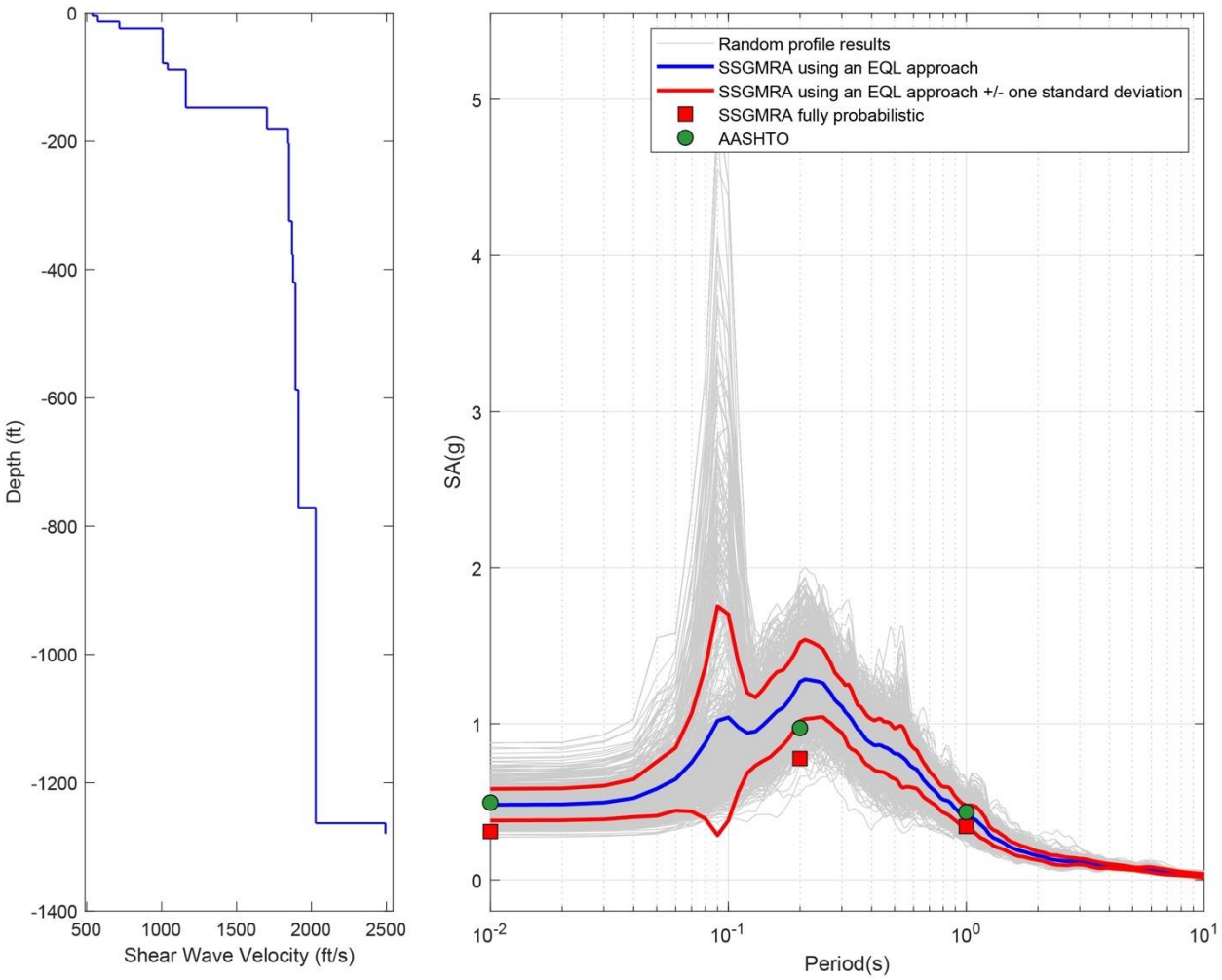


**Figure B-71. Left Panel: Shear-Wave Velocity Profile for Site 18 (Based on Peninsular Soil Model); and Right Panel: Results of SSGMRA Using a Fully Probabilistic Approach, SSGMRA Using an Equivalent Linear Approach, SSGMRA Using an Equivalent Linear Approach Plus and Minus One Standard Deviation, and AASHTO General Approach**

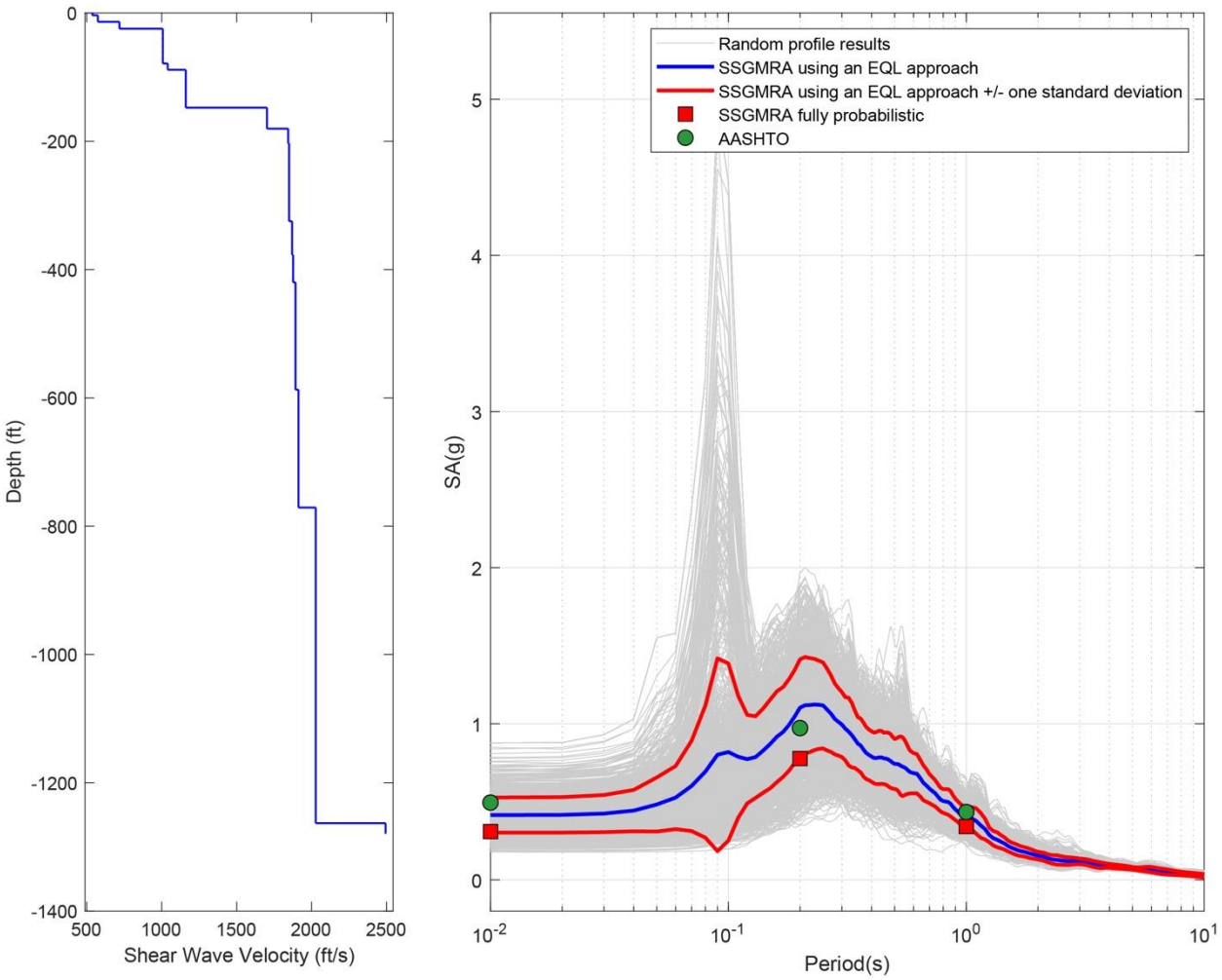


**Figure B-72. Left Panel: Shear-Wave Velocity Profile for Site 18 (Combined); and Right Panel: Results of SSGMRA Using a Fully Probabilistic Approach, SSGMRA Using an Equivalent Linear Approach, SSGMRA Using an Equivalent Linear Approach Plus and Minus one Standard Deviation, and AASHTO General Approach**

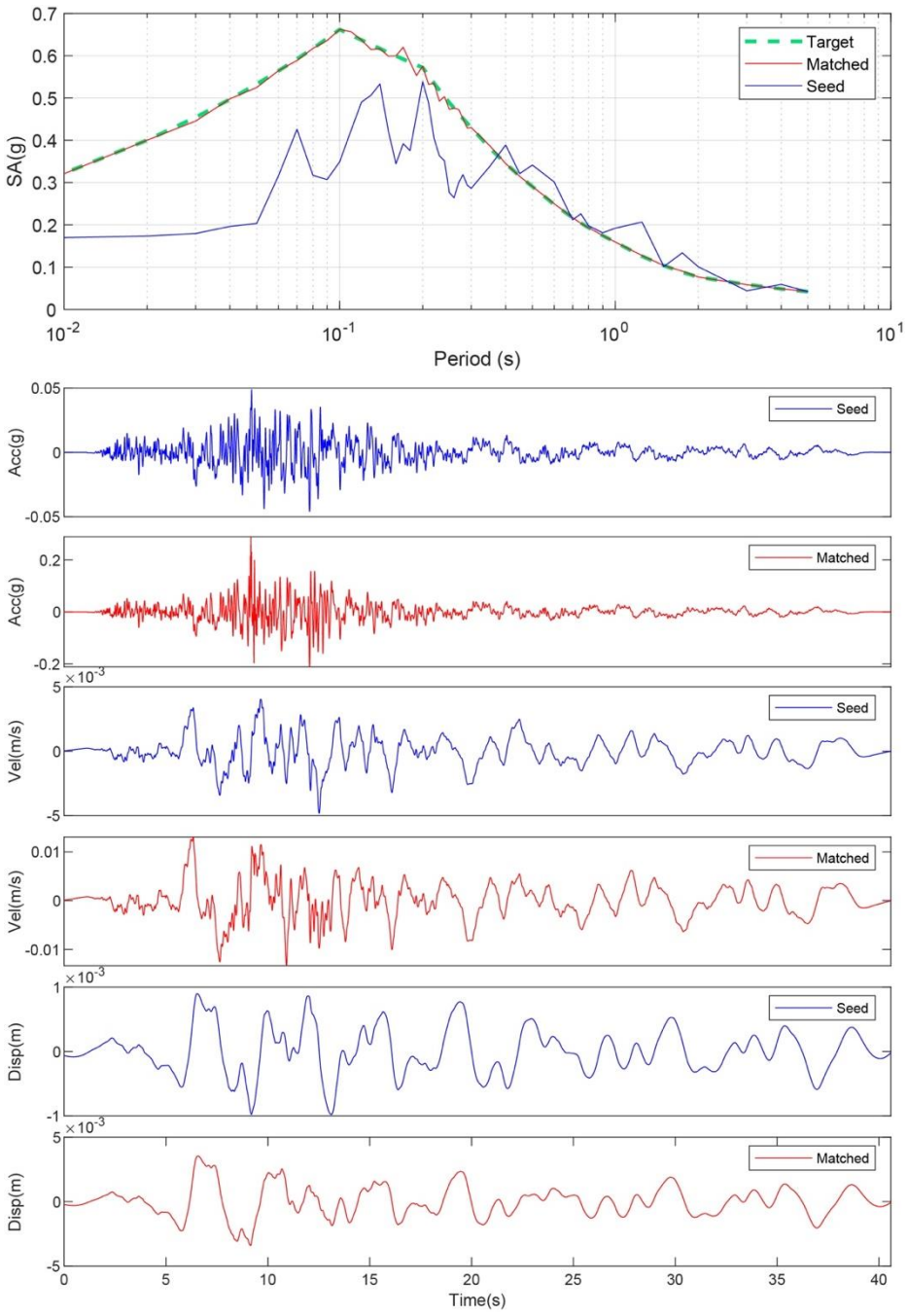


**Figure B-73. Matching Spectrum of Seed Motion (RSN774-LOMAP-HYN064) to the Target Spectrum (UHS) at Site 19. The Middle Subplot Shows the Seed Motion, and the Bottom Subplot Indicates the Matched Motion**

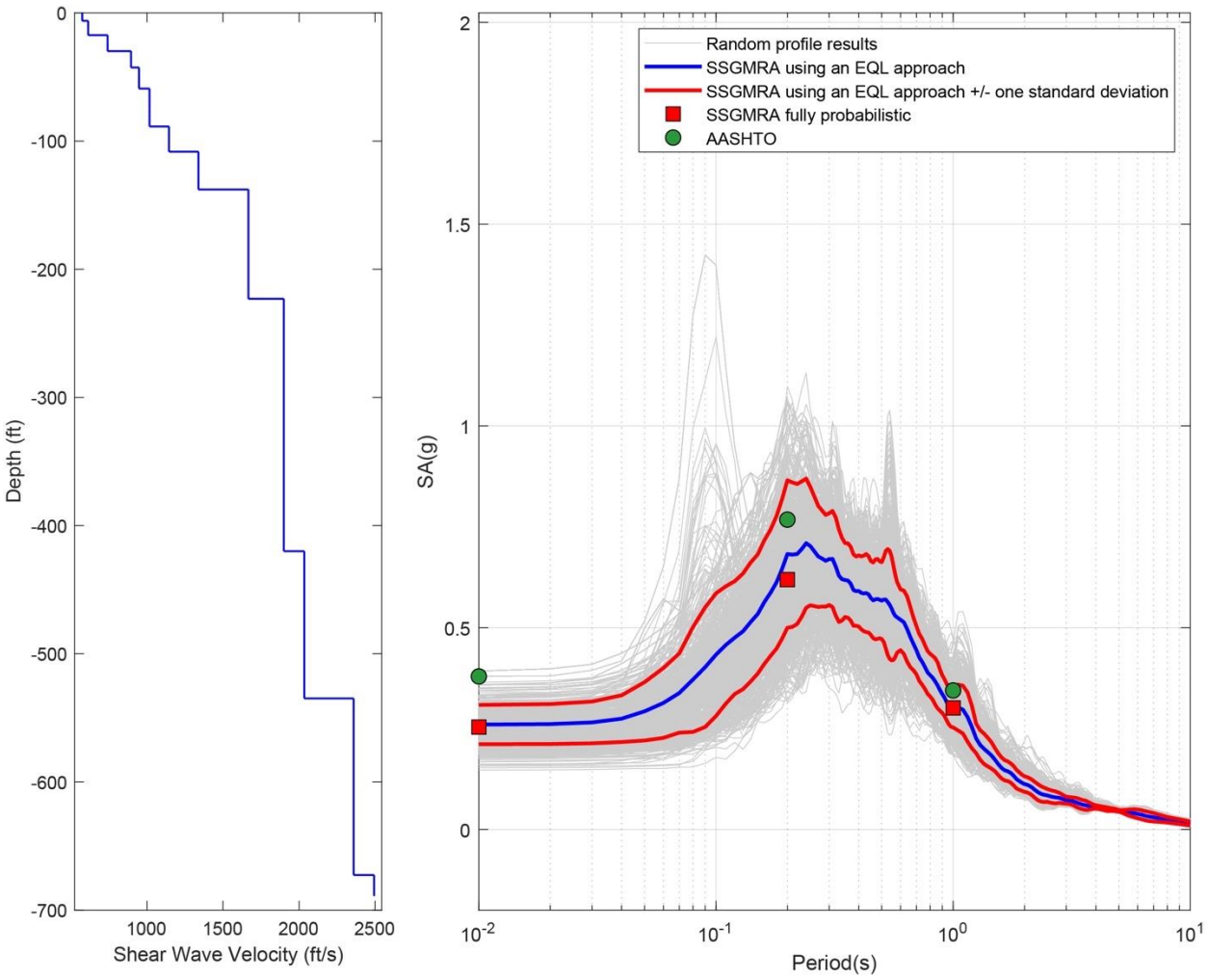


**Figure B-74. Left Panel: Shear-Wave Velocity Profile for Site 19 (Based on EPRI Soil Model); and Right Panel: Results of SSGMRA Using a Fully Probabilistic Approach, SSGMRA Using an Equivalent Linear Approach, SSGMRA Using an Equivalent Linear Approach Plus and Minus One Standard Deviation, and AASHTO General Approach**

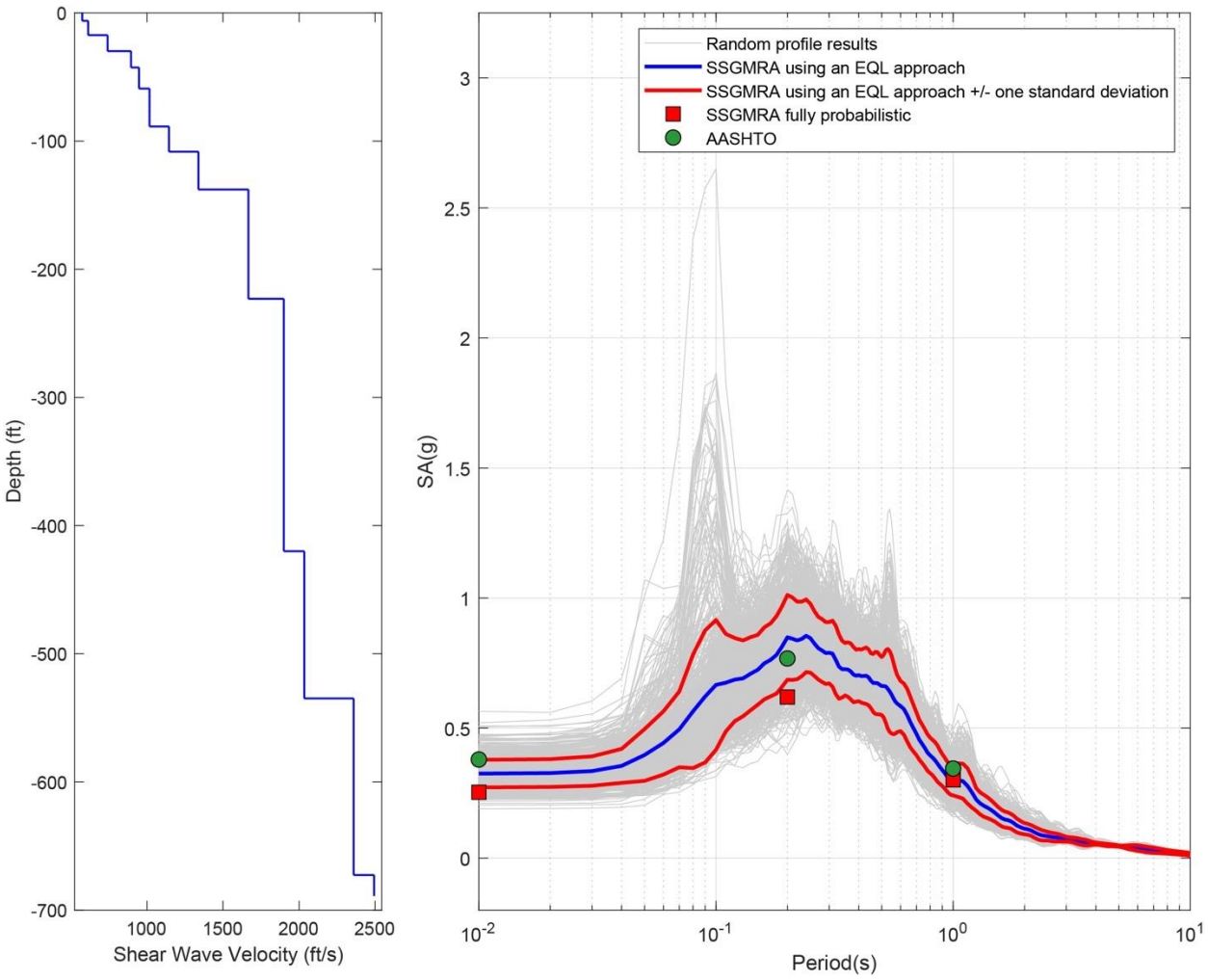


**Figure B-75. Left Panel: Shear-Wave Velocity Profile for Site 19 (Based on Peninsular Soil Model); and Right Panel: Results of SSGMRA Using a Fully Probabilistic Approach, SSGMRA Using an Equivalent Linear Approach, SSGMRA Using an Equivalent Linear Approach Plus and Minus One Standard Deviation, and AASHTO General Approach**

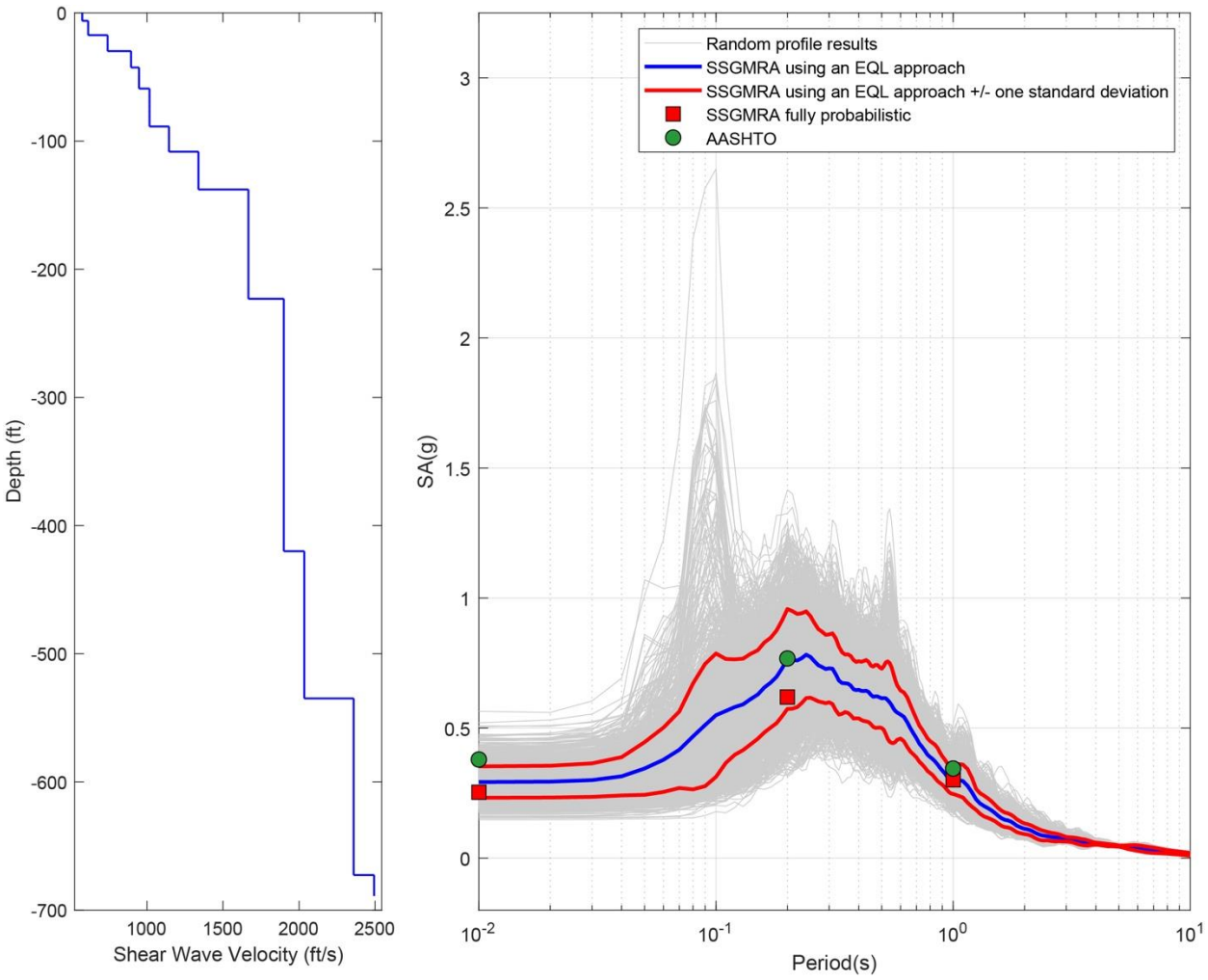


**Figure B-76. Left Panel: Shear-Wave Velocity Profile for Site 19 (Combined); and Right Panel: Results of SSGMRA Using a Fully Probabilistic Approach, SSGMRA Using an Equivalent Linear Approach, SSGMRA Using an Equivalent Linear Approach Plus and Minus One Standard Deviation, and AASHTO General Approach**

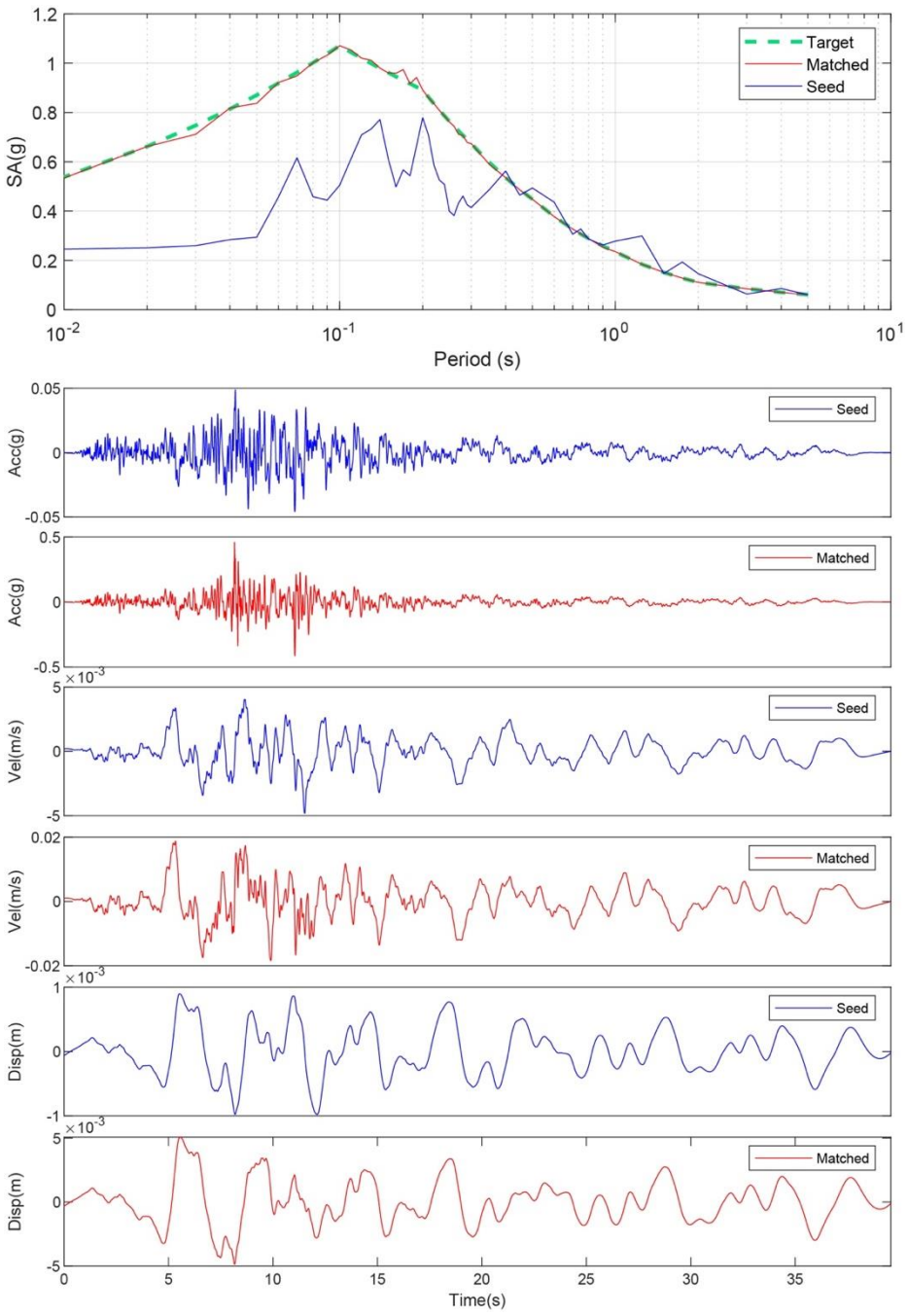


**Figure B-77. Matching Spectrum of Seed Motion (RSN774-LOMAP-HYN064) to the Target Spectrum (UHS) at Site 20. The Middle Subplot Shows the Seed Motion, and the Bottom Subplot Indicates the Matched Motion**

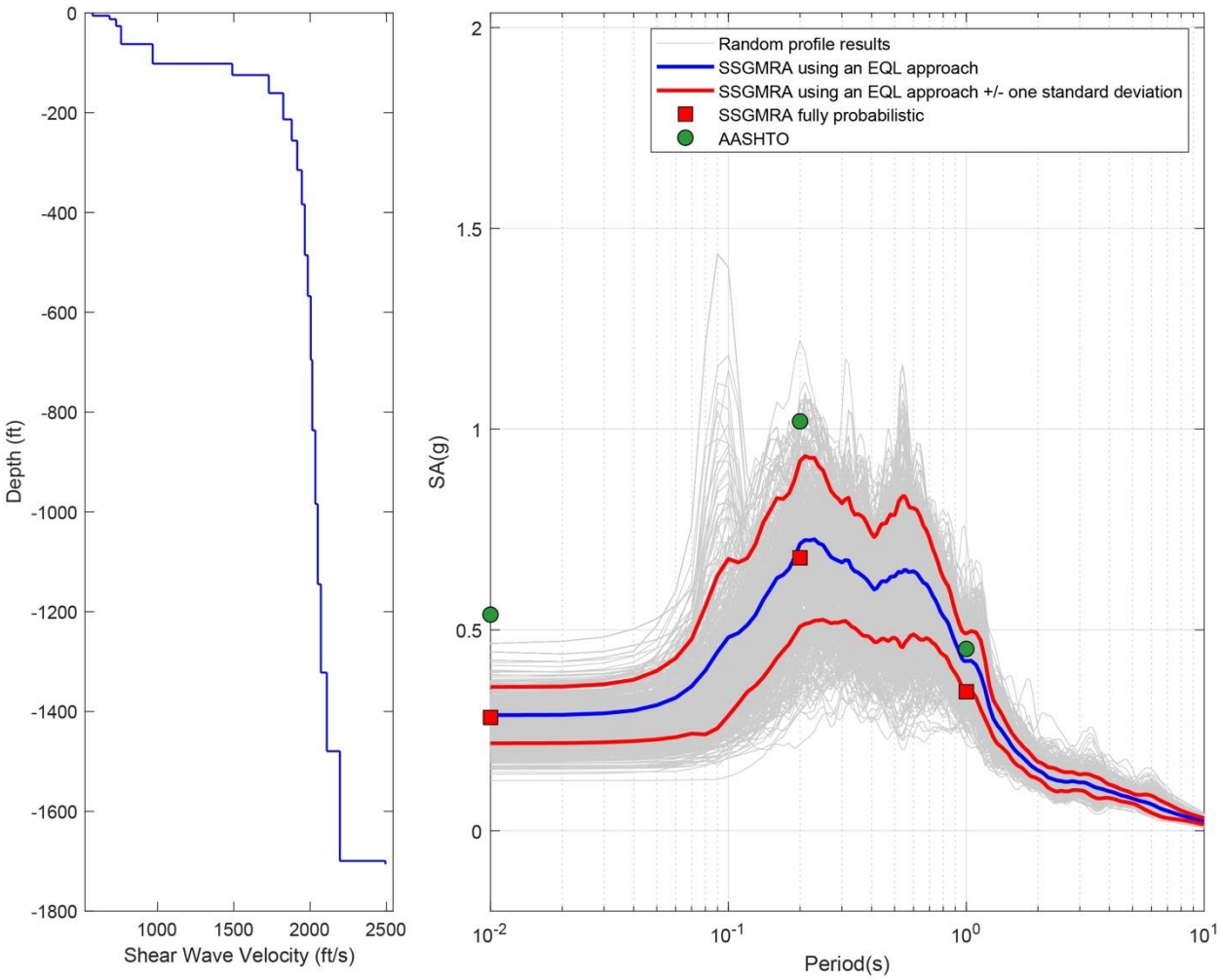


**Figure B-78. Left Panel: Shear-Wave Velocity Profile for Site 20 (Based on EPRI Soil Model); and Right Panel: Results of SSGMRA Using a Fully Probabilistic Approach, SSGMRA Using an Equivalent Linear Approach, SSGMRA Using an Equivalent Linear Approach Plus and Minus One Standard Deviation, and AASHTO General Approach**

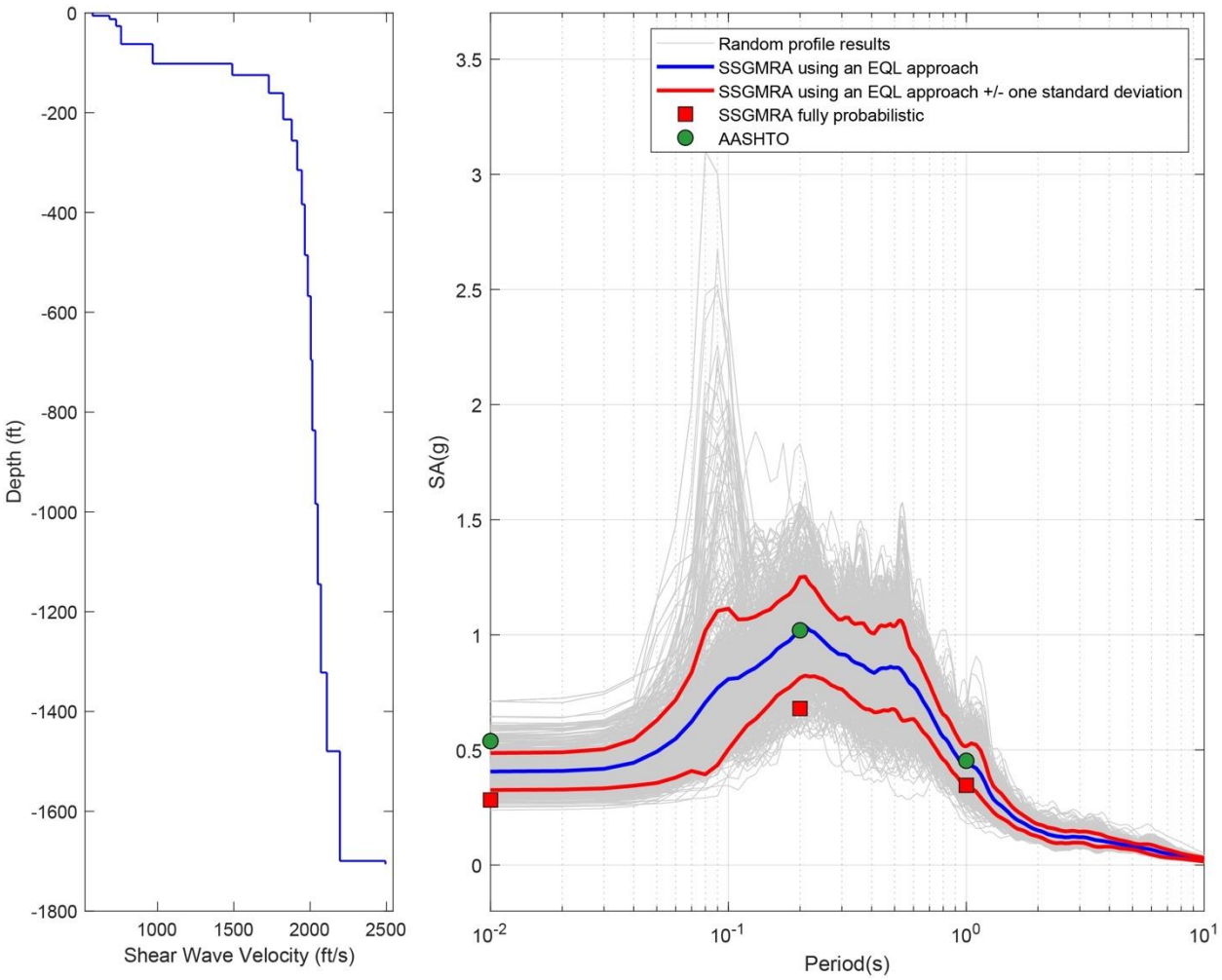


**Figure B-79. Left Panel: Shear-Wave Velocity Profile for Site 20 (Based on Peninsular Soil Model); and Right Panel: Results of SSGMRA Using a Fully Probabilistic Approach, SSGMRA Using an Equivalent Linear Approach, SSGMRA Using an Equivalent Linear Approach Plus and Minus One Standard Deviation, and AASHTO General Approach**

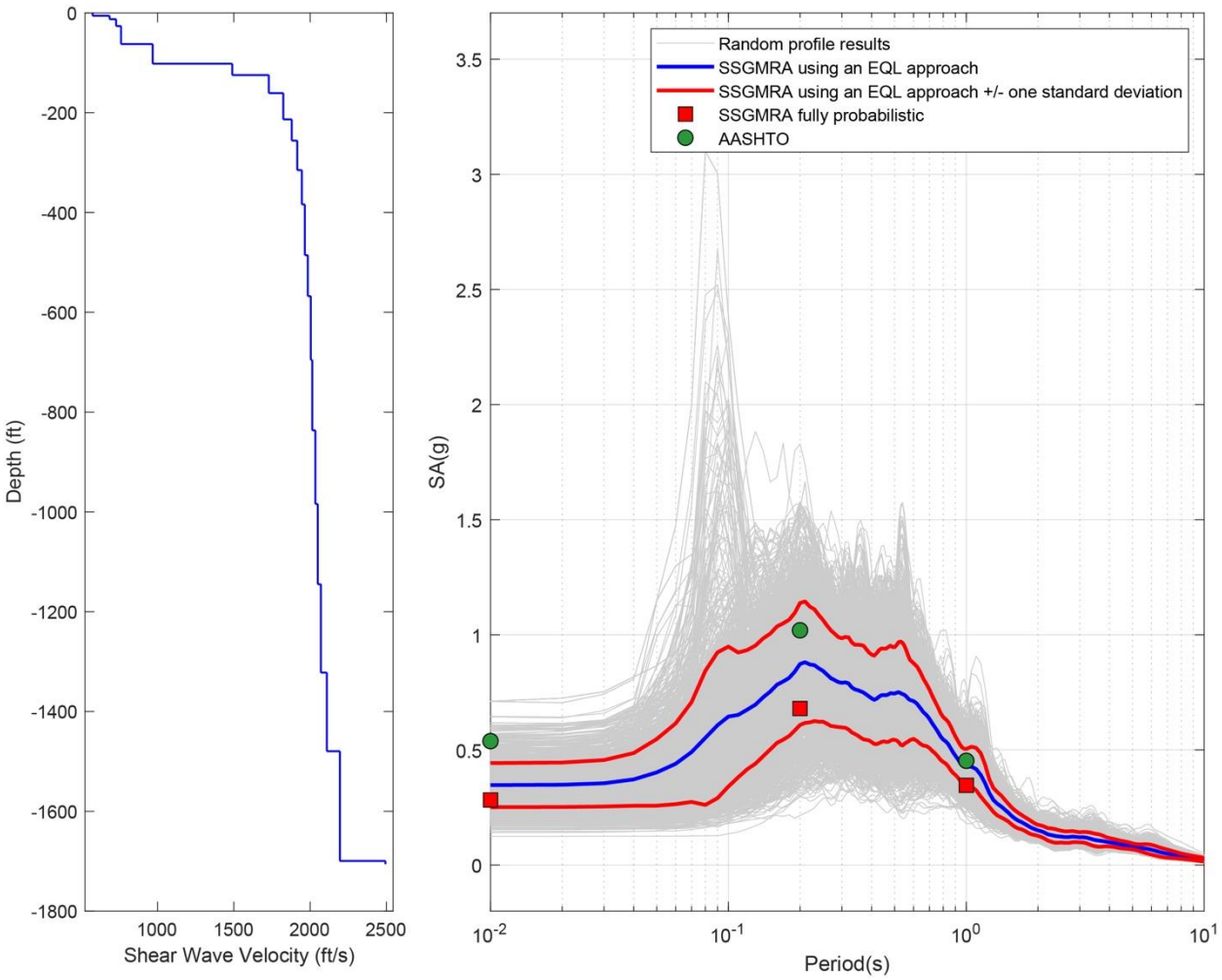


**Figure B.80 Left Panel: Shear-Wave Velocity Profile for Site 20 (Combined); and Right Panel: Results of SSGMRA Using a Fully Probabilistic Approach, SSGMRA Using an Equivalent Linear Approach, SSGMRA Using an Equivalent Linear Approach Plus and Minus One Standard Deviation, and AASHTO General Approach**

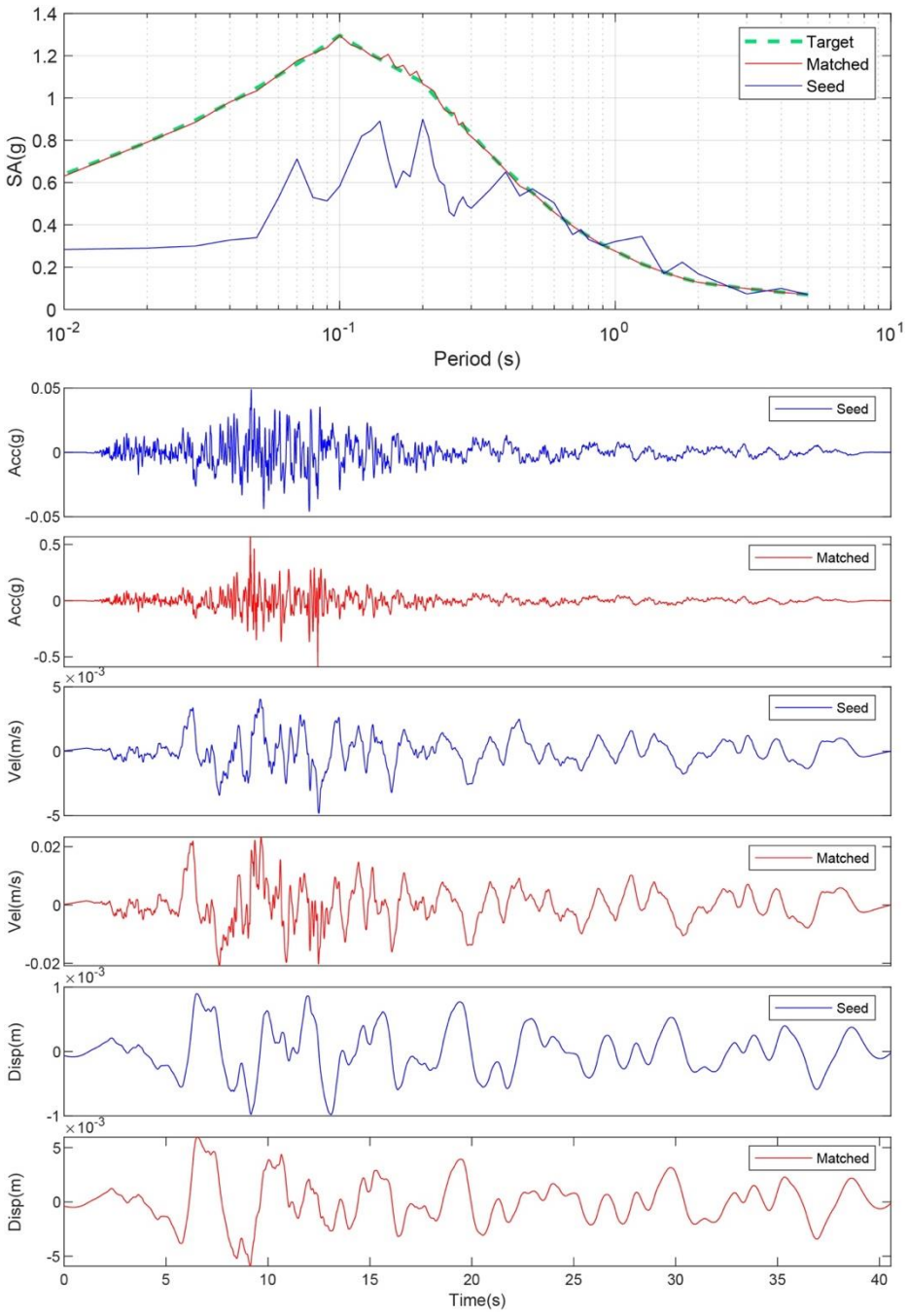


**Figure B-81. Matching Spectrum of Seed Motion (RSN774-LOMAP-HYN064) to the Target Spectrum (UHS) at Site 21. The Middle Subplot Shows the Seed Motion, and the Bottom Subplot Indicates the Matched Motion**

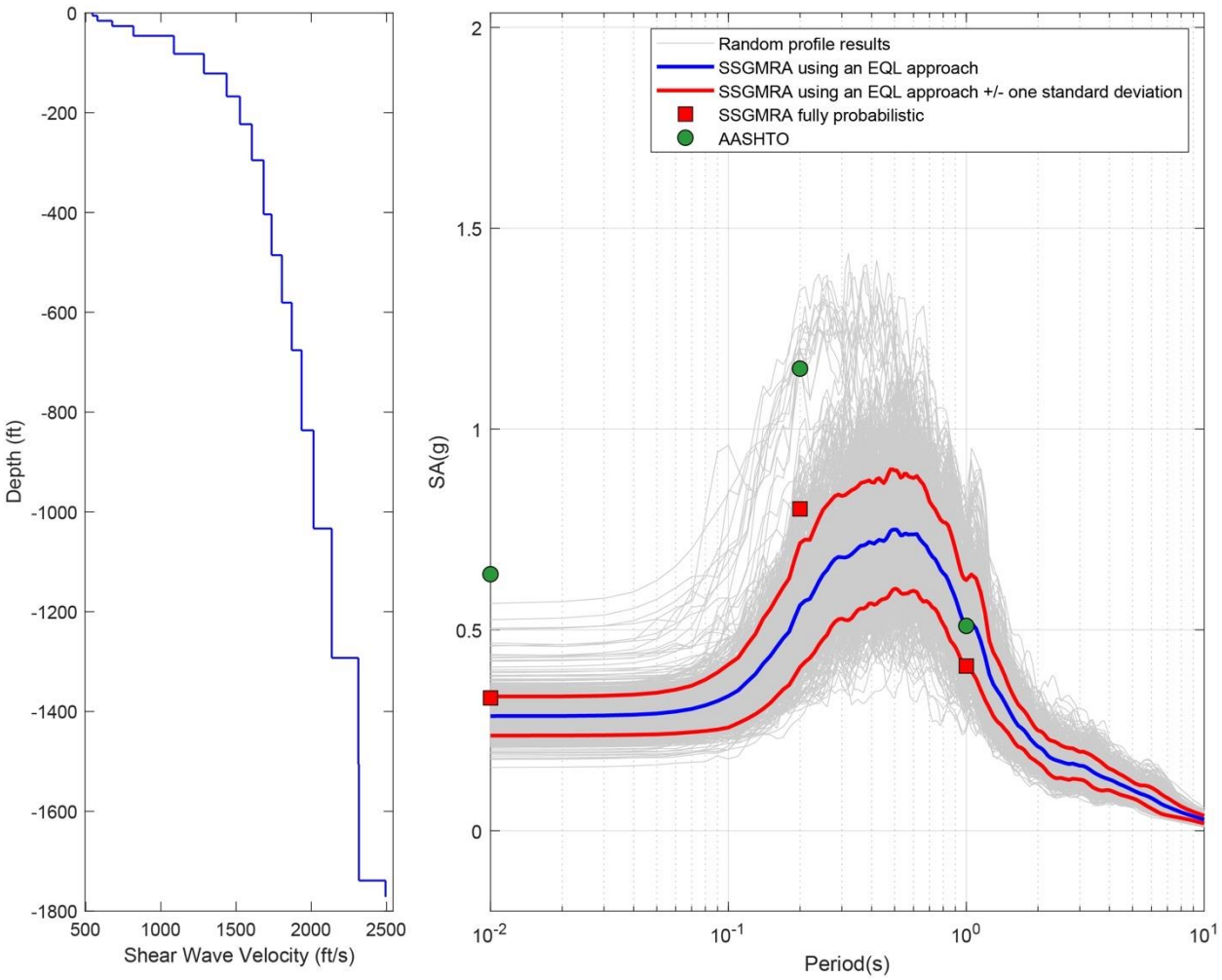


**Figure B-82. Left Panel: Shear-Wave Velocity Profile for Site 21 (Based on EPRI Soil Model); and Right Panel: Results of SSGMRA Using a Fully Probabilistic Approach, SSGMRA Using an Equivalent Linear Approach, SSGMRA Using an Equivalent Linear Approach Plus and Minus One Standard Deviation, and AASHTO General Approach**

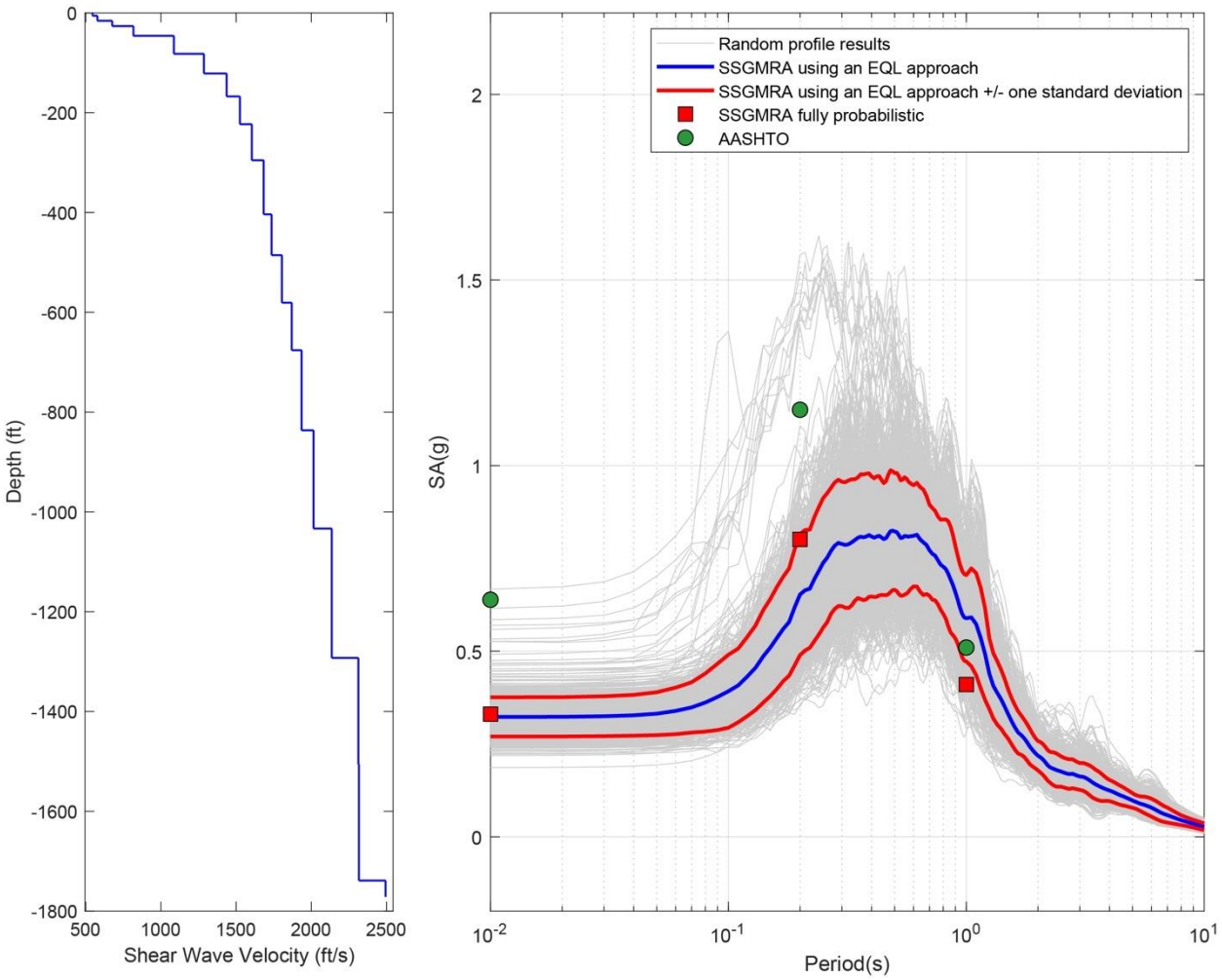


**Figure B-83. Left Panel: Shear-Wave Velocity Profile for Site 21 (Based on Peninsular Soil Model); and Right Panel: Results of SSGMRA Using a Fully Probabilistic Approach, SSGMRA Using an Equivalent Linear Approach, SSGMRA Using an Equivalent Linear Approach Plus and Minus One Standard Deviation, and AASHTO General Approach**

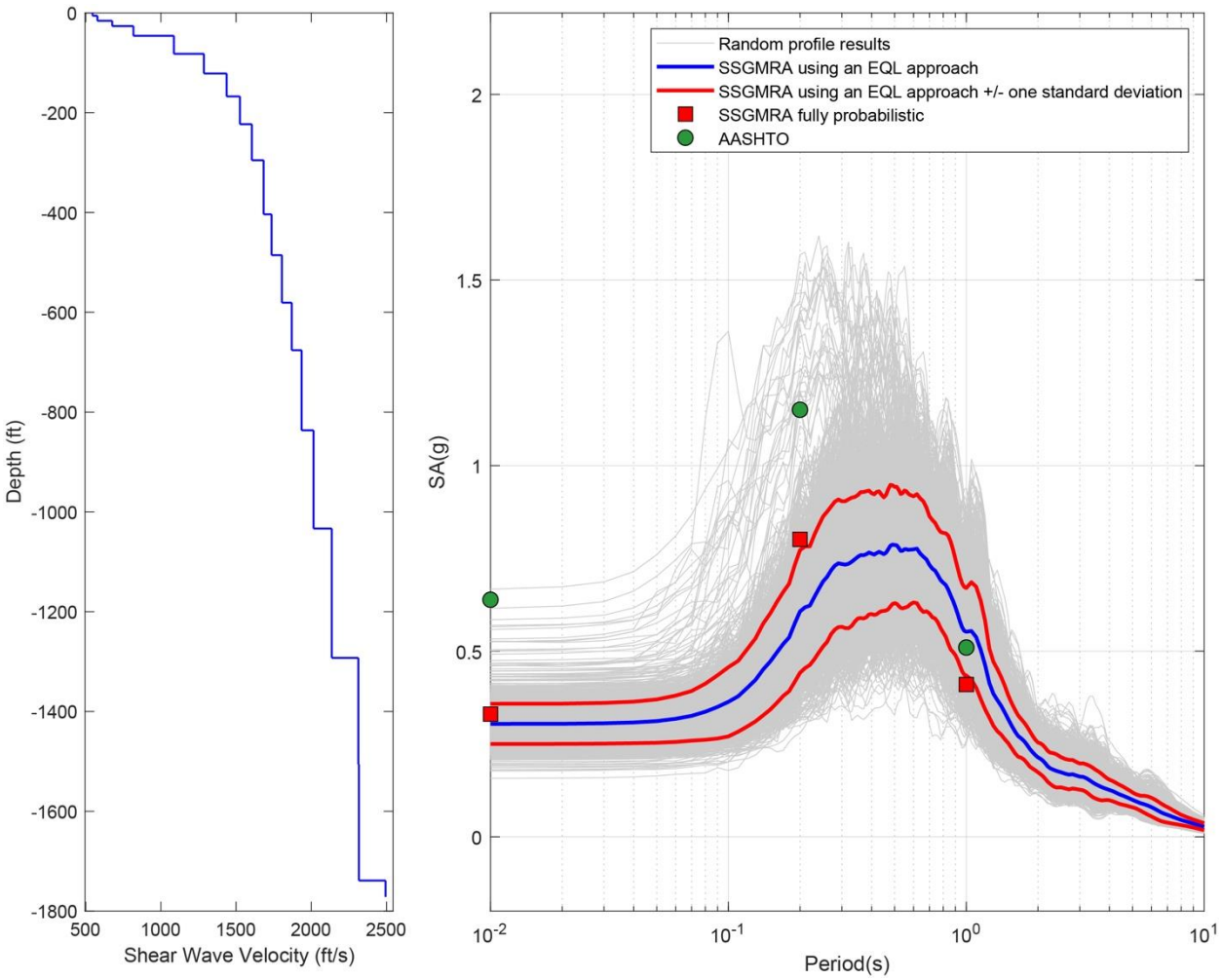


**Figure B-84. Left Panel: Shear-Wave Velocity Profile for Site 21 (Combined); and Right Panel: Results of SSGMRA Using a Fully Probabilistic Approach, SSGMRA Using an Equivalent Linear Approach, SSGMRA Using an Equivalent Linear Approach Plus and Minus One Standard Deviation, and AASHTO General Approach**

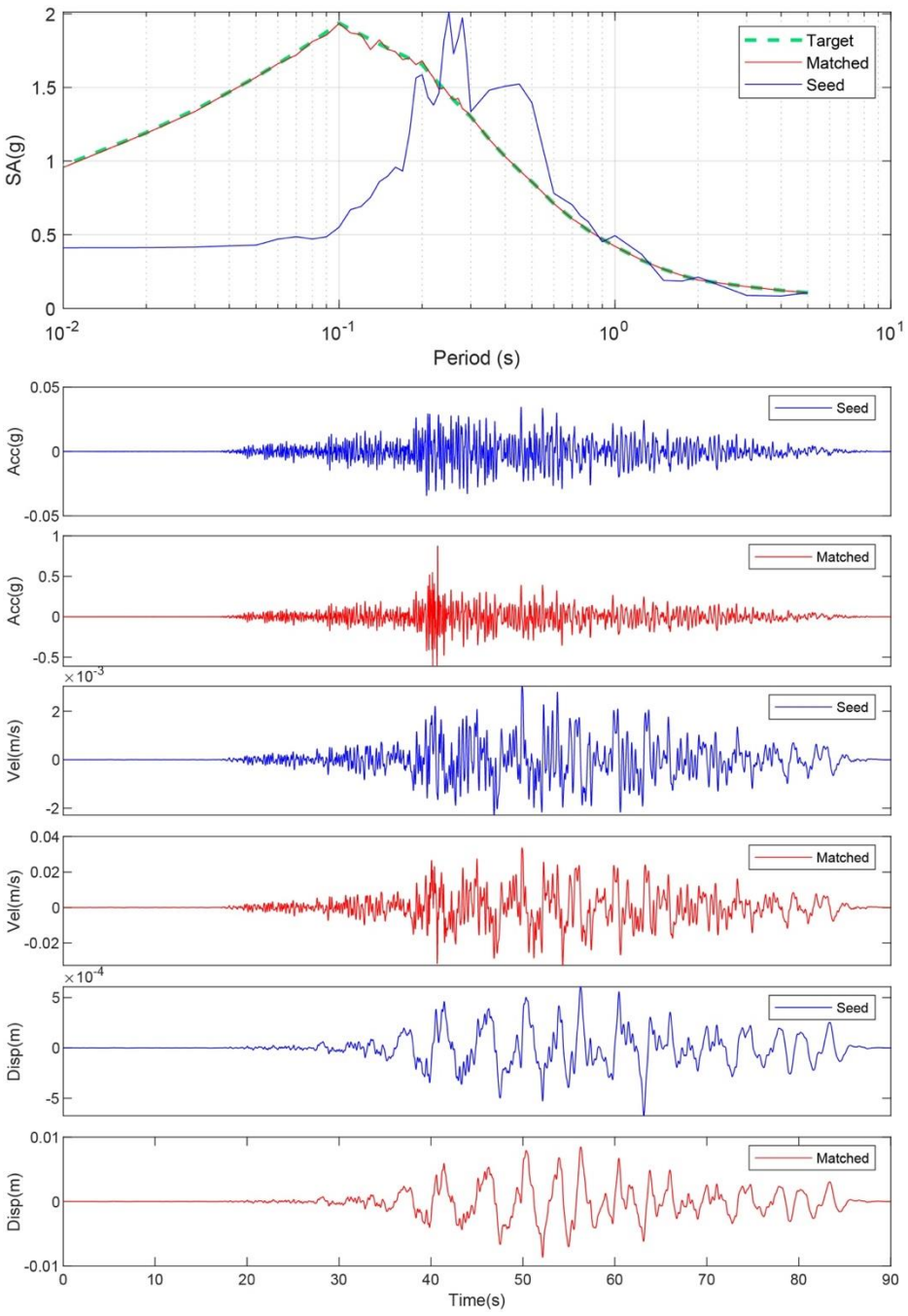


**Figure B-85. Matching Spectrum of Seed Motion (RSN1577-CHICHI-TTN025-E) to the Target Spectrum (UHS) at Site 22. The Middle Subplot Shows the Seed Motion, and the Bottom Subplot Indicates the Matched Motion**

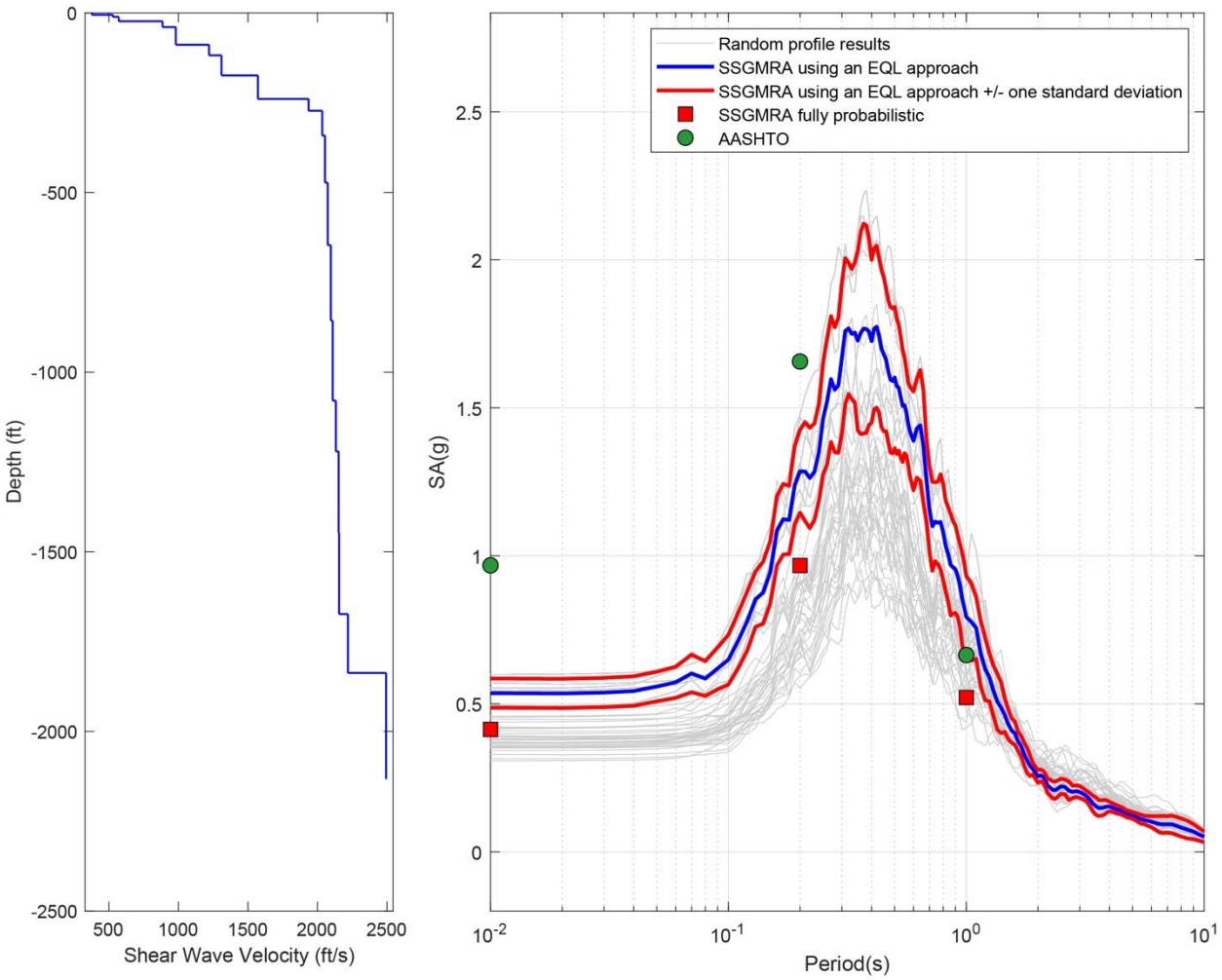


**Figure B-86. Left Panel: Shear-Wave Velocity Profile for Site 22 (Based on EPRI Soil Model); and Right Panel: Results of SSGMRA Using a Fully Probabilistic Approach, SSGMRA Using an Equivalent Linear Approach, SSGMRA Using an Equivalent Linear Approach Plus and Minus One Standard Deviation, and AASHTO General Approach**

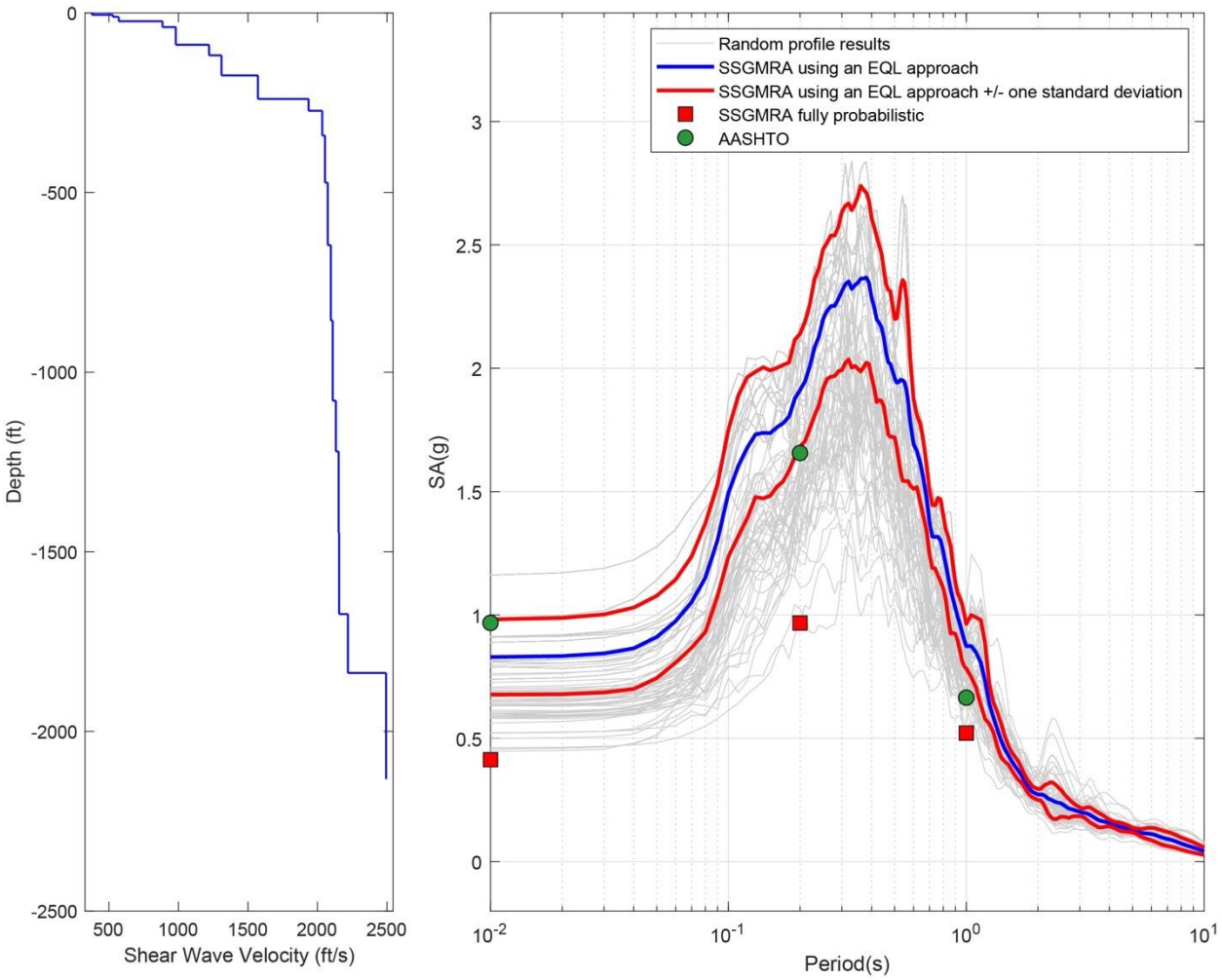


**Figure B-87. Left Panel: Shear-Wave Velocity Profile for Site 22 (Based on Peninsular Soil Model); and Right Panel: Results of SSGMRA Using a Fully Probabilistic Approach, SSGMRA Using an Equivalent Linear Approach, SSGMRA Using an Equivalent Linear Approach Plus and Minus One Standard Deviation, and AASHTO General Approach**

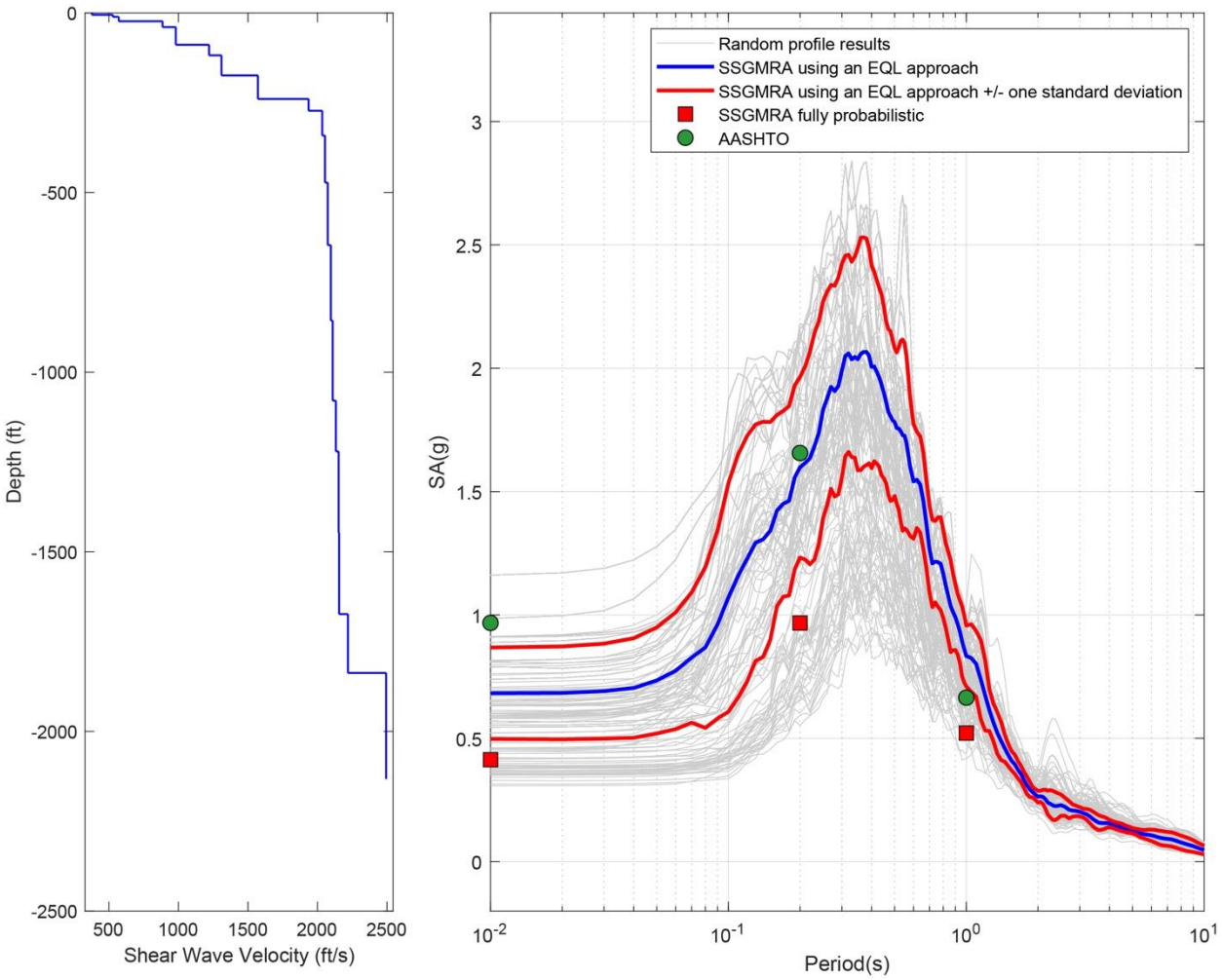


**Figure B-88. Left Panel: Shear-Wave Velocity Profile for Site 22 (Combined); and Right Panel: Results of SSGMRA Using a Fully Probabilistic Approach, SSGMRA Using an Equivalent Linear Approach, SSGMRA Using an Equivalent Linear Approach Plus and Minus One Standard Deviation, and AASHTO General Approach**

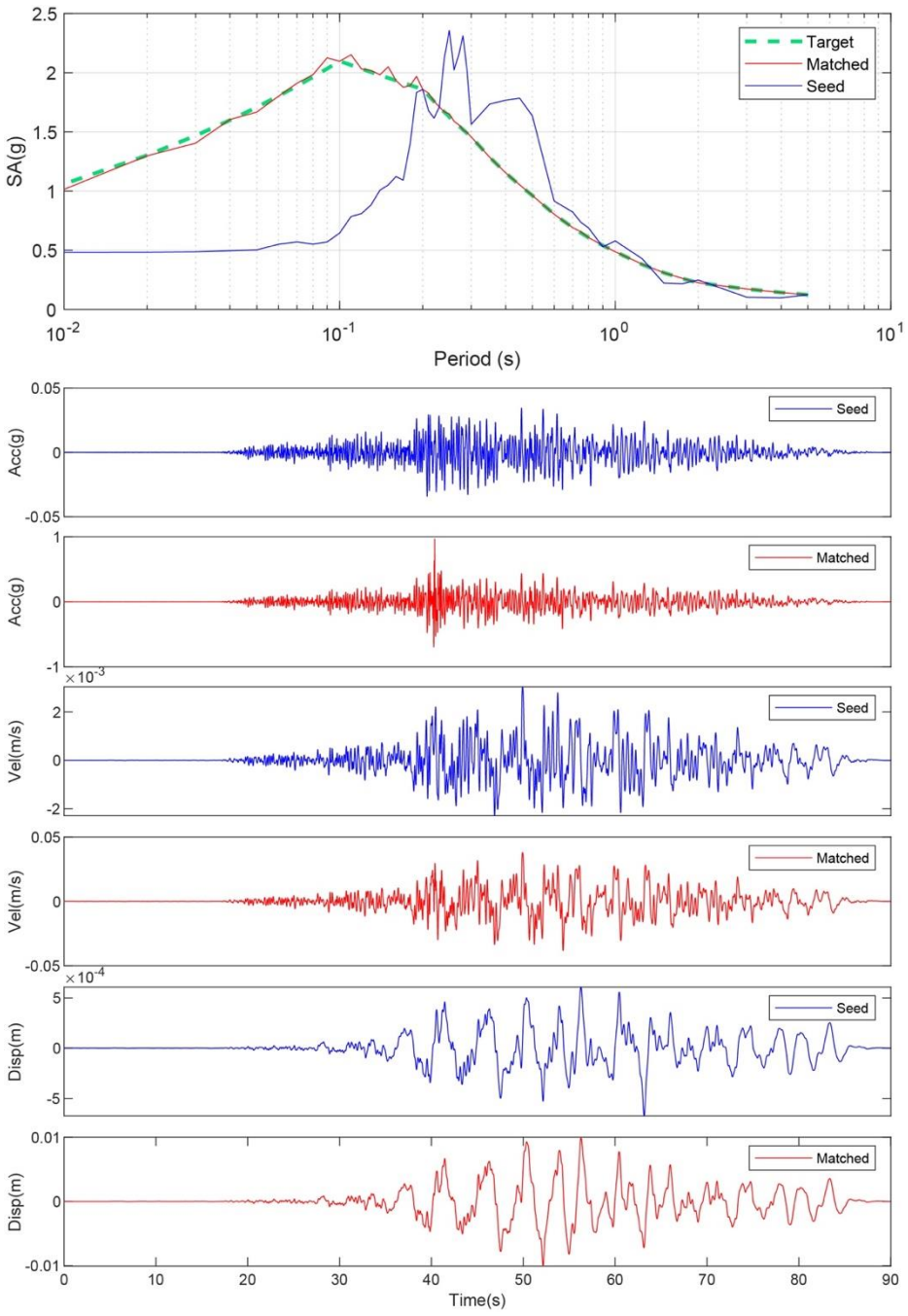


**Figure B-89. Matching Spectrum of Seed Motion (RSN1577-CHICHI-TTN025-E) to the target Spectrum (UHS) at Site 23. The Middle Subplot Shows the Seed Motion, and the Bottom Subplot Indicates the Matched Motion**

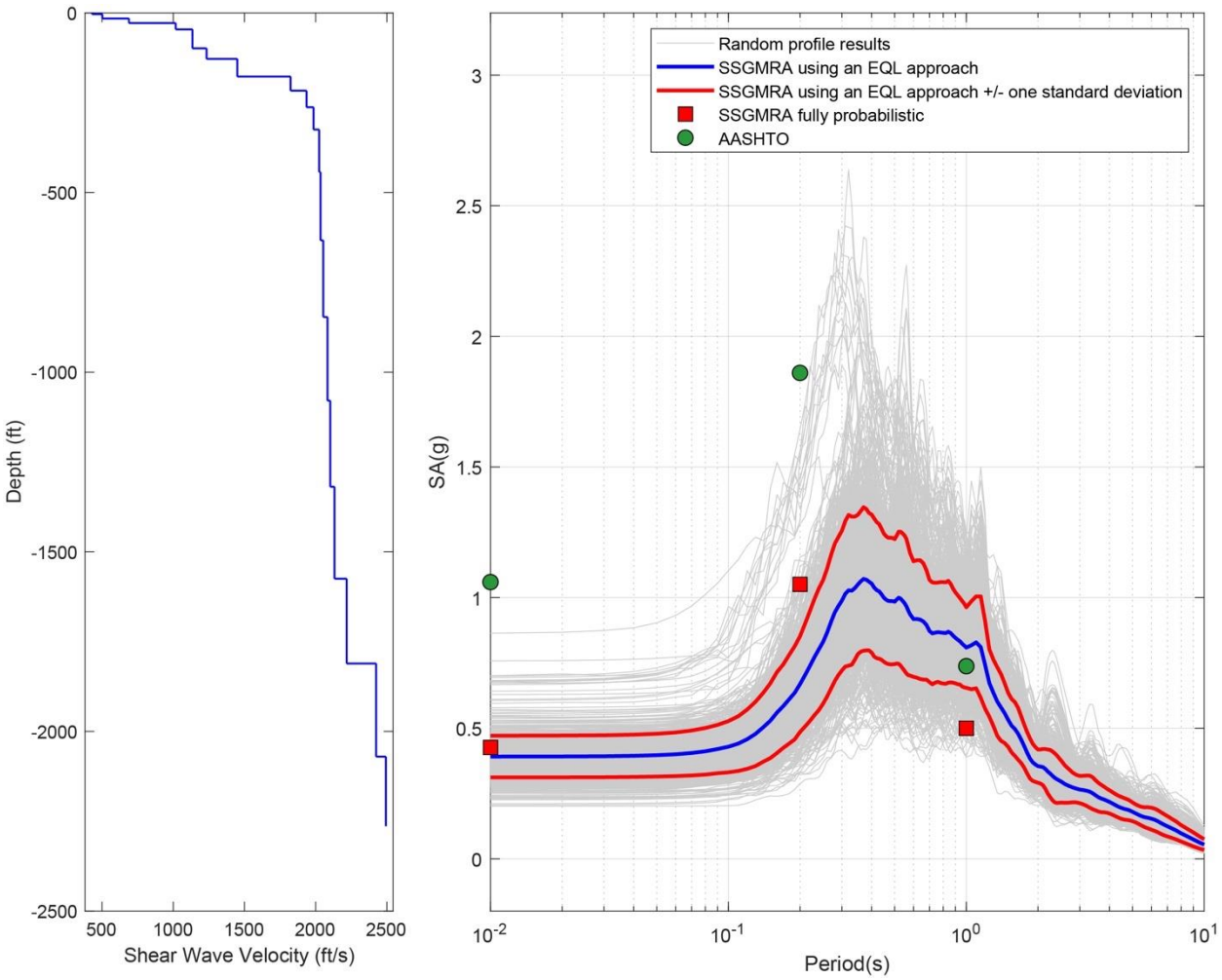


**Figure B-90. Left Panel: Shear-Wave Velocity Profile for Site 23 (Based on EPRI Soil Model); and Right Panel: Results of SSGMRA Using a Fully Probabilistic Approach, SSGMRA Using an Equivalent Linear Approach, SSGMRA Using an Equivalent Linear Approach Plus and Minus One Standard Deviation, and AASHTO General Approach**

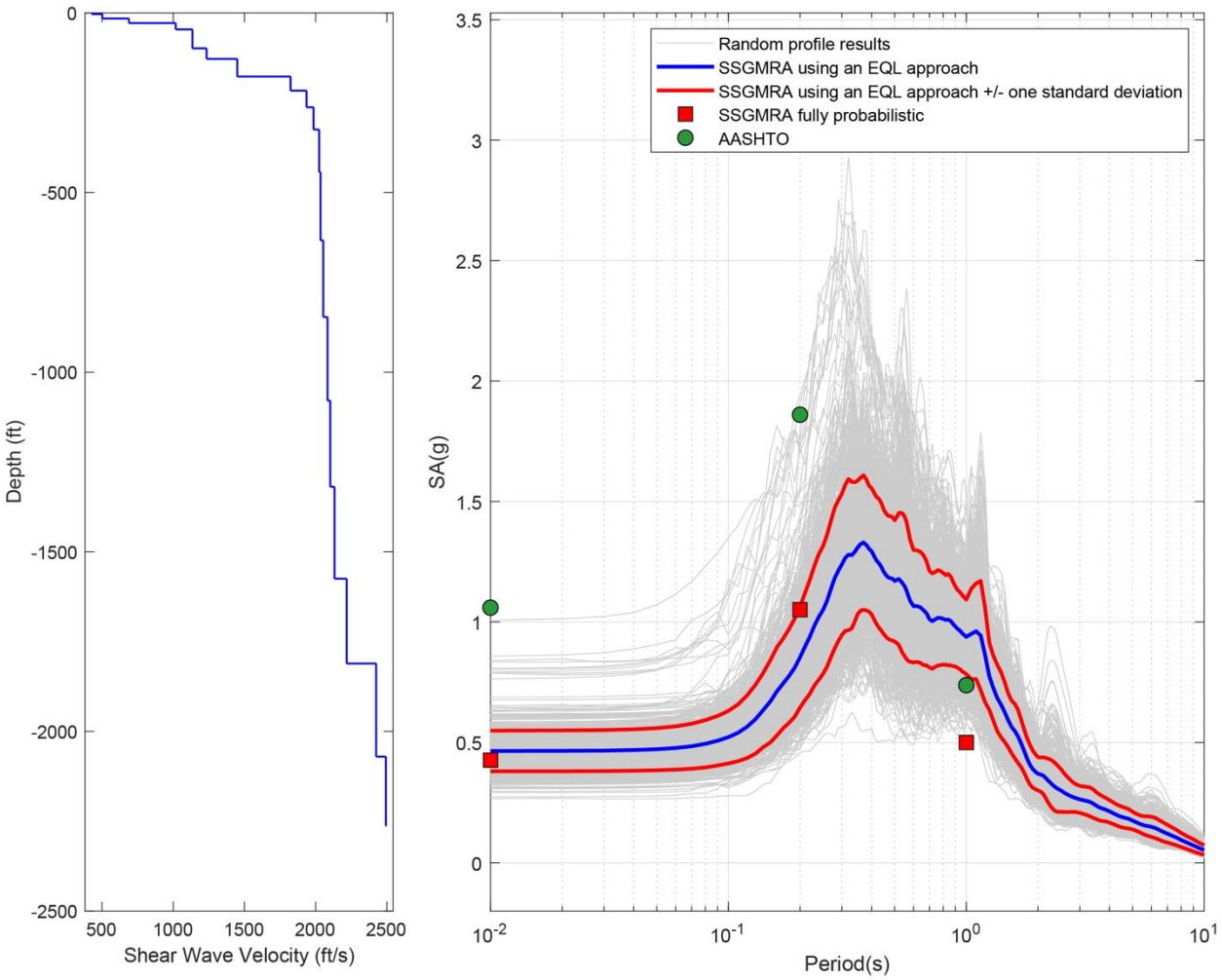


**Figure B-91. Left Panel: Shear-Wave Velocity Profile for Site 23 (Based on Peninsular Soil Model); and Right Panel: Results of SSGMRA Using a Fully Probabilistic Approach, SSGMRA Using an Equivalent Linear Approach, SSGMRA Using an Equivalent Linear Approach Plus and Minus One Standard Deviation, and AASHTO General Approach**

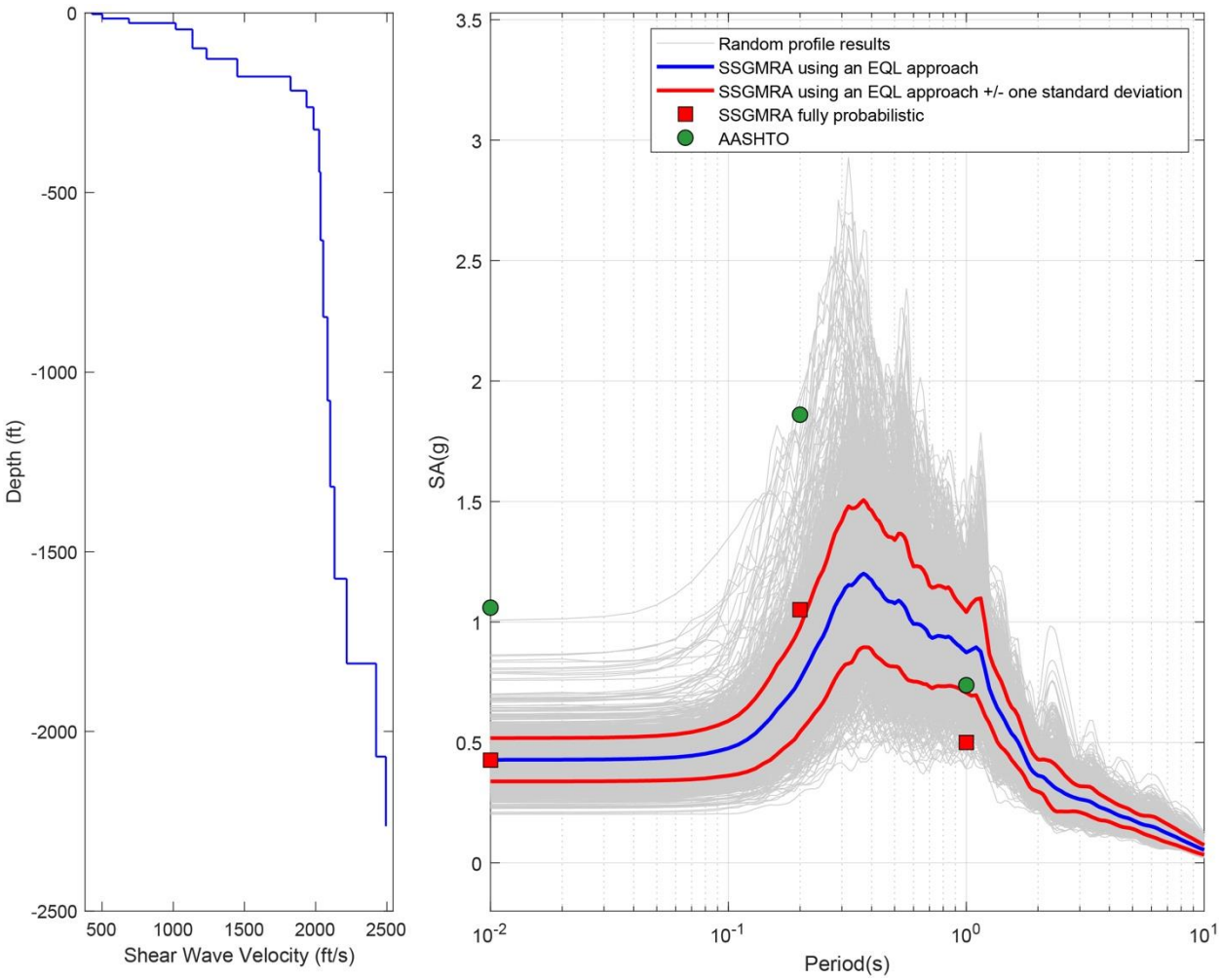


**Figure B-92. Left Panel: Shear-Wave Velocity Profile for Site 23 (Combined); and Right Panel: Results of SSGMRA Using a Fully Probabilistic Approach, SSGMRA Using an Equivalent Linear Approach, SSGMRA Using an Equivalent Linear Approach Plus and Minus One Standard Deviation, and AASHTO General Approach**

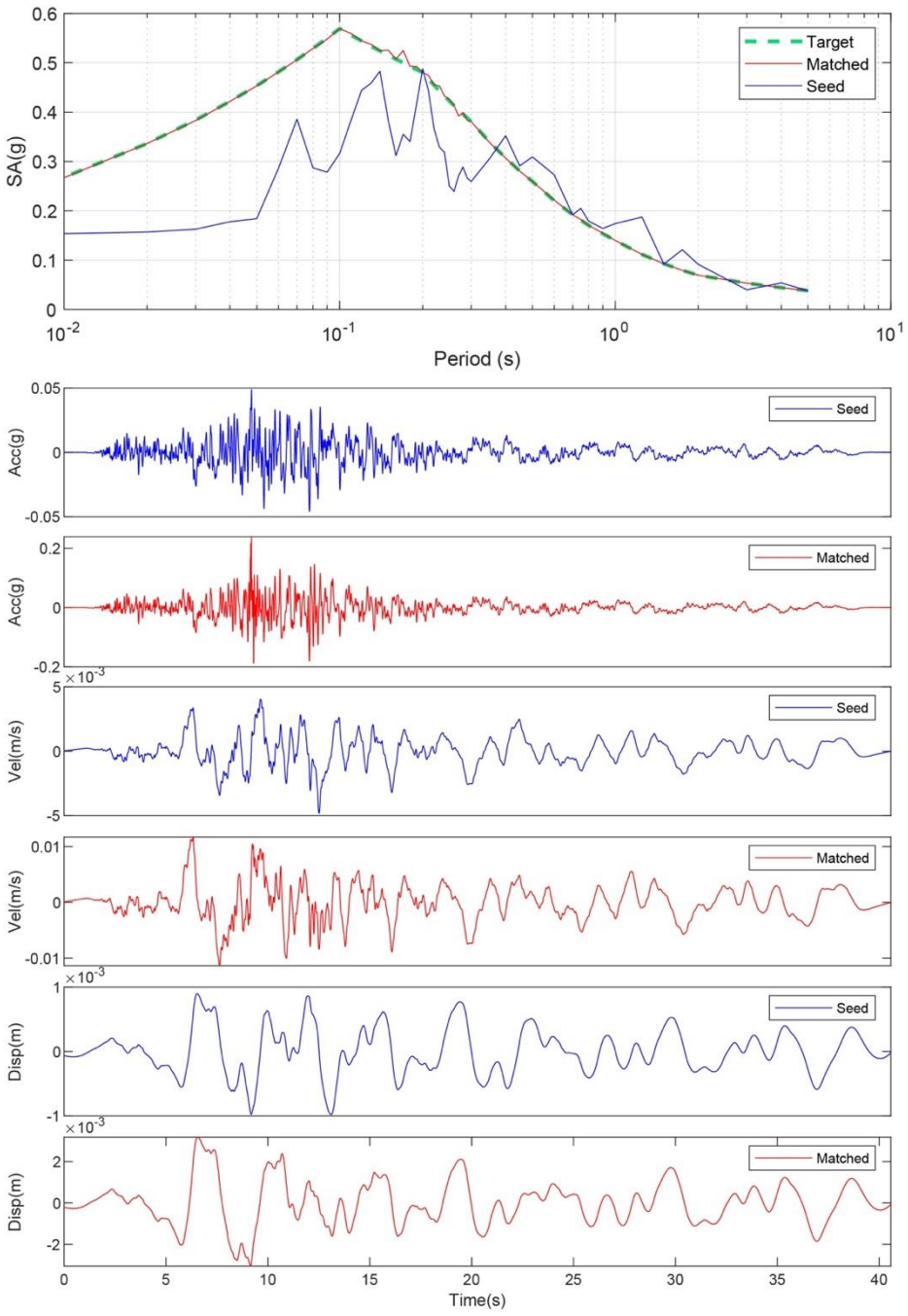


**Figure B-93. Matching Spectrum of Seed Motion (RSN774-LOMAP-HYN064) to the Target Spectrum (UHS) at Site 24. The Middle Subplot Shows the Seed Motion, and the Bottom Subplot Indicates the Matched Motion**

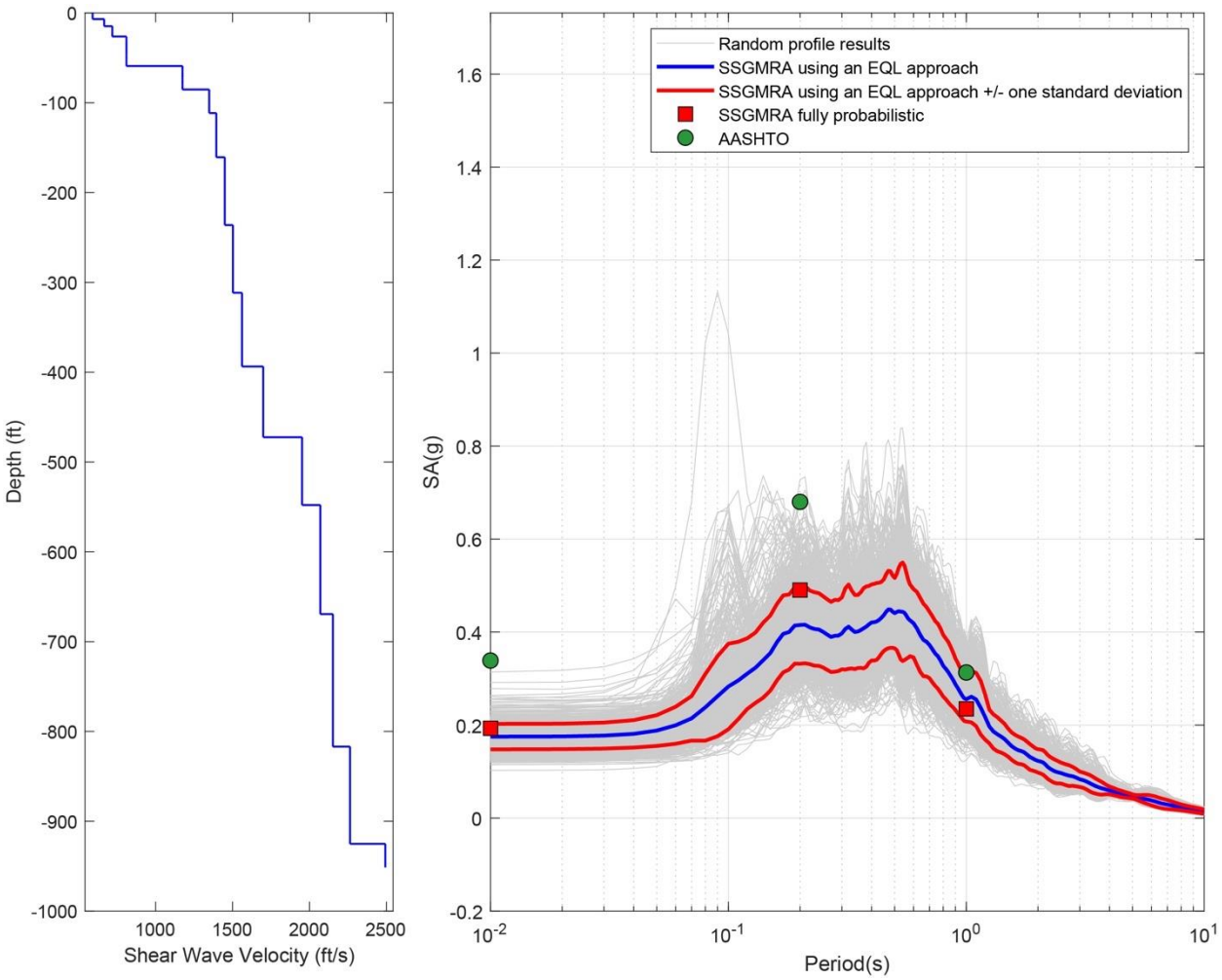


**Figure B-94. Left Panel: Shear-Wave Velocity Profile for Site 24 (Based on EPRI Soil Model); and Right Panel: Results of SSGMRA Using a Fully Probabilistic Approach, SSGMRA Using an Equivalent Linear Approach, SSGMRA Using an Equivalent Linear Approach Plus and Minus One Standard Deviation, and AASHTO General Approach**

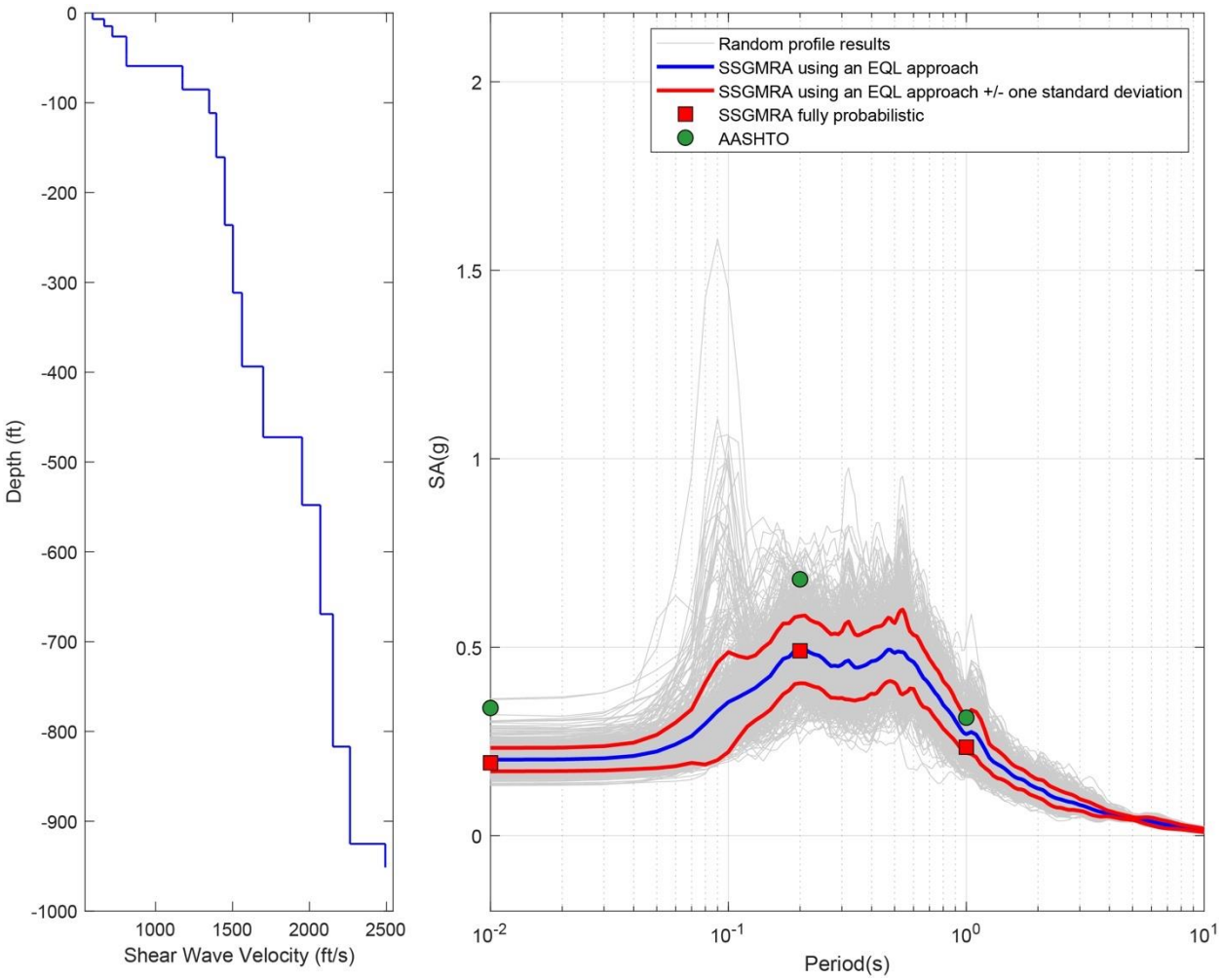


**Figure B-95. Left Panel: Shear-Wave Velocity Profile for Site 24 (Based on Peninsular Soil Model); and Right Panel: Results of SSGMRA Using a Fully Probabilistic Approach, SSGMRA Using an Equivalent Linear Approach, SSGMRA Using an Equivalent Linear Approach Plus and Minus One Standard Deviation, and AASHTO General Approach**

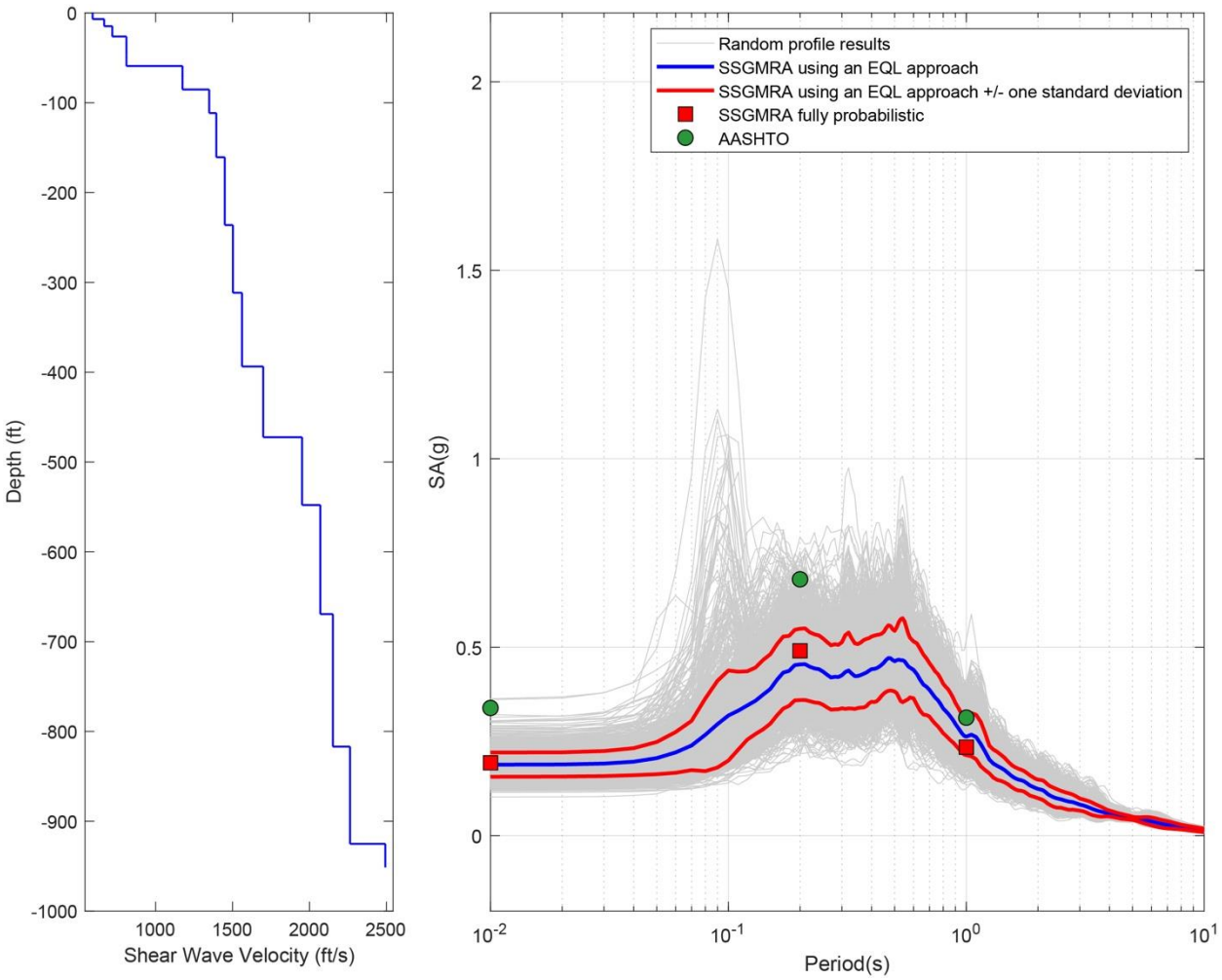


**Figure B-96. Left Panel: Shear-Wave Velocity Profile for Site 24 (Combined); and Right Panel: Results of SSGMRA Using a Fully Probabilistic Approach, SSGMRA Using an Equivalent Linear Approach, SSGMRA Using an Equivalent Linear Approach Plus and Minus One Standard Deviation, and AASHTO General Approach**

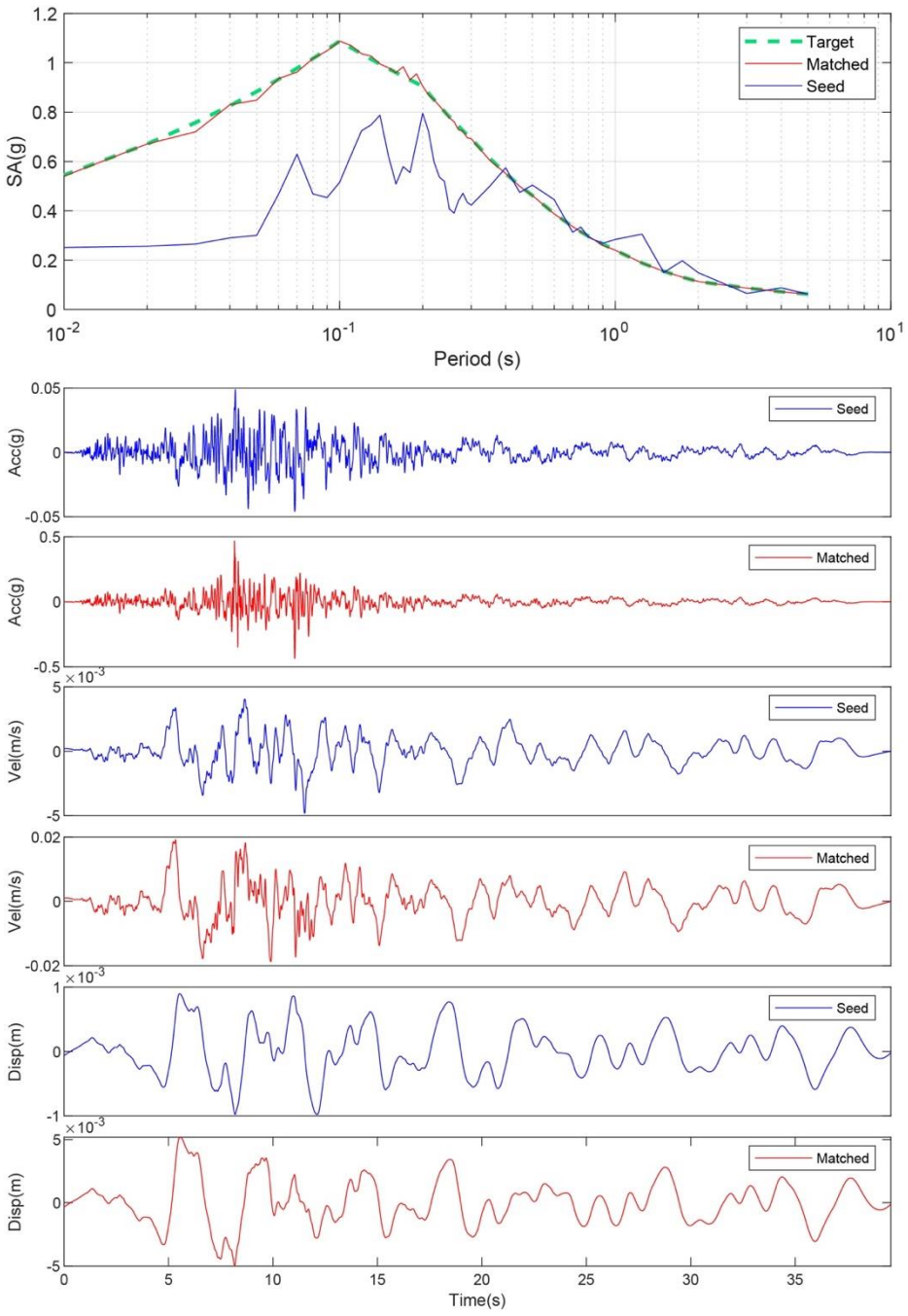


**Figure B-97. Matching Spectrum of Seed Motion (RSN774-LOMAP-HYN064) to the Target Spectrum (UHS) at Site 25. The Middle Subplot Shows the Seed Motion, and the Bottom Subplot Indicates the Matched Motion**

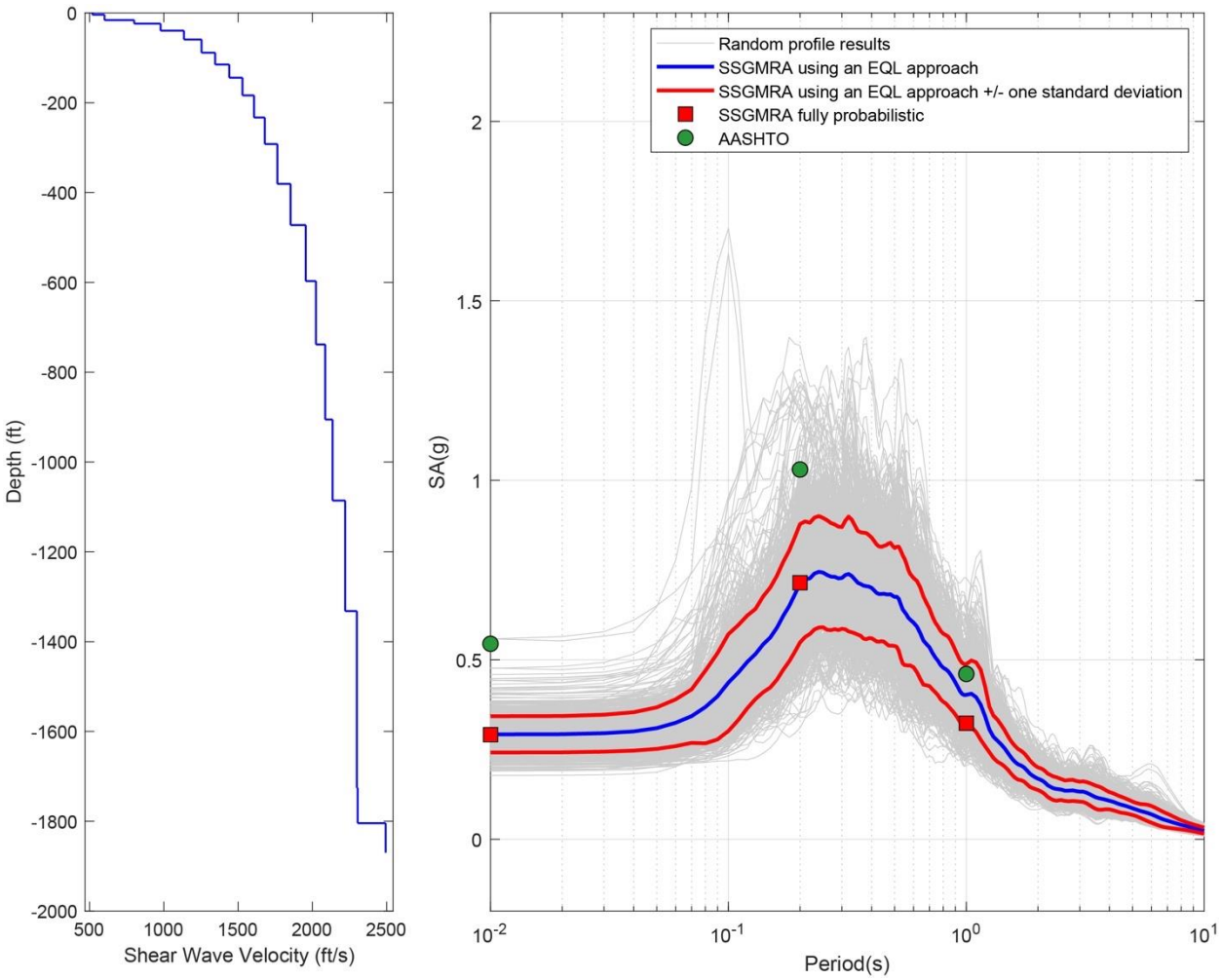


**Figure B-98. Left Panel: Shear-Wave Velocity Profile for Site 25 (Based on EPRI Soil Model); and Right Panel: Results of SSGMRA Using a Fully Probabilistic Approach, SSGMRA Using an Equivalent Linear Approach, SSGMRA Using an Equivalent Linear Approach Plus and Minus One Standard Deviation, and AASHTO General Approach**

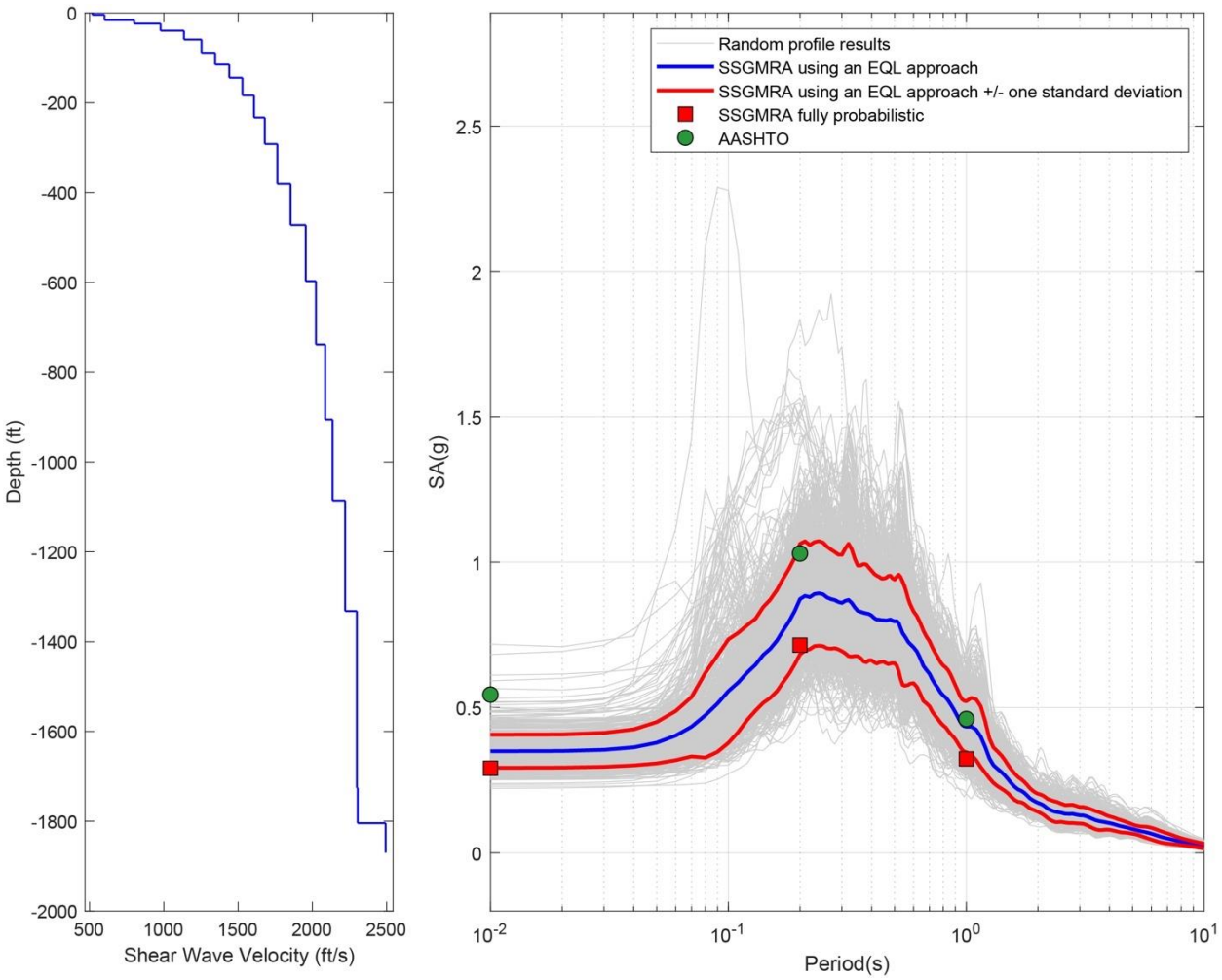


**Figure B-99. Left Panel: Shear-Wave Velocity Profile for Site 25 (Based on Peninsular Soil Model); and Right Panel: Results of SSGMRA Using a Fully Probabilistic Approach, SSGMRA Using an Equivalent Linear Approach, SSGMRA Using an Equivalent Linear Approach Plus and Minus One Standard Deviation, and AASHTO General Approach**

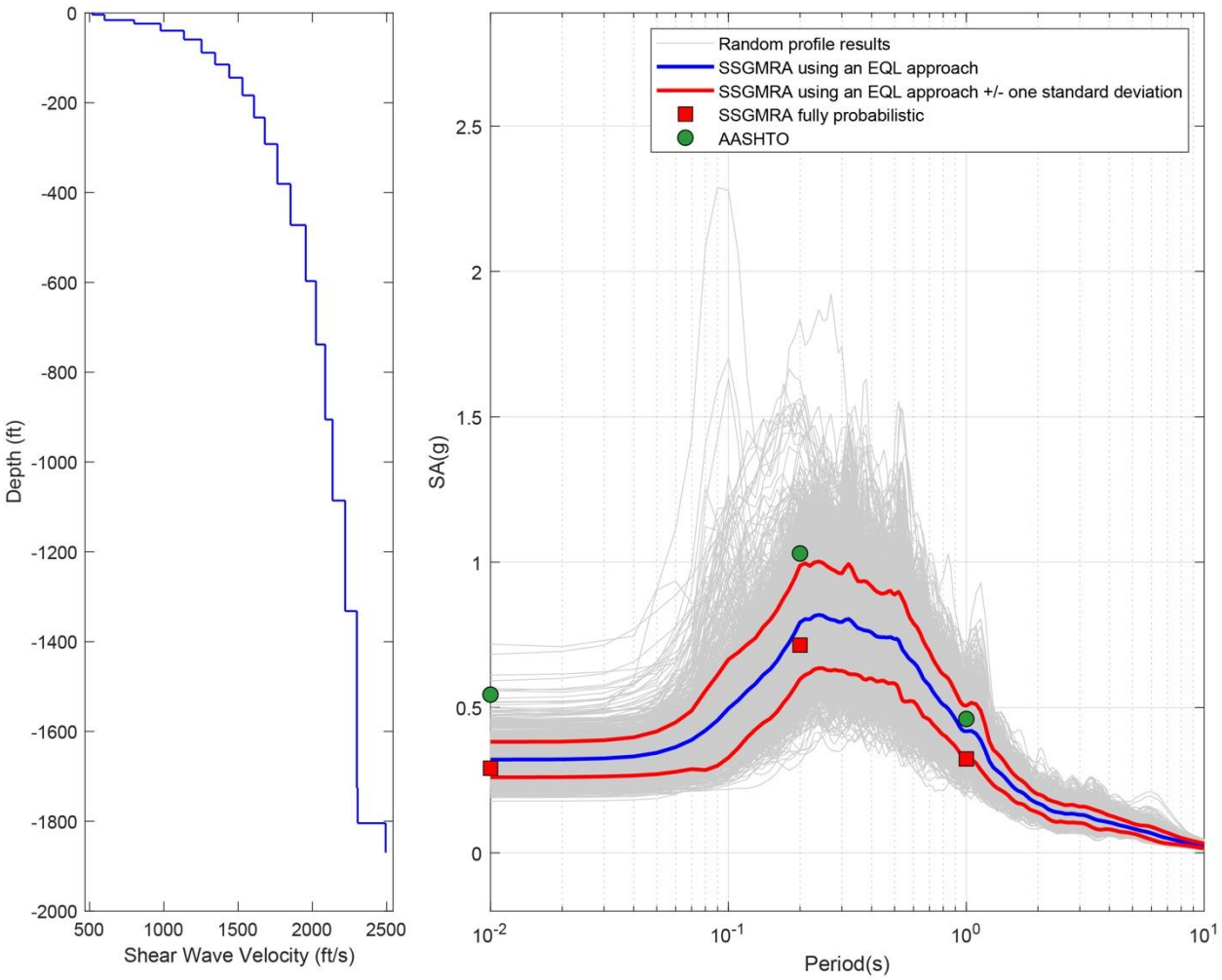


**Figure B-100. Left Panel: Shear-Wave Velocity Profile for Site 25 (Combined); and Right Panel: Results of SSGMRA Using a Fully Probabilistic Approach, SSGMRA Using an Equivalent Linear Approach, SSGMRA Using an Equivalent Linear Approach Plus and Minus One Standard Deviation, and AASHTO General Approach**

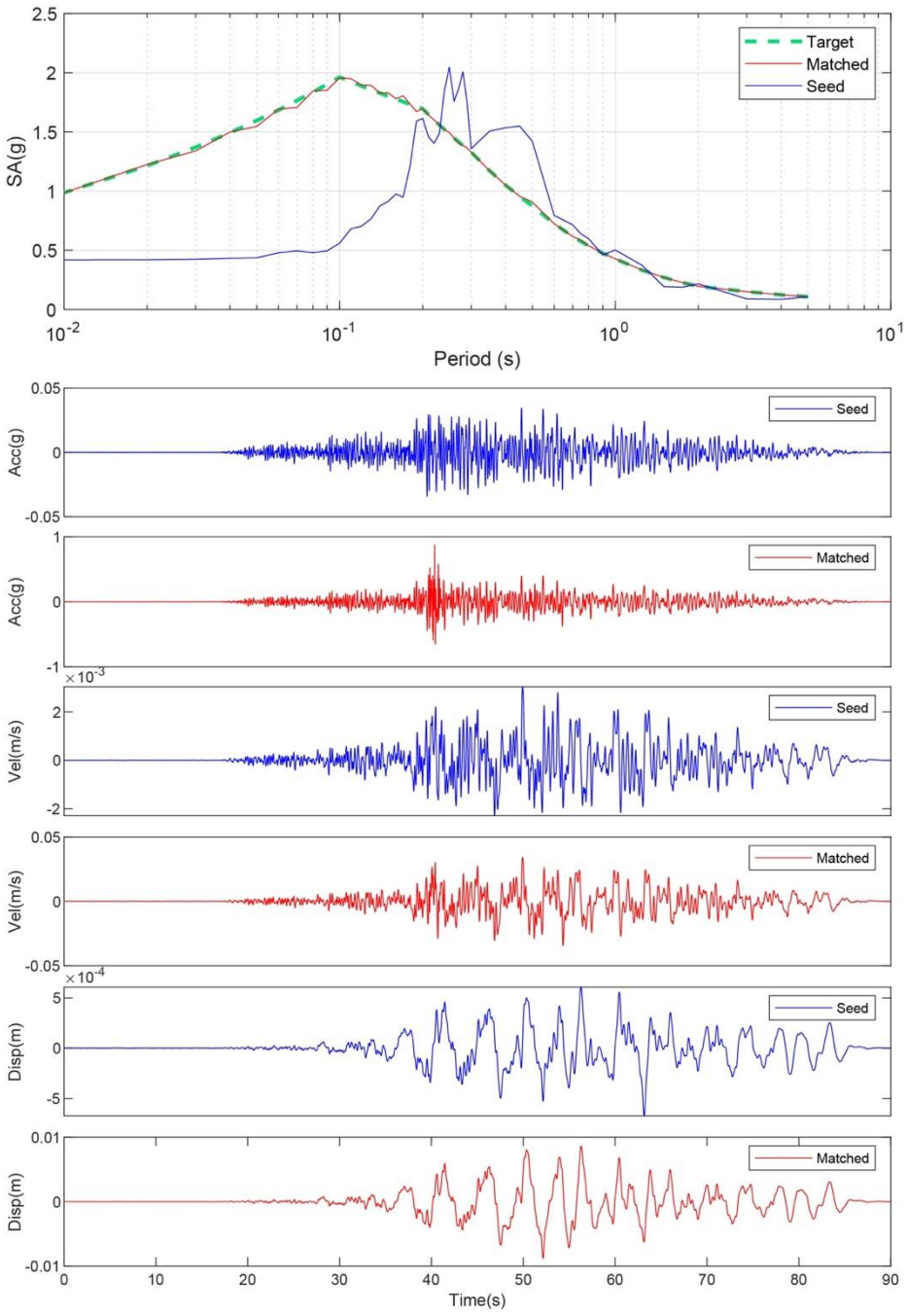


**Figure B-101. Matching Spectrum of Seed Motion (RSN1577-CHICHI-TTN025-E) to the Target Spectrum (UHS) at Site 26. The Middle Subplot Shows the Seed Motion, and the Bottom Subplot Indicates the Matched Motion**

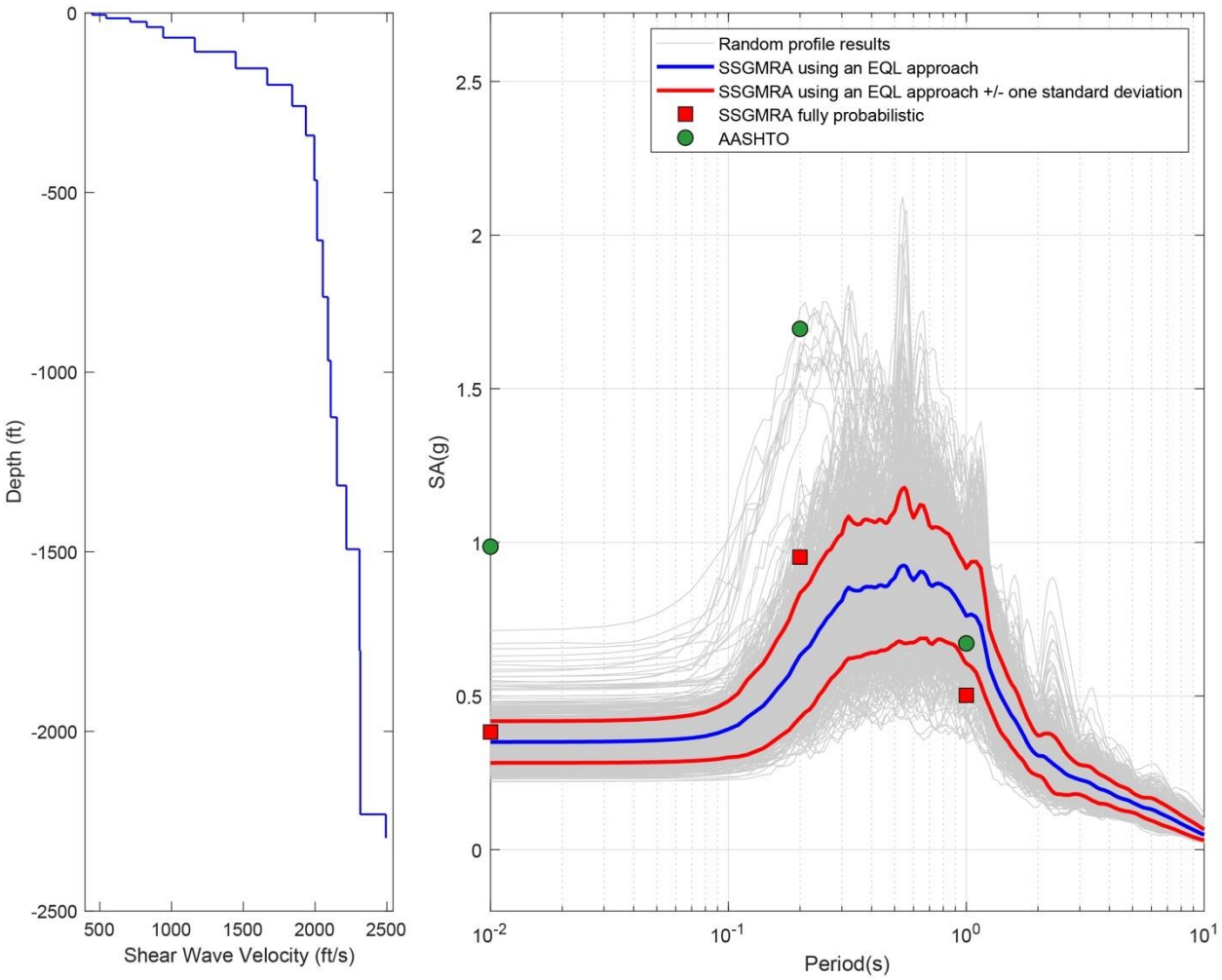


**Figure B-102. Left Panel: Shear-Wave Velocity Profile for Site 26 (Based on EPRI Soil Model); and Right Panel: Results of SSGMRA Using a Fully Probabilistic Approach, SSGMRA Using an Equivalent Linear Approach, SSGMRA Using an Equivalent Linear Approach Plus and Minus One Standard Deviation, and AASHTO General Approach**

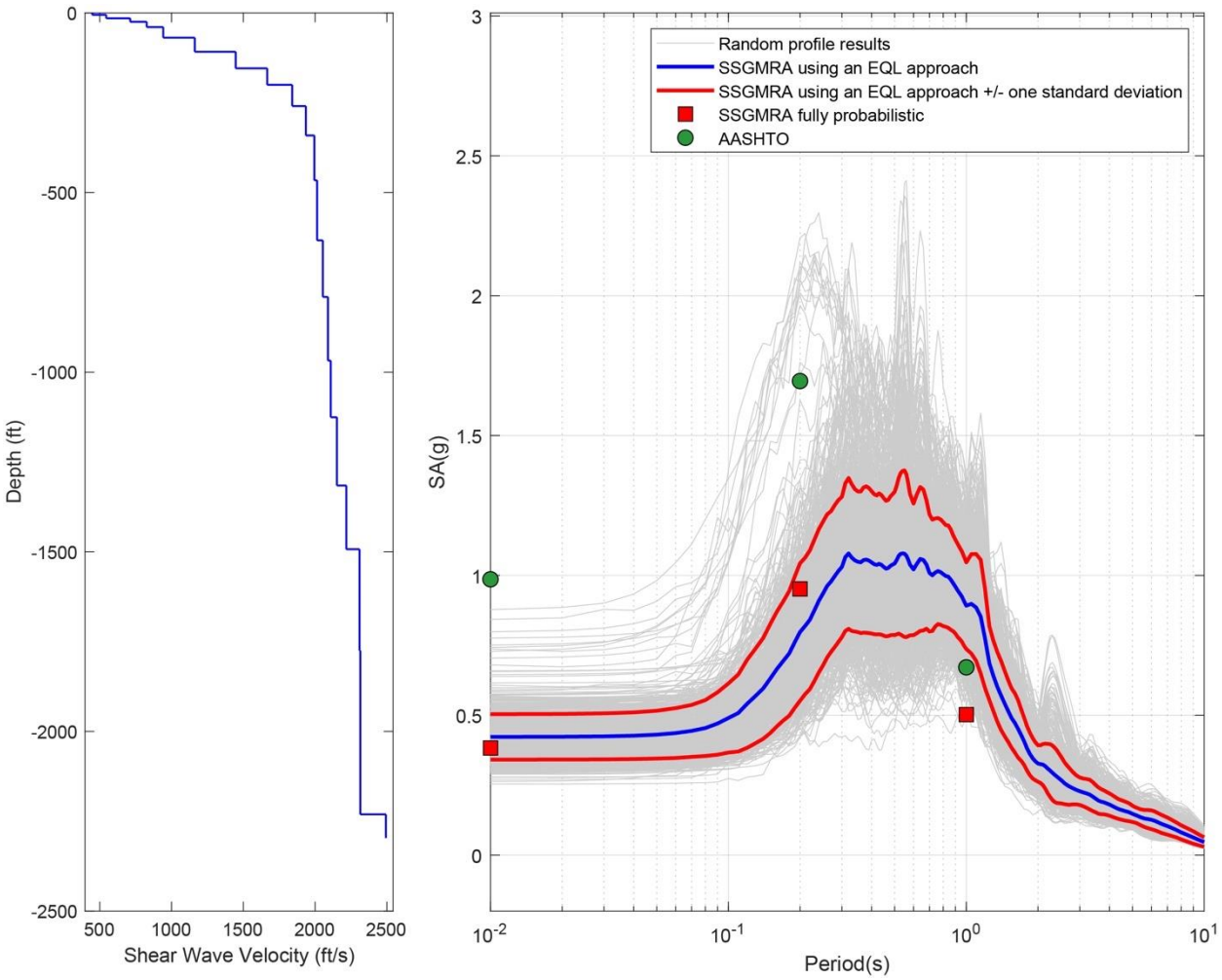


**Figure B-103. Left Panel: Shear-Wave Velocity Profile for Site 26 (Based on Peninsular Soil Model); and Right Panel: Results of SSGMRA Using a Fully Probabilistic Approach, SSGMRA Using an Equivalent Linear Approach, SSGMRA Using an Equivalent Linear Approach Plus and Minus One Standard Deviation, and AASHTO General Approach**

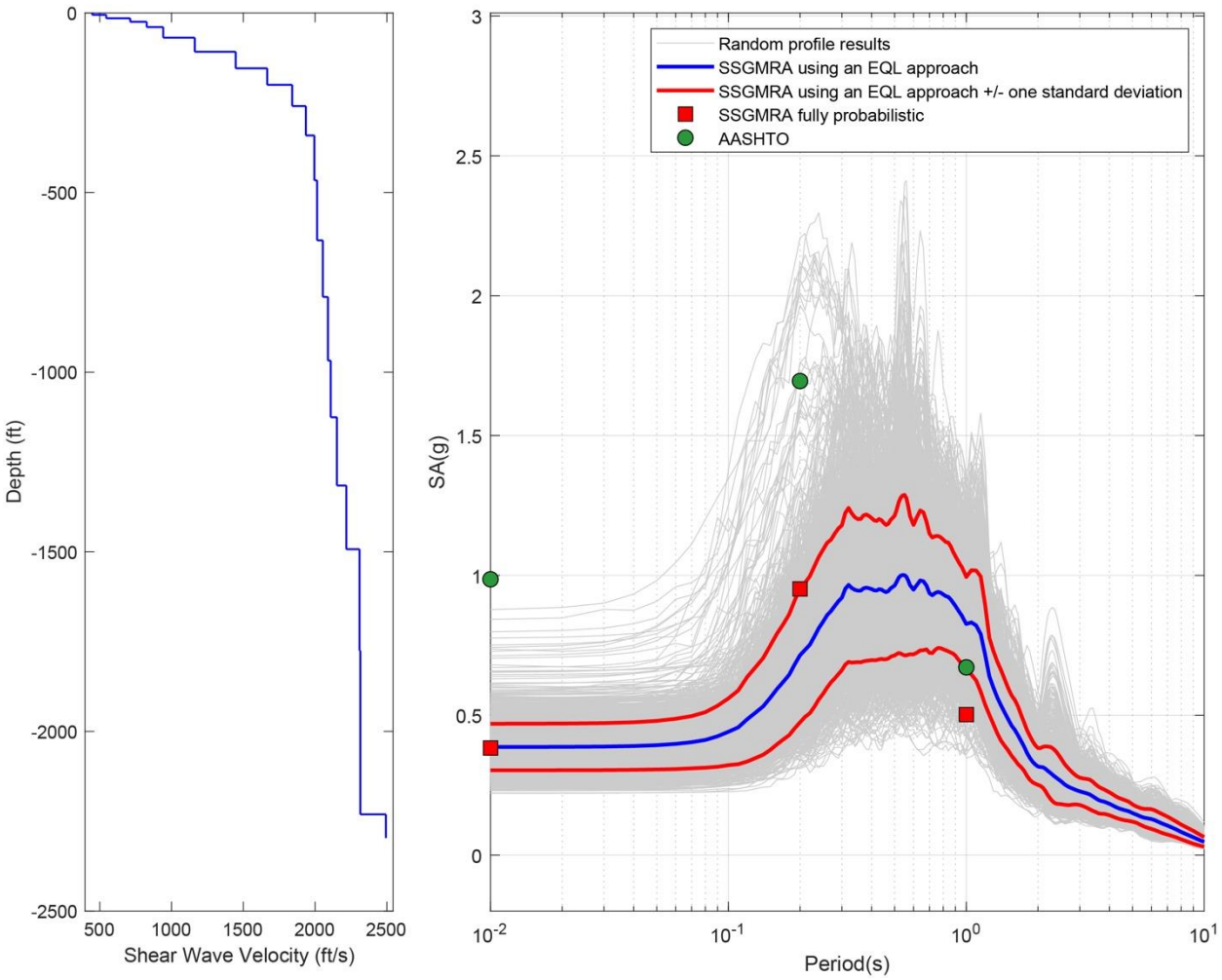


**Figure B-104. Left Panel: Shear-Wave Velocity Profile for Site 26 (Combined); and Right Panel: Results of SSGMRA Using a Fully Probabilistic Approach, SSGMRA Using an Equivalent Linear Approach, SSGMRA Using an Equivalent Linear Approach Plus and Minus One Standard Deviation, and AASHTO General Approach**

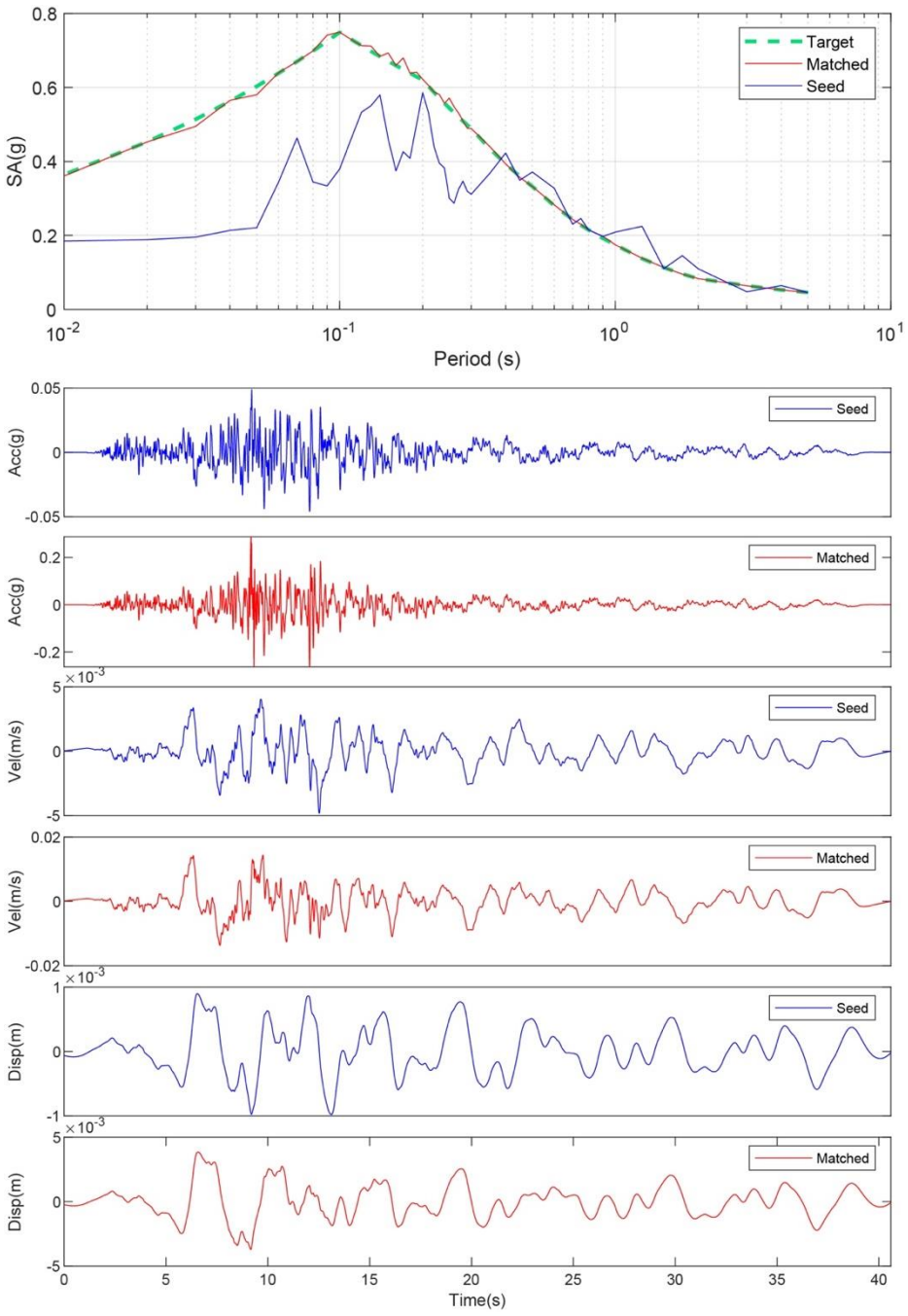


**Figure B-105. Matching Spectrum of Seed Motion (RSN774-LOMAP-HYN064) to the Target Spectrum (UHS) at Site 27. The Middle Subplot Shows the Seed Motion, and the Bottom Subplot Indicates the Matched Motion**

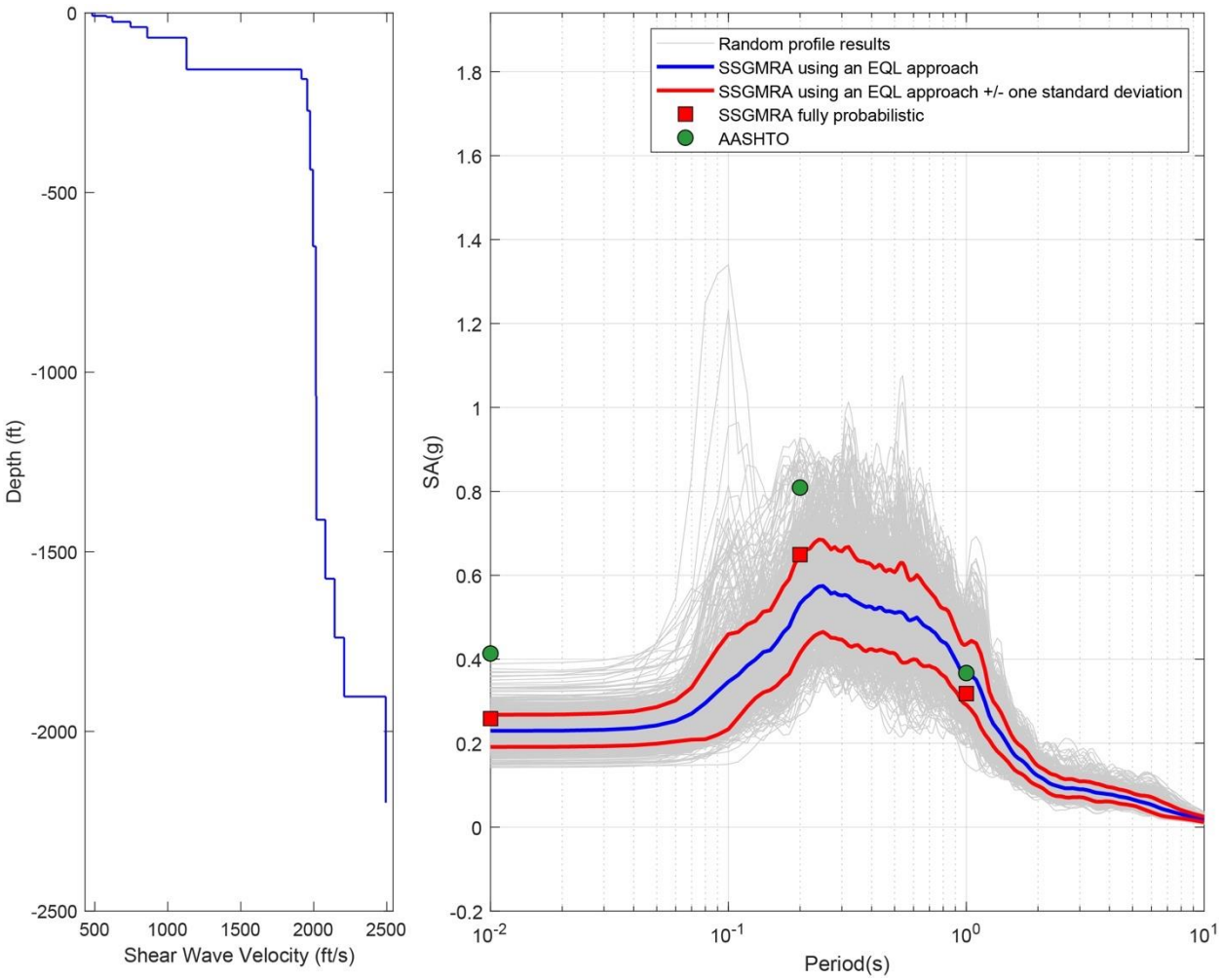


**Figure B-106. Left Panel: Shear-Wave Velocity Profile for Site 27 (Based on EPRI Soil Model); and Right Panel: Results of SSGMRA Using a Fully Probabilistic Approach, SSGMRA Using an Equivalent Linear Approach, SSGMRA Using an Equivalent Linear Approach Plus and Minus One Standard Deviation, and AASHTO General Approach**

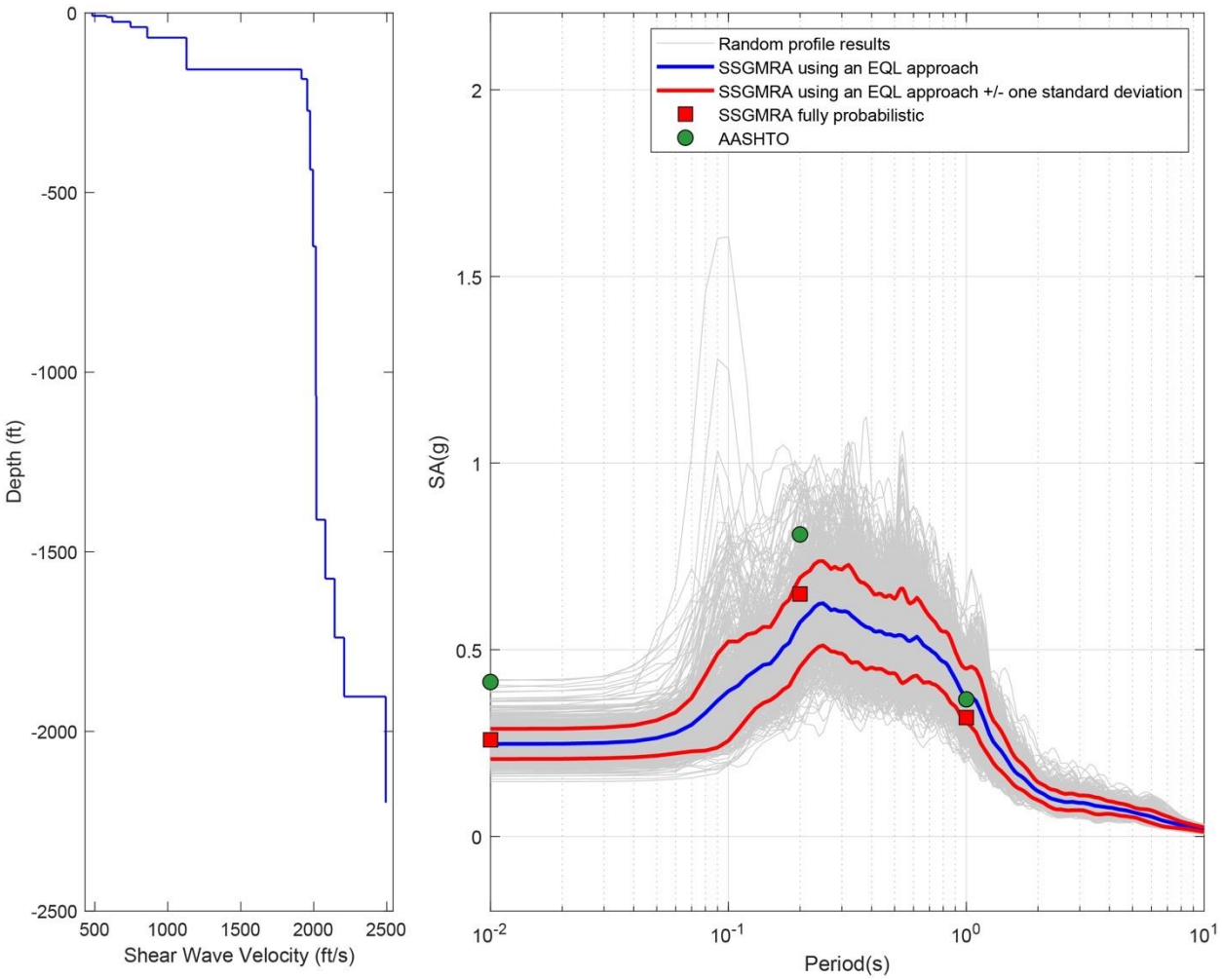


**Figure B-107. Left Panel: Shear-Wave Velocity Profile for Site 27 (Based on Peninsular Soil Model); and Right Panel: Results of SSGMRA Using a Fully Probabilistic Approach, SSGMRA Using an Equivalent Linear Approach, SSGMRA Using an Equivalent Linear Approach Plus and Minus One Standard Deviation, and AASHTO General Approach.**

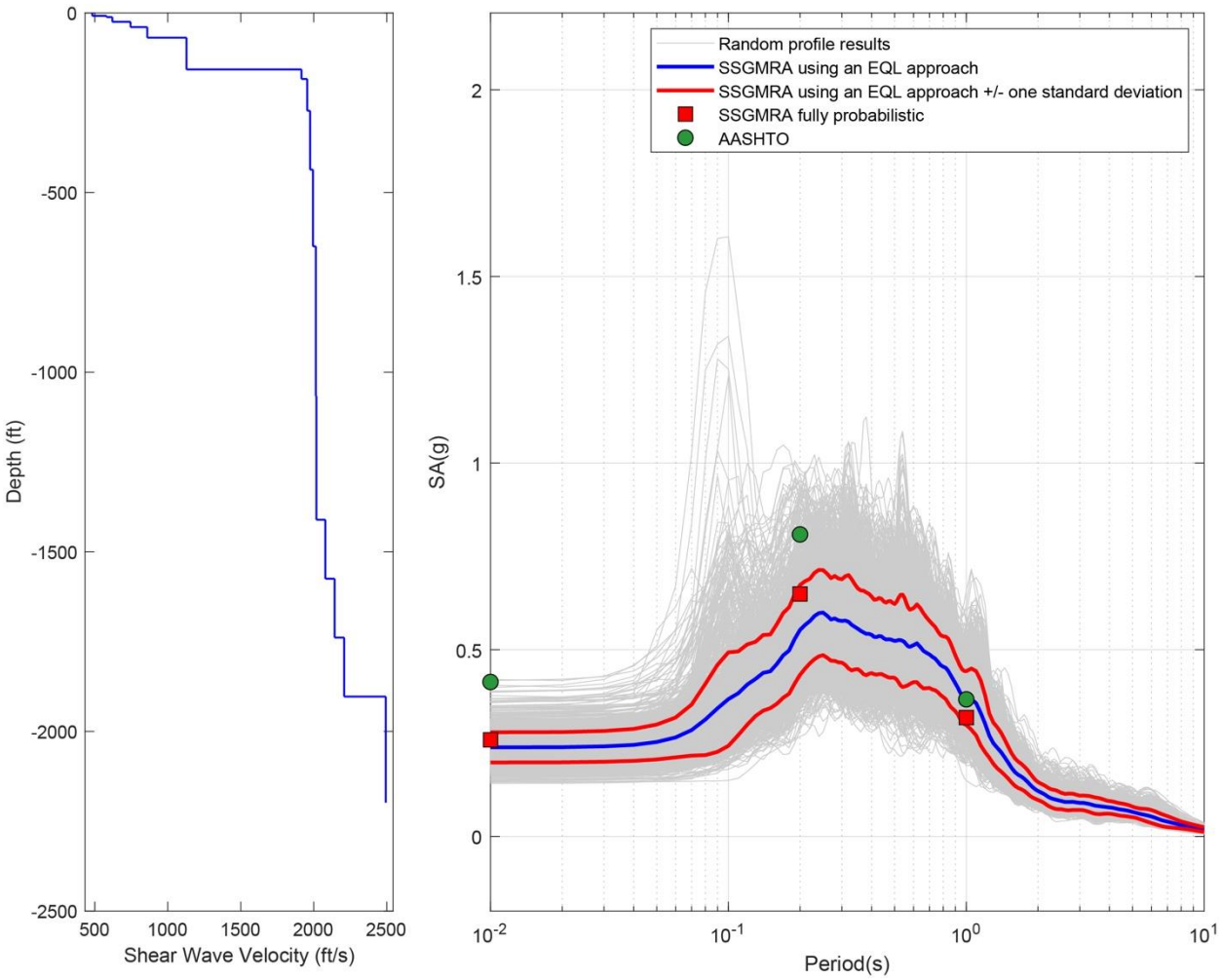


**Figure B-108. Left Panel: Shear-Wave Velocity Profile for Site 27 (Combined); and Right Panel: Results of SSGMRA Using a Fully Probabilistic Approach, SSGMRA Using an Equivalent Linear Approach, SSGMRA Using an Equivalent Linear Approach Plus and Minus One Standard Deviation, and AASHTO General Approach**

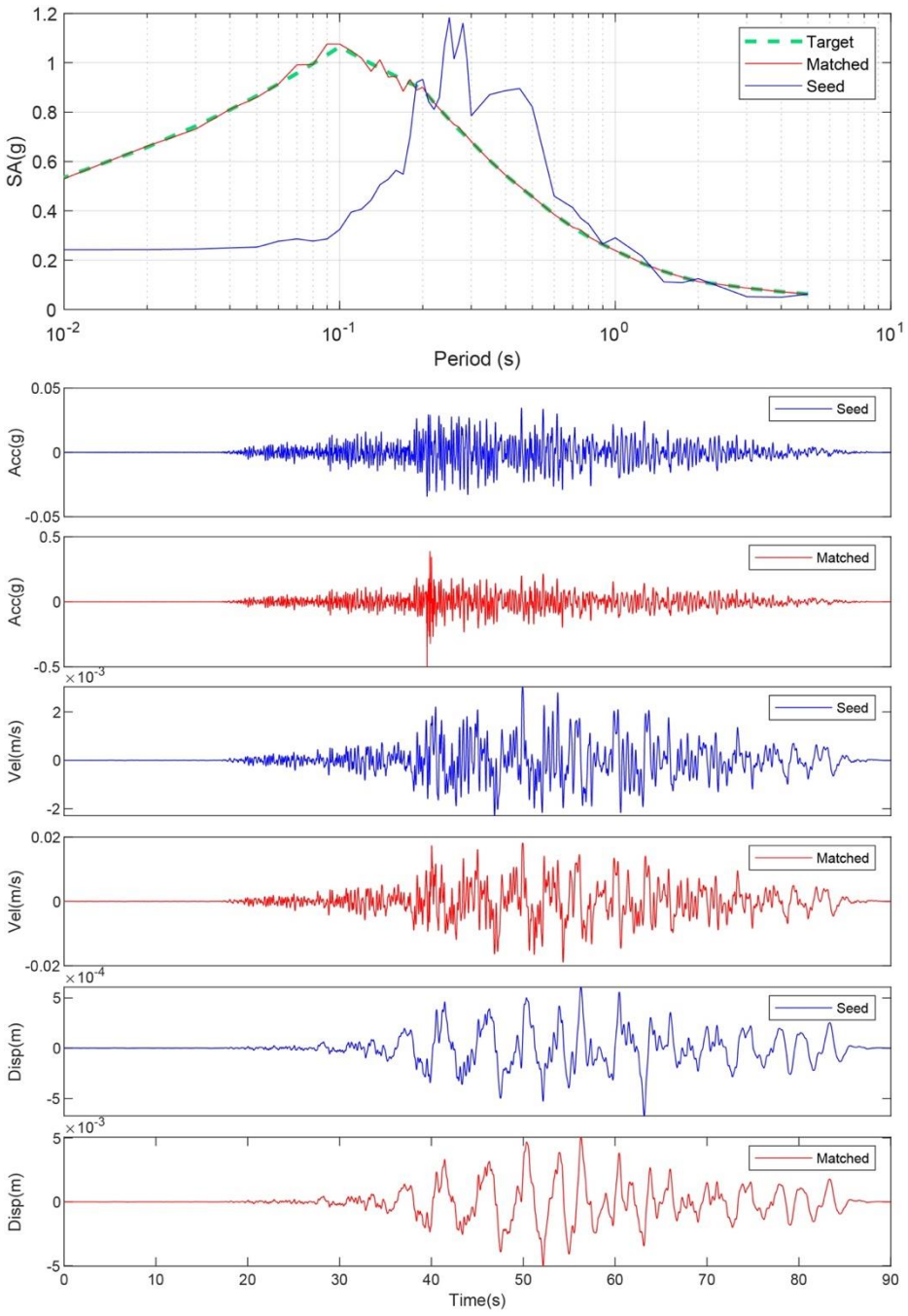


**Figure B-109. Matching Spectrum 0f Seed Motion (RSN1577-CHICHI-TTN025-E) to the Target Spectrum (UHS) at Site 28. The Middle Subplot Shows the Seed Motion, and the Bottom Subplot Indicates the Matched Motion**

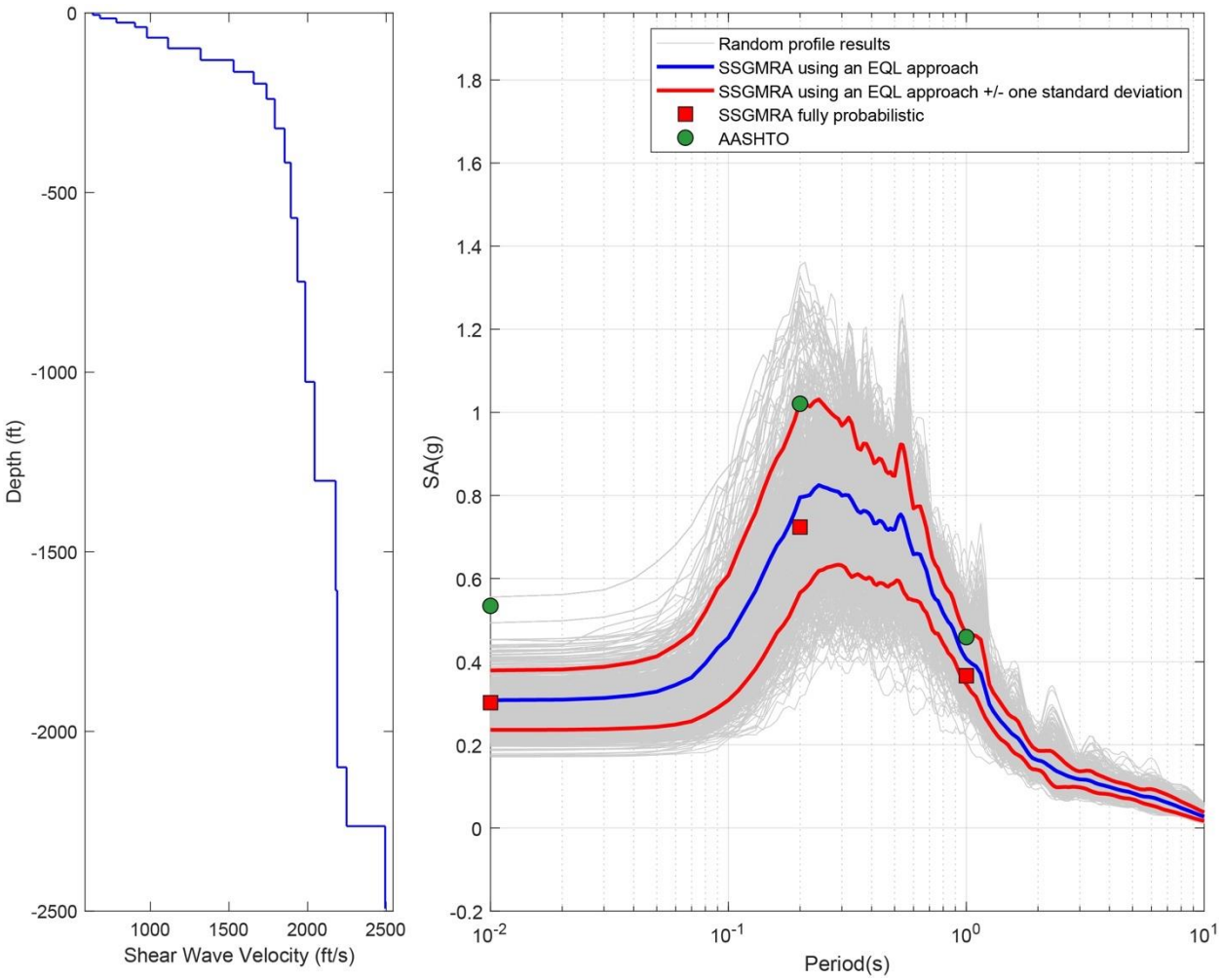


**Figure B-110. Left Panel: Shear-Wave Velocity Profile for Site 28 (Based on EPRI Soil Model); and Right Panel: Results of SSGMRA Using a Fully Probabilistic Approach, SSGMRA Using an Equivalent Linear Approach, SSGMRA Using an Equivalent Linear Approach Plus and Minus One Standard Deviation, and AASHTO General Approach**

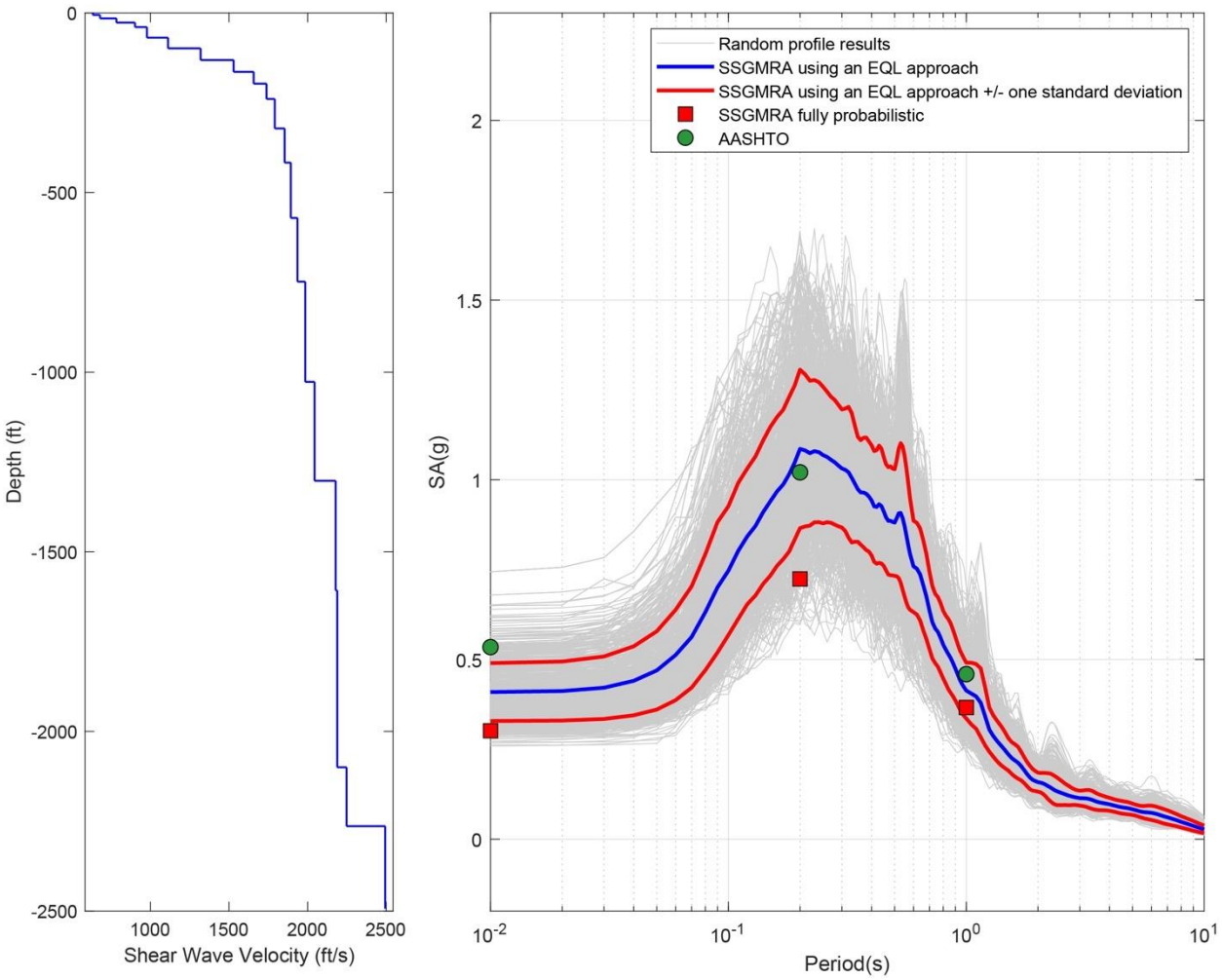


**Figure B-111. Left Panel: Shear-Wave Velocity Profile for Site 28 (Based on Peninsular Soil Model); and Right Panel: Results of SSGMRA Using a Fully Probabilistic Approach, SSGMRA Using an Equivalent Linear Approach, SSGMRA Using an Equivalent Linear Approach Plus and Minus One Standard Deviation, and AASHTO General Approach**

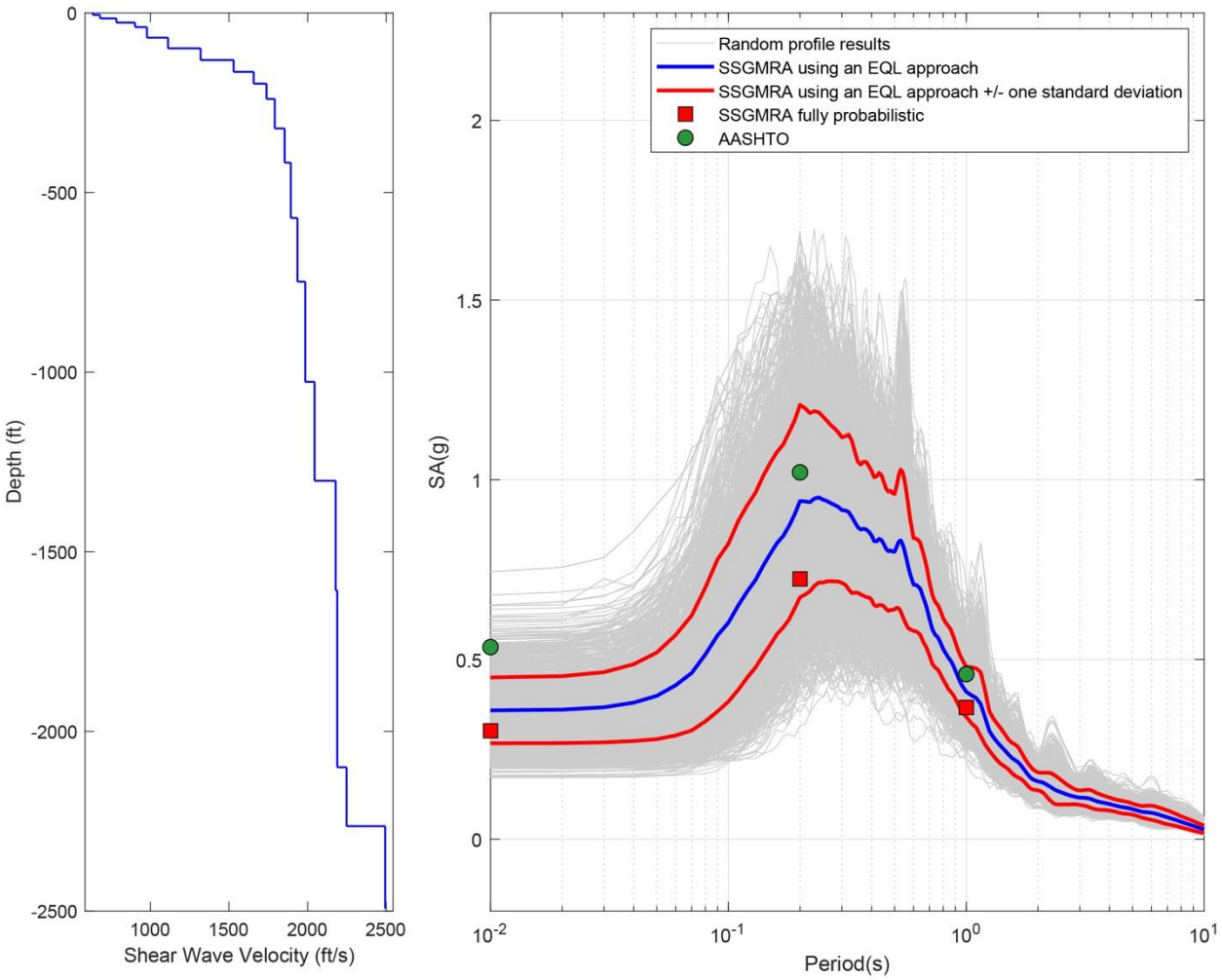


**Figure B-112. Left Panel: Shear-Wave Velocity Profile for Site 28 (Combined); and Right Panel: Results of SSGMRA Using a Fully Probabilistic Approach, SSGMRA Using an Equivalent Linear Approach, SSGMRA Using an Equivalent Linear Approach Plus and Minus One Standard Deviation, and AASHTO General Approach**

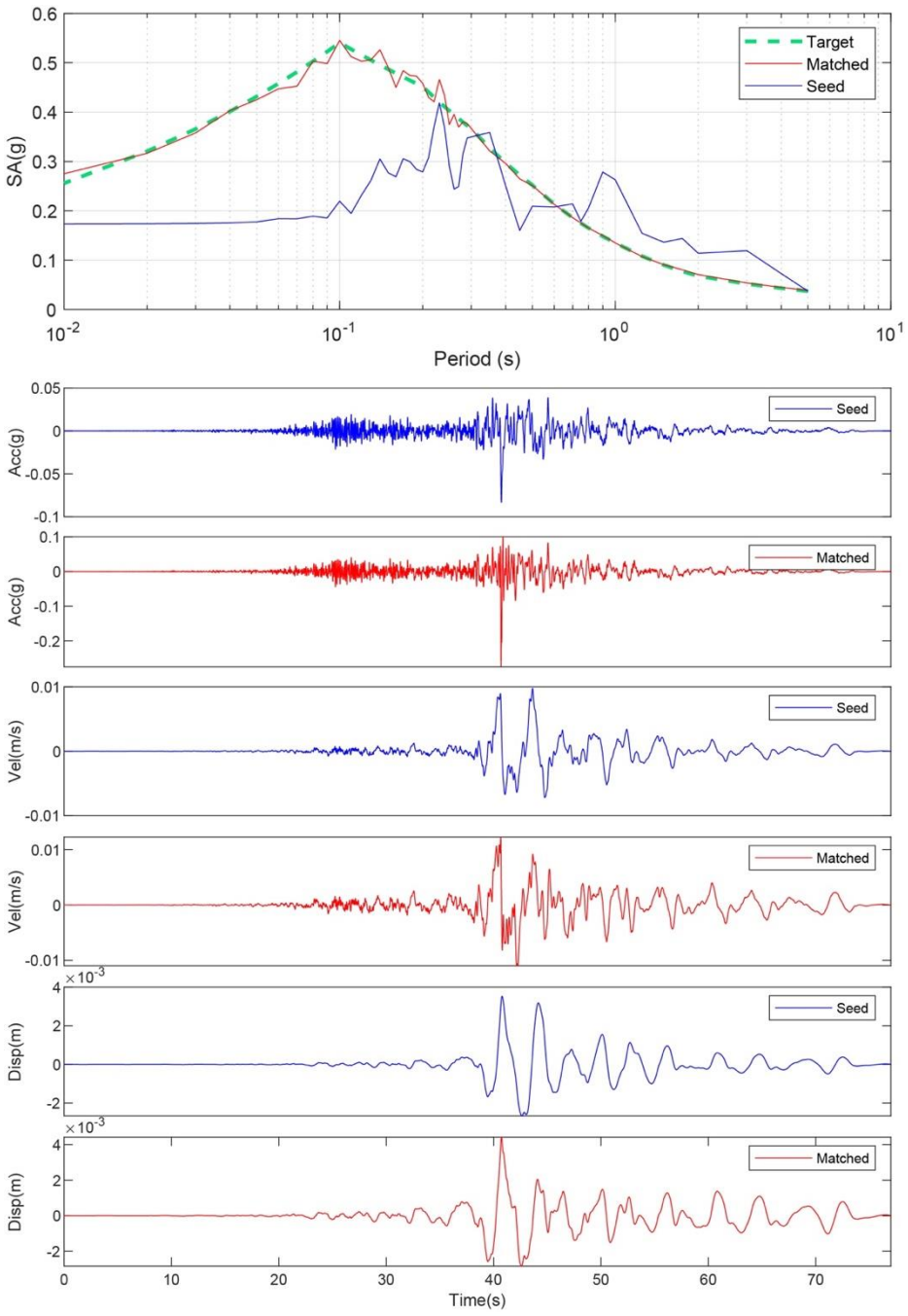


**Figure B-113. Matching Spectrum of Seed Motion (RSN1432-CHICHI-TAP046-E) to the Target Spectrum (UHS) at Site 29. The Middle Subplot Shows the Seed Motion, and the Bottom Subplot Indicates the Matched Motion**

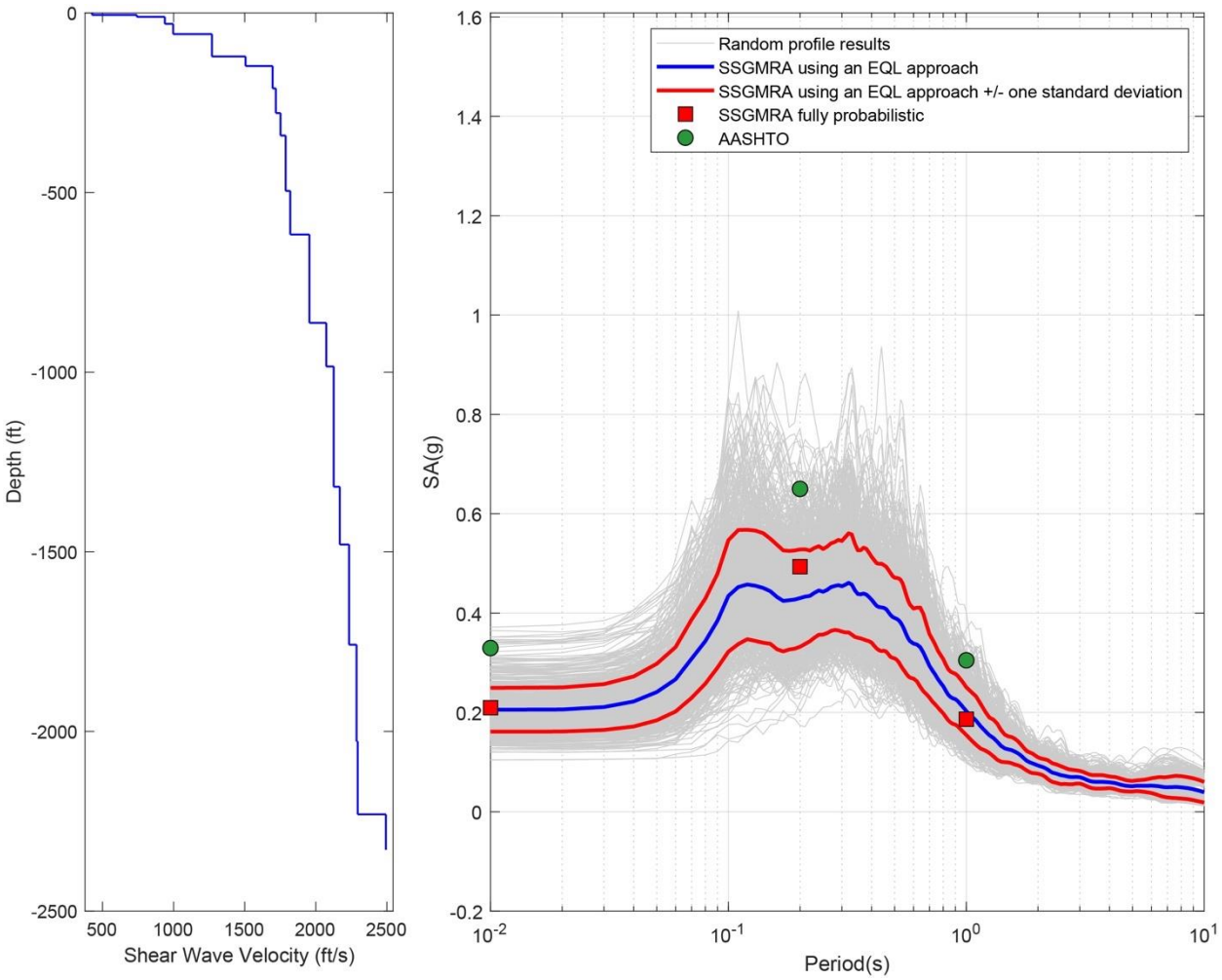


**Figure B-114. Left Panel: Shear-Wave Velocity Profile for Site 29 (Based on EPRI Soil Model); and Right Panel: Results of SSGMRA Using a Fully Probabilistic Approach, SSGMRA Using an Equivalent Linear Approach, SSGMRA Using an Equivalent Linear Approach Plus and Minus One Standard Deviation, and AASHTO general approach**

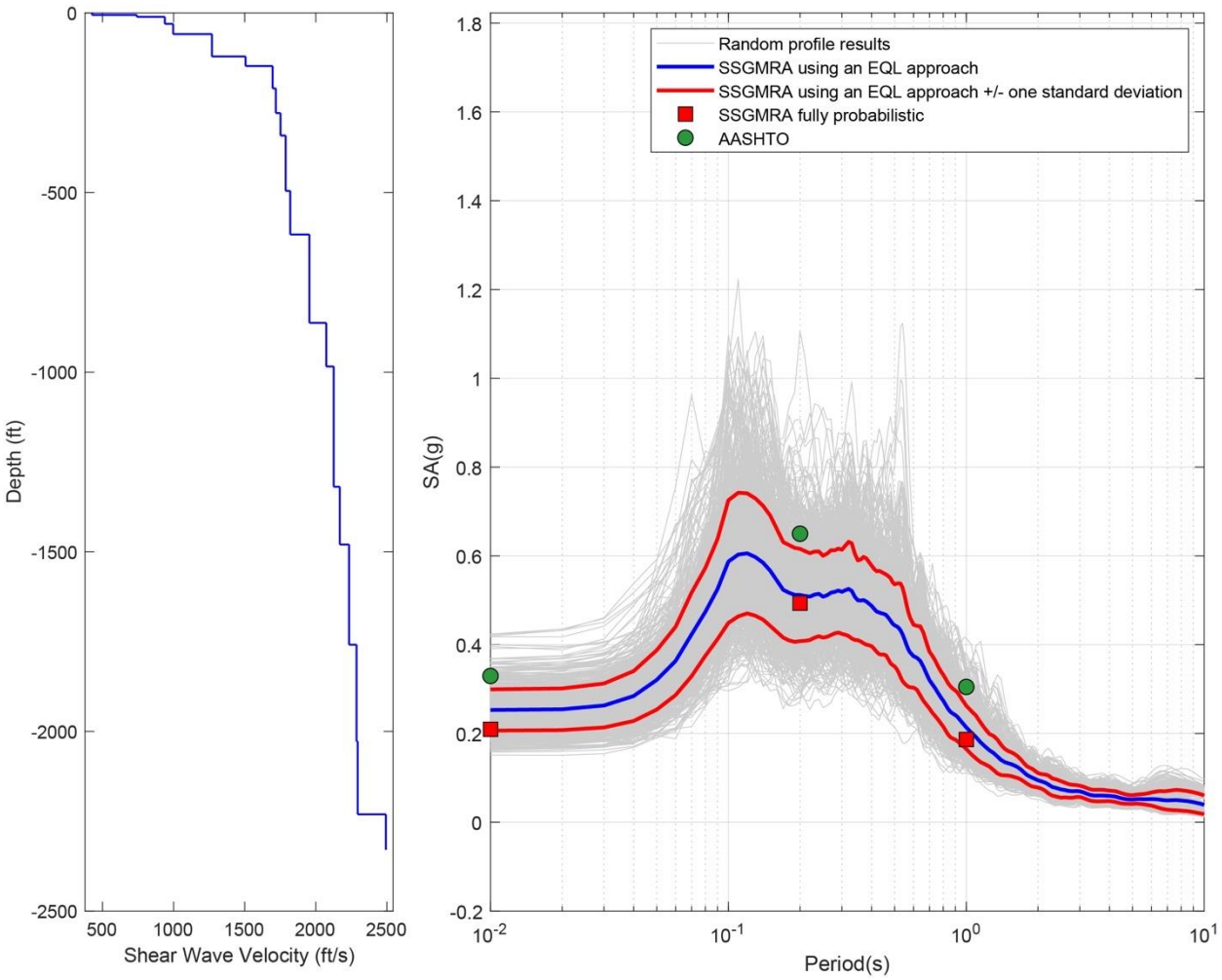


**Figure B-115. Left Panel: Shear-Wave Velocity Profile for Site 29 (Based on Peninsular Soil Model); and Right Panel: Results of SSGMRA Using a Fully Probabilistic Approach, SSGMRA Using an Equivalent Linear Approach, SSGMRA Using an Equivalent Linear Approach Plus and Minus One Standard Deviation, and AASHTO General Approach**

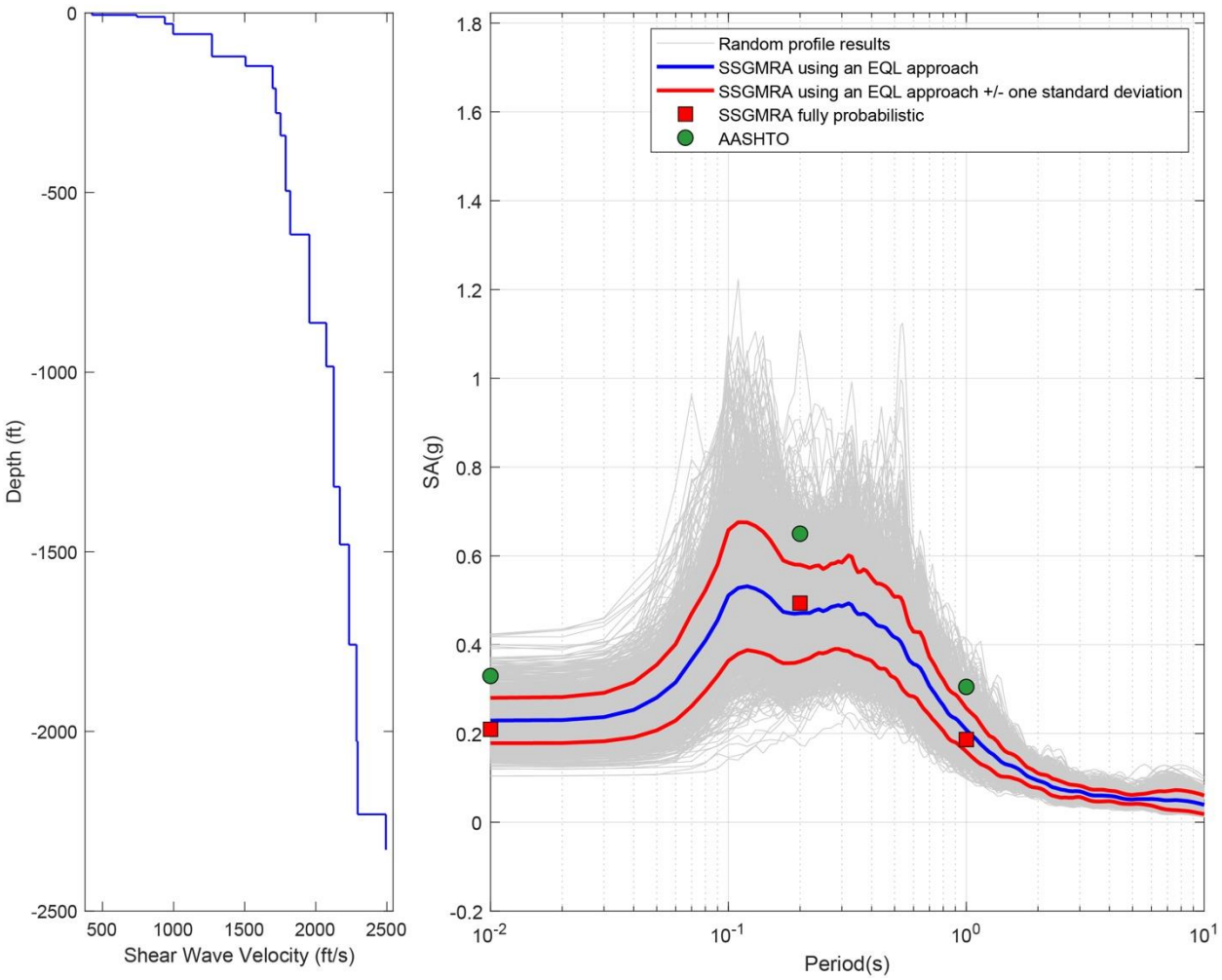


**Figure B-116. Left Panel: Shear-Wave Velocity Profile for Site 29 (Combined); and Right Panel: Results of SSGMRA Using a Fully Probabilistic Approach, SSGMRA Using an Equivalent Linear Approach, SSGMRA Using an Equivalent Linear Approach Plus and Minus One Standard Deviation, and AASHTO General Approach**

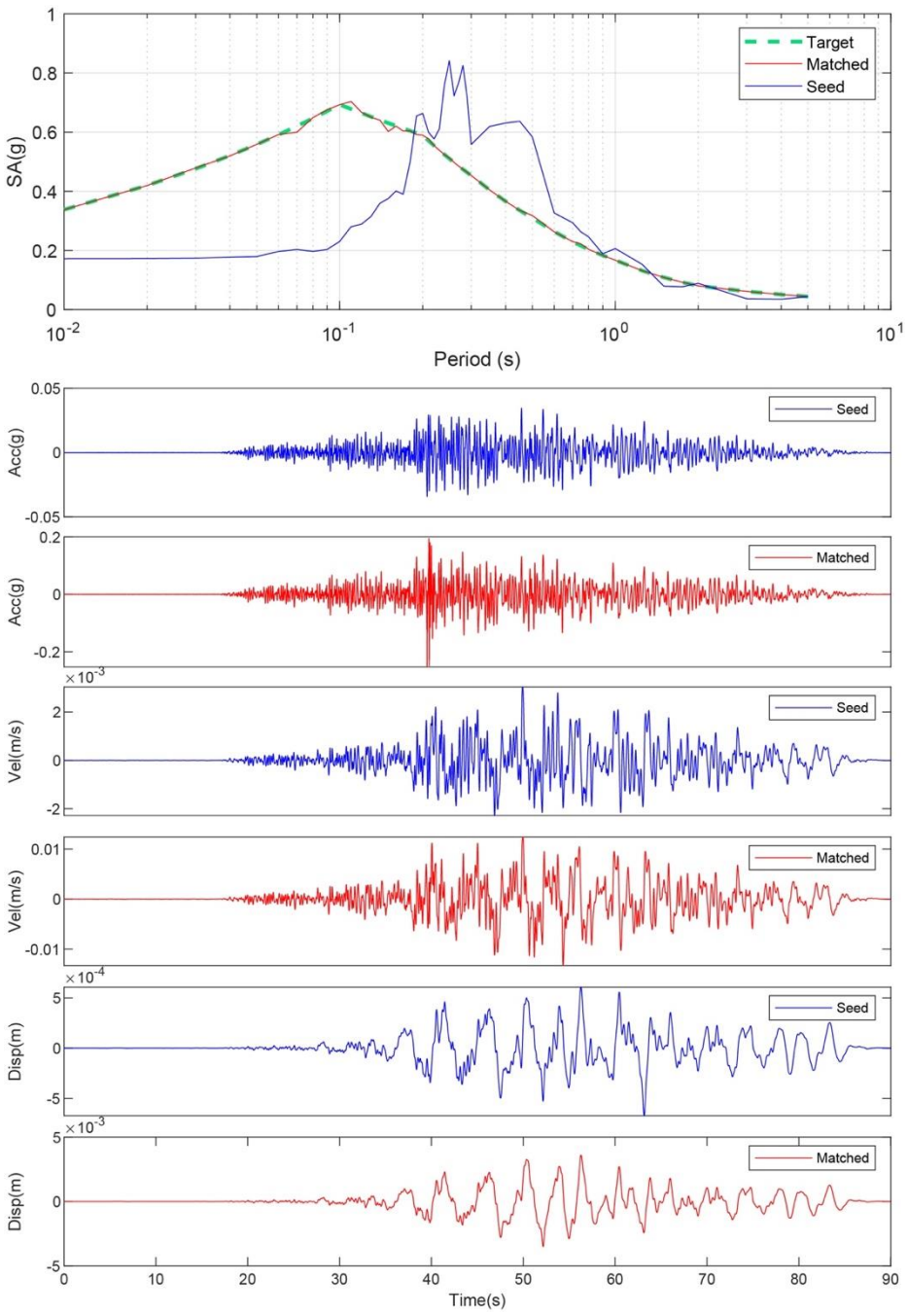


**Figure B-117. Matching Spectrum of Seed Motion (RSN1577-CHICHI-TTN025-E) to the Target Spectrum (UHS) at Site 30. The Middle Subplot Shows the Seed Motion, and the Bottom Subplot Indicates the Matched Motion**

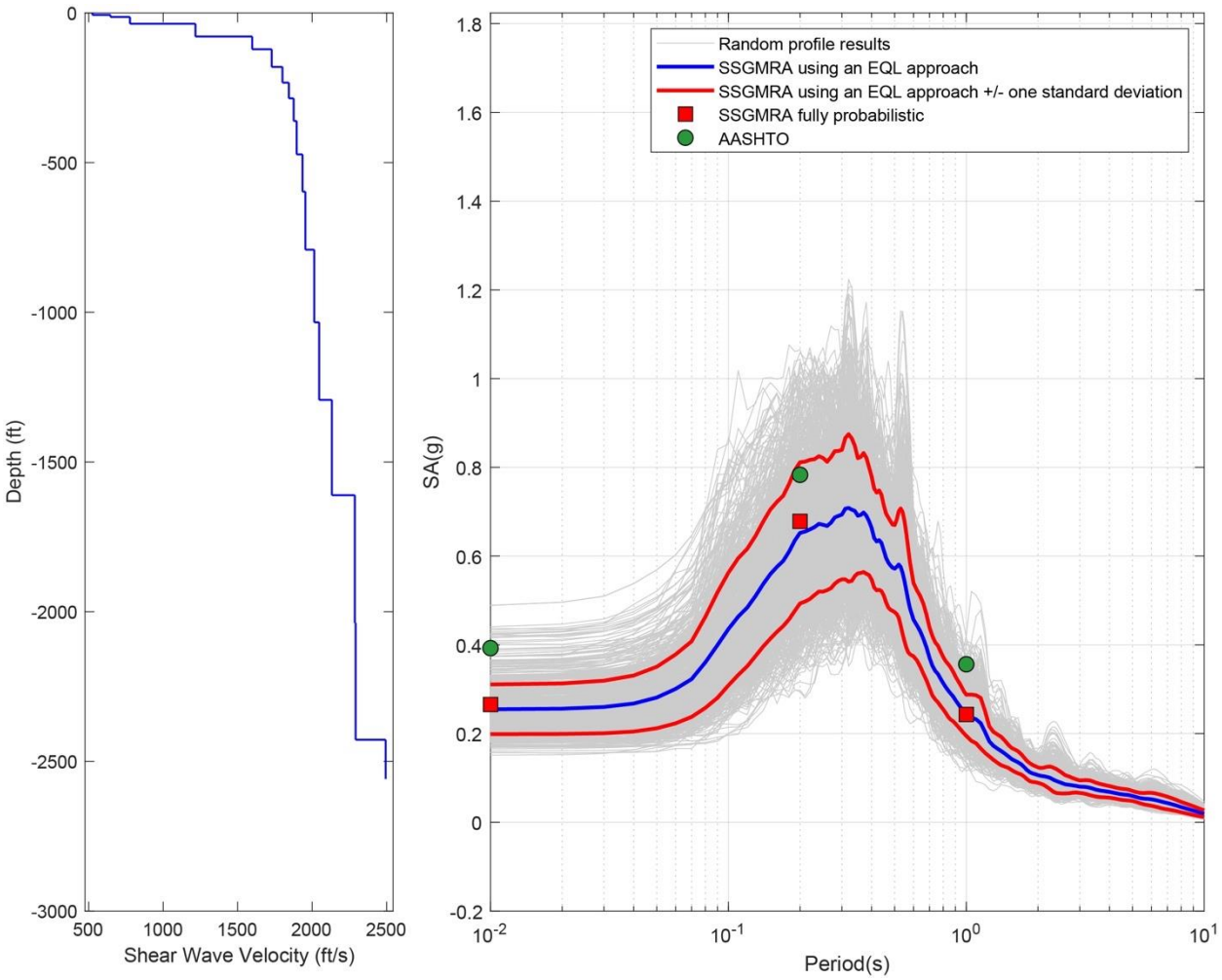


**Figure B-118. Left Panel: Shear-Wave Velocity Profile for Site 30 (Based on EPRI Soil Model); and Right Panel: Results of SSGMRA Using a Fully Probabilistic Approach, SSGMRA Using an Equivalent Linear Approach, SSGMRA Using an Equivalent Linear Approach Plus and Minus One Standard Deviation, And AASHTO General Approach**

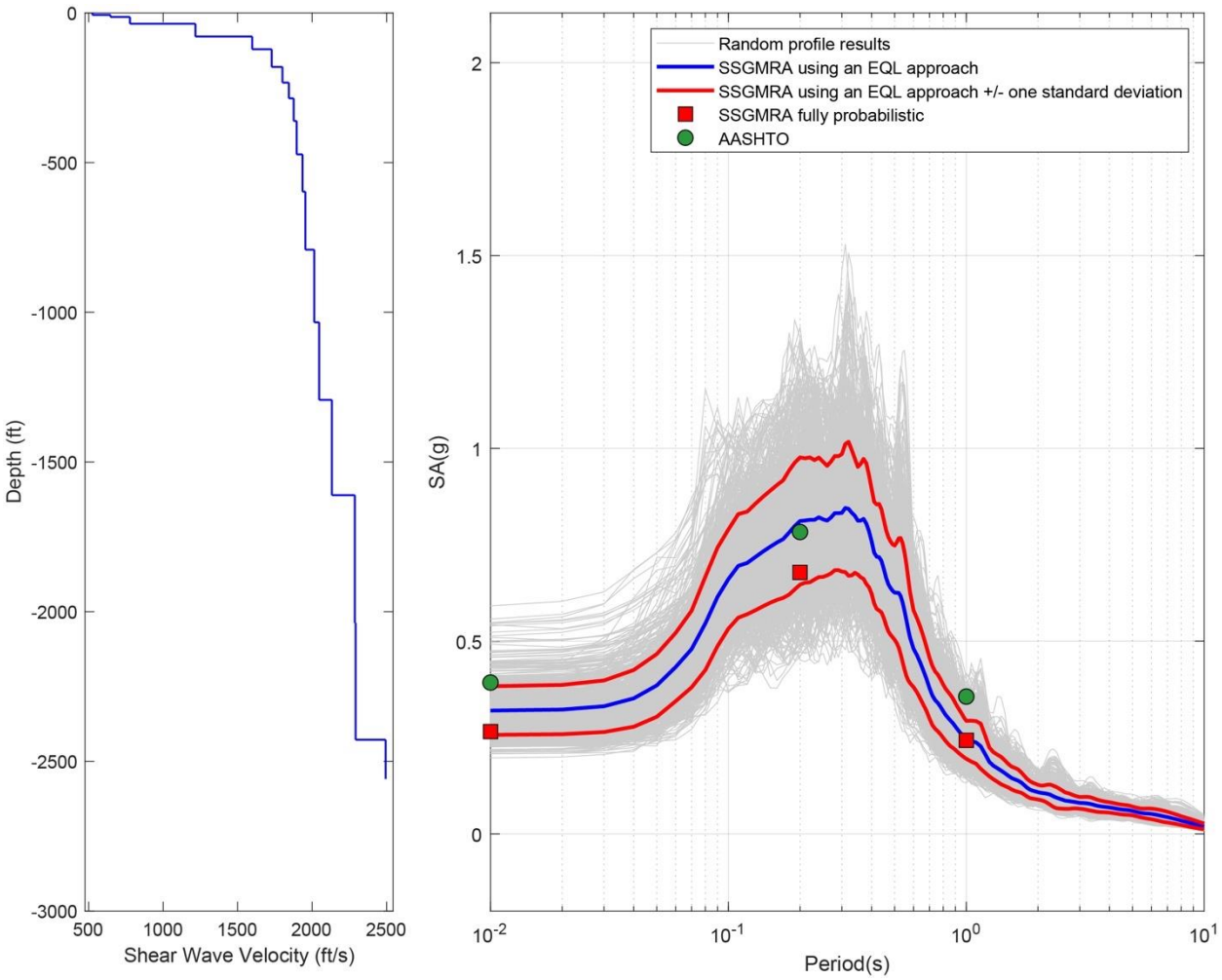


**Figure B-119. Left Panel: Shear-Wave Velocity Profile for Site 30 (Based on Peninsular Soil Model); and Right Panel: Results of SSGMRA Using a Fully Probabilistic Approach, SSGMRA Using an Equivalent Linear Approach, SSGMRA Using an Equivalent Linear Approach Plus and Minus One Standard Deviation, and AASHTO General Approach**

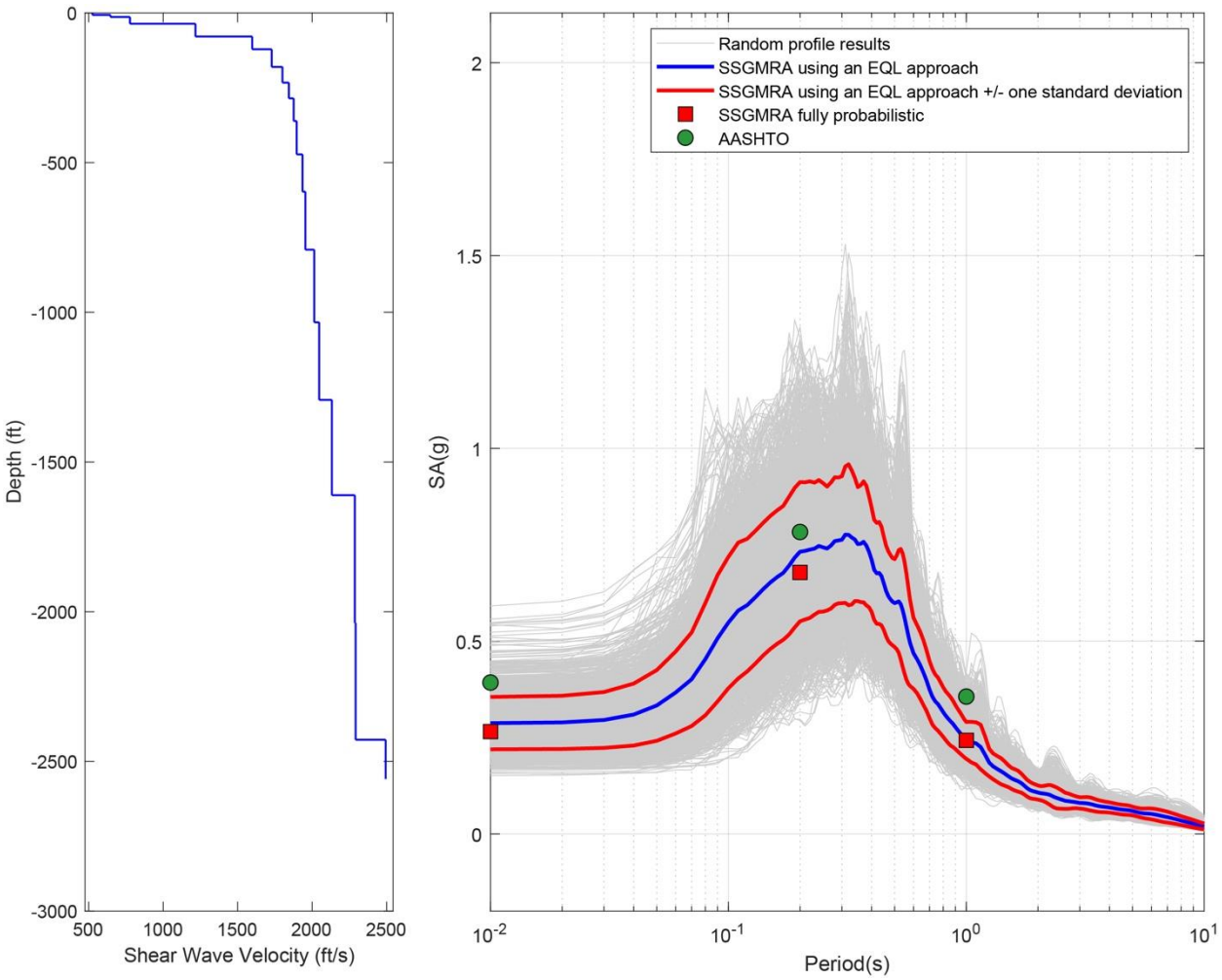


**Figure B-120. Left Panel: Shear-Wave Velocity Profile for Site 30 (Combined); and Right Panel: Results of SSGMRA Using a Fully Probabilistic Approach, SSGMRA Using an Equivalent Linear Approach, SSGMRA Using an Equivalent Linear Approach Plus and Minus One Standard Deviation, and AASHTO General Approach**

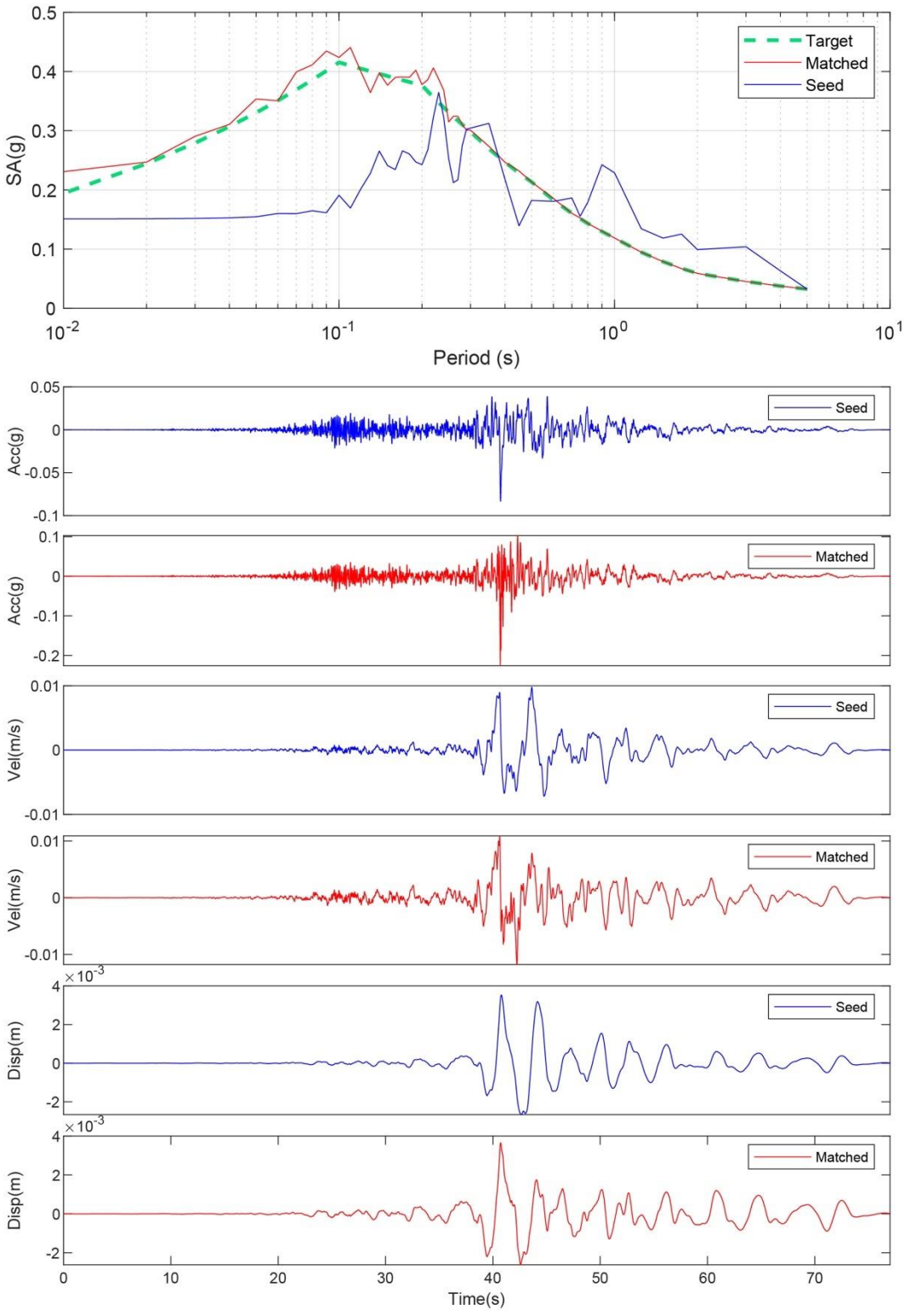


**Figure B-121. Matching Spectrum of Seed Motion (RSN1432-CHICHI-TAP046-E) to the Target Spectrum (UHS) at Site 31. The Middle Subplot Shows the Seed Motion, and the Bottom Subplot Indicates the Matched Motion**

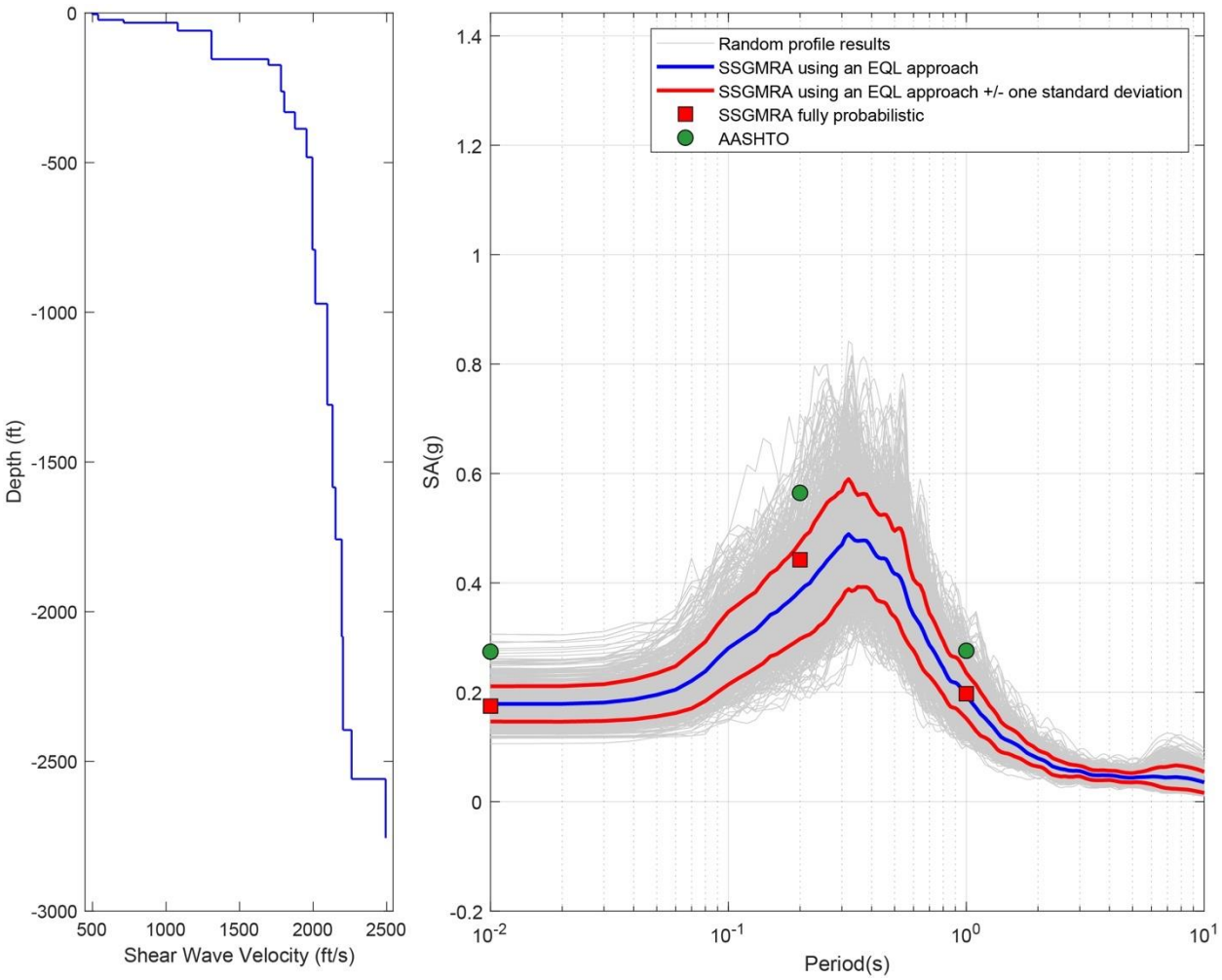


**Figure B-122. Left Panel: Shear-Wave Velocity Profile for Site 31 (Based on EPRI Soil Model); and Right Panel: Results of SSGMRA Using a Fully Probabilistic Approach, SSGMRA Using an Equivalent Linear Approach, SSGMRA Using an Equivalent Linear Approach Plus and Minus One Standard Deviation, and AASHTO General Approach**

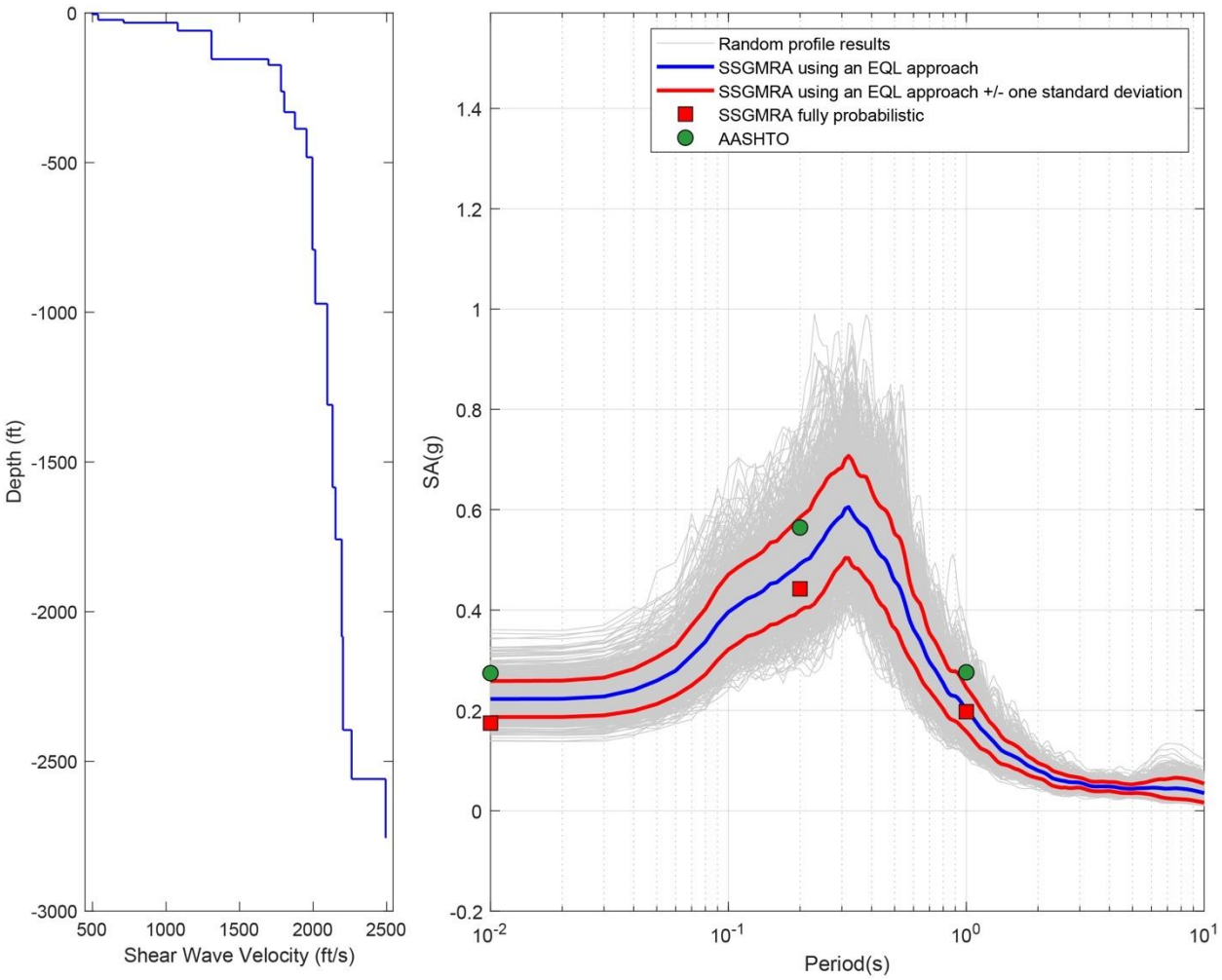


**Figure B-123. Left Panel: Shear-Wave Velocity Profile for Site 31 (Based on Peninsular Soil Model); and Right Panel: Results of SSGMRA Using a Fully Probabilistic Approach, SSGMRA Using an Equivalent Linear Approach, SSGMRA Using an Equivalent Linear Approach Plus and Minus One Standard Deviation, and AASHTO General Approach**

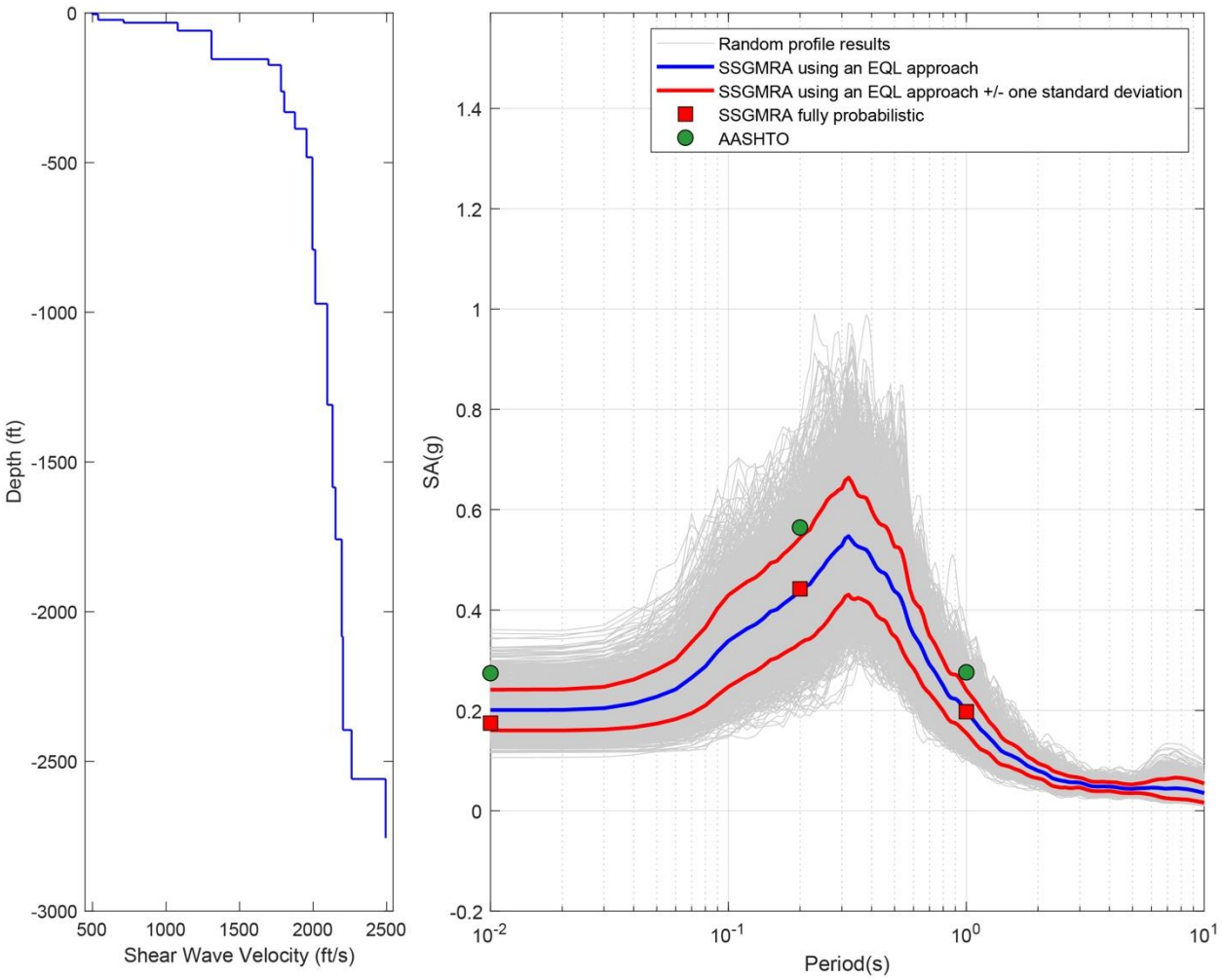


**Figure B-124. Left Panel: Shear-Wave Velocity Profile for Site 31 (Combined); and Right Panel: Results of SSGMRA Using a Fully Probabilistic Approach, SSGMRA Using an Equivalent Linear Approach, SSGMRA Using an Equivalent Linear Approach Plus and Minus One Standard Deviation, and AASHTO General Approach**

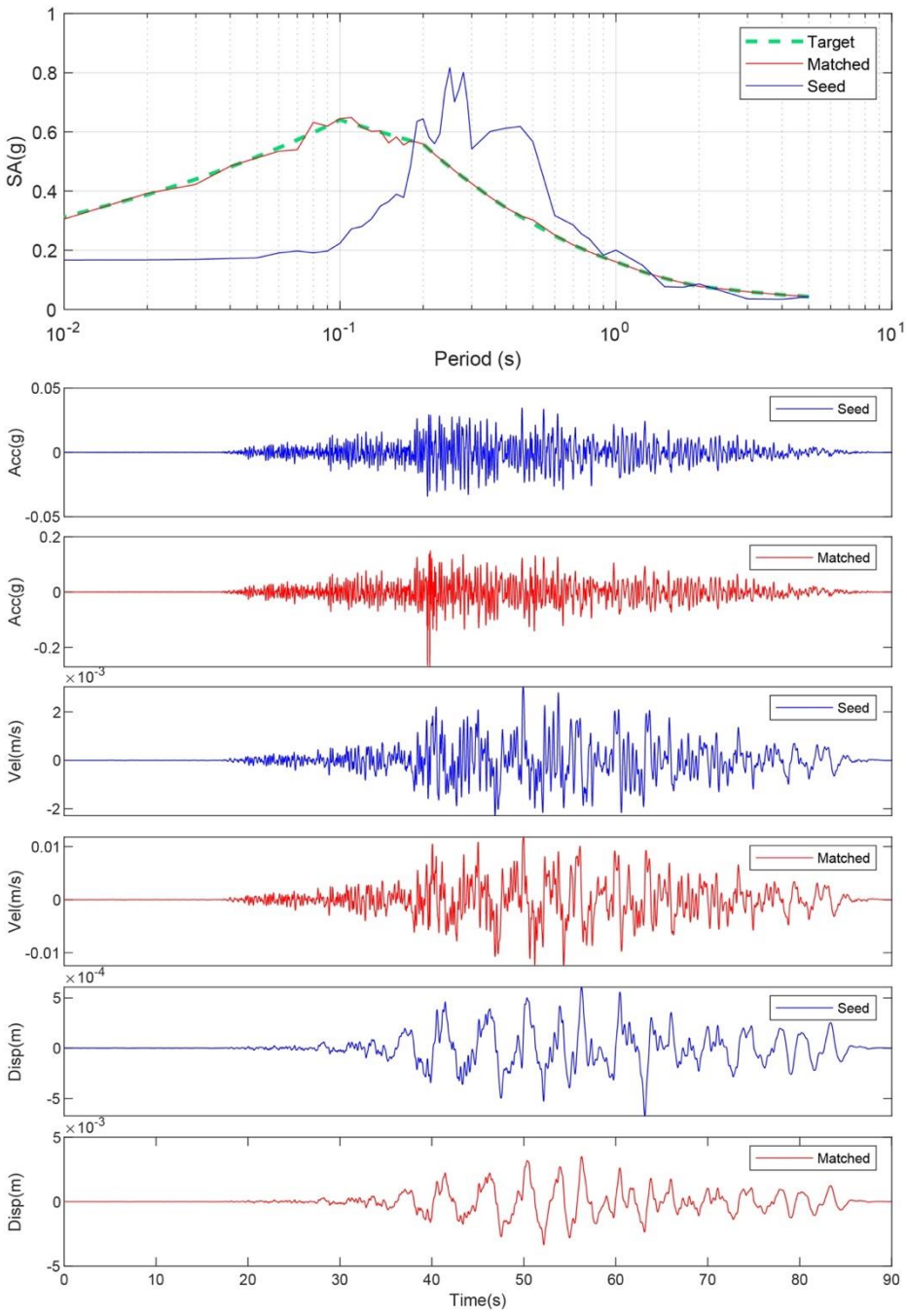


**Figure B-125. Matching Spectrum of Seed Motion (RSN1577-CHICHI-TTN025-E) to the Target Spectrum (UHS) at Site 32. The Middle Subplot Shows the Seed Motion, and the Bottom Subplot Indicates the Matched Motion**

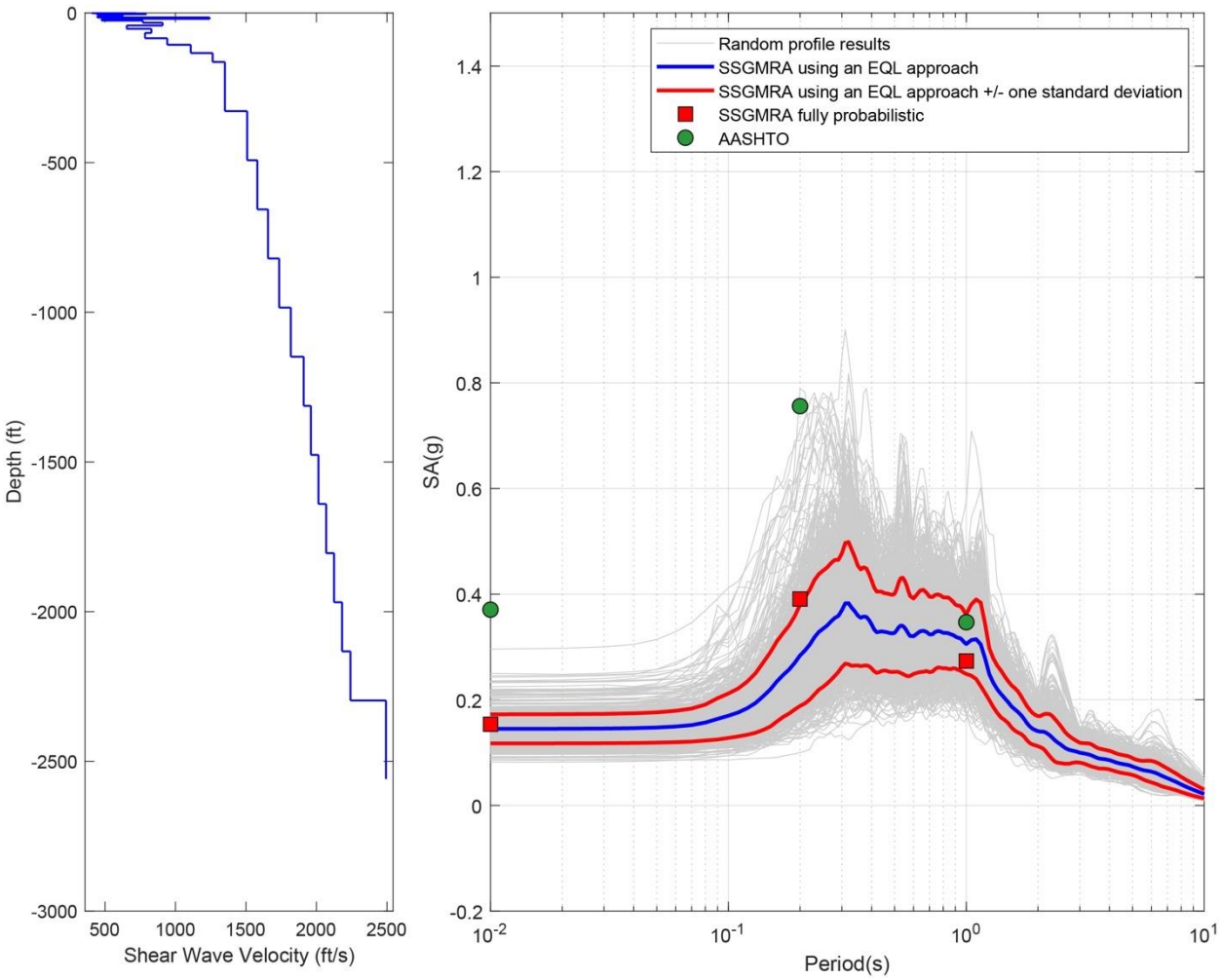


**Figure B-126. Left Panel: Shear-Wave Velocity Profile for Site 32 (Based on EPRI Soil Model); and Right Panel: Results of SSGMRA Using a Fully Probabilistic Approach, SSGMRA Using an Equivalent Linear Approach, SSGMRA Using an Equivalent Linear Approach Plus and Minus One Standard Deviation, and AASHTO General Approach**

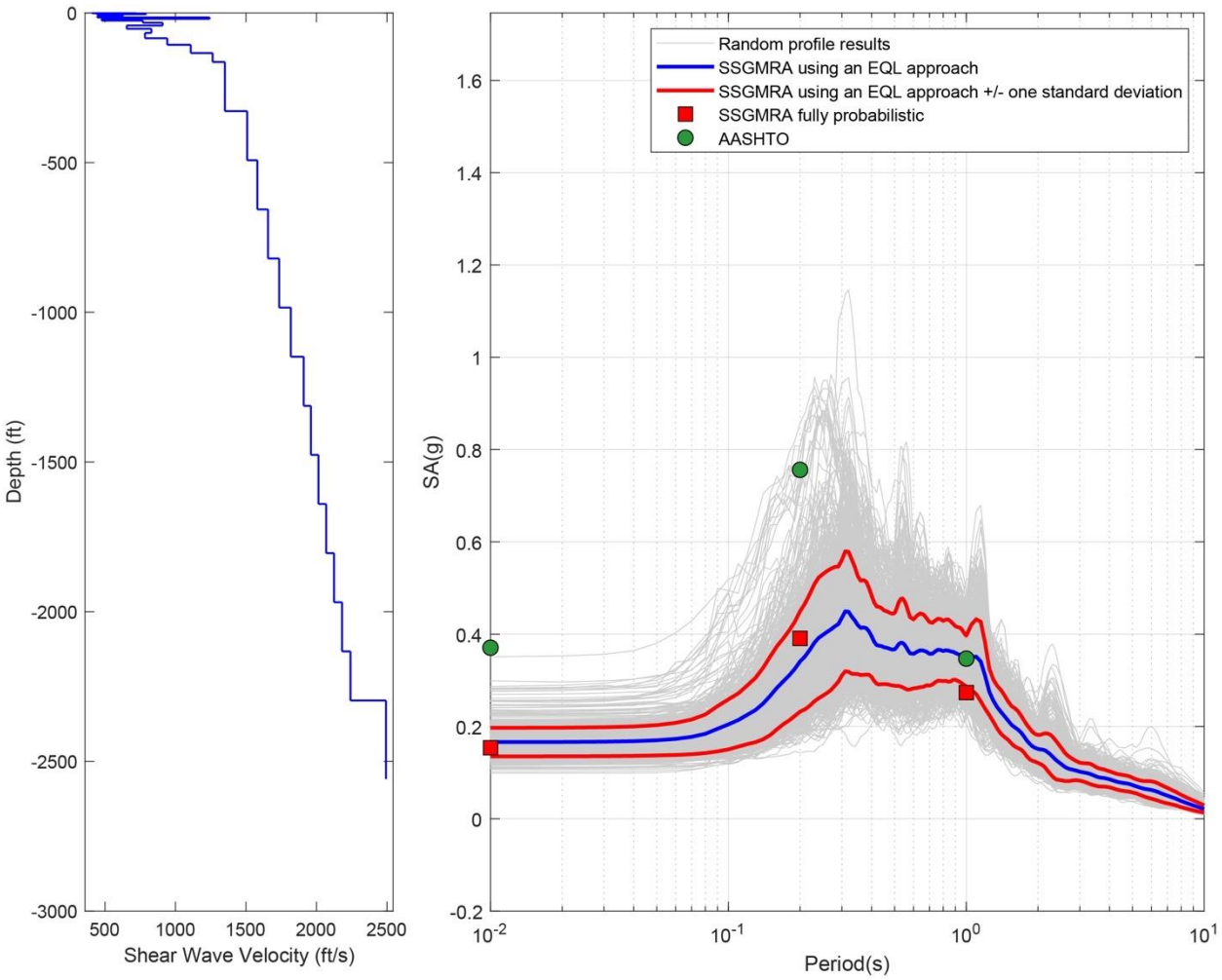


**Figure B-127. Left Panel: Shear-Wave Velocity Profile for Site 32 (Based on Peninsular Soil Model); and Right Panel: Results of SSGMRA Using a Fully Probabilistic Approach, SSGMRA Using an Equivalent Linear Approach, SSGMRA Using an Equivalent Linear Approach Plus and Minus One Standard Deviation, and AASHTO General Approach**

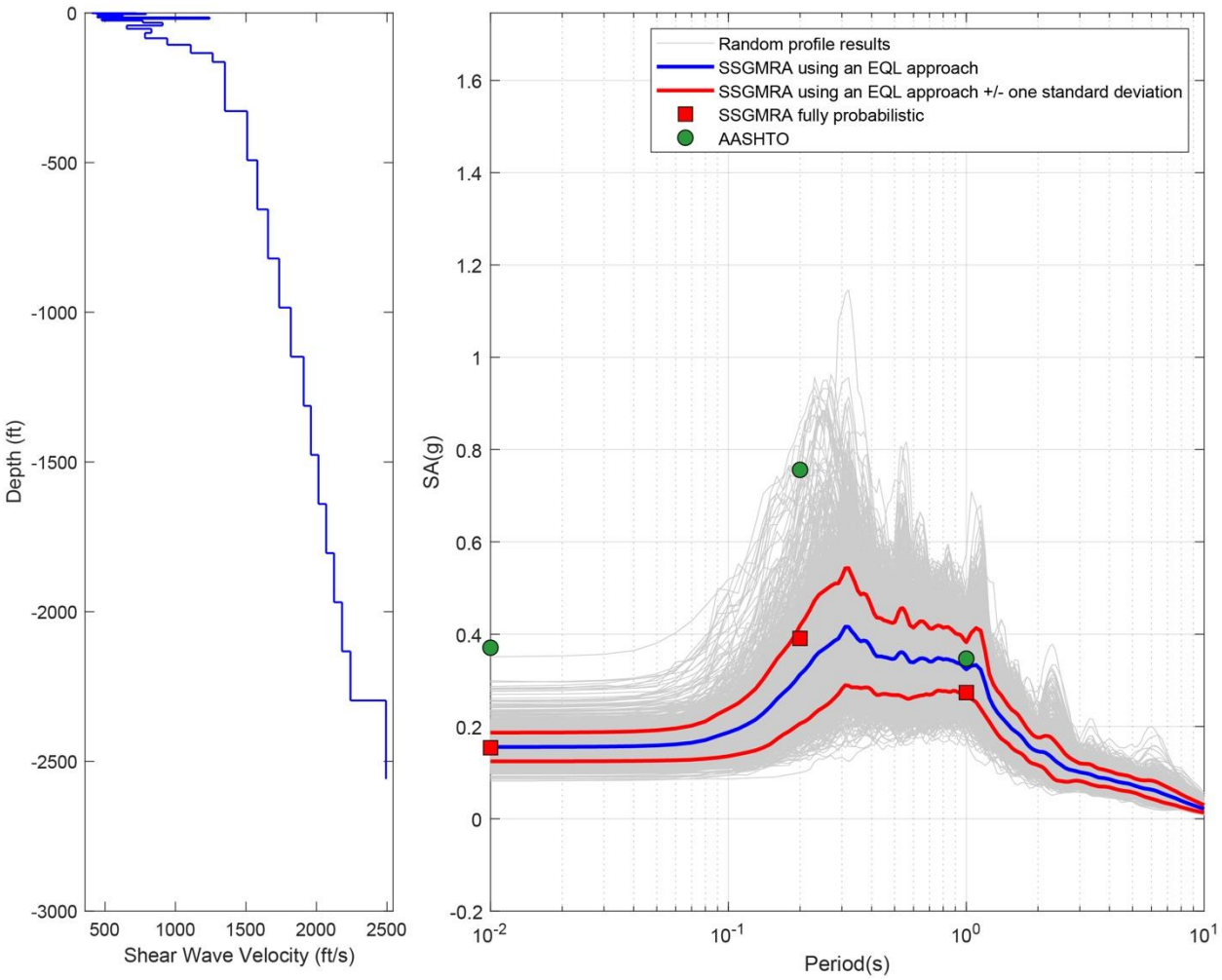


**Figure B-128. Left Panel: Shear-Wave Velocity Profile for Site 32 (Combined); and Right Panel: Results of SSGMRA Using a Fully Probabilistic Approach, SSGMRA Using an Equivalent Linear Approach, SSGMRA Using an Equivalent Linear Approach Plus and Minus One Standard Deviation, and AASHTO General Approach**

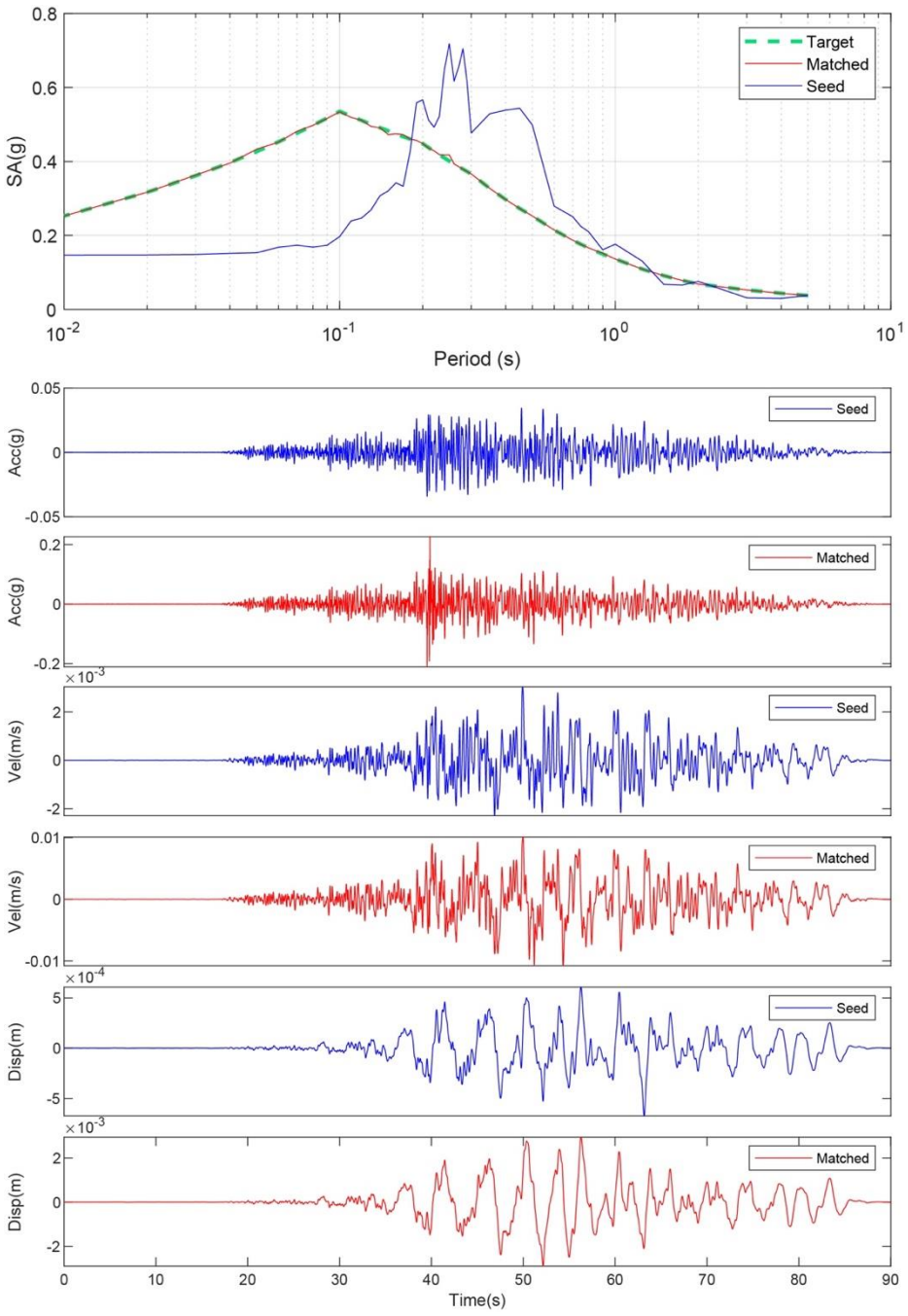


**Figure B-129. Matching Spectrum of Seed Motion (RSN1577-CHICHI-TTN025-E) to the Target Spectrum (UHS) at Site 33. The Middle Subplot Shows the Seed Motion, and the Bottom Subplot Indicates the Matched Motion**

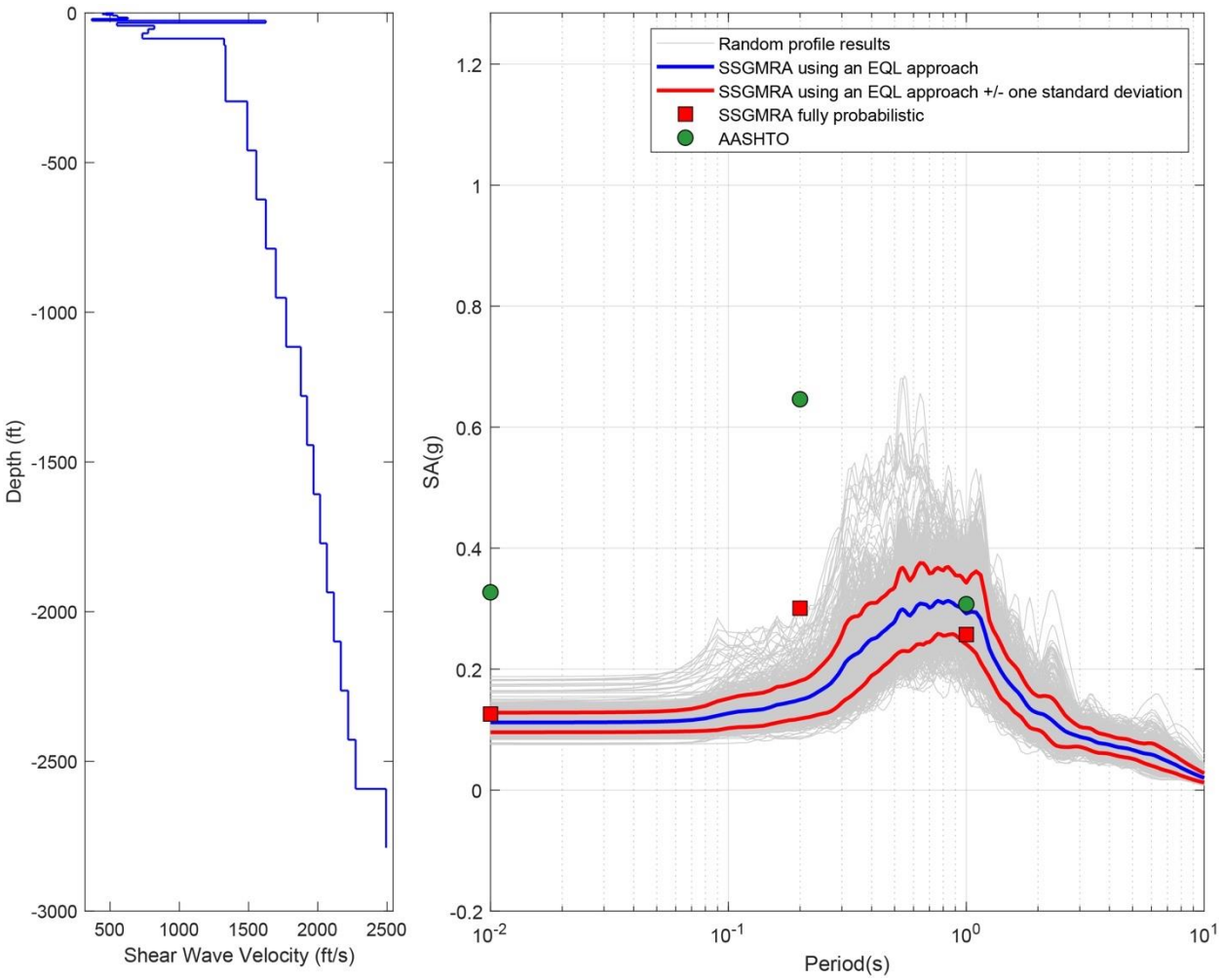


**Figure B-130. Left Panel: Shear-Wave Velocity Profile for Site 33 (Based on EPRI Soil Model); and Right Panel: Results of SSGMRA Using a Fully Probabilistic Approach, SSGMRA Using an Equivalent Linear Approach, SSGMRA Using an Equivalent Linear Approach Plus and Minus One Standard Deviation, and AASHTO General Approach**

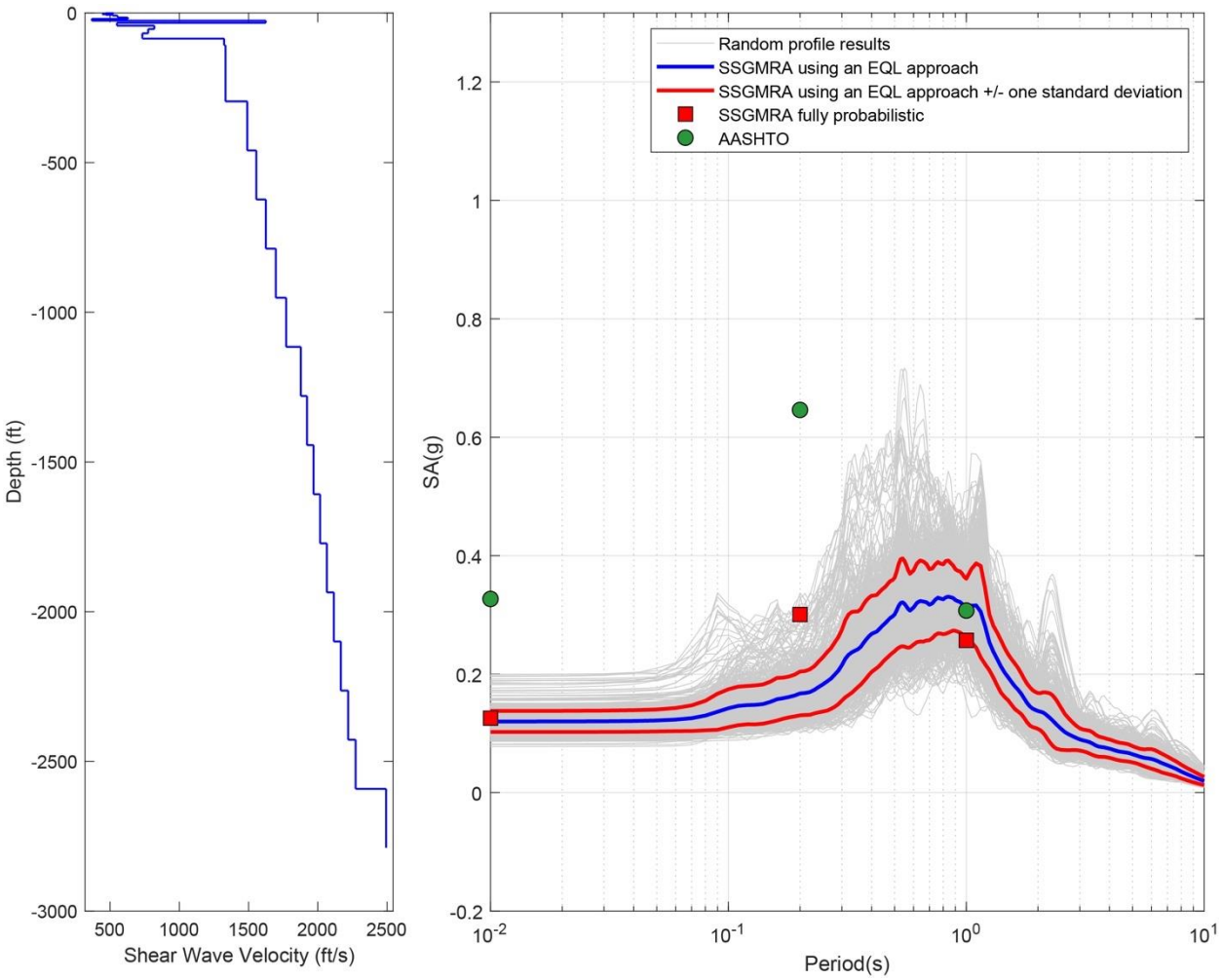


**Figure B-131. Left Panel: Shear-Wave Velocity Profile for Site 33 (Based on Peninsular Soil Model); and Right Panel: Results of SSGMRA Using a Fully Probabilistic Approach, SSGMRA Using an Equivalent Linear Approach, SSGMRA Using an Equivalent Linear Approach Plus and Minus One Standard Deviation, and AASHTO General Approach**

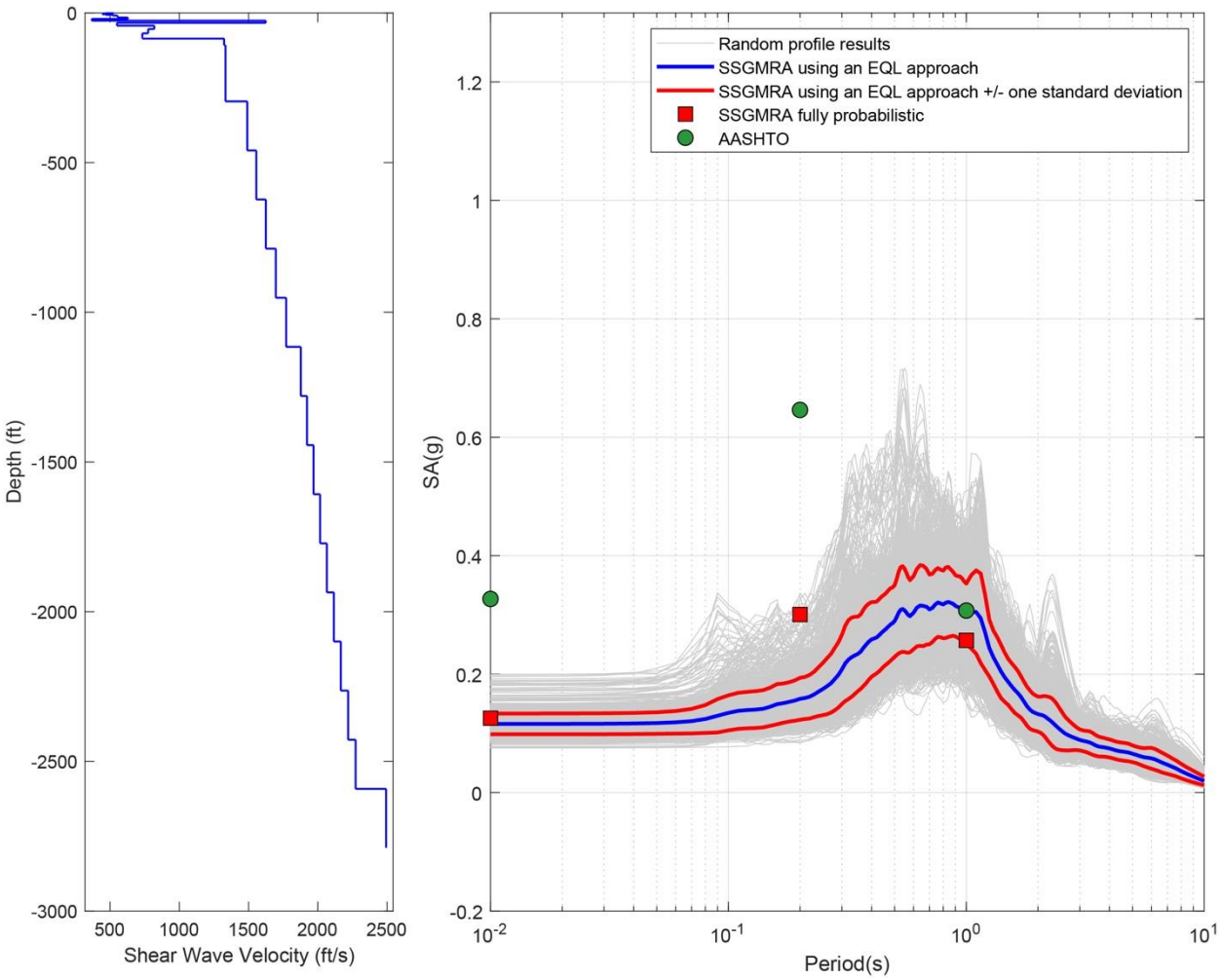


**Figure B-132. Left Panel: Shear-Wave Velocity Profile for Site 33 (Combined); and Right Panel: Results of SSGMRA Using a Fully Probabilistic Approach, SSGMRA Using an Equivalent Linear Approach, SSGMRA Using an Equivalent Linear Approach Plus and Minus One Standard Deviation, and AASHTO General Approach**

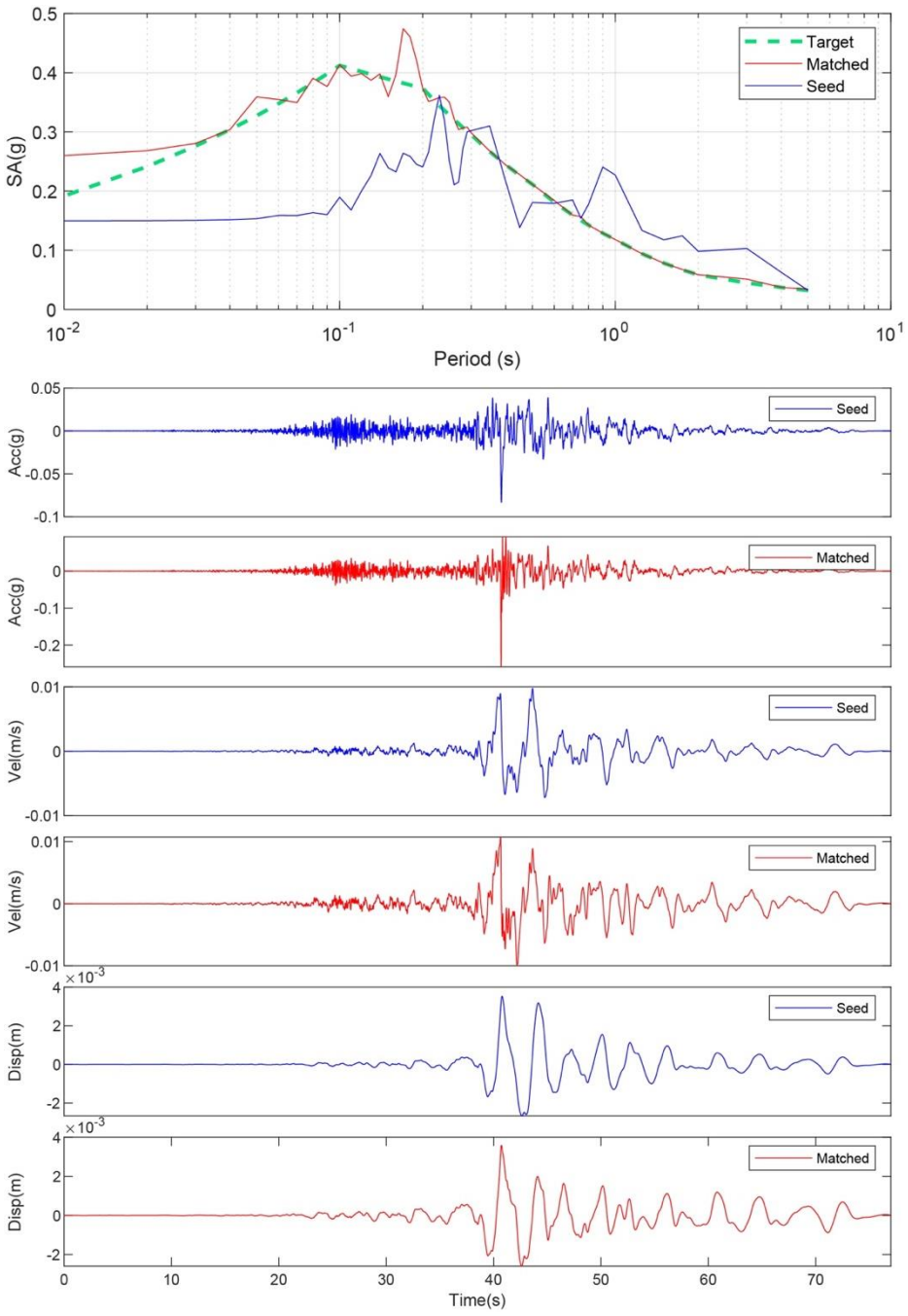


**Figure B-133. Matching Spectrum of Seed Motion (RSN1432-CHICHI-TAP046-E) to the Target Spectrum (UHS) at Site 34. The Middle Subplot Shows the Seed Motion, and the Bottom Subplot Indicates the Matched Motion**

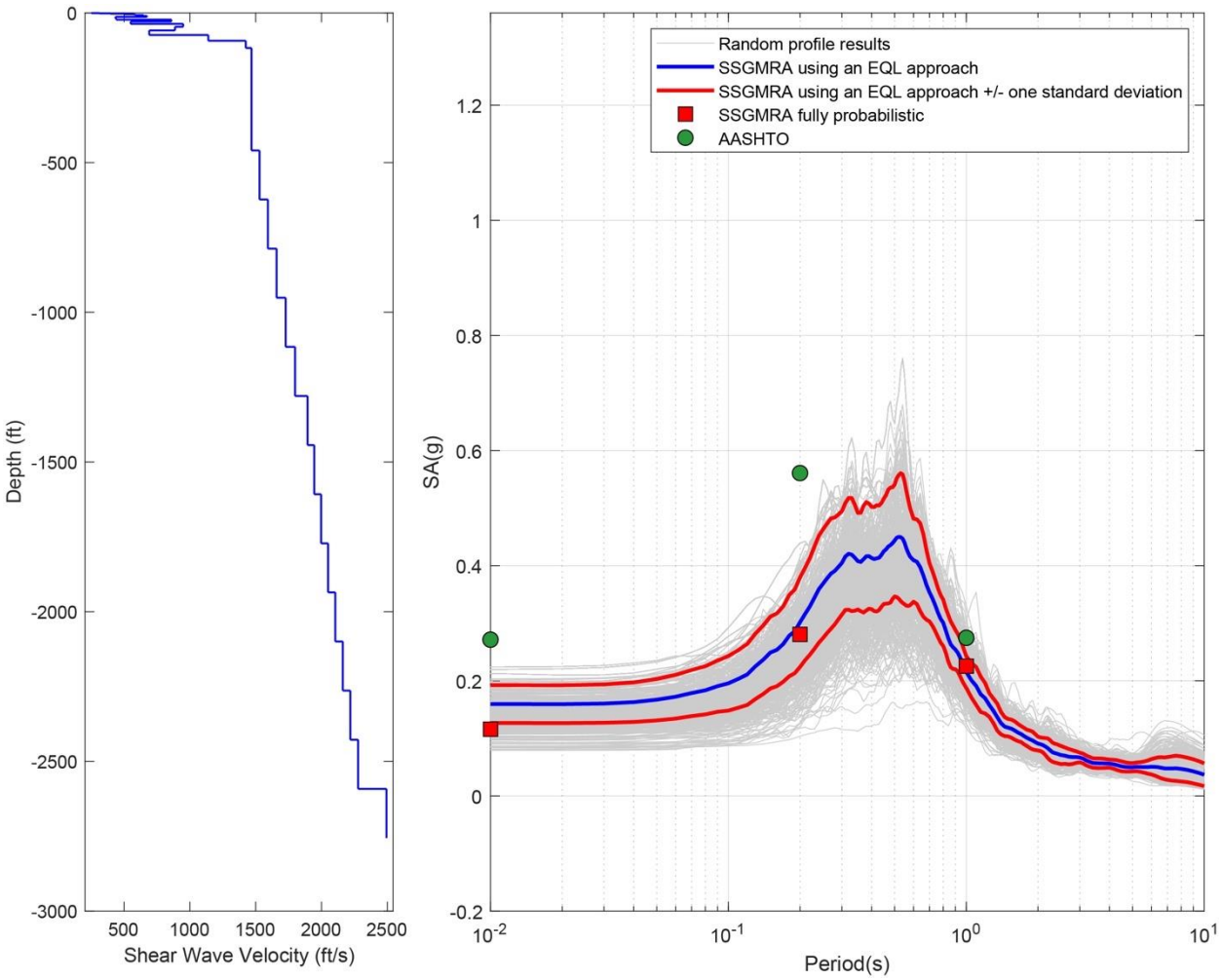


**Figure B-134. Left Panel: Shear-Wave Velocity Profile for Site 34 (Based on EPRI Soil Model); and Right Panel: Results of SSGMRA Using a Fully Probabilistic Approach, SSGMRA Using an Equivalent Linear Approach, SSGMRA Using an Equivalent Linear Approach Plus and Minus One Standard Deviation, and AASHTO General Approach**

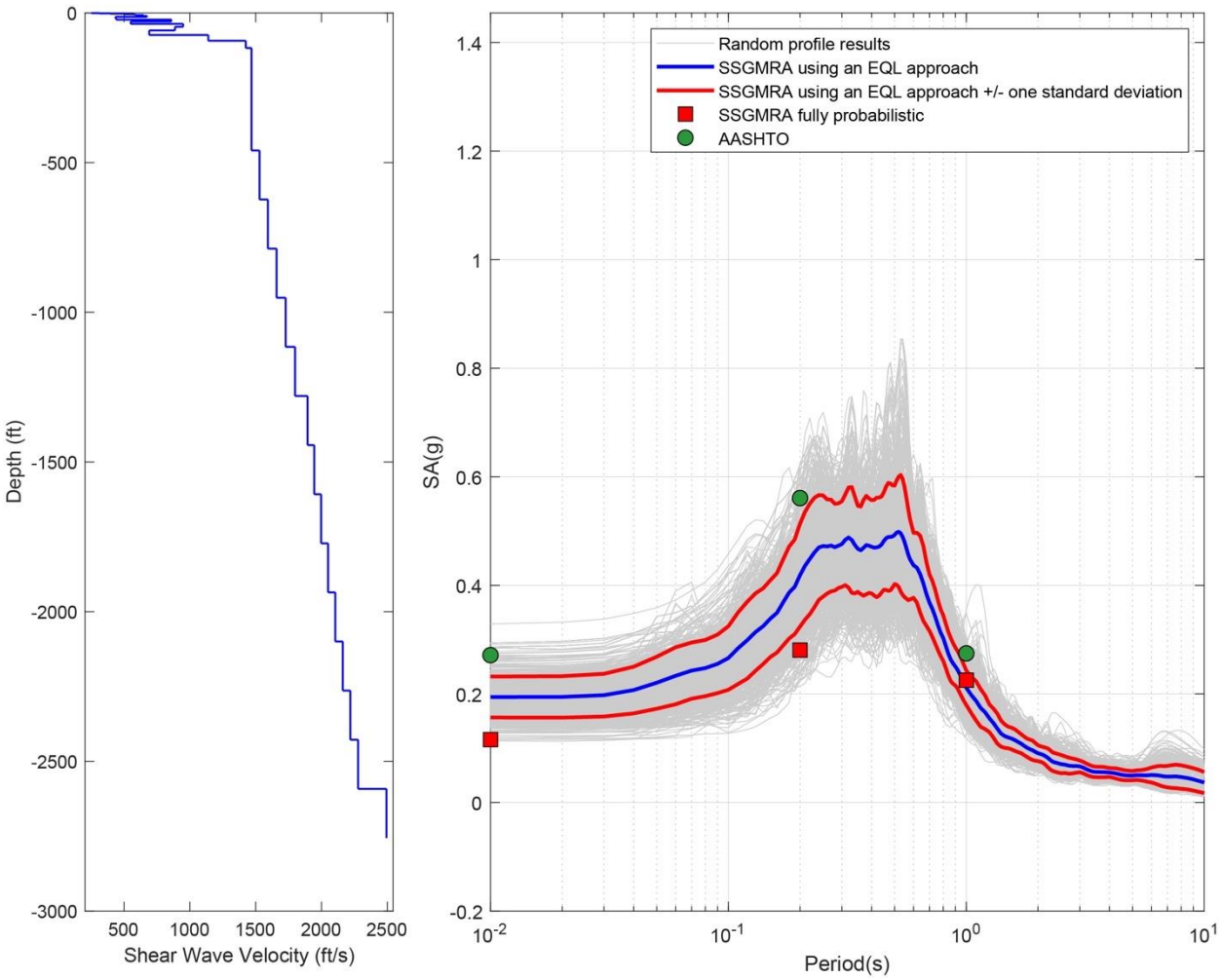


**Figure B-135. Left Panel: Shear-Wave Velocity Profile for Site 34 (Based on Peninsular Soil Model); and Right Panel: Results of SSGMRA Using a Fully Probabilistic Approach, SSGMRA Using an Equivalent Linear Approach, SSGMRA Using an Equivalent Linear Approach Plus and Minus One Standard Deviation, and AASHTO General Approach**

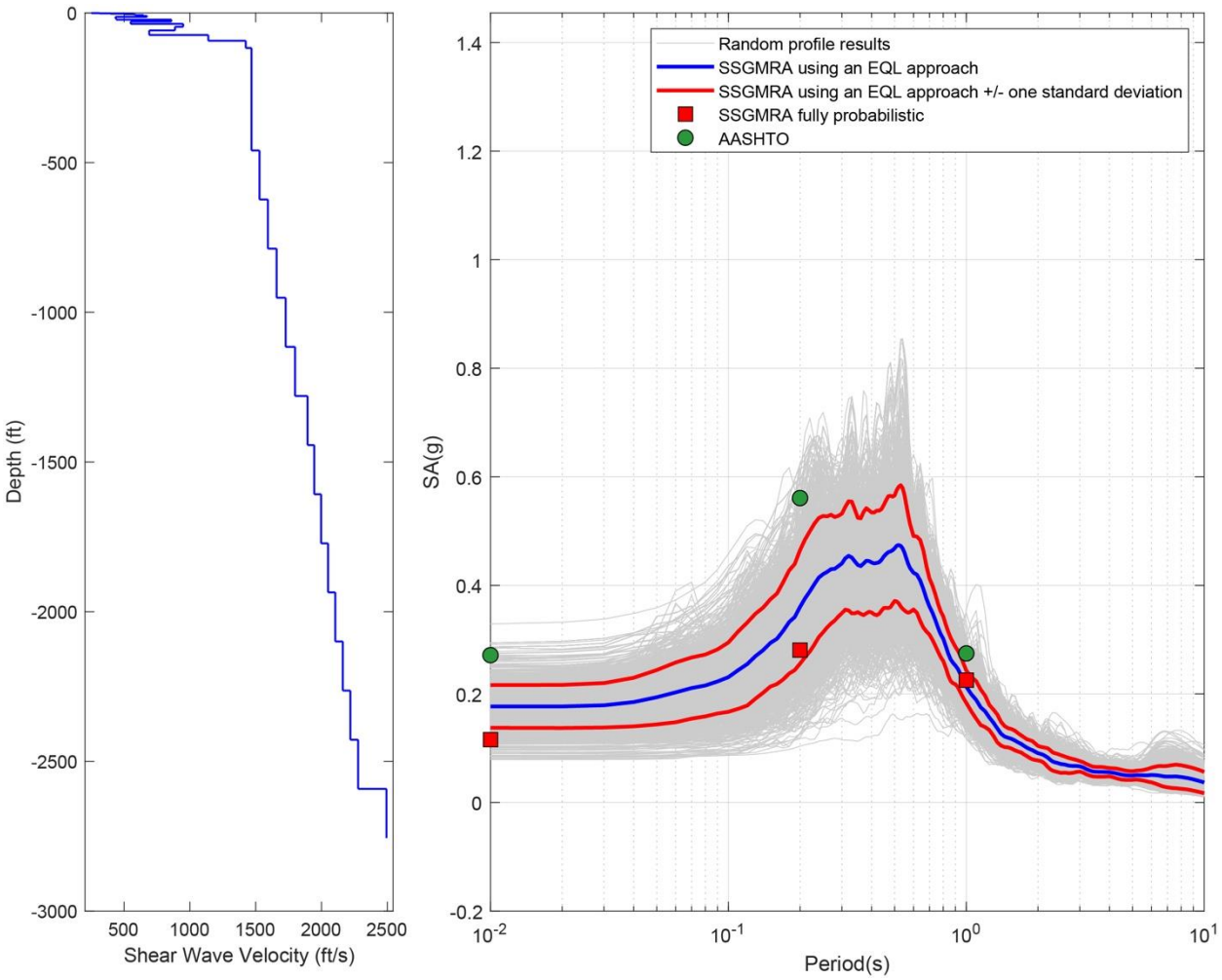


**Figure B-136. Left Panel: Shear-Wave Velocity Profile for Site 34 (Combined); and Right Panel: Results of SSGMRA Using a Fully Probabilistic Approach, SSGMRA Using an Equivalent Linear Approach, SSGMRA Using an Equivalent Linear Approach Plus and Minus One Standard Deviation, and AASHTO General Approach**

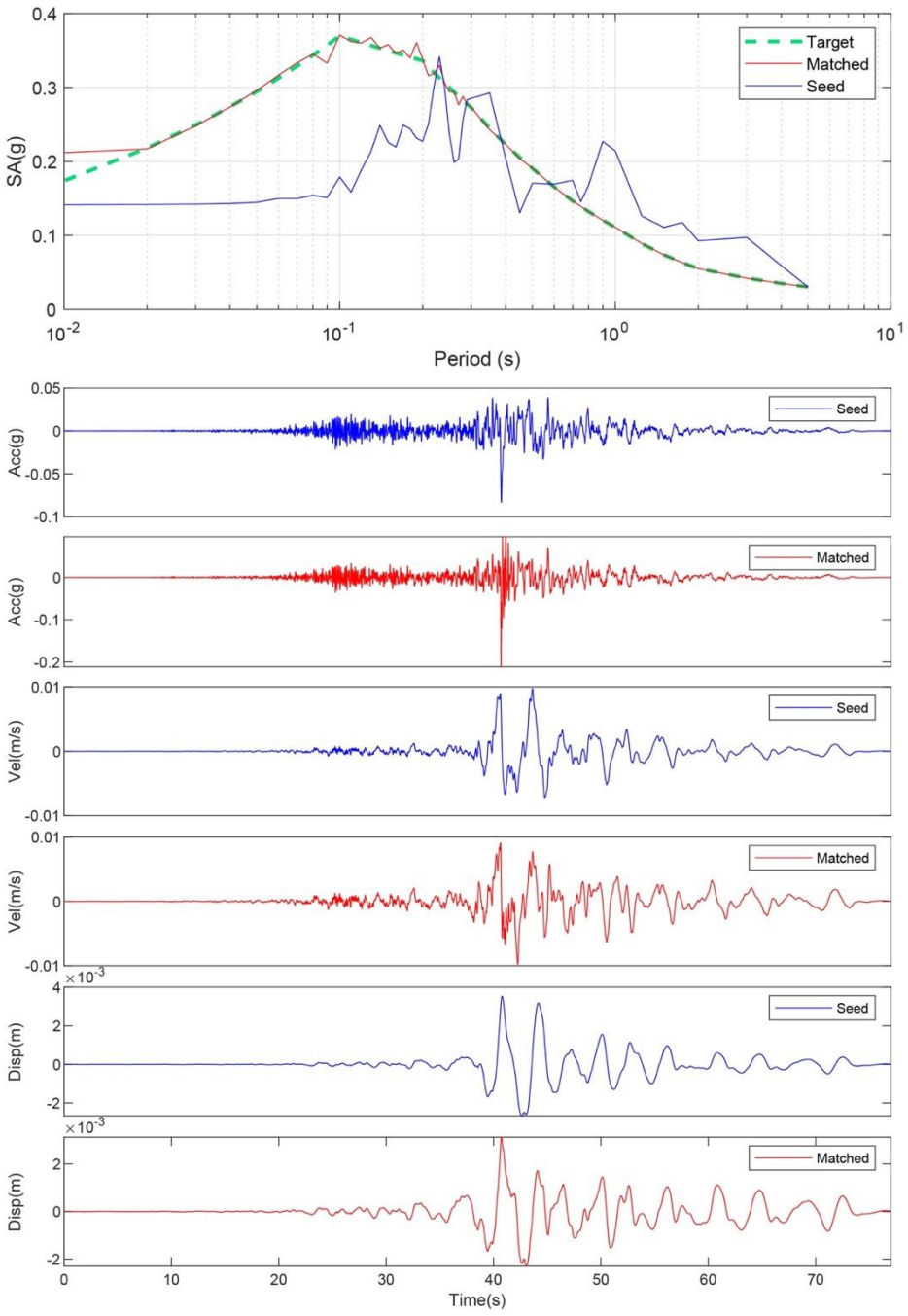


**Figure B-137. Matching Spectrum of Seed Motion (RSN1432-CHICHI-TAP046-E) to the Target Spectrum (UHS) at Site 35. The Middle Subplot Shows the Seed Motion, and the Bottom Subplot Indicates the Matched Motion**

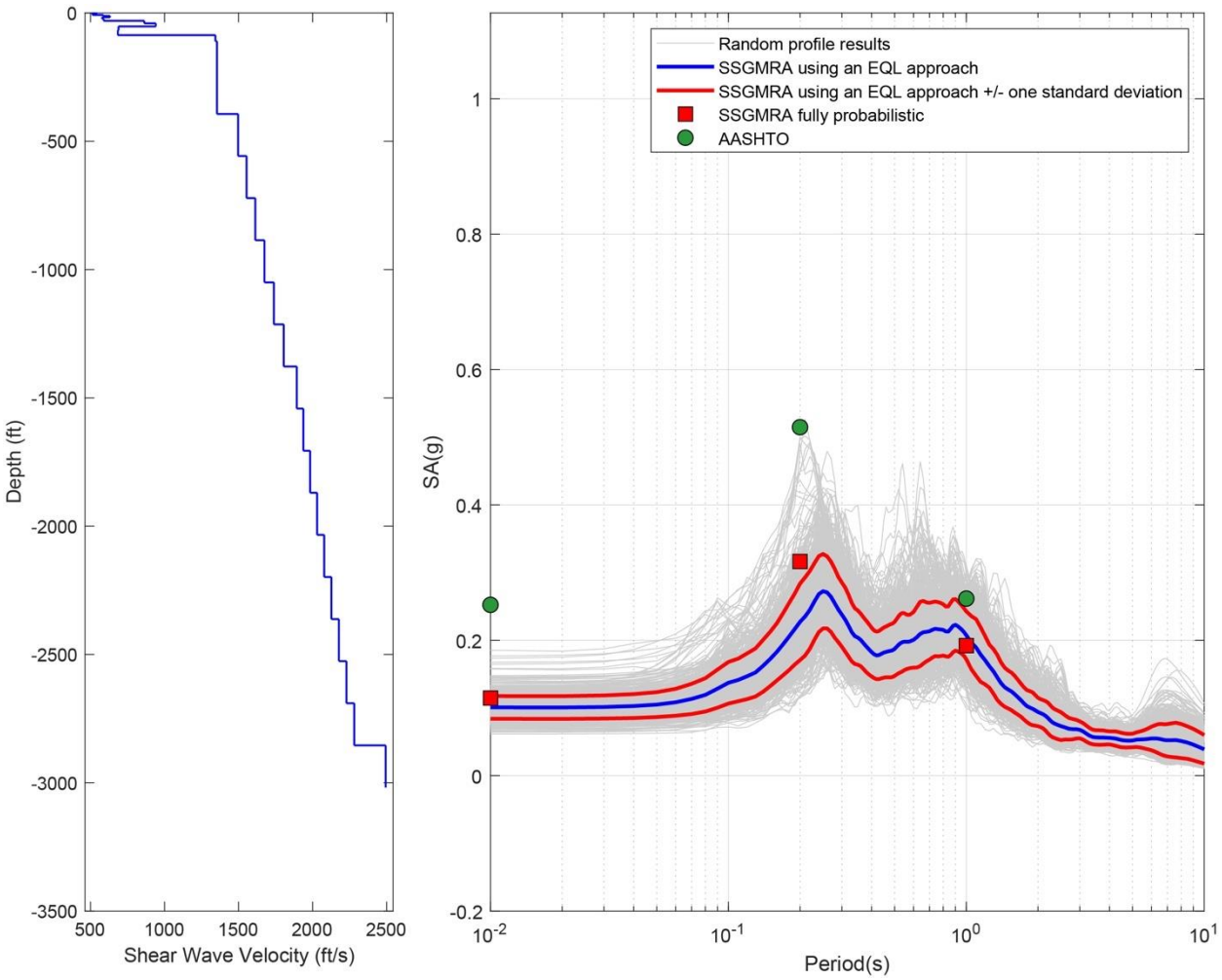


**Figure B-138. Left Panel: Shear-Wave Velocity Profile for Site 35 (Based on EPRI Soil Model); and Right Panel: Results of SSGMRA Using a Fully Probabilistic Approach, SSGMRA Using an Equivalent Linear Approach, SSGMRA Using an Equivalent Linear Approach Plus and Minus One Standard Deviation, and AASHTO General Approach**

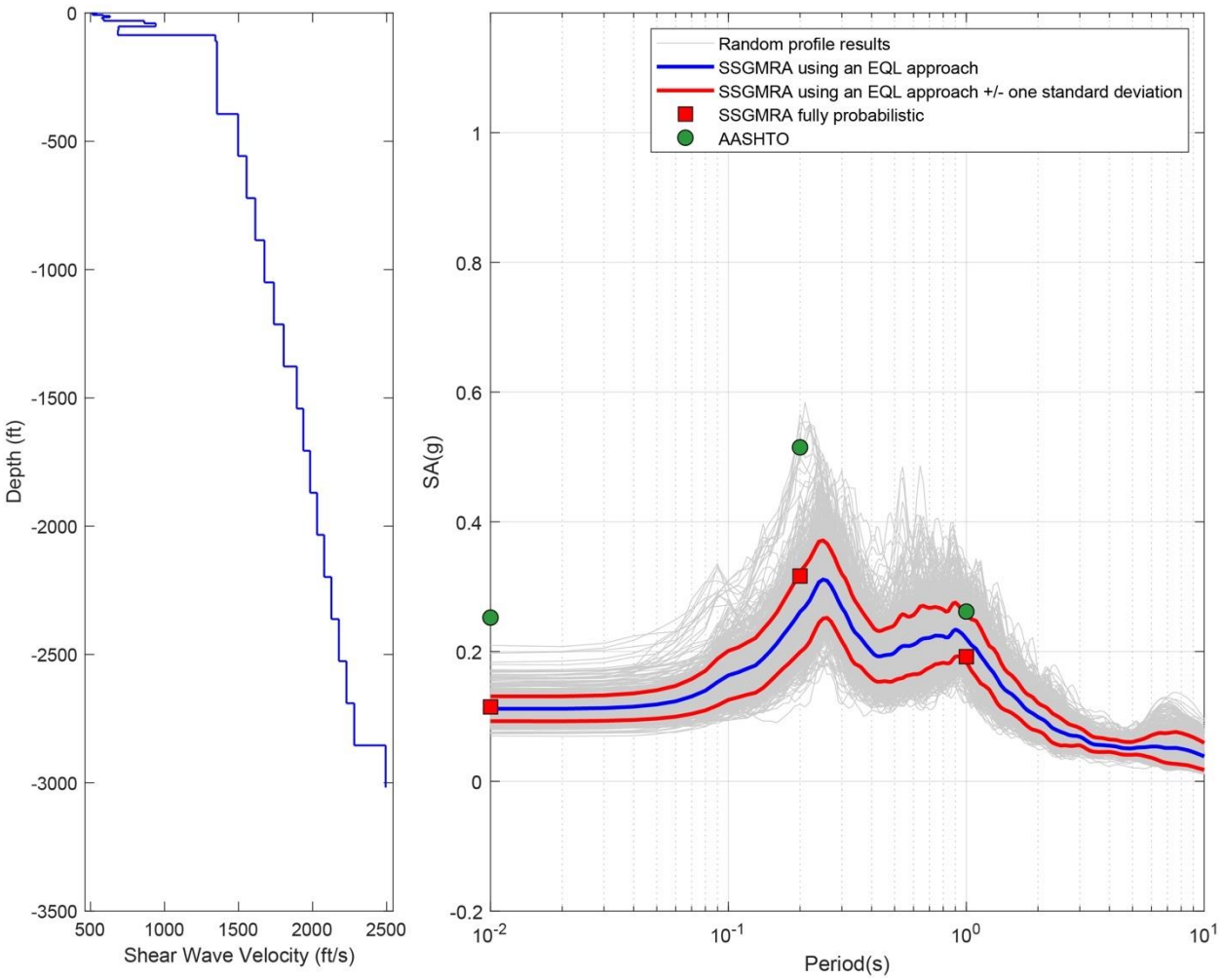


**Figure B-139. Left Panel: Shear-Wave Velocity Profile for Site 35 (Based on Peninsular Soil Model); and Right Panel: Results of SSGMRA Using a Fully Probabilistic Approach, SSGMRA Using an Equivalent Linear Approach, SSGMRA Using an Equivalent Linear Approach Plus and Minus One Standard Deviation, and AASHTO General Approach**

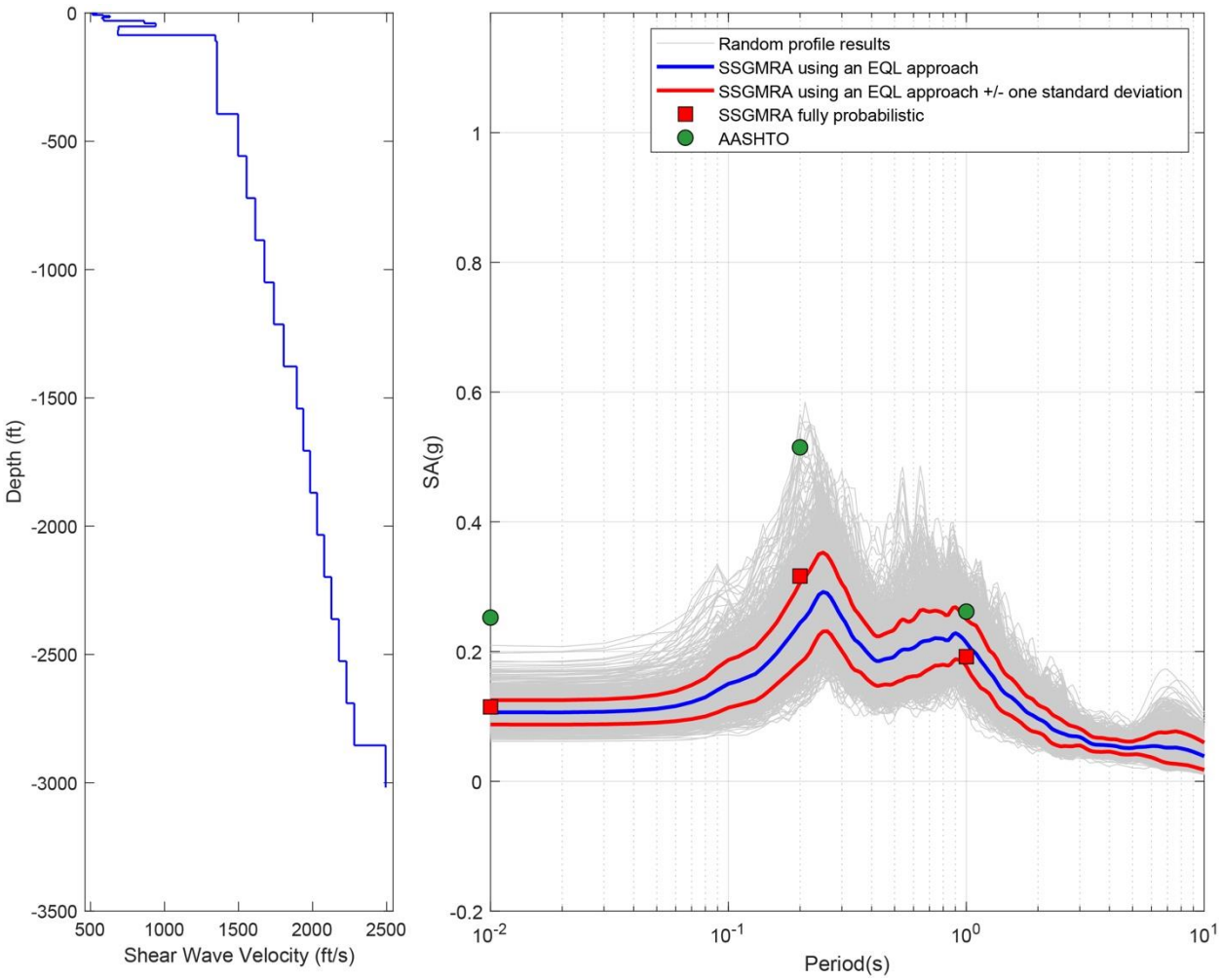


**Figure B-140. Left Panel: Shear-Wave Velocity Profile for Site 35 (Combined); and Right Panel: Results of SSGMRA Using a Fully Probabilistic Approach, SSGMRA Using an Equivalent Linear Approach, SSGMRA Using an Equivalent Linear Approach Plus and Minus One Standard Deviation, and AASHTO General Approach**

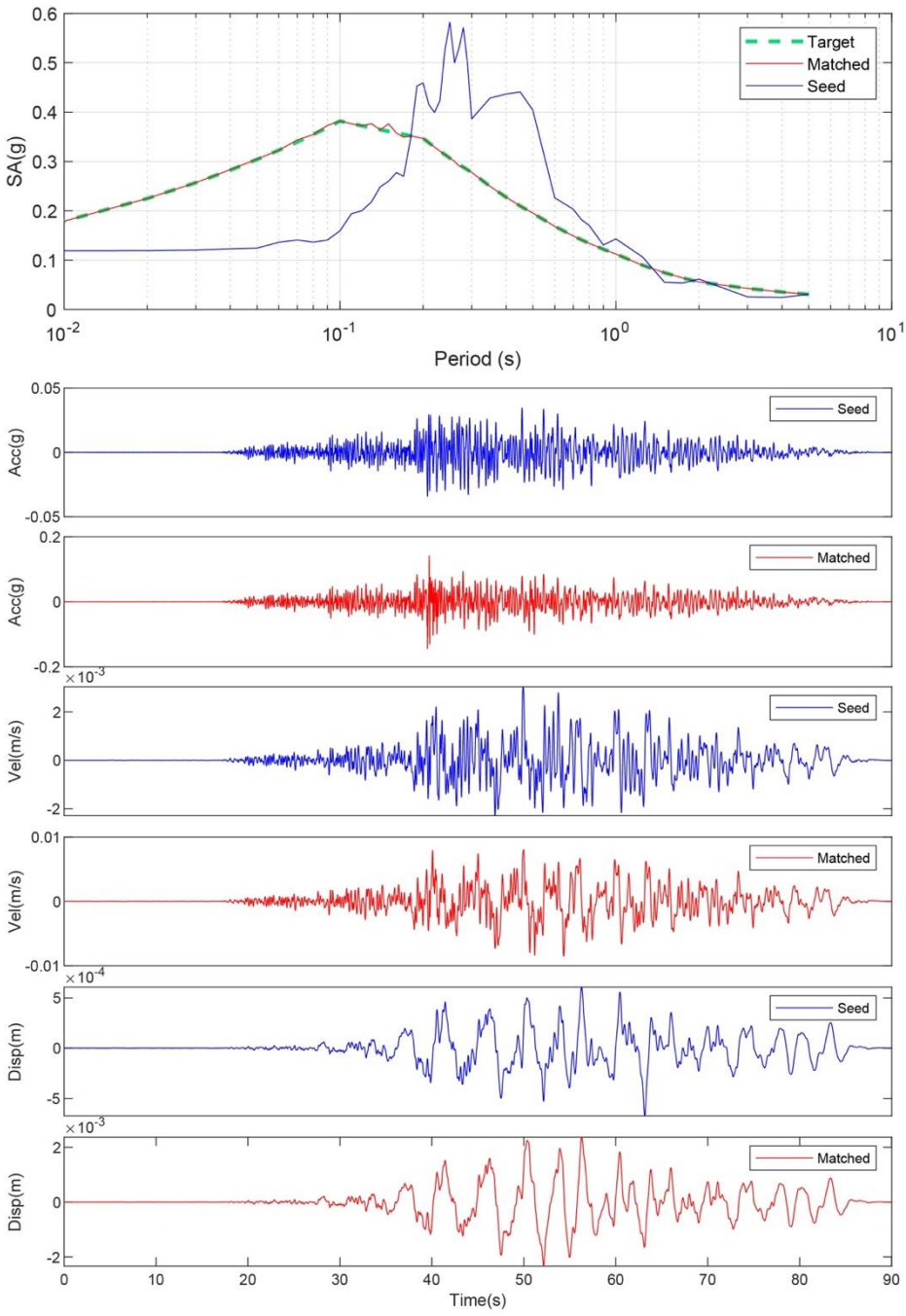


**Figure B-141. Matching Spectrum of Seed Motion (RSN1577-CHICHI-TTN025-E) to the Target Spectrum (UHS) at Site 36. The Middle Subplot Shows the Seed Motion, and the Bottom Subplot Indicates the Matched Motion**

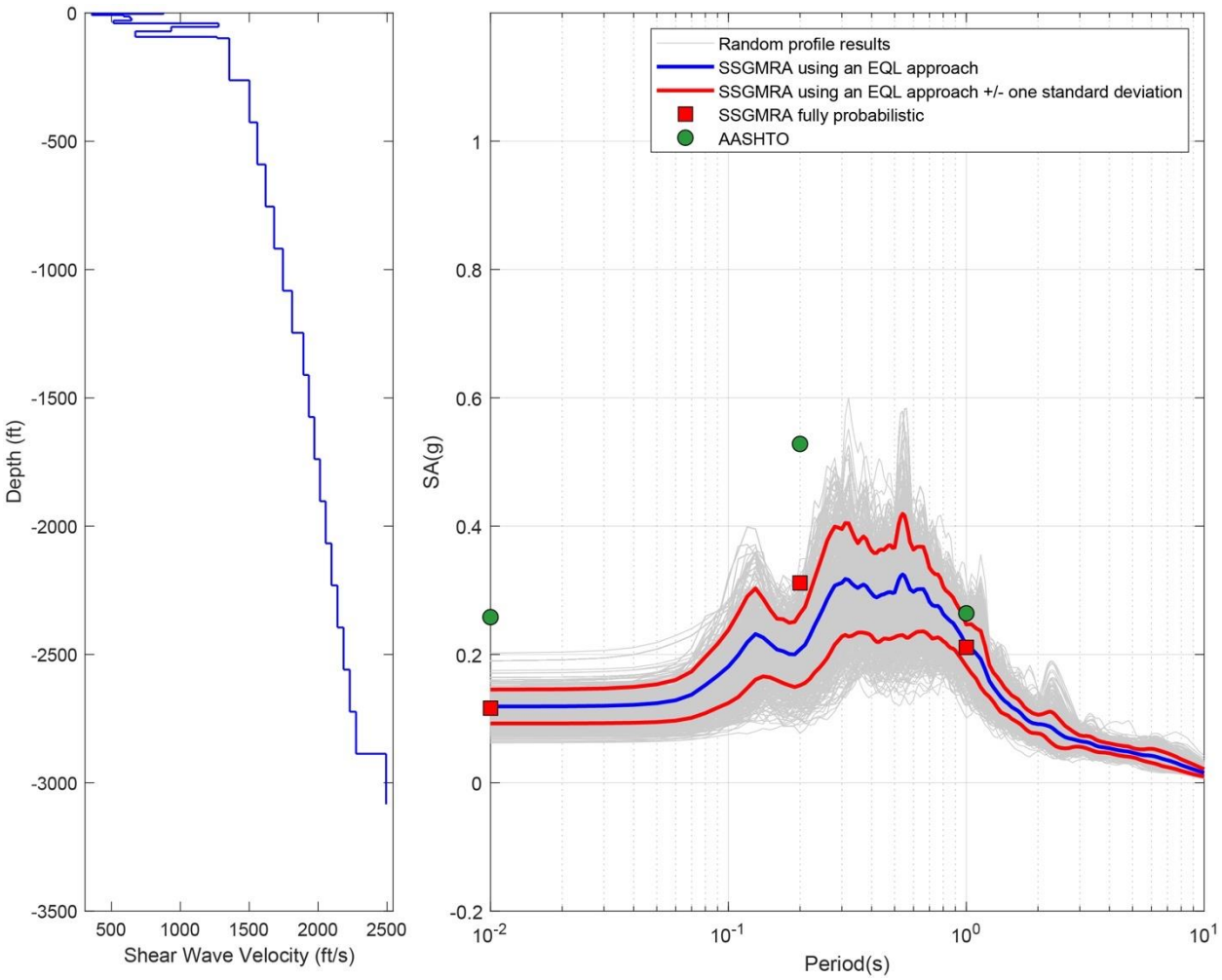


**Figure B-142. Left Panel: Shear-Wave Velocity Profile for Site 36 (Based on EPRI Soil Model); and Right Panel: Results of SSGMRA Using a Fully Probabilistic Approach, SSGMRA Using an Equivalent Linear Approach, SSGMRA Using an Equivalent Linear Approach Plus and Minus One Standard Deviation, and AASHTO General Approach**

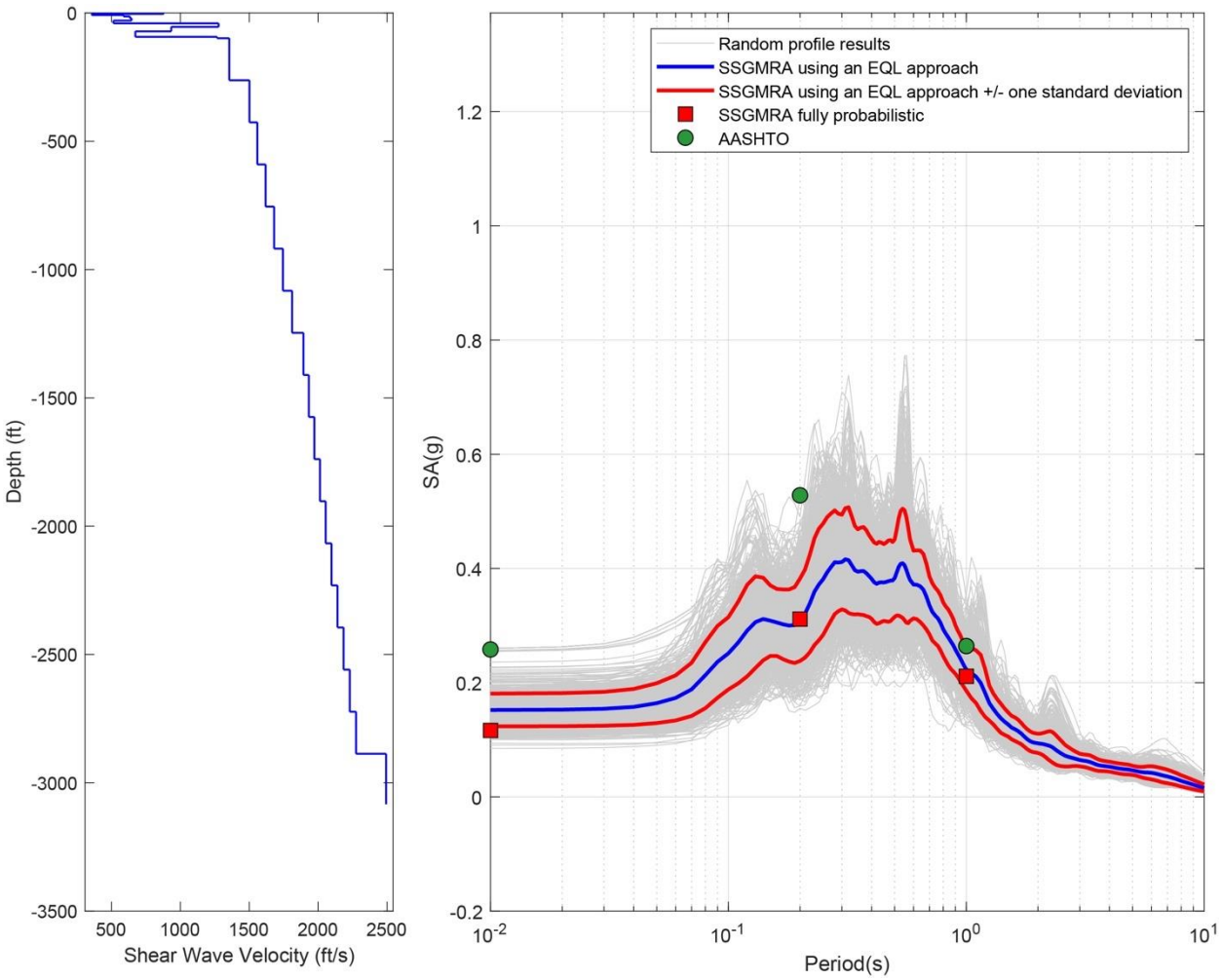


**Figure B-143. Left Panel: Shear-Wave Velocity Profile for Site 36 (Based on Peninsular Soil Model); and Right Panel: Results of SSGMRA Using a Fully Probabilistic Approach, SSGMRA Using an Equivalent Linear Approach, SSGMRA Using an Equivalent Linear Approach Plus and Minus One Standard Deviation, and AASHTO General Approach**

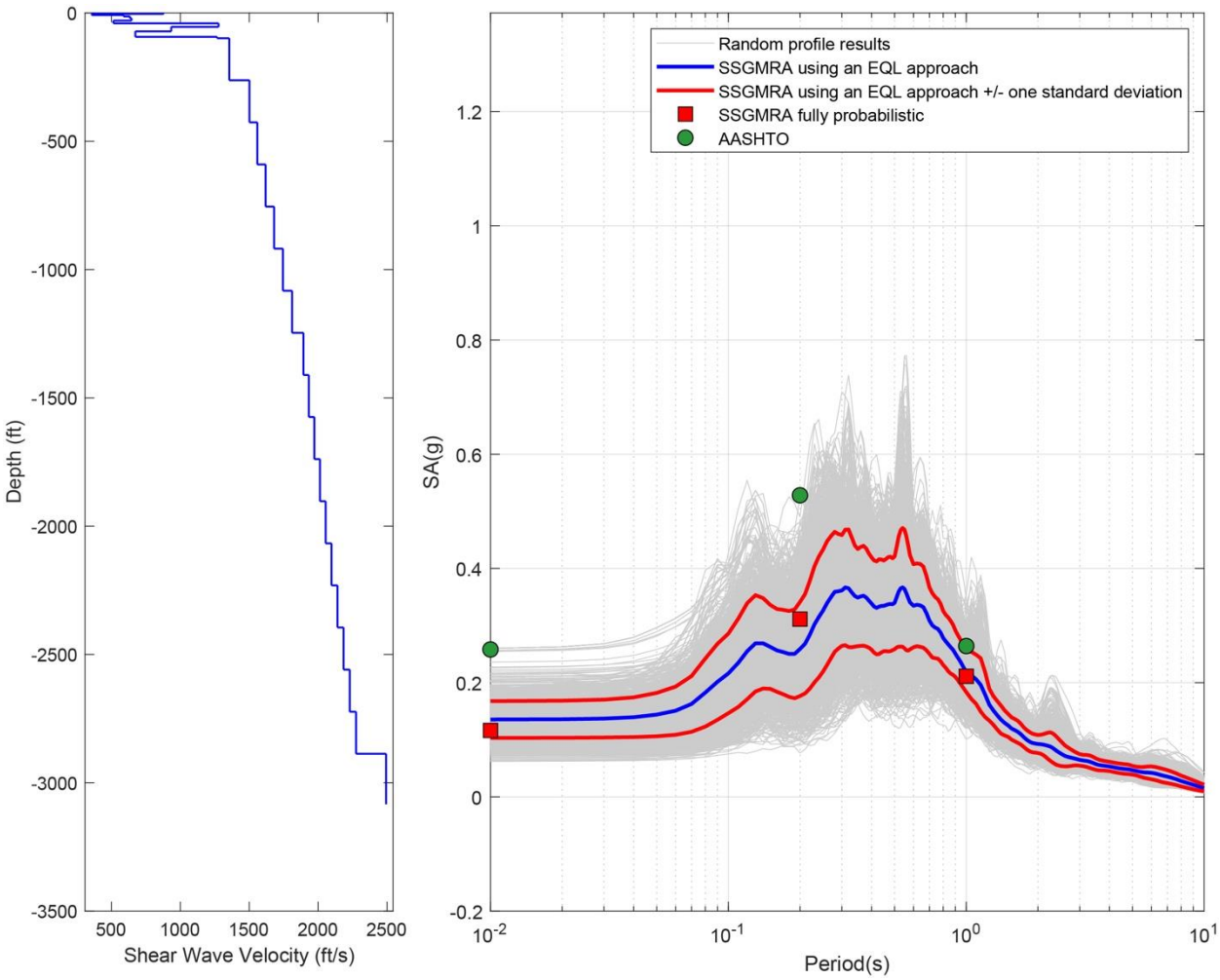


**Figure B-144. Left Panel: Shear-Wave Velocity Profile for Site 36 (Combined); and Right Panel: Results of SSGMRA Using a Fully Probabilistic Approach, SSGMRA Using an Equivalent Linear Approach, SSGMRA Using an Equivalent Linear Approach Plus and Minus One Standard Deviation, and AASHTO General Approach**

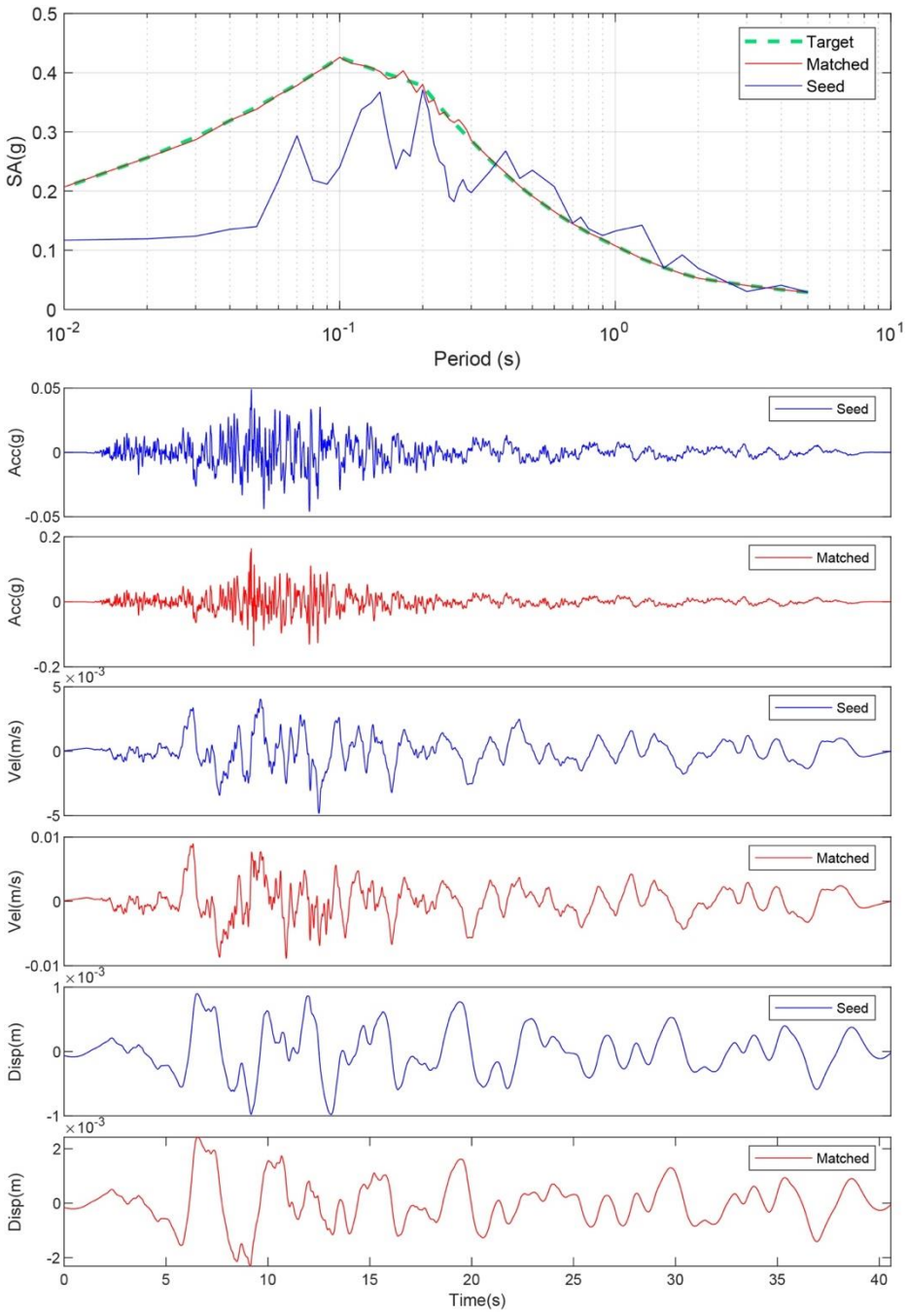


**Figure B-145. Matching Spectrum of Seed Motion (RSN774-LOMAP-HYN064) to the Target Spectrum (UHS) at Site 37. The Middle Subplot Shows the Seed Motion, and the Bottom Subplot Indicates the Matched Motion**

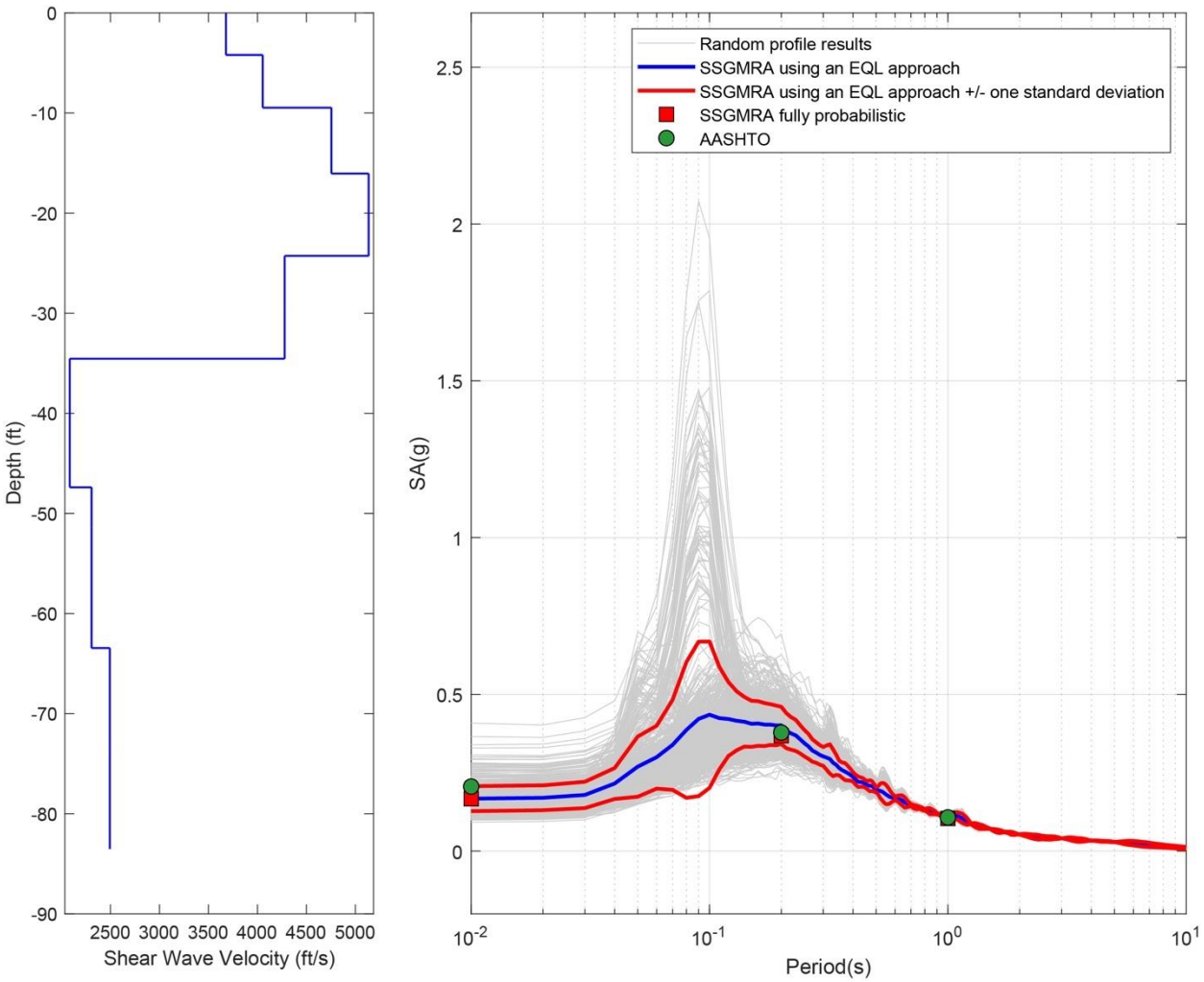


**Figure B-146. Left Panel: Shear-Wave Velocity Profile for Site 37 (Based on EPRI Soil Model); and Right Panel: Results of SSGMRA Using a Fully Probabilistic Approach, SSGMRA Using an Equivalent Linear Approach, SSGMRA Using an Equivalent Linear Approach Plus and Minus One Standard Deviation, and AASHTO General Approach**

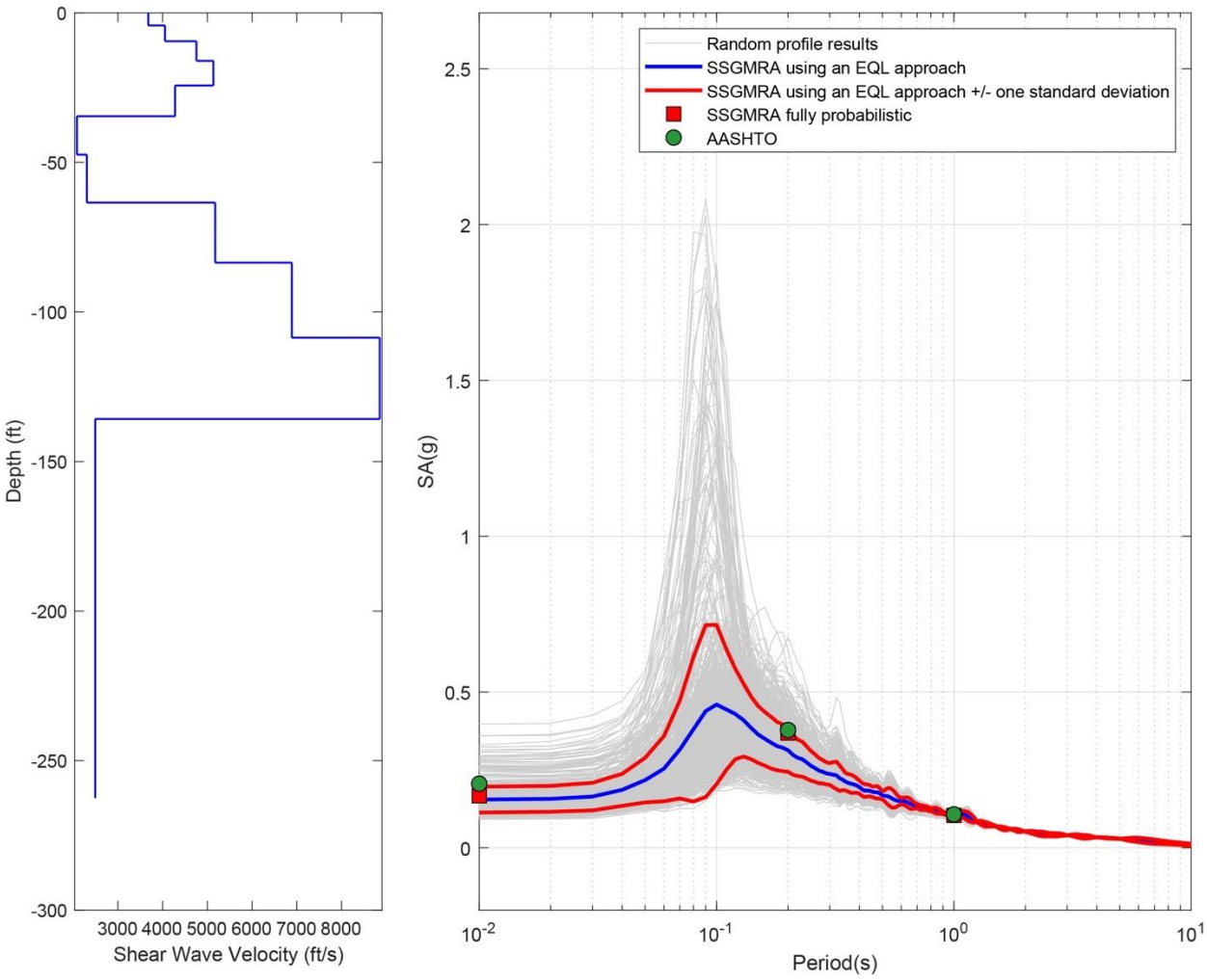


**Figure B-147. Left Panel: Shear-Wave Velocity Profile for Site 37 (Based on Peninsular Soil Model); and Right Panel: Results of SSGMRA Using a Fully Probabilistic Approach, SSGMRA Using an Equivalent Linear Approach, SSGMRA Using an Equivalent Linear Approach Plus and Minus One Standard Deviation, and AASHTO General Approach**

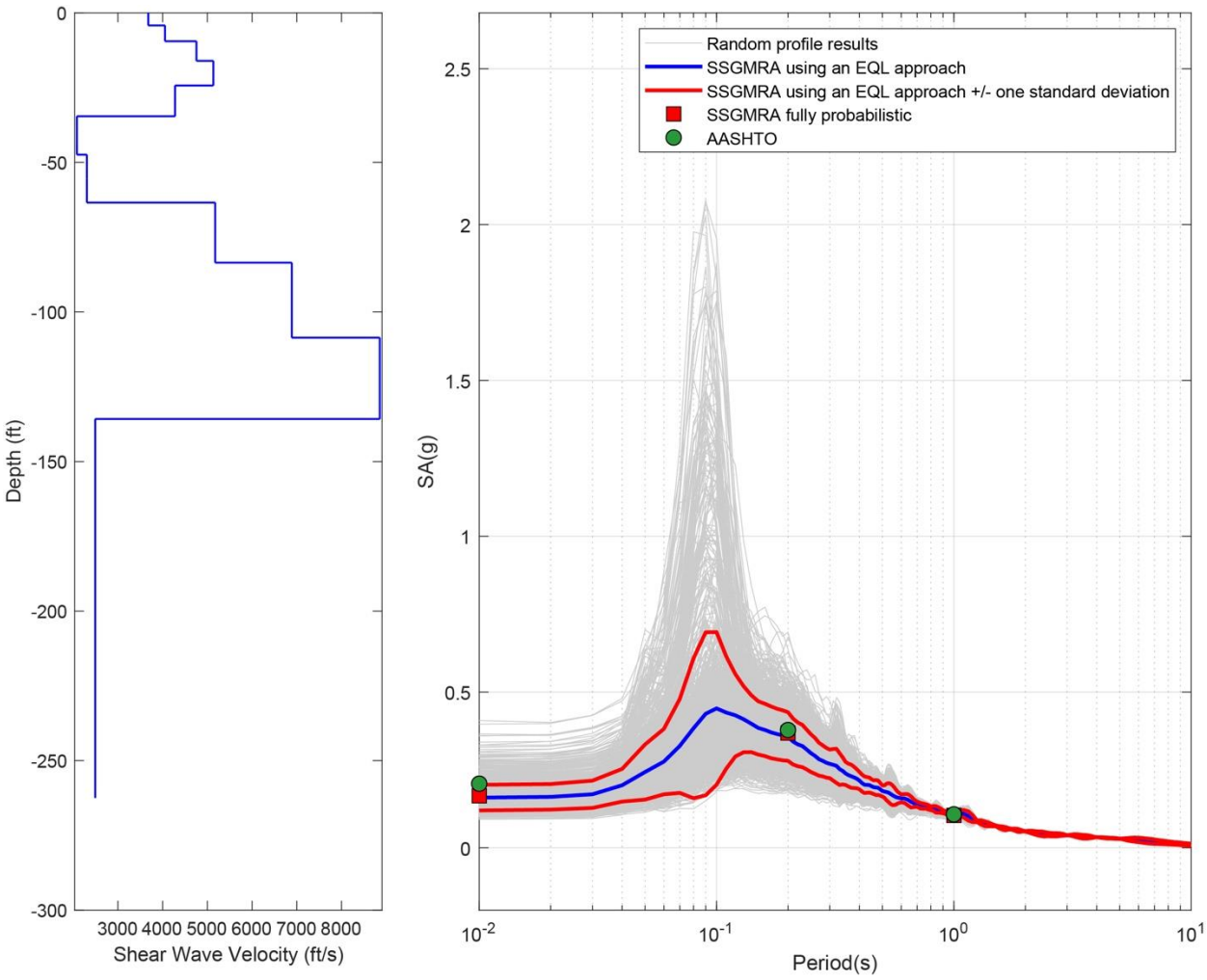


**Figure B-148. Left Panel: Shear-Wave Velocity Profile for Site 37 (Combined); and Right Panel: Results of SSGMRA Using a Fully Probabilistic Approach, SSGMRA Using an Equivalent Linear Approach, SSGMRA Using an Equivalent Linear Approach Plus and Minus One Standard Deviation, and AASHTO General Approach**

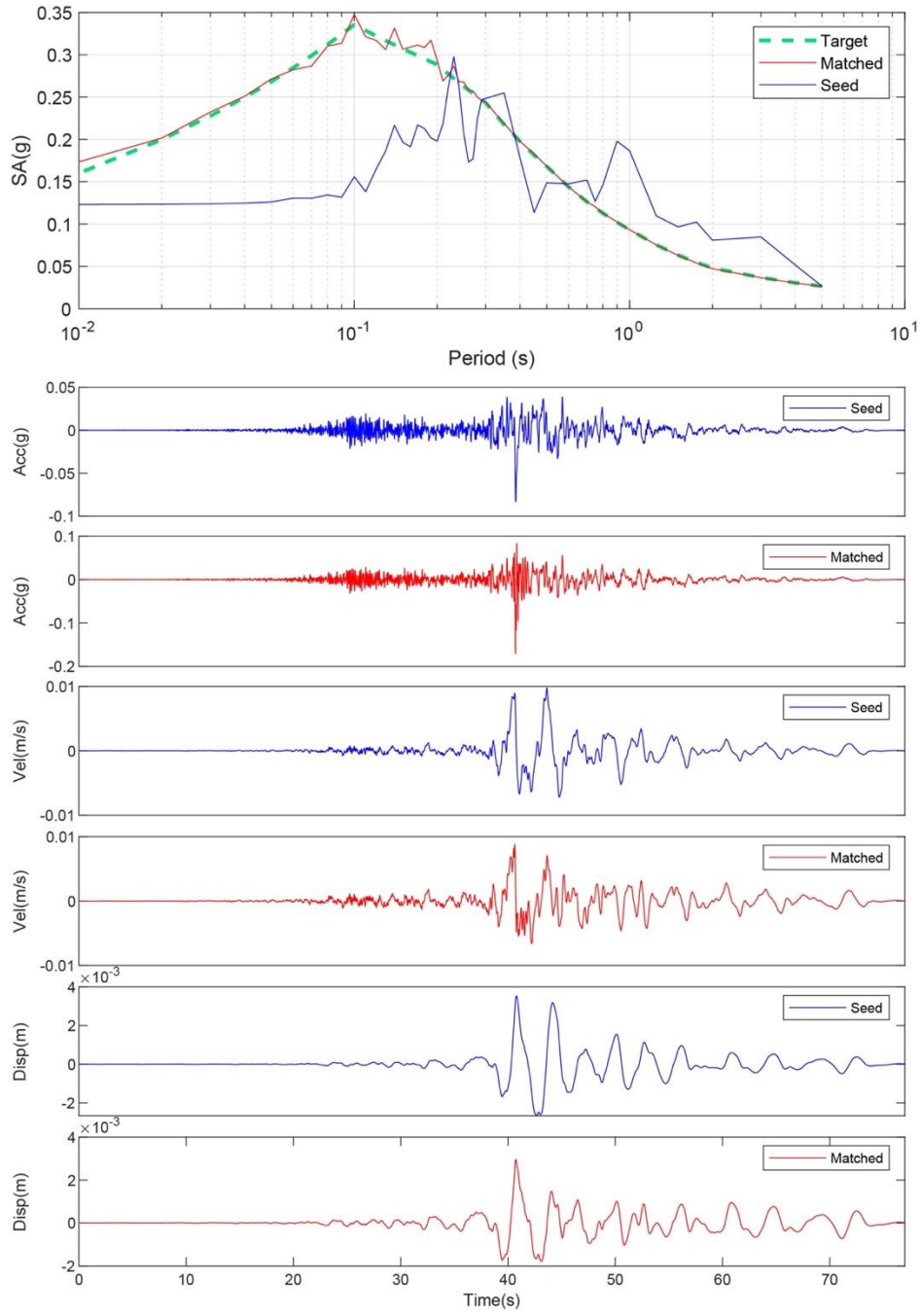


**Figure B-149. Matching Spectrum of Seed Motion (RSN1432-CHICHI-TAP046-E) to the Target Spectrum (UHS) at Site 38. The Middle Subplot Shows the Seed Motion, and the Bottom Subplot Indicates the Matched Motion**

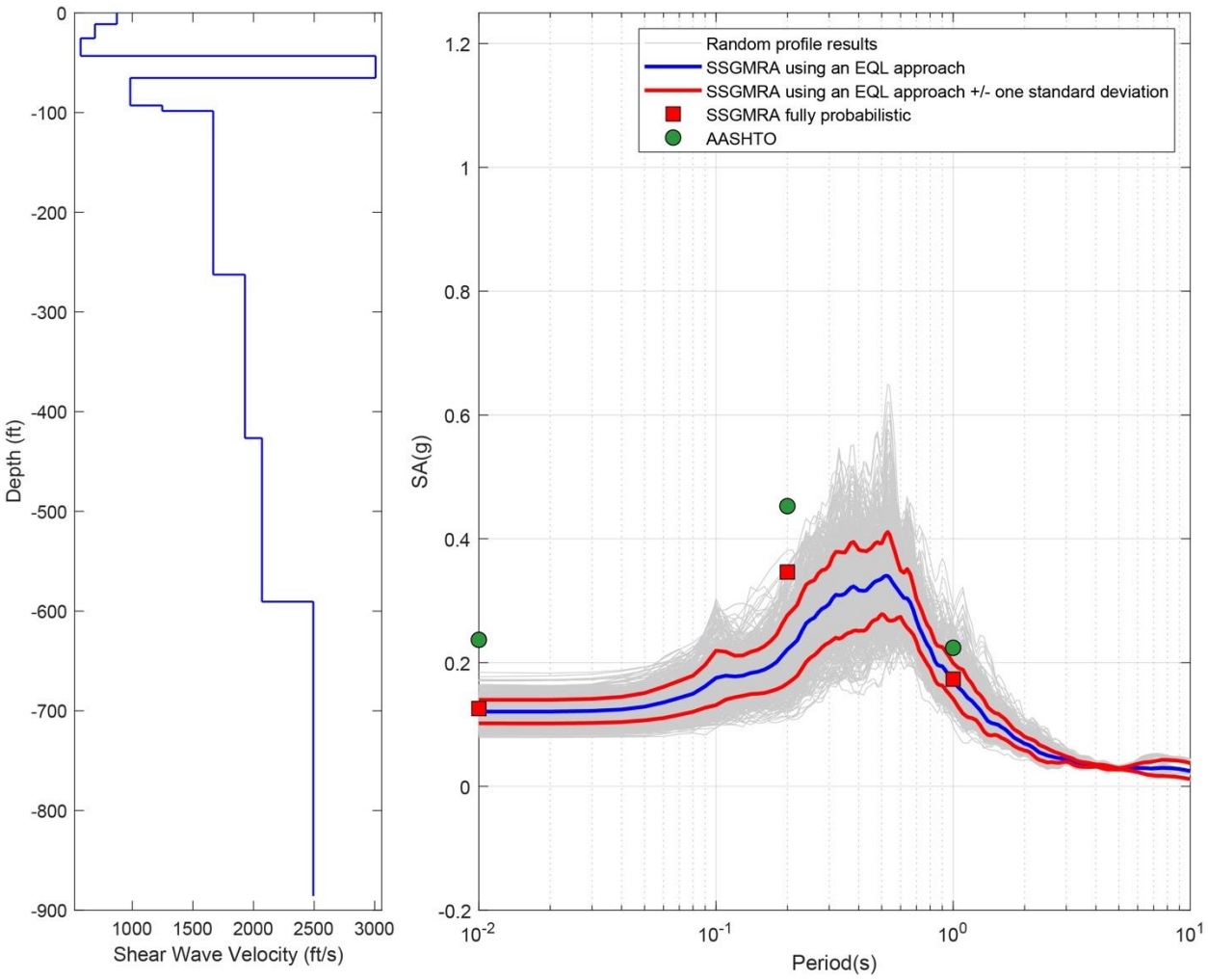


**Figure B-150. Left Panel: Shear-Wave Velocity Profile for Site 38 (Based on EPRI Soil Model); and Right Panel: Results of SSGMRA Using a Fully Probabilistic Approach, SSGMRA Using an Equivalent Linear Approach, SSGMRA Using an Equivalent Linear Approach Plus and Minus One Standard Deviation, and AASHTO General Approach**

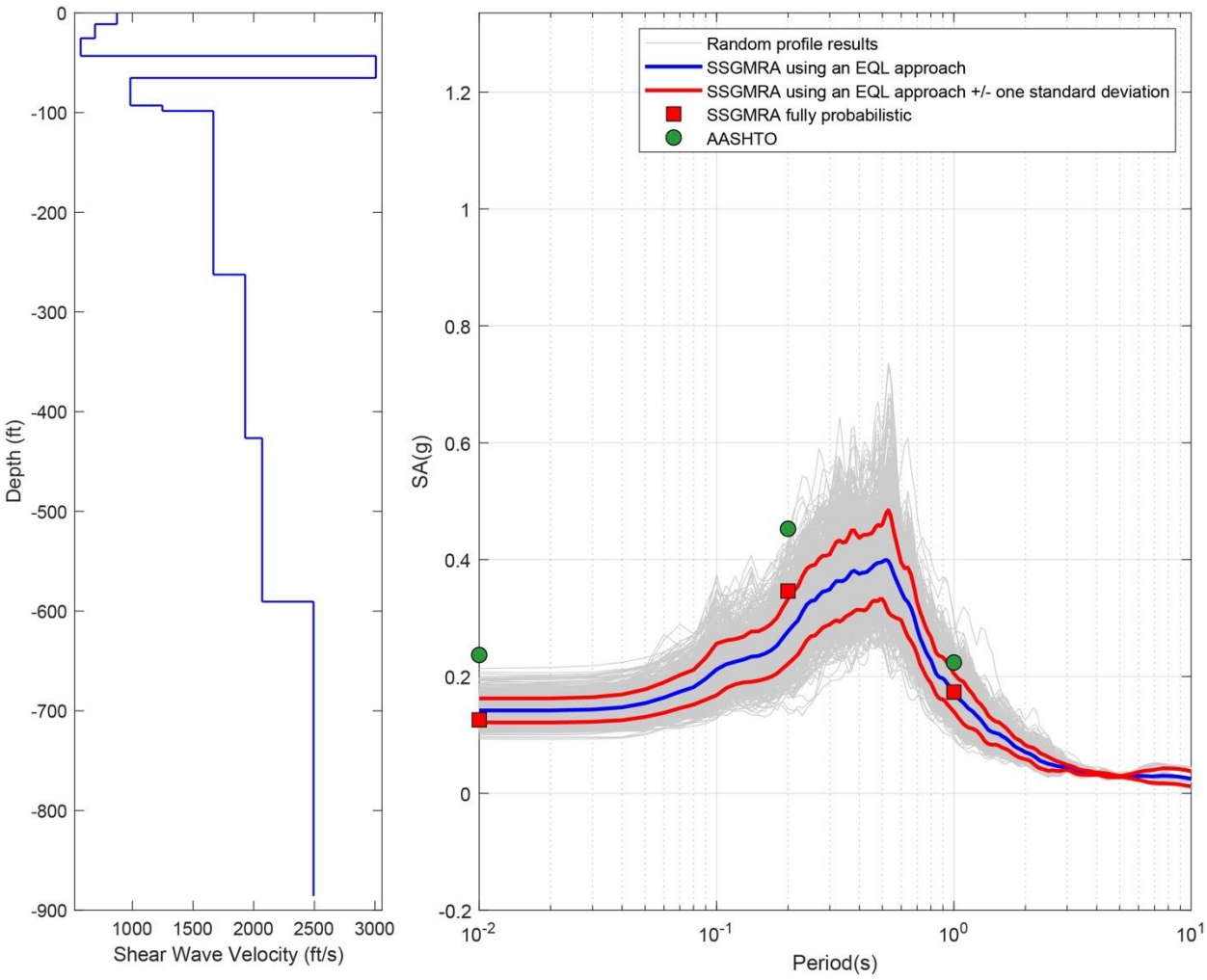


**Figure B-151. Left Panel: Shear-Wave Velocity Profile for Site 38 (Based on Peninsular Soil Model); and Right Panel: Results of SSGMRA Using a Fully Probabilistic Approach, SSGMRA Using an Equivalent Linear Approach, SSGMRA Using an Equivalent Linear Approach Plus and Minus One Standard Deviation, and AASHTO General Approach**

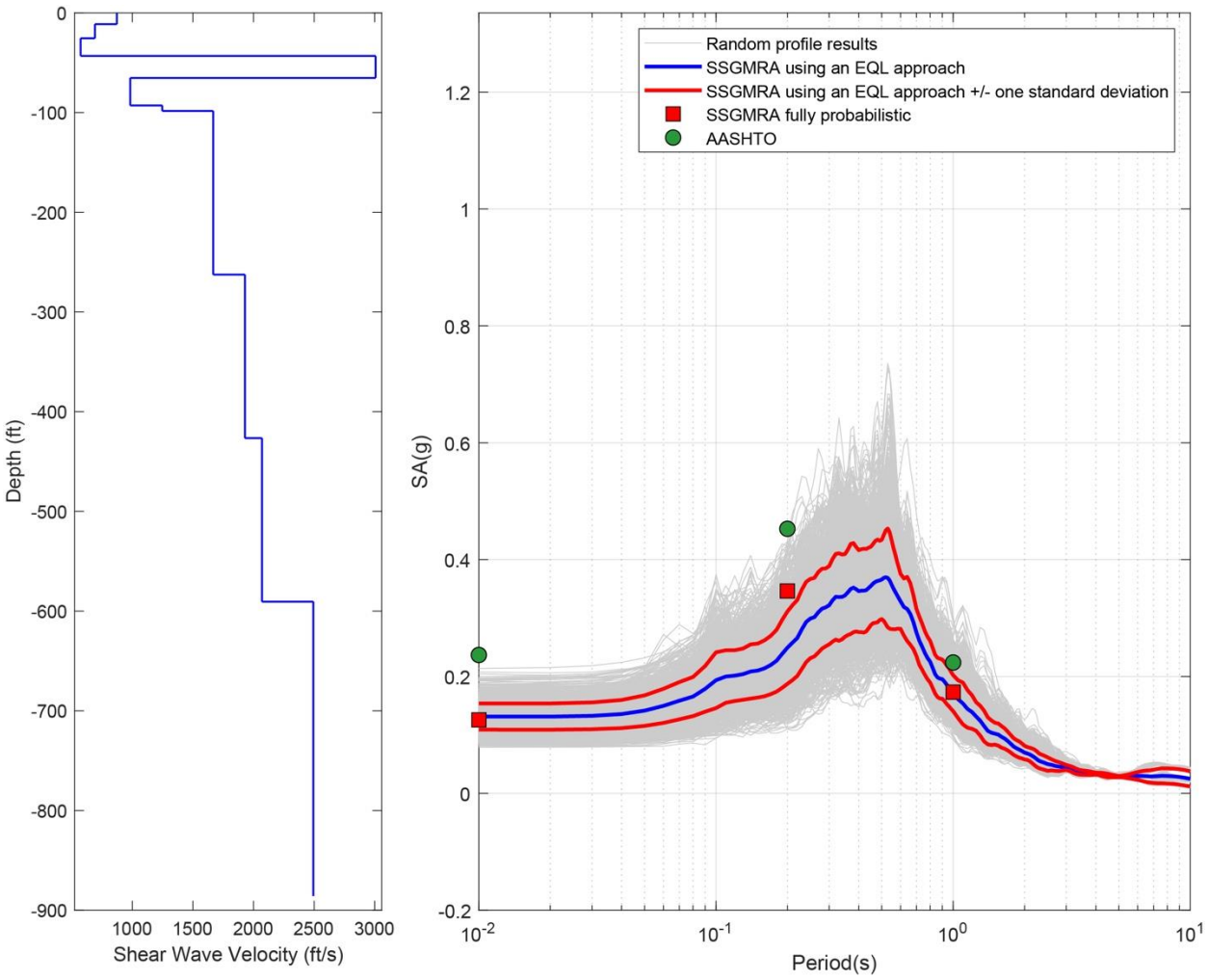


**Figure B-152. Left Panel: Shear-Wave Velocity Profile for Site 38 (Combined); and Right Panel: Results of SSGMRA Using a Fully Probabilistic Approach, SSGMRA Using an Equivalent Linear Approach, SSGMRA Using an Equivalent Linear Approach Plus and Minus One Standard Deviation, and AASHTO General Approach**

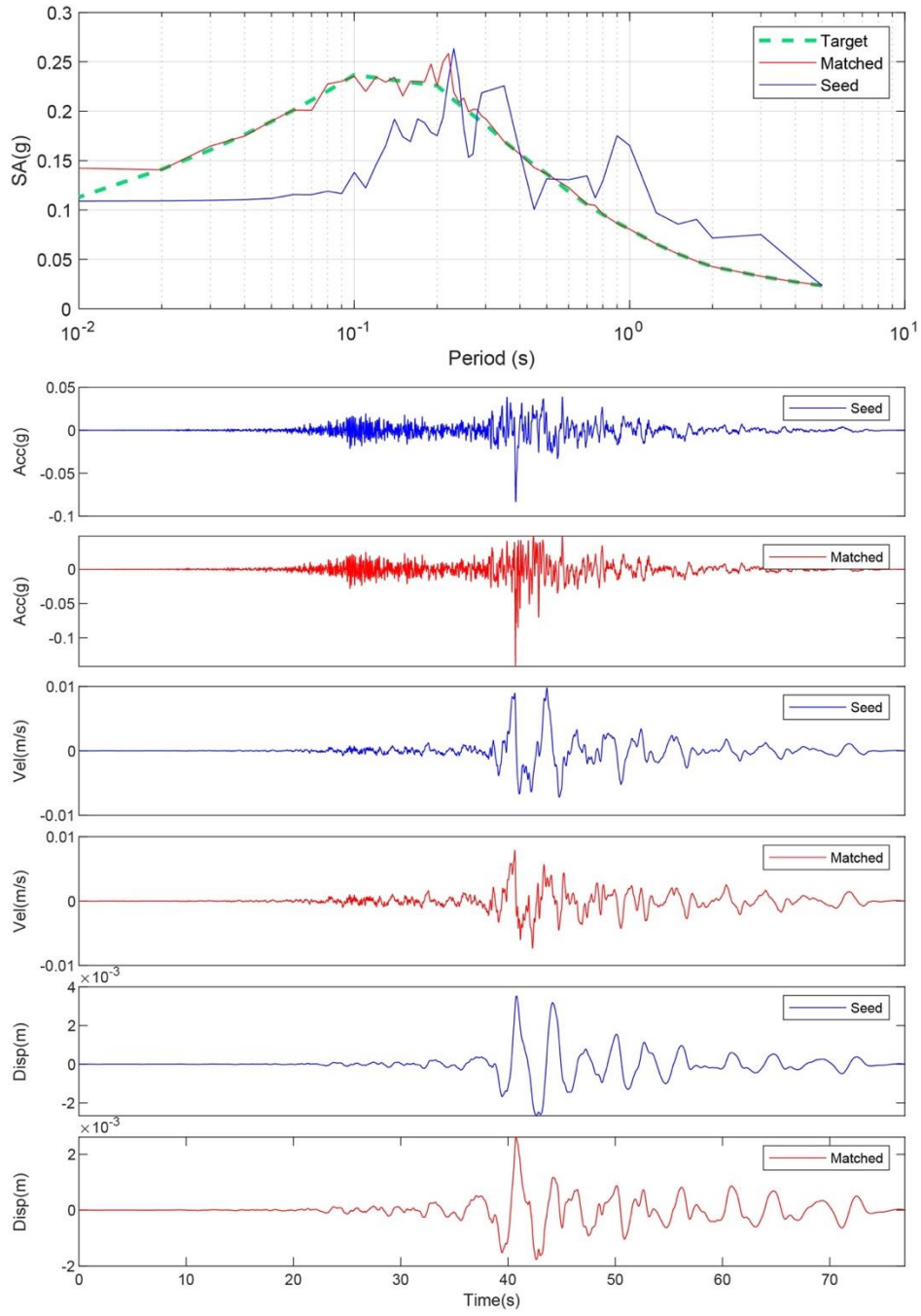


**Figure B-153. Matching Spectrum of Seed Motion (RSN1432-CHICHI-TAP046-E) to the Target Spectrum (UHS) at Site 39. The Middle Subplot Shows the Seed Motion, and the Bottom Subplot Indicates the Matched Motion**

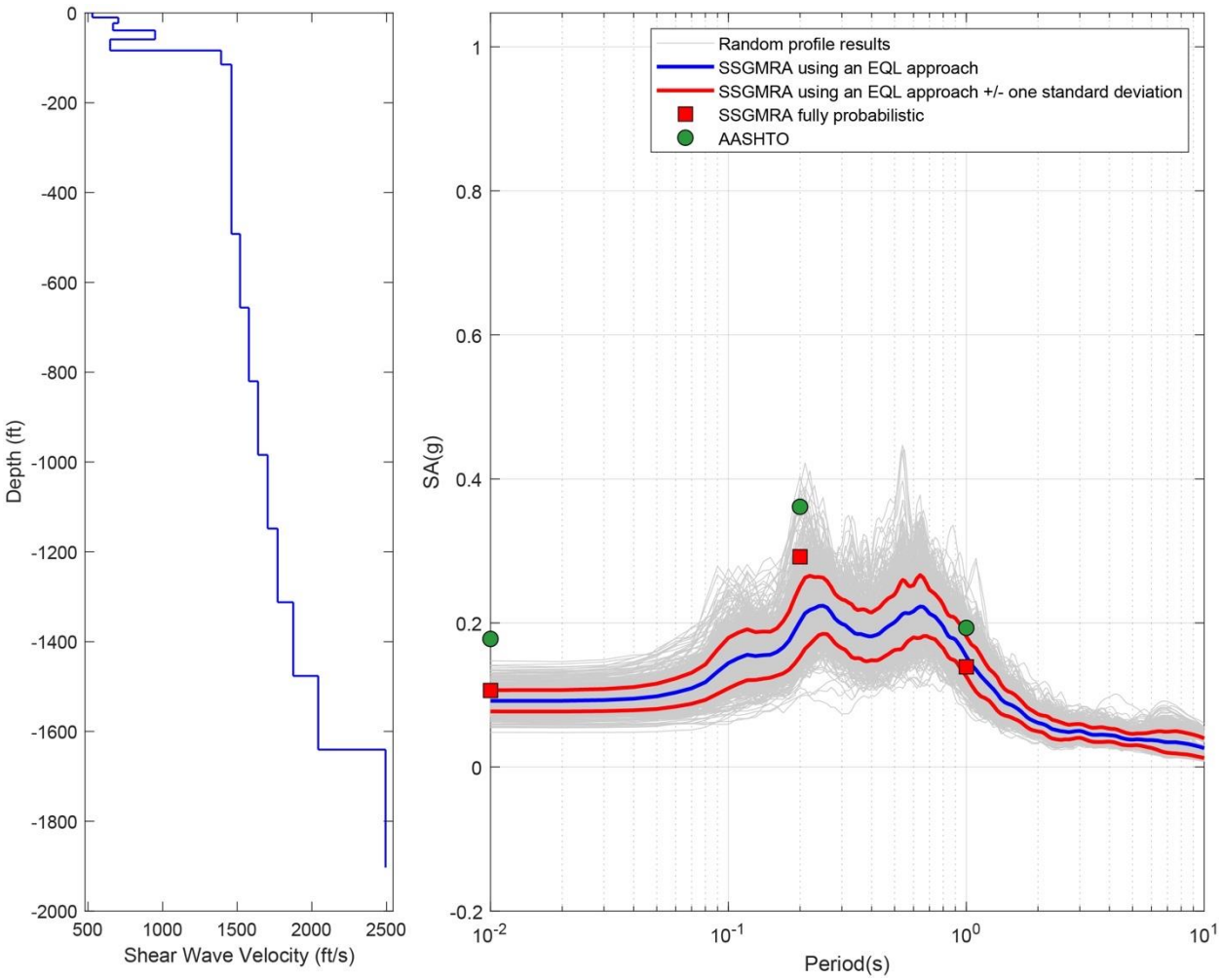


**Figure B-154. Left Panel: Shear-Wave Velocity Profile for Site 39 (Based on EPRI Soil Model); and Right Panel: Results of SSGMRA Using a Fully Probabilistic Approach, SSGMRA Using an Equivalent Linear Approach, SSGMRA Using an Equivalent Linear Approach Plus and Minus One Standard Deviation, and AASHTO General Approach**

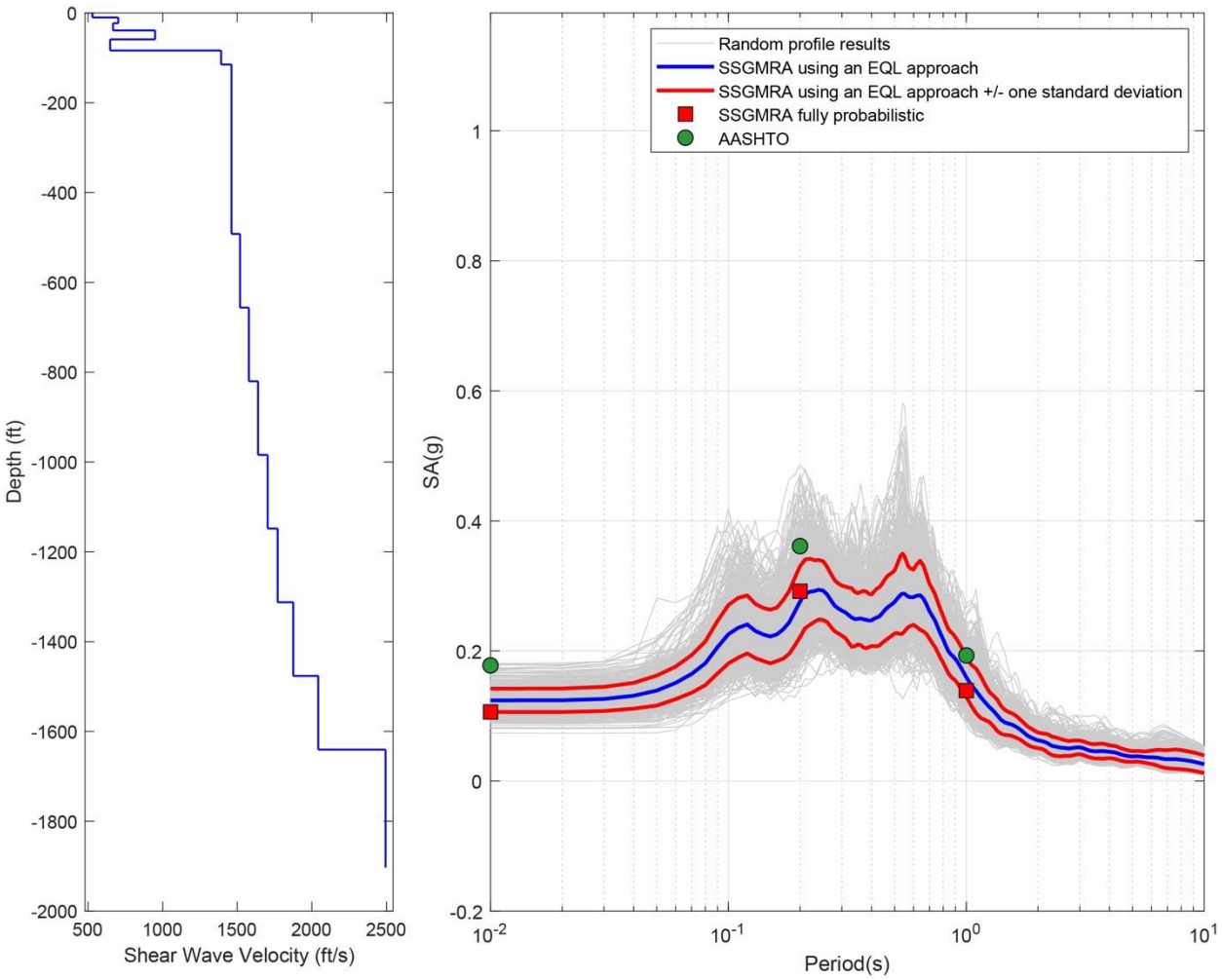


**Figure B-155. Left panel: Shear-wave velocity profile for Site 39 (Based on Peninsular soil model); and Right Panel: results of SSGMRA using a fully probabilistic approach, SSGMRA using an equivalent linear approach, SSGMRA using an equivalent linear approach plus and minus one standard deviation, and AASHTO general approach**

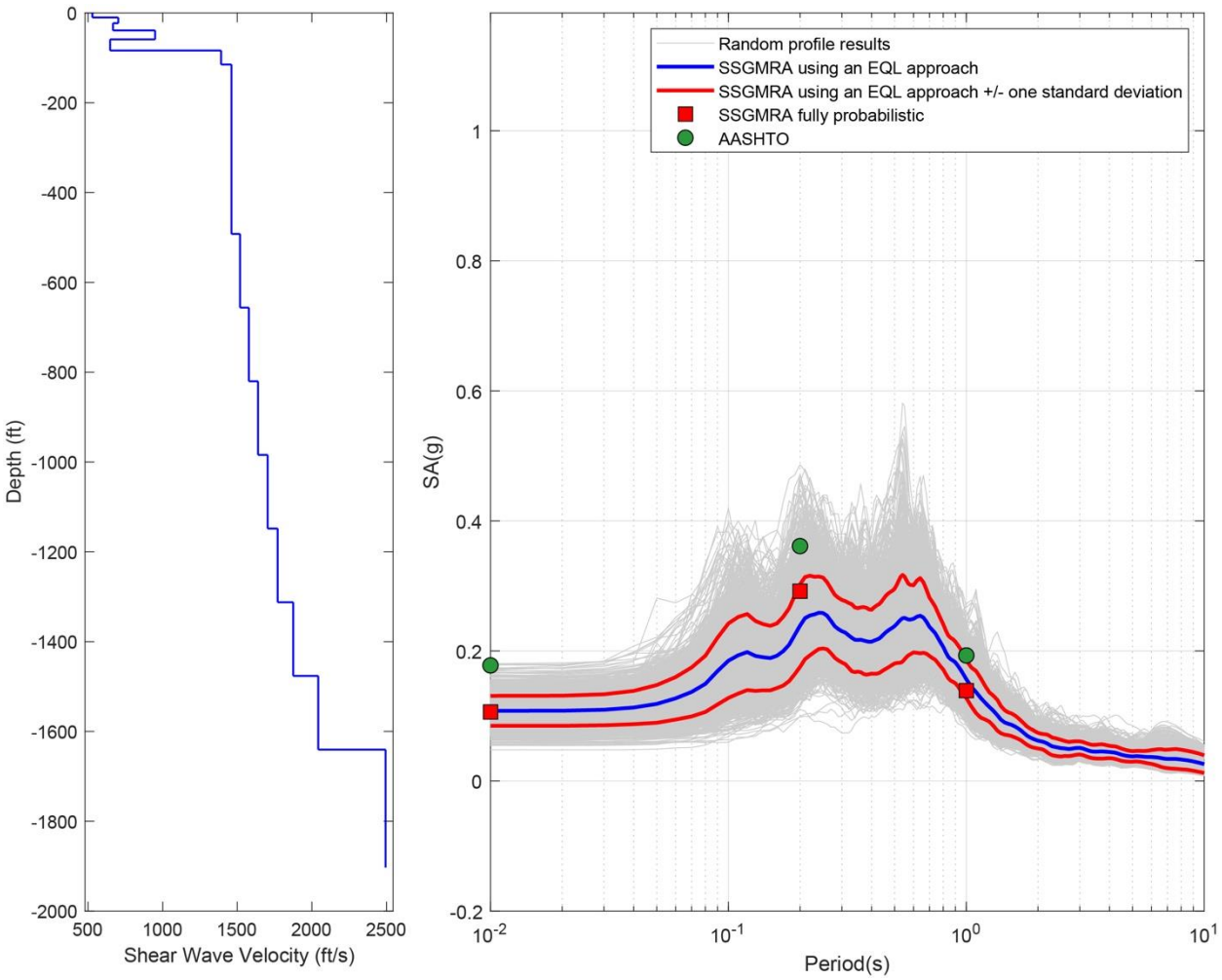


**Figure B-156. Left Panel: Shear-Wave Velocity Profile for Site 39(Combined); and Right Panel: Results of SSGMRA Using a Fully Probabilistic Approach, SSGMRA Using an Equivalent Linear Approach, SSGMRA Using an Equivalent Linear Approach Plus and Minus One Standard Deviation, and AASHTO General Approach**

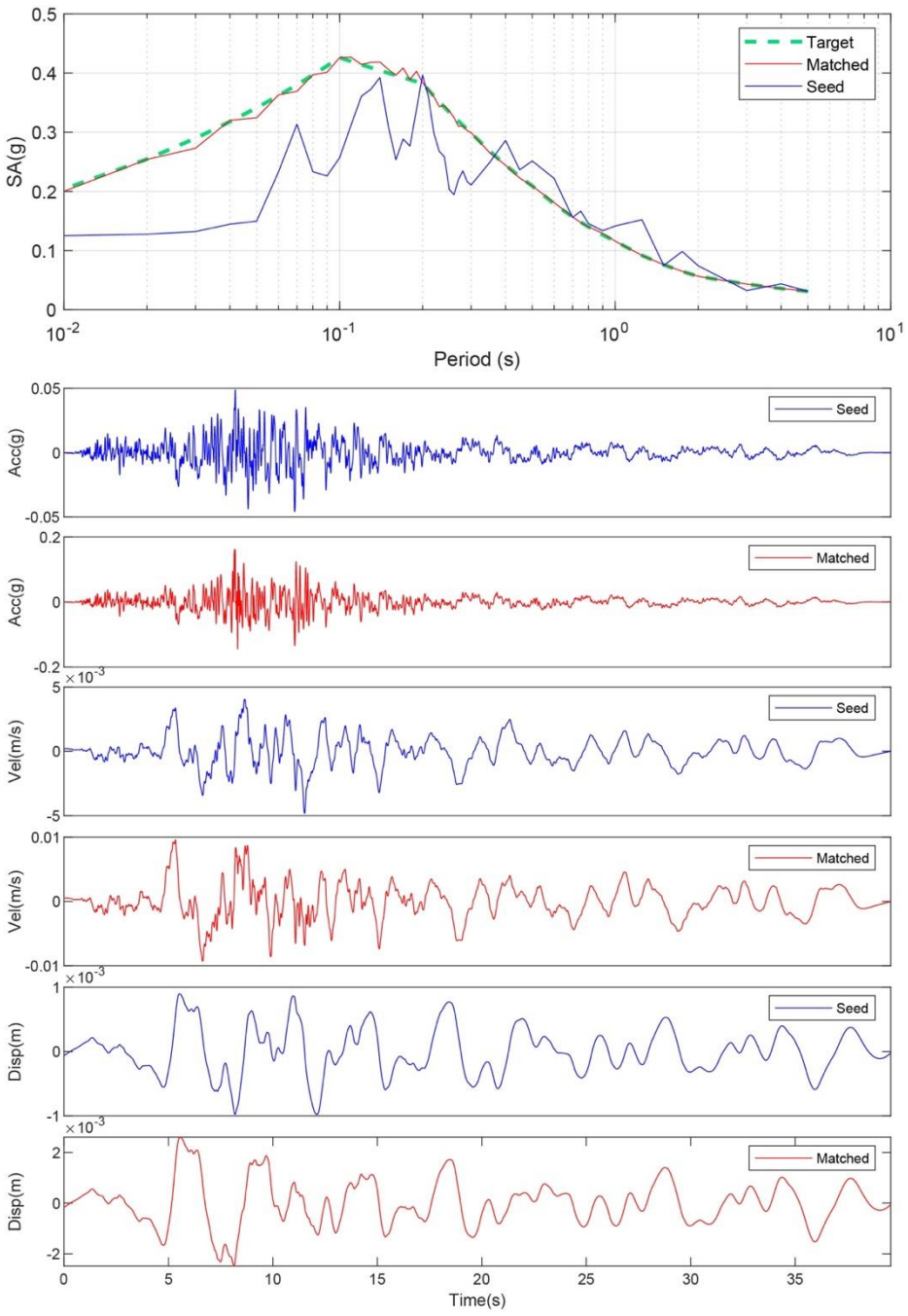


**Figure B-157. Matching Spectrum of Seed Motion (RSN774-LOMAP-HYN064) to the Target Spectrum (UHS) at Site 40. The Middle Subplot Shows the Seed Motion, and the Bottom Subplot Indicates the Matched Motion**

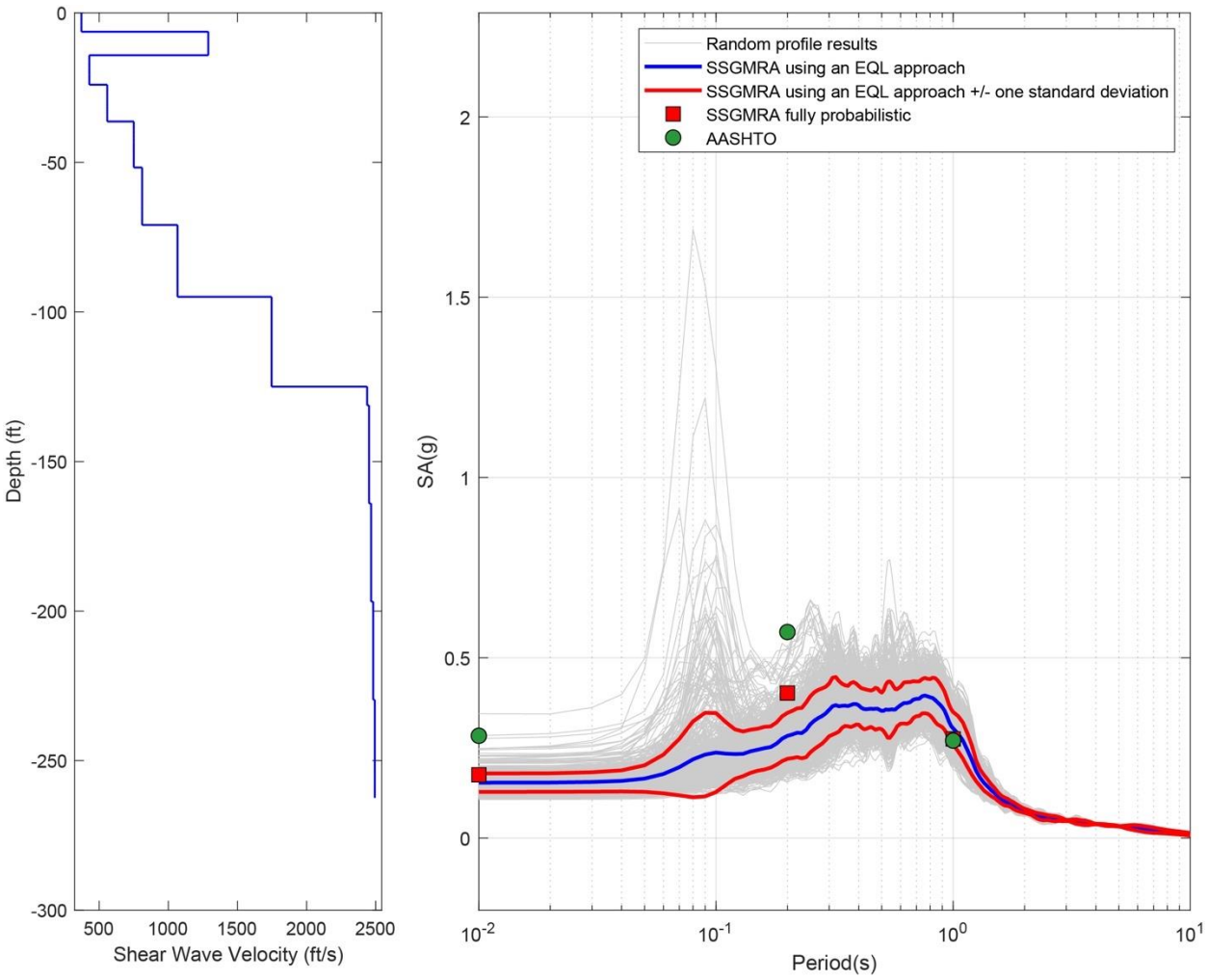


**Figure B-158. Left Panel: Shear-Wave Velocity Profile for Site 40 (Based on EPRI Soil Model); and Right Panel: Results of SSGMRA Using a Fully Probabilistic Approach, SSGMRA Using an Equivalent Linear Approach, SSGMRA Using an Equivalent Linear Approach Plus and Minus One Standard Deviation, and AASHTO General Approach**

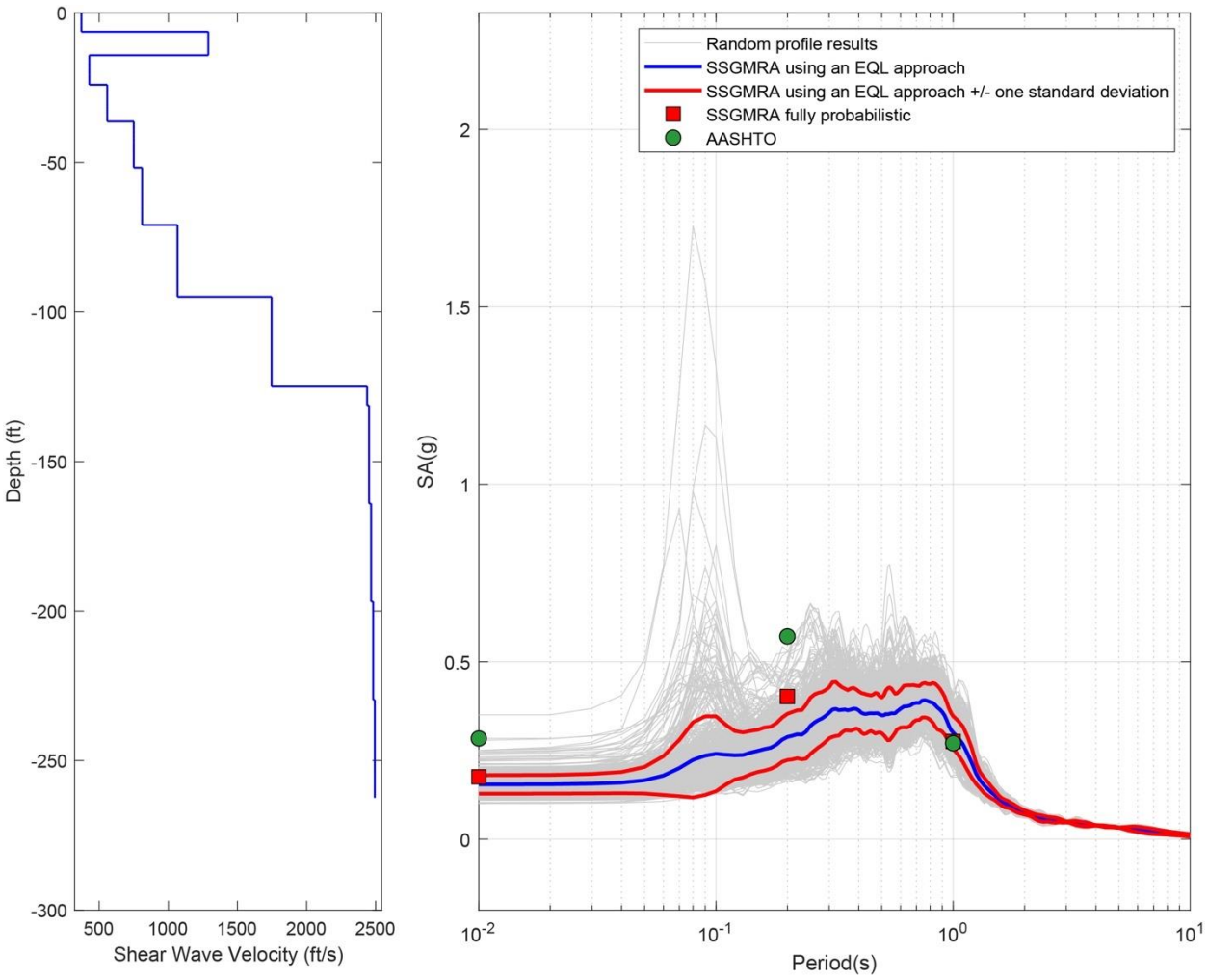


**Figure B-159. Left Panel: Shear-Wave Velocity Profile for Site 40 (Based on Peninsular Soil Model); and Right Panel: Results of SSGMRA Using a Fully Probabilistic Approach, SSGMRA Using an Equivalent Linear Approach, SSGMRA Using an Equivalent Linear Approach Plus and Minus One Standard Deviation, and AASHTO General Approach**

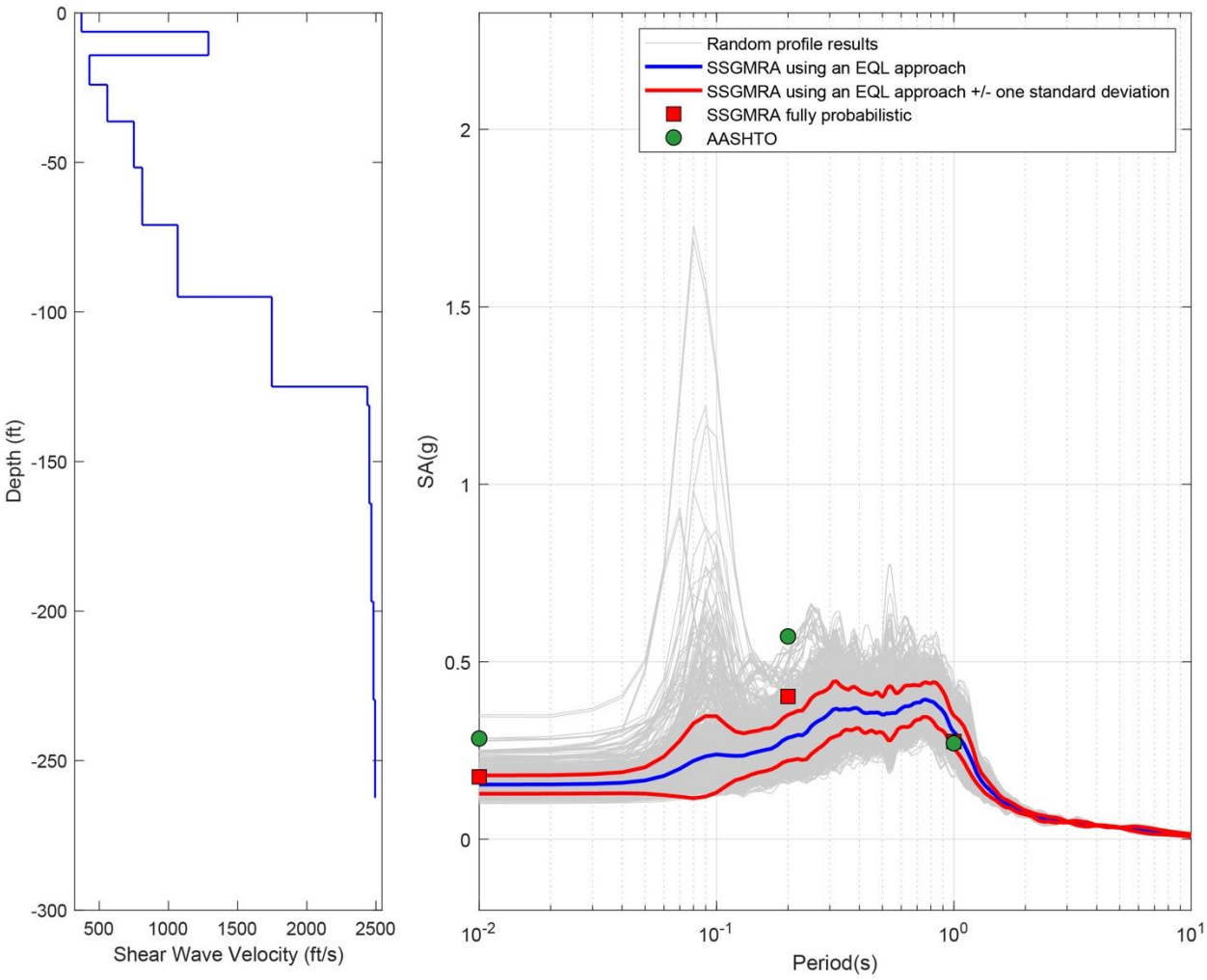


**Figure B-160. Left Panel: Shear-Wave Velocity Profile for Site 40 (Combined); and Right Panel: Results of SSGMRA Using a Fully Probabilistic Approach, SSGMRA Using an Equivalent Linear Approach, SSGMRA Using an Equivalent Linear Approach Plus and Minus One Standard Deviation, and AASHTO General Approach**

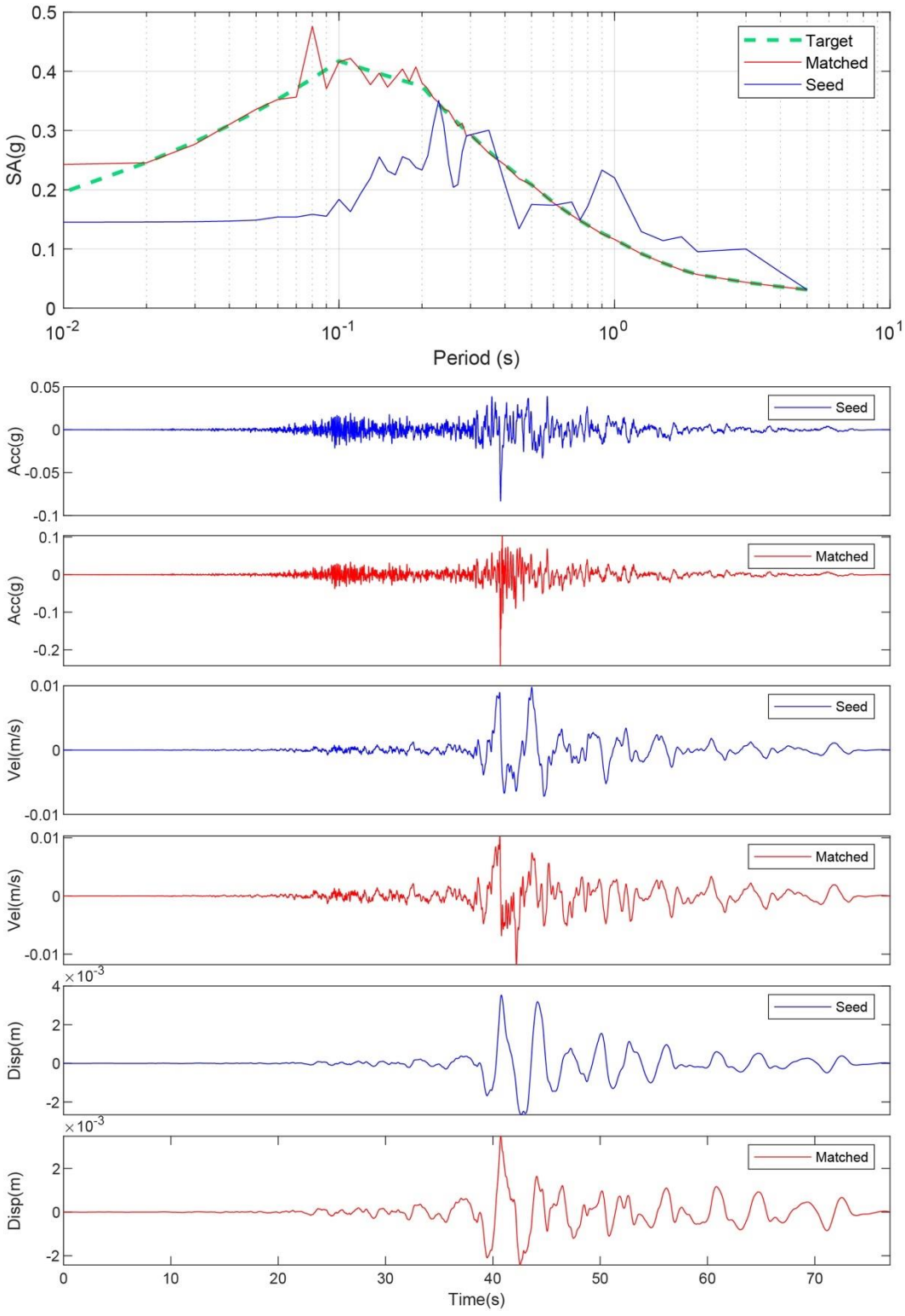


**Figure B-161. Matching Spectrum of Seed Motion (RSN1432-CHICHI-TAP046-E) to the Target Spectrum (UHS) at Site 41. The Middle Subplot Shows the Seed Motion, and The Bottom Subplot Indicates the Matched Motion**

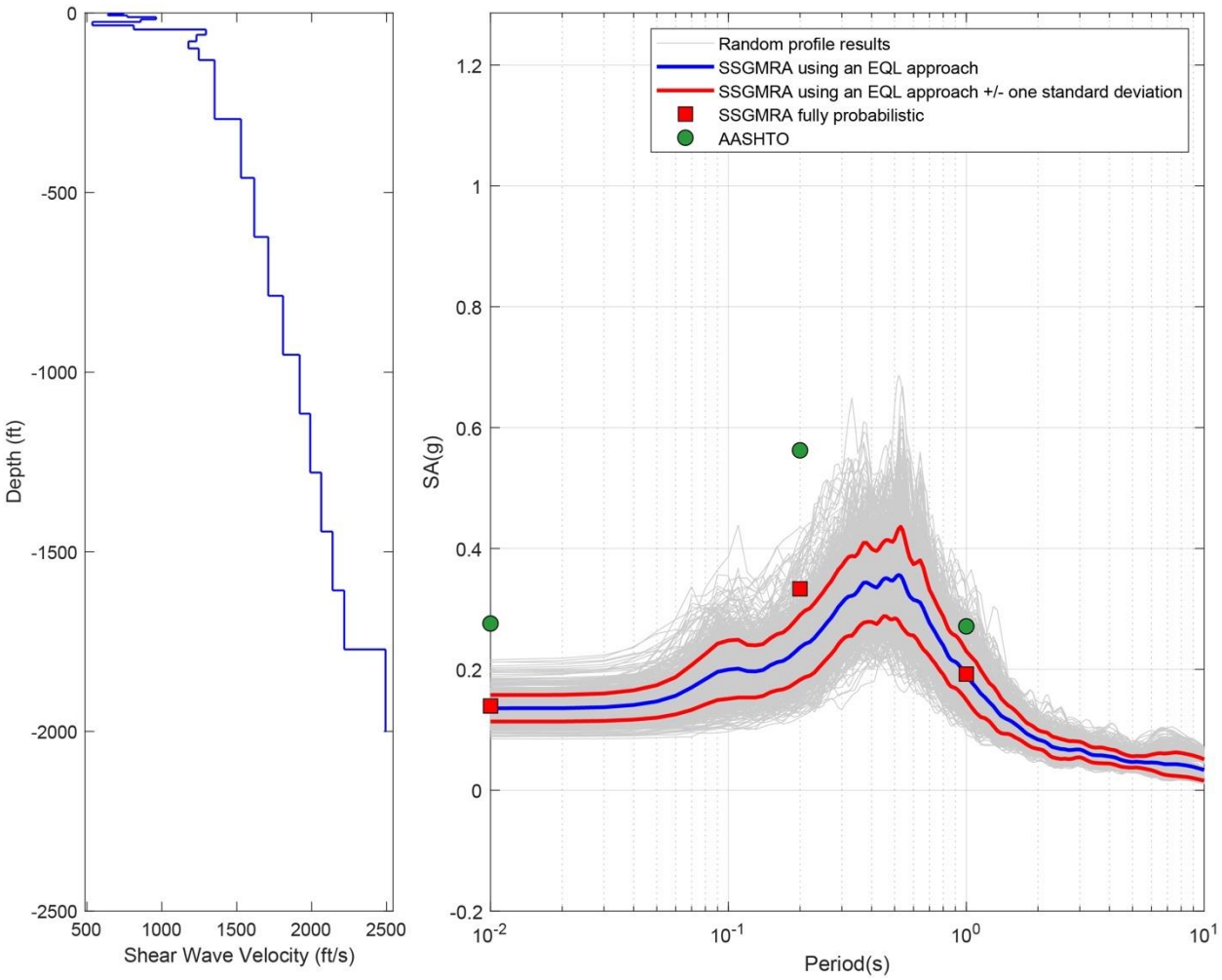


**Figure B-162. Left Panel: Shear-Wave Velocity Profile for Site 41 (Based on EPRI Soil Model); and Right Panel: Results of SSGMRA Using a Fully Probabilistic Approach, SSGMRA Using an Equivalent Linear Approach, SSGMRA Using an Equivalent Linear Approach Plus and Minus One Standard Deviation, and AASHTO General Approach**

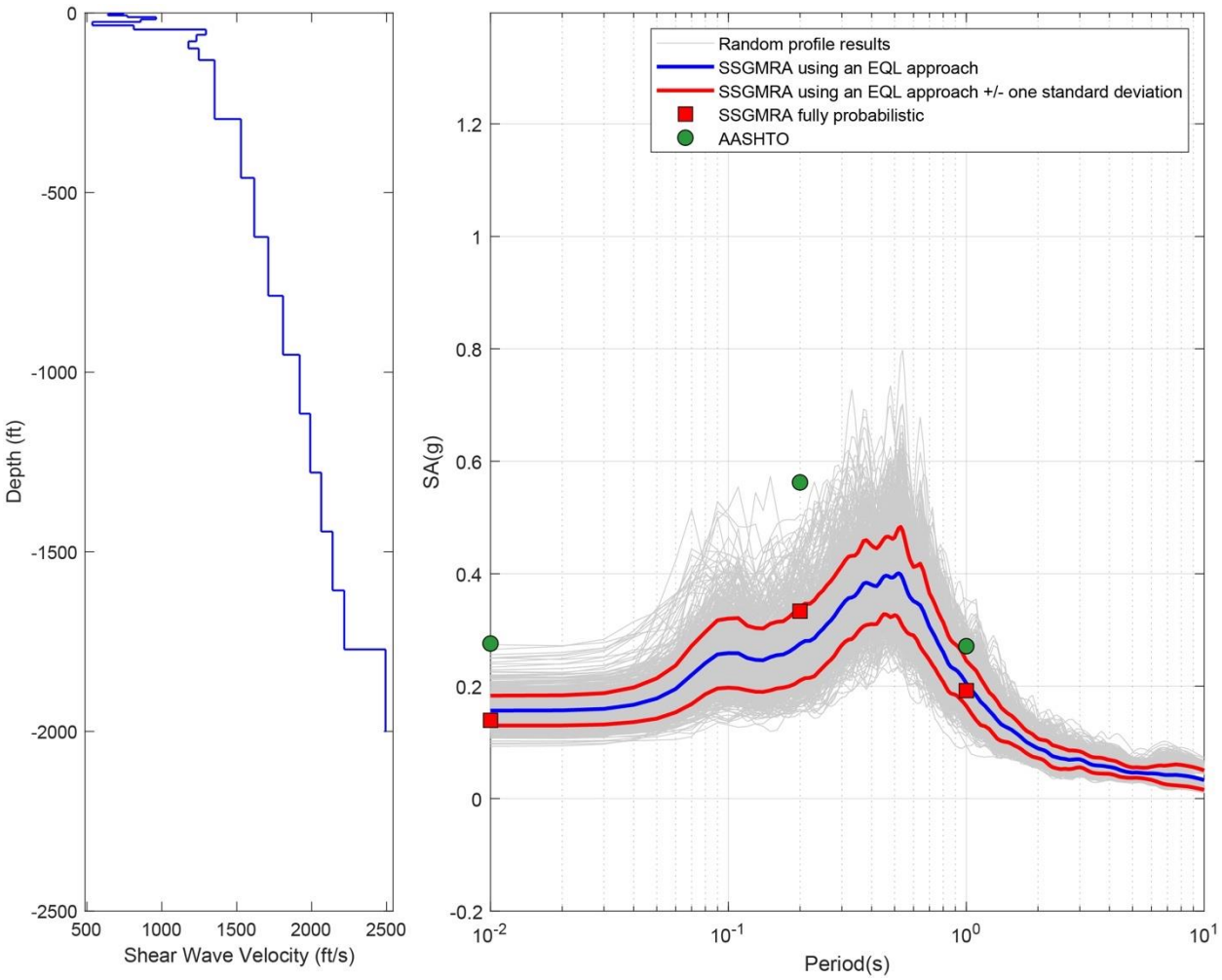


**Figure B-163. Left Panel: Shear-Wave Velocity Profile for Site 41 (Based on Peninsular Soil Model); and Right Panel: Results of SSGMRA Using a Fully Probabilistic Approach, SSGMRA Using an Equivalent Linear Approach, SSGMRA Using an Equivalent Linear Approach Plus and Minus One Standard Deviation, and AASHTO General Approach**

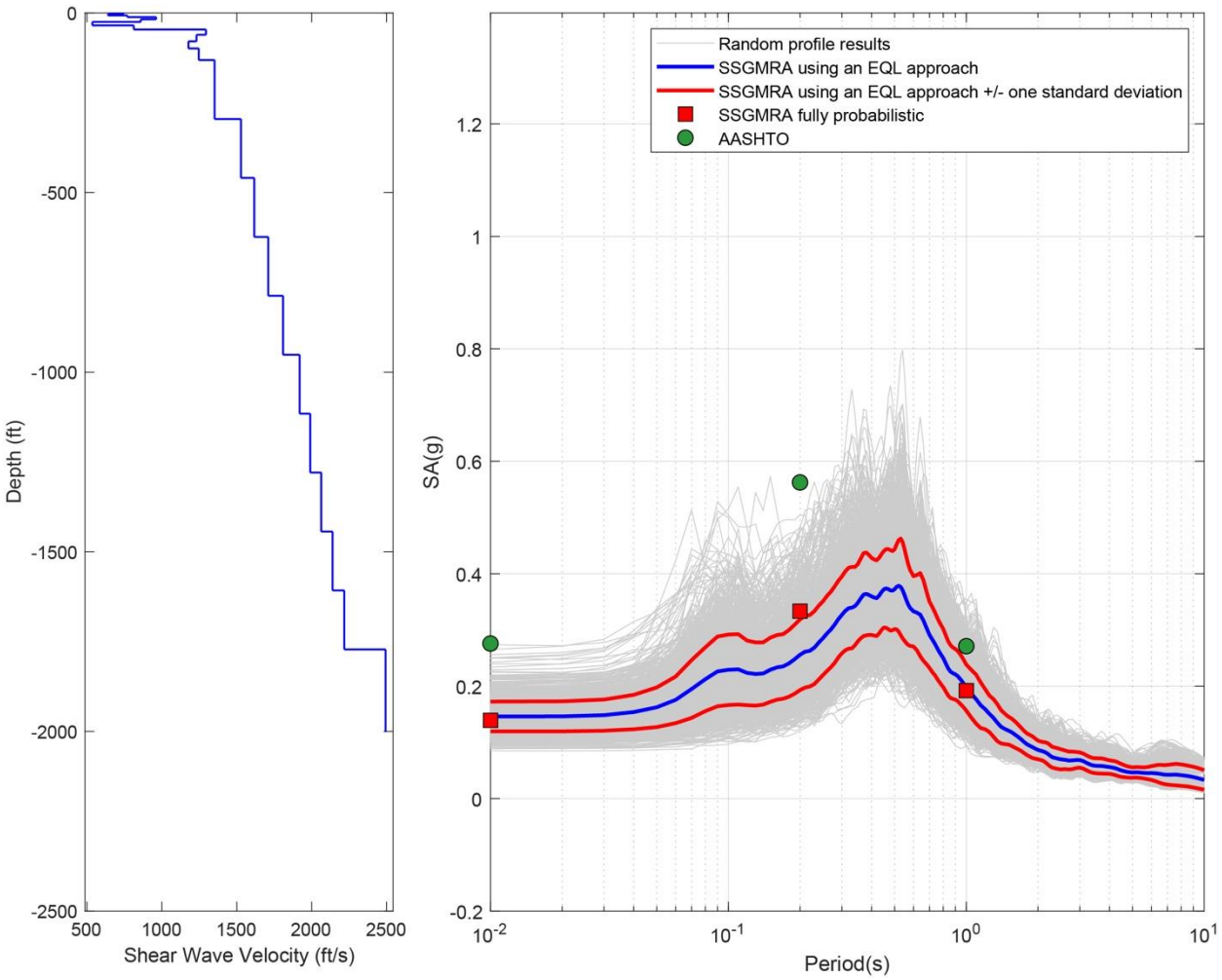


**Figure B-164. Left Panel: Shear-Wave Velocity Profile for Site 41 (Combined); and Right Panel: Results of SSGMRA Using a Fully Probabilistic Approach, SSGMRA Using an Equivalent Linear Approach, SSGMRA Using an Equivalent Linear Approach Plus and Minus One Standard Deviation, and AASHTO General Approach**

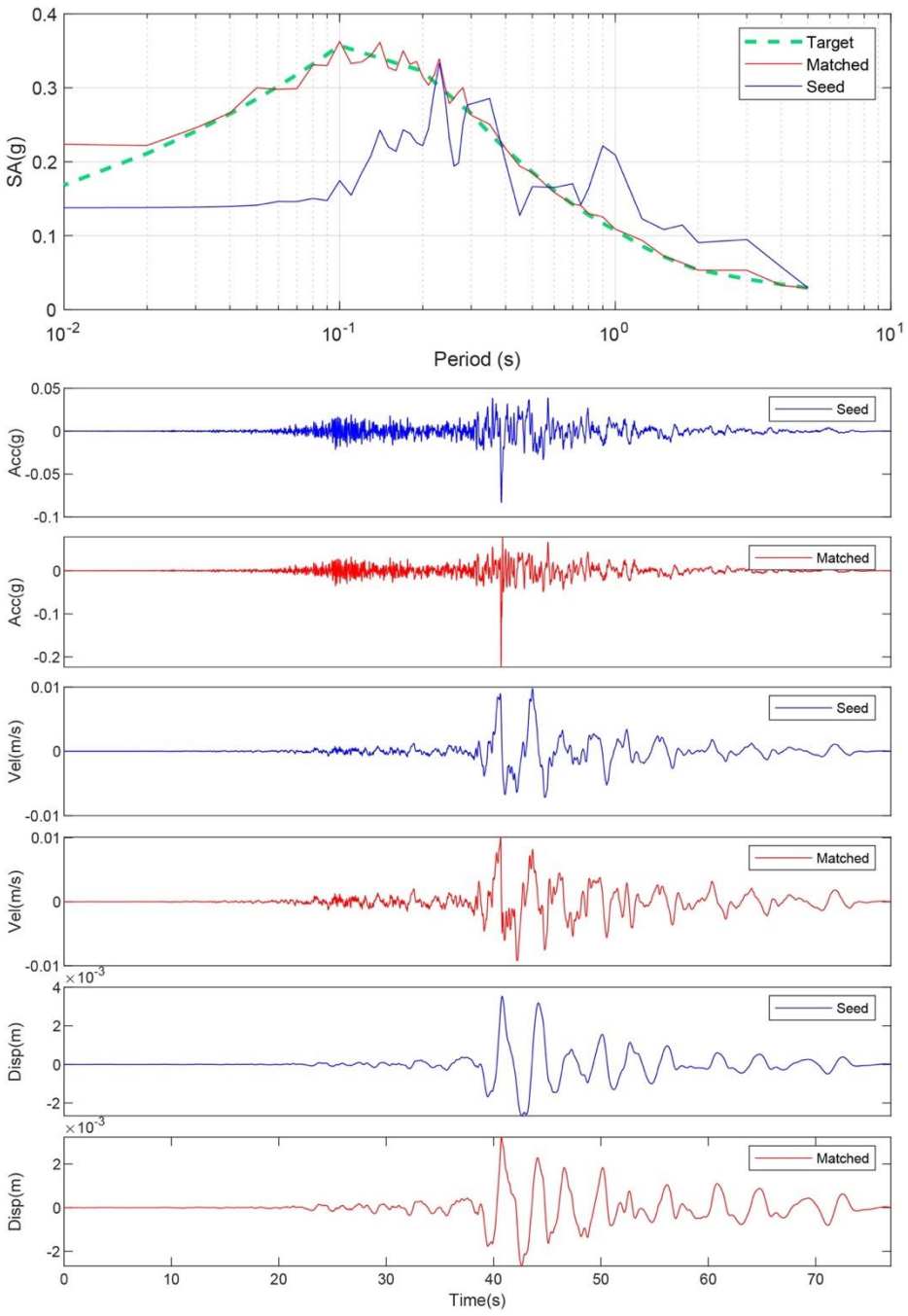


**Figure B-165. Matching Spectrum of Seed Motion (RSN1432-CHICHI-TAP046-E) to the Target Spectrum (UHS) at Site 42. The Middle Subplot Shows the Seed Motion, and the Bottom Subplot Indicates the Matched Motion**

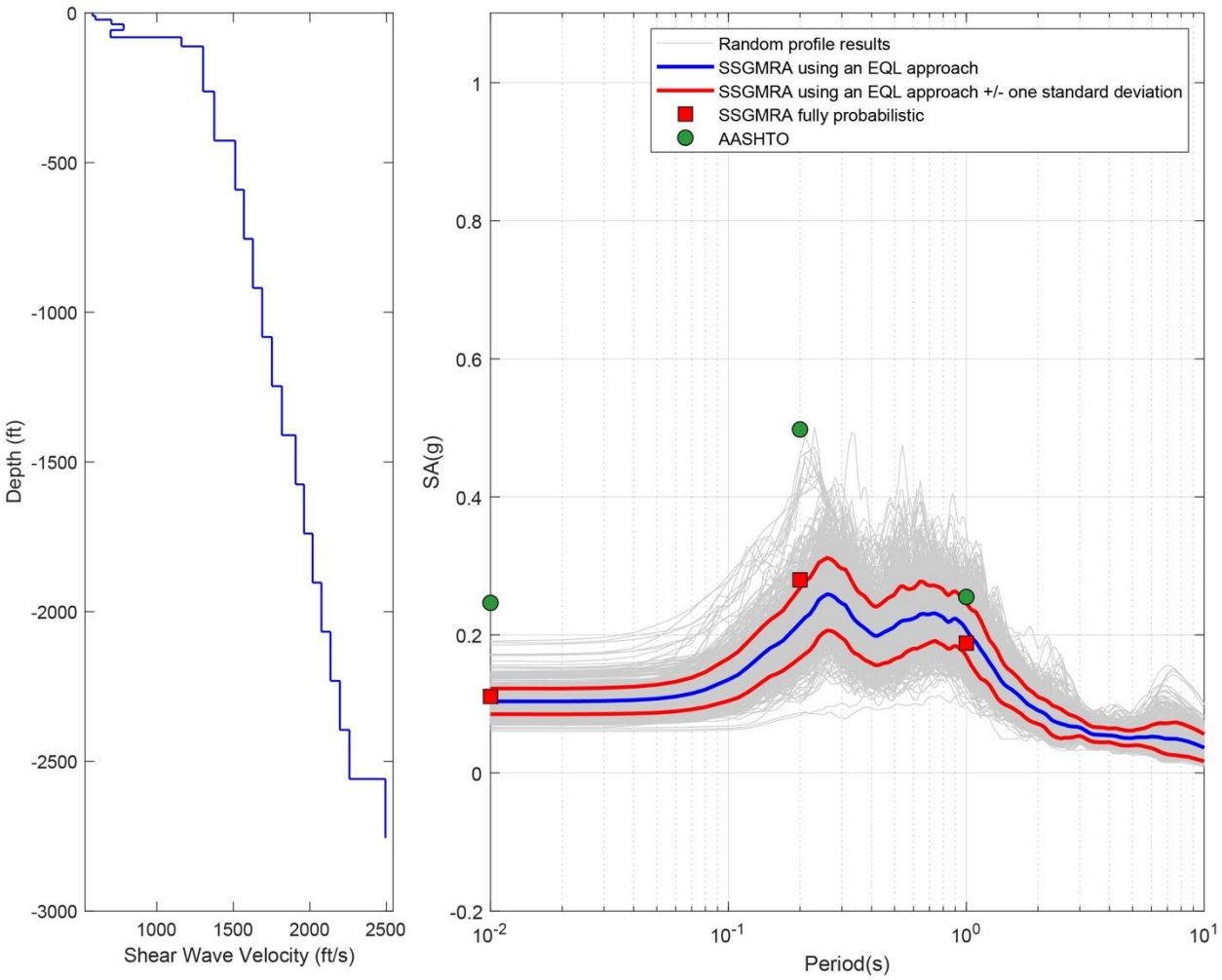


**Figure B-166. Left Panel: Shear-Wave Velocity Profile of Site 42 (Based on EPRI Soil Model); and Right Panel: Results of SSGMRA Using a Fully Probabilistic Approach, SSGMRA Using an Equivalent Linear Approach, SSGMRA Using an Equivalent Linear Approach Plus and Minus One Standard Deviation, and AASHTO General Approach**

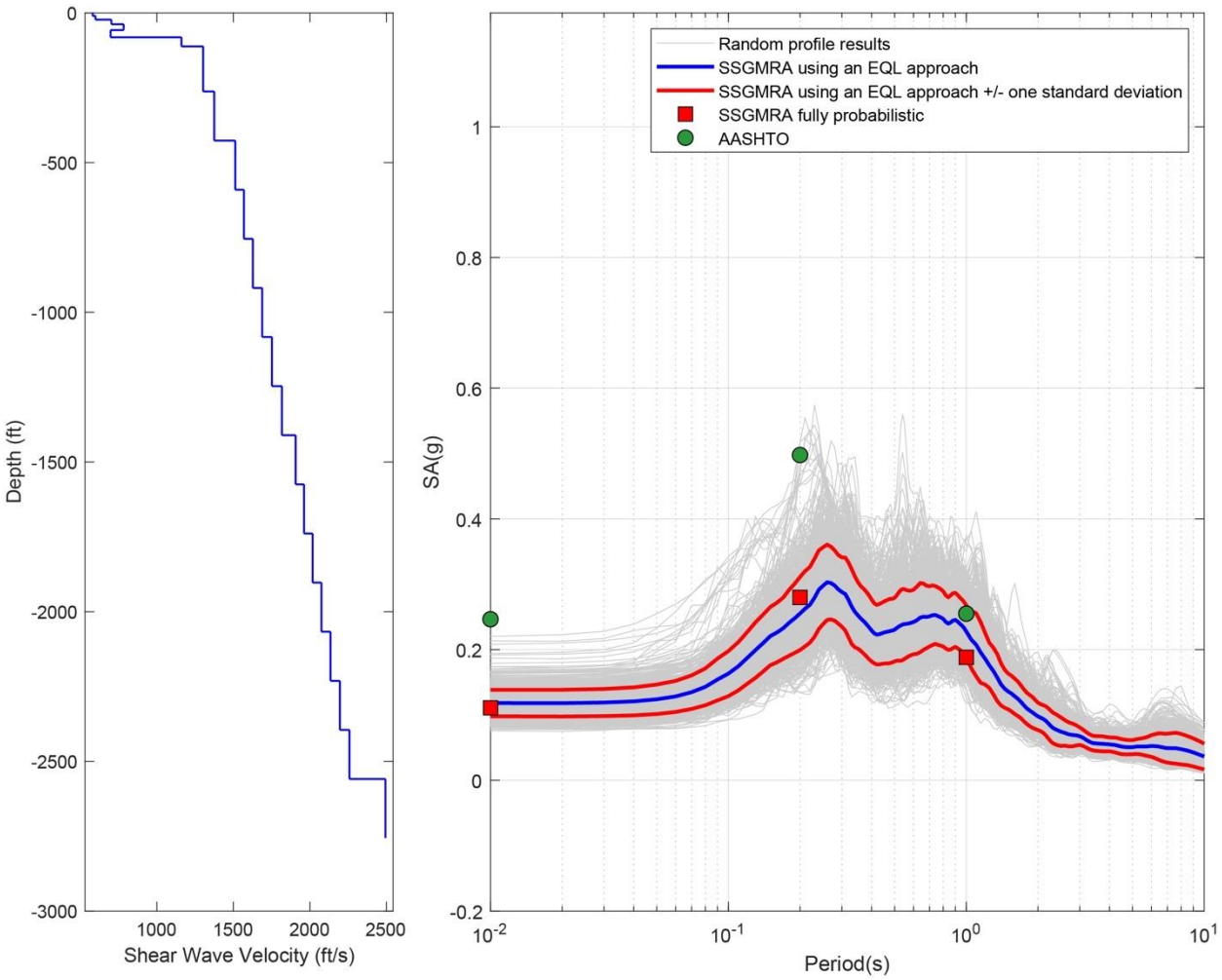


**Figure B-167. Left Panel: Shear-Wave Velocity Profile for Site 42 (Based on Peninsular Soil Model); and Right Panel: Results of SSGMRA Using a Fully Probabilistic Approach, SSGMRA Using an Equivalent Linear Approach, SSGMRA Using an Equivalent Linear Approach Plus and Minus One Standard Deviation, and AASHTO General Approach**

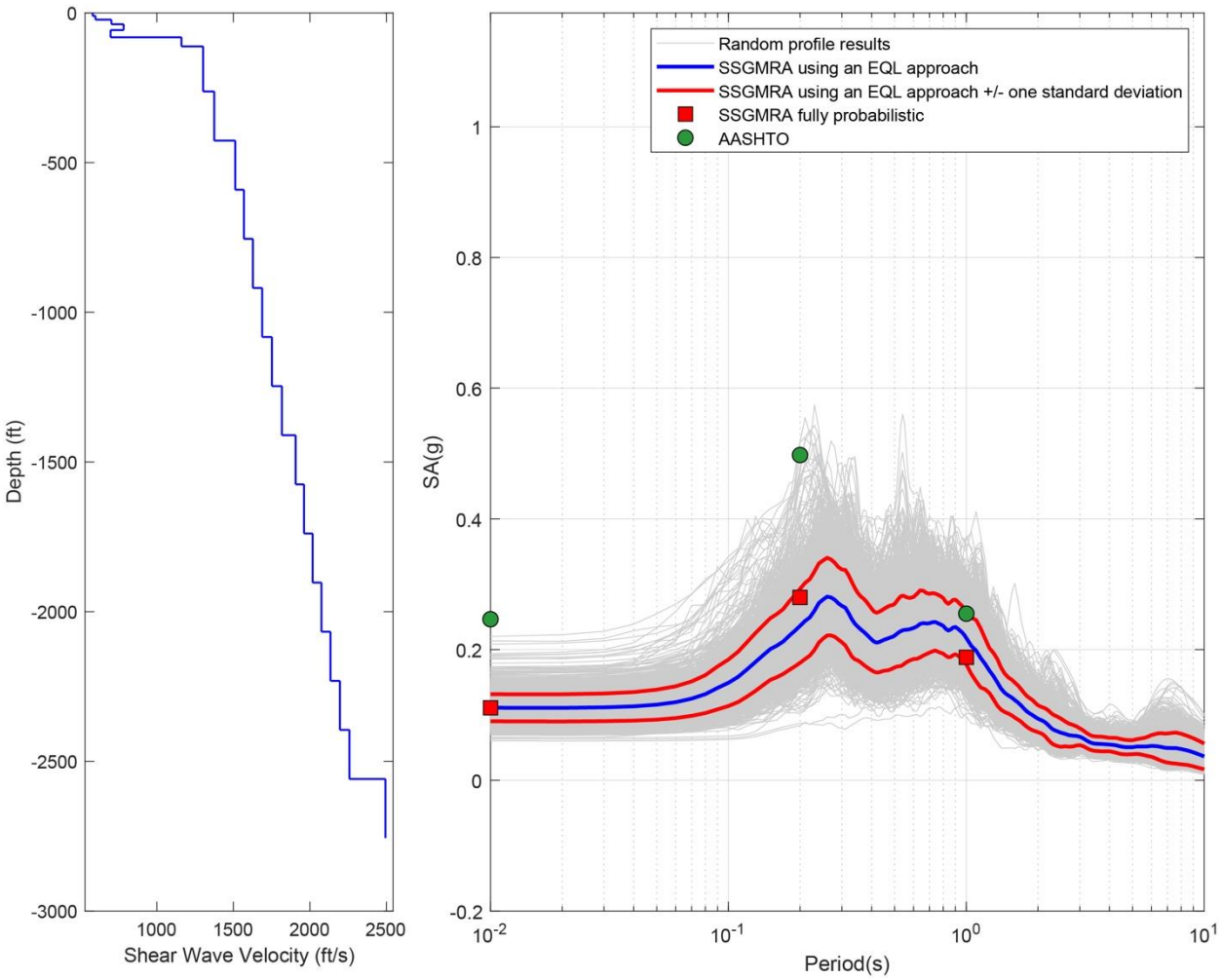


**Figure B-168. Left Panel: Shear-Wave Velocity Profile for Site 42 (Combined); and Right Panel: Results of SSGMRA Using a Fully Probabilistic Approach, SSGMRA Using an Equivalent Linear Approach, SSGMRA Using an Equivalent Linear Approach Plus and Minus One Standard Deviation, and AASHTO General Approach**

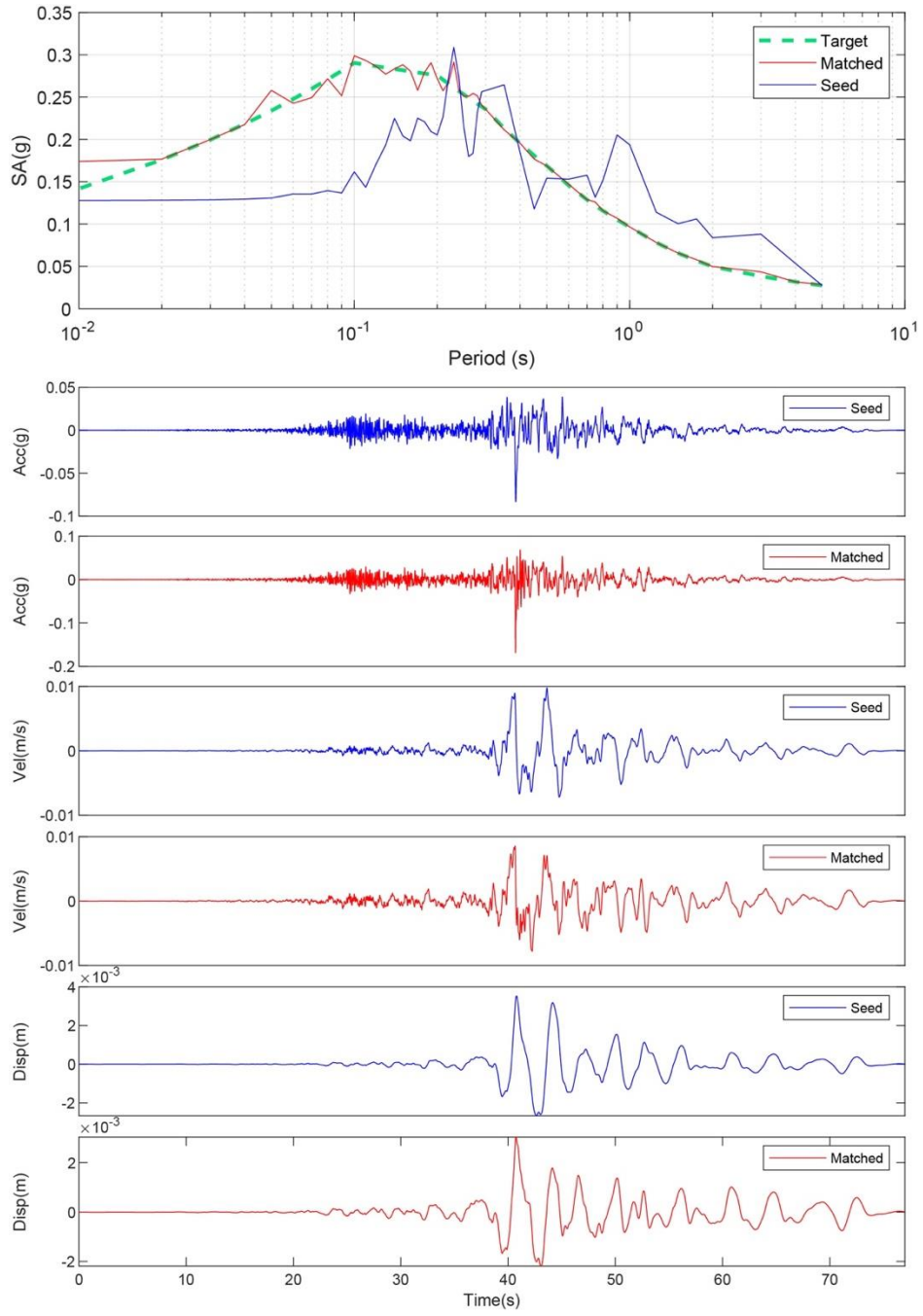


**Figure B-169. Matching Spectrum of Seed Motion (RSN1432-CHICHI-TAP046-E) to the Target Spectrum (UHS) at Site 43. The Middle Subplot Shows the Seed Motion, and The Bottom Subplot Indicates the Matched Motion**

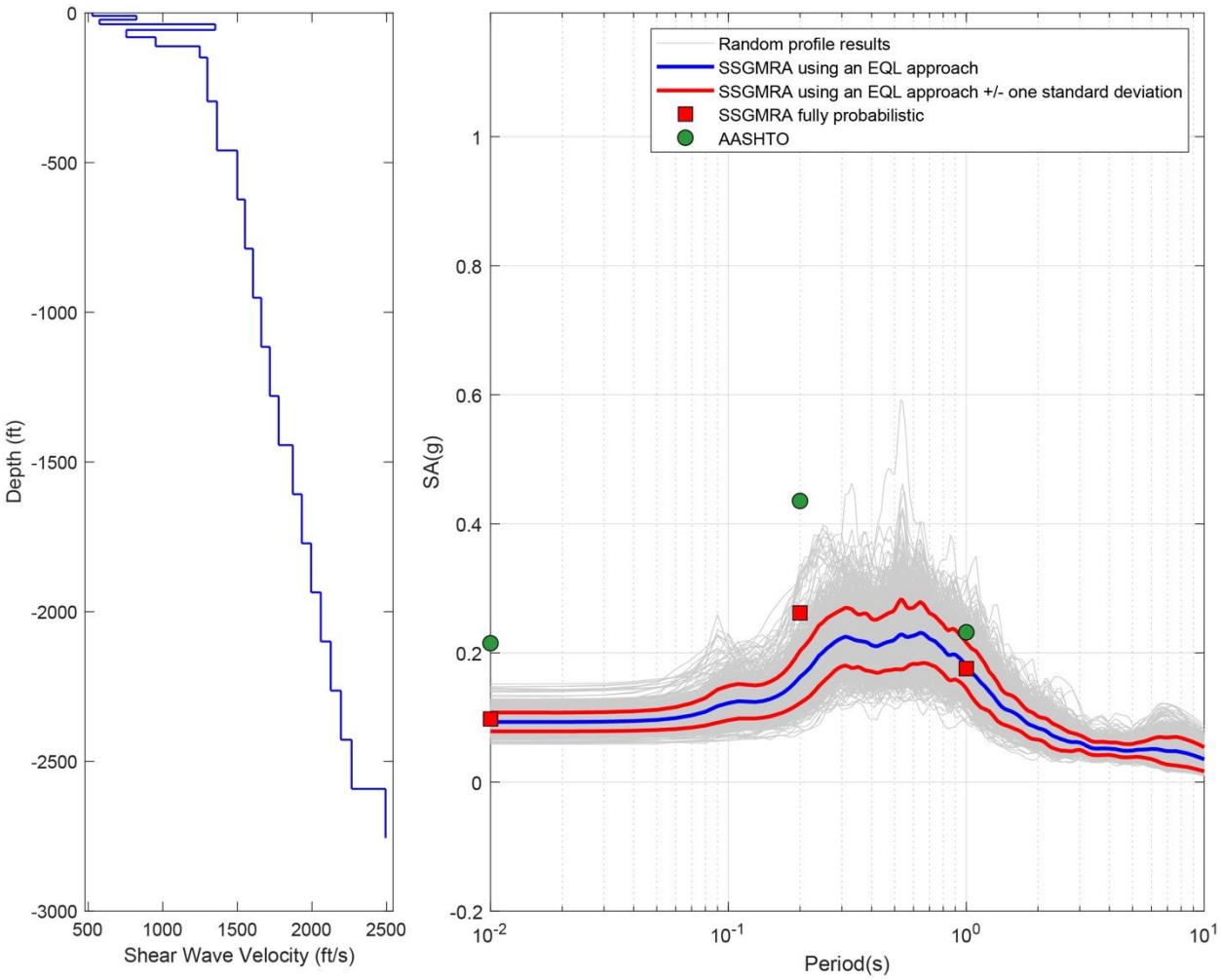


**Figure B-170. Left Panel: Shear-Wave Velocity Profile for Site 43 (Based on EPRI Soil Model); and Right Panel: Results of SSGMRA Using a Fully Probabilistic Approach, SSGMRA Using an Equivalent Linear Approach, SSGMRA Using an Equivalent Linear Approach Plus and Minus One Standard Deviation, and AASHTO General Approach**

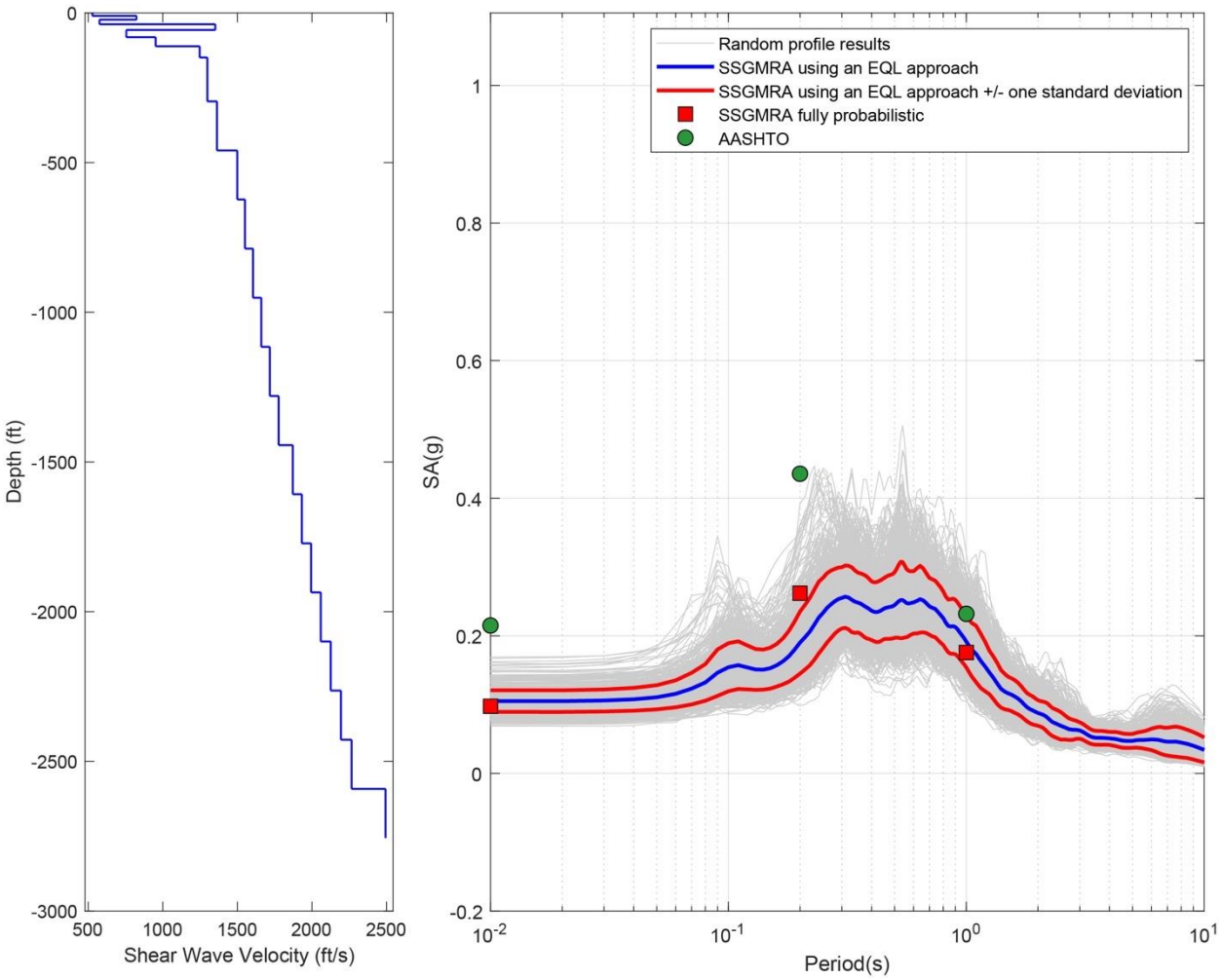


**Figure B-171. Left Panel: Shear-Wave Velocity Profile for Site 43 (Based on Peninsular Soil Model); and Right Panel: Results of SSGMRA Using a Fully Probabilistic Approach, SSGMRA Using an Equivalent Linear Approach, SSGMRA Using an Equivalent Linear Approach Plus and Minus One Standard Deviation, and AASHTO General Approach**

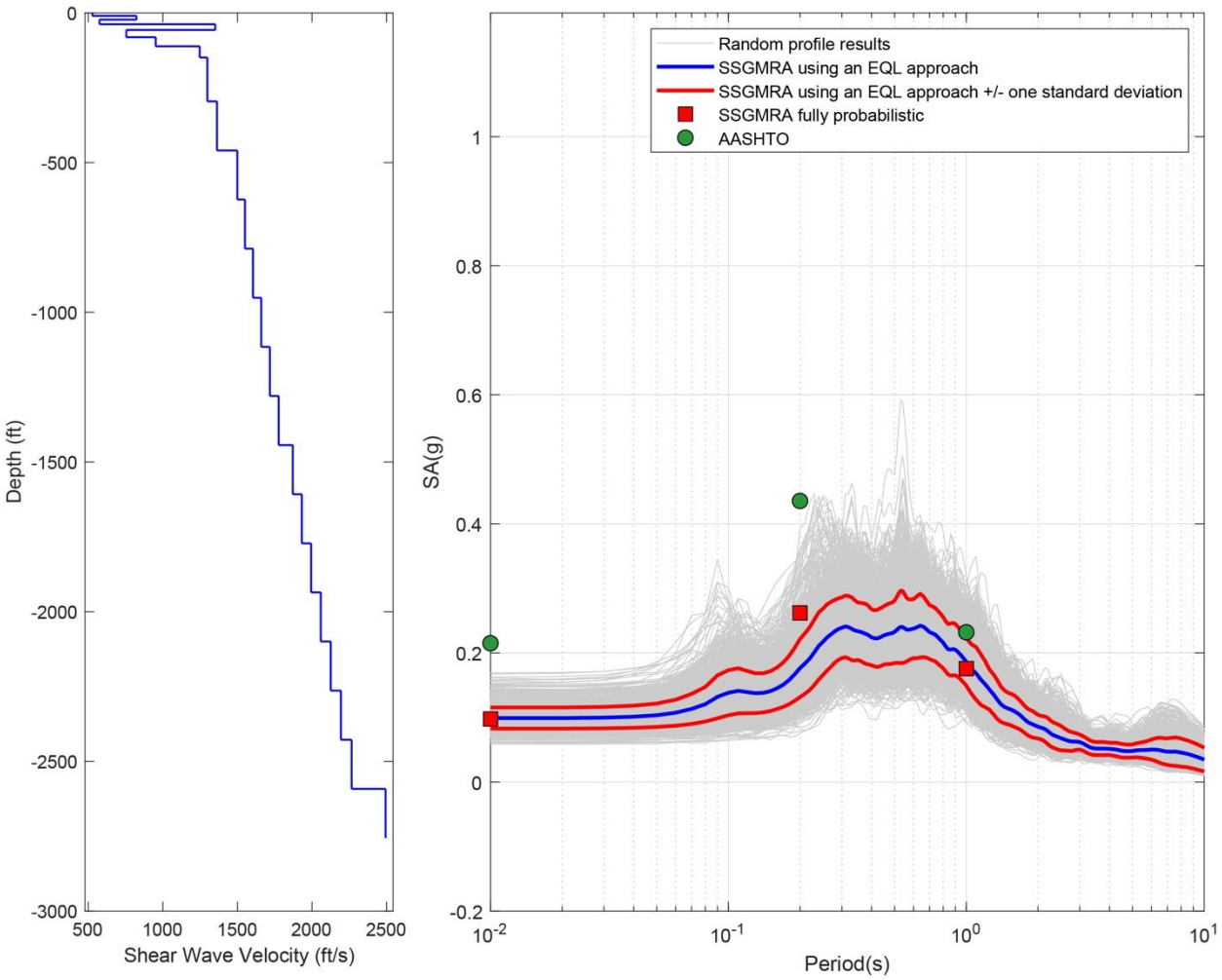


**Figure B-172. Left Panel: Shear-Wave Velocity Profile for Site 43 (Combined); and Right Panel: Results of SSGMRA Using a Fully Probabilistic Approach, SSGMRA Using an Equivalent Linear Approach, SSGMRA Using an Equivalent Linear Approach Plus and Minus One Standard Deviation, and AASHTO General Approach**

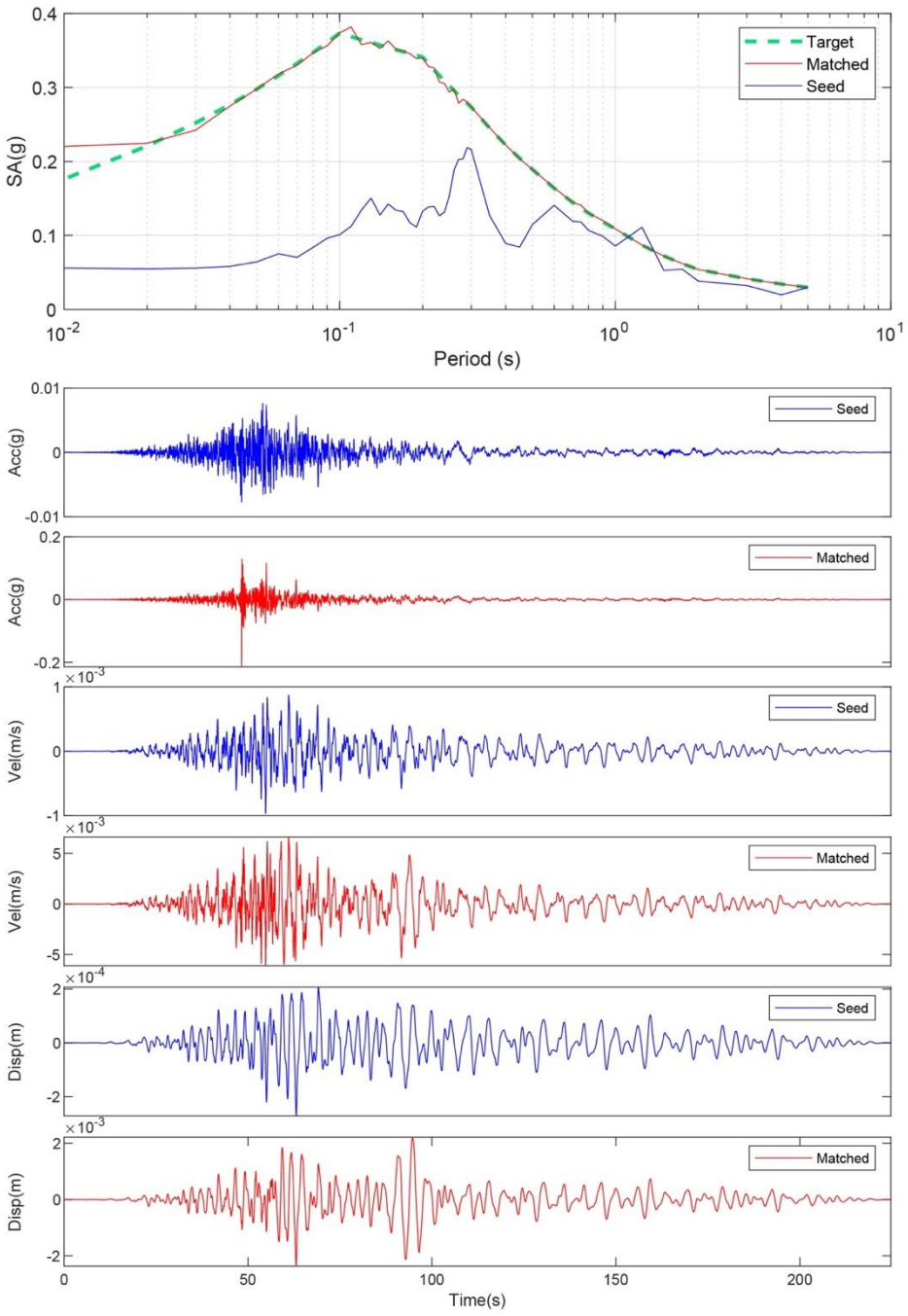


**Figure B-173. Matching Spectrum of Seed Motion (RSN5965-SIERRA.MEX-BC3360) to the Target Spectrum (UHS) at Site 44. The Middle Subplot Shows the Seed Motion, and the Bottom Subplot Indicates the Matched Motion**

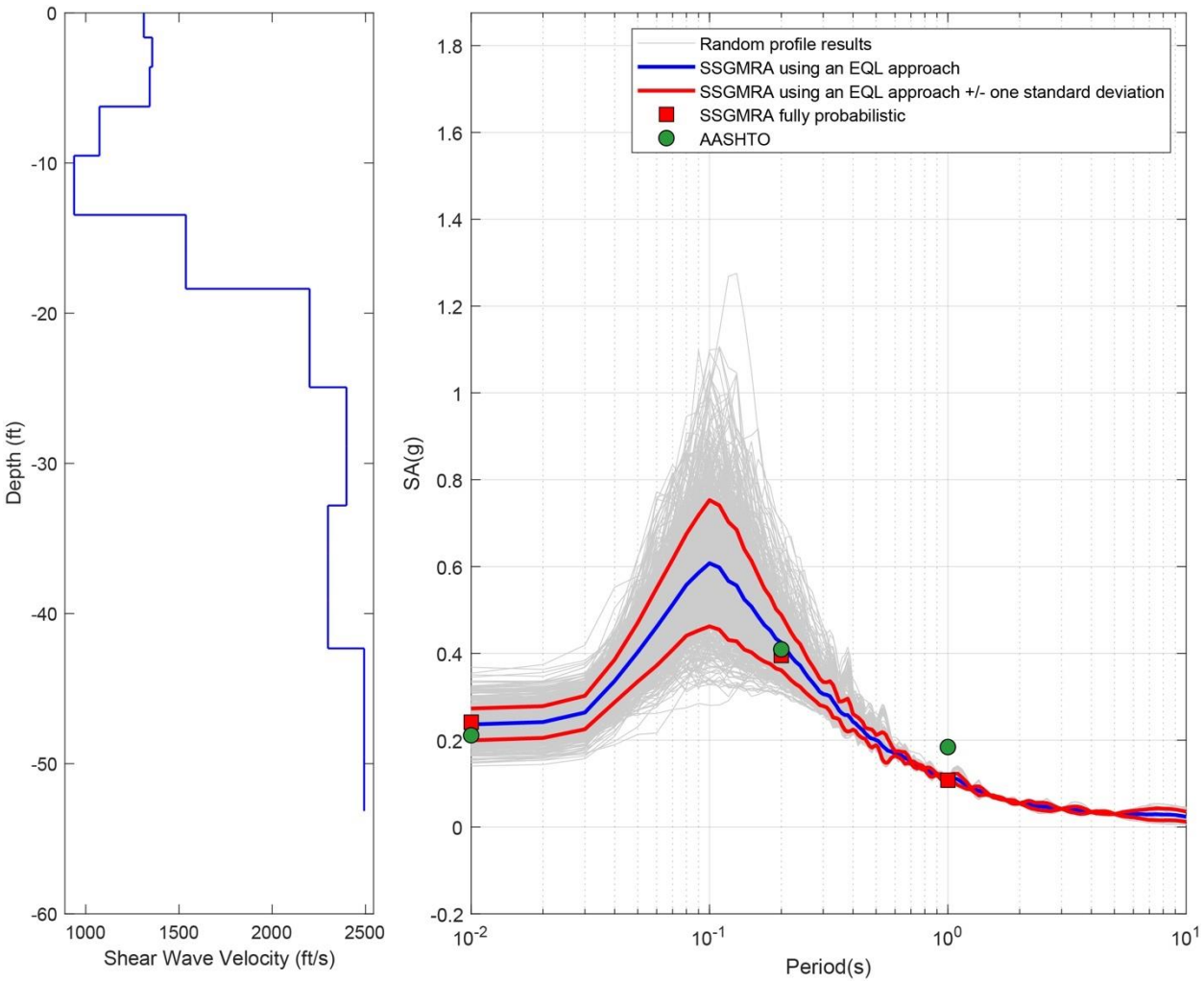


**Figure B-174. Left Panel: Shear-Wave Velocity Profile for Site 44 (Based on EPRI Soil Model); and Right Panel: Results of SSGMRA Using a Fully Probabilistic Approach, SSGMRA Using an Equivalent Linear Approach, SSGMRA Using an Equivalent Linear Approach Plus and Minus One Standard Deviation, and AASHTO General Approach**

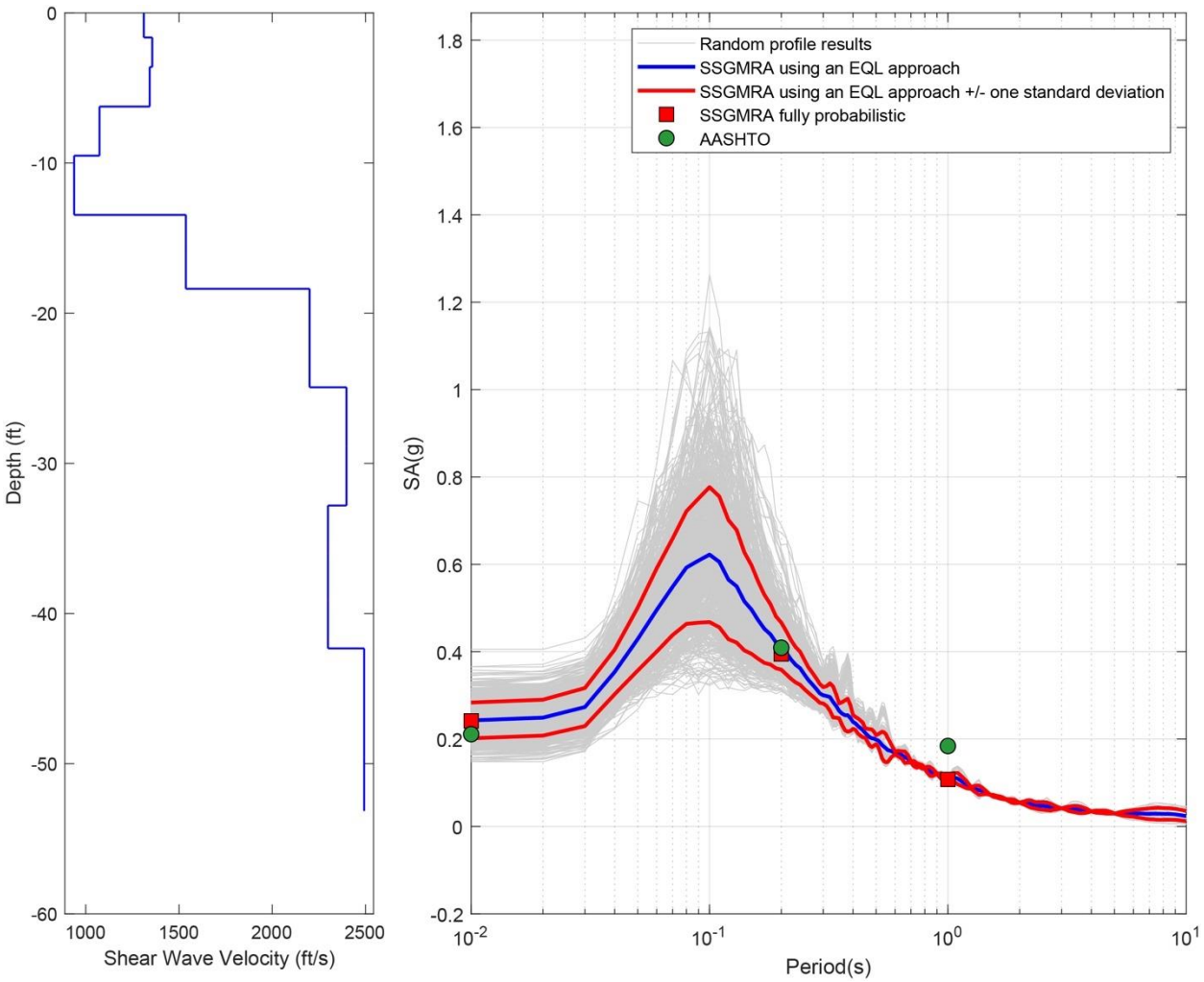


**Figure B-175. Left Panel: Shear-Wave Velocity Profile for Site 44 (Based on Peninsular Soil Model); and Right Panel: Results of SSGMRA Using a Fully Probabilistic Approach, SSGMRA Using an Equivalent Linear Approach, SSGMRA Using an Equivalent Linear Approach Plus and Minus One Standard Deviation, and AASHTO General Approach**

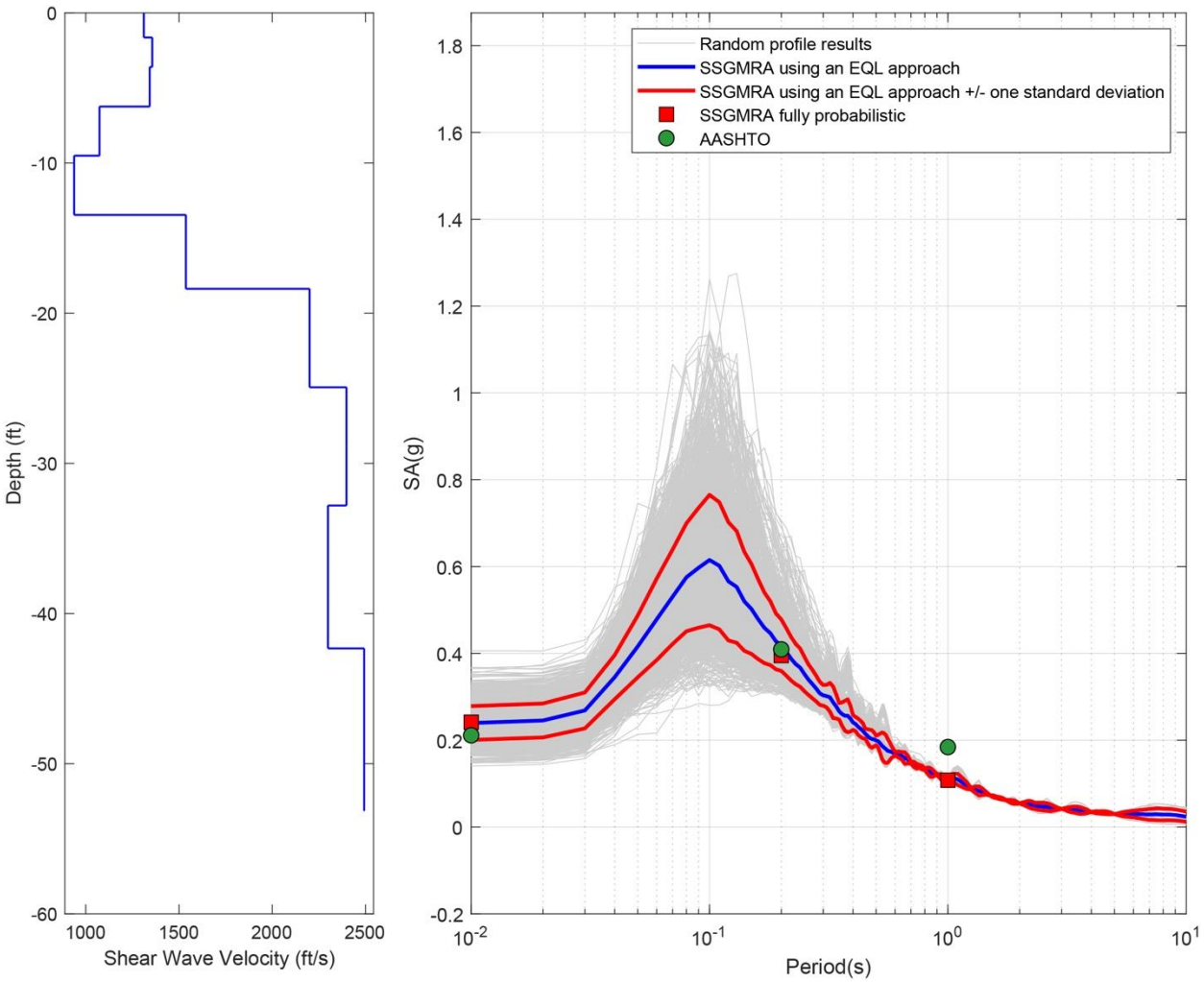


**Figure B-176. Left Panel: Shear-Wave Velocity Profile for Site 44 (Combined); and Right Panel: Results of SSGMRA Using a Fully Probabilistic Approach, SSGMRA Using an Equivalent Linear Approach, SSGMRA Using an Equivalent Linear Approach Plus and Minus One Standard Deviation, and AASHTO General Approach**

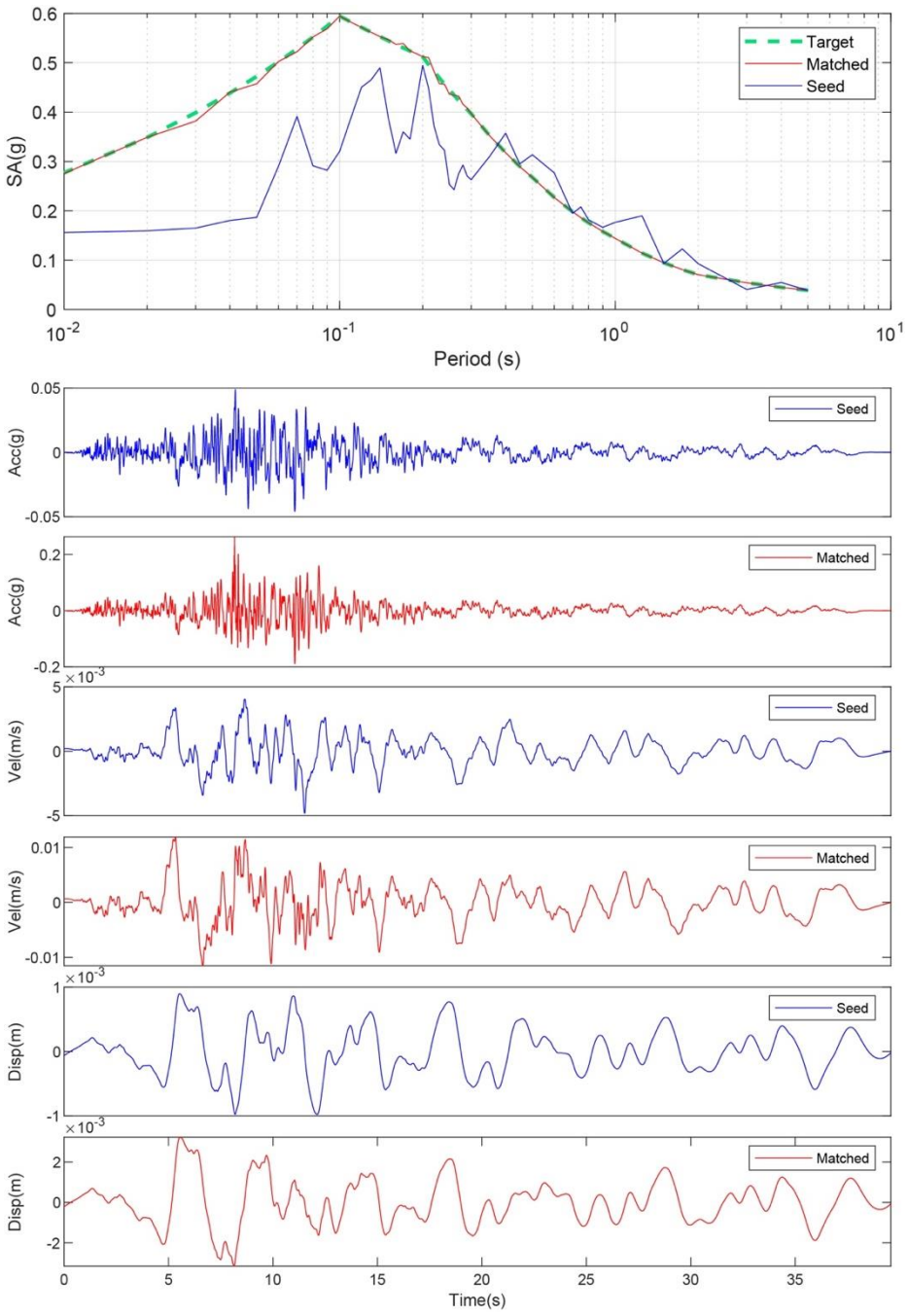


**Figure B-177. Matching Spectrum of Seed Motion (RSN774-LOMAP-HYN064) to the Target Spectrum (UHS) at Site 45. The Middle Subplot Shows the Seed Motion, and The Bottom Subplot Indicates the Matched Motion**

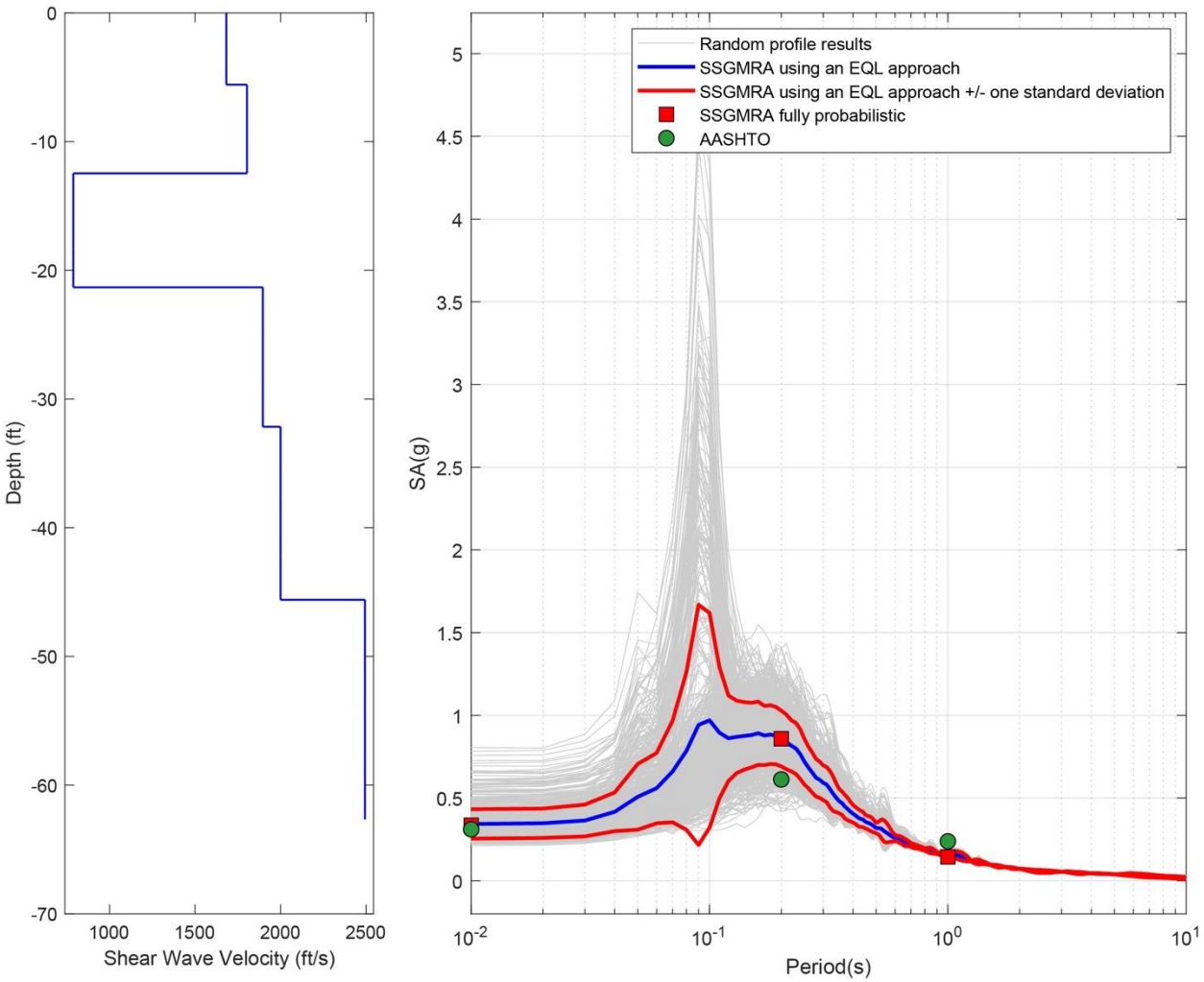


**Figure B-178. Left Panel: Shear-Wave Velocity Profile for Site 45 (Based on EPRI Soil Model); and Right Panel: Results of SSGMRA Using a Fully Probabilistic Approach, SSGMRA Using an Equivalent Linear Approach, SSGMRA Using an Equivalent Linear Approach Plus and Minus One Standard Deviation, and AASHTO General Approach**

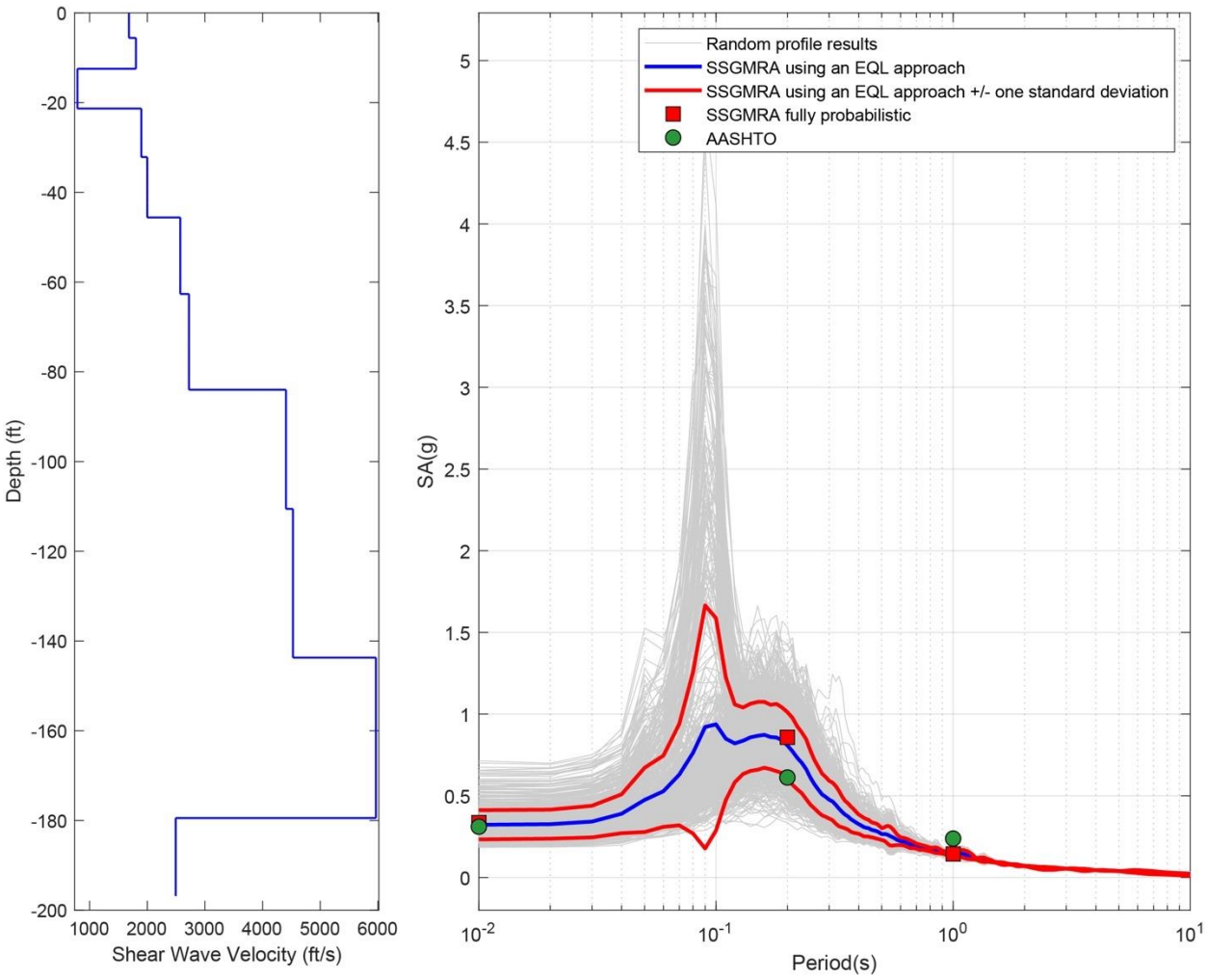


**Figure B-179. Left Panel: Shear-Wave Velocity Profile for Site 45 (Based on Peninsular Soil Model); and Right Panel: Results of SSGMRA Using a Fully Probabilistic Approach, SSGMRA Using an Equivalent Linear Approach, SSGMRA Using an Equivalent Linear Approach Plus and Minus One Standard Deviation, and AASHTO General Approach**

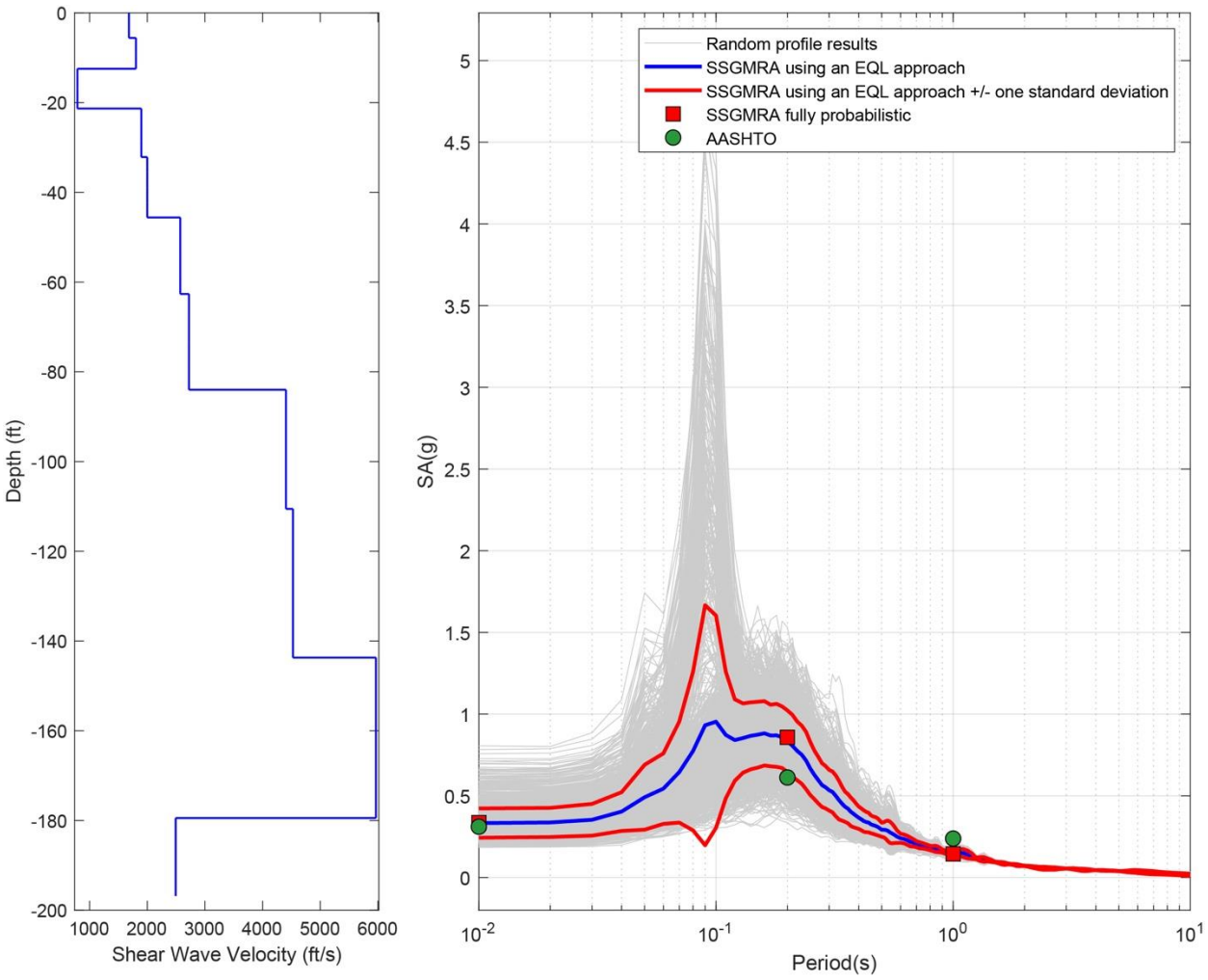


**Figure B-180. Left Panel: Shear-Wave Velocity Profile for Site 45 (Combined); and Right Panel: Results of SSGMRA Using a Fully Probabilistic Approach, SSGMRA Using an Equivalent Linear Approach, SSGMRA Using an Equivalent Linear Approach Plus and Minus One Standard Deviation, and AASHTO General Approach**

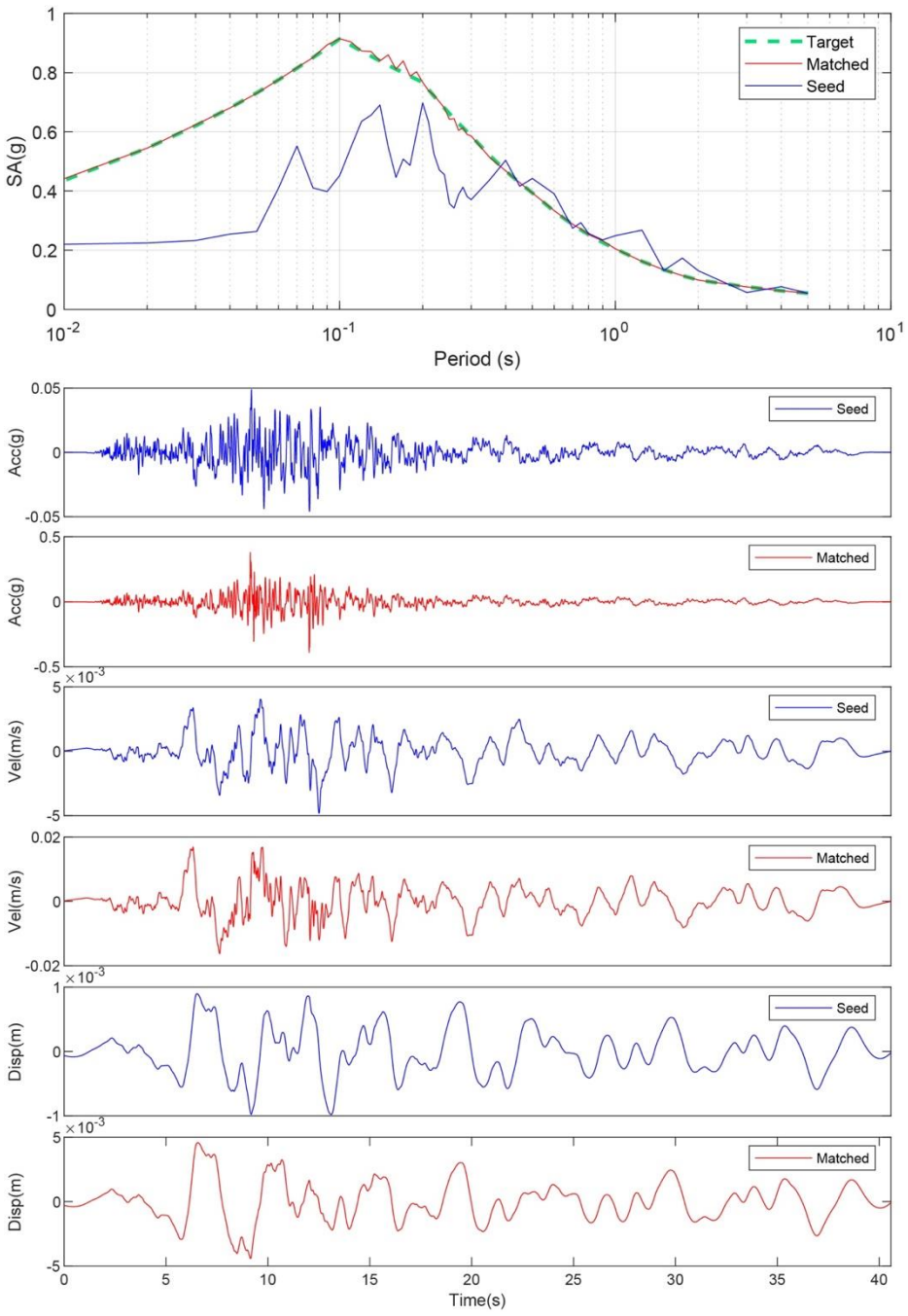


**Figure B-181. Matching Spectrum of Seed Motion (RSN774-LOMAP-HYN064) to the Target Spectrum (UHS) at Site 46. The Middle Subplot Shows the Seed Motion, and the Bottom Subplot Indicates the Matched Motion**

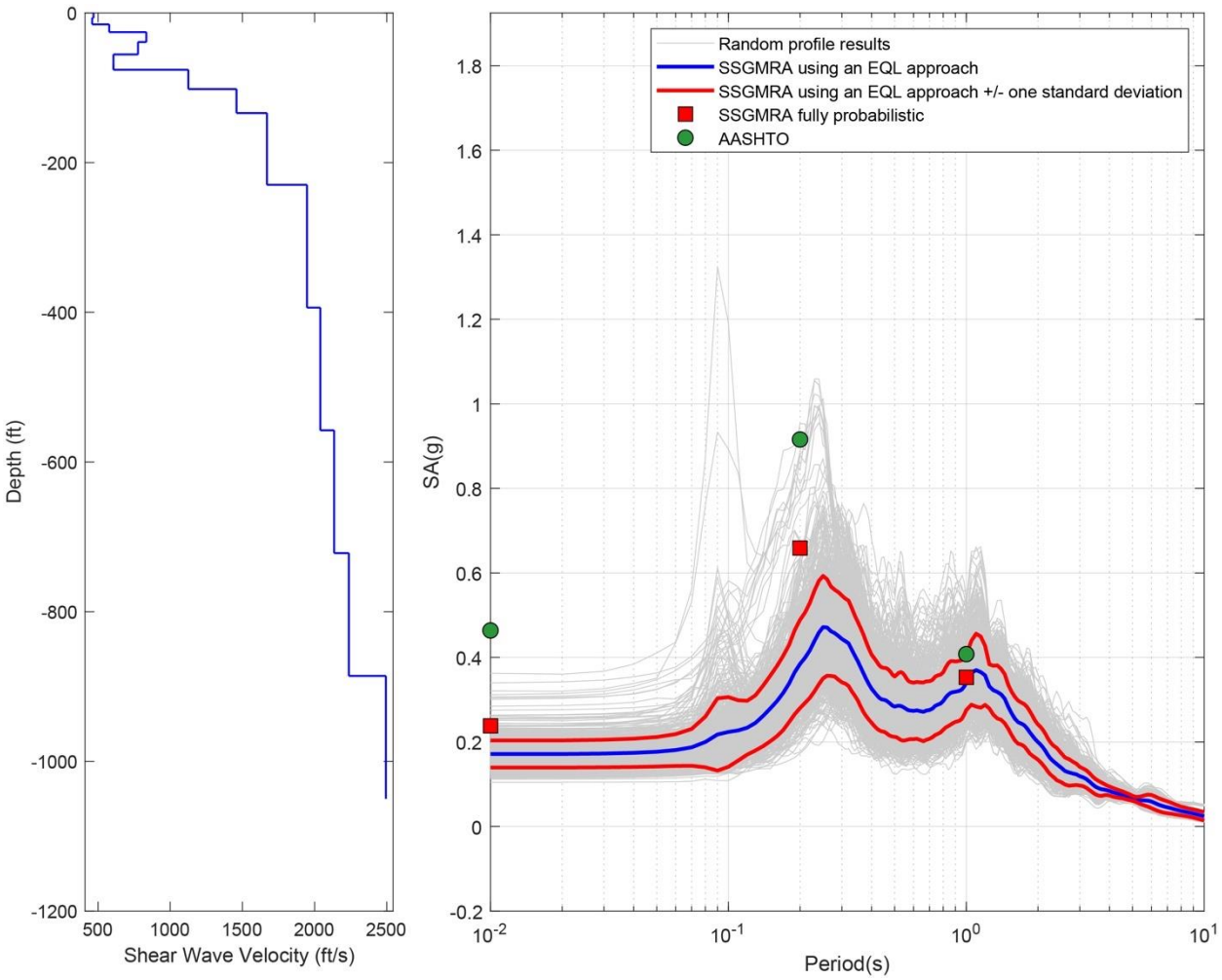


**Figure B-182. Left Panel: Shear-Wave Velocity Profile for Site 46 (Based on EPRI Soil Model); and Right Panel: Results of SSGMRA Using A Fully Probabilistic Approach, SSGMRA Using an Equivalent Linear Approach, SSGMRA Using an Equivalent Linear Approach Plus and Minus One Standard Deviation, and AASHTO General Approach**

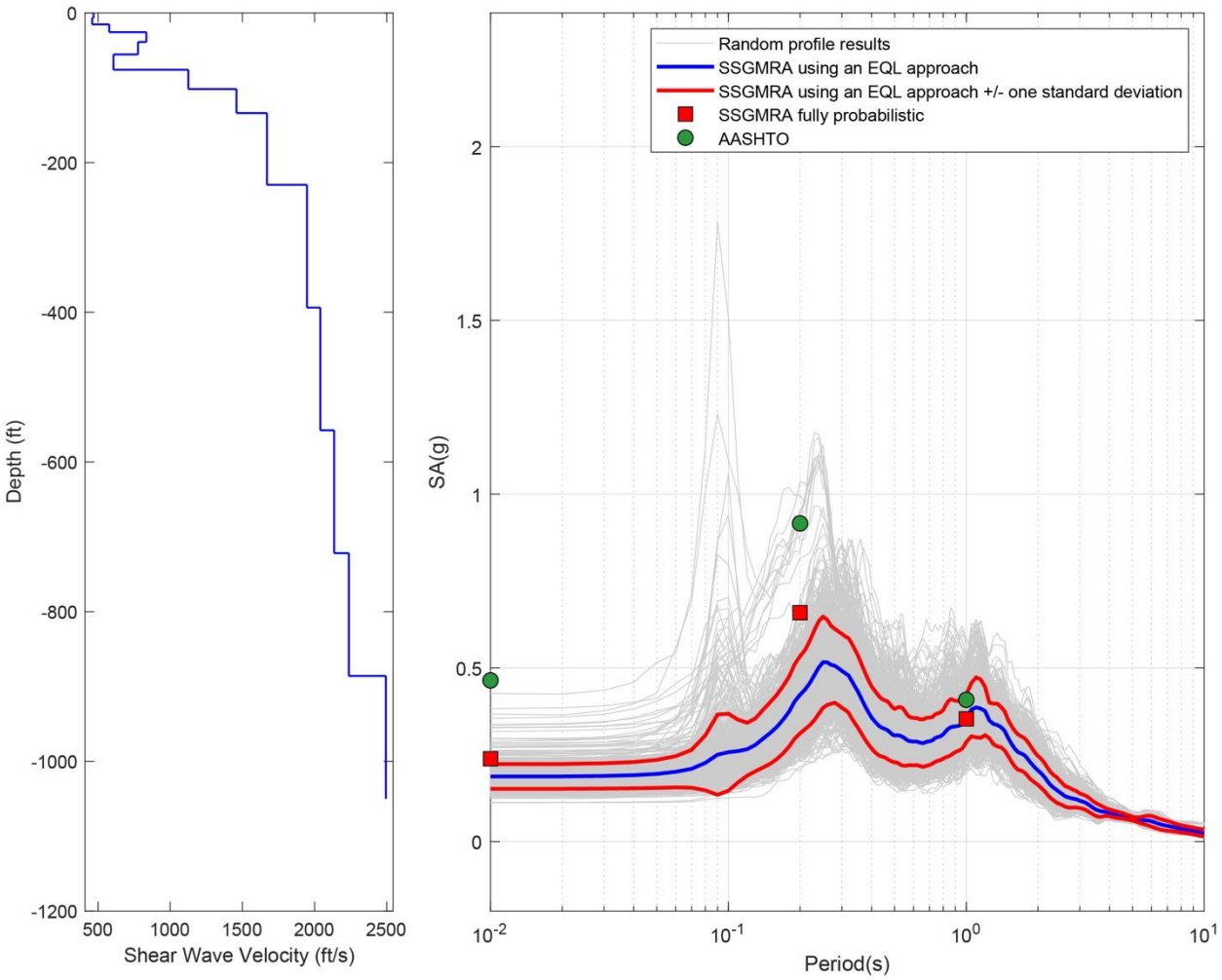


**Figure B-183. Left Panel: Shear-Wave Velocity Profile for Site 46 (Based on Peninsular Soil Model); and Right Panel: Results of SSGMRA Using a Fully Probabilistic Approach, SSGMRA Using an Equivalent Linear Approach, SSGMRA Using an Equivalent Linear Approach Plus and Minus One Standard Deviation, and AASHTO General Approach**

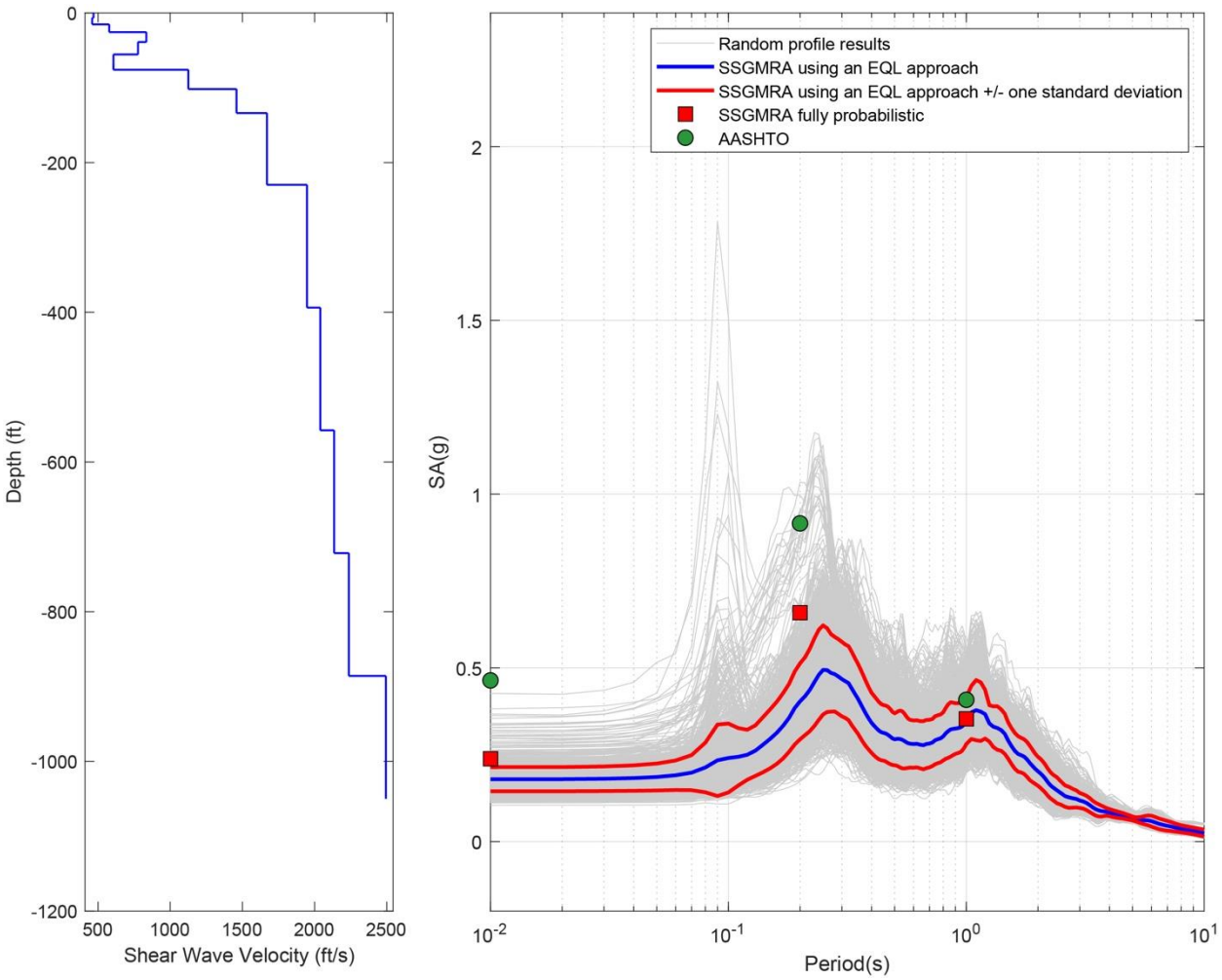


**Figure B-184. Left Panel: Shear-Wave Velocity Profile for Site 46 (Combined); and Right Panel: Results of SSGMRA Using a Fully Probabilistic Approach, SSGMRA Using an Equivalent Linear Approach, SSGMRA Using an Equivalent Linear Approach Plus and Minus One Standard Deviation, and AASHTO General Approach**

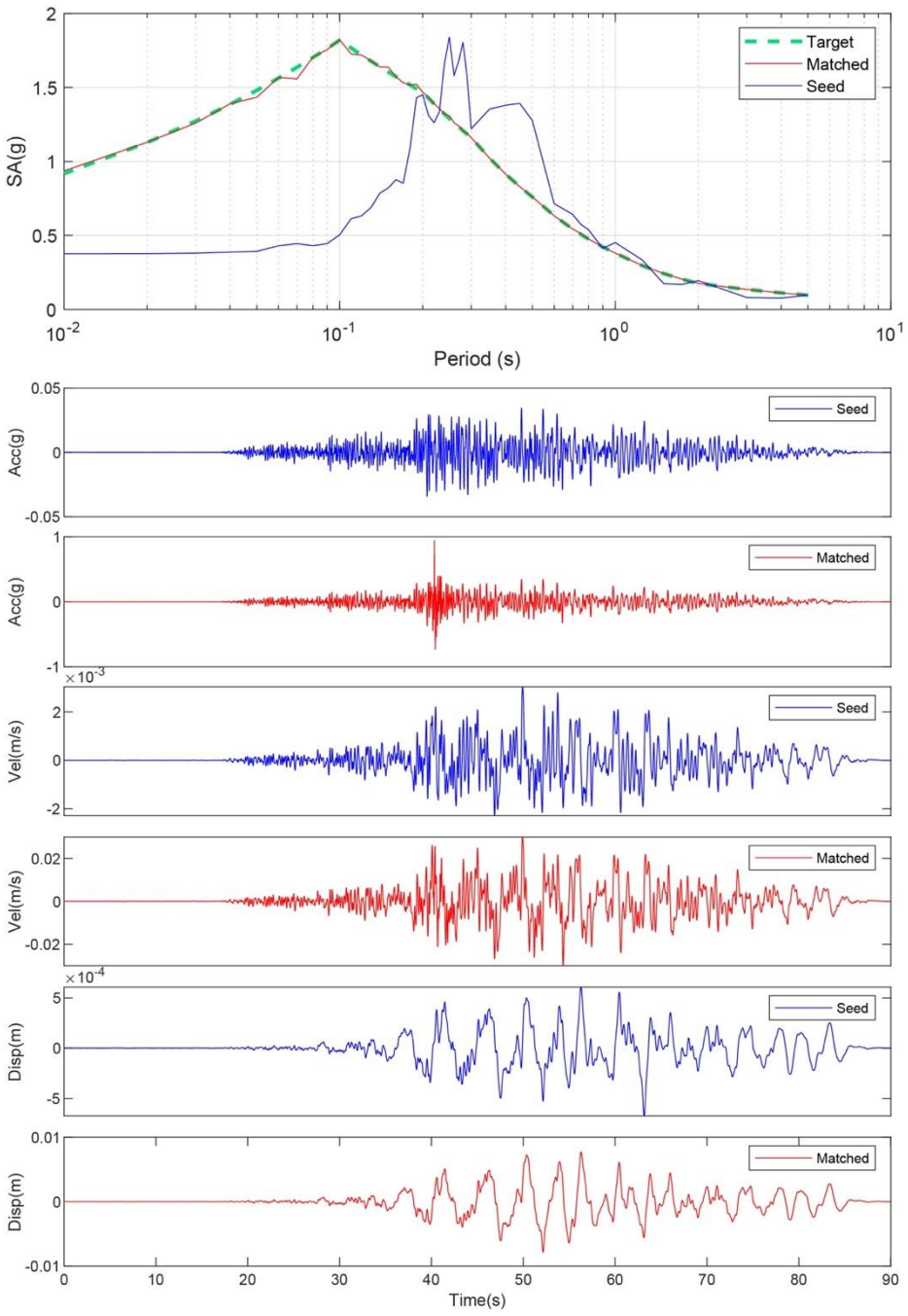


**Figure B-185. Matching Spectrum of Seed Motion (RSN1577-CHICHI-TTN025-E) to the Target Spectrum (UHS) at Site 47. The Middle Subplot Shows the Seed Motion, and the Bottom Subplot Indicates the Matched Motion**

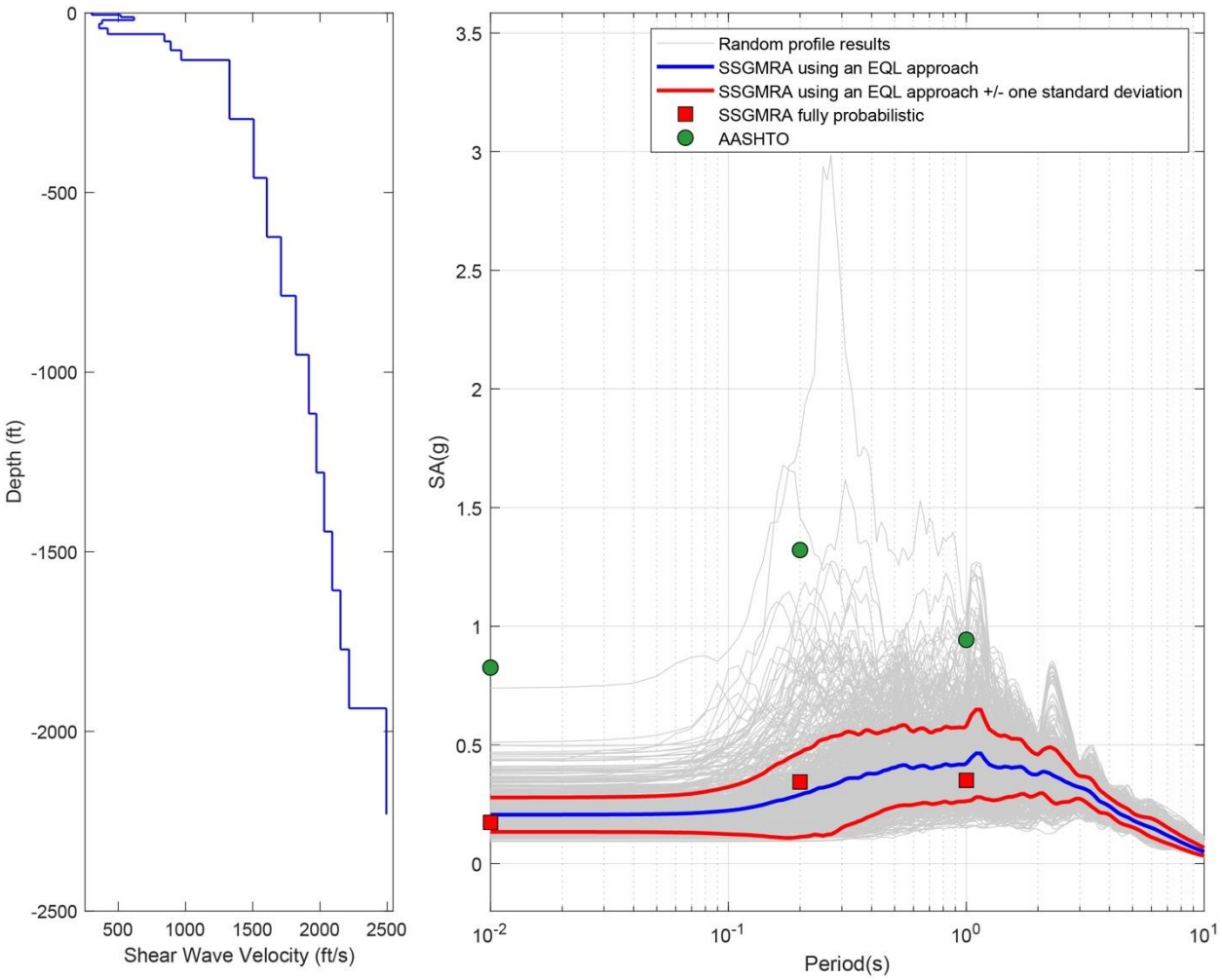


**Figure B-186. Left Panel: Shear-Wave Velocity Profile for Site 47 (Based on EPRI Soil Model); and Right Panel: Results of SSGMRA Using a Fully Probabilistic Approach, SSGMRA Using an Equivalent Linear Approach, SSGMRA Using an Equivalent Linear Approach Plus and Minus One Standard Deviation, and AASHTO General Approach**

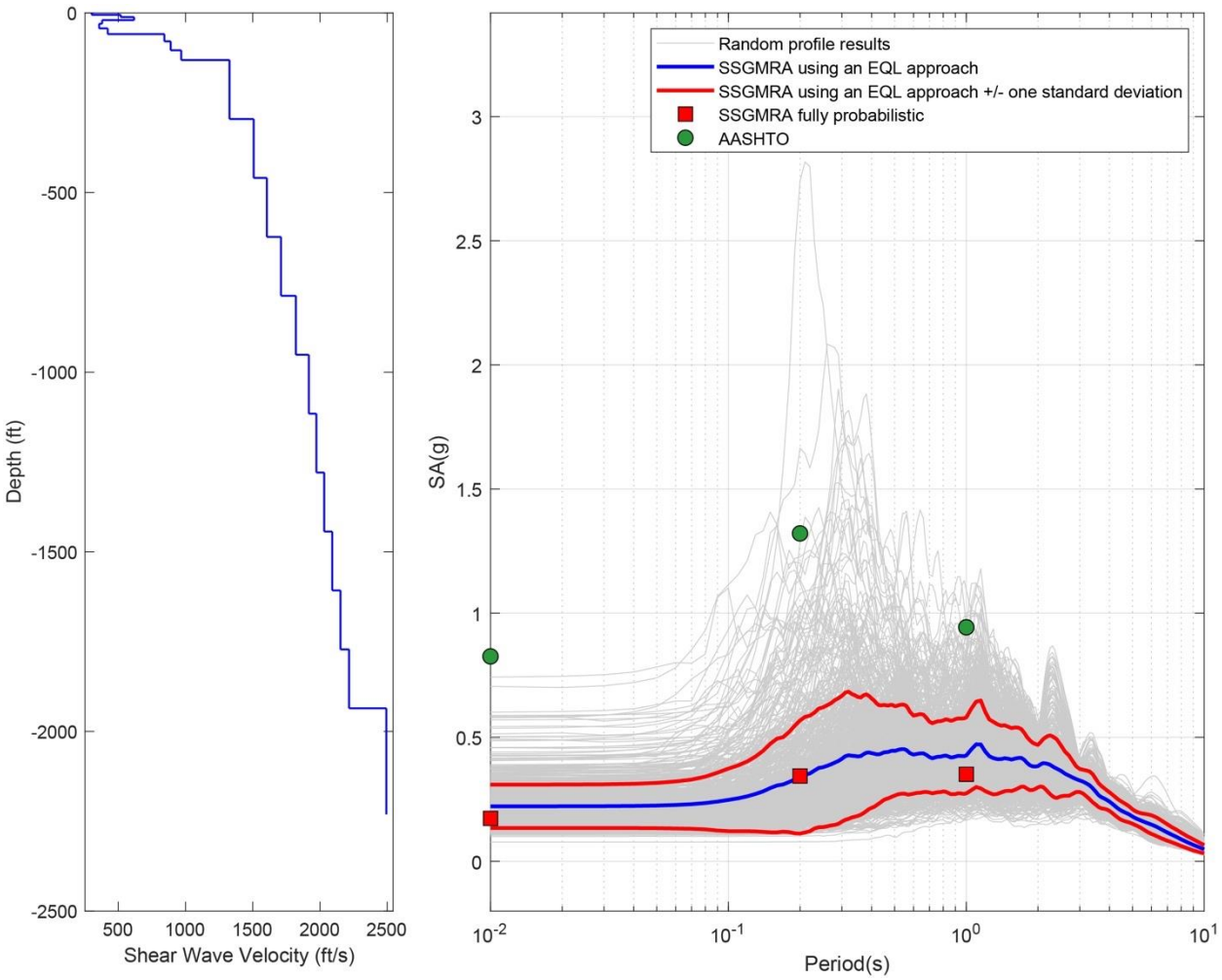


**Figure B-187. Left Panel: Shear-Wave Velocity Profile for Site 47 (Based on Peninsular Soil Model); and Right Panel: Results of SSGMRA Using a Fully Probabilistic Approach, SSGMRA Using an Equivalent Linear Approach, SSGMRA Using an Equivalent Linear Approach Plus and Minus One Standard Deviation, and AASHTO General Approach**

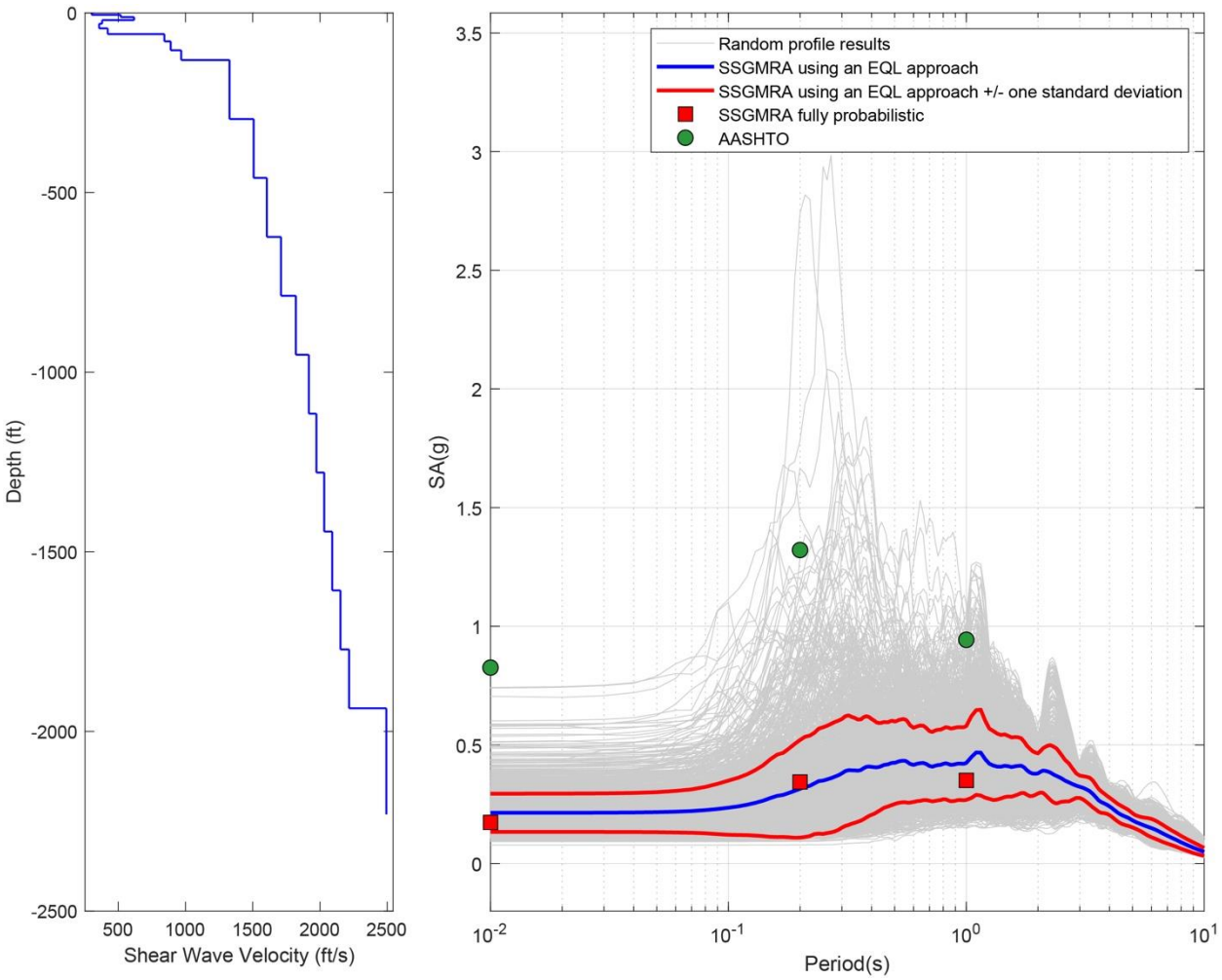


**Figure B-188. Left Panel: Shear-Wave Velocity Profile for Site 47 (Combined); and Right Panel: Results of SSGMRA Using a Fully Probabilistic Approach, SSGMRA Using an Equivalent Linear Approach, SSGMRA Using an Equivalent Linear Approach Plus and Minus One Standard Deviation, and AASHTO General Approach**

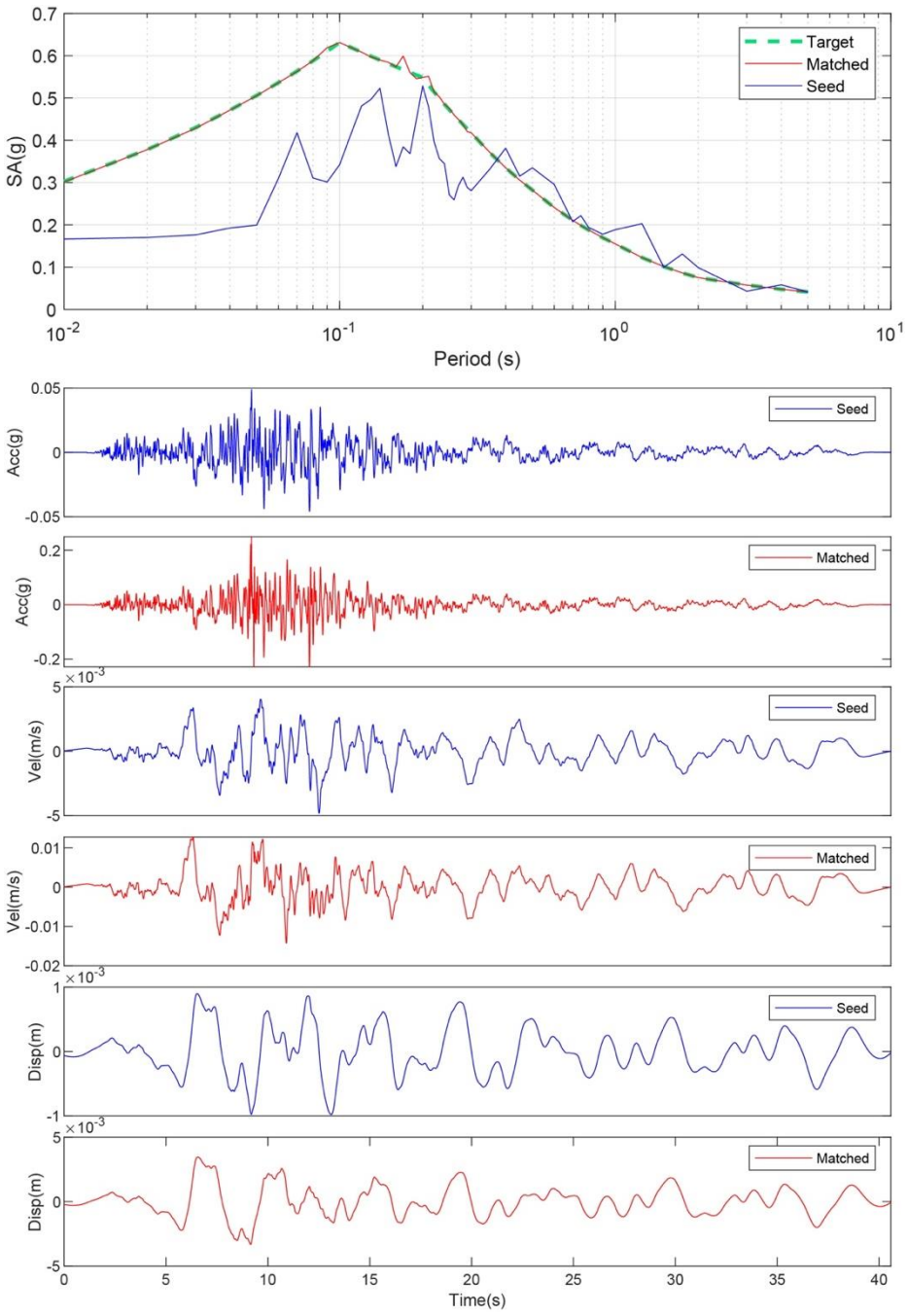


**Figure B-189. Matching Spectrum of Seed Motion (RSN774-LOMAP-HYN064) to the Target Spectrum (UHS) at Site 48. the Middle Subplot Shows the Seed Motion, and the Bottom Subplot Indicates the Matched Motion**

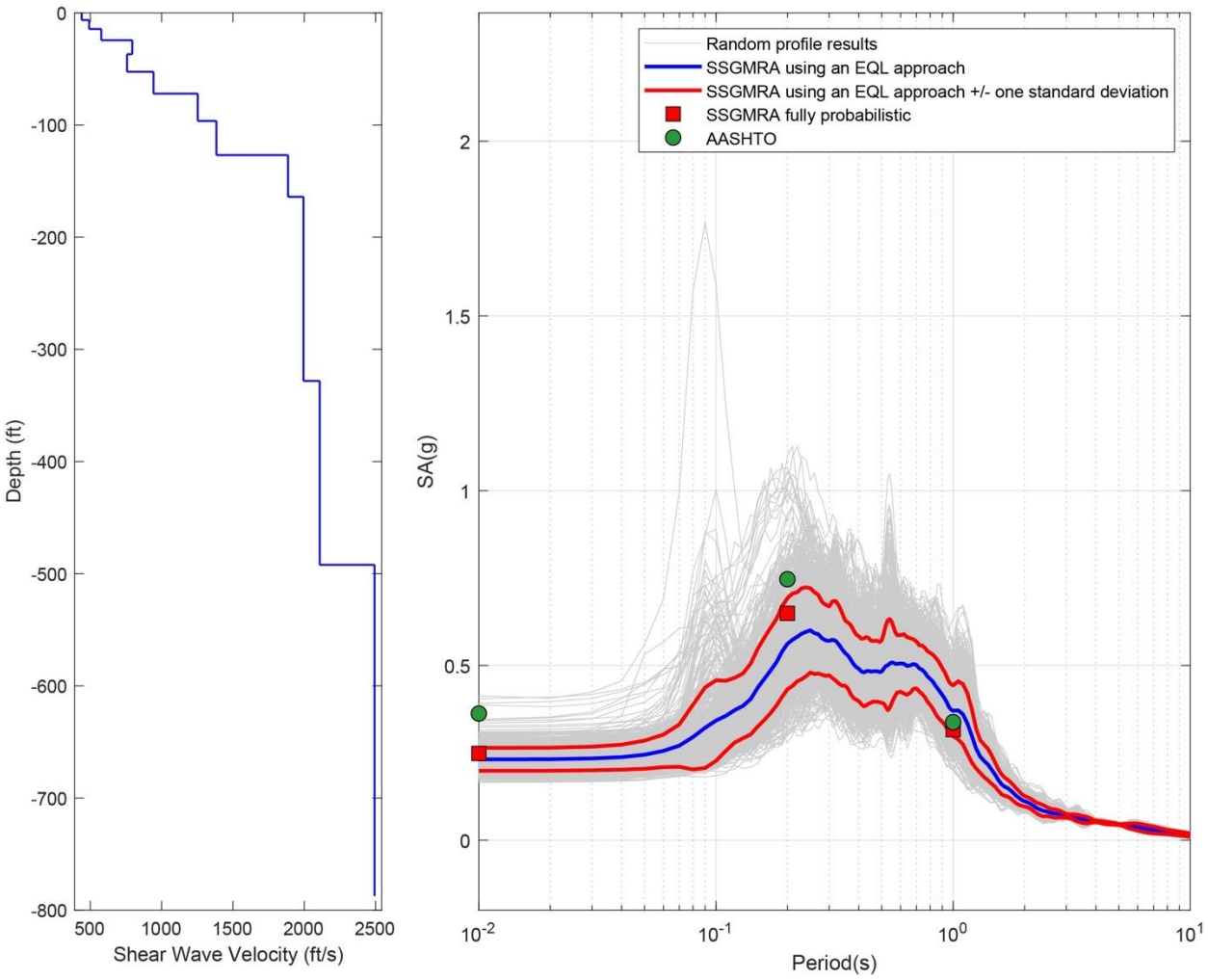


**Figure B-190. Left Panel: Shear-Wave Velocity Profile for Site 48 (Based on EPRI Soil Model); and Right Panel: Results of SSGMRA Using a Fully Probabilistic Approach, SSGMRA Using an Equivalent Linear Approach, SSGMRA Using an Equivalent Linear Approach Plus and Minus One Standard Deviation, and AASHTO General Approach**

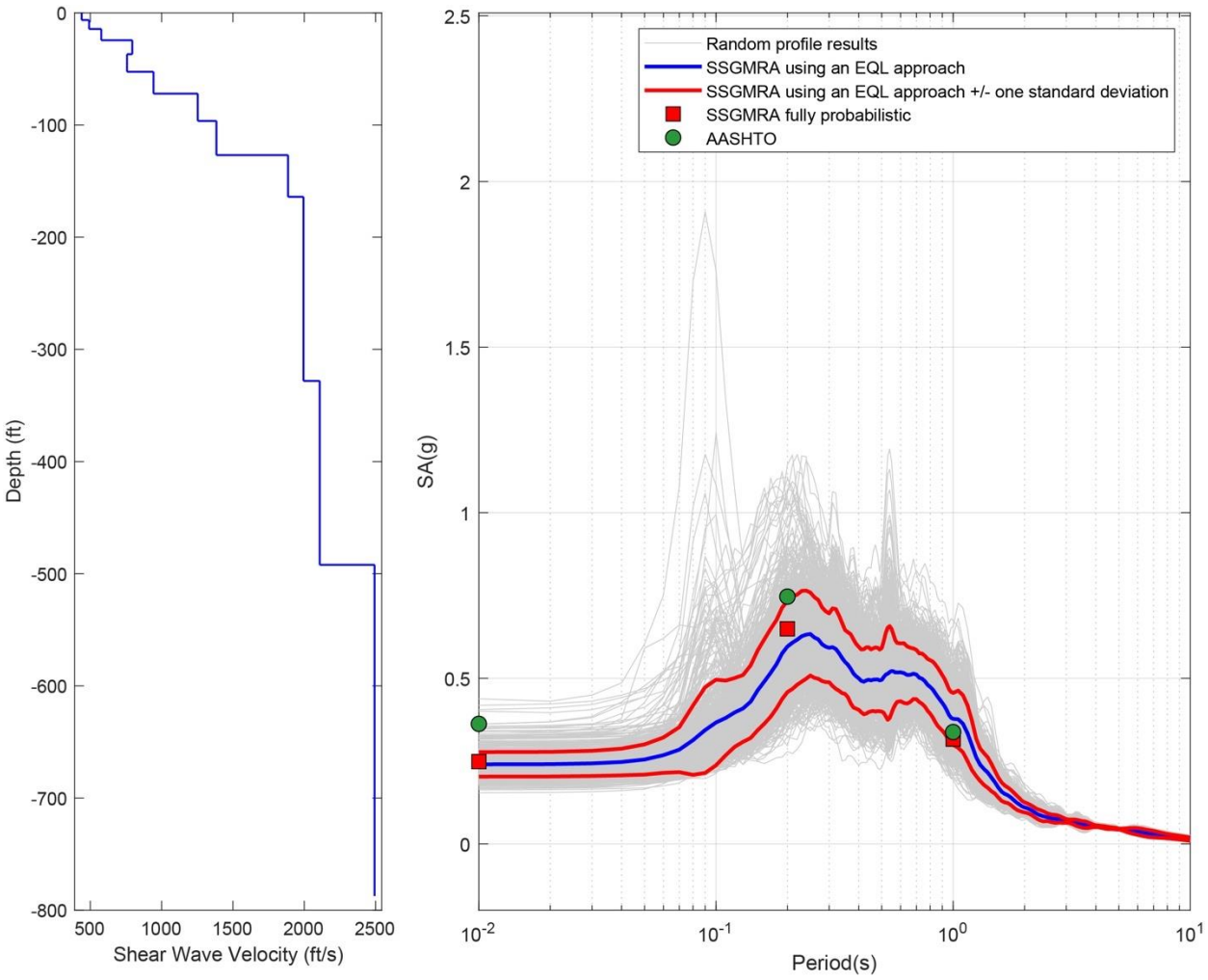


**Figure B-191. Left Panel: Shear-Wave Velocity Profile for Site 48 (Based on Peninsular Soil Model); and Right Panel: Results of SSGMRA Using a Fully Probabilistic Approach, SSGMRA using an Equivalent Linear Approach, SSGMRA Using an Equivalent Linear Approach Plus and Minus One Standard Deviation, and AASHTO General Approach**

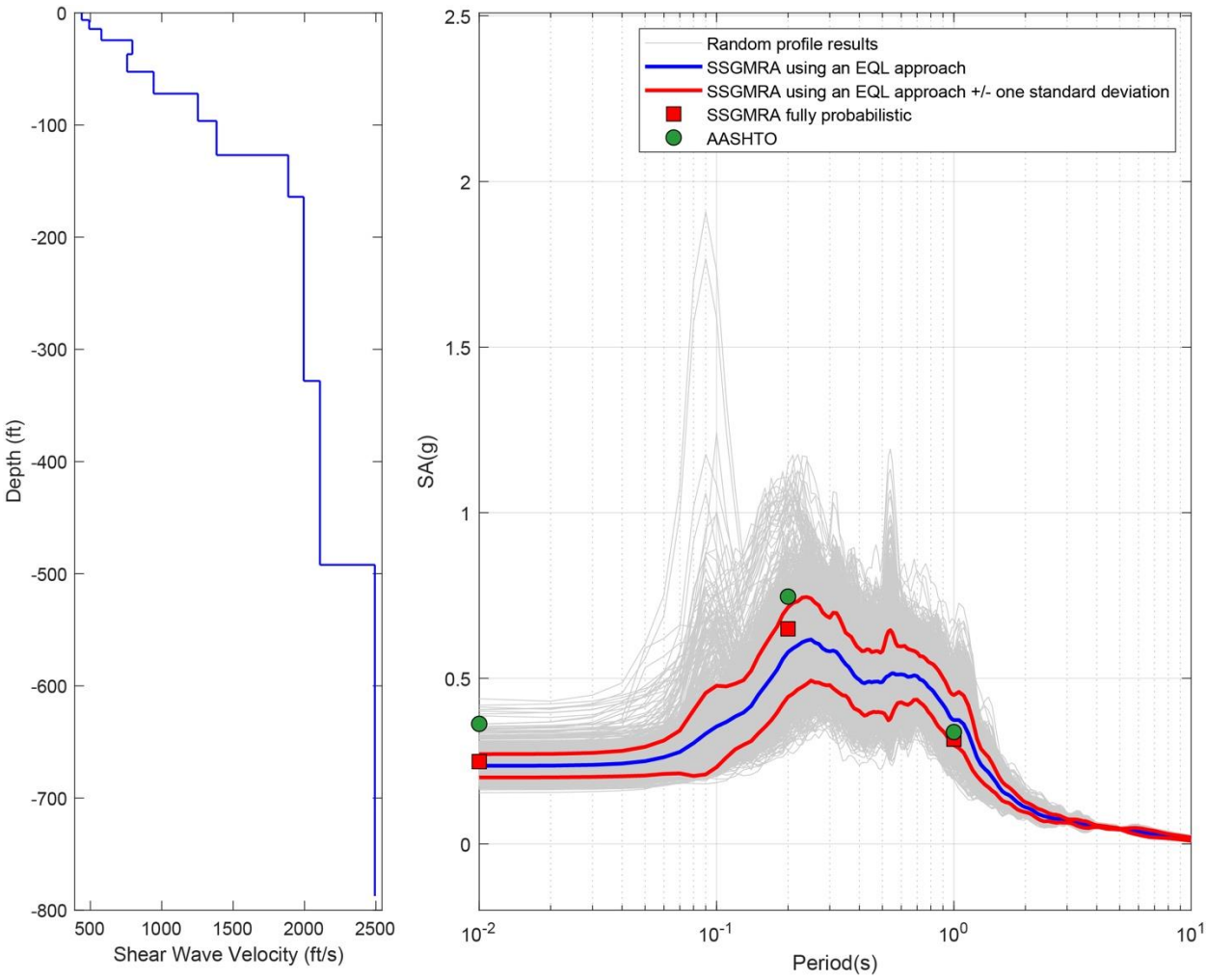


**Figure B-192. Left Panel: Shear-Wave Velocity Profile for Site 48 (Combined); and Right Panel: Results of SSGMRA Using a Fully Probabilistic Approach, SSGMRA Using an Equivalent Linear Approach, SSGMRA Using an Equivalent Linear Approach Plus and Minus One Standard Deviation, and AASHTO General Approach**

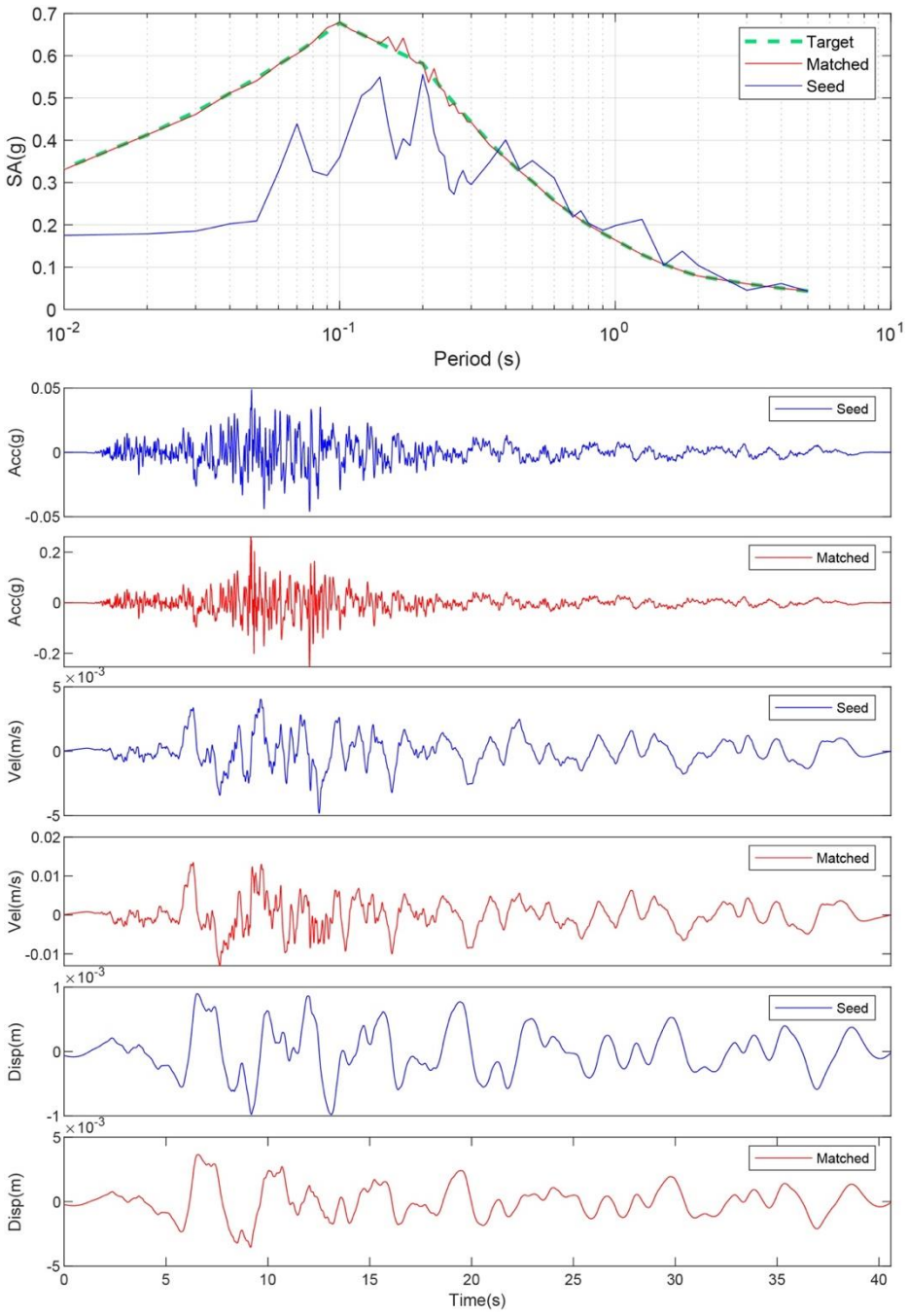


**Figure B-193. Matching Spectrum of Seed Motion (RSN774-LOMAP-HYN064) to the Target Spectrum (UHS) at Site 49. the Middle Subplot Shows the Seed Motion, and the Bottom Subplot Indicates the Matched Motion**

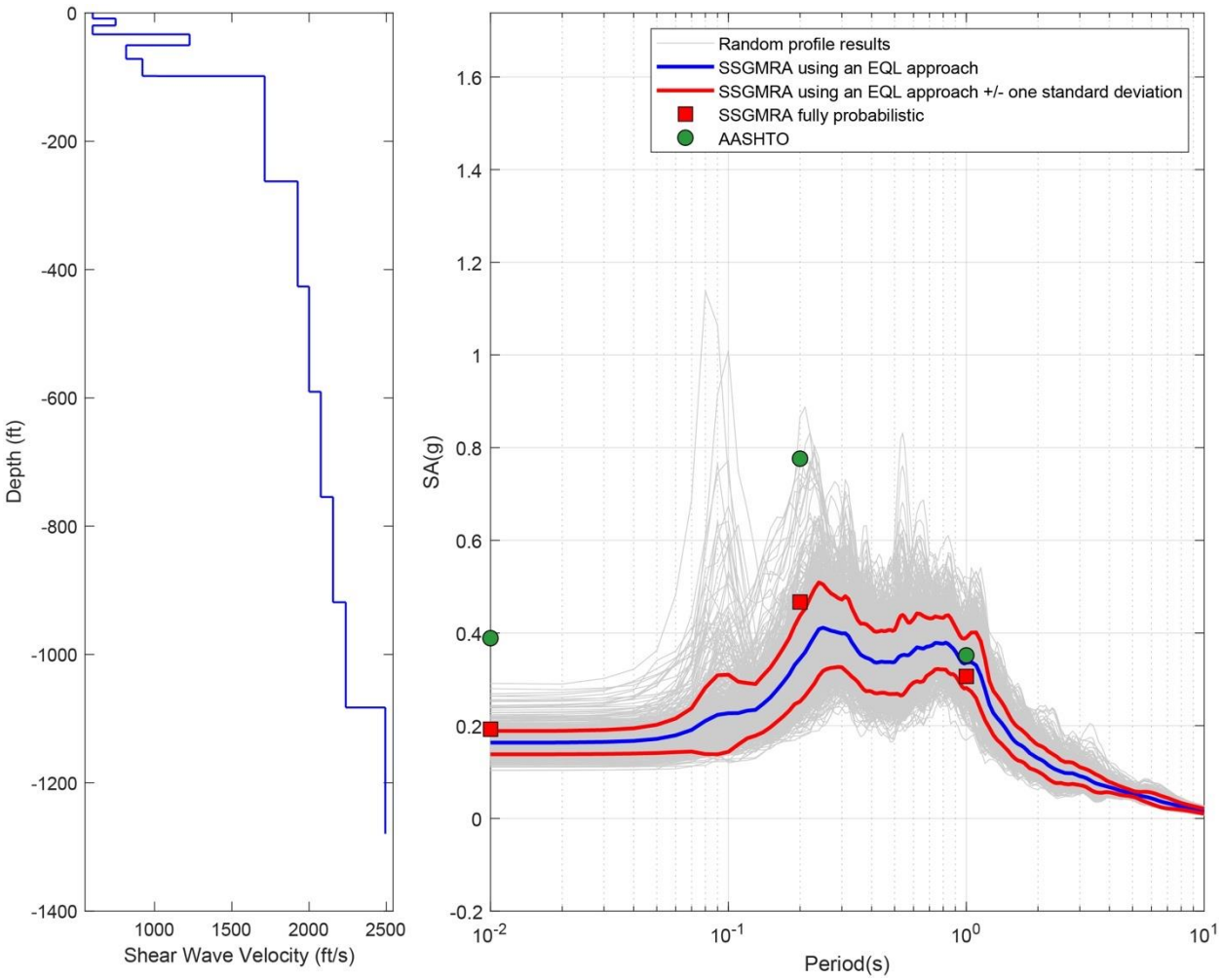


**Figure B-194. Left Panel: Shear-Wave Velocity Profile for Site 49 (Based on EPRI Soil Model); and Right Panel: Results of SSGMRA Using a Fully Probabilistic Approach, SSGMRA Using an Equivalent Linear Approach, SSGMRA Using an Equivalent Linear Approach Plus and Minus One Standard Deviation, and AASHTO General Approach**

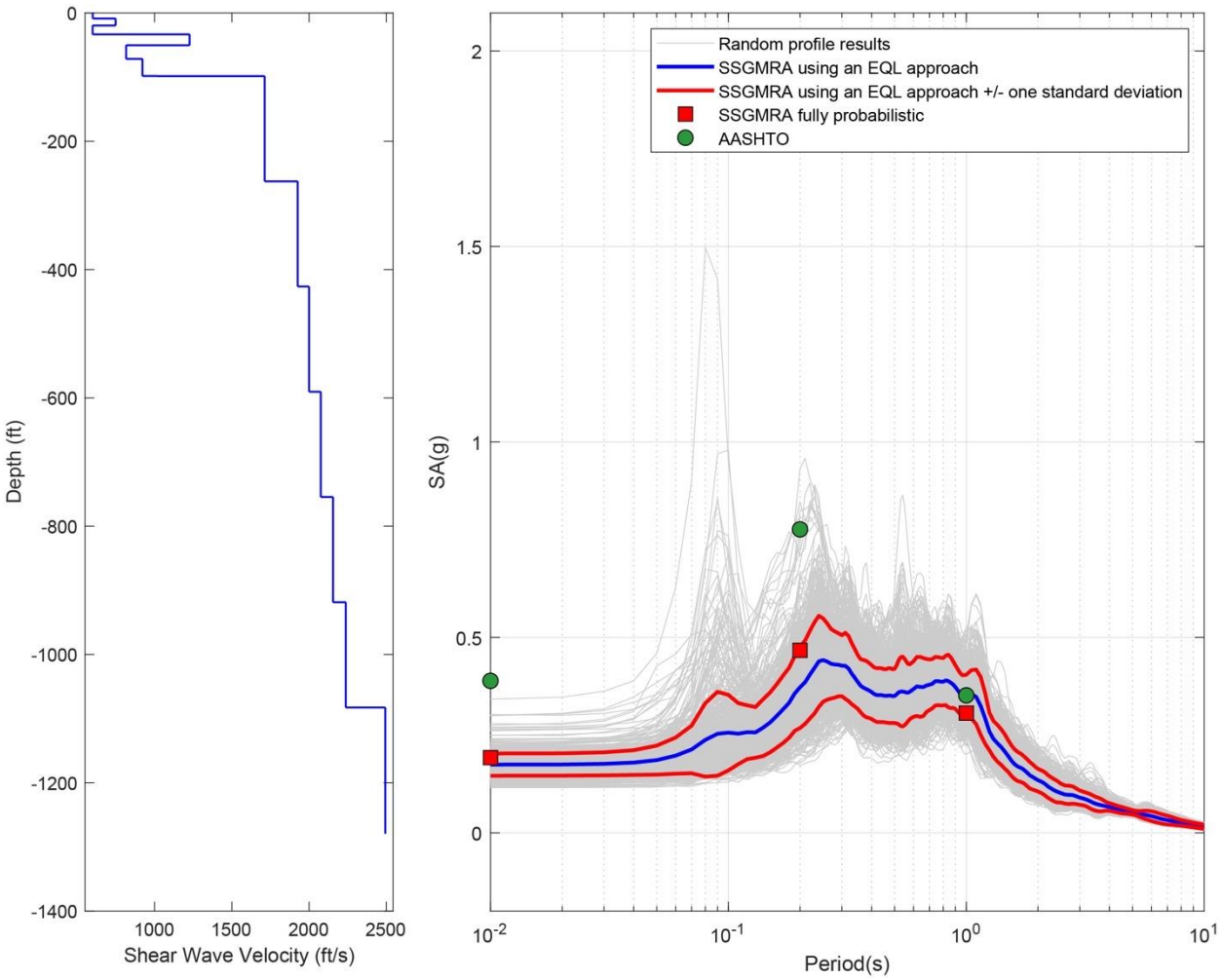


**Figure B-195. Left Panel: Shear-Wave Velocity Profile for Site 49 (Based on Peninsular Soil Model); and Right Panel: Results of SSGMRA Using a Fully Probabilistic Approach, SSGMRA Using an Equivalent Linear Approach, SSGMRA Using an Equivalent Linear Approach Plus and Minus One Standard Deviation, and AASHTO General Approach**

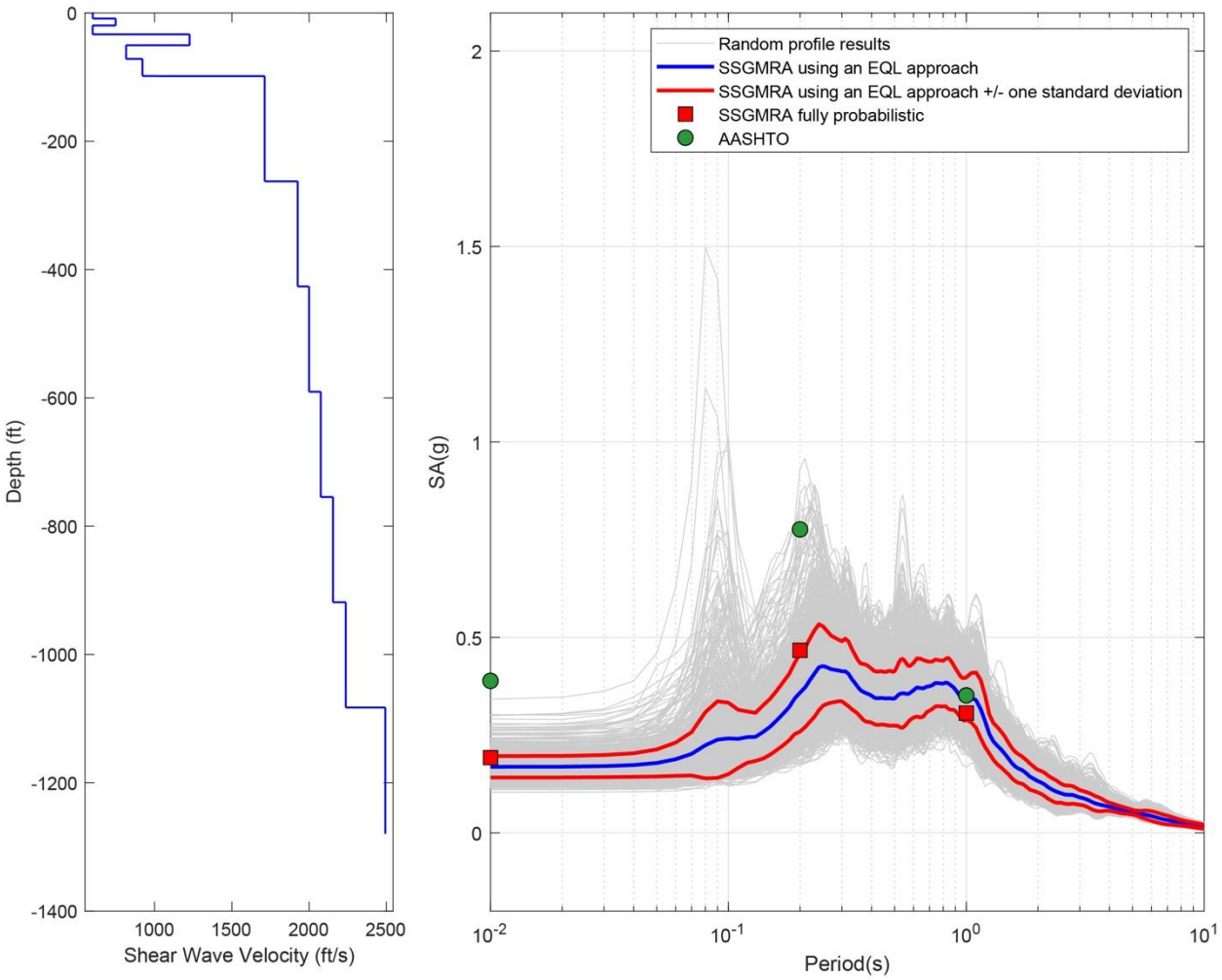


**Figure B-196. Left Panel: Shear-Wave Velocity Profile for Site 49 (Combined); and Right Panel: Results of SSGMRA Using a Fully Probabilistic Approach, SSGMRA Using an Equivalent Linear Approach, SSGMRA Using an Equivalent Linear Approach Plus and Minus One Standard Deviation, and AASHTO General approach**

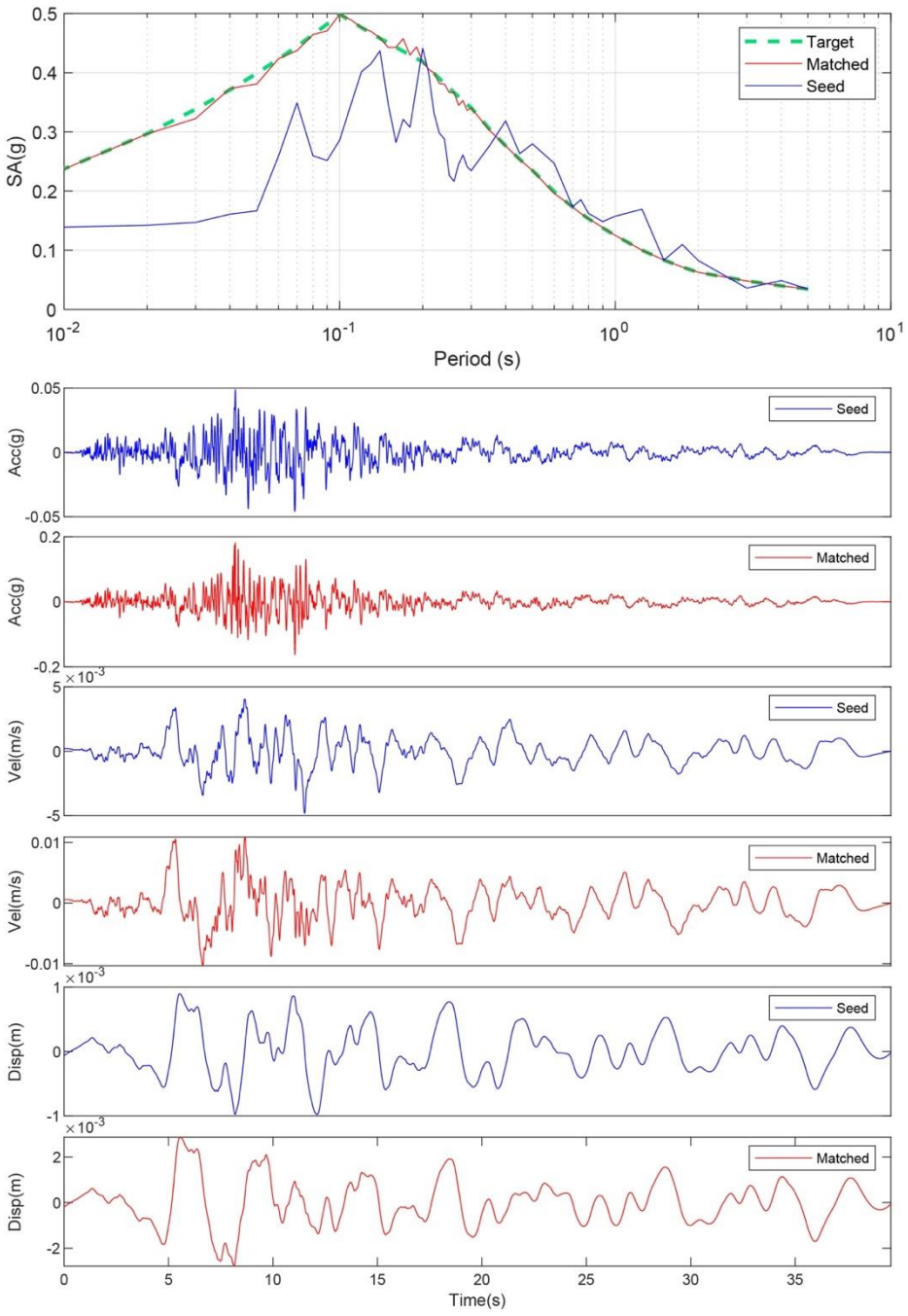


**Figure B-197. Matching Spectrum of Seed Motion (RSN774-LOMAP-HYN064) to the Target Spectrum (UHS) at Site 50. the Middle Subplot Shows the Seed Motion, and the Bottom Subplot Indicates the Matched Motion**

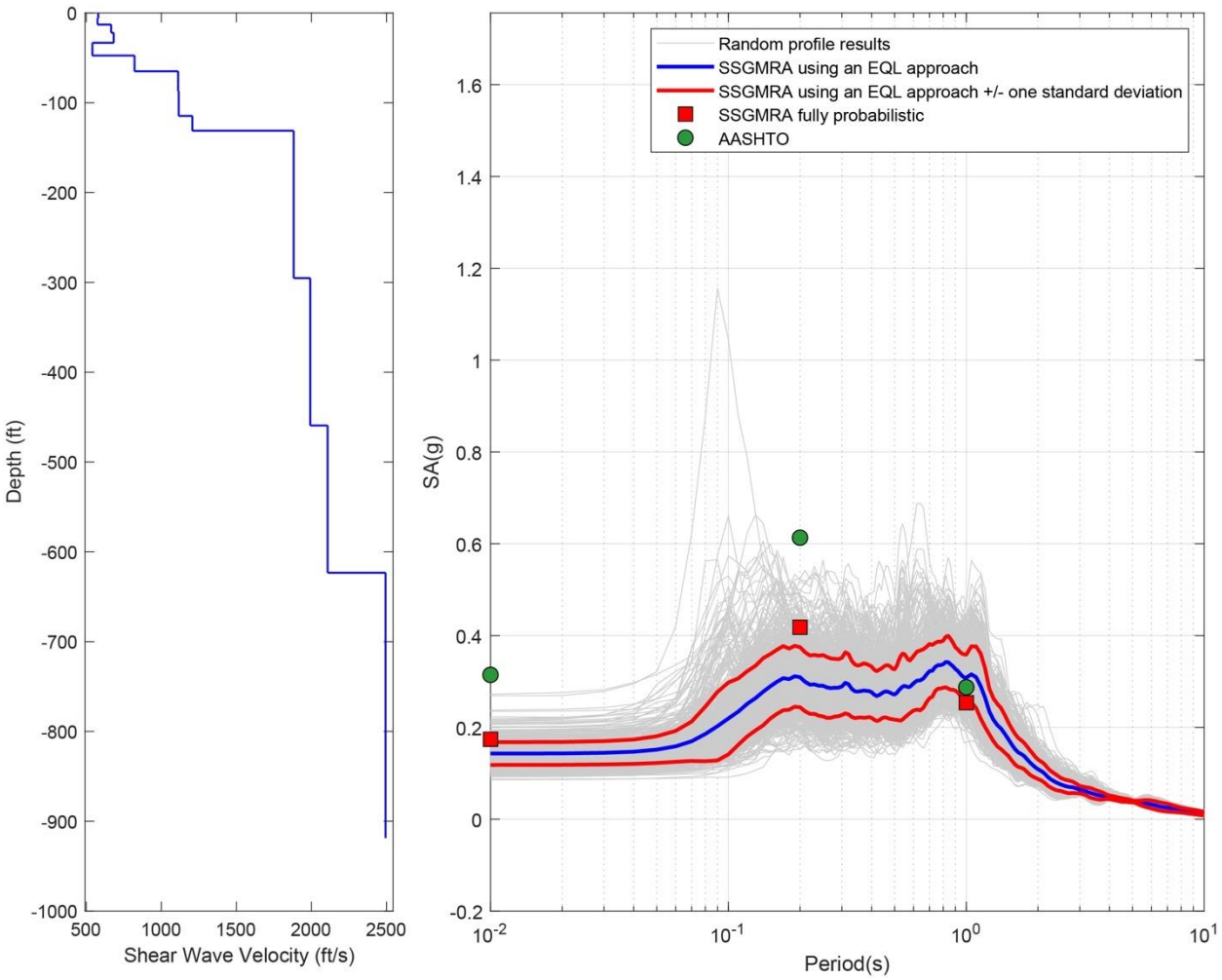


**Figure B-198. Left Panel: Shear-Wave Velocity Profile for Site 50 (Based on EPRI Soil Model); and Right Panel: Results of SSGMRA Using a Fully Probabilistic Approach, SSGMRA Using an Equivalent Linear Approach, SSGMRA Using an Equivalent Linear Approach Plus and Minus One Standard Deviation, and AASHTO General Approach**

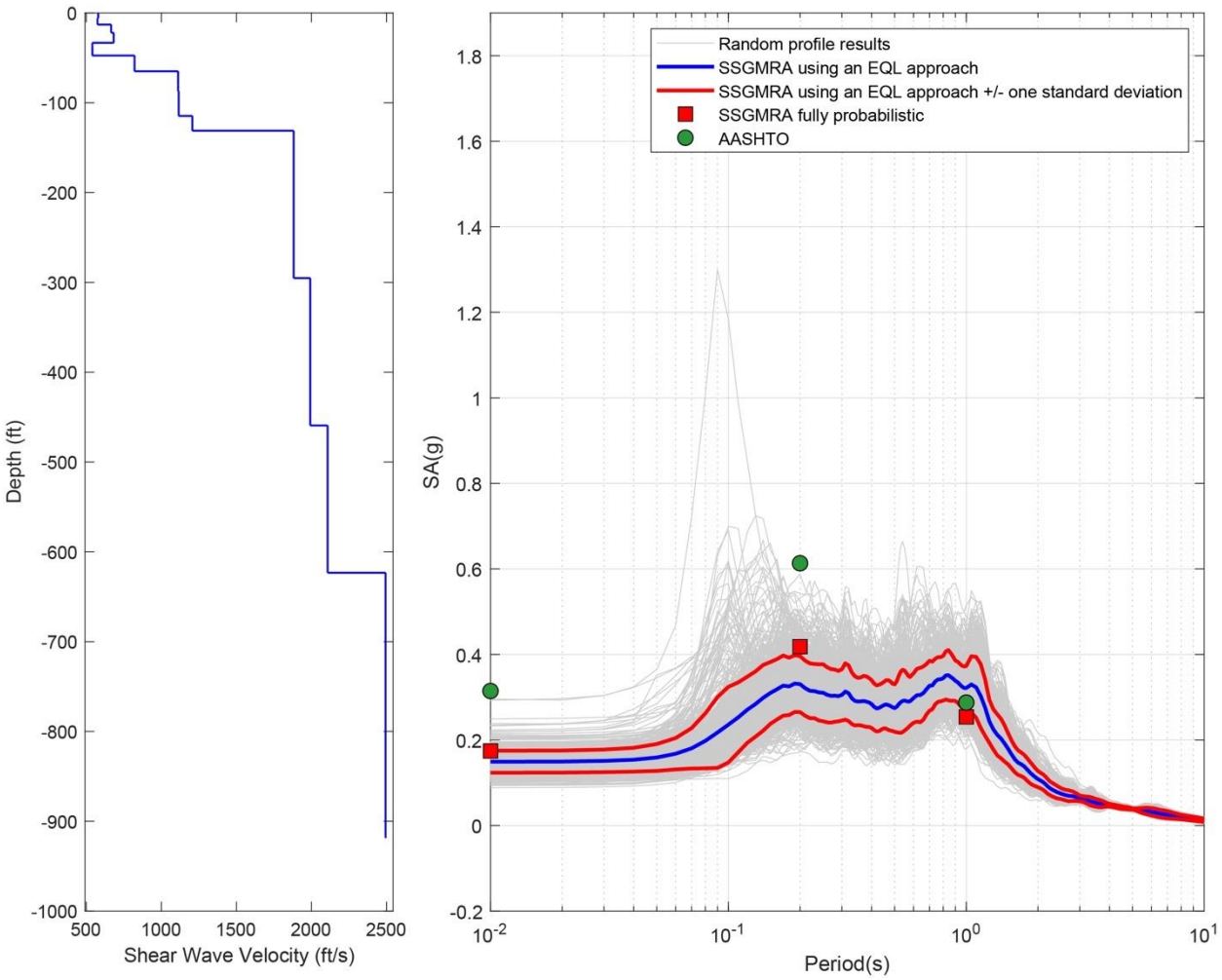


**Figure B-199. Left Panel: Shear-Wave Velocity Profile for Site 50 (Based on Peninsular Soil Model); and Right Panel: Results of SSGMRA Using a Fully Probabilistic Approach, SSGMRA Using an Equivalent Linear Approach, SSGMRA Using an Equivalent Linear Approach Plus and Minus One Standard Deviation, and AASHTO GENERAL APPROACH**

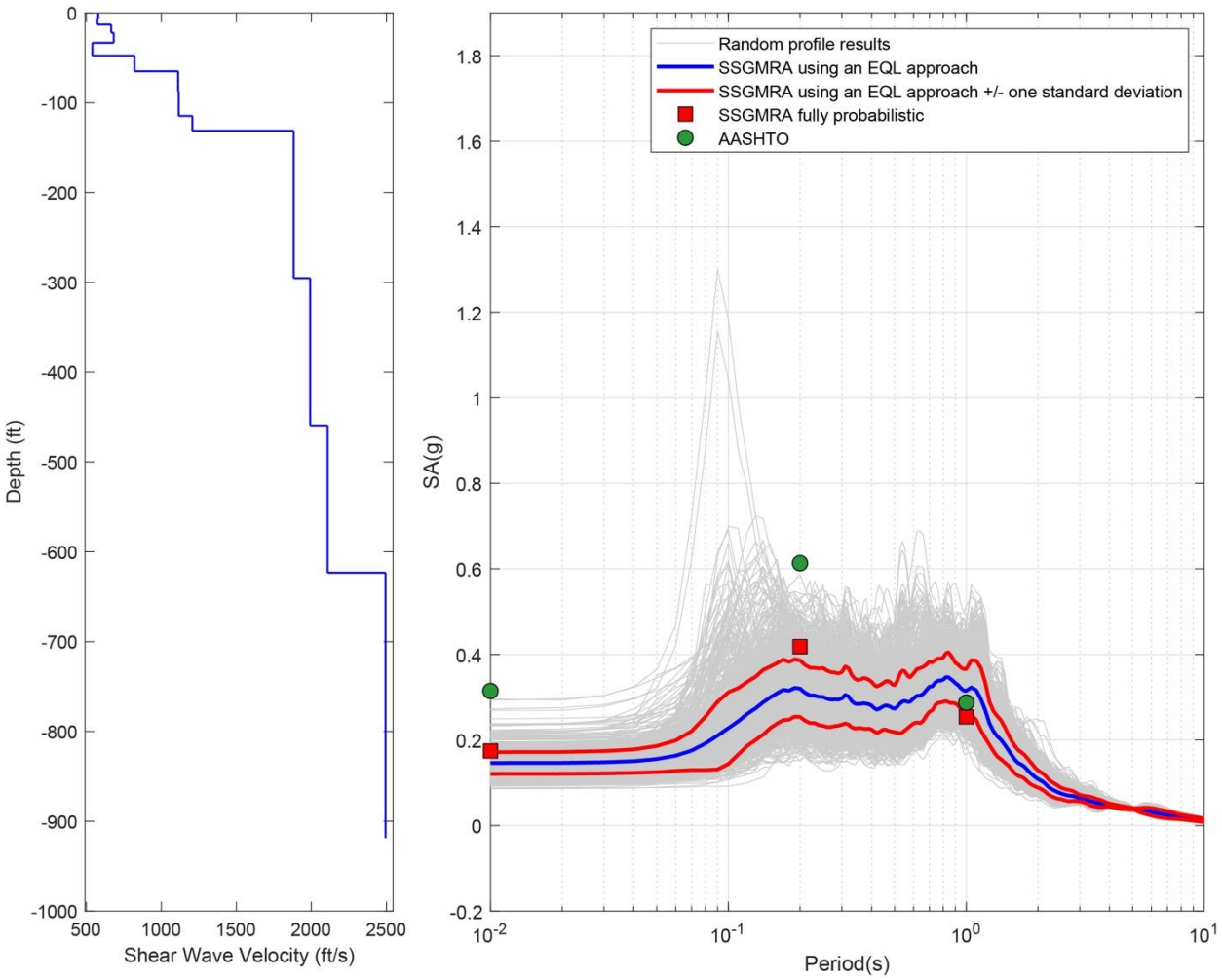


**Figure B-200. Left Panel: Shear-Wave Velocity Profile for Site 50 (Combined); and Right Panel: Results of SSGMRA Using a Fully Probabilistic Approach, SSGMRA Using an Equivalent Linear Approach, SSGMRA Using an Equivalent Linear Approach Plus and Minus One Standard Deviation, and AASHTO General Approach**

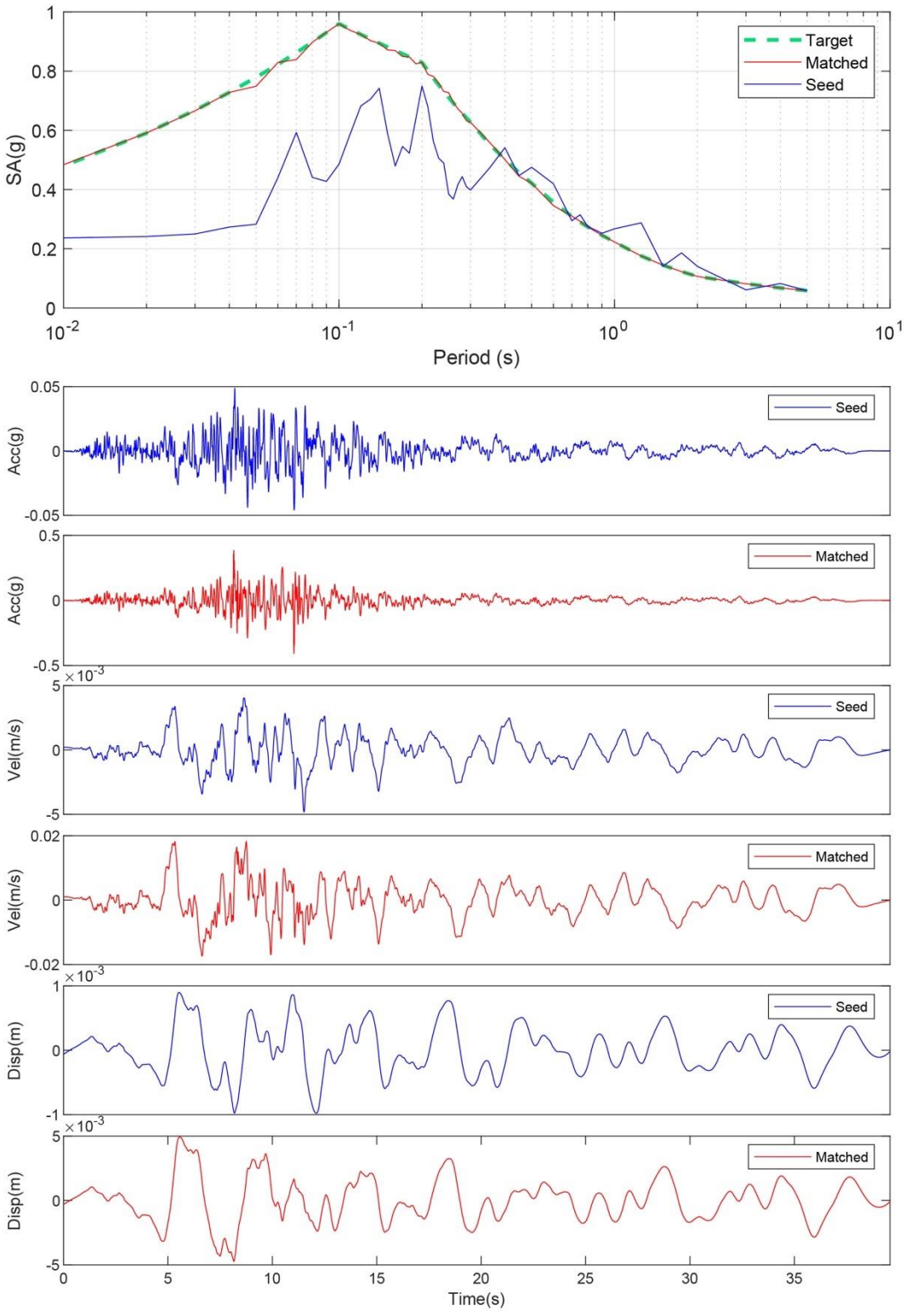


**Figure B-201. Matching Spectrum of Seed Motion (RSN774-LOMAP-HYN064) to the Target Spectrum (UHS) at Site 51. The Middle Subplot Shows the Seed Motion, and the Bottom Subplot Indicates the Matched Motion**

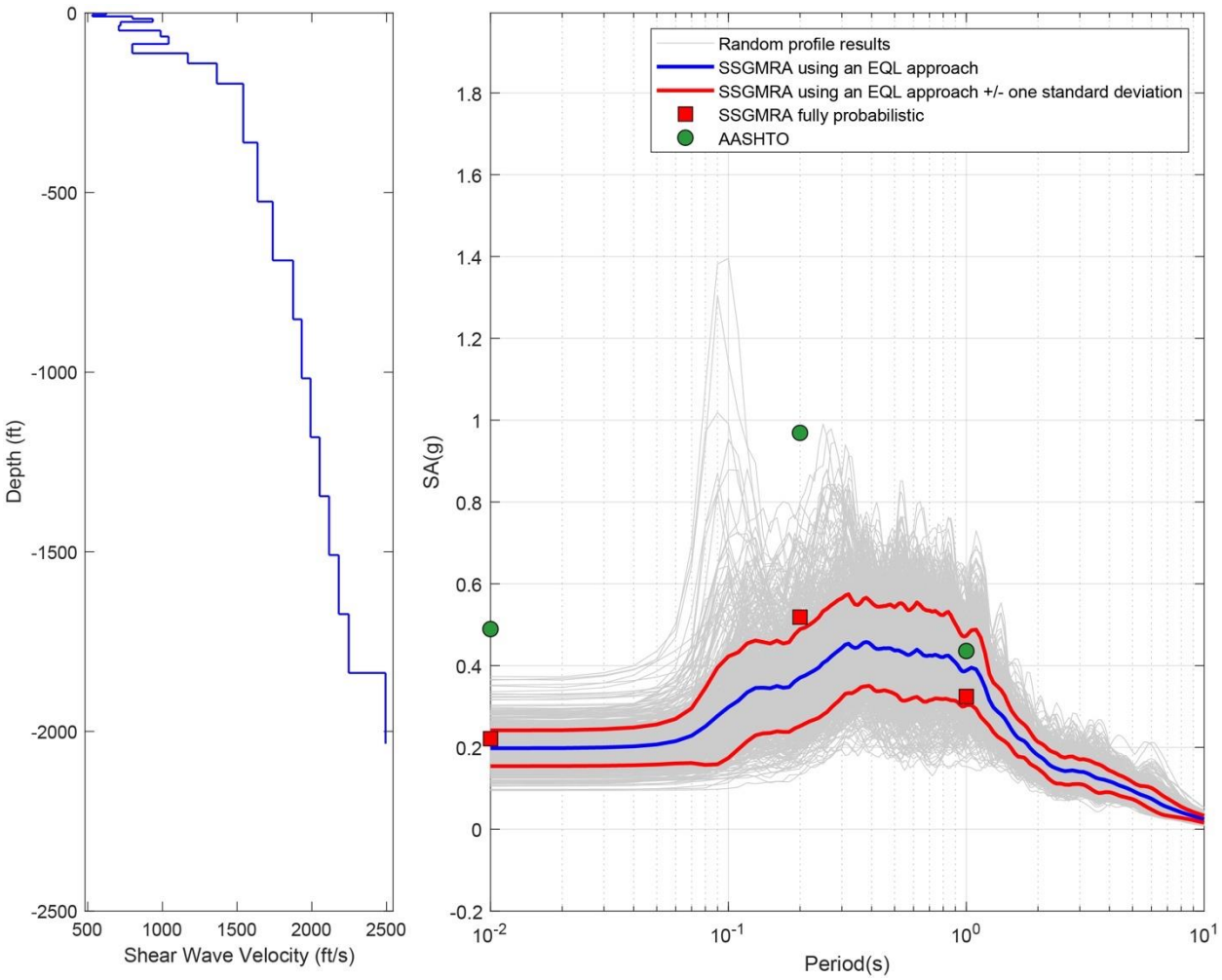


**Figure B-202. Left Panel: Shear-Wave Velocity Profile for Site 51 (Based on EPRI Soil Model); and Right Panel: Results of SSGMRA Using a Fully Probabilistic Approach, SSGMRA Using an Equivalent Linear Approach, SSGMRA Using an Equivalent Linear Approach Plus and Minus One Standard Deviation, and AASHTO General Approach**

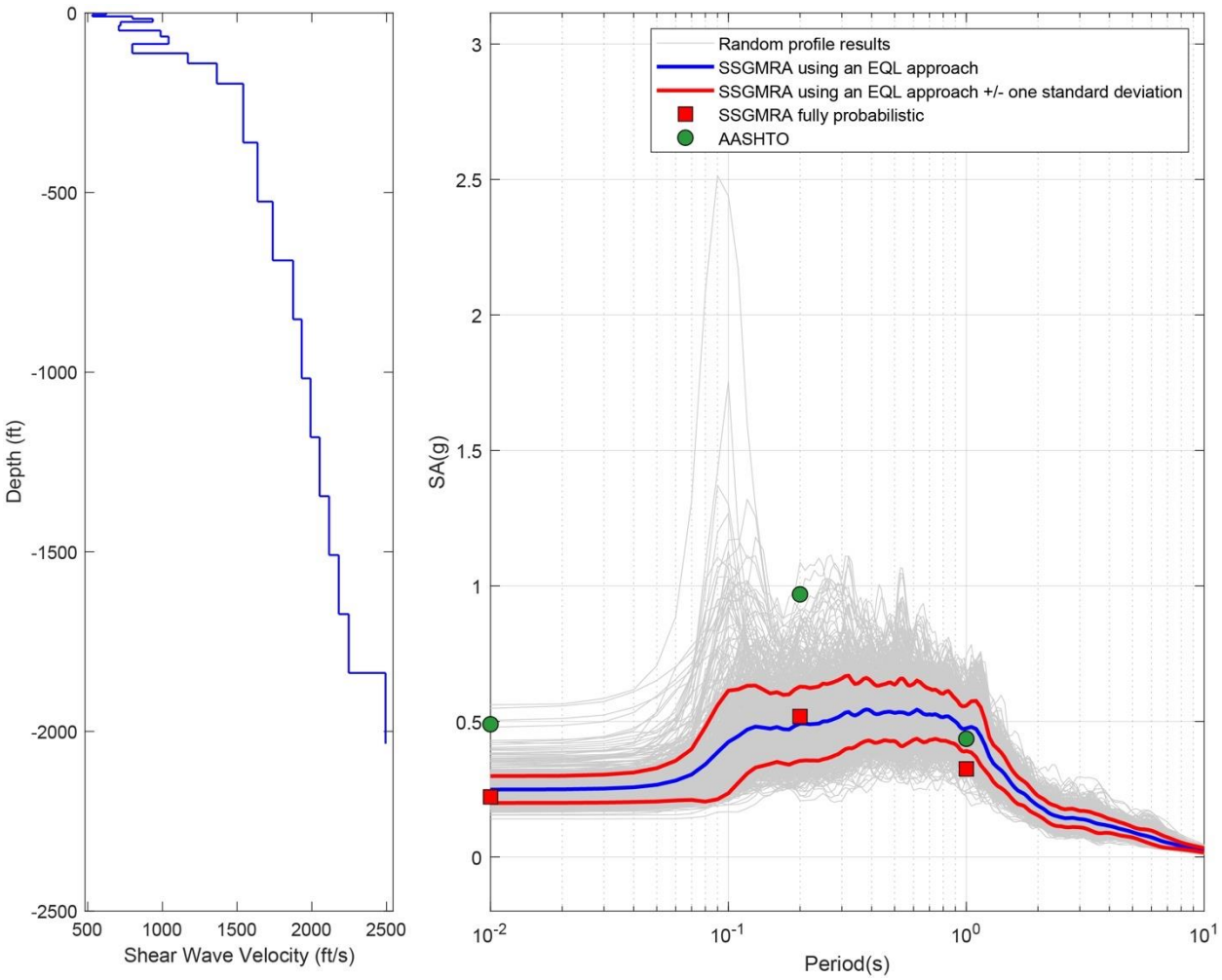


**Figure B-203. Left Panel: Shear-Wave Velocity Profile for Site 51 (Based on Peninsular Soil Model); and Right Panel: Results of SSGMRA Using a Fully Probabilistic Approach, SSGMRA Using an Equivalent Linear Approach, SSGMRA Using an Equivalent Linear Approach Plus and Minus One Standard Deviation, and AASHTO General Approach**

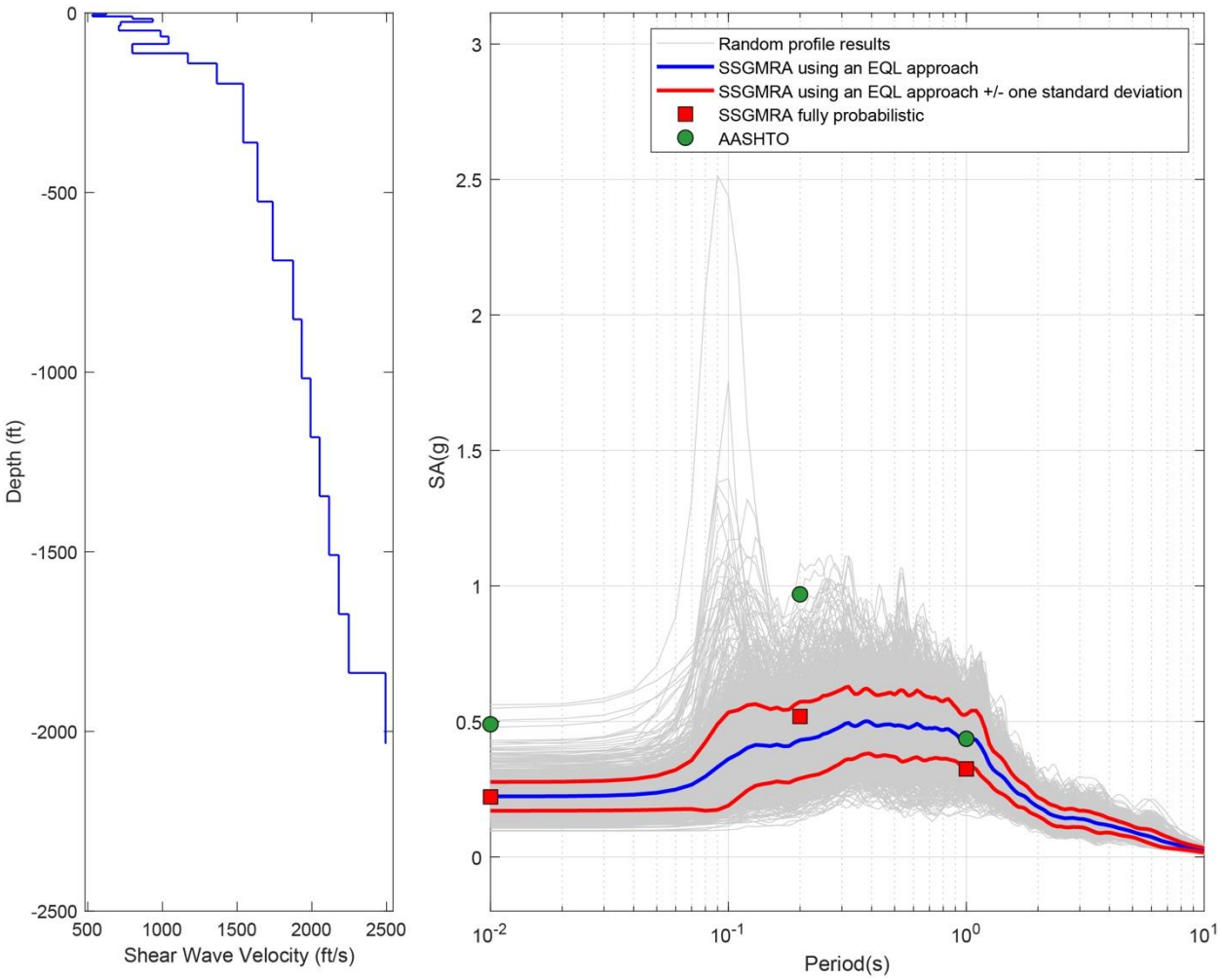


**Figure B-204. Left Panel: Shear-Wave Velocity Profile for Site 51 (Combined); and Right Panel: Results of SSGMRA Using a Fully Probabilistic Approach, SSGMRA Using an Equivalent Linear Approach, SSGMRA Using an Equivalent Linear Approach Plus and Minus One Standard Deviation, and AASHTO General Approach**